THE INFLUENCE OF GEOMETRY ON THE PERFORMANCE OF BREAKWATER ARMOUR UNITS

A thesis submitted for the degree of
Doctor of Philosophy of the University of London

S.S.L. Hettiarachchi, B.Sc. (Eng.)

Hydraulics Section,
Department of Civil Engineering,
Imperial College of Science and Technology.

May 1987

TO MY PARENTS

ABSTRACT

This study is mainly concerned with the influence of voids and geometry of armour on the performance of breakwaters and other coastal structures used in port construction and for sea defence purposes. In particular, attention is focused on armour units of a hollow-block form used for breakwater construction. Wave action on coastal structures is investigated from a viewpoint of the hydraulics of flow through porous media.

Extensive experimental investigations were performed on a variety of porous media under steady flow, oscillatory flow and unidirectional accelerated flow conditions to study the influence of the geometry of the voids matrix on overall hydraulic behaviour. The different structures investigated were broadly classified into vertical-faced rectangular structures and sloping structures, both containing homogeneous fill, conventional trapezoidal breakwaters with layered fill and armoured with hollow block armour units, and vertical pile structures. By varying the external configuration and internal material layout it was possible to generate a wide spectrum of porous coastal structures of practical interest.

The study identified both geometric and hydraulic governing parameters to classify porous media in general and hollow-block armour units in particular. The importance of area blockage at the wave-structure interface, volumetric porosity and tortuosity of the structure, dimension and shape of voids was established in relation to the performance of different porous media. Investigations were conducted on both permeability characteristics and force coefficients to study their behaviour as the flow was changed from steady to accelerated conditions including both unidirectional and oscillatory flow regimes.

The study provides extensive information on wave reflection, wave transmission and energy loss coefficients for a wide range of structures, thus providing a base for their performance to be assessed. Wave steepness, front slope and overall effective length of the structure and the degree of submergence were found to be important parameters which had to be considered together with the material layout of a porous structure.

Reflection, run-up and run-down coefficients were found for breakwaters armoured with different types of hollow block armour unit and measurements were made of along-slope and lift forces acting on a single unit. The upward along-slope force associated with wave impact was found to be the

dominant loading mechanism and the positive lift force – tending to extract an armour unit from the slope – was found to be within acceptable limits, not endangering the stability of the structure.

Analytical and numerical techniques were developed to predict reflection and transmission coefficients and to monitor internal wave decay in porous structures consisting of homogeneous fill. Because of the complexity of the problem, the study was limited to small-amplitude long waves normally incident to the structure. The respective coefficients were predicted in terms of the incident wave conditions and the hydraulic and geometric properties of the porous medium. The Forchheimer equation was used for the hydraulic gradient – velocity relationship. An assessment was also made of interface losses and scale effects on wave transmission through porous structures. The analysis of sloping embankments is performed by transforming them to an equivalent rectangular section and the physical significance of this concept was investigated experimentally. Satisfactory agreement was obtained between experimental and predicted values.

The study was relatively fundamental in nature but the results obtained are relevant to practical problems of breakwater design and also provide a basis for further work on this topic.

ACKNOWLEDGEMENTS

I wish to express my thanks to Professor P. Holmes for his supervision, encouragement and guidance provided during the course of the research study.

My thanks are also due to the members of the academic staff and colleagues of the Hydraulics Section for their advice and cooperation. I am grateful to Dr. R. Wing for his assistance with instrumentation and to Mr. N.W.H. Allsop of Hydraulics Research Ltd. for his keen interest and assistance.

Assistance given to me in laboratory work by Geoff Thomas, John Audsley, members of the technical staff and colleagues, Robert Shih and Y. Yang, is greatly appreciated. I am thankful to Patricia O'Connell for typing the manuscript and for her assistance.

I am very grateful to my parents for their constant encouragement and for providing funds for my studies. I acknowledge with thanks the financial assistance given to me from the Mountbatten Memorial Trust and the Leche Trust. I am also thankful to Hydraulics Research Ltd. for providing a bursary.

My sincere thanks are also due to Mildred and Arthur Madanayake and Dr. Priyan Dias for their invaluable support during my stay in U.K.

Finally, I wish to express my gratitude to Premini, my wife, for her assistance at all times. In spite of being busy with her own studies, she always found time to help me.

CONTENTS

	Page
ABSTRACT	3
ACKNOWLEDGEMENTS	5
LIST OF TABLES	9
LIST OF FIGURES	11
LIST OF PLATES	25
LIST OF SYMBOLS	26
CHAPTER 1 - INTRODUCTION	28
CHAPTER 2 - REVIEW OF PREVIOUS INVESTIGATIONS	44
2.1. Introduction	44
2.2. Flow through porous media	46
2.3. Hydraulic gradient - velocity relationships for steady non-Darcy flow in porous media	53
2.4. Time dependent flow in porous media	57
2.5. Wave action on porous structures	62
CHAPTER 3 - APPROACH TO THE PROBLEM	92
3.1. Introduction	92
3.2. Relevant conclusions from the literature review	92
3.3. Governing parameters for porous media and hollow block units	94
3.4. Selection of experimental media	97
3.5. Type of tests and experimental techniques	103
3.6. Theoretical considerations	113
CHAPTER 4 - EXPERIMENTAL APPARATUS, FLOW ENVIRONMENT AND PROCEDURES	127
4.1. Introduction	127
4.2. Steady flow tests	127
4.3. Oscillatory flow tests	131
4.4. Unidirectional acceleration tests	140
4.5. Tests on a model breakwater section	146

		Page
4.6.	Measurement of physical properties of random porous media	151
CHAPTER 5 -	THEORETICAL DEVELOPMENTS	164
5.1.	Introduction	164
5.2.	Governing equations	164
5.3.	Analytical developments	166
5.4.	Numerical developments	177
5.5.	Properties of finite difference schemes	185
CHAPTER 6 -	STEADY FLOW PERMEABILITY TESTS AND OSCILLATORY FLOW TESTS	194
6.1.	Introduction	194
6.2.	Physical properties of porous media	195
6.3.	Steady flow permeability tests	196
6.4.	Oscillatory flow tests	202
6.5.	Tests to determine interface losses	212
6.6.	Evaluation of the theoretical analyses	213
CHAPTER 7 -	CONSTANT ACCELERATION AND VELOCITY TESTS FOR MOVING POROUS BLOCK	269
7.1.	Introduction	269
7.2.	Method of analysis	271
7.3.	Discussion of results	274
7.4.	Concluding remarks	279
CHAPTER 8 -	ADDITIONAL TESTS UNDER OSCILLATORY FLOW CONDITIONS	309
8.1.	Introduction	309
8.2.	Performance of closed block structures (porous wave absorbers)	309
8.3.	Performance of porous submerged structures	318
8.4.	Performance of an open block structure with a sloping front	319

Page

8.5. Performance of a porous trapezoidal structure 323
8.6. Influence of length of open and closed block structures in relation to their overall performance 324
8.7. Evaluation of the theoretical analyses 326

CHAPTER 9 - TESTS ON A BREAKWATER SLOPING SECTION 363

9.1. Introduction 363
9.2. Reflection, run-up and run-down studies 363
9.3. Measurement of lift and along-slope forces 374

CHAPTER 10 - SCALE EFFECTS IN MODELS OF POROUS COASTAL STRUCTURES 435

10.1. Introduction 435
10.2. Modelling for transmission and reflection on undistorted scale 435
10.3. Methods of determining the scale ratio for particle size 437
10.4. Objectives of the present study 438
10.5. Analytical development, its application and discussion 439
10.6. Scale effect tests on wave transmission and reflection 447

CHAPTER 11 - SUMMARY, CONCLUSIONS AND RECOMMENDATIONS 462

11.1. Summary 462
11.2. Conclusions 463
11.3. Recommendations 467

REFERENCES 469

LIST OF TABLES

	Page
Table 1.1 - Classification of breakwater armour units	37
Table 2.1 - Structure of the literature survey	45
Table 2.2 - Flow coefficients for Engelund's (1953) equation	54
Table 2.3 - Comparison of Engelund's (1953) and LeMehaute's (1957) equations	84
Table 2.4 - Wave action on porous structures	85
Table 3.1 - Experimental techniques	115
Table 6.1 - Summary of the experimental programme	222
Table 6.2 - Physical properties of experimental media	223
Table 6.3 - Results from steady flow permeability tests	225
Table 6.4 - Results from selected investigations on steady flow permeability tests	226
Table 6.5 - Results from oscillatory flow tests Relative magnitude of transmission (K_t), reflection (K_r) and energy loss (K_d) coefficients	227
Table 6.6 - Cross-comparison studies with experimental media	228
Table 7.1 - Results from unidirectional constant acceleration tests	282
Table 7.2 - Results from constant velocity tests	283
Table 8.1 - Numerical solution for the internal transmission coefficients for different porous media	333
Table 8.2 - Response of the numerical solution to variations in laminar and turbulent flow coefficients	334
Table 8.3 - Sensitivity of the numerical solution to variations in wave period	335

Page

Table 9.1 - Equations for reflection, run-up and run-down coefficients based on data from the present study 393

Table 9.2 - Equations for reflection, run-up and run-down coefficients based on data from tests performed by Stickland (1969) 394

Table 9.3 - Equations for reflection, run-up and run-down coefficients (Losada and Gimenez-Curto 1981) 395

Table 9.4 - Results from breakwater section with a permeable underlayer 396

Table 9.5 - Results from breakwater section with a permeable underlayer 397

Table 9.6 - Results from breakwater section with a permeable underlayer 398

Table 9.7 - Results from breakwater section with an impermeable underlayer 399

Table 9.8 - Results from breakwater section with an impermeable underlayer 400

Table 9.9 - Comparison of results from breakwater sections with and without a permeable underlayer 401

Table 10.1 - Steady flow laminar and turbulent coefficients 440

Table 10.2 - Steady flow coefficients for cylindrical lattice structures 445

Table 10.3 - Steady flow coefficients for spheres and rounded stones 447

Table 10.4 - Details of selected investigations on the influence of scale effects on wave transmission and reflection 451

Table 10.5 - Details of the present study on the influence of scale effects on wave transmission and reflection 452

LIST OF FIGURES

	Page
Fig. 1.1 - Coastal structures	38
Fig. 1.2 - Bulky type of armour units	39
Fig. 1.3 - Slender interlocking type of armour units	40
Fig. 1.4 - Hollow block type of armour units	41
Fig. 1.5 - Relationship between armour block stability and voids ratio	42
Fig. 1.6 - Important aspects of wave action on a rubble mound breakwater	43
Fig. 2.1 - Variation of Friction factor with Reynolds number	86
Fig. 2.2 - Effects of unsteady flow	88
Fig. 2.3 - Effects of air entrainment	89
Fig. 2.4 - Influence of different core material on the stability of rubble mounds	90
Fig. 2.5 - Field investigations on porous coastal structures	91
Fig. 3.1 - Geometric parameters for hollow block armour units	116
Fig. 3.2 - Details of the Cob armour unit	117
Fig. 3.3 - Details of the Shed armour unit	118
Fig. 3.4 - Details of the Stolk armour unit	119
Fig. 3.5 - Details of the Hobo (Hollow Block) armour unit	120
Fig. 3.6 - Details of the Hexagonal armour unit (Hexo)	121
Fig. 3.7 - Details of the Cylindrical lattice structure	122
Fig. 3.8 - Plan views of pile structures used for the study	123
Fig. 3.9 - Details of the structures consisting of spheres and rounded stones	124
Fig. 3.10 - Details of the Dolos armour unit	125
Fig. 3.11 - Details of the Stabit armour unit	125
Fig. 3.12 - Details of the structures used for additional tests under oscillatory flow conditions	126
Fig. 4.1 - Experimental equipment for steady flow permeability tests	153
Fig. 4.2 - Experimental equipment for oscillatory flow tests	154

Page

Fig. 4.3 - Cross-sectional elevation of the moving porous block for unidirectional acceleration tests 155
Fig. 4.4 - Details of the force transducer used for acceleration tests 156
Fig. 4.5 - Experimental equipment for unidirectional acceleration tests 157
Fig. 4.6 - Experimental equipment for reflection, run-up and run-down tests on a breakwater section 158
Fig. 4.7 - Cross-sectional elevation of the model breakwater 159
Fig. 4.8 - Plan view of the model breakwater - Section A-A, Fig. 4.7 160
Fig. 4.9 - Details of the force transducer 161
Fig. 4.10 - Detailed view of the instrumented armour unit 162
Fig. 4.11 - Experimental equipment for measurement of lift and along-slope force on the breakwater section 163

Fig. 5.1 - Structural configurations used for analyses 164
Fig. 5.2 - Open block structure 170
Fig. 5.3 - Closed block structure 173
Fig. 5.4 - Closed block structure (wave absorber) 178

Fig. 6.1.a - Hydraulic gradient vs Mean velocity for Cob units 230
Fig. 6.1.b - Loss coefficient vs Reynolds number for Cob units 230
Fig. 6.2.a - Hydraulic gradient vs Mean velocity for Shed units 231
Fig. 6.2.b - Loss coefficient vs Reynolds number for Shed units 231
Fig. 6.3.a - Hydraulic gradient vs Mean velocity for Hobo (20 mm) units 232
Fig. 6.3.b - Loss coefficient vs Reynolds number for Hobo (20 mm) units 232
Fig. 6.4.a - Hydraulic gradient vs Mean velocity for Hobo (25 mm) units 233
Fig. 6.4.b - Loss coefficient vs Reynolds number for Hobo (25 mm) units 233

Page

Fig. 6.5.a - Hydraulic gradient vs Mean velocity for Cylindrical lattice structure (15 mm) 234

Fig. 6.5.b - Loss coefficient vs Reynolds number for Cylindrical lattice structure (15 mm) 234

Fig. 6.6.a - Hydraulic gradient vs Mean velocity for Cylindrical lattice structure (20 mm) 235

Fig. 6.6.b - Loss coefficient vs Reynolds number for Cylindrical lattice structure (20 mm) 235

Fig. 6.7.a - Hydraulic gradient vs Mean velocity for Cylindrical lattice structure (30 mm) 236

Fig. 6.7.b - Loss coefficient vs Reynolds number for Cylindrical lattice structure (30 mm) 236

Fig. 6.8.a - Hydraulic gradient vs Mean velocity for randomly packed spheres (19 mm) 237

Fig. 6.8.b - Loss coefficient vs Reynolds number for randomly packed spheres (19 mm) 237

Fig. 6.9.a - Hydraulic gradient vs Mean velocity for randomly packed spheres (25 mm) 238

Fig. 6.9.b - Loss coefficient vs Reynolds number for randomly packed spheres (25 mm) 238

Fig. 6.10.a - Hydraulic gradient vs Mean velocity for rounded stones (34.8 mm) 239

Fig. 6.10.b - Loss coefficient vs Reynolds number for rounded stones (34.8 mm) 239

Fig. 6.11.a - Hydraulic gradient vs Mean velocity Fitted curves ($I = au + bu^2$) for hollow block units and cylindrical lattice structures 240

Fig. 6.11.b - Hydraulic gradient vs Mean velocity Fitted curves ($I = au + bu^2$) for randomly packed spheres and rounded stones 241

Fig. 6.12.a - Hydraulic gradient vs Mean velocity Fitted curves ($I = cu^m$) for hollow block units and cylindrical lattice structures 242

Fig. 6.12.b - Hydraulic gradient vs Mean velocity Fitted curves ($I = cu^m$) for randomly packed spheres and rounded stones 243

		Page
Fig. 6.13.a	- Loss coefficient vs Reynolds number Fitted curves ($C_1 = C_2/Re + C_3$) for hollow block units and cylindrical lattice structures	244
Fig. 6.13.b	- Loss coefficient vs Reynolds number Fitted curves ($C_1 = C_2/Re + C_3$) for randomly packed spheres and rounded stones	245
Fig. 6.14.a	- I_T/I_L vs Velocity for hollow block units and cylindrical lattice structures	246
Fig. 6.14.b	- I_T/I_L vs Velocity for randomly packed spheres and rounded stones	247
Fig. 6.15	- Turbulent coefficent (b in $I = au + bu^2$) vs Diameter for cylindrical lattice structures	248
Fig. 6.16	- K_t, K_r and K_d vs Steepness for Cob units	249
Fig. 6.17	- K_t, K_r and K_d vs Steepness for Shed units	249
Fig. 6.18	- K_t, K_r and K_d vs Steepness for Hobo (16 mm) units	250
Fig. 6.19	- K_t, K_r and K_d vs Steepness for Hobo (20 mm) units	250
Fig. 6.20	- K_t, K_r and K_d vs Steepness for Hobo (25 mm) units	251
Fig. 6.21	- K_t, K_r and K_d vs Steepness for Dolos units	252
Fig. 6.22	- K_t, K_r and K_d vs Steepness for Stabit units	252
Fig. 6.23	- K_t, K_r and K_d vs Steepness for Cylindrical lattice (15 mm)	253
Fig. 6.24	- K_t, K_r and K_d vs Steepness for Cylindrical lattice (20 mm)	253
Fig. 6.25	- K_t, K_r and K_d vs Steepness for Cylindrical lattice (30 mm)	254
Fig. 6.26	- K_t vs Wave height/Depth (H_i/D) for Cylindrical lattice structures	255
Fig. 6.27	- K_t, K_r and K_d vs Steepness for Pile structure (15 mm) (members aligned in both directions)	256
Fig. 6.28	- K_t, K_r and K_d vs Steepness for Pile structure (15 mm) (alternate rows staggered)	256
Fig. 6.29	- K_t, K_r and K_d vs Steepness for Spherical lattice (38 mm)	257

		Page
Fig. 6.30	- K_t, K_r and K_d vs Steepness for Spherical lattice (51 mm)	257
Fig. 6.31	- K_t, K_r and K_d vs Steepness for randomly packed spheres (19 mm)	258
Fig. 6.32	- K_t, K_r and K_d vs Steepness for randomly packed spheres (25 mm)	258
Fig. 6.33	- K_t, K_r and K_d vs Steepness for rounded stones (34.76 mm)	259
Fig. 6.34	- K_t vs Wave height/Depth (H_i/D) for spherical lattice structures and randomly packed spheres	260
Fig. 6.35	- Results from selected investigations on wave reflection and transmission through porous structures	261
Fig. 6.36	- K_t, K_r and K_d vs Steepness Interface losses for Cob units	262
Fig. 6.37	- K_t, K_r and K_d vs Steepness Interface losses for Shed units	262
Fig. 6.38	- Comparison of experimental and theoretical values: K_t, K_r and K_d for porous block consisting of Cob units	263
Fig. 6.39	- Comparison of experimental and theoretical values: K_t, K_r and K_d for porous block consisting of Shed units	263
Fig. 6.40	- Comparison of experimental and theoretical values: K_t, K_r and K_d for porous block consisting of Hobo (20 mm) units	264
Fig. 6.41	- Comparison of experimental and theoretical values: K_t, K_r and K_d for porous block consisting of Hobo (25 mm) units	264
Fig. 6.42	- Comparison of experimental and theoretical values: K_t, K_r and K_d for Cylindrical lattice structure (15 mm)	265

		Page
Fig. 6.43	- Comparison of experimental and theoretical values: K_t, K_r and K_d for Cylindrical lattice structure (20 mm)	265
Fig. 6.44	- Comparison of experimental and theoretical values: K_t, K_r and K_d for Cylindrical lattice structure (30 mm)	266
Fig. 6.45	- Comparison of experimental and theoretical values: K_t, K_r and K_d for randomly packed spheres (19 mm)	267
Fig. 6.46	- Comparison of experimental and theoretical values: K_t, K_r and K_d for randomly packed spheres (25 mm)	267
Fig. 6.47	- Comparison of experimental and theoretical values: K_t, K_r and K_d for rounded stones (34.8 mm)	268
Fig. 7.1.a	- Force (measured) vs Time for Cob units under acceleration	284
Fig. 7.1.b	- Force (smoothed) vs Time for Cob units under acceleration	284
Fig. 7.1.c	- Spectral analysis of residual force for Cob units under acceleration	285
Fig. 7.1.d	- Force (measured) vs Velocity for Cob units under acceleration	285
Fig. 7.1.e	- Velocity time profile for the trolley for Cob units under acceleration	286
Fig. 7.1.f	- Force vs Velocity for Cob units under uniform velocity	286
Fig. 7.2.a	- Force (measured) vs Time for Shed units under acceleration	287
Fig. 7.2.b	- Force (smoothed) vs Time for Shed units under acceleration	287
Fig. 7.2.c	- Spectral analysis of residual force for Shed units under acceleration	288

		Page
Fig. 7.2.d	- Force (measured) vs Velocity for Shed units under acceleration	288
Fig. 7.2.e	- Velocity time profile for the trolley for Shed units under acceleration	289
Fig. 7.2.f	- Force vs Velocity for Shed units under uniform velocity	289
Fig. 7.3.a	- Force (measured) vs Time for Hobo units under acceleration	290
Fig. 7.3.b	- Force (smoothed) vs Time for Hobo units under acceleration	290
Fig. 7.3.c	- Spectral analysis of residual force for Hobo units under acceleration	291
Fig. 7.3.d	- Force (measured) vs Velocity for Hobo units under acceleration	291
Fig. 7.3.e	- Velocity time profile for the trolley for Hobo units under acceleration	292
Fig. 7.3.f	- Force vs Velocity for Hobo units under uniform velocity	292
Fig. 7.4.a	- Force (measured) vs Time for Hobo units under acceleration	293
Fig. 7.4.b	- Force (smoothed) vs Time for Hobo units under acceleration	293
Fig. 7.4.c	- Spectral analysis of residual force for Hobo units under acceleration	294
Fig. 7.4.d	- Force (measured) vs Velocity for Hobo units under acceleration	294
Fig. 7.4.e	- Velocity time profile for the trolley for Hobo units under acceleration	295
Fig. 7.5.a	- Force (measured) vs Time for Cylat under acceleration	296
Fig. 7.5.b	- Force (smoothed) vs Time for Cylat under acceleration	296
Fig. 7.5.c	- Spectral analysis of residual force for Cylat under acceleration	297
Fig. 7.5.d	- Force (measured) vs Velocity for Cylat under acceleration	297
Fig. 7.5.e	- Velocity time profile for the trolley for Cylat under acceleration	298

		Page
Fig. 7.5.f	- Force vs Velocity for Cylat under uniform velocity	298
Fig. 7.6	- Force vs Velocity for Cob units Fitted curves for experimental observations	299
Fig. 7.7	- Force vs Velocity for Shed units Fitted curves for experimental observations	300
Fig. 7.8	- Force vs Velocity for Hobo units Fitted curves for experimental observations	301
Fig. 7.9	- Force vs Velocity for Cylat units Fitted cuves for experimental observations	302
Fig. 7.10.a and b	- Difference in force vs Velocity for Cob units	303
Fig. 7.11.a and b	- Difference in force vs Velocity for Shed units	304
Fig. 7.12.a and b	- Difference in force vs Velocity for Hobo units	305
Fig. 7.13.a and b	- Difference in force vs Velocity for Cylat units	306
Fig. 7.14	- Drag force coefficient vs Acceleration (b in $F = bu^2 + c\dot{u}$ for constant acceleration and $F = bu^2$ for constant velocity)	307
Fig. 7.15	- Force vs Velocity Fitted curves for experimental observations for Cob, Shed, Hobo and Cylat units under constant velocity	308
Fig. 8.1	- Open and closed block structures	336
Fig. 8.2	- Wave decay in a porous absorber consisting of Cob armour units Experimental values for T = 1.0, 1.5 and 2.0 secs	337
Fig. 8.3	- Wave decay in a porous absorber consisting of Cob armour units Experimental values for T = 1.0 sec	338
Fig. 8.4	- Wave decay in a porous absorber consisting of Cob armour units Experimental values for T = 1.5 secs	338

		Page
Fig. 8.5	- Wave decay in a porous absorber consisting of Cob armour units Experimental values for T = 2.0 secs	339
Fig. 8.6.a	- Reflection coefficient (K_r) vs Steepness For porous absorber consisting of Cob armour units	340
Fig. 8.6.b	- Reflection coefficient (K_r) vs Wave height/ Depth (H_i/d) ratio for porous absorber consisting of Cob armour units	340
Fig. 8.7	- Wave decay in an open block structure consisting of Shed armour units Experimental values for T = 1.5 secs	341
Fig. 8.8	- Wave decay in an absorber (closed block structure) consisting of Shed armour units Experimental values for T = 1.5 secs	341
Fig. 8.9	- Wave decay in an open block structure consisting of Shed armour units Experimental values for T = 1.0, 1.5 and 2.0 secs	342
Fig. 8.10	- Wave decay in an absorber (closed block structure) consisting of Shed armour units Experimental values for T = 1.0, 1.5 and 2.0 secs	342
Fig. 8.11	- K_t and K_r vs Steepness Comparison of performance of a rectangular block of Shed armour units with and without an impermeable face at the back	343
Fig. 8.12.a	- K_d (energy loss coefficient) vs Steepness Comparison of performance of a rectangular block of Shed armour units with and without an impermeable face at the back	344
Fig. 8.12.b	- K_d (energy loss coefficient) vs Steepness Performance of a rectangular absorber consisting of Cob armour units	345
Fig. 8.13	- Different types of wave absorbers	346
Fig. 8.14	- K_t, K_r and K_d vs Steepness for a rectangular block of Cob armour units (non-submerged)	347

		Page
Fig. 8.15	- K_t, K_r and K_d vs Steepness for a rectangular block of Cob armour units (just-submerged)	347
Fig. 8.16	- K_t, K_r and K_d vs Steepness for a rectangular block of Cob armour units (fully-submerged)	348
Fig. 8.17	- Results from selected investigations on wave reflection from sloping surfaces	349
Fig. 8.18	- K_t, K_r and K_d vs Steepness Influence of a sloping front face at T = 1.5 secs for a structure consisting of rounded stones	350
Fig. 8.19	- K_r vs ξ^* ($= \sin\alpha/\sqrt{H_i/L_o}$) for sloping and vertical faced structures consisting of rounded stones	351
Fig. 8.20	- K_t, K_r and K_d vs Steepness for the porous trapezoidal structure consisting of Cob armour units	352
Fig. 8.21	- K_t, K_r and K_d vs Steepness for the equivalent rectangular structure based on equal submerged volume	353
Fig. 8.22	- K_t, K_r and K_d vs Steepness for the equivalent rectangular structure based on equal length at still water depth	354
Fig. 8.23	- K_t, K_r and K_d vs Steepness Influence of length of structure at T = 1.5 secs for structures consisting of rounded stones	355
Fig. 8.24	- K_t vs Steepness for varying structural geometry (porous media consisting of rounded stones)	356
Fig. 8.25	- Comparison of experimental and theoretical values: Reflection coefficients for porous absorber consisting of Cob armour units	357
Fig. 8.26	- Wave decay in a porous absorber Comparison of experimental and theoretical values for T = 2.0 secs and A_o = 2.28 cm	358

		Page
Fig. 8.27	- Wave decay in a porous absorber Comparison of experimental and theoretical values for T = 2.0 secs and A_o = 3.82 cm	358
Fig. 8.28	- Wave decay in a porous absorber Comparison of experimental and theoretical values for T = 1.5 secs and A_o = 2.81 cm	359
Fig. 8.29	- Wave decay in a porous absorber Comparison of experimental and theoretical values for T = 1.0 secs and A_o = 2.62 cm	359
Fig. 8.30	- Porous trapezoid and its equivalent rectangular structures	360
Fig. 8.31	- Comparison of experimental and theoretical values: K_t, K_r and K_d for porous rectangular block of length 52.0 cm consisting of Cob armour units	361
Fig. 8.32	- Comparison of experimental and theoretical values: K_t, K_r and K_d for porous rectangular block of length 33.3 cm consisting of Cob armour units	361
Fig. 8.33	- Comparison of experimental and theoretical values: K_t, K_r and K_d for porous trapezoidal block consisting of Cob armour units	362
Fig. 9.1	- Results from Cob armour units	402
Fig. 9.2	- Results from Shed armour units (regular arrangement)	403
Fig. 9.3	- Results from Shed armour units (staggered arrangement)	404
Fig. 9.4	- Results from Hobo (16 mm) armour units	405
Fig. 9.5	- Results from Hobo (20 mm) armour units	406
Fig. 9.6	- Results from Hobo (25 mm) armour units	407
Fig. 9.7	- Results from Hexo armour units	408
Fig. 9.8	- Results from porous trapezoid consisting of Cob armour units	409

		Page
Fig. 9.9	- K_r vs tanα/(H_i/L)**0.5 for slopes (1:1 1/3) of varying armour	410
Fig. 9.10	- R_u/H_i vs tanα/(H_i/L)**0.5 for slopes (1:1 1/3) of varying armour	411
Fig. 9.11	- R_d/H_i vs tanα/(H_i/L)**0.5 for slopes (1:1 1/3) of varying armour	412
Fig. 9.12.a	- K_r vs tanα/(H_i/L)**0.5 for slopes consisting of Cob armour units Re-analysis of Stickland (1969)	413
Fig. 9.12.b	- K_r vs tanα/$H_i/L)$**0.5 for breakwater slope and complete section (1:1 1/3) Re-analysis of Stickland (1969)	414
Fig. 9.12.c	- K_r vs tan α/$H_i/L)$**0.5 for slopes consisting of Dolos armour units. Re-analysis of HRS (1970)	415
Fig. 9.13	- R_u/H_i vs tanα/(H_i/L)**0.5 for slopes consisting of Cob armour units. Re-analysis of Stickland (1969)	416
Fig. 9.14	- R_d/H_i vs tanα/(H_i/L)**0.5 for slopes consisting of Cob armour units. Re-analysis of Stickland (1969)	417
Fig. 9.15	- Typical schematization of time-dependent wave impact forces by periodic water waves	418
Fig. 9.16	- Position of the instrumented armour unit for varying depth	419
Fig. 9.17	- Sign convention for wave height and force measurements	419
Fig. 9.18	- Wave height and force measurements Measured values for breakwater section with a permeable underlayer (T = 1.0 sec)	420
Fig. 9.19	- Wave height and force measurements Measured values for breakwater section with a permeable underlayer (T = 1.5 secs)	421
Fig. 9.20	- Wave height and force measurements Measured values for breakwater section with a permeable underlayer (T = 2.0 secs)	422

		Page
Fig. 9.21	- Wave height and force measurements Smoothed values for breakwater section with a permeable underlayer (T = 1.0 sec)	423
Fig. 9.22	- Variation of along-slope force Measured values for different incident wave conditions	424
Fig. 9.23	- Variation of along-slope force Smoothed values for different incident wave conditions	425
Fig. 9.24	- Wave height and force measurements Measured values for breakwater section with an impermeable underlayer (T = 1.0 sec)	426
Fig. 9.25	- Wave height and force measurements Measured values for breakwater section with an impermeable underlayer (T = 1.5 secs)	427
Fig. 9.26	- Wave height and force measurements Smoothed values for breakwater section with an impermeable underlayer (T = 1.0 sec)	428
Fig. 9.27.a	- $F_{slope(+)}/W_{ss}$ vs Steepness	429
Fig. 9.27.b	- $F_{slope(+)}/W_{ss}$ vs Water depth	429
Fig. 9.28.a	- $F_{lift(+)}/W_{sl}$ vs Steepness	430
Fig. 9.28.b	- $F_{lift(+)}/W_{sl}$ vs Water depth	430
Fig. 9.29	- Measurement of bending moments in model Tetrapod armour units (Ligteringen and Heydra 1984)	431
Fig. 9.30	- Measurement of acceleration in model Tetrapod armour units (Ligteringen 1983)	432
Fig. 9.31	- Measurement of bending moments in model Dolos armour units (Scott, Turcke, Baird and Readshaw 1987)	433
Fig. 10.1	- Results from field studies on wave transmission	453
Fig. 10.2	- Enlargement factor (k) vs Porosity (for constant Reynolds number)	454
Fig. 10.3	- Enlargement factor (k) vs Porosity (for constant scale ratio)	455

		Page
Fig. 10.4	- Enlargement factor (k) vs Scale ratio (for constant porosity)	456
Fig. 10.5	- Results from previous investigations on the influence of scale effects on wave transmission	457
Fig. 10.6.a	- K_t vs Steepness Scale effect tests for Cylindrical lattice structures	458
Fig. 10.6.b	- K_r vs Steepness Scale effect tests for Cylindrical lattice structures	459
Fig. 10.6.c	- K_d vs Steepness Scale effect tests for Cylindrical lattice structures	460
Fig. 10.7	- K_t, K_r and K_d vs Steepness Scale effect tests for Spherical lattice structures	461

LIST OF PLATES

Page

Plate 1 - Wave action on the model breakwater 434

LIST OF SYMBOLS

The most important symbols used in the text are listed below. Variables which have been used locally are not listed but are defined in the text. Some symbols have more than one meaning and it is evident from the text which meaning is intended.

a	steady laminar flow coefficient in the Forchheimer equation
A_o	amplitude of the standing wave at the front interface
b	steady turbulent flow coefficient in the Forchheimer equation
b	drag coefficient under constant acceleration
b'	drag coefficient under constant velocity
c	wave celerity
c	acceleration coefficient
d, D	water depth
d_m	characteristic dimension in the model
d_p	characteristic dimension in the prototype
D, d	characteristic dimension of the porous medium
exp	exponential
f	linearized friction factor
f_L	steady laminar flow resistance coefficient
f_T	steady turbulent flow resistance coefficient
F	non-Darcy friction factor (= $a + b\|u\|$)
F	force
F_{lift}	lift force
F_{slope}	along-slope force
g	acceleration due to gravity
h_o	constant depth outside the structure
H	total fluid head
H_i	incident wave height
H_r	reflected wave height
H_{max}	anti-node (loop) height
H_{min}	node height
H_o	height of the standing wave at the front interface
H_o	deep water wave height
H_{st}	height of structure
ΔH	difference in total fluid head
I	hydraulic gradient
I	$\sqrt{-1}$
I_L	laminar flow component of the hydraulic gradient

I_T	turbulent flow component of the hydraulic gradient
k	wave number ($k = 2\pi/L$)
k	enlargement factor applied to the linear scale
k	coefficient of permeability
k_o	$\omega/\sqrt{gh_o}$
K_d	energy loss coefficient
K_r	reflection coefficient
K_t	transmission coefficient
K_t'	internal transmission coefficient
l	length of structure
L	wave length
L_o	deep water wave length
L_r	linear scale ($= L_m/L_p$)
n	porosity
P	pressure
Re	Reynolds number
R_d	run-down
R_u	run-up
R.D.	relative density
t	time
T	wave period
u	horizontal component of the macroscopic velocity (discharge velocity)
u_p	pore fluid velocity ($u = nu_p$)
W_{sl}	component of the submerged weight of an armour unit in the direction perpendicular to the slope
W_{ss}	component of the submerged weight of an armour unit in the direction parallel to the slope
$\bar{x}$	mean value
γ_w	relative density of water
η	free surface elevation relative to the still water level
γ	kinematic viscosity of water
ξ	$I_{turbulent}/I_{laminar}$
ξ	surf similarity parameter (Iribarren number)
ρ_a	density of armour unit
ρ_w	density of water
σ_n	coefficient of variation
τ_b	bed shear stress
φ	phase angle for the reflected and transmitted wave
ω	frequency ($\omega = 2\pi/T$)

CHAPTER 1 - INTRODUCTION

Wave action on porous coastal structures has been a subject of extensive investigations, of which many have been limited to hydraulic model investigations at typical laboratory scales. Although mathematical models have been used to study this subject, most of the available models are of a semi-empirical nature. These models have been developed based on simplifying assumptions most of which are necessary due to the absence of quantitative expressions to identify and describe some of the complex interactions between wave motion and porous coastal structures.

Of various types of coastal structures, the rubble mound breakwater is one of the main forms of construction used to protect harbours. Other forms of breakwater construction include caisson, wave absorbers and composite types of structure. Vertical pile structures with and without horizontal bracings have also been used for various purposes in the construction of ports and harbours. Some of these structures are illustrated in Fig. 1.1.

Although breakwaters have been used for thousands of years it has been only in the last two decades that the design of these structures has developed on a more systematic basis. This has led to a better understanding of the wave mechanics principles related to the design and construction of breakwaters and, in the case of rubble mound structures, greater emphasis being given to the functions and performance of primary armour, secondary armour and the core.

The need to construct breakwaters in deep water exposed to more severe conditions imposed limitations on the use of natural rock as the primary armour. It often happens that the size of rock needed for the protection against large waves is impossible to obtain in the quantities required. This has led to the development of artificial concrete armour units. Although these units are an improvement on natural rock armour, their performance depends on, amongst other factors, the voids between the units to dissipate wave energy.

The emphasis in most research work on rubble mound breakwaters has been on the hydraulic stability of armour units and to a lesser extent on dynamic forces under wave attack, material properties of the units and the hydraulics of wave motion within the porous structure. Breakwater cross-sections constructed with model armour units are subjected to design wave conditions in the laboratory in order to justify their use in the prototype. A major design consideration is the

stability of individual model armour units with reference to their displacements from the original position. This enables the identification of different levels of damage and the definition of stability coefficients (K_D) for different types of armour units (Hudson 1959).

Breakwater designers have developed various shapes of artificial armour units in order to obtain high hydraulic stability at a relatively small armour block weight. It was expected that these armour units would withstand the design wave height without significant damage to individual armour units or to the breakwater as a whole.

The different types of artificial armour units used in practice can be broadly classified into three types.

(1) Bulky
(2) Slender, interlocking
and (3) Hollow block

The bulky type of armour units rely mainly on their weight for stability and are usually placed at random. However, there have been cases in which solid cubes were placed in a predetermined manner resulting in a structure similar to a sloping wall.

The slender, interlocking type of units have the advantage of greater hydraulic stability due to interlocking effects. However, armour units of this type develop greater static and dynamic forces under wave action. These armour units which have a relatively reduced block weight are normally placed at random although there are instances when these units have been placed in a predetermined layout.

It is important to note that in the case of both bulky and slender interlocking type of units the voids which contribute to the dissipation of wave energy are generated between the armour units in a random manner. For all practical purposes, this is even valid when slender interlocking type of armour units are placed in a predetermined form.

The hollow block type of armour units which are of more recent origin, are somewhat different to the other two types in that the voids are built into the individual units in the required form. Armour units belonging to this type are always placed in a predetermined manner and thus the resulting voids matrix of the

primary armour is geometrically well-defined, in contrast to those belonging to the other two types for which the voids matrices are generated randomly by irregular voids between the armour units.

It is evident that the stability of a breakwater consisting of hollow block armour units does not depend on the degree of interlocking between the units and as a result the weight of the individual armour units can be reduced considerably. The characteristic feature of a hollow block unit is the presence of a large volume of void in the unit relative to the volume of solid material. These armour units are designed to have the minimum volume of solid material and surface area which in practice would give the largest overall armour block size, minimising cost provided stability requirements are satisfied. Hollow block armour units have been produced in various external shapes of which the cubic form has been more popular in relation to placing of units.

Hollow block armour units can be broadly classified into three types, as given below, based on the presence of lateral porosity and the method of placing.

(1) Armour units without lateral porosity
(2) Armour units with lateral porosity
(3) Armour units with lateral porosity and placed in sets of two or more units.

In the case of the first group when the armour units are placed in the prescribed manner on the breakwater slope, the resulting voids matrix is not interconnected laterally although individual armour units have a void in the direction normal to the slope.

In contrast to the first group, units belonging to the second group generate a laterally interconnected voids matrix. By adopting a method of placement in which alternate rows are staggered by a length of half an armour unit it is possible to generate a voids matrix of equal porosity but with increased tortuosity.

Armour units categorised into the third group are very similar to those belonging to the second group but are placed in sets of two or more armour units. They have been designed on the basis that three-dimensional symmetry of individual units is not an essential requirement in relation to the top surface of the armour layer and that having parallel edges of adjacent blocks is uneconomical with regard to material usage. It has been also pointed out that the latter generates

long narrow spaces in which wave pressure can concentrate, resulting in abrasion. It is evident that the armour units belonging to this group will have a rather complex geometry in contrast to those belonging to the first and second groups. Care has to be exercised when placing hollow block armour units to a given overall layout pattern to ensure proper and close alignment.

Water entering a hollow block unit having lateral porosity spills in four directions within the unit and out into the adjacent units where it encounters water moving, generally, in opposite directions. Wave energy is thus dissipated in turbulence within the block. Since these units are placed close to each other forces of appreciable magnitude do not act to force apart adjoining blocks and this is assisted by the relatively small surface area of the blocks.

Table 1.1 summarises the classification of armour units used for breakwater construction. Figs. 1.2 to 1.4 illustrate the three dimensional geometry of selected armour units belonging to the different categories identified earlier. They also illustrate typical cross–sections of breakwaters consisting of different types of armour units.

The important aspect of the hollow block concept is the systematic analysis of the voids matrix of the primary armour layer. This concept permits the absolute control of varying the geometry of the voids within the confined boundaries of an individual armour unit or a group of units to produce a cost–effective primary armour layer which is very efficient with respect to wave energy dissipation. When the armour units are correctly placed they exhibit hardly any movement, with contact forces uniformly distributed. These units represent optimum use of concrete for wave energy dissipation.

The importance of the voids matrix of the primary armour layer in relation to the performance of concrete armour units was first highlighted by Whillock (1981) and several others thereafter. This aspect can be further illustrated by applying Hudson's formula to a solid cube and to a typical interlocking type of armour unit both designed to withstand the same design conditions.

For example, the relationship between weight (W) and stability coefficient (K_D) of a solid cube and the interlocking type of armour unit will, under the conditions specified, be given by

$$W_c K_{Dc} = W_b K_{Db} = \ldots . \frac{\gamma_a H^3}{(s_a - 1)^3 \cot\alpha} \qquad (1.1)$$

where

W = weight of armour unit
H = wave height
K_D = stability coefficient

s_a = relative density of armour unit = $\frac{\rho_a}{\rho_w}$

$\gamma_a = \rho_a g$
ρ_a = density of armour unit
ρ_w = density of water
g = acceleration due to gravity
α = slope angle

Suffices c and b refer to the solid cube and the interlocking type of armour block respectively.

If both armour units have the same relative density it is evident that the volumes (V) of both armour units are related by

$$\frac{V_c}{V_b} = \frac{K_{Db}}{K_{Dc}} \qquad (1.2)$$

Previous investigations have indicated that the values of K_{Db} corresponding to the interlocking type to be always greater than K_{Dc}, the corresponding value of the solid cube.

In relation to the dimensions given in Fig. 1.5.1, if it is assumed that

$$L_b = \epsilon L_c \qquad (1.3)$$

where ($\epsilon < 1$)
it can be shown that the increase in K_D given by

$$\Delta K_{Db} = K_{Db} - K_{Dc} \qquad (1.4)$$

is related to the volume V_v by the relationship

$$\frac{\Delta K_{Db}}{K_{Dc}} = \frac{1}{\epsilon^3}\left[\frac{V_v}{V_b} + 1\right] - 1 \qquad (1.5)$$

In this case the volume V_v represents the material removed when carving out the armour unit from its circumscribing cube. This illustrates to a certain extent that the increase in the stability coefficient is closely associated to the void it creates. However the voids matrix generated by the random placement of the same armour units is somewhat different to that described by the volume V_v and a typical illustration of a random assembly is given in Fig. 1.5.2.

A plot of K_D in Hudson's equation versus voids ratio for different armour unit assemblies is presented in Fig. 1.5.3. The plot indicates that armour unit stability increases as at least the fourth power as the voids ratio. Whillock (1981) points out that the lower value of K_D for the Dolos armour unit is from tests on a slope with a lower permeability than usually assumed. This observation indicates that maximum benefit from increased voids can only be obtained by making necessary improvements in the interior parts of the structure. This plot to a certain extent illustrates the direct importance of voids in relation to stability realizing that porosity also reflects to an ill-defined degree the interlocking between armour units.

Even very recent studies on the performance of rubble mound structures (van der Meer 1985) have not produced satisfactory relationships in relation to the influence of porosity and permeability on wave energy dissipation. It has been left to the designer's judgement to choose an appropriate value for the parameters relating to these variables.

One of the main difficulties in using hollow block armour units is establishing a design criterion. Unlike other types of armour units they have proved to be extremely stable during hydraulic model tests and as such the definition of a stability coefficient on the basis of Hudson's approach is not applicable. Values of K_D greater than 80 have been observed for the Cob armour unit. These armour units have been found to be more stable on steeper slopes, rather than less stable.

When attempts were made to identify the failure mechanism it was observed that excessive overtopping of a breakwater having a relatively mild slope and with an unsupported crest dislodged several units. However, this problem was

overcome by using appropriate restraining measures. A comparatively loose laying pattern also resulted in the movement of a few units mainly by rocking or lifting at high incident wave amplitudes.

Some of the important aspects associated with wave action on a rubble mound breakwater are summarised in Fig. 1.6. As pointed out earlier the main emphasis in most of the investigations on rubble mound breakwaters has been on stability, run-up and run-down. Some of the more fundamental aspects have not been investigated in detail.

The necessity to consider in detail the structural integrity of artificial armour for breakwaters in deep water is now widely accepted. It is only in the recent past, after a series of failures, that breakwater designers have given due consideration to the strength of concrete armour units. Until this stage designs were based only on hydraulic stability tests for which the strength of armour units was not scaled. This led to the development and use of comparatively large interlocking type of armour units. Recent failures indicate that the limits of applicability of these units have been exceeded mainly because due consideration was not given to other aspects particularly dynamic forces and the capability of armour units to withstand such loads.

In view of the above observations it was considered necessary to investigate some of the critical design aspects identified in Fig. 1.6. In doing so it was required to ensure that the investigations were not limited to a particular structural configuration but that it encompassed different types of coastal structures used in practice.

From a geometric point of view a coastal structure can be characterized by its external configuration and the internal layout of the constituent material or materials. The first defines its overall shape and the second defines the size of and inter-relationship between solid materials and voids. The hydraulic properties of the structure will be dependent on these factors. Thus an assessment of overall performance with respect to wave energy dissipation can be made by a systematic study of these parameters with due consideration given to material properties.

In formulating the project, attention was primarily focused on the influence of voids and geometry in relation to the performance of coastal structures from a view point of both internal and external configuration.

The importance of this aspect in relation to hollow block armour units

was presented earlier in this chapter. It is observed that the design of hollow block armour units is based on the concept of optimum utilization of both the individual void in the armour unit and the overall voids matrix of primary armour layer, thus producing an armour block which is more efficient and economical with respect to material usage. To investigate these aspects further it was necessary that this study concentrated on structures consisting of this type of unit. In addition, different types of porous media and structural configurations which have characteristic geometric features compatible with those used in practice were also included in the study.

Some of the design aspects which were investigated both experimentally and theoretically as part of the work included the following.

(1) Hydraulic properties of different materials selected for the study.

(2) The influence of unsteady flow on forces acting on armour units.

(3) Investigation of external and internal flow in relation to coastal structures.
   (a) wave reflection;
   (b) wave transmission through a structure and by overtopping;
   (c) internal wave decay;
   (d) wave run-up and run-down.

(4) Study of wave forces on a typical armour unit of a breakwater slope.

(5) Study of scale effects in hydraulic modelling of wave action on coastal structures.

For the purposes of the study it was necessary to perform detailed tests under steady flow, oscillatory flow and accelerated flow for selected structures having a specific external geometry and internal layout. Both non-submerged and submerged conditions were used. Theoretical aspects relevant to these phenomena were considered separately and the predictive ability of the mathematical formulations was assessed by comparing with experimental values.

Chapter 2 presents a detailed literature review on the different aspects which were investigated in this study.

Formulation of the problem and how it was approached are described in Chapter 3. This chapter deals with the selection of experimental media and justifies the reasons for adopting different approaches for the investigation of the selected phenomena. It also establishes a relationship between the different phases of the project.

Technical details of experimental apparatus, flow environment and procedures are presented in Chapter 4. This chapter identifies the scale and limitations of the experimental techniques in order to assess the quality of the measurements.

Chapter 5 presents the theoretical developments, both analytical and numerical in relation to wave action on coastal structures.

The results from experimental investigations are classified into four groups and are presented in Chapters 6, 7, 8 and 9. A summary of the entire experimental programme is given at the beginning of Chapter 6. At the end of each of these chapters an evaluation is made of the relevant theoretical analysis by comparing the predicted values with those measured experimentally.

Chapter 6 deals with the results from steady flow permeability tests and oscillatory flow tests performed on several porous media having the same external geometry. Chapter 7 concentrates on the results from constant acceleration and velocity tests which are used to assess the influence of unsteady flow. Results from additional tests under oscillatory flow conditions performed on different structures of varying external geometry are presented in Chapter 8. Results from different studies performed on breakwater sections consisting of different hollow block armour units are presented in Chapter 9.

Chapter 10 deals with scale effects in models of porous structures with particular attention focused on wave transmission through them.

Finally Chapter 11 presents the summary, conclusions and recommend-ations of this study on the influence of geometry on the performance of breakwater armour units.

CLASSIFICATION OF BREAKWATER ARMOUR UNITS

ARMOUR UNITS	METHOD OF PLACING	VOID STRUCTURE OF THE PRIMARY ARMOUR LAYER
Natural rock	- at random	
Artificial armour		
1) Bulky type	-normally at random -sometimes in a regular pattern	voids are created between the armour units in a random manner
2) Slender interlocking type	-normally at random -sometimes in a regular pattern	
3) Hollow block type	-in a regular pattern	
a)without lateral porosity b)with lateral porosity c)with lateral porosity and placed in sets of two or more units		voids are created within the armour units in a pre-determined manner

TABLE 1.1 CLASSIFICATION OF BREAKWATER ARMOUR UNITS

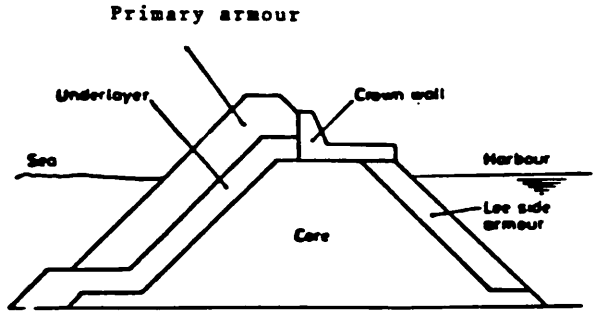


Fig.1.1.1 Rubble mound breakwater

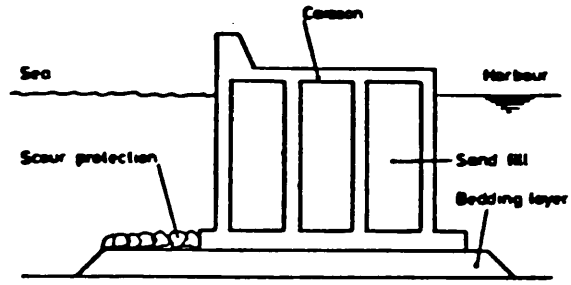


Fig.1.1.2 Caisson breakwater

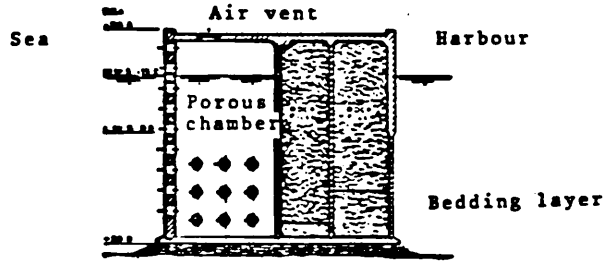


Fig.1.1.3 Porous wave absorber

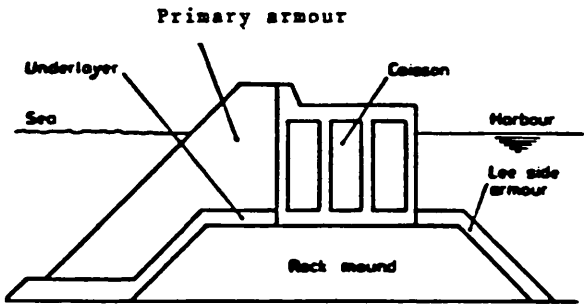


Fig.1.1.4 Composite breakwater

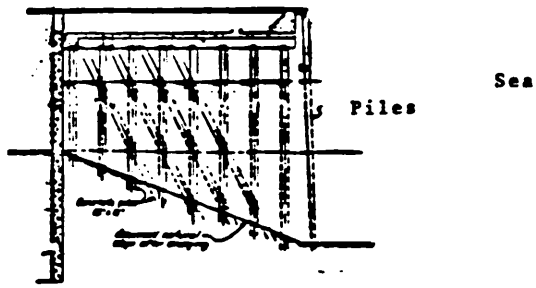


Fig.1.1.5 Pile structure

FIG.1.1 COASTAL STRUCTURES

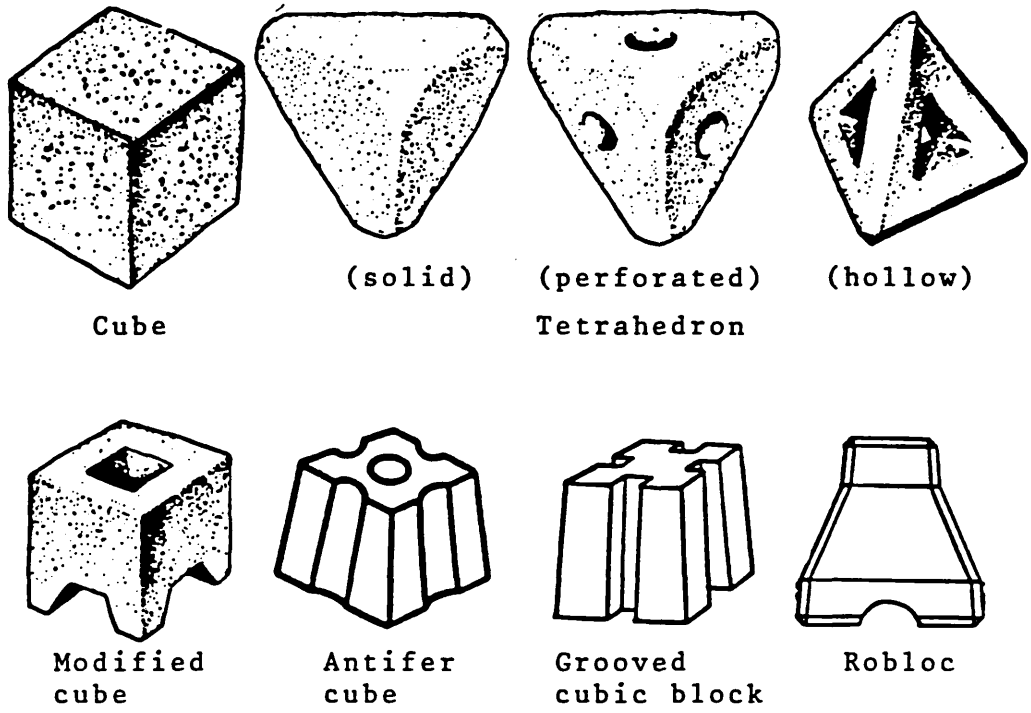


Fig.1.2.1 Selected armour units

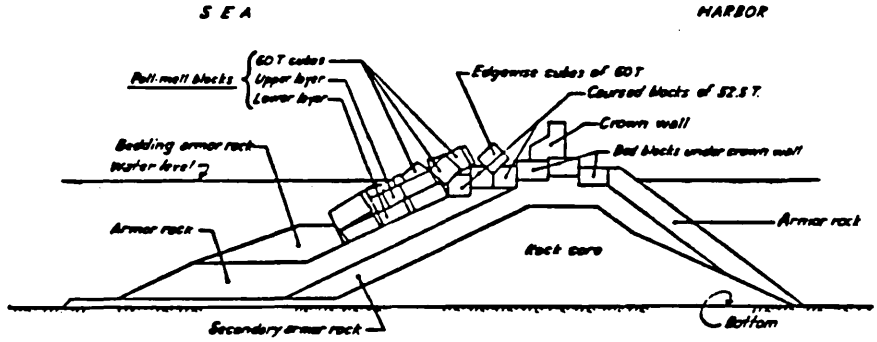


Fig.1.2.2 Concrete blocks placed randomly

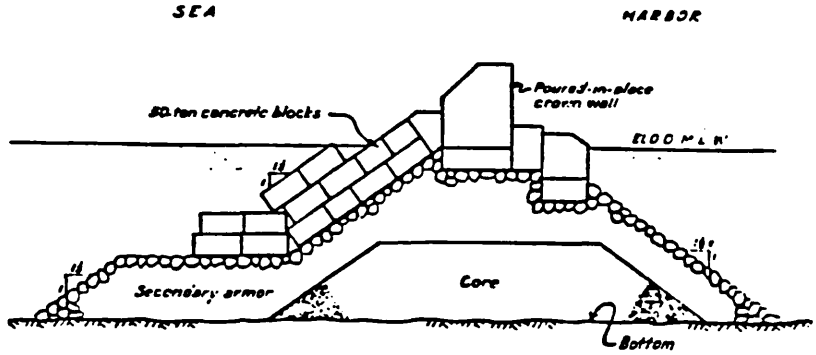
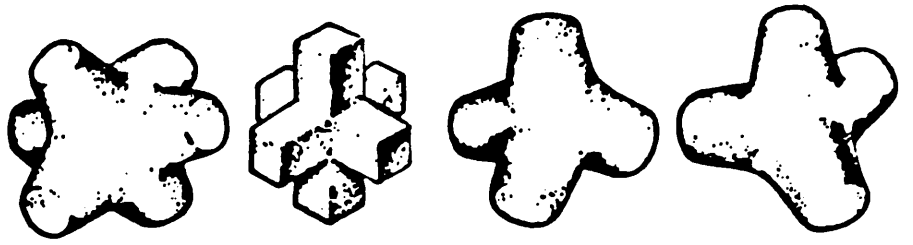
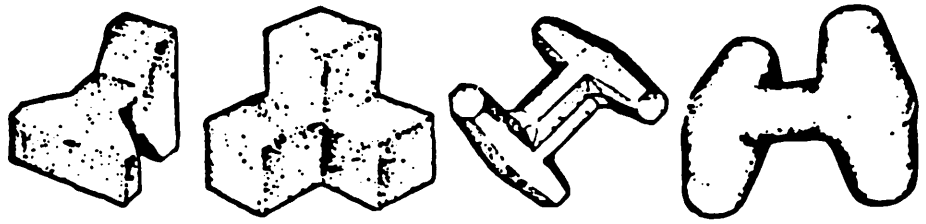


Fig.1.2.3 Concrete blocks placed to a predetermined layout

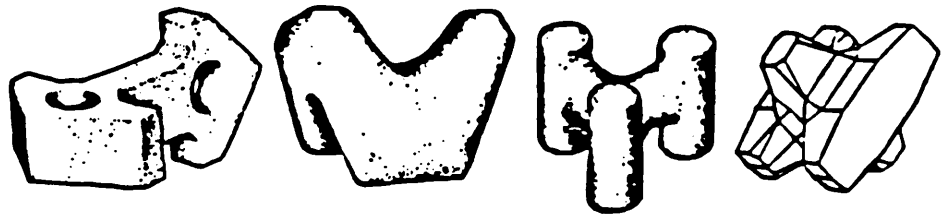
FIG.1.2 BULKY TYPE OF ARMOUR UNITS



Hexapod Hexaleg Tetrapod Quadripod



Akmon Tri-pod Dolos Sta-bar



Toskane Stabit Tribar Accropode

Fig.1.3.1 Selected armour units

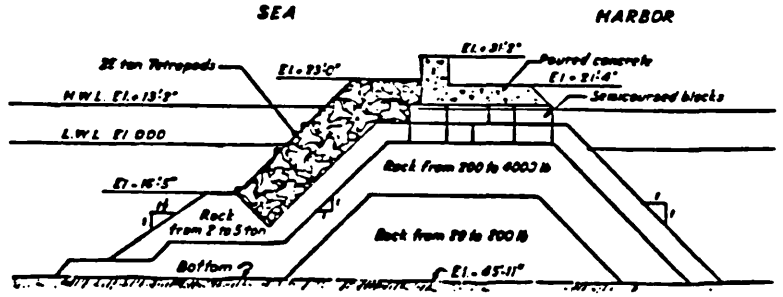


Fig.1.3.2 Tetrapods placed randomly

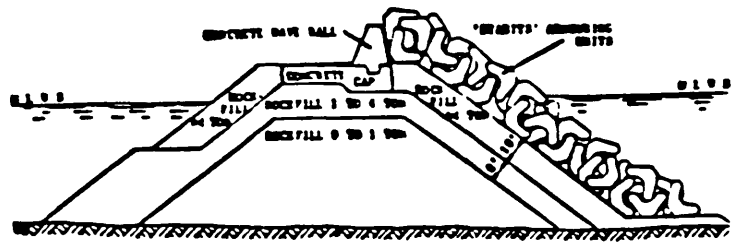
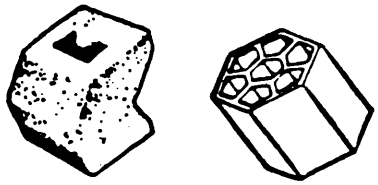


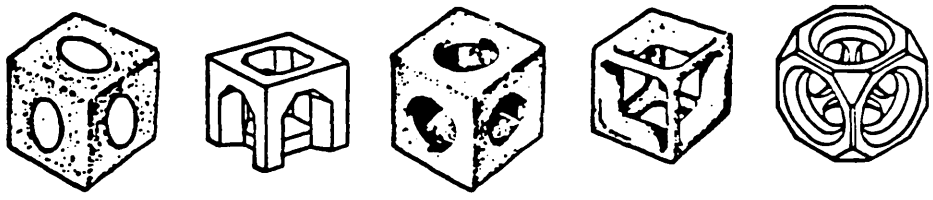
Fig.1.3.3 Stabits placed to a predetermined layout

FIG.1.3 SLENDER INTERLOCKING TYPE OF ARMOUR UNITS



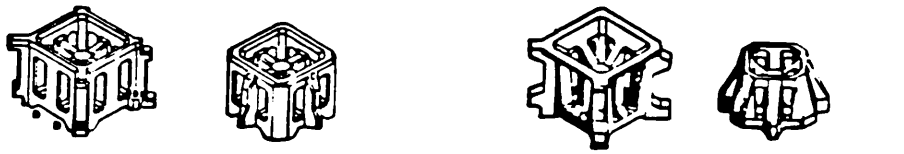
Svee block Seabee

Hollow block units without lateral porosity



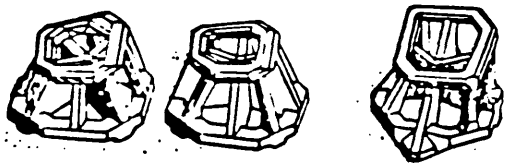
Stolk Cobwebb Hobo Cob Shed

Hollow block units with lateral porosity



Primary unit Secondary unit Primary unit Secondary unit

Diode Reef I



Primary unit Secondary unit Terrace unit

Reef II

Hollow block units with lateral porosity and placed in sets of two or more units

Fig.1.4.1 Selected armour units

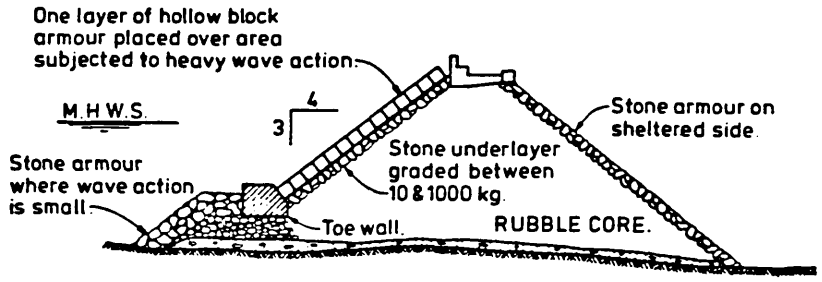
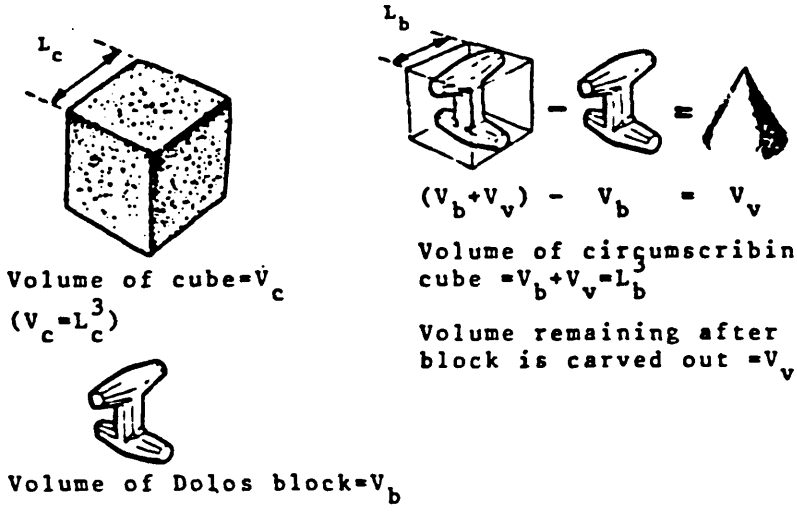


Fig.1.4.2 Breakwater section consisting of Cob armour units

FIG.1.4 HOLLOW BLOCK TYPE OF ARMOUR UNITS



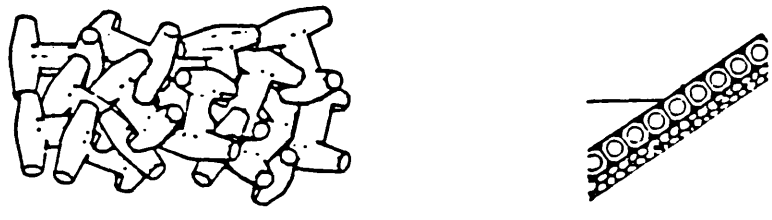
Volume of cube=V_c
$(V_c=L_c^3)$

Volume of circumscribing cube $=V_b+V_v=L_b^3$

Volume remaining after the block is carved out $=V_v$

Volume of Dolos block=V_b

Fig.1.5.1 Armour blocks carved out of cubes



Randomly placed Dolos armour units

Shed armour units placed on a slope

Fig.1.5.2 Geometry of the primary armour layer

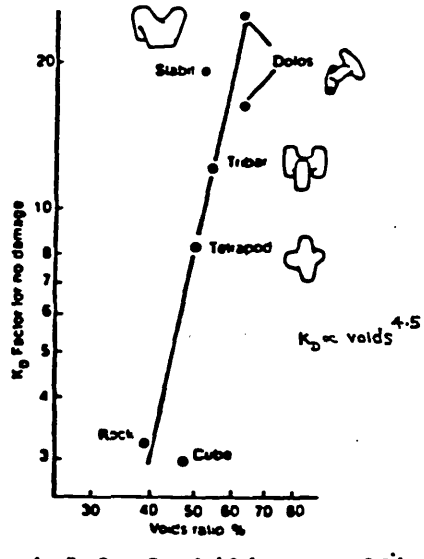


Fig.1.5.3 Stability coefficient(K_D) vs Voids ratio(%) (Whillock 1981)

FIG.1.5 RELATIONSHIP BETWEEN ARMOUR BLOCK STABILITY AND VOIDS RATIO

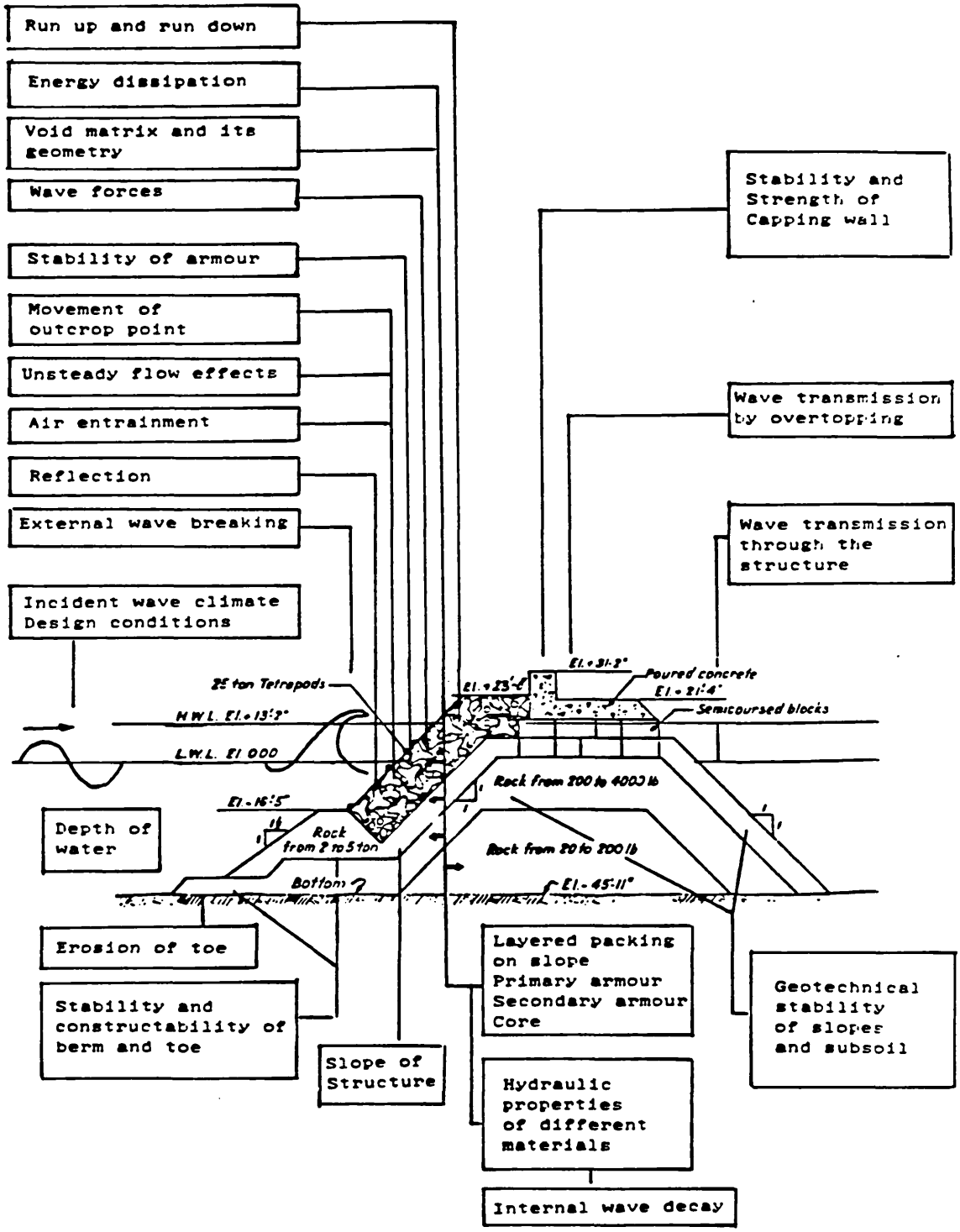


FIG.1.6 IMPORTANT ASPECTS OF WAVE ACTION ON A RUBBLE MOUND BREAKWATER

CHAPTER 2 - REVIEW OF PREVIOUS INVESTIGATIONS

2.1. Introduction

A preliminary review of the relevant literature indicated that an extensive study of the influence of voids ratio and geometry of armour on energy dissipation had not been undertaken previously. However, numerous investigations of flow through porous media have been performed in various disciplines associated with fluid mechanics and hydraulics. Thus it was necessary to identify areas of specific interest in which an extensive literature review could be carried out. The present work primarily focuses its attention on the performance of hollow block armour units from a viewpoint of flow through porous media. This requires the subject of flow through porous media and its application to coastal structures to be discussed in detail. In doing so it is possible to identify two areas of interest, namely: steady and unsteady flow, and in each area a broad classification could be made under the following three sections.

(1) Theoretical developments
(2) Experimental work
(3) Field studies

In addition, attention will be focused on relevant studies of Rubble Mound Breakwaters particularly in relation to selected hydraulic model investigations.

Before considering the details of previous investigations it is appropriate to discuss briefly the structure of the literature review in relation to the specific areas identified earlier.

The primary objective of discriminating between steady and unsteady flow is to differentiate between work on steady, Darcy and non-Darcy flow regimes and that on wave action through porous media.

Unsteady flow conditions also include unidirectional accelerated flow and oscillatory (or reversing) flow which is established in U-tube oscillators and in pulsating water tunnels. Tests pertaining to these two flow conditions and steady flow regimes are classified into one group where most of the work has been performed from a strictly hydraulics point of view. They provide information on resistance coefficients under steady flow conditions and deviations which are observed as the flow becomes unsteady.

The second group relates to wave action through porous structures which is of direct interest from a coastal engineering point of view. Transmission, reflection and energy loss coefficients will be used to assess the performance of different types of coastal structures.

Theoretical, experimental and field investigations pertaining to both groups will be reviewed within the framework of the principal objectives of the study.

The structure of the literature review is given in Table 2.1.

Structure of the literature survey

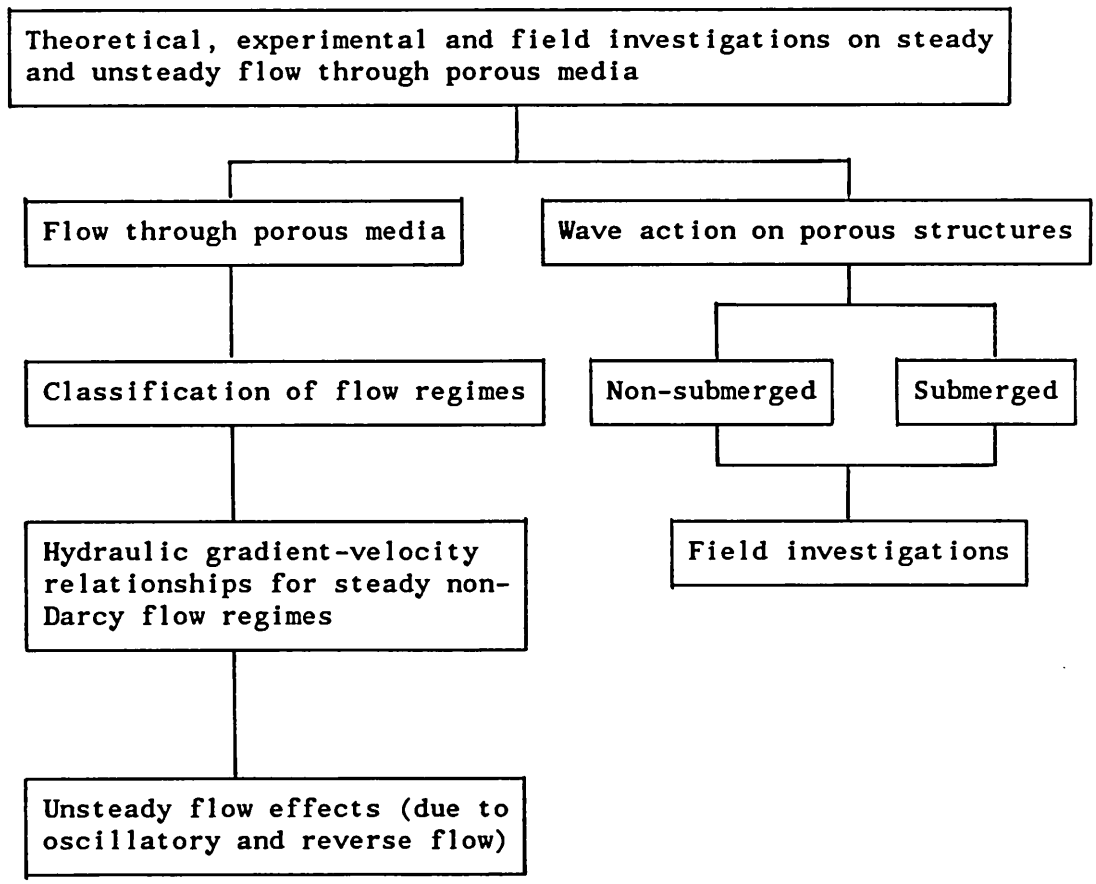


TABLE 2.1. STRUCTURE OF THE LITERATURE SURVEY

2.2. Flow through porous media

2.2.1. Flow regimes in porous media

The hydraulic gradient - velocity relationship for the flow of fluids through porous media has long been a subject of discussion. Although a number of papers on this subject have been published no general agreement has yet been reached as to its form. The practical difficulties of covering an extensive range of flow conditions for a particular porous medium and the frequently large scatter of experimental results have contributed to the appearance of a number of different equations for the relationship.

Problems involving flow of fluids through porous media have traditionally been solved on the assumption of Darcy's equation relating head loss and velocity (Darcy 1856), given by

$$u = - k \frac{\partial H}{\partial s} = ki \qquad (2.1)$$

where

- u = discharge velocity (also identified as bulk or macroscopic velocity).
- k = coefficient of permeability in the 's' direction, dependent on properties of the fluid and the medium.
- H = total fluid head.
- s = distance measured in the direction of the resultant velocity at the point under consideration.
- i = the negative total head gradient $(= - \frac{\partial H}{\partial s})$.

It should be observed that in a medium of porosity 'n' the discharge per unit area in a particular direction is given by

$$u = n u_p \qquad (2.2)$$

where u_p is the actual mean velocity of the pore fluid.

The relationship between discharge velocity and the actual mean velocity through the pore fluid given by eq. 2.2 can be established as follows. If the total cross-sectional area of the porous medium is A and the discharge traversing it is Q, the discharge velocity is

$$u = Q/A \tag{2.3}$$

In this cross-section there are numerous openings of total area A_o ($A_o < A$). The mean value of the velocity through these openings (pores) is

$$u_p = Q/A_o \tag{2.4}$$

The volume occupied by the porous medium between two sections Δs apart is $A.\Delta s$. Assuming that A_o remains constant along the length Δs, the void space in the same volume is given by $A_o.\Delta s$. Denoting porosity, 'n' as

$$n = A_o/A \tag{2.5}$$

the relationship given by eq. 2.2 is obtained. This discussion focuses attention on the practical limitations of this relationship particularly for randomly packed porous media.

Darcy's law represents a linear relationship between head loss and velocity and it satisfactorily describes the flow conditions, provided the velocities are small, for example, in seepage flow. It has been realized that this law fails to hold for high flow velocities for which more general flow equations must be used to describe the flow correctly. Any deviation from Darcy's law represents non-Darcian flows, for which a fundamental approach could be adopted by seeking the physical causes underlying the deviations from linearity. A review of literature reveals that such deviations may arise for several reasons of which high flow rates, molecular effects, ionic effects and non-Newtonian behaviour of the percolating fluid have been investigated by previous researchers.

The deviation from Darcy's law at high flow rates has been attributed to both inertial effects and the onset of turbulence. Experimental evidence on the dispersion of dye streams supports this view. At very low rates of flow, the validity of Darcy's law has been questioned for fine-grained porous media, particularly clays. Deviations have been attributed to electro-chemical surface effects between the fluid and the solid particles. There has, however, been a wide range of values of Reynolds number reported for the upper limit of validity of the law. Scheidegger (1974) quotes values ranging from 0.1 to 75. It should be noted that there exists no unique definition for Reynolds number and various forms have been used by different investigators. For the present investigation deviations due to high flow rates demand closer examination.

Saturated flow in porous media may be characterized by one of the following flow regimes.

Microseepage: when non-Newtonian flow is observed at extremely small velocities.

Darcy flow: laminar Newtonian flow characterized by stable streamlines in the pores; a regime in which viscous forces dominate and inertial effects are negligible. The head loss is directly proportional to the first power of the velocity.

Non-linear laminar flow: which could be identified as a steady inertial regime in which both viscous and inertial terms influence the flow. Stable streamlines are present in the pores. The head loss deviates from a linear relationship with velocity.

Turbulent transitional flow: in this regime some of the streamlines in the pores become unstable and inertial effects emerge to play a dominant role with viscous effects being less prominent. The head loss gradually becomes proportional to the square of the velocity.

Fully turbulent regime: where inertial effects govern the flow with negligible viscous effects. Stable streamlines no longer exist in the pores and the head loss varies approximately with the square of the velocity.

Apart from porosity another important parameter in relation to flow through porous media is tortuosity. This is defined as the ratio of the length of the flow channel for a fluid particle to the length of the porous medium. For a randomly-packed porous medium the length of one flow channel varies from another and as a consequence it is very difficult to define tortuosity. In this case it is also very difficult to identify the respective flow paths. However the importance of this geometrical parameter can be closely examined in relation to well-defined porous media. Although this aspect has been discussed by several investigators it is a property which is very difficult to quantify for a porous medium and quantification of its influence is problematical.

2.2.2. Classification of steady non-Darcy flow equations

Several investigations have been made in different disciplines in order to establish resistance equations for the description of non-linear flow through porous media. Scheidegger (1974) presents detailed information on the research on the subject and Hannoura and Barends (1981) review the work on the same subject in

a way that is more beneficial in relation to coastal hydraulics.

In non-Darcy flows the main problem is to establish a relationship between two measurable parameters namely the pressure head gradient and the velocity of the pore fluid. The limited validity of Darcy's law led to the suggestion of relationships that would be accurate over all the flow ranges encountered. Several representations have emerged which can be categorized under any of the following formulae.

(i) The Forchheimer form $I = au + bu^2$ (2.6)

(ii) The general form $I = au + c_o u^{m_o} + bu^2$ (2.7)

(iii) The exponential form $I = c_1 u^{m_1}$ (2.8)

(iv) Friction factor - Reynolds number correlations such as

$$\lambda = c_2 / R_e^{m_2} n^{m_3} \quad (2.9)$$

where

I = magnitude of the hydraulic gradient.

u = bulk or macroscopic velocity.

R_e = Reynolds number.

n = porosity.

a, b, c_o, c_1, c_2, m_o, m_1, m_2, m_3, are constants for a particular medium, fluid and flow regime.

λ = friction factor, for which several definitions similar to eq. 2.9 have been presented by different investigators.

From amongst these relationships many authors have supported the Forchheimer (1901) relation (eq. 2.6) on the basis of experimental evidence. It should be noted that the Forchheimer equation was originally postulated from semi-theoretical reasoning by analogy with the flow phenomena occurring in tubes. Theoretical developments supporting the validity of this equation have been presented by Ahmed and Sunanda (1969) and McCorquodale (1970).

Experimental and analytical investigations of flow through idealized media show that 'a' and 'b' are not strictly constants and depend on the Reynolds number of the flow. However, for all practical purposes it can be assumed that 'a' and 'b' remain constant over a range of Reynolds number and this view is held by many who have investigated the subject. The importance of this formula is that laminar and turbulent terms are expressed separately which permits the determination of their relative influence by evaluating the ratio of respective terms given by

$$\frac{I_T}{I_L} = \frac{b}{a} u \qquad (2.10)$$

In some cases, the Forchheimer equation has been modified by the inclusion of a third term proportional to velocity-cubed in order to obtain a better fit to experimental values.

Forchheimer (1901) was probably the first to suggest a series form to describe the non-linear relationship between the hydraulic gradient and macroscopic velocity. He realized that Darcy's law was not universally valid for flow through porous media and noted that for high velocities the linear relationship breaks down.

The general form of the equation (eq. 2.7) contains an additional term $c_o u^{m_o}$, not present in the Forchheimer equation. m_o is assumed to have a value of approximately 1.5. In general it can be stated that this term accounts for a transitional term intermediate between fully laminar and fully turbulent flow. Although this equation is presented as an improvement on the Forchheimer equation, Nasser and McCorquodale (1974) quote Ng (1969) who found that in the Reynolds number range 600 - 4000, the Forchheimer equation gave correlation with his experimental values equally as good as did the three term general formula. In this case the Reynolds number was based on the geometric mean diameter of the rockfill media.

The high-velocity flow phenomena occurring in porous media can be expressed in mathematical terms in several ways. Without attempting to understand the physics of the phenomena, one can simply fit, heurestically, curves or equations to the experimental data so as to obtain a correlation. The exponential relation (eq. 2.8) belongs to this category. This equation is completely empirical and has not been given a theoretical basis by its numerous users. It is also observed that both laminar and turbulent terms are incorporated into one term thus providing no opportunity for a closer examination of their relative effects.

Friction factor - Reynolds number correlations and other relationships based on similar concepts have been presented by various authors and an excellent review of such formulae is given by Scheidegger (1974). Unfortunately, all such correlations are subject to limitations as the Reynolds number and friction factor depend significantly upon the definition of a general characteristic length associated with the porous medium. The average grain diameter, the pore diameter or some other length corresponding to the hydraulic radius theory is often adopted. It should be noted that in most cases the characteristic length in a random porous

matrix is not really defined either geometrically or by detailed statistical reasoning. Hence it is evident that results obtained under these conditions must be regarded as subject to a major shortcoming in that a length parameter is employed for which no universal definition exists.

Among other variables that would have an influence, porosity plays a significant dual role. If the idea of a Reynolds number is maintained, it is apparent that the pore velocity (u_p) and not the discharge velocity (u), is significant for the onset of turbulence. Apart from the generally accepted relationship between the two variables $u = nu_p$ (eq. 2.2), which introduces porosity (n) into the final equation, it has been argued that porosity should be accounted for differently, for example, by its incorporation into the friction factor as a separate entity.

There have also been attempts to establish correlations between the flow variables involving the porosity and particle diameter, without their being represented by the friction factor and Reynolds number. Similarly some authors have introduced the shape of particles and related parameters as factors influencing fluid flow. The definition of a shape factor for single particles – as the ratio of the surface of a sphere having the same volume as the particle to the surface of the particle – is one example of such a development.

Darcy's law and its correlation with Reynolds number was chosen originally on the assumption of an analogy between flow in tubes and flow in a porous medium. The latter was considered to be equivalent to an assemblage of capillaries and a phenomenon was sought in porous media similar to the onset of turbulence in tubes, which takes place at a definite Reynolds number. However, experimental evidence shows that for porous media there exists a great discrepancy regarding this value. The uncertainty in the critical Reynolds number partly reflects the indeterminacy of the characteristic length.

It should be noted that even in tubes, the dependence of the pressure drop on the flow velocity becomes non-linear as the inertia term becomes important. An interesting result of experimental evidence, noted by Scheidegger (1974), is that the critical Reynolds number above which turbulence is believed to occur is much lower for porous media, varying from 0.1 to 75, than for straight tubes for which it is approximately 2000. It was concluded that deviation from Darcy's law at high velocities is primarily due to the emergence of inertia effects in laminar flow owing to the curvature of the flow channel and not due to the onset of turbulence. Only at very high Reynolds numbers will true turbulence occur and this causes the second change in the flow regime observed experimentally.

It is evident that the critical Reynolds number for the emergence of inertia effects is very much influenced by the curvature of the flow channels and therefore it must be expected that there exists no such parameter as a universal Reynolds number for a porous medium at which non-linearity would set in. Depending on the curvature of the channels, the critical Reynolds number will vary from one flow channel to another even if the cross-sections are identical or if the flow channels are assembled together to form a porous medium of identical porosity and tortuosity. This discussion illustrates that there is no proper physical basis for assuming that flow behaviour and therefore friction factors should be the same for identical Reynolds numbers, unless very careful consideration is given to the definition of variables associated with such numbers as well as the inclusion of curvature in a definite form.

2.2.3. Other aspects of flow in porous media

The previous section of this chapter considered steady, saturated flow through porous media. In this section a brief introduction is given to the subject of unsteady, unsaturated flow. The influence of unsteady flow in porous media on the non-Darcy hydraulic conductivity has often been assumed to be negligible, an assumption which may be valid in the case of low Reynolds number flow through highly compacted fine porous media.

Polubarinova-Kochina (1962) generalized the Forchheimer relation to include a time dependent term, $c\frac{\partial u}{\partial t}$, so that the hydraulic gradient for unsteady non-Darcy flows could be expressed as

$$I = au + bu^2 + c\frac{\partial u}{\partial t} \qquad (2.11)$$

Many investigators have not considered the influence of this additional term and consequently very little research has been carried out on either acceleration effects or air entrainment. At a later stage in this chapter, reference will be made in more detail to recent developments in this field.

The subject under investigation demands a very detailed review of wave action within porous media. When a progressive wave collides with a porous structure, reflection and transmission of the wave take place on and across the interface. The resultant flow is often non-Darcy and may be single or two phase. Two phase flow may occur due to external and internal wave breaking. These flow conditions in combination generate a complicated flow system which will

influence the effective conductivity of the structure, reducing wave transmission and increasing reflection. At the same time constituent elements of the structure will be subjected to unsteady wave forces. Wave - structure interactions associated with rubble mound breakwaters and porous coastal structures are typical examples in which the above-mentioned complex flow system is observed. Comparatively little attention has been focused on this type of phenomenon.

The mathematical treatment of this subject has only been possible under simplifying assumptions. However in view of the complex nature of the problem most of these assumptions are reasonably justified. Some have been necessary because of the lack of quantitative expressions to describe the different complicated aspects associated with wave motion on a porous slope.

In the above review some of the fundamental aspects related to the mechanics of the phenomena were presented. Attention is now focused on some of the investigations, both pioneering and of recent origin, that have been carried out in this field. These were selected on the basis of their close relationship and applicability to the subject under investigation. It should be appreciated that the work of some researchers is not limited to one specific domain, but encompasses several areas of interest. Although the investigations reviewed are classified under different headings, it is evident from the above reasoning that in some instances reference to a particular contribution will be made on more than one occasion.

2.3. Hydraulic gradient - velocity relationships for steady non-Darcy flow in porous media

Engelund (1953) proposed that the hydraulic gradient I of flow through homogeneous sand can be written as $I = au + bu^2$ and developed this equation to the form :

$$I = \alpha_o \frac{(1-n)^3}{n^2} \frac{\gamma}{gd^2} u + \beta_o \frac{(1-n)}{n^3} \frac{1}{gd} u^2 \qquad (2.12)$$

in which α_o and β_o are constants depending upon the shape of the grains.

n = porosity
γ = kinematic viscosity
d = grain size
g = gravitational constant

It was found from experiments and a literature study, that the following values of the constants α_o and β_o are valid.

	Laminar coefficient α_o	Turbulent coefficient β_o
uniform, spherical particles.	≃ 780	≃ 1.8
uniform, rounded sand grains	≃ 1000	≃ 2.8
irregular, angular grains	up to 1500 or more	up to 3.6 or more

TABLE 2.2. FLOW COEFFICIENTS FOR ENGELUND'S (1953) EQUATION

All the measurements on which Engelund based his recommendations were obtained in sand, where the flow, although turbulent, corresponds to a much smaller Reynolds number than that which would be observed in a rubble mound structure.

LeMehaute (1957) as part of a detailed study on wave transmission through permeable structures developed the following expression.

$$I = \frac{c}{n^5}\,\frac{1}{d}\,\frac{u^2}{2g} \qquad (2.13)$$

in which

$$c = \frac{c_2}{(ud/\gamma)} + c_3 \qquad (2.14)$$

Values of $c_2 = 28.0$ and $c_3 = 0.20$ were recommended. It is observed that the equations of both Engelund (1953) and LeMehaute (1957) are of identical form except for the coefficient and the influence of porosity.

A comparison of laminar and turbulent terms in equations of Engelund and LeMehaute is given in Table 2.3. It illustrates the relative magnitude of these two terms and its variation with porosity. The computations were made using typical values for the respective coefficients as suggested by both authors.

In LeMehaute's equation the ratio $\frac{I_T}{I_L}$ is independent of porosity whereas it reaches a minimum when using Engelund's equation. This minimum value is greater than that of the constant value given by LeMehaute's equation. The relative importance of laminar and turbulent terms at a given porosity can be assessed by multiplying the values in Table 2.3 by the Reynolds number characterizing the flow.

Ward (1964) developed an equation for both laminar and turbulent flow in porous media, based on a dimensional analysis, to express the pressure gradient as follows

$$\frac{dP}{dl} = \frac{\mu v}{k} + \frac{c\rho v^2}{\sqrt{k}} \qquad (2.15)$$

This leads to $$f_k = \frac{1}{R_k} + c \qquad (2.16)$$

in which $$R_k = \frac{\rho v \sqrt{k}}{\mu} \qquad (2.17)$$

and $$f_k = \frac{dP}{dl} \frac{\sqrt{k}}{v^2 \rho} \qquad (2.18)$$

All experiments were represented on a plot of the friction factor (f_k) for the porous media versus the Reynolds number (R_k), in which the characteristic length in both cases is the square root of the permeability ($\sqrt{k}$) of the porous medium. Fig. 2.1.a indicates a smooth transition from laminar to turbulent flow. Ward was of the opinion that Reynolds number (R_k) as defined by eq. 2.17 appeared to be satisfactory for characterizing flow in porous media.

This method of presentation was also adopted by Sollitt and Cross (1972) who performed tests on gravel. Their plot is shown in Fig. 2.1.b. In comparison with Ward (1964) who presented a single curve for different media consisting of glass beads, ion exchange resin, sand, gravel and granular activated carbon, Sollitt and Cross (1972) presented three different curves, on the basis of different diameters of stones.

Arbhabhirama and Dinoy (1973) used the same parameters to analyse results on sand, angular gravel and large gravel. However the plot presented is different and is modelled on the pipe friction diagram known as the Moody

diagram. This plot, illustrated in Fig. 2.1.c substantiates the validity of the hydraulic gradient – velocity relationship as observed by Sollitt and Cross (1972) for a number of different materials. The experiments verify that resistance becomes pure Darcian at low Reynolds numbers and fully turbulent, at high Reynolds numbers. Although the scatter in the results of Arbhabhirama and Dinoy (1973) is less than that observed by Sollitt and Cross (1972), it should be observed that all materials tested were not subjected to the same flow range. Hence doubt exists with regard to the extrapolation of the results in either direction.

Results of tests performed on cylindrical lattice structures by Kondo and Toma (1972) are presented in Fig. 2.1.d. For each structure not more than eight readings were obtained. By using structures of different diameter within a limited flow range the results show a linear relationship on the log scale.
This relationship is expressed by

$$c_1 = \frac{0.54}{R_e^{1/6}} \qquad (2.19)$$

In the same plot relationships obtained by several others are incorporated. Kondo and Toma (1972) adopted friction coefficients developed by LeMehaute (1957) for their analysis of results.

Kamel (1969) and Keulegan (1973) based their analyses on similar parameters and the results of the latter are given in Fig. 2.1.e. This is another example where results from different media have been represented by a single curve.

Extensive and well-documented studies on the hydraulic conductivity of crushed rock and river gravel have also been presented by Dudgeon (1966) and McCorquodale, Hannoura and Nasser (1978). In a recent study Gupta (1985) discussed the use of angularity of aggregate particles as a measure of their shape and hydraulic resistance. An angularity number for rockfill was defined as the actual porosity minus 33%. This was based on the assumption that most rounded gravels had a porosity of 33% and a relationship between the angularity number and the size of particles (average size) for materials of different shape was investigated.

The selected data discussed above illustrates the different ways in which the subject of steady flow through porous media has been investigated. In most cases no single porous medium has been subjected to an extensive range of flow velocities. Instead by using media of different characteristic length, Reynolds

number ($\propto$ d) has been varied within a limited flow range. The scatter of the results and the lack of results at close intervals of velocity are noted.

Although the velocity – hydraulic gradient relationship for flow of fluids through porous media has been investigated by many authors, no general agreement has yet been reached as to its form. The main reasons for the appearance of a number of conflicting equations for their relationship could be attributed to the following:

(i) Practical difficulties of covering an extensive range of flow conditions for a particular porous medium. The experimental arrangements used were best suited only to a limited flow range in which they performed well with minimum experimental errors.

(ii) Frequently large scatter of experimental results and the limited number of readings for a given experiment.

(iii) Use of different governing equations and various parameters for the analyses of experimental data. Some authors presented equations for individual materials, for example, a particular type of stone of given diameter, while others preferred a general equation for all data covering a wide range of materials.

For these reasons it is also difficult to perform a detailed comparative study either by using the data in its present form or by normalizing it to a set of common parameters. However, it should be noted that steady flow permeability coefficients play an important role in the mathematical modelling of wave transmission through porous media. These steady flow coefficients are assumed to be valid under time dependent conditions and have been incorporated into all mathematical formulations. The validity of these models will be discussed at a later stage in this chapter.

2.4. Time dependent flow in porous media

2.4.1. Effects of unsteady flow

In comparison with the vast amount of information available on the hydraulic gradient – velocity relationship for steady flow conditions, very few investigations have been performed under unsteady flow conditions.

In porous media, the unsteady flow problem is very complex. Accelerating flow can cause a change in the expected flow regime for a particular Reynolds number and may cause a delay in the onset of turbulence in coarse porous media. Any change in flow regime will affect the flow resistance. In a porous medium the virtual mass of a particle is restricted by the presence of neighbouring particles. The limitation on wake growth due to limited pore volume downstream of each grain will influence the effective virtual mass of the particles. In addition most porous media experience some distortion under an applied force, therefore, during the acceleration phase the grains of the media may experience an acceleration albeit small.

The increase of off-shore construction activities yielded considerable development and understanding of virtual mass forces under wave action on submerged pipelines, pile arrays and plate forms. However similar advances have not been made in areas related to coastal engineering. The available analysis of case histories of breakwater failure are based on the Hudson's formula (Hudson 1959), which does not include the effects of inertia. Although acceleration effects were considered in a study on the stability of rubble mounds by Bruun and Johannesson (1976), values of virtual mass coefficients were not given.

Pioneering experimental work in this field was performed by Keulegan (1968) in a study of the damping effects of wave screens. Keulegan used an oscillatory flow tank to study the coefficients of resistance of wire mesh screens.

Shuto and Hashimoto (1978) used similar apparatus to study the hydraulic resistance of artificial concrete blocks. Theoretical analyses and experimental work involving both steady and unsteady flow were used to clarify the mechanism by which wave energy is absorbed by block structures. Three kinds of armour units namely the tetrapod, hollow tetrahedron and the hexaleg were investigated. In order to express the hydraulic resistance of each kind of unit, three different theoretical models were proposed. Unsteady flow tests were performed on various size models of the armour units in a large U-tube oscillator which generated periods varying from 3.4 secs to 4.9 secs. Free oscillations were induced by imposing an instantaneous head difference across the ends of the U-tube. From these tests it was concluded that resistance coefficients obtained under steady flow and oscillatory flow show almost no difference for periods of oscillation greater than 3.4 secs. It was also recommended that, for the armour units investigated, it is advisable to use units heavier than 500 gm and that experiments should be carried out with Reynolds numbers greater than 1000. Because of the relatively long periods of oscillation used in these tests the results have important implications for

prototype wave excitation but the recommended model criteria may not necessarily apply to all small scale laboratory conditions.

The most significant contribution in this field has been made by Hannoura and McCorquodale (1978a) who considered inertia effects in relation to materials such as crushed rock, a common construction material for breakwaters. Both steady and accelerated flow tests were performed in essentially the same apparatus with modifications to suit both test conditions. For steady flow tests the apparatus performs similar to that of a permeameter placed in a horizontal position. For acceleration tests the principle of the U-tube oscillator was adopted and for rapid acceleration the free water surface was depressed by compressed air and then suddenly released. Variations in fluid velocity and pressure difference across the porous media were recorded from a laser anemometer and a differential pressure transducer respectively. Details of the apparatus are given in Fig. 2.2.a.

Hannoura and McCorquodale (1978a) adopted a semi-empirical representation of one dimensional unsteady flow in porous media expressed in the form

$$I = (a + b|u|)u + \frac{(1+c)}{g}\frac{du}{dt} \qquad (2.20)$$

where a, b = steady flow coefficients

$c = (\frac{1-n}{n})c_n$ = acceleration coefficient

c_n = inertia coefficient

n = porosity

However, in determining 'c', it was assumed that the steady flow coefficients 'a' and 'b' were valid for unsteady flow conditions.

Figs. 2.2.a to 2.2.c illustrate the results of this work. From Fig. 2.2.b, it is observed that the acceleration effect on the resistance was restricted to the first 0.25 secs of the acceleration test for a 4.4 cm diameter rock and about 0.10 secs for 1.6 cm diameter rock. The diameter in this case refers to the mean geometric value. During this initial period the total resistance to the flow through the porous media was found to be as much as three times the corresponding steady flow resistance. The value of 'c' varied from negative to approximately +6, with the most significant positive results occurring for the largest rock size. Fig. 2.2.c is a further comparison between the steady and unsteady flow resistance, indicating the influence of the accelerating head (initial difference in the water level in the

U-tube oscillator). It shows that flow resistance approaches the steady flow resistance as the acceleration head decreases.

In general it is observed that a comparatively large scatter is present in the experimental results. The duration of each test was very short and made accurate measurements of the virtual mass effect very difficult. Due to the physics of the flow regime, the steady flow drag coefficients may not be applicable to unsteady flow conditions. Possible distortions of the porous matrix will have an influence by reducing the effect of acceleration because some of the applied force is used to accelerate the grains. The authors concluded that a statistical analysis yielded evidence of the existence of a virtual mass effect in porous media for the 4.4 cm rock but the scatter was too great to comment on the smaller sized materials.

The overall validity of the semi-empirical governing equation, 2.20, the assumption of the validity of the steady flow coefficients under unsteady flow conditions and the measurement difficulties encountered in the laboratory studies contribute to the large scatter in the experimental values. The scatter also reflects to a certain extent the limitations of the experimental set-up used for the study.

Burcharth and Thompson (1983) investigated a similar problem from a different view point. The objectives of this study were to explain some of the differences in the hydraulic stability of slender and bulky armour units and to examine scale effects that might be present in rubble mound breakwater models of different sizes. Horizontal beds of Dolosse and stones which represent two extremities in the variety of units were subjected to sinusoidal oscillatory flows parallel to the cover layer. In studying hydraulic stability the authors observed the displacement and rocking of the units. The threshold of movement was observed for the units weighing from 14 gm to 130 gm and the experiments were performed in the pulsating water tunnel at the Hydraulics Research Station, Wallingford, U.K. The test results revealed that no significant differences exist between the hydraulic stability of Dolosse and rocks of the same weight. Furthermore, units of different sizes showed the same stability and no viscous scale effect was observed.

2.4.2. Air entrainment studies

The phenomenon of air entrainment due to wave-breakwater interaction has received very little attention. Few investigators have dealt with the problem of air entrainment in waves. Fuhrboter (1970) investigated the effect of air entrainment in waves in the breaking zone and found that the effect of aeration

cannot be neglected.

The hydraulic conductivity of a porous structure such as a rubble mound breakwater has been shown to affect the wave reflection, transmission and run-up. However, with short period or breaking waves, air may be entrained in the flow within the porous structure, thus reducing the wave transmission and increasing the reflection. Although saturated flow in a porous structure can be classified in detail, a similar classification does not exist for two-phase flow in porous media.

McCorquodale, Nasser and Hannoura (1977) investigated this phenomenon and observations were made on air-water flow in wave absorbers consisting of crushed rock. The relative hydraulic conductivity in the unsaturated flow region was defined by the authors as

$$\frac{K}{K_o} = \frac{q_w \Delta z \, (a + b|q_w|)_o}{\Delta H_f} \qquad (2.21)$$

in which K = two-phase conductivity

K_o = single phase (saturated) conductivity

q_w = Darcy velocity

ΔH_f = two phase friction head loss through a distance of Δz

$(a + b|q_w|)_o$ = single phase (saturated) resistance

The flow tests were performed in an apparatus consisting of a closed-loop of 10.16 cm diameter pipe having a recirculating flow system together with a removable test section. The loop included an air diffuser capable of injecting air bubbles into the flow. Both co-current and counter-current air flows were investigated. A laser anemometer and an orifice meter were used to measure the water discharges while a rotometer was used to measure air flow to the diffuser. All experiments were conducted under steady flow conditions. Details of the apparatus is given in Fig. 2.3.a.

Some of their results are presented in Figs. 2.3.b and 2.3.c. They show typical results for co-current and counter-current flow of an air water mixture in crushed rock. The counter-current flows were found to be very unstable for high values of discharge. The reduction in the conductivity was found to be much greater for counter-current flow due to the blockage provided by the entrained air.

Subsequently Hannoura and McCorquodale (1978b) performed further tests on counter-current flow. In particular, conceptual models and semi-empirical

equations were proposed to describe the nature of the flow and the hydraulic conductivity of air–water flow through coarse porous media. The flows in the tests were primarily on a vertical axis.

2.5. Wave action on porous structures

The ability to predict wave transmission through and reflection from a porous structure plays an important role in assessing the overall effectiveness of such a structure. These characteristics are closely related to the amount of protection afforded by the structure against incident wave energy. The overall influence of porosity on the stability of the armour layer and on the structural integrity of the complete rubble mound breakwater demands closer examination.

It is observed that the work of most researchers is not limited to one specific domain but encompasses several areas of interest. It includes theoretical, experimental and field studies on both non–submerged and submerged structures of varying geometry and a variety of wave environments.

In discussing theoretical developments emphasis will be placed on empirical, semi–empirical, analytical and numerical work on flow through porous media with special attention being given to internal and external flow associated with wave action on permeable structures. Most of the analytical models have been developed for regular waves and only in the recent past have random waves been incorporated into the computation process. Numerical models have either used the finite difference or the finite element method of analysis and on a few occasions hybrid models using both methods have been presented.

Numerous experiments, some in support of theoretical developments and others investigating the performance of various structural forms, have been carried out on both non–submerged and submerged porous structures.

In comparison with theoretical and experimental work the number of reported field investigations is very few and in most of them the structures have been exposed to mild wave conditions.

Wave action on non–submerged and submerged porous structures can be classified into several topics as illustrated in (Table 2.3) and a review will be made of each topic.

2.5.1. Analytical and experimental studies on non-submerged porous structures using regular waves

Early work on porous structures was directed towards a better understanding of the hydraulic behaviour and performance of wave filters which are placed in front of laboratory wave generators. In a way they are similar to breakwaters in that they cause partial reflection and reduced transmission of the incident wave.

Biesel (1950) presented one of the first analytical approaches to investigate wave filters by considering the equations of motion through a hypothetical wave filter resisting motion according to Darcy's law for unsteady flow. Biesel showed that the motion decays exponentially in the direction of wave propagation. The rate of decay and wave length were described by a pair of dispersion equations. The significant contribution made by Biesel was the identification of the form of the spatial and temporal functions which describe a linearly damped, periodic, free surface motion.

Straub and Herbich (1956) presented an artificial viscosity theory in order to account for wave damping in a filter. A Navier-Stokes laminar dispersion function together with a velocity field derived from linear progressive wave theory were used to determine the power consumed by the filter. The true kinematic viscosity was replaced by an effective viscosity the value of which was adjusted until agreement was obtained between theory and experiment. In this study wave reflections were not given detailed consideration. Subsequently a brief laboratory investigation was made by Straub in which reflection coefficients were determined for absorbers of varying porosity.

LeMehaute (1957) was one of the first to present a detailed study on the subject of flow through porous media. It was recognised that the resistance forces in large scale granular media are not prescribed by Darcy's law. However in order to obtain an analytical solution the author assumed a resistance law such that head loss was proportional to the local velocity. The intention was to derive a constant of proportionality by comparing the theoretical solution to experimental results. LeMehaute recognized that any imbalance of pressure and resistance forces in the flow resulted in an increase in the pore velocity rather than in the local gross flow rate. This enables account to be taken of the effect of porosity in the equations of motion. An irrotational velocity field was prescribed which results in a boundary value problem similar to that of Biesel (1950) whose solution to the problem was accepted by LeMehaute. The experimental results showed that the reflection

coefficient was approximately constant at 0.6 and that part of the theory which predicts exponential decay in the internal wave amplitude was modified to formulate an empirical equation for the transmission coefficient.

In the same study LeMehaute presented the results of an extensive experimental programme which covered both homogeneous crib style breakwaters and multi-layered sloping faced breakwaters. However the hydraulic properties of the media composing the models were not determined. If these properties were available they could have been used for experimental verification of other theories.

Although the studies of Biesel (1958) and LeMehaute (1957) have been critically evaluated by some investigators, they represent pioneering work in understanding the behaviour of wave motion within porous media. In the absence of detailed information, many investigators (Kondo and Toma 1972, Kogami 1978) continue to use expressions developed by LeMehaute (1957).

Goda and Ippen (1963) conducted both experimental and theoretical studies of wave filters composed of wire mesh screens. In this analysis the mesh was resolved into sets of horizontal and vertical cylinders. Linear wave theory was used and the power loss was computed from the drag force relationship on circular cylinders. Partial reflection from individual screens was not considered and the change in energy flux across each screen was equated to the power loss at the screen. The theory is to an extent dependent on experimental work because it had to be calibrated against experimental results in order to determine appropriate unsteady drag coefficients. Neglecting wave reflections will naturally enforce a limitation when applying the method to less porous structures.

Keulegan (1968) analysed wave damping in composite filters using an energy dissipation approach. This method of analysis is different to that of Goda and Ippen (1963). Instead of superimposing the drag force on rows and columns of cylinders to evaluate the effective screen resistance coefficient, Keulegan measured the drag in separate tests which were performed in oscillatory flow in a U-tube. With regard to wave damping effects, both cnoidal and linear wave theory were used to relate the particle velocity to the wave amplitude between adjacent screens. Assuming the local wave energy to be proportional to the square of the local amplitude, a differential equation was developed to express the rate of change of amplitude as a function of the power lost via filter resistance forces. The solution requires certain parameters to be evaluated by comparison with experimental results. Since wave reflection is not accounted for, the solution is not readily applicable to less porous structures.

Kamel (1969) adopted a modified version of Keulegan's (1968) theory for wave filters to analyse idealized homogeneous crib style breakwaters. The experimental structures consisted of vertical walled wire baskets filled with spheres or cubes. Although high reflection coefficients were observed, the theory developed does not include reflection analyses. A parameter is used to calibrate the theoretical development against experimental values. Apart from transmission tests, Kamel also performed steady flow permeability tests on several media to obtain resistance equations.

Lean (1967) presented an analysis which allows the reflection of waves from permeable wave absorbers of simple shape to be calculated when the resistance coefficient of the material composing the absorber is known. It was assumed that the waves were sufficiently long and of low amplitude for the linear theory of long waves to be applicable. The equations used were

$$\frac{\partial \eta}{\partial t} = - \frac{\partial}{\partial x} (du) \qquad (2.22)$$

$$\frac{\partial u}{\partial t} = - g \frac{\partial \eta}{\partial x} - \frac{k' u|u|}{d} \qquad (2.23)$$

where

u = horizontal velocity

k' = resistance coefficient

Lean then linearized the quadratic friction term in the second equation through the transformation.

$$f' = \frac{8}{3\pi} \frac{k'}{d} U \qquad (2.24)$$

in which f' = constant

and U = amplitude of the local wave particle velocity.

The factor f' is chosen such that the above term will yield the same energy loss per unit plan area per cycle as the non-linear friction term. Hence eq. 2.23 becomes :

$$\frac{\partial u}{\partial t} = - g \frac{\partial \eta}{\partial x} - f'u \qquad (2.25)$$

It is apparent that Lean's solution is strictly applicable to long waves of low amplitude which do not break at the entry to the absorber.

It should be noted that linearization is performed by using the Lorentz approximation to the quadratic friction law. The essential feature of this method is the replacement of the quadratic term by a fictitious resistance term which is proportional to the velocity, the constant of proportionality (f') being chosen to give the same energy loss per unit plan area per cycle. In eq. 2.24, U is the local wave particle velocity amplitude. Thus in general f' varies from point to point within the absorber depending on the local wave height and depth. However, to linearize the momentum equation it is assumed that f' is independent of x and equal to its mean value for a given absorber and incident wave condition. The reason for this being stressed is because the above approximation has been made in most of the analytical techniques used to solve the problem of wave transmission through porous structures.

Kondo (1970) treated the problem of wave transmission and reflection for permeable structures in a manner similar to that of Lean (1967). An analytical approach was developed to study long wave interaction with homogeneous, vertical faced breakwaters. The one dimensional equation of motion for periodic, linearly damped free surface flow was solved. The linearized equations of momentum and continuity are given below.

$$\frac{\tau}{ng}\frac{\partial u}{\partial t} + \frac{u}{k^*} + \frac{\partial \eta}{\partial x} = 0 \qquad (2.26)$$

$$n\frac{\partial u}{\partial t} + (d + \eta)\frac{\partial u}{\partial x} = 0 \qquad (2.27)$$

in which τ = square root of tortuosity
k^* = effective permeability

Kondo expressed k^* in terms of laminar and turbulent flow coefficients of the Forchheimer equation (a and b in $I = au + bu^2$) and a representative value of the velocity (u^*) applicable for the entire structure. This value was evaluated at the centre of the structure.

$$k^* = \left[\frac{1}{a + b\theta u^*}\right] \qquad (2.28)$$

in which θ is a linearizing factor. However Kondo did not give a specific definition for tortuosity.

The similarity of the work of Lean (1967) and Kondo (1970) is that both solutions yield an exponential decay of wave amplitude in the direction of wave propagation. Lean's work mainly involves the computation of reflection coefficients for high porosity, wire mesh absorbers. Kondo assumes linear wave theory to apply outside the porous structure and the external–internal solutions are combined via the continuity of horizontal velocity and pressure at the liquid–structure interface in order to obtain reflected and transmitted wave amplitudes.

Kondo and Toma (1972) modified the previous theory in order to obtain a better prediction of the reflection coefficient. In the earlier development of Kondo (1970) only the wave energy reflected by the front face of the structure was considered and as a consequence the reflection did not vary with the length of the structure. Owing to internal reflections, experimental values were not in good agreement particularly for smaller values of the ratio, length of structure to wave length. This modification assumed that the porous structure consisted of a number of vertical layers and reflection from each boundary surface was considered.

Kondo, Toma and Yano (1976) made further modifications to the existing theory in order to study multi–layered breakwaters. However it was assumed that the breakwater was composed of rectangular vertical layers. The reflections were restricted to one from each boundary and that reflection was carried back to the sea. This development although somewhat idealized permitted the theory to be applied to breakwaters of trapezoidal cross–section.

Kondo and Toma (1972) also performed experimental studies to assess the influence of incident wave characteristics and thickness of structure on reflection and transmission. An idealized porous medium, comprising a cylindrical lattice structure was used for this investigation. The results indicate that whilst the transmission decreases with increasing wave steepness, reflection was not significantly dependent upon this parameter.

It was observed that an increase in the ratio of the structure's width to the wave length causes an almost exponential decrease in transmission whereas the

reflection coefficient reaches a maximum when this ratio is approximately 0.2 to 0.3. Thereafter the coefficient decreases and remains almost uniform when the ratio is greater than 0.6. Kondo and Toma also observed the presence of a standing wave pattern within the porous medium when the width/wave length ratio equalled or exceeded 0.25.

Sollitt and Cross (1972) presented investigations on wave transmission through porous structures. Similar to previous work by Lean (1967) and Kondo (1970), a linearizing technique was used to solve small amplitude wave motion in three breakwater configurations, namely, crib style, pile array and trapezoidal sections. This method yields a potential flow problem solved by an eigen–series solution. Linear theory was assumed outside the structure and a solution was obtained by adopting appropriate boundary conditions at the liquid–structure interface. From experimental work it was observed that transmission decreases with decreasing wave length and breakwater porosity, and increasing wave height and breakwater width. Reflection was found to decrease with increasing wave length and breakwater porosity and decreasing breakwater width.

In order to apply the theoretical development to trapezoidal breakwaters, Sollitt and Cross considered an equivalent rectangular section to replace the trapezoidal section. This was done such that both sections have the same submerged volume. An estimate of the energy loss due to waves breaking on the seaward slope was obtained by modifying the wave breaking criterion proposed by Miche (1951) for impermeable slopes. The final solution was obtained by combining breaking losses and internal damping.

Keulegan (1973) applied energy methods for long waves travelling through a porous structure consisting of rocks of uniform size in order to develop an expression for the coefficient of transmission. When energy dissipation in the voids is due partly to turbulent forces, the transmission was expressed by a power formula which was modified by a parametric factor to correspond to the short wave conditions normally applied in model studies. The form of this factor was determined from observations made with waves of different periods. With the reflections not being amenable to an analytical treatment, test results were consolidated in a single curve, irrespective of the rock sizes, with the porosity remaining constant.

A similar method to that of Kondo (1970) was adopted by Madsen (1974) in analysing the reflection–transmission phenomenon in porous structures. Madsen adopted an approach which was of physical significance rather than a pure

mathematical derivation. The governing equations were derived for the case of linear shallow water waves and a homogeneous, isotropic porous structure confined between vertical walls. The simple closed-form solution employed (in conjunction with Lorentz principle of equivalent work) resulted in a relatively simple explicit solution for the friction factor in terms of the breakwater geometry, the hydraulic properties of the breakwater material and the incident wave-characteristics. This result meant a considerable reduction in the computational procedure compared with the rather tedious iterative procedure suggested by Sollitt and Cross (1972). It should be noted that Madsen's simplified solution was obtained only after making several assumptions which led to a reduction in mathematical complexity. Engelund's (1953) equations were recommended to determine the non-Darcy hydraulic parameters.

Madsen and White (1976b) extended the theory to analyse flow through trapezoidal breakwaters. An equivalent breakwater was defined by considering the flow through horizontal layers and the theoretical work in this development was based on steady flow turbulent discharges.

In a subsequent publication, Madsen, Shusang and Hanson (1978) analysed the flow through a trapezoidal breakwater in more detail by dividing it into three regions, two of which had sloping faces and the third was of rectangular form. This enabled a differentiation to be made between the two sloping faces of the breakwater and the central part. The dividing lines were at the points where the mean water level met the breakwater. The results from this more elaborate method provided better agreement with experimental results.

In the last two investigations reviewed, energy dissipation on rough slopes was assessed by using the method presented by Madsen and White (1976a).

Svendsen (1976) proposed an analytical method to predict the reflection coefficient from rubble mound breakwaters with an impermeable core. The assumptions are long linear waves and linearized friction forces, based on a purely turbulent friction law. The theory forms an extension of Madsen's (1974) work. Svendsen was of the opinion that for practical purposes reflection from a multi-layered breakwater with rock armour could be determined by assuming that the second layer was impermeable. In effect the analysis related to a wave absorber of rectangular section with a vertical impermeable face at the back of the structure. A modification was then proposed to account for the sloping front face, but the work was not supported by experimental investigations.

Madsen, P.A. (1983) presented the most recent analytical development for the reflection of linear shallow water waves from a vertical porous wave absorber on a horizontal bottom. This approach was very similar to that of Svendsen (1976) in that the governing equations were the same as those adopted by Madsen and White (1976b). Instead of making simplified assumptions to reduce the computational effort, a rigorous analytical approach was adopted to determine an expression for the reflection coefficient as a function of parameters describing the incoming waves and the absorber characteristics. To evaluate the linearized friction factor a refined numerical iterative scheme was used. The influence of porosity, wave steepness and structure width was examined for various wave environments. Madsen also pointed out omissions made by Lean (1967) and Svendsen (1976) in their theoretical developments. In the absence of any experimental data pertaining to rectangular wave absorbers, a comparison was made with measurements from an almost rectangular absorber having a sloping surface.

2.5.2. Analytical and experimental studies on non-submerged porous structures using random waves

The analytical developments presented so far were based on regular wave theories. In all of these studies the incident waves were assumed to be sinusoidal and the effect of damping was represented empirically by a term quadratic in the local velocity. With proper choice of the empirical constants, these theoretical developments seem to be reasonably supported by laboratory experiments. However in the natural ocean environment the wind generated waves are seldom sinusoidal and a more realistic description involving statistical methods is required.

Massel and Mei (1977) in a study on transmission of random wind waves through porous media applied spectral theory to wave scattering by perforated or slotted and porous breakwaters. Semi-empirical solutions were derived for random waves passing these structures with the quadratic damping term treated by the stochastic equivalent linearization technique. The statistical transmission and reflection coefficients were introduced in terms of their standard deviations and the wave spectrum.

Massel and Mei's solution is approximate for the shallow coastal zone where the energy of the incident wave energy is concentrated in the long wave part of the spectrum. Massel and Butowski (1980) presented an analysis extending this theory which included a more rigorous analysis of wave motion inside the breakwater space where the incident wave spectrum may be arbitrary. The basic non-linear equation of motion in a porous structure was linearized using a

statistical linearization technique and the reflection and transmission coefficients were found by adopting a similar method to that of Massel and Mei (1977). Making use of simplifying assumptions, the predictive ability of this model was tested against prototype measurements and calculations performed by Thornton and Calhoun (1972). One such assumption is the use of an equivalent rectangular cross-section for the trapezoidal prototype. In addition, hydraulic properties pertaining to permeability coefficients have to be determined using a suitable formula. Comparison of numerical calculations and field measurements indicated that the transmitted energy in the field is higher than that predicted by theory. Agreement on reflection coefficient was satisfactory. This method may be used in practical applications but it is necessary to have further good quality experimental data to determine the range of applicability of the solution.

2.5.3. Numerical and experimental studies on non-submerged porous structures using regular waves

Both finite difference and finite element techniques have been used in numerical analysis of wave action on porous media. In comparison with analytical models, relatively few studies involving numerical models have been presented.

For one dimensional flow, the equation for unsteady non-Darcy flow may be written as

$$I = aq + bq^2 + c\frac{\partial q}{\partial t} \qquad (2.11)$$

in which q = bulk or macroscopic velocity
a, b, and c are constants

With the limitation that convergence, divergence and curvature of the macroscopic streamlines have negligible effects on the conductivity, McCorquodale (1970) generalized equation 2.11 to describe two and three dimensional flow. He examined the Navier-Stokes equation and with the aid of a number of assumptions, arrived at the following :

$$\vec{q} = -\left(\frac{1}{a + bq}\right)\left(\nabla\varphi + \frac{1}{gn}\frac{\partial \vec{q}}{\partial t}\right) \qquad (2.29)$$

in which n is porosity.

Eq. 2.9 together with the continuity equation

$$\nabla . \vec{q} = 0 \tag{2.30}$$

yields the governing equation for two and three dimensional unsteady non-Darcy flow as

$$\nabla . \left\{ \frac{1}{(a + bq)} \left(\nabla \varphi + \frac{1}{gn} \frac{\partial \vec{q}}{\partial t} \right) \right\} = 0 \tag{2.31}$$

McCorquodale solved eq. 2.31 for rapid drawdown in rockfill using a finite element technique, using a Lagrangian method to compute the free surface position at the end of each time increment. The inertia term was assumed to be small when compared to friction and a series of experiments with rock sizes up to 4 cm was performed to support this assumption. The numerical solution was confirmed by rapid drawdown laboratory tests.

McCorquodale (1972) presented a modified rapid drawdown finite element model and applied it to the problem of wave propagation through a rectangular rockfill embankment with an impervious core. The solution was based on eq. 2.31 assuming that the term $\frac{1}{gn} \frac{\partial \vec{q}}{\partial t}$ is small compared to $|\nabla \varphi|$ and has nearly the same line of action as $\nabla \varphi$ and $\vec{q}$. On this basis the transformation

$$\nabla \xi = \nabla \varphi + \frac{1}{gn} \frac{\partial \vec{q}}{\partial t} \tag{2.32}$$

reduces the governing equation to

$$\nabla . \left\{ k \, (|\nabla \xi|) \nabla \, \xi \right\} = 0 \tag{2.33}$$

$$\text{in which } k(|\nabla \xi|) = \frac{a}{2b} \left\{ \frac{\sqrt{1 + 4b|\nabla \xi|/a^2} - 1}{|\nabla \xi|} \right\} \tag{2.34}$$

This was then expressed in variational form

$$\partial X = \int_{t_o}^{t} \int_{A(T)} \delta\left\{k(|\nabla\xi|)(|\nabla\xi|)^2 + G(|\nabla\xi|)\right\} dA dT = 0 \qquad (2.35)$$

where t_o = initial time

$A(T)$ = solution domain

and $G(|\nabla\xi|)$ is a function introduced to ensure that continuity requirements are satisfied.

McCorquodale represented the tailwater piezometric boundary condition by a periodic time function and used triangular elements in discretizing the solution domain. At the end of each time increment the position of the free surface was calculated from the known previous value and the surface particle velocity during that increment.

Nasser and McCorquodale (1975) presented a mathematical simulation of the internal wave propagation for non-Darcy flow in a rockfill embankment using the method of characteristics together with a finite difference scheme. The characteristic directions were used to control the discretization of the solution domain. An explicit scheme with central differences in space and forward differences in time was used to discretize the governing equations for non-linear, long, shallow-water waves.

It has been observed by several investigators that when water flows into a porous body, for example during run-up stage on a breakwater, the phreatic line and the free water level meet at the same point on the boundary. However when the water flows out from the porous body, during run down, a seepage surface may be interposed between the free water level and the phreatic level. The point at which the phreatic line joins the seepage surface is defined as the outcrop point. The movement of the outcrop point will only be identical with the movement of the free water level under certain conditions.

Two boundary conditions have to be satisfied : An entrance boundary condition which prescribes the time dependent movement of the outcrop point and a downstream condition indicating a zero normal velocity at the impervious core. The model traces phreatic line profiles with time. In the analysis the movement of the outcrop point was considered in detail. The authors pointed out that during run-up (rising phase) the outcrop point coincides with the external water level whereas during run-down (falling phase) this need not necessarily occur. In the

falling phase, the outcrop point will only coincide with the outside water level if the latter drops at a rate equal to or slower than the maximum internal fall velocity. If this condition is not satisfied a seepage face is created and this phenomenon is known as the fast drop. The movement of the outcrop point was incorporated into the solution based on a theory developed by Dracos (1969) for Darcy flow. The fast drop case undergoes different stages, one of which is governed by a damped, non-linear ordinary differential equation. Thus the authors identified a new classification for waves running up slopes by defining them as either "fast" or "slow" rising, depending on the uprush speed being faster or slower than the internal seepage rate.

The analysis of sloping embankments was simplified by utilizing an equivalent rectangular section and allowing for possible additional energy losses in the internal, immediate vicinity of the embankment face. Nasser and McCorquodale also found that the best correlation with experimental results was obtained when transformation of a sloping embankment to its rectangular equivalent was based on the concept of both structures having equal length at still water depth. It should be pointed out that Sollitt and Cross (1972) preferred the use of a rectangular section based on the concept of both structures having equal submerged volume. These concepts will be considered in detail in the next chapter.

In addition to the above contribution, Nasser and McCorquodale (1973, 1974), McCorquodale and Nasser (1974) and Nasser (1979) presented a series of papers concerned with different aspects of both numerical and experimental studies. A notable feature is the consideration of the flow outside the structure in order to couple the external and internal wave motion. To achieve this the shallow-water wave dynamic equation and the associated continuity equation were discretized and used to advance the solution, in the external region, in a similar manner to that used for the internal equations. Experimental work was performed on rockfill structures consisting of four different media. At a later stage their properties will be discussed and compared with those used for the present study.

Hannoura (1980) analysed the internal flow due to wave action on a porous structure with an impervious core. The problem was formulated in two phases.

In the first phase the governing equations for unsteady non-Darcy flow in rubble mounds were developed and simplified to a set of one dimensional unsteady equations which were solved using a finite difference technique to obtain the

instantaneous phreatic surface. A system of hyperbolic differential equations was obtained and solved by the method of characteristics. The equations of the charactertistics were used to determine the maximum time step required to ensure the stability and convergence of the finite difference solution.

In the second phase of the solution the finite element method was used to analyse the flow domain after every time step or after a predetermined number of time steps. This compensates for the simplifications assumed in the first phase of the overall solution. The introduction of the finite element method yielded representative values of the actual pressure distribution and the hydraulic conductivity of the rubble mound matrix. The solution domain was divided into a number of vertical sub-domains and then weighted averages for pressure and hydraulic conductivity were obtained and transferred to the finite difference solution.

Several studies pertaining to this hybrid model which uses the finite difference method for time integration and the finite element for space integration have been presented by Hannoura and McCorquodale (1978c, 1979a, 1985a, 1985b) and Hannoura and Barends (1982). In the latest contribution, provisions were included in the model to account for added mass and to detect and correct for internal wave breaking and the entrainment of air near the air-water interface. These modifications were based on the authors previous studies on unsteady effects and air entrainment which were reviewed earlier in this chapter.

Koutitas (1982) presented a numerical model of the stability of rubble mound breakwaters. The model which used finite difference methods describes the flow on the sloping face and inside the structure. It consists of two parts, the first considers a quantitative description of wave run-up on a permeable slope and the second describes the unsteady two dimensional unconfined flow in the voids of a rubble mound section. The first phase was based on a model presented by Gopalakrishnan and Tung (1980) and the second phase was based on a model previously developed by Koutitas. The coupling of the two models for simultaneous application was achieved through a staggered numerical solution of the open channel and groundwater models at successive locations in the time domain. It should be noted that this study adopted Darcy's assumption with special attention being paid to the estimation of the permeability coefficient. This model was not supported by experimental investigations.

One of the more recent studies on wave reflection and transmission at permeable breakwaters of arbitrary cross-section was presented by Sulisz (1985). The theoretical approach used in this study was based on the unsteady Forchheimer

equation of motion in the pores of a coarse, granular medium. The equation was linearized using Lorentz's hypothesis of equivalent work. Linear wave theory was applied and the excitation was provided by a monochromatic wave with normal incidence to the structure. The boundary value problem was solved by using a hybrid method which employs boundary element methods in the breakwater body and in the vicinity of the breakwater with a boundary solution procedure in the exterior regions. Numerical results were compared with experimental data and the agreement was satisfactory.

An extensive model system developed by Abbot, Skovgaard and Petersen (1978) was used by Madsen, P.A. and Warren (1984) to investigate reflection and transmission from vertical porous structures. This system was based on the time-dependent, vertically-integrated Boussinesq equations of conservation of mass and momentum and is able to simulate unsteady two-dimensional flows in vertically homogeneous fluids. The use of these equations is of particular importance in the simulation of short waves. They account for, amongst other phenomena, the deviation from a hydrostatic pressure distribution due to vertical accelerations and make it possible to consider a wide range of water waves which are not restricted by linear assumptions. The equations also include porosity which makes it possible to simulate the reflection-transmission phenomena in porous breakwaters.

The numerical model was set up to simulate the physical model of Keulegan (1973). Comparison of numerical and experimental results indicated that transmission coefficients were in satisfactory agreement whereas a significant discrepancy was observed with regard to the reflection coefficients. Similar observations were made when comparing the numerical solution with the analytical solution developed by Madsen and White (1976b). Investigations were also performed on the influence of the grid size and time step of the finite difference scheme. Finally, numerical model tests were performed on wave absorbers and the computational results compared with those of an analytical solution to the same problem by Madsen, P.A. (1983). For small values of the reflection coefficient the agreement was satisfactory whereas deviations were observed for larger values. This was attributed to non-linear effects which have a considerable influence on the experimental technique used to determine the reflection coefficients.

Mizumuara (1985) presented an analysis of wave induced currents in an idealized rubble mound breakwater. Particular consideration was given to the modelling of flow channels and solutions were obtained by use of the method of characteristics. The computed results showed that vertical currents are generated in the breakwater and these currents play an important role in wave damping.

2.5.4. Experimental studies on submerged porous structures using regular waves

A submerged breakwater is a barrier which is constructed so that its crest is at, or slightly below, the still-water level. Such structures absorb some of the wave energy by causing the waves to break prematurely. Part of the remaining energy is reflected and some is transmitted shoreward. The submerged breakwater, though seldom used in a permanent harbour development, affords limited protection against wave action.

Several semi-empirical theories have been proposed to express the coefficient of transmission for wave action on a submerged breakwater. Many of these theories relate to impermeable structures. In this review attention will be focused on studies pertaining to porous submerged structures. The influence of porosity on wave transmission and reflection will be discussed to assess the performance of such structures and a comparison will be made with similar but impermeable structures. Analytical developments will not be considered in this review. A brief summary on this topic is given by Khader and Rai (1980).

Dick and Brebner (1968) performed one of the first laboratory investigations on permeable and impermeable submerged breakwaters when exploring the possibility of improving the effectiveness of a submerged breakwater by increasing turbulence and wave interference. A permeable rectangular structure consisting of nested tubes with their axes parallel to the incident wave direction was used for the study. A rigid horizontal flat plate was placed on top of the tubes.

The authors observed that in both permeable and impermeable cases a major portion of the wave attenuation results from energy losses caused by turbulence and wave breaking at the structure. At least 50% of the incident wave energy was lost to turbulence. A substantial proportion, 30% to 60% of the energy transmitted was transferred to frequencies higher than that of the incident wave. This property was exhibited by both types of structures.

It was also noted that submerged impermeable breakwaters cause a maximum wave reflection when the incident wave has the same period as a standing wave on top of the structure with a wave length equal to the crest width. It was found that submerged permeable breakwaters transmitted less wave energy than an impermeable type over a certain frequency range for depths of submergence greater than 5% of the total depth. Minimum energy was transmitted over and through permeable breakwaters when the criteria noted above for impermeable breakwaters

are met. A fairly well-defined minimum coefficient of transmission was observed for permeable breakwaters. The impermeable counterpart did not exhibit this property and the investigation provided sufficient justification for the use of porous submerged structures.

Dattari, Raman and Shanker (1978) performed a series of experiments on both impermeable and permeable structures of various shapes, using crushed stones for the latter. It was observed that incident wave steepness has an important influence on the wave breaking phenomenon. Waves near critical steepness may be induced to break by the submerged breakwater and since this process is always accompanied by energy losses, steep waves are likely to be attenuated more than waves of lesser steepness.

It was also found that an increase in the crest width over the minimum necessary to initiate breaking did not have any significant influence on the transmission characteristics which were observed to be independent of the structural form. In contrast to the findings of Dick and Brebner (1968), Dattari et al. revealed that both permeable and impermeable submerged structures behaved in very similar fashion.

Khader and Rai (1980) who performed a series of experiments on impermeable submerged structures observed the existence of a critical value of relative height (height of structure/water depth) for each of the structures. Its value varied from 0.43 to 0.66. For values less than the critical value the structure was not effective in damping waves. As the relative height increased the damping effect increased significantly. It was also observed that a relatively wide barrier exhibited better damping characteristics than a narrower one and of the shapes investigated, the rectangular cross-section breakwater, was the most effective.

A comparison of three investigators reviewed indicate that there exists a degree of uncertainty with regard to some of the final conclusions. In two of the studies porosity was considered as a separate variable and its influence assessed. From the conclusions of Dick and Brebner (1968) it is evident that porous submerged structures could be more effective and further research is required to determine the type of porous media to be used.

In recent developments of this subject the performance of low crest rubble mound breakwaters has been investigated by Allsop and Ojo (1982) and Allsop (1983). Rock armoured low crest rubble breakwater sections were investigated in random waves. Observations and measurements were made of the

number of overtopping waves, the transmitted waves and of the damage to the armour on both front and rear slopes of the breakwater. Allsop identified the importance of several free-board parameters in relation to overtopping and subsequent damage.

2.5.5. Selected experimental studies relating to specific structural configurations and wave environment

In this section attention is focused on a few selected studies which relate to wave action on porous media and which concentrate on areas most relevant to the present study. The majority of these are experimental investigations on different structural forms but illustrate the importance of the voids matrix and permeability. The first part of this section relates to the performance of rubble mound structures and the second part analyses the results of investigations on vertical pile structures.

Sawaragi (1966) presented one of the earlier studies on scouring due to wave motion at the toe of a permeable coastal structure, investigating the relationship between the reflection coefficient (K_r) and porosity and the influence of K_r on scouring.

It was shown that K_r changed remarkably with voids ratio when the latter was less than 20%, but the change of K_r was small for voids ratio greater than 20% for any slope of the permeable face. With regard to scouring depth and K_r it was observed that the former becomes larger in proportion to the increment of the coefficient when K_r is greater than 25%. When K_r is less than this value, the scouring depth becomes small and in some cases the final topography at the toe revealed sediment accumulation. It was also observed that structures installed at shallower depths were not necessarily stable against scouring. With regard to the subsidence of armour blocks it was concluded that for a seaward slope greater than 30 degrees subsidence could be influenced by scouring depth. The results from this study are of importance in relation to the design of toe structures.

Fallon (1972) performed an experimental study on discontinuous composite wave absorbers. This study concentrated on the influence of a berm which is often used in rubble mound structures. Wave energy absorption was determined, based on the properties of the input wave and the absorber. The experimental model consisted of an impervious lower slope which terminated at a berm supporting a stone filled, upper slope. A study of the reflection coefficients was made by varying wave length, wave height, water depth, average stone

diameter, depth and width of berm as well as the constituent materials of the slopes.

Fallon concluded that wave absorption increases with wave steepness, berm width and with decreasing angles of the upper and lower slopes. Enlarging the width of the berm beyond five stone diameters does not cause a significant change in wave absorption nor does varying the stone size or water depth. The experimental data indicated that minimum reflection occurred when the berm depth was between 0.25 and 0.50 of the water depth and that greater water depth over the berm increased reflection. This study provides information required for the efficient design of a berm from a view point of both its geometry and porosity.

The influence of different permeabilities of the core material on the stability of a breakwater was investigated by Bruun and Johannesson (1976). In a series of tests three different core materials (22.5 mm - 30.0 mm, 6.1 mm - 11.5 mm and 3.2 mm - 6.1 mm) were used with the same armour layer (60 mm granite) resting on the same underlayer (20 mm - 30 mm stones). For comparative tests an impermeable slope made of a wooden slab was also used.

Results from these investigations are presented in Figs. 2.4.a and b. For very low permeabilities, the highest water elevation in the core occurred after maximum uprush on the armour slope and was located just inside the sublayer with an elevation slightly below that of the maximum uprush. For low permeability, hydrostatic pressure builds up in the core during water outflow in the backwash phase. For high permeability of the core, the situation reversed, because the water level in the structure followed the retreating wave more closely. The water elevation within the structure measured at the time of maximum wave run up is shown in Fig. 2.4.a. The damage ratio based on the percentage of blocks which moved plotted against the wave height for various core material is presented in Fig. 2.4.b. It demonstrates that damage is more pronounced and occurs earlier with finer core material than with a coarser core. This is particularly noticeable for higher damage ratios. Therefore, within certain limits, stability seems to increase with increasing permeability. This investigation clearly illustrates the importance of porosity of core material in relation to the stability of the structure. However it must be noted that the use of a relatively permeable core will increase wave transmission through the structure particularly for waves of long period and low amplitude.

Groups of cylindrical piles arranged in specific geometric patterns have been investigated experimentally for various purposes one of which is their

performance as a porous wave absorber in the construction of ports and harbours. Most experiments in the past concentrated on wave transmission characteristics with little reference to wave reflection and energy losses. In relation to the present study, groups of cylindrical piles represent porous structures with specific porosities, surface area and tortuosity.

Early work in this field indicates that if a group or configuration of piles having more than one row is used, the problem of calculating the power transmitted becomes relatively complicated. This is due to a number of factors varying from reflection and scattering of wave energy to energy dissipation by skin-friction and form drag. It has also been found that mutual interference between piles has an effect on the transmitted and reflected wave characteristics if the spacing is less than two pile diameters.

Costello (1952), in a study of dense pile structures, compared the effects of spacing between piles transverse to the wave front to the effects of longitudinal spacing of piles. The results of this study indicated that the relative depth (depth/wave length) may be neglected in the comparison of various transmission capacities. It was also noted that increasing the number of rows by 100% resulted in an average decrease in wave transmission of only 18%, irrespective of the configuration and density of the cylinders. Furthermore approximately 50% of the total decrease in wave transmission occurred within a distance of less than one quarter of the wave length measured from the incident face of the group of cylinders.

A detailed investigation on this subject was carried out by Van Weele and Herbich (1972) who tested a group of piles for various longitudinal and transverse spacing. Although no mention was made of porosity, these represented structures whose porosity varied from 0.82 to 0.92 in a systematic way.

Van Weele and Herbich concluded that transmission through a particular pile group decreased with increase in steepness of the waves passing through the group. The variation of transmission between different pile groups was found to be dependent on the spacing between the piles. It was observed that the reflection coefficient decreased with increase in steepness as well as with increase in the longitudinal and transverse spacing between piles. Furthermore, staggering the pile rows resulted in a decrease in transmission whereas no significant change was observed in the reflection coefficient. Although Van Weele and Herbich covered a wide spectrum of structures with different spacing combinations, it should be noted that the number of readings for each case was limited to three. This limitation

imposes a restriction in arriving at positive conclusions from the experimental results. However these studies illustrated that the overall performance of pile groups is very much dependent on the spacing between the piles.

Grune and Kohlhase (1974) investigated the behaviour of vertical slotted walls which represent a particular form of porous medium. Porosity is related to the spacing of the individual elements. The uniqueness of this study in comparison to similar studies done previously was that the angle of wave direction was taken as a variable. The investigators expressed the opinion that this type of structure can be adopted in situations where the construction should be permeable with respect to currents and sediments while giving sufficient protection against wave action.

The main topics of Grune and Kohlhase's investigation involved the ratio of the impermeable area of the wall to the total wall area, shape of wall elements and the direction of wave approach. It was observed that the transmission coefficient depends only slightly on the relative depth (depth/wave length) and wall thickness. The wave steepness, the shape of wall elements, their spacing and the wave direction were important factors. A slight decrease of transmission coefficient with increasing wave steepness was observed. However, the experiments seemed to have been affected to a certain degree by diffraction effects.

2.5.6. Field investigations on non-submerged and submerged porous structures

Thornton and Calhoun (1972) performed one of the few field studies on the subject of wave reflection and transmission for a rubble mound breakwater. The Monterey breakwater in California, U.S.A. was the structure investigated (Fig. 2.5.a.). Two wave sensors seaward of the structure and another inside the harbour were installed for data collection. The three sensors were placed on a line normal to the breakwater. The measurements were taken only when the incoming waves had their crests approximately parallel to the breakwater thus ensuring normal wave incidence. Although the measurements were taken at fixed locations, the authors developed a method to separate incident and reflected wave components, based on linear wave theory. It was observed that reflection and transmission coefficients displayed a dependence on wave frequency, tidal stage and incident wave amplitude. They were of the opinion that, at least under moderate wave conditions, it is justifiable to treat wave reflection and transmission as a linear, stationary, random process. Under such conditions this type of analysis could be considered a reliable and useful technique.

Ludwick et al. (1975) presented the results of an extensive study which assessed the field performance of a permeable breakwater made of open-work steel used to control beach erosion at Virginia Beach, U.S.A. (Fig. 2.5.b). For a period of a year after installation, the submerged structure and the adjacent surf zone and beach were monitored to detect changes. During the monitoring period observations were made of the velocity and direction of longshore currents, wave height and breaker angle. Bottom topography and shoreline configuration were measured and samples of beach sand were analysed for particle size distribution. These data were taken at locations along the beach near the breakwater. Wave induced vibrations led to the collapse of part of the structure within a period of two months and following repairs no structural failure was observed during the study period which was free from storms of great force.

The performance of this structure was not very satisfactory. Within the detection limits of the methods employed, there was no conclusive evidence that the structure influenced any of the following desirable phenomena:

(i) Diminution in wave height or speed of longshore currents at beach stations in the lee of the device.

(ii) Producing a wave shadow zone and deposition of sand preferentially in the lee of the structure.

(iii) Change in average beach width.

With the device extending vertically through 45% of the water column at mean low water and through 33% of the water column at mean high water, it is believed that most of the incident wave energy passed over or through the structure, or both, on to the beach. The device as installed undoubtedly presents an impedance to the energy of the waves moving onshore, but evidently the amount of reduction in wave action was too small to produce any desirable or detectable effects. Installation of the same device in shallow water, nearer to shore, would on one hand certainly result in a larger dissipation and reflection of incident wave energy, but on the other it could locate the device at the plunge point of some waves which would have induced greater loading on the structure. This detailed study highlights some of the problems associated with highly permeable structures when used as shore protection devices in submerged conditions.

	$\frac{I_{Turbulent}}{I_{Laminar}} = \xi$	The values of c in $\xi = c * Re$, for varying porosity ($\times 10^{-3}$)			
		Porosity (n)			
		0.10	0.20	0.30	0.40
Engelund (1953)	$\xi = \frac{\beta_o}{\alpha_o n(1-n)^2} \cdot \frac{Ud}{\upsilon}$ $\xi = c * Re$ $\alpha_o = 1500$ $\beta_o = 3.6$	29.63	18.75	16.3	16.67
Le Mehaute (1957)	$\xi = \frac{c_3}{c_2} \cdot \frac{Ud}{\upsilon}$ $\xi = c * Re$ $c_3 = 0.2$ $c_2 = 28$	7.14	7.14	7.14	7.14

TABLE 2.3 COMPARISON OF ENGELUND'S (1953) AND LE MEHAUTE'S (1957) EQUATIONS

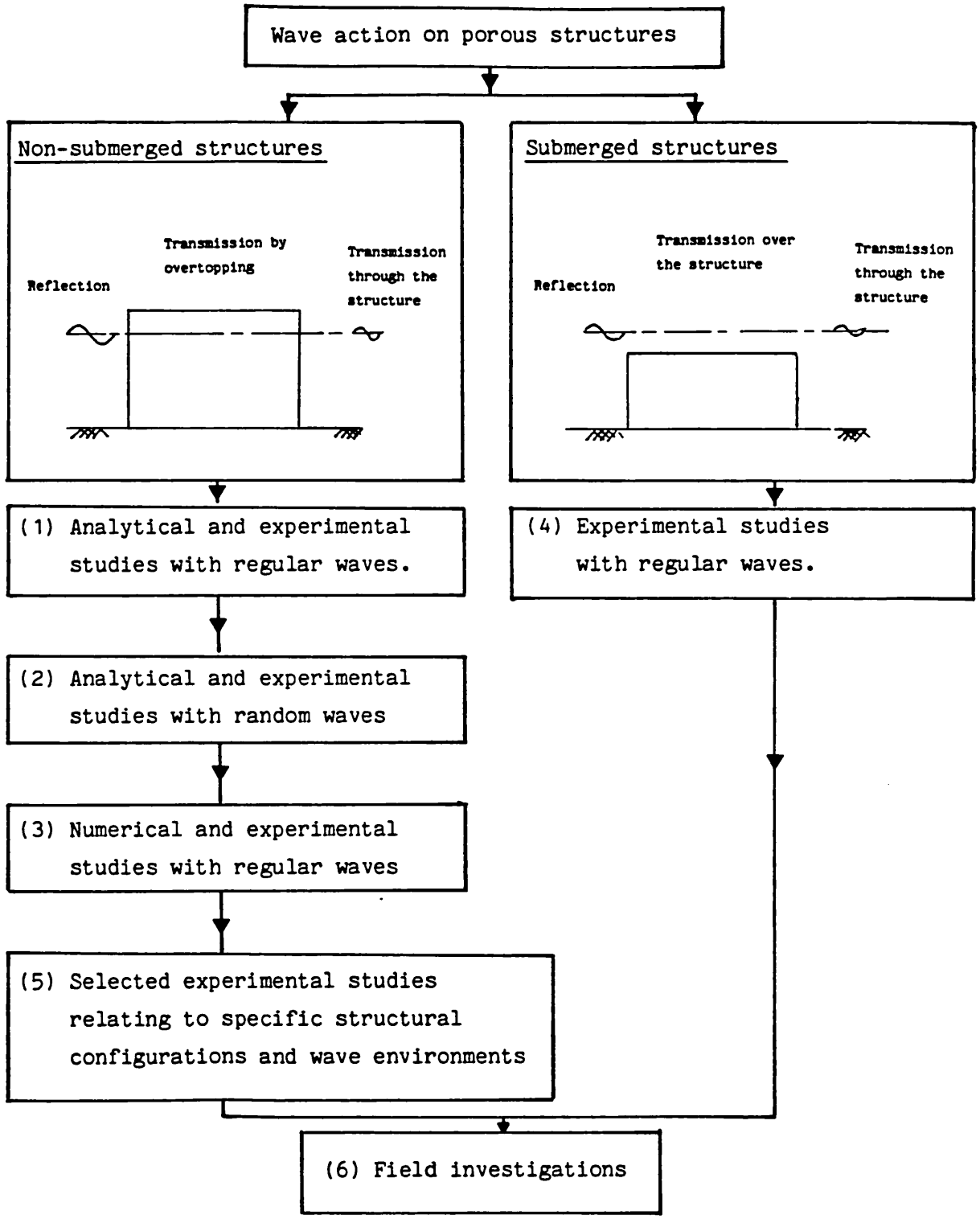


TABLE 2.4 WAVE ACTION ON POROUS STRUCTURES

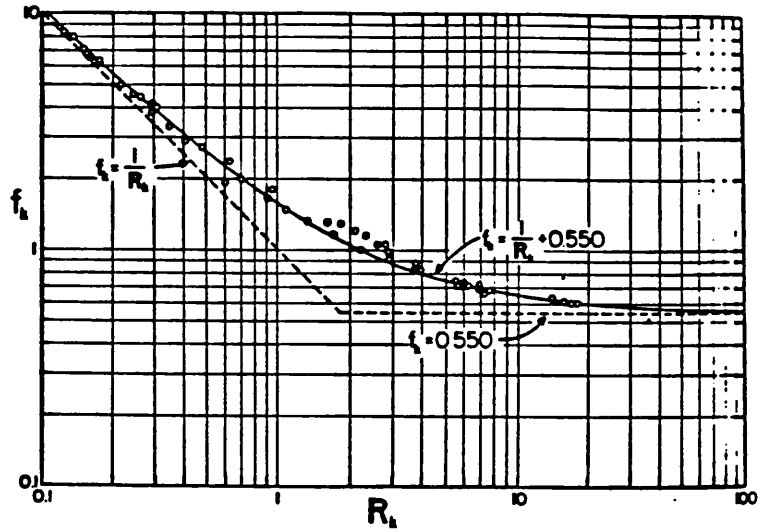


Fig.2.1.a Friction factor vs Reynolds number (Ward 1964)

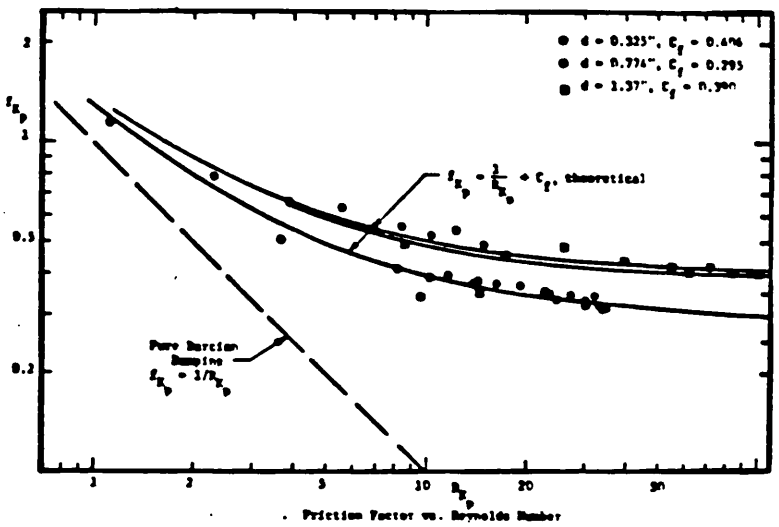


Fig.2.1.b Friction factor vs Reynolds number (Sollitt and Cross 1972)

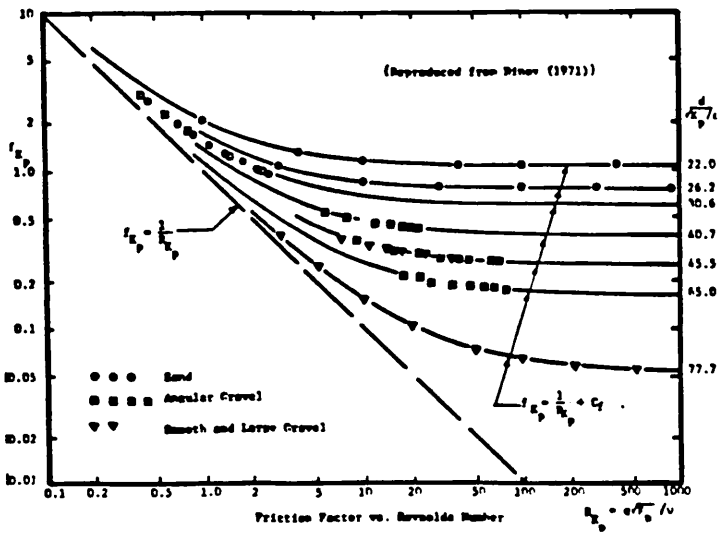


Fig.2.1.c Friction factor vs Reynolds number (Arbhabhirama and Dinoy 1973)

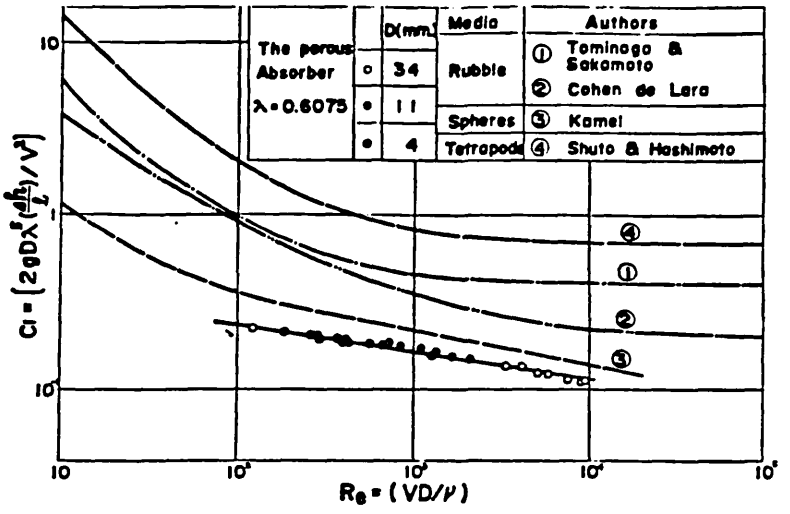


Fig.2.1.d Friction factor vs Reynolds number (Kondo and Toma 1972)

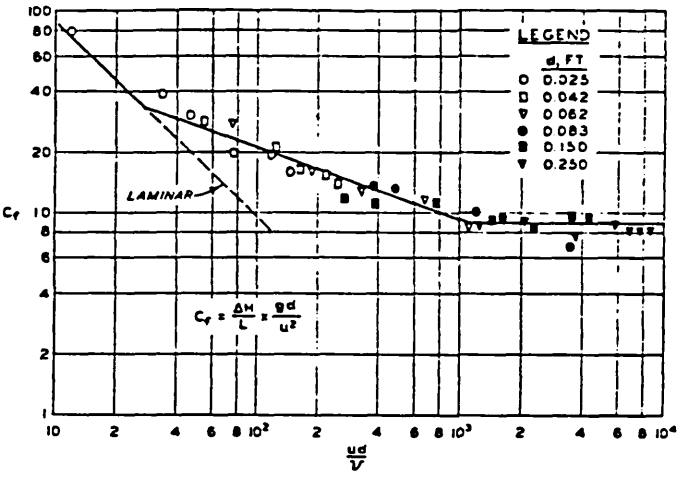


Fig.2.1.e Friction factor vs Reynolds number (Keulegan 1973)

FIG.2.1 VARIATION OF FRICTION FACTOR WITH REYNOLDS NUMBER

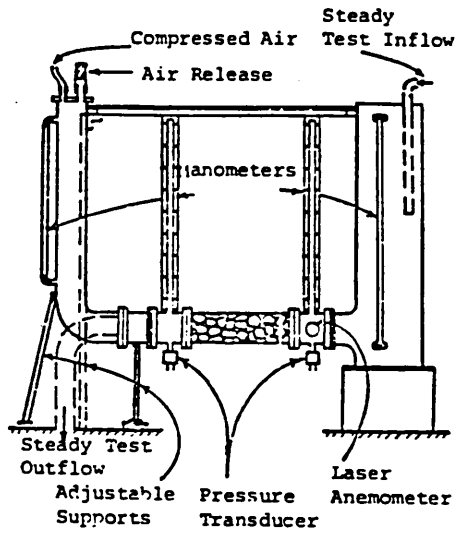


Fig.2.2.a Experimental apparatus

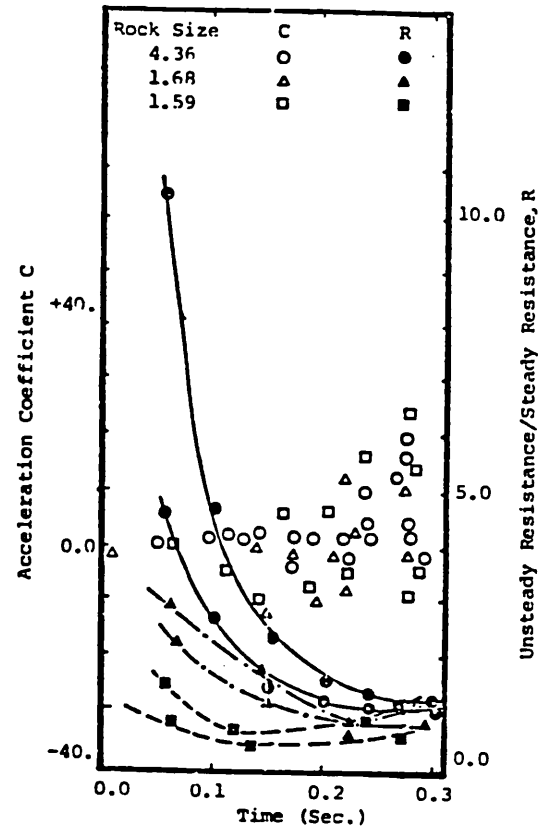


Fig.2.2.b Acceleration coefficient vs time

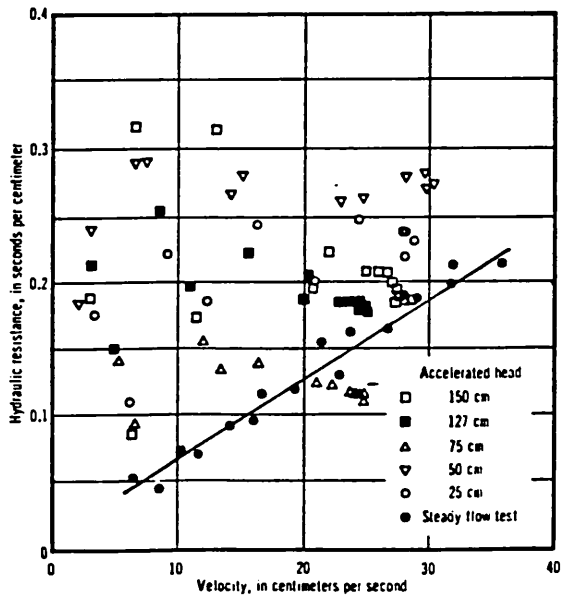


Fig.2.2.c Hydraulic resistance vs velocity

FIG.2.2 EFFECTS OF UNSTEADY FLOW

(Hannoura and McCorquodale 1978a)

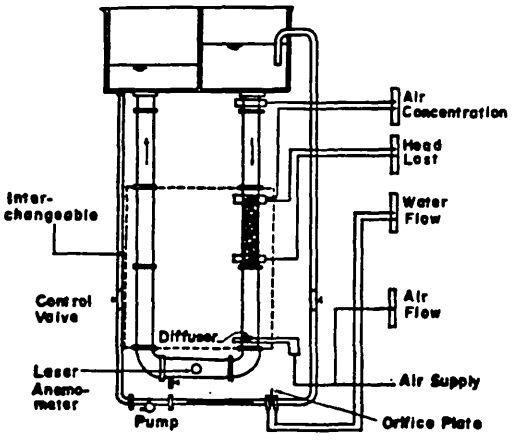


Fig.2.3.a Experimental apparatus

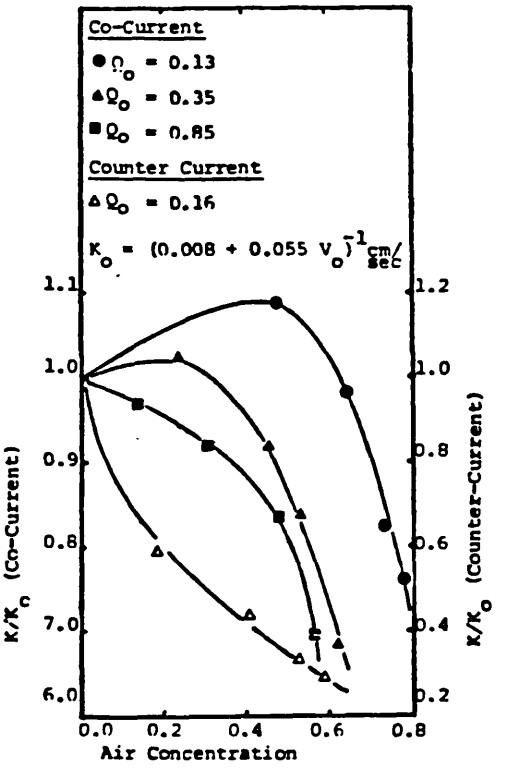


Fig.2.3.b Effect of air concentration on conductivity

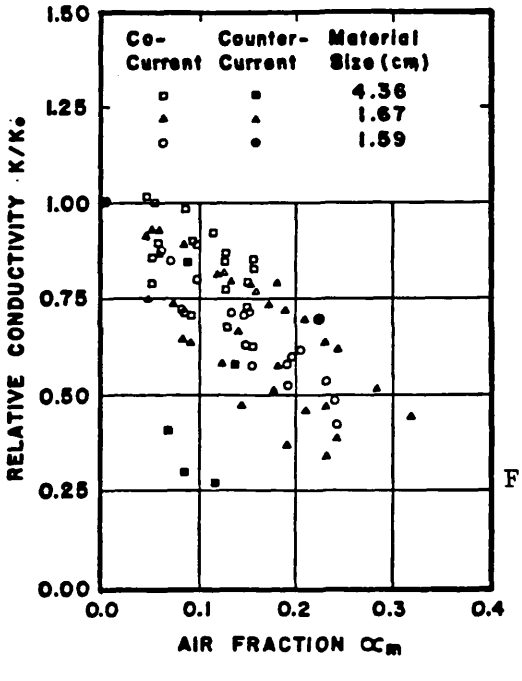


Fig.2.3.c Relative conductivity vs air fraction

FIG.2.3 EFFECTS OF AIR ENTRAINMENT

(Hannoura and McCorquodale 1978b)

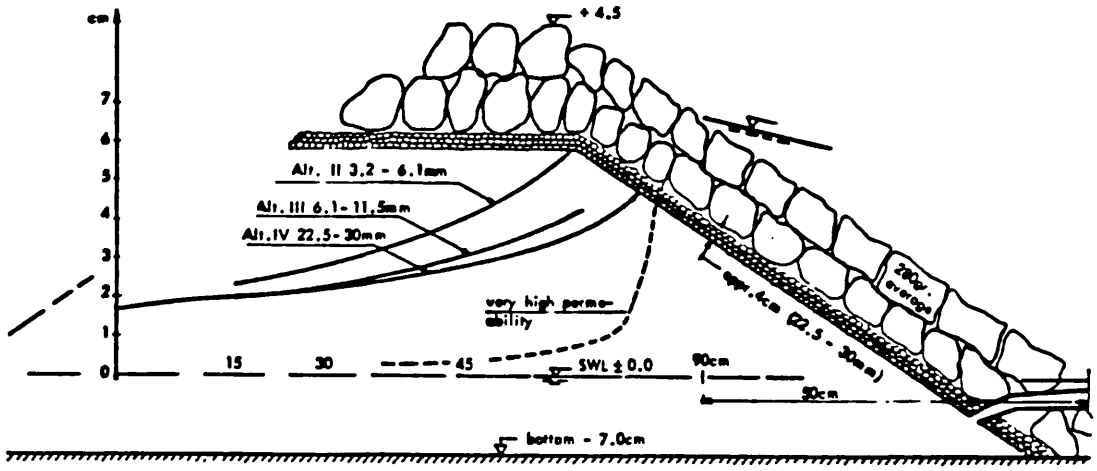


Fig.2.4.a Water elevation in core at maximum uprush for varying permeability

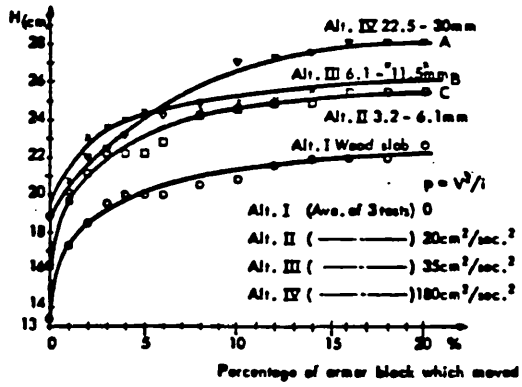


Fig.2.4.b Wave height vs Damage ratio for different core material

FIG.2.4 INFLUENCE OF DIFFERENT CORE MATERIAL ON THE STABILITY OF RUBBLE MOUNDS

(Bruun and Johannesson 1976)

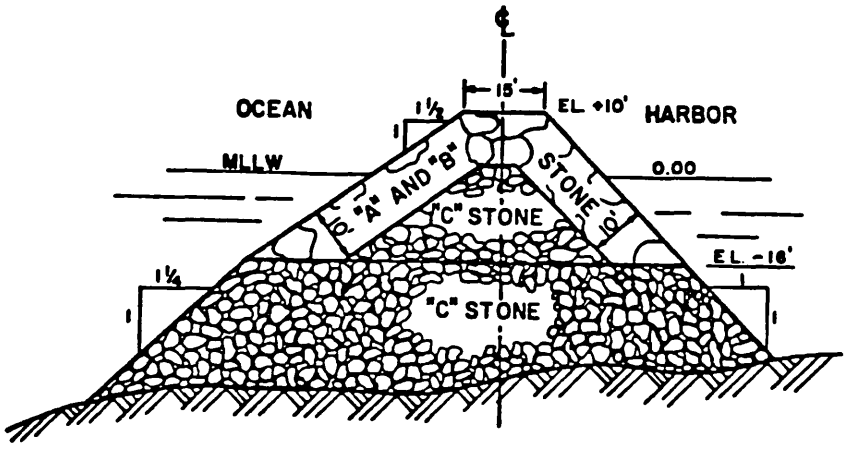


Fig.2.5.a Monterey breakwater cross section
(Thornton and Calhoun 1972)

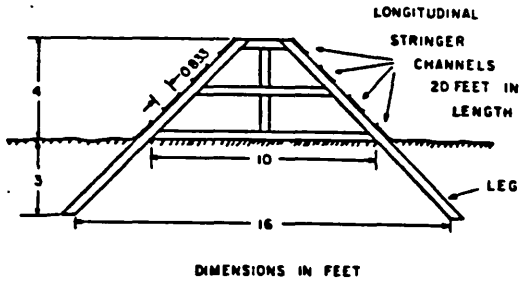


Fig.2.5.b Permeable breakwater cross section
(Ludwick,Fleischer,Johnson and Shideler 1975)

FIG.2.5 FIELD INVESTIGATIONS ON POROUS COASTAL STRUCTURES

CHAPTER 3 - APPROACH TO THE PROBLEM

3.1. Introduction

This chapter is presented with three objectives. Firstly it discusses the factors which were considered in identifying the areas to be investigated. Secondly it outlines the reasoning which led to the selection of experimental media and appropriate experimental techniques. Thirdly the underlying concepts relating to the theoretical developments are introduced in order to provide an appreciation of the whole project. The relationship between each phase of the project is assessed within the framework of the principal objectives of the investigation.

With reference to the first objective, it was necessary to decide on the most appropriate approach to investigate the subject - the influence of voids and geometry of armour with regard to energy dissipation. In order to formulate the framework as well as to define the scope of the investigation, due consideration had to be given to several factors. Relevant conclusions from the literature review and the laboratory facilities available for experimental studies formed the background to this exercise. In addition attention had to be focused on the availability of and access to suitable experimental media for the proposed study.

3.2. Relevant conclusions from the literature review

The literature review revealed that flow through porous media has been investigated in various contexts. Although several porous structures of coastal engineering interest have been subjected to experiments, the absence of a systematic study covering a wide range of materials is obvious. As a result it is difficult to extract any reliable information pertaining to the subject under investigation. The use of different experimental techniques and various definitions of governing parameters makes this task even more complex. Under such circumstances the conclusions obtained from a comparative study of existing data and solutions may not prove to be very reliable, as has been shown in Chapter 2.

The majority of previous studies have been performed on rockfill media for which the terms porosity and geometry are applicable only in an overall and statistical sense, with voids and flowpaths being randomly created. This holds true for any porous medium consisting of randomly-packed, irregular-shaped constituent elements.

It is clear that many researchers have given less attention to the

experimental determination of hydraulic properties. Those who have determined such properties as part of their investigation on transmission and reflection through porous media performed only limited studies. Many investigators who undertook theoretical studies accepted the applicability of formulae for hydraulic gradient, such as those given by Engelund (1953) or LeMehaute (1957). It should be observed that some of the formulae discussed in Chapter 2 were determined for different types of porous media, for example, Engelund (1953) focused on the steady flow of groundwater through homogeneous sand. Hence it was evident that tests pertaining to the hydraulic properties and therefore the permeability characteristics of different media had to be incorporated into the experimental programme.

Additionally it is most appropriate and consistent with previous studies to include detailed tests on reflection by and transmission through porous structures selected for the project. Although some studies have been performed in specific unsteady flow conditions using U-tube oscillators (Shuto and Hashimoto 1970, Hannoura and McCorquodale 1978a), it was considered relevant and compatible to include an experimental programme to assess the performance of porous media under unidirectional accelerated flow conditions. This is most justified in the light of considerable scatter observed in the results of previous investigations. It should be observed that tests under constant acceleration have an advantage with the immediate consequence being that the equations characterizing the motion may be logically reduced to a workable form dependent only on a few variables.

From a viewpoint of the present breakwater studies, it is essential to perform selected two-dimensional tests on a model breakwater section consisting of hollow block units. This is necessary to estimate reflection, run-up and run-down characteristics when energy transmission through the structure is not a critical factor. Although several studies on stability have been performed in the evolutionary process of different kinds of armour units, comparatively less effort has been devoted to the forces acting on them.

Whenever possible it is advisable to investigate the presence of scale effects and to assess their influence on the phenomenon under investigation. For this purpose it is necessary to perform a separate test series. On wave transmission, experimental studies on scale effects have been limited to a few investigations (Johnson, Kondo and Wallihan 1966, Delmonte 1972, Wilson and Cross 1972).

The preceding discussion and the literature review on which it is based determined a broad framework for the experimental programme. Furthermore the

suggested studies could well be considered as a continuation of the present state of knowledge and are in every way compatible with previous investigations, thus providing an opportunity for a detailed comparison.

3.3. Governing parameters for porous media and hollow block units

3.3.1. Parameters for porous media in general

In order to select appropriate experimental media it is essential to identify governing parameters which are characteristic of any given porous media. Obviously, no detailed comparison could be made between two porous media if consistent parameters are not recognized.

A porous medium could be generated either by a completely random process or in a predetermined manner. Randomly packed stones and spheres are typical examples of the first type whereas spherical and cylindrical lattice structures are representative of the latter.

Whatever definitions are used to classify the first type, they are only applicable in an overall sense, implying average values. Other statistical definitions may also be included. For example, it is difficult to describe in microscopic terms the porous matrix formed by the random packing of spheres. If the packing procedure is repeated it would be very difficult to use simple geometric parameters to compare the newly-formed porous matrix with that of the previous one, although the overall porosity may be approximately the same. The randomness itself accounts for the lack of precise definitions of such media.

On the other hand porous media belonging to the second category could be subjected to very detailed definitions and for uniform media it is easy to identify a basic constituent element (or unit). The media could then be imagined as a regular, defined assembly of these basic elements. It is observed that an insight into the different properties of the assemblage could be obtained by considering the corresponding properties of the basic element. In effect these elements placed in repetition, conforming to a predetermined layout, generate the porous medium.

From the conclusions of the literature review and from logical reasoning the following governing parameters are identified.

1. Overall porosity
2. Shape (geometry) of the void
3. Size of the void
4. Characteristic dimension of the void
5. Tortuosity
6. Properties of the leading interface (two dimensional porosity, shape, roughness).

Of these a close correlation exists between parameters (3) and (4) for the type of porous media associated with hollow block units but they are classified separately so that the above concepts could be applied in general.

All the parameters are related to the geometry of the structure. It is relevant to extend the same line of thought to identify parameters associated with the hydraulics of the porous media. For this purpose it is appropriate to use the steady flow laminar and turbulent coefficients 'a' and 'b' in the eq. $I = au + bu^2$ (eq. 2.6). The present state of knowledge on the subject does not permit the inclusion of an unsteady flow coefficient. In contrast to the geometric properties, the hydraulic properties are to a certain extent dependent on the experimental technique and flow range adopted in respective steady flow experiments. Thus a particular medium tested under different conditions may not produce the same values of 'a' and 'b'. Hence when quoting these two parameters it is essential to specify the experimental conditions. The absence of a parameter describing the unsteady flow characteristics is considered a limitation. Although it is desirable to include such a parameter, the uncertainty associated with results pertaining to unsteady flow tests does not permit the recognition of an acceptable term.

3.3.2. Parameters for hollow block armour units

Apart from the above classification for porous media in general, it is necessary to examine the basic structural form of a hollow block armour unit. The purpose of this exercise is to identify critical factors which influence the flow and thereby provide a common base for comparison of different types of such armour.

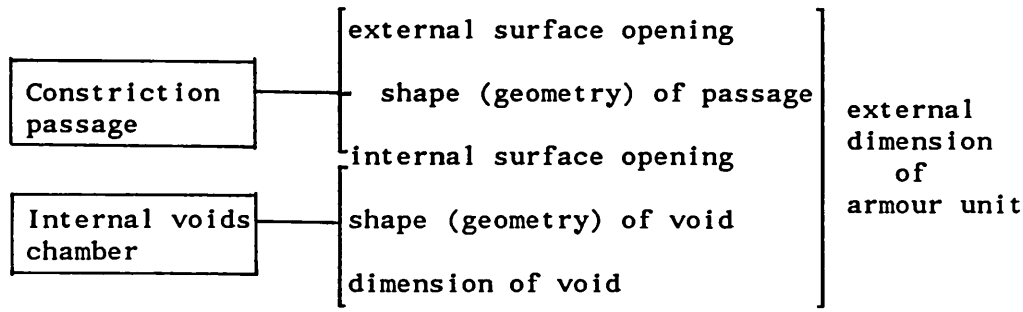
It was mentioned earlier that there are essentially two types of hollow block armour units : with and without lateral porosity when placed on a slope. The Cob and Shed belong to the first category whereas the Seabee and Svee Block are examples of the second. The Diode and Reef Block which belong to a third type are in effect an extension of the first type having a comparatively complicated geometry and being placed in sets of two units or more. Hollow block armour

units may or may not have three dimensional symmetry.

In the present study it was decided to concentrate on the first type of units which are of cubic form. However for cross-comparison it is beneficial to incorporate the second type. Hence it is necessary to identify parameters which are common to both types.

Fig. 3.1 illustrates the details of a Cob armour unit. When analyzing the flow through the unit it is possible to isolate two important regions namely the constriction passage (ABCD) and the internal voids chamber (CDEF). Flow enters the first region across AB and the second region across CD. Hence both cross-sectional shape and dimensions corresponding to AB and CD are relatively critical and are termed the external and internal surface openings. The impinging water flows through the constriction passage and converges into the internal voids chamber where much dissipation occurs. This chamber is characterized by shape (geometry) and an appropriate dimension (size).

It will be realized in the course of discussion of other units that these properties are generally applicable to all hollow block armour units and serve as useful criteria for comparison. Hence the governing parameters for such units are summarized as follows.



Hydraulic properties used to classify porous media will also be used to classify hollow block units.

In this section sufficient parameters both geometric and hydraulic have been introduced to classify porous media in general. The importance of these parameters is evident when they are applied to porous media with well-defined porous matrices. In addition, further parameters have been identified to describe commonly-used hollow block armour units. It was expected that the above parameters could effectively be used in the classification of all porous media selected for the present study.

3.4. Selection of experimental media

The preceding discussion implied a necessity for a systematic study covering a wide range of media whose physical and geometric properties are such that they would be consistent with the objectives of the study. Selection of experimental media required careful consideration, particularly in view of the broad area of investigation. They should be representative of the numerous porous media and structures used under different circumstances in coastal engineering practice.

3.4.1. Hollow block armour units with lateral porosity

Since the study is primarily based on the hollow block concept it was necessary to experiment with at least two types of such armour units currently being used. With the assistance of the Hydraulics Research Limited (HRL) - Wallingford, Cob and Shed armour units introduced by Coode and Partners and Shephard Hill Ltd., respectively, were made available for the present study. Model tests on the Cob have been previously performed in the Wimpey Laboratories (Stickland 1969) and at HRL (HRS - EX632 1973) and the Shed was also tested at HRL (HRS - EX1124 1983). The details of these two units are given in Fig. 3.2 and Fig. 3.3.

Shed armour units have been modelled in a loaded plastic by injection moulding and have been made in two identical halves with locating pins and holes so that they could be simply pressed together. A carefully controlled mix of nylon and barium ferrite was used to give a mean relative density of 2.29. This low value of relative density has been used to correct for model tests conducted in fresh water (R.D. = 1.0) as opposed to prototype structures located in sea water (R.D. $\approx$ 1.026). The unit has an overall porosity of 0.614 and side length 40 mm. Accurate simulation of specific gravity is a necessary requirement for model studies pertaining to stability.

Measurements in the HRS-EX1124(1983) report were scaled to a prototype unit of 2 tonne Sheds. The objective was to test at the largest model scale possible to minimise potential scale effects and to maximise the accuracy of any measurements made. It was also hoped to be able to generate waves large enough to achieve failure of the cover layer. Considerations were also given to the production of reasonable quantities with accuracy and economy. Under these circumstances the model units at a geometric scale 1:32.5 were equivalent to prototype units of relative density 2.35, weighing 2.00 tonnes, having side length of

1.3 m.

The model Cob units were made of thermo-plastic loaded with zinc powder using similar techniques to that of the Shed. The model Cob unit had an overall porosity 0.627 and side length 41.6 mm with a volume of 26.85 cc. The mean relative density was 2.4.

It should be noted that the original two dimensional studies on the Cob (Stickland 1969) were performed on a larger model unit at a scale 1:24. The length of the model units was 5.93 cm and they were formed from a cement sand mix using a liquid rapid hardener in order to achieve well-shaped units of relative density 2.4.

Comparison of the projected area of both model units, as observed in side elevation, shows that the Cob has a central square opening of minimum side length 19.00 mm, whereas the Shed has a central circular opening of minimum diameter 21.54 mm. The Cob and the Shed are very similar units with approximately same porosity and void dimensions. However, the structure of the internal voids differs in that the Cob has a square constriction section with a cubic voids chamber whereas the Shed has a circular constriction section with a spherical voids chamber.

When using Cobs and Sheds as breakwater armour blocks, they are placed in a pre-determined pattern, for example, adjacent units being aligned in both directions in order to maintain maximum lateral porosity. This generates a well-defined interconnected porous matrix. Another possible arrangement is the staggering of alternate rows by half a unit. This too creates a porous matrix similar to the previous one but with increased tortuosity which may increase energy dissipation. The importance of this type of unit is that it permits flow in all three directions.

The literature survey also revealed the existence of another hollow block armour unit named the Stolk (Hakkeling 1971). It is essentially a solid cube having three centrally located cylindrical bores in the three mutually perpendicular directions parallel to the edge of the cube (Fig. 3.4). This unit, although having lateral porosity, does not have an enlarged voids chamber similar to that of the Cob and Shed. The constriction passage is also of constant dimension. Hence in comparison, the Stolk may not be that effective in dissipating wave energy when placed in pre-determined manner. However the unit has been used only as a randomly placed armour. No recent references are available on the performance

of the Stolk.

In contrast to the structure of the Stolk, one could imagine a hollow cube of a specified thickness having centrally located circular openings on all six sides (Fig. 3.5). For identification this unit is named Hobo, an abbreviation of hollow block. If such a unit is made with relatively thin walls it would possess high overall porosity which will have minimum dependence on the diameter of the circular opening. Hence this type of unit provides an excellent opportunity of investigating the influence of shape and dimension of the surface opening while maintaining approximately constant overall porosity.

For this project it was possible to create three plastic units made from the same material with same external dimensions but having circular openings of varying diameter. Thus the influence of the diameter of the external opening could be examined at constant porosity. These units were named Hobo 1, Hobo 2 and Hobo 3 in ascending order of the diameter. All three Hobo units used for this investigation have a side length of 45 mm with the diameters of the surface openings being 16, 20 and 25 mm respectively. The variation in overall porosity was only 0.033 with the two extreme values corresponding to the largest and smallest diameters being 0.823 and 0.790 respectively. For all practical purposes it may be assumed that the units are of porosity 0.80 with ± 0.02 variation. In comparison with Cobs and Sheds, the Hobo has an enlarged internal voids chamber with a constriction passage of negligible length.

3.4.2. Hollow block armour units without lateral porosity

In order to include a hollow block unit not having lateral porosity it was decided to use a hexagonal shape block with a circular opening through the full length of the unit. It was named Hexo an abbreviation of hexagonal unit. When these units are placed on a slope the void pattern created is not inter-connected and there is no lateral porosity. It should be noted that this unit is similar in shape to that of the Seabee. In classifying the Hexo, it is observed that there is no difference between the constriction passage and the voids chamber, both having same shape and size with flow restricted in one direction only. The details of the unit are given in Fig. 3.6.

3.4.3. Cylindrical lattice structures

Another structural form which was included in the experimental programme was that of a cylindrical lattice. It essentially consists of horizontal

and vertical cylindrical members joined together to maintain the required spacing in the three directions. The basic constituent element for this structure is shown in Fig. 3.7 and is named Cylat for identification purpose. A cylindrical lattice can be considered as a three dimensional assembly of Cylat units. The spacing between members used for this investigation is equal to the diameter of the cylinder.

In this study the Cylat was introduced for several reasons. Firstly, structures consisting of vertical cylindrical members with or without horizontal or inclined bracing have been frequently used in coastal, port and oil terminal projects. As such, from a coastal engineering point of view, the inclusion is justified. Secondly, the Cylat unit (Fig. 3.7) has a well-defined geometry with a porosity of 0.607, compatible with Cobs and Sheds, thus allowing cross-comparison studies. Hence by using three lattice structures consisting of Cylat units of different diameter, it is possible to investigate the influence of the size of the void while maintaining constant porosity and constant shape of the void. Thirdly, it should be recalled that rectangular and trapezoidal shaped cylindrical lattice structures of different dimensions were used by Kondo and Toma (1972) for experimental studies on reflection and transmission. Although the objectives of that study were different to those of the present study, the data provides an opportunity for comparison.

For these reasons it was decided to test three cylindrical lattice structures consisting of Cylat units of diameters 15, 20 and 30 mm respectively. The first was made of wooden dowels whereas perspex tubes with closed ends were used for the latter two. The size of the voids chamber and the constriction passage of the Cylat is of the same order as that of Cobs and Sheds, although the structural form of the constriction passage is somewhat different.

It should be appreciated that the basic Cylat concept when used in conjunction with varying diameter and spacing generates an infinite series of void systems of different shape (geometry), size, porosity and surface area. By selecting the variables in an appropriate manner it is possible to vary one of the properties while keeping the others constant. Three units from this vast series were included in the present study.

3.4.4. Pile structures

In view of the importance of vertical pile arrays in coastal works, it was decided to include two such structures in the present study. The first pile

structure consists of vertical cylindrical members aligned in both directions. The second was similar to the first but with alternate rows staggered. The purpose of the staggered arrangement is to investigate the influence of tortuosity which is greater for the second case. In order to compare the performance of these two structures with that of a cylindrical lattice structure which has additional horizontal members, it was decided to use 15 mm wooden dowels for the pile structures. This provided a group of three structures for comparison purpose. Fig. 3.8 illustrates the important details.

3.4.5. Spherical lattice structures

To supplement the cylindrical lattice structures it was thought advisable to test two spherical lattice structures (Fig. 3.9a). These structures which are assembled by placing spheres on top of each other and aligned in all three directions have an overall porosity of 0.476 which is independent of the diameter of the sphere. The basic repetitive element in this case is named Sphelat for identification. The two structures used for this study were made of polystyrene spheres of diameters 38 and 51 mm respectively.

3.4.6. Slender, interlocking type of armour units

Although this work deals particularly with hollow block armour units, it was thought appropriate to include at least two types of conventional, randomly-packed artificial armour units. Since several investigations have been already performed on such units when placed at random, it was decided to adopt a pre-determined packing form to be consistent with the objectives of the present project.

Carver and Davidson (1978) studied the performance of Dolos units for three different pre-determined packing arrangements and observed that one of them proved to be more stable than the normally adopted random packing arrangement. In this arrangement the first layer of units is placed with shanks parallel to the slope and the vertical legs all upslope (parallel to the direction of wave attack) or downslope on alternating columns. The second layer of units is placed in the same manner to yield the complete structure. The second layer finds itself in a stable position on top of the first layer. The porosity of this packing form was found by them to be 0.5. In view of the general philosophy of the experimental programme, it was decided to investigate Dolos units (Fig. 3.10) packed in the above arrangement. It is evident that if a block structure is to be investigated, this packing arrangement could be repeated on top of each layer. It should be

observed that no information is available on whether this stable packing form has ever been used in practice.

In addition to the Dolos units, it was decided to include Stabit units (Fig. 3.11) in the present study. These are classified as slender units but are always placed in a pre-determined manner. Singh (1968) in his introductory presentation of this unit proposed two methods of placement for the Stabit. In the double layer method the Stabits are positioned to a pre-determined grid in two layers with the top layer being displaced from the bottom layer by half the grid spacing in both directions. The upper Stabits then sit in cradles formed by lower Stabits. The second method is the brickwall placing method which closely follows the principle of bonded brickwork construction. Both methods of placing have been used and it has been found that the latter method results in good interlocking on slopes steeper than 1 in 2. Singh recommended that the Stabits should be placed using the double layer method on the sole-plate on the sea bed at the toe of the slope while the brickwall method be adopted for armouring the side slopes of the breakwater itself. It has been found from both experimental and field investigations that the overall porosity of the voids matrix generated by the double layer method and the brickwall method was 0.52 and 0.55 respectively. For this investigation it was decided to adopt the double layer method which can also be extended to block structures.

With reference to the Dolos and Stabit which are both classified as slender units it should be realized that in general Dolos units are placed at random but have been laboratory tested for pre-determined packing forms of which one has proved to be more stable. On the other hand Stabits are normally placed according to a specific layout. In both cases the porous matrix generated is random for all practical purpose, with voids created between the units.

3.4.7. Randomly packed stones and spheres

In addition to the above media, it was considered appropriate to include media which are truly random. This could be achieved by using porous media consisting of rockfill and glass spheres packed at random.

Most previous investigations on flow through porous media included at least one consisting of rockfill or stone. Apart from that it should be recognized that prior to the development of artificial armour units, most breakwaters were constructed using rockfill only and in spite of the developments in the former, rockfill is still widely used as main armour. Even breakwaters constructed with

artificial armour require the use of rockfill for the underlayer. Therefore a porous medium consisting of rounded stones of equivalent spherical diameter 34.8 mm, relative density 2.69 and overall porosity 0.362 was included in the study.

Irregularity of the constituent elements and the random placing are both contributory factors to the random porous matrix present in rockfill. However the influence of the irregularity of elements can be eliminated by using spherical elements. Porous media consisting of randomly packed spheres belong to this category. Two such media of glass spheres 19 and 25 mm were included in the test programme. The overall porosities for the two cases were 0.350 and 0.394 respectively. This also provides an opportunity for comparison with spherical lattice structures referred to earlier. Fig. 3.9.b illustrates porous media consisting of spheres and stones.

This concludes the discussion on the reasoning which led to the selection of porous media for this study. The discussion was limited to the relevant properties of the media and no mention was made of the external geometry and actual structural forms which were adopted for the experimental programme. This is considered in the next two sections in conjunction with type of tests and the experimental techniques.

3.5. Type of tests and experimental techniques

3.5.1. Type of test

Considering the relevant conclusions from the literature review, it was necessary to identify the type of tests that would be most appropriate to determine the influence of voids and geometry of armour with regard to energy dissipation.

For the selected porous media it was decided to perform tests under the following flow conditions :

1. Steady flow
2. Oscillatory flow (with regular waves)
3. Unidirectional constant acceleration

In addition, it was necessary to perform a series of two dimensional tests on a model breakwater section with different hollow block armour.

Finally, it was desirable to perform selected tests to study the influence of model scale effects.

Once the type of tests had been identified, the next phase was the selection of appropriate experimental techniques with due consideration being given to the principal objectives associated with each such type. Concepts underlying the techniques and the reasoning which led to their selection are discussed below together with comments on the quantities to be measured, with special reference to their fundamental relationship to the phenomenon under investigation. Technical details of the experimental apparatus, conditions under which the experiments were performed and procedures adopted, are presented in Chapter 4.

The experimental investigation was performed in various phases and it was important to ensure that continuity existed not only between fundamental concepts associated with each phase but also between different experimental techniques adopted for each phase.

3.5.2. Experimental techniques

On a broad classification there are two experimental techniques which are generally adopted in the investigation of various flow phenomena. In the first technique the object under investigation is kept stationary in a flowing fluid, whereas in the second technique the object is moved in accordance with a prescribed motion in initially still fluid. A summary of these techniques and their application to various flow phenomena is presented in Table 3.1 together with references for selected studies.

3.5.3. Steady flow tests

The objective of steady flow tests is to determine the hydraulic properties of each medium and in the present investigation this mainly consists of determining steady flow permeability coefficients.

Most previous investigations on steady flow through porous media have been performed in vertical or horizontal permeameters of various cross-sections. Measurements have been made of the discharge and head loss across the experimental medium which is packed in the permeameter. However, for the present study it was decided to assemble the media in a horizontal flume, and to measure the heads upstream and downstream of the structure.

This method ensures the presence of free surface conditions in contrast to flow with closed boundaries as observed in permeameters. When applying steady flow permeability coefficients for theoretical studies on wave action on porous structures, it is more realistic to employ coefficients obtained under free surface conditions than those obtained by other techniques. Thus the method of experimentation and the conditions under which the steady flow tests were performed were consistent with the objectives of the research programme as a whole.

In order to compare the permeability coefficients of different media, it was decided to perform all tests on rectangular blocks of constant length and width. The latter was equal to the width of the flume, 30 cm., and the length was fixed at 30 cm. The height of these vertical-faced blocks was approximately 40 cm., governed by the height of the glass sides of the flume.

3.5.4. Oscillatory flow tests

To maintain comparability with the tests under steady flow conditions, oscillatory flow tests were initially performed on the same block structures. For these tests the structures were placed on a horizontal bed flume and subjected to regular waves. The objectives of these tests were to determine, under non-submerged conditions, reflection characteristics on the seaward side, transmission characteristics on the leeward side and internal wave decay.

Apart from the block structures which were common to both test programmes, additional block structures were investigated under oscillatory flow conditions. Hence this test series formed a major component of the experimental programme involving more than fifteen different media. For each medium tested, it was possible to evaluate flow characteristics for different wave heights, wave periods and still water depths, within the limits imposed by the experimental facilities.

The experimental techniques adopted for the two test programmes were designed to be consistent with each other. In addition, by employing identical structures, a closer relationship was established between the two test series.

3.5.5. Additional tests under oscillatory flow conditions

In addition to the basic test programme, it was decided to perform tests with regular waves, for selected media, to investigate the following phenomena:

1. The performance, under varying conditions, of block structures backed by an impervious vertical face (wave absorbers), to provide a comparison with similar but open block structures used for oscillatory flow tests.

2. The influence of the length of the structure.

3. The response to the introduction of a front slope.

4. The influence of submerged porous media.

5. The performance of trapezoidal porous block structures and of equivalent rectangular blocks of the same structure.

The essential difference between open block structures (wave transmitters) and closed block structures (wave absorbers) is the presence of an impermeable vertical face at the rear of an absorber which will reflect the incoming waves. Structures used in the construction of ports and harbours can be classified as either open or closed block structures. In the first type the important parameters are the reflection, internal wave damping and transmitted wave height. For the second type external wave transmission is not applicable and only the first two need to be considered, together with the effects due to the presence of the rear face.

Both theoretical and experimental investigations on the influence of the length of porous structures have been performed by many authors (Kondo and Toma 1972, Nasser 1979 and Madsen, P.A. 1983). In coastal and port works the dimensions of porous structures are critical not only on economic considerations but also from a viewpoint of optimum use of available space.

For open block structures the major criterion is to determine under critical service conditions the minimum length required to attenuate transmitted waves to permissible levels. Additional information pertaining to changes in reflection and transmission that would occur due to variations in the wave environment as well as due to limited variation in the length of structure is useful from a design point of view.

In contrast, reflection characteristics dominate the design of wave absorbers and a criterion based on considerations similar to that of open block structures could be adopted in the selection of structure length. For given wave conditions it is important to determine the optimum length of absorber which would dissipate the required percentage of energy. Extension of the length of the

structure beyond a certain limit will not increase the efficiency but would involve greater costs. It should also be noted that closed–end structures are susceptible to seiche motion due to reflection from the rear face and precautions have to be taken to accommodate such effects.

It is important to realize that optimum lengths referred to in the previous paragraphs depend very much on the porous matrix of the structure concerned. In this context results from the present study, which cover a variety of porous media, can be adopted to obtain a better understanding of the wave dissipation process. Therefore, a series of tests was performed on wave absorbers constructed with Cobs and Sheds as part of the experimental programme.

Most coastal structures are constructed with sloping surfaces and it was thought appropriate to investigate this aspect in relation to one of the porous media. For this purpose sloping faces of different inclinations were introduced in front of an open block structure. This study was limited to porous media consisting of rounded stones to give a continuous slope. Both the sloping front and the main rectangular block structure were assembled with the same type of stone. The main objective in this study was to determine, for different slopes, the reflection and transmission coefficients – of which the latter will not be subjected to much change.

Under certain conditions it is possible to employ submerged porous structures which may provide an economic solution to a given problem. In this respect it is necessary to study the changes which occur in the reflection–transmission characteristics in response to a gradual decrease in the height of the structure, varying from the non–submerged condition to different levels of submergence. It is evident that below a certain level the structure would be ineffective with most of the energy being transmitted over it. Results from this type of study can also be used to study the possible effects which may arise when non–submerged structures are overtopped. Hence information from this type of test can effectively be used for both submerged and non–submerged structures.

Although several experimental investigations have been undertaken on both solid and permeable submerged structures, no information is available on the performance of hollow block armour units under these conditions. Hence selected studies on Cob armour units were included in this study.

Since the oscillatory flow tests were performed on rectangular porous structures, it was appropriate to incorporate a trapezoidal porous structure to

compare its performance. The length of the former could either be based on the concept of equal submerged volume or such that both structures intercept the still water level at the same point. It is evident that trapezoidal structures with a sloping surface will exhibit much lower reflection coefficients than those with vertical surfaces.

The concept of equivalent rectangular section has been widely used by those who have performed theoretical studies on wave transmission through trapezoidal structures.

For this study a trapezoidal porous structure consisting of Cob units and its two rectangular equivalents were tested under the action of regular waves to measure reflection, transmission and loss coefficients.

Fig. 3.12 illustrates the geometry of structures that were included for additional tests under oscillatory flow conditions.

3.5.6. Constant acceleration tests

Hitherto, tests under unidirectional constant acceleration have not been performed in relation to armour units. It was thought relevant to study the force field under such conditions in preference to permeability characteristics. The tests were limited to selected hollow block units, to provide information on the loading on such units under steady and accelerated flow conditions.

This test series is somewhat different from the previous two and posed several conceptual problems in adopting a suitable experimental technique. The main difficulty lies in imposing a constant acceleration on a volume of fluid while being able to measure its magnitude. Apart from Sarpkaya and Garrison (1963) who performed a similar test on a cylindrical member inside a vertical tank of rectangular cross-section, no other reference is available on this type of study.

However, the problem can be viewed from a frame of reference in which the body is uniformly accelerated in initially still water. This technique was adopted for the present study with provisions made for the measurement of force and velocity with time. It should be noted that the flow past a stationary object is hydrodynamically equivalent to the same object moved in the otherwise still fluid as long as the fluid is incompressible. However, the forces experienced by the object differ due to the presence of a pressure gradient in the fluid on the one hand and to the inertia of the object itself on the other. In the case of a moving

fluid, the object experiences an extra force which is equal to the displaced mass of the fluid times the acceleration, due to the pressure field necessary to accelerate the fluid. Consequently it is only necessary to study the case of relative motion and either of the two techniques could be adopted.

In the present study, which was limited to hollow block armour units, it was decided that in each case a pack of model units would be accelerated in initially still water. The model units were assembled to form a cubic pack and the horizontal force acting on the centre unit was measured, together with the velocity-time profile of the motion. By incorporating a dual facility to repeat these tests under constant velocity it is possible to compare the imposed forces in the two states of flow. Hence both steady and accelerated flow conditions are achieved in the same experimental facility.

There have been several investigations based on this technique where objects have been moved in a prescribed motion. Almost all such studies have concentrated on cylindrical members or structural components related to the offshore industry. Attention will be focused on some of the relevant features of these studies when analysing the results of the present study.

3.5.7. Two dimensional tests with a breakwater section

The widely acceptable methods of conducting hydraulic model tests on breakwaters are to perform either two dimensional studies in a wave flume or three dimensional studies in a wave basin. The method to be used naturally depends on the objectives of the investigation.

Since the primary objective of this study is to determine reflection, run-up and run-down characteristics the first method was adopted. It was also assumed that under these conditions wave transmission on the leeward side is not a critical factor. For this purpose it was necessary to construct in a wave flume, a model breakwater section with hollow blocks as main armour. It was also decided to use the same section for the measurement of forces on one of the armour units. This study on a breakwater section forms a logical continuation of similar studies performed on different porous structures of varying geometry. It also extends the present investigation to encompass rubble mound structures commonly used in practice.

Most real breakwaters are not constructed as a homogeneous structure but consist of several layers with a central core of fine materials. Thus in most

typical breakwaters, wave transmission through the structure is very limited. Hence it was not considered necessary to concentrate on wave transmission measurements on the rear side of the breakwater. In view of this it was decided to build the seaward half of a trapezoidal breakwater in preference to a complete structure. However, a porous metal plate was used as the rear vertical face and it was assumed that this arrangement would be an acceptable simulation for the continuity in the hydraulic behaviour of underlayers.

It should be noted that some of the previous studies on hollow block armour were performed without a core and the underlayer has been founded on either impermeable (Stickland 1969) or permeable (HRS-EX1124 1983) metal sheets. This permitted the construction of a test frame which could be rotated to vary the slope. However, when using a complete breakwater section it is not possible to vary the slope without major alterations to the basic model structure. Hence the model tests in the present work were limited to a slope angle θ of 36.9 deg (cot θ = 1.33) equal to one of the slope angles investigated by both Stickland and HRS.

The breakwater section used for the present study consisted of the armour layer, a secondary layer and the central core. The armour layer was of hollow block units; the secondary layer was made of randomly packed glass spheres of diameter 19 mm and the core consisted of fine crushed stone. The glass spheres were the same diameter as those used in both steady and oscillatory flow tests. The dimensions of the hollow block armour unit and the diameter of the spheres were in the correct proportion as required by the relationship between primary and secondary armour.

A wooden toe structure was used for the breakwater. It should be noted that stability of the toe is a critical factor for breakwaters built with hollow block armour because the units rest on the toe structure which has to withstand the force component of the weight acting down the slope.

With regard to the model breakwater section it should be appreciated that hydraulic properties pertaining to permeability of both armour layer (hollow block unit) and the secondary layer (glass spheres) would be known from the first part of the experimental project. This provides the foundation for potential application of theoretical considerations to understanding the mechanics of the phenomena.

It was decided that the breakwater section be used to test the armour

block arrangements listed below. In this context 'regular' arrangement is used to define the laying pattern in which the units are placed with their central axes aligned in both directions. This generates regular horizontal rows and continuous vertical joints.

1. Cobs (regular)
2. Sheds (regular)
3. Sheds (staggered: alternate rows staggered by half unit)
4. Hobo 16 mm (regular)
5. Hobo 20 mm (regular)
6. Hobo 25 mm (regular)
7. Hexo (adjacent faces in contact with each other, no voids present between the units).

In this test series, the primary objective was the study of reflection, run-up and run-down for different armour material and not the stability. Even if stability is to be considered it could only be done in the case of Cobs and Sheds which have been manufactured with materials having the required density for simulation of prototype conditions. However, in comparison with previous studies on the same model Cobs and Sheds, (HRS-EX632 1973, HRS-EX1124 1983) it was evident that comparatively small wave heights used in the present work would not permit a detailed study on stability. With regard to the Hobo and Hexo, it was not possible to consider stability because the weights of these units were not modelled. Hence the units were stable and it was possible to study the flow characteristics under the action of regular waves.

The force measurement tests were limited to Shed units placed in a regular manner. The objectives of these tests were to determine the forces acting on a single Shed unit, perpendicular and parallel to the slope. These two forces were identified as lift and along-slope force.

When randomly-packed armour units of different shapes are placed on a slope they are free to move in almost any direction around any of their axes. However, the same is not applicable in the case of hollow block units most of which are cubical with rectangular vertical faces and are placed in a pre-determined compact form. Under such circumstances the study of lift and along slope force is adequate to understand the forces acting on such a unit.

Model studies on Cob and Shed units (Stickland 1969 and HRS-EX1124 1983) have shown that assemblies of hollow block units on slopes have

demonstrated considerable stability even under extreme conditions. Model tests on 2 tonne Shed-armoured slopes have been run with incident waves upto 8.4 m significant wave height. When provided with adequate support at the toe and crest these Shed-armoured slopes suffered minimal armour unit movement with no extractions of units. Model tests on Cob units performed with regular waves showed that two units each having an equivalent prototype weight of 2.9 tonnes and placed on a slope of 1:1 1/3, were dislodged by a 7.0 m wave having a period of 8.8 s. In view of these observations, stability tests were not performed as part of the present experimental programme.

A loose laying pattern had indicated certain amount of instability for larger wave heights. This instability was characterized by lifting and falling in positions of a few units with none being extracted from the armour layer. It should be noted that hollow block units placed at the boundaries of the breakwater such as the crest demands closer examination particularly with regard to adequate support and overtopping. Such a unit does not represent a typical unit for force analysis. Hence the measurement of forces were made on a unit positioned near still water level. This unit will be subjected to wave impact forces.

Previous model studies have illustrated that under extreme conditions of incident wave climate or due to a loose laying pattern, hollow blocks may be displaced by lifting. Once a unit is extracted from the armour assembly there exists an opportunity for other units to fall over or to be lifted from their positions. The resulting instability will be characterized by lifting, rocking and rolling of armour units. This state corresponds to one of the possible failure mechanisms for hollow block armour units provided the crest and the toe wall of the breakwater remain stable.

The foregoing discussion establishes that the study of lift and along-slope forces are appropriate in relation to hollow block units and will provide information on forces acting on the unit and the relative magnitude of the two components. Although the lift forces corresponding to critical states of instability would not be achieved due to limited wave heights under the available laboratory conditions, the results would correspond to service loads encountered by the armour unit.

3.6. Theoretical considerations

From the literature review it was evident that numerous theoretical studies, both analytical and numerical, have been performed on wave reflection and transmission.

Almost all analytical techniques are based on linear, shallow-water waves acting on non-submerged homogeneous structures of rectangular cross-section, open on the seaward side and either open or closed on the rear side. A simplified form of the governing equations has always been adopted. Equations for flow within the structure were coupled with those outside by requiring continuity of horizontal velocity and pressure at the interface thus yielding reflection and transmission coefficients. The main feature of all analytical techniques is the use of an appropriate linearizing technique to approximate the turbulent flow resistance term. The Lorentz principle has been frequently used for this purpose (refer Chapter 2, Section 2.5.1).

Based on this general solution, several modifications have been incorporated to account for multi-layered breakwaters. This introduces the equivalent rectangular concept, various forms of which have been presented by different authors. It should also be observed that some of the models can only be applied after they have been calibrated against experimental data in order to determine certain constants. Analytical studies on submerged breakwaters involve a high degree of empiricism.

Analytical solutions are based on simplified governing equations and in order to obtain explicit results further simplifying assumptions are adopted to reduce the computational complexity. This, of course, is done at the expense of accuracy of the final results. If the analysis is to be applied to general cases of intermediate or short wave excitation it is necessary to rewrite the equations of motion incorporating depth-dependent terms which in turn will preclude an analytical solution even in the presence of further simplifications.

Hence when applying analytical methods to the problem of reflection-transmission through porous media it is appropriate to use the simplified governing equation but adopt a more rigourous method of solution by making minimum use of further assumptions. This method of approach was adopted in the present study to investigate both open block (wave transmitter) and closed block (wave absorber) structures. An evaluation was made on the application of such formulations to sloping porous structures, supported by experimental investigations on similar

structures as well as their 'equivalent rectangular' counterparts.

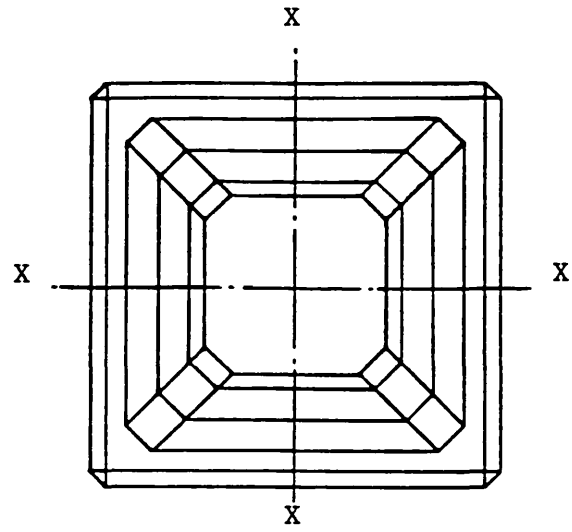
Both finite difference and finite element methods have been used to analyze the problem numerically. Although advances in computer technology have allowed numerical modelling of porous structures using relatively complex governing equations, it has been necessary at some stage to incorporate simplifying assumptions. Use of steady flow permeability coefficients under time-dependent conditions, limited knowledge on acceleration effects and air entrainment due to internal and external wave breaking are some of them. On occasions the steady flow coefficients used have been obtained from general expressions, determined for different media than those used for breakwaters.

To be consistent with the analytical approach adopted for this study, numerical methods using the finite difference techniques were used to study the flow behaviour of wave absorbers, the primary objective being to predict wave decay inside such structures.

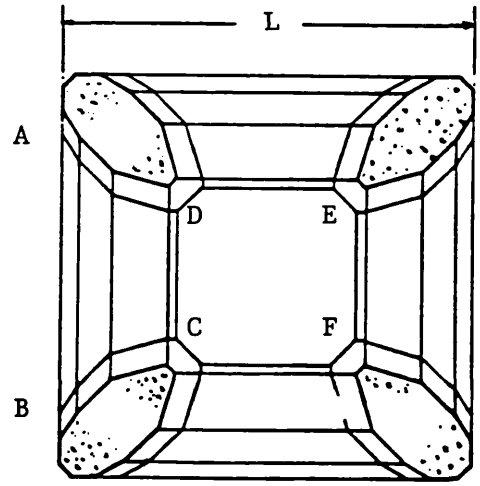
The predictive ability of both analytical and numerical models was tested against the results from different porous media to obtain an understanding of the range of applicability of the models.

State or Type	Experimental Technique (1) Object fixed in flowing fluid	Experimental Technique (2) Object moved in initially still fluid
steady (uni-directional) flow/motion.	- constant discharge in a horizontal bed flume.	- object moved at uniform speed
	- constant discharge in an enclosed permeameter.	
oscillatory flow/motion.	- regular waves generated in a horizontal bed flume.	- object moved with a prescribed oscillatory motion. Goring and Raichlen (1979)
	- use of U-tube oscillatory flow principle by using special apparatus. Sarpkaya(1975)	
	- use of pulsating channel. Burcharth and Thompson (1983)	
	- object placed under a node of a standing wave. Keulegan and Carpenter (1958)	
circular rotation flow/motion.		- object moved around a circular orbit. Holmes and Chaplin (1978)
uni-directional acceleration. flow/motion.	- fluid moved with constant acceleration Sarpkaya and Garrison (1963)	- object moved with constant acceleration. Gibson and Wang (1977)
uni-directional steady velocity or acceleration together with oscillatory flow/motion.		- object oscillated while mounting the oscillatory mechanism on towing carriage.
	- Towing the object in a wave field. Teng and Nath (1985) - Oscillating the object in a pre determined flow. Verley and Moe (1979)	

TABLE 3.1 EXPERIMENTAL TECHNIQUES



Elevation of any face of the Cob unit



section x-x

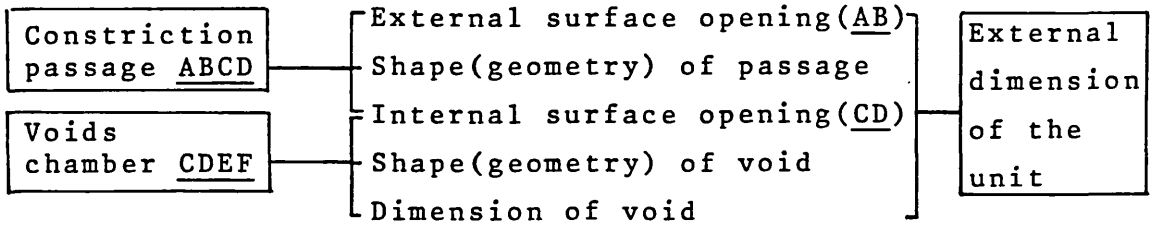
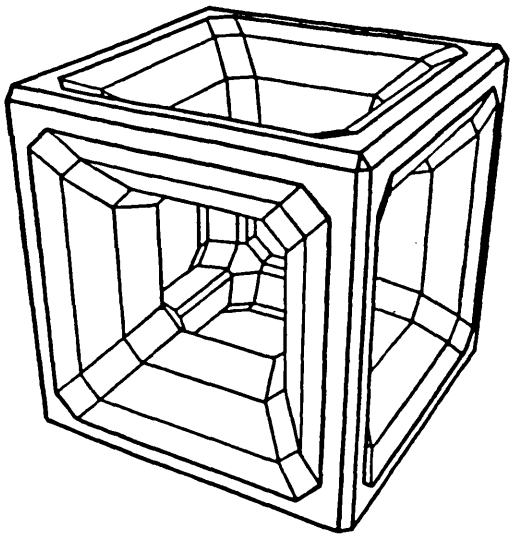
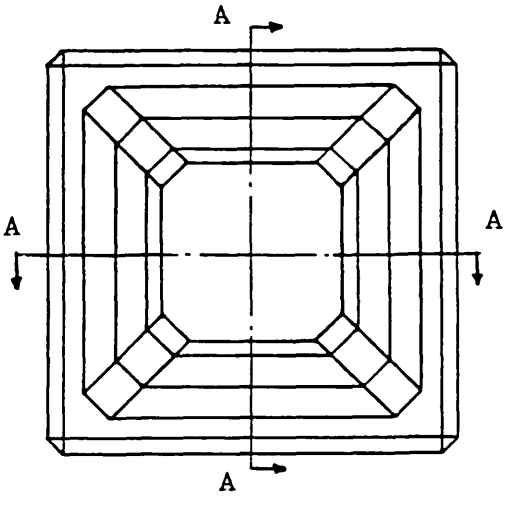


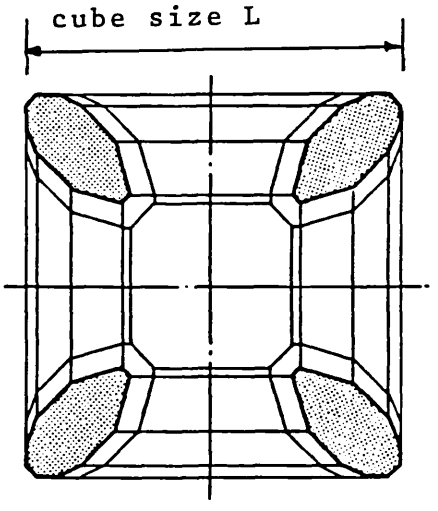
FIG.3.1 GEOMETRIC PARAMETERS FOR HOLLOW BLOCK ARMOUR UNITS



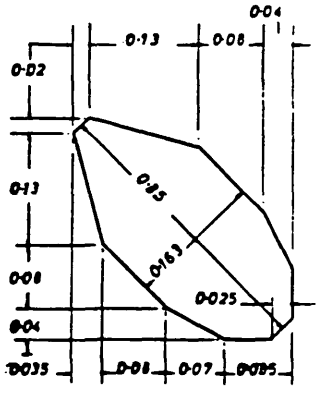
Perspective view of a typical Cob unit



Elevation of any face

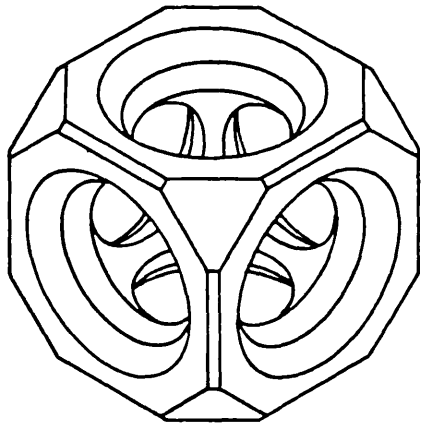


section A-A

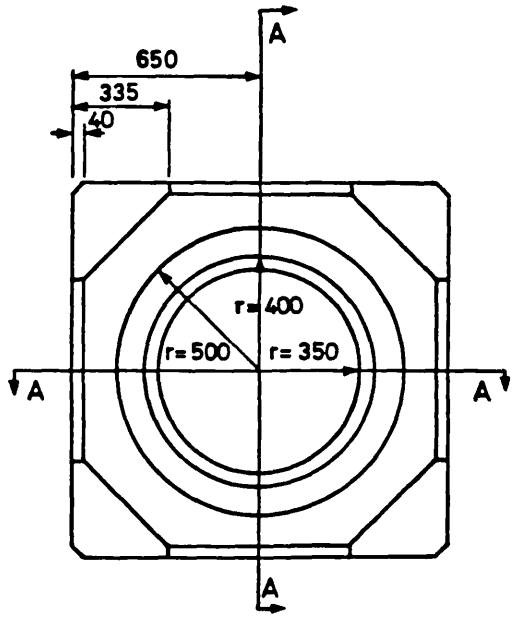


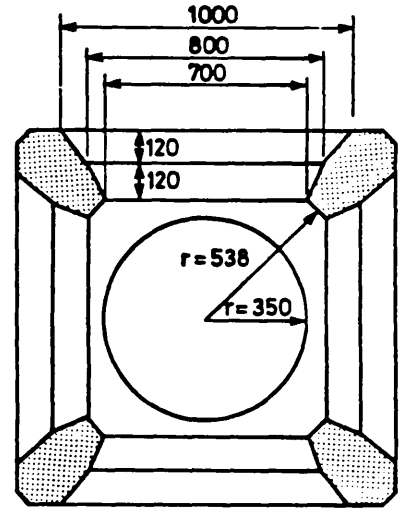
Limb section
(dimensions as proportions of L)

FIG.3.2 DETAILS OF THE COB ARMOUR UNIT



Perspective view of a typical Shed unit

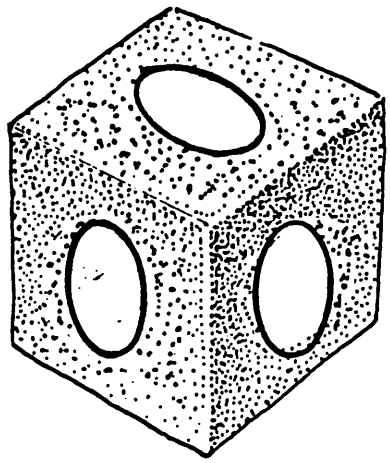




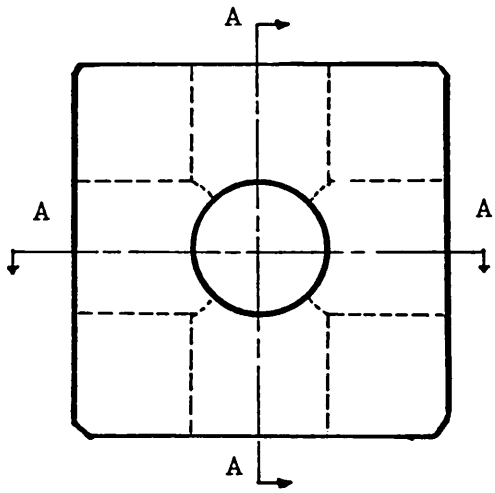
Side elevation and plan view section A-A

Dimensions in mm corresponding to a 2 tonne unit

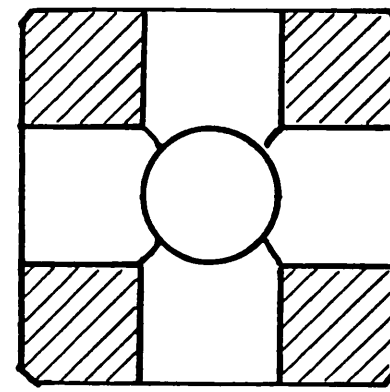
FIG.3.3 DETAILS OF THE SHED ARMOUR UNIT



Perspective view of a typical Stolk unit

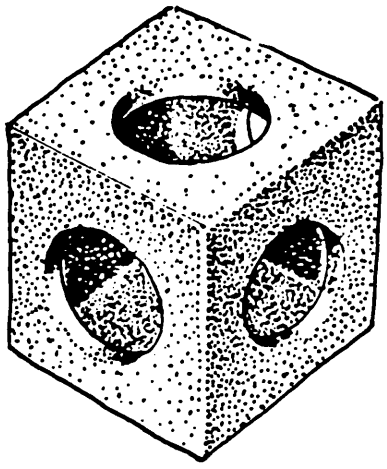


Side elevation and plan view

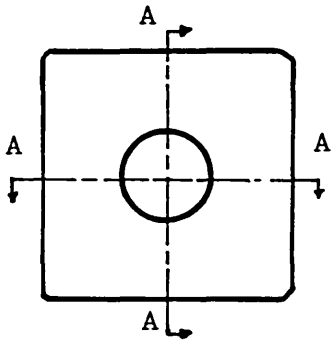


section A-A

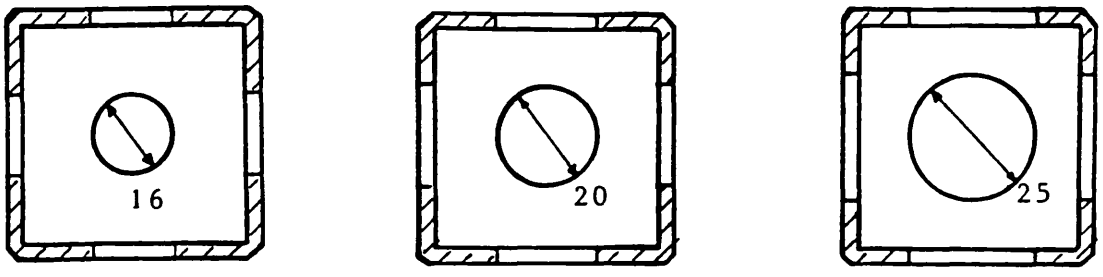
FIG.3.4 DETAILS OF THE STOLK ARMOUR UNIT



Perspective view of a typical Hobo unit

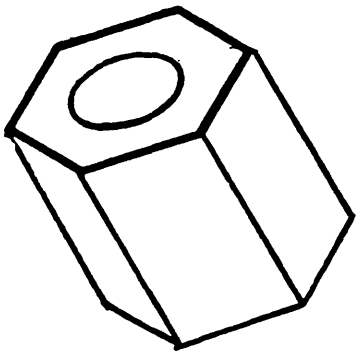


Side elevation and plan view

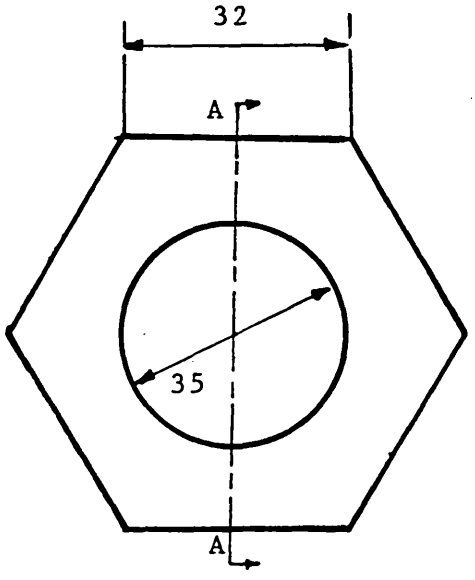


Sectional elevation A-A of the three units used for this study
(dimensions in mm)

FIG.3.5 DETAILS OF THE HOBO (HOLLOW BLOCK) ARMOUR UNIT

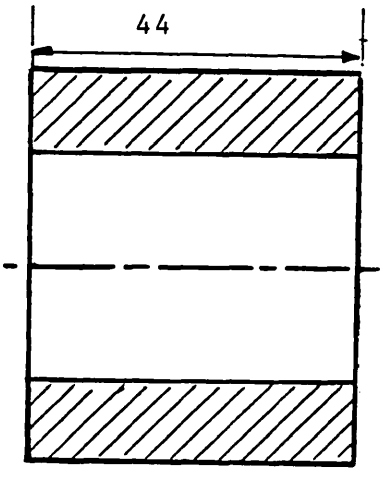


Perspective view of a typical Hexo unit



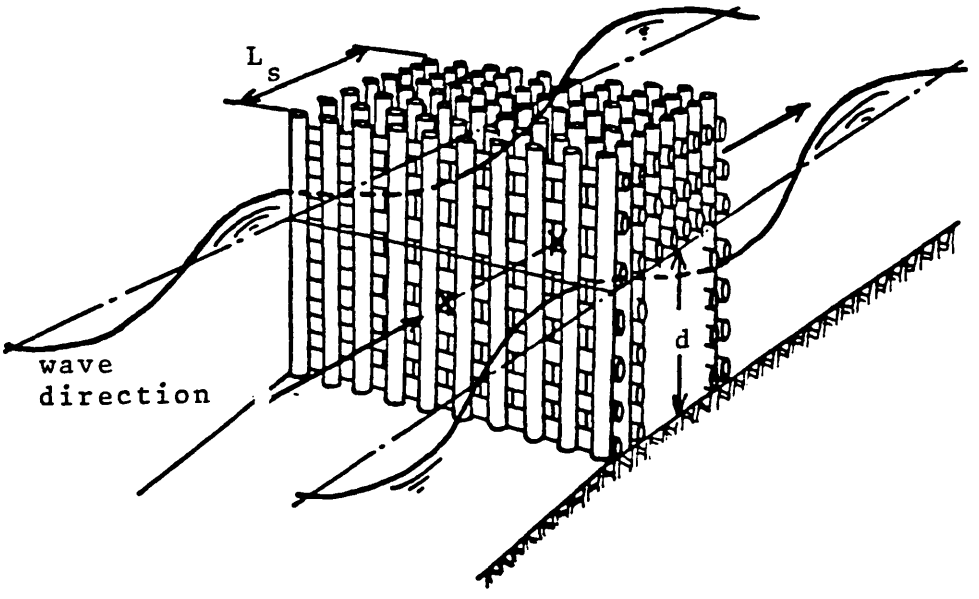
Front elevation of model unit

(dimensions in mm)

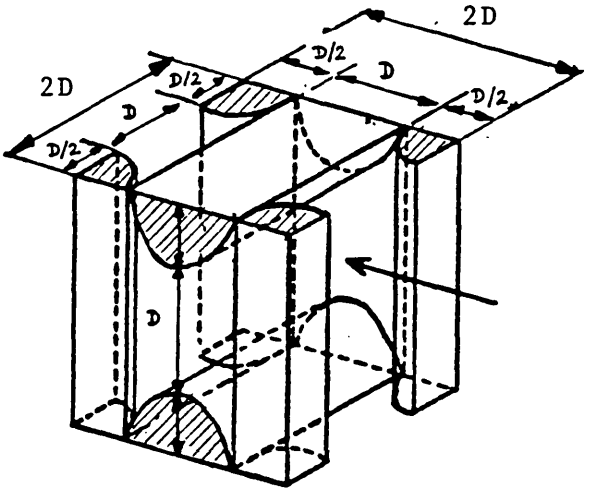


section A-A

FIG.3.6 DETAILS OF THE HEXAGONAL ARMOUR UNIT (HEXO)



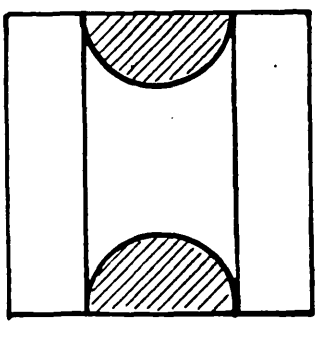
Perspective view of a typical cylindrical lattice



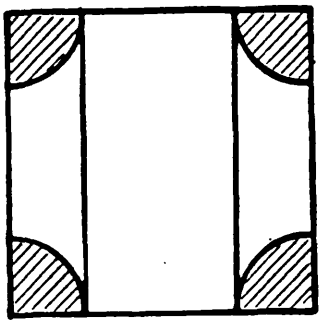
Repetitive element of the cylindrical lattice structure (Cylat)

D is the diameter of cylinder

Details of the void

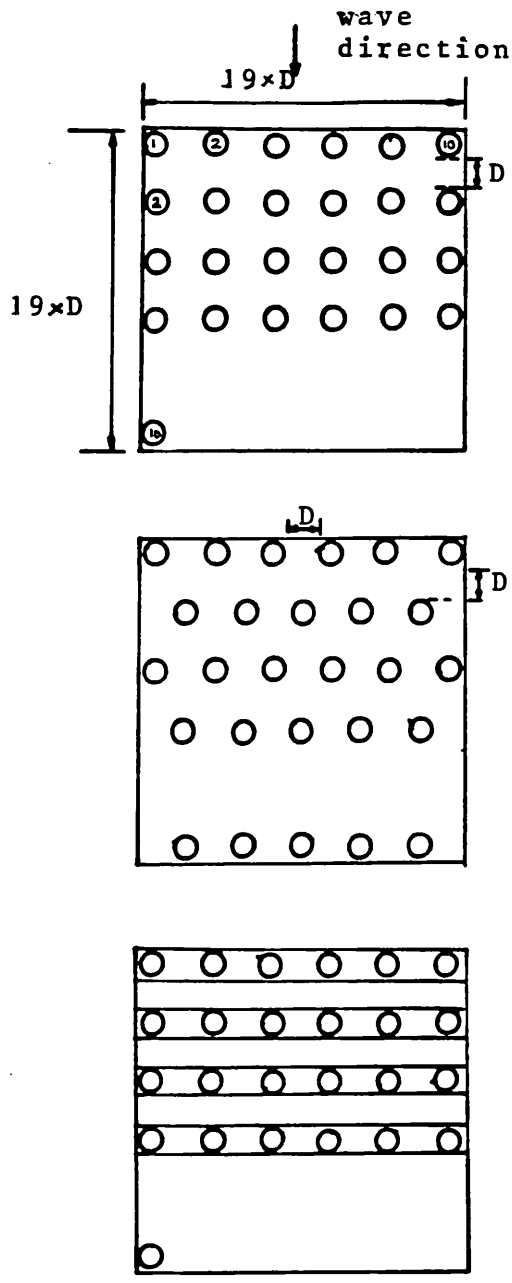


sectional elevation



sectional plan view

FIG.3.7 DETAILS OF THE CYLINDRICAL LATTICE STRUCTURE



Vertical pile structure

(members aligned in both directions)

Vertical pile structure

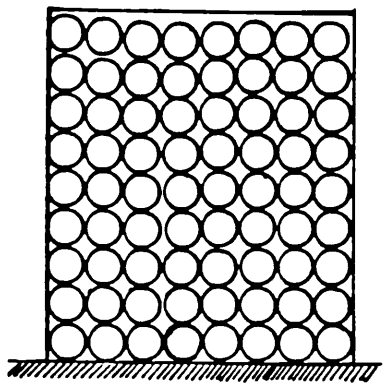
(alternate rows staggered)

Vertical pile structure with horizontal cylindrical members

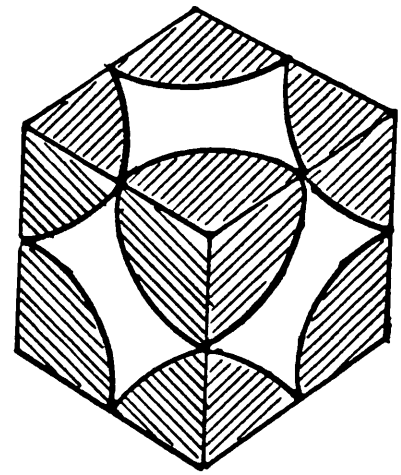
(cylindrical lattice)

D is the diameter of the cylinder(15 mm)

FIG.3.8 PLAN VIEWS OF PILE STRUCTURES USED FOR THE STUDY



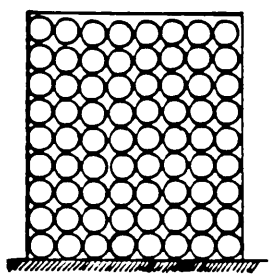
side elevation



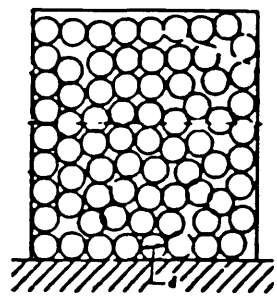
Repetitive element of the spherical lattice structure (Sphelat)

Details of the void

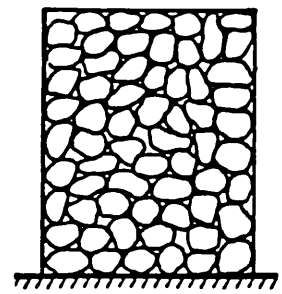
Fig.3.9.a Details of the Spherical lattice structure



spherical lattice



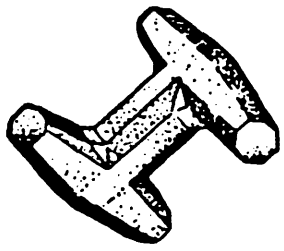
randomly packed spheres



randomly packed stones

Fig.3.9.b Porous media consisting of spheres and rounded stone

FIG.3.9 DETAILS OF THE STRUCTURES CONSISTING OF SPHERES AND ROUNDED STONES



Perspective view of the Dolos unit

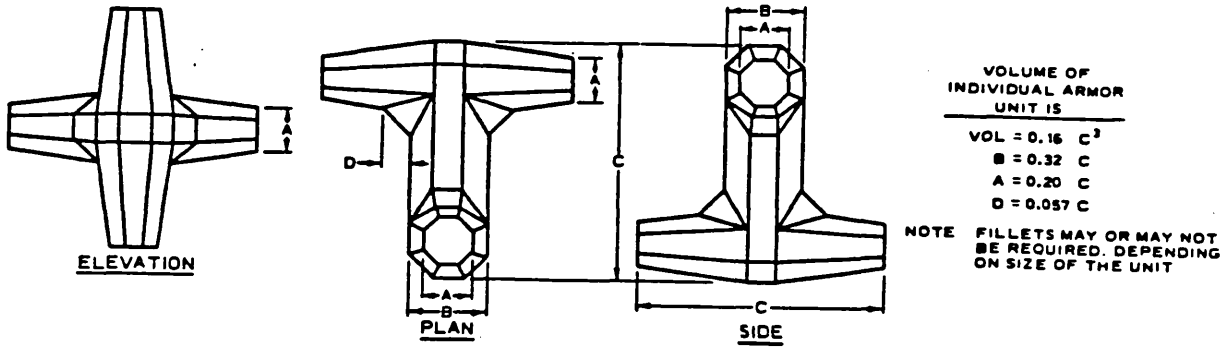
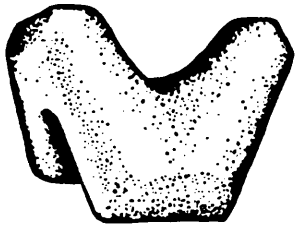
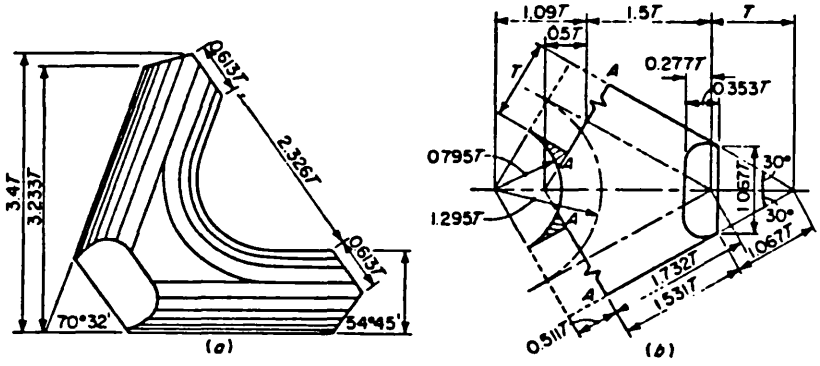


FIG.3.10 DETAILS OF THE DOLOS ARMOUR UNIT

(Carver and Davidson 1978)



Perspective view of the Stabit unit



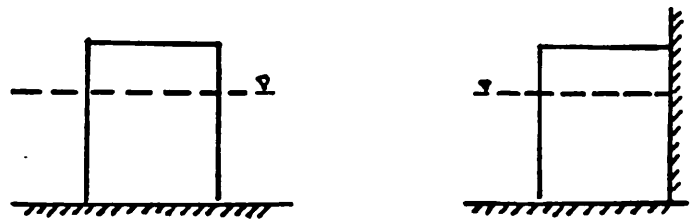
Side elevation of Stabit sitting on two limbs

Part plan of Stabit showing corner

Stabit proportional dimensions

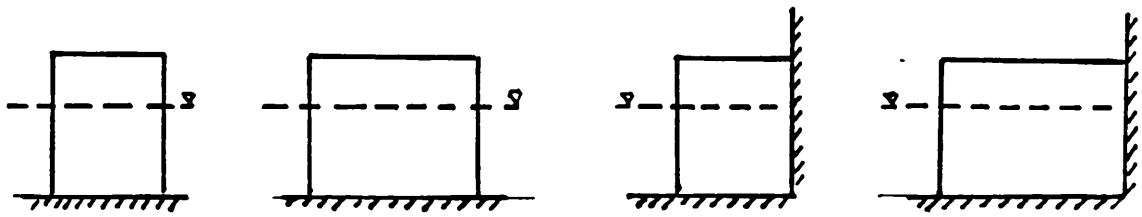
FIG.3.11 DETAILS OF THE STABIT ARMOUR UNIT

(Singh 1968)



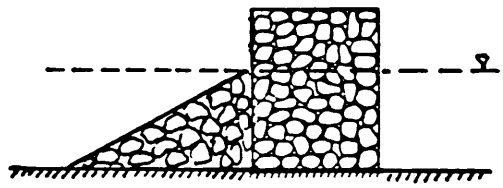
open block structure closed block structure

Comparison of open and closed block structures

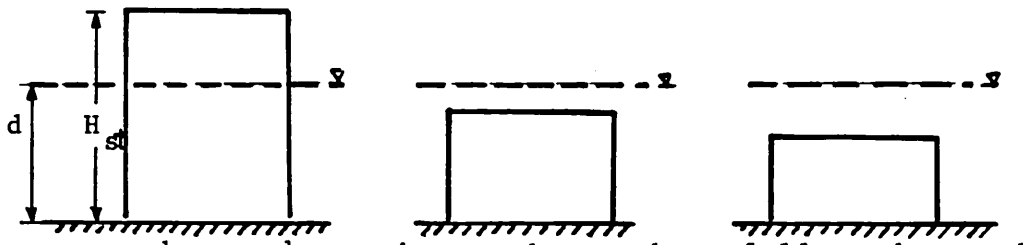


open block structures closed block structures

Influence of length of structures

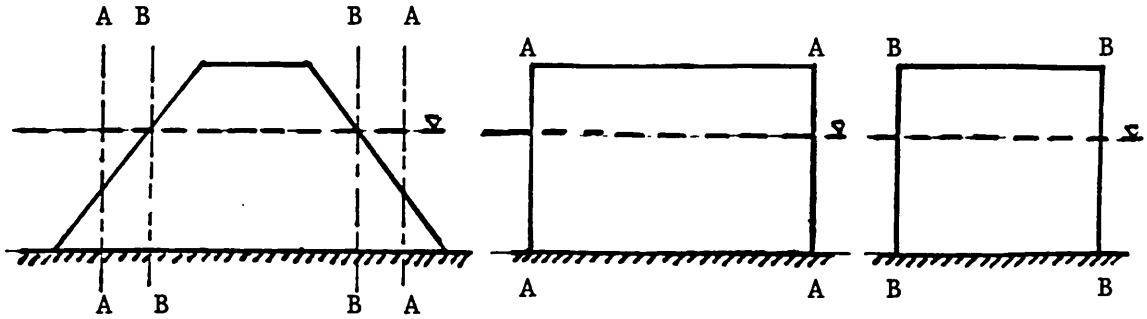


Response to the introduction of a front slope



non submerged just submerged fully submerged

Influence of submerged porous media



Performance of a trapezoidal porous block structure and its rectangular equivalents

FIG.3.12 DETAILS OF THE STRUCTURES USED FOR ADDITIONAL TESTS UNDER OSCILLATORY FLOW CONDITIONS

CHAPTER 4 - EXPERIMENTAL APPARATUS, FLOW ENVIRONMENT AND PROCEDURES

4.1. Introduction

In the previous chapter the basic underlying concepts relating to the different experimental techniques used for each phase of the project were discussed.

The objectives of this chapter are to present

(i) relevant technical details of the experimental apparatus,
(ii) important features of the flow (or wave) environment,
(iii) some of the precautionary measures adopted, and
(iv) experimental procedures followed.

Limitations of the apparatus, uncertainty and inaccuracy of the measurements, and data evaluation techniques are all integral parts of any experimental programme and these will be assessed in order to obtain an understanding of the range of applicability of the results.

4.2. Steady flow tests

4.2.1. Details of apparatus

Steady flow permeability tests on porous rectangular block structures were carried out in a 30 cm wide, 12 m long straight glass-sided flume supplied with water from the laboratory re-circulating system. A constant head tank with a weir (3.44 m in length), placed immediately above the upstream end of the flume and supplying no other apparatus ensured accurate control of the flow rate.

The bed of the channel was maintained as far as possible, horizontal throughout the length of the flume as required for the experiment (Fig. 4.1).

A variable height downstream weir controlled the tail-water depth, enabling normal flow to be used for all experimental runs. The tail water could then be directed by a pair of connected open-shut valve systems into either the sump or an underfloor measuring tank. If this arrangement was not suitable, particularly for low discharges, it was possible to place a measuring tank on a weighing scale at the downstream end of the flume and direct water into this tank.

4.2.2. Placing of porous structures

The porous media under investigation occupied the full width of the flume and were located 6 m from the head of the flume, maintaining upstream and downstream faces of the structure vertical. The length of all porous structures was kept approximately constant at 30 cm with ± 1 cm variation depending on the particular medium, thus permitting a comparative study to be made on all structures tested. Porous honeycomb materials were inserted at the head of the flume to eliminate surface ripples and possible distortions of the water surface. It was important to ensure that no space was left between the glass sides of the flume and the vertical side face of the porous structure. For this purpose it was necessary to use very thin packing material that prevented any leakage from the sides thus eliminating 'side effects' which would have had an unfavourable influence on the final result.

4.2.3. Special considerations for randomly packed media

In the case of randomly packed material, it was necessary to use a cage made of thin wire mesh to assemble the media and to accommodate it when the tests were in progress. The cages, fabricated to the required dimensions, were first placed in the flume and then the porous media were assembled by pouring in the constituent elements randomly. Side packing as well as water-proof tape were used to prevent side leakage and to guide the flowing water into the structure.

To assess the influence of the cages, a separate steady flow test was performed with the empty cage in position. It was found that the hydraulic losses were negligible and could not be detected by the measuring apparatus. The presence of the cage was therefore not considered in the subsequent analysis.

The side effects of randomly packed material in a cage are more significant in comparison with a truly rectangular block structure placed in a similar position across the full width of the flume. In addition a phenomenon identified as a 'wall effect' is also present. This is a factor responsible for the variation in velocity near the wall of a permeameter due to changes in porosity. In a permeameter filled with non-cohesive granular materials a zone of high porosity of the order of half a particle diameter is created against the wall. Being dependent on porosity, the velocity in this zone will be different to that of the average velocity in the centre portion, thereby causing the mean velocity of the whole cross-section to differ from the true velocity in an infinite medium. Studies on this subject were performed by Dudgeon (1967) who proposed a formula to correct

for this effect based on the exponential resistance equation.

In the present investigation the steady flow tests were performed in a horizontal bed channel in preference to a permeameter. The rectangular cross-section normal to the flow is comparatively large compared with the circular cross-sections of permeameters used in previous investigations. An increase in the cross-section area of flow is equivalent to reducing the influence of wall effects. Use of porous media assembled from cubic or rectangular shaped elements which generate well-defined vertical side faces when placed against the sides of the flume eliminates this effect altogether.

In this study the media which would have been subjected to wall effects are randomly packed spheres and rounded stones. It is assumed that the experimental technique adopted would have reduced its influence to a minimum. One simple way of overcoming the problem to a great extent is to attach on the sides of the flume, elements cut in the shape of half stones or spheres to simulate the effect which would otherwise be present when a randomly packed porous medium is intersected by a vertical plane.

4.2.4. Experimental procedure

The experimental procedure was straightforward in that for a given discharge, the difference in the levels of the water surface upstream and downstream of the test structure was noted. In view of the comparatively large scatter observed in previous investigations it was decided to obtain readings at close intervals of discharge. The lowest value was dependent on careful visual observation. Once it was realized that water was flowing effectively through the structure, it was possible to take the first reading. The highest value was governed by the depth of the flume which if exceeded would cause overflow. Before any new reading was taken, water was allowed to flow freely through the structure for at least ten to fifteeen minutes to ensure flow stabilization which is a critical factor in this experiment.

4.2.5. Measurement of surface elevation and discharge

Surface elevation measurements in front of and behind the structure were made using a system of static head tubes with point gauges attached. Vertical oscillations of the free surface rendered direct point gauge measurements inaccurate, particularly for high flows. Almost all depth measurements were made with static head tubes connected by 5 mm tubing to 30 mm diameter stilling wells. Depth

gauges attached to the stilling wells were aligned and calibrated against still water depth measurements. Normal flow was used for all runs and the depth, checked before and after each run, was never found to vary more than 0.1 mm during any single experiment.

Water flow rates had to be measured by two different methods depending on whether the flow rate was high or low.

For high flow rates the discharge from the model was measured volumetrically over a pre-determined time interval with the water being collected in an underfloor tank of constant rectangular section with plan area 10.80 m^2. With the aid of two valves which opened and closed simultaneously, water flow could be cut off from the underfloor tank and discharged into the laboratory sump. The water levels in the underfloor tank were measured by a battery operated depth recorder mounted on a tripod which read water level changes to within 0.1 mm. To eliminate the influence of surface disturbances which occur in the underfloor tank, a stilling well made of smooth iron pipe with openings at the bottom was placed vertically to enclose the point gauge. In addition, care was taken to leave the water in the tank for several minutes before measuring the level to ensure that all seiche motion had subsided. The time for discharges was measured by a stop watch with the measurement having an uncertainty of ± 0.5 sec. It should also be noted that a maximum error of ± 0.5 sec. could occur in the operation of the valve system.

For low flow rates the water was directed into a measuring tank placed on a weighing scale and the time taken to collect a specified weight was noted. This method proved to be very effective for low discharges.

On all occasions, for a given discharge, the measurements were repeated at least four times and the arithmetic mean was considered as the reliable value for computation. If considerable variation was observed in the four values, measurements were taken after an additional five minutes giving an opportunity for the flow to stabilize further. The total uncertainty in the discharge measurement is within 1%.

During the test programme it was noted that a considerable time elapsed before steady conditions were reached for a given discharge and for extreme cases of very low and very high flow rates it was almost impossible to achieve this state. This observation is attributed to the overall limitation and sensitivity of the experimental set-up. Unstable measurements obtained under such conditions were

not used for computations.

For each media a few readings were taken again at the end of an experimental run to check the repeatability of the results. It was found that they were reproducible on every occasion to within 1%.

4.3. Oscillatory flow tests

4.3.1. Details of apparatus

Oscillatory flow tests on porous structures were performed in a horizontal bed flume, 30 cm in width, 40 cm in depth and 10 m in length. These tests were performed on all media tested under steady flow conditions and on additional media identified earlier.

A plunger type wave generator was located at one end of the flume driven by a constant speed electric motor through a continuously variable gear box. The wave frequency was varied by altering the setting on the dial which controls the speed of the motor. The period of the generator could thus be varied from 0.5 secs to 2.0 secs and the wave amplitude for a given period was altered by changing the eccentricity of the drive. At the other end of the flume was a beach made of a frame of aluminium angles onto which was mounted perspex sheeting. The beach was at a slope 1 in 8.33 for a length of 3 m.

A filter system was placed in front of the wave plunger for several purposes. The filter reduces surface ripples, helps to smooth the incident waves and damps any free or forced harmonics generated by the plunger. Once the incident wave is reflected by the structure under test, it proceeds back to the plunger and part of the energy is absorbed by the filter. This arrangement proved to be very effective in producing a desirable standing wave system between the filter and the structure. Reference to this wave system will be made at a later stage in this chapter. The filter in this study essentially consists of a box made of thin wire mesh accommodating a number of rolls of wire mesh made from the same material. It had approximate dimensions of 30 cm in width, 40 cm in depth and 60 cm in length, thus occupying the full width of the flume. It is natural that such a system will reduce the wave height to a certain extent. However this was the most suitable method of achieving a well-defined incident-reflected wave system which is desirable for subsequent analysis.

The energy in waves which impinge on a porous structure, such as a

rubble mound breakwater, can thereafter be divided into reflected energy, transmitted energy and dissipated energy. The energy dissipated has two components of which the first is that dissipated on the face of the structure and the second is due to the turbulence within the structure.

The parameters defining this process are the characteristics of the wave environment, and the geometric and hydraulic properties of the porous media. With regard to the first, the governing parameters when testing with regular waves are the wave height (H), period (T) and water depth (d). The basic experimental programme covered all media selected for the investigation. In each case the experimental medium was assembled in the form of a rectangular block structure with the water depth maintained at a constant value of 20 cm. For selected wave periods, wave height was varied to obtain different values of wave steepness. In subsequent tests the water depth was varied and different structural forms tested.

In the experiments the porous structures were assembled and located firmly in the flume 5 m from the filter system. The structures extended across the full width of the flume, simulating the condition of an infinitely wide structure. Sufficient care was exercised as before to minimize side and wall effects.

A separate test programme was performed to investigate the influence of the cages used for randomly packed media. The webbing of the screens was sparse and the diameter of the wires was so small that the screens did not have any effect on the measured wave reflection and transmission. Thus the negligible influence of the screens was not considered in the analysis of results.

4.3.2. Wave environment in front of the structure

When performing model tests with regular waves in a wave flume it is often difficult to determine the height of the incident waves which impinge on the model. The model generates reflected waves which move backwards towards the wave generator and by superposition give rise to a composite wave train. In most flumes, the distance from the wave generator to the model is of such a length as not to permit the incident wave height to be measured without being disturbed by the influence of the reflected wave. In general within a short distance from the wave generator, disturbances from the wave generation make accurate recording impossible. This is eliminated by introducing wave filters close to the wave generator. In the remaining part of the flume upto the model, the length is normally limited and as such there exists no point where the waves have grown to the full height without the influence of the returning reflected wave.

In many cases, it is therefore necessary to record the composite wave in an appropriate way and then separate the incident and reflected wave components. With regard to porous structures the composite wave essentially consists of a partial standing wave characterized by nodes and anti-nodes, the distances between which is one quarter of a wave length.

The standing wave envelope profile does not propagate relative to a fixed reference system. If such a profile is to be measured, a wave probe has to be moved in an appropriate manner perpendicular to the crest line to record the amplitudes of the oscillations at successive positions. By adopting this technique it is possible to measure the relative maxima and minima every quarter wave length in the envelope.

4.3.3. Analysis of the standing wave system

Assuming that the incident and reflected waves are of sinusoidal form, i.e., consistent with linear wave theory, both must have the same period and can be expressed as,

$$\eta_i = a_i \sin(\omega t - kx) \qquad (4.1)$$

$$\eta_r = a_r \sin(\omega t + kx) \qquad (4.2)$$

where η refers to the water surface elevation above mean water level.

a_i and a_r are the amplitudes of the incident and reflected wave.

$$\omega = \frac{2\pi}{T} \quad \text{where T is the wave period} \qquad (4.3)$$

$$k = \frac{2\pi}{L} \quad \text{where L is the wave length} \qquad (4.4)$$

Hence a reflection coefficient can be defined as the ratio between the amplitudes as

$$K_r = \frac{a_r}{a_i} \quad (\leqslant 1) \qquad (4.5)$$

$K_r = 1$ corresponding to complete reflection.

Values of K_r less than 1 frequently occur during model experiments with rough

vertical or inclined faces which may be permeable or impermeable.

The combined wave motion can be expressed as

$$\eta = \eta_i + \eta_r \tag{4.6a}$$

$$\eta = (a_i + a_r) \sin \omega t \cos kx - (a_i - a_r) \cos \omega t \sin kx \tag{4.6b}$$

Differentiating eq. 4.6.b with respect to time t and setting the result equal to zero, the time at which this combined wave system produces maximum and minimum amplitude is given by

$$\tan \omega t^* = \left(\frac{K_r + 1}{K_r - 1}\right) \cot kx \tag{4.7}$$

Substituting the values of $\sin\omega t^*$ and $\cos\omega t^*$ obtained from eq. 4.7 in eq. 4.6.b, the equation for the variation of wave amplitude with distance is

$$|\eta_x| = a_i \left[(1 + K_r)^2 \cos^2 kx + (1 - K_r)^2 \sin^2 kx\right]^{\frac{1}{2}} \tag{4.8}$$

Differentiating eq. 4.8 with respect to x and setting the result equal to zero, the maximum and minimum values of η_x are given by

$$|\eta_x|_{max} = a_i + a_r \quad \text{when } kx = n\pi \quad n = 0,1,2,3 \tag{4.9}$$

$$|\eta_x|_{min} = a_i - a_r \quad \text{when } kx = \left(\frac{2n+1}{2}\right)\pi \quad n = 0,1,2,3 \tag{4.10}$$

From eq. 4.9 and eq. 4.10

$$a_i = \frac{|\eta_x|_{max} + |\eta_x|_{min}}{2} \tag{4.11}$$

$$a_r = \frac{|\eta_x|_{max} - |\eta_x|_{min}}{2} \tag{4.12}$$

Since the wave height (H), according to linear wave theory is twice the amplitude, the above expressions can be written in terms of wave height.

$$H_i = \frac{H_{max} + H_{min}}{2} \tag{4.13}$$

$$Hr = \frac{H_{max} - H_{min}}{2} \tag{4.14}$$

Thus the first order approximation to K_r is

$$K_r (= \frac{H_r}{H_i}) = \frac{H_{max} - H_{min}}{H_{max} + H_{min}} \tag{4.15}$$

Hence it is possible to determine K_r by merely seeking out a node and anti-node along the length of the flume.

The theoretical variation of the wave amplitude (eq. 4.8) relative to the maximum wave amplitude (eq. 4.9) can be expressed as,

$$\frac{|\eta_x|}{|\eta_x|_{max}} = \frac{H_x}{H_{max}} = \left[1 + \frac{2K_r}{(1 + K_r)^2} (\cos 2kx - 1)\right]^{\frac{1}{2}} \tag{4.16}$$

As discussed by Ursell et al (1960) the above formulae are also valid when the wave motion is weakly non-linear, that is, when it contains a small second harmonic component in addition to the primary first harmonic motion of period equal to that of the wave generator.

It should be appreciated that the above development is based on linear theory which implies waves of low steepness and sinusoidal profiles. Waves of finite amplitude have narrow crests and broad shallow troughs. If the above equations are applied under such conditions the results will not be correct; the steeper the waves, the larger the error. The use of the theory is only valid if the wave pattern conforms to the underlying assumptions and, if computations are to be based on this theory, sufficient care must be taken from an experimental point of view to ensure the presence of such a wave pattern.

4.3.4. Methods of monitoring the standing wave envelope

In model studies the standing wave pattern developed can be traced by several methods. That most frequently used is to move the wave probe at a slow speed along the wave train thus detecting the anti-node and node heights. This method has been successfully adopted by Kamel (1969), Kondo and Toma (1972), Sollitt and Cross (1972) and Nasser and McCorquodale (1974).

Another method is to measure wave heights within this region at several locations, preferably at close intervals, over a considerable length in order to ensure that both anti-node and node heights are included in detectable form. Once the wave heights are obtained it is possible to construct the composite wave system. This method was used by Madsen and White (1976b) for their studies on porous rubble mound breakwaters. In analysing their results, they used a precise technique based on Fourier methods to determine the required wave height. Reference to this method will be made later in this chapter.

Sandstrom (1974a) recommended the use of two probes assembled at a fixed distance of quarter of a wave length. The accuracy of the method in relation to the location of the probes and wave parameters was investigated using linear and second order wave theory.

For this investigation it was decided to use the first method while exercising sufficient care to obtain a well-defined standing wave pattern consistent with the theoretical requirements presented earlier. The main reason for selecting this method of recording was because of the extensive experimental programme. More than thirty different porous structures with varying geometries were investigated for two or more wave periods. For each wave period a minimum of six readings was obtained with varying wave amplitude.

In each experiment the wave probe monitoring the standing wave system was moved so that it would cover at least three or four anti-nodes and nodes depending on the wave period. Measurements were duplicated to ascertain the repeatability of the experimental values, average values being used for computations. Regions immediately adjacent to the structure, where local modes distort the free surface, were avoided. Close examination of the wave records was carried out for every run in order to detect any second harmonic motion whose presence manifests itself clearly due to the disappearance of the first harmonic motion at the nodes as well as other distortions in the wave profile. It was noticed that waves of very high frequency particularly at high amplitudes introduced lateral oscillations in the

flume and these contributed to surface distortions. If any distortions were observed, the profile was obtained after a further period had elapsed thus giving more time for flow stabilization. If no improvement was observed, the particular reading was rejected.

In almost all the cases investigated in this study it was observed that the porous structures caused a change in wave amplitude and phase but not frequency and it was also possible to obtain a well-defined partial standing wave system consistent with the theoretical development to be used for its analysis. Only a few readings, corresponding to large wave heights at low periods had to be eliminated on this account.

It was realized that sufficient time had to be given for flow stabilization and this was found to be in the order of 5 - 10 minutes. It was also evident that this method of experimentation would not have been possible if not for the use of an appropriate filter placed in front of the wave generator. The wave records obtained without the filter were distorted and included second harmonics which in combination invalidated the theory developed for analysis. The speed of the carriage on which the wave probe was attached had an influence on the recorded wave pattern, particularly with regard to the node height. Wave records obtained at high speeds were not suitable for analysis. After a few runs it was possible to ascertain the appropriate speed for manual operation to obtain desired results. Close examination of the wave profile corresponding to every reading is considered essential when adopting this technique.

At this stage reference is made to the technique adopted by Madsen and White (1976b). At each station along the flume, where the free surface variation with time was recorded, the amplitude of the motion with a period equal to that of the wave generator was extracted from the wave record by means of Fourier series analysis. The authors obtained improved data on the variation of the amplitude of the first harmonic motion with distance along the flume. The apparent disorder observed when plotting the raw data was no longer present. Furthermore this technique provided excellent agreement with the theoretical prediction offered by linear theory.

It should be mentioned that the wave records of Madsen and White (1976b) indicated pronounced second harmonics at nodes and for this reason it was necessary to adopt the Fourier analysis technique. In the present study, it was observed that the wave records were free from such effects and the technique was not required. In addition, for an extensive experimental programme it would not

be convenient to adopt such a time-consuming procedure. For this reason all precautions were taken to obtain a well-defined partial standing wave system. However, frequency analysis was performed on selected readings and it was proved that no second harmonics which may influence the analysis were present. It was found that a visual inspection of the recorded wave profile in each case generally led to an accurate assessment whether or not the wave profile was consistent with the assumptions made in the theory. The few readings which were affected by this phenomena were not used in the subsequent analysis.

4.3.5. Wave environment behind the structure

So far attention has been focused on the wave pattern in front of the structure. A 3 m long beach of slope 1 in 8.33 was utilized as the wave absorber, located at the closed end of the flume. When the same node/anti-node technique was adopted to investigate the interaction of the transmitted wave with the beach, it was observed that the resulting reflections were very low, of the order of 5% or less. Therefore the effect of reflection was ignored and the transmitted wave height was measured at a location behind the structure. In general the transmission coefficients observed in this investigation were very low and the highest value was recorded for the vertical pile structure with its members aligned in both directions. Even in this case, a standing wave pattern was not formed between the structure and the beach.

4.3.6. Regularity of wave surface profiles

In order to assess the regularity of the wave surface profiles, a test was performed in which measurements were taken at half-hourly intervals up to 3 hours for waves corresponding to shortest and longest periods that could be generated. It was observed that the profiles remained constant during this period of investigation thus exhibiting satisfactory profiles with time. In selected experiments, readings were retaken at the end to check for repeatability and they proved to be very satisfactory.

4.3.7. Instrumentation for wave height measurements

Wave heights were measured by employing wave probes together with appropriate electronic monitor modules. The instrument works on the principle of measuring the current flowing in a probe which consists of a pair of parallel stainless steel wires, the resistance of which changes with water surface elevation. The standard form of the probe consists of a pair of stainless steel wires, 1.5 mm

in diameter and spaced 12.5 mm apart. The associated wave monitor module provides energising and sensing circuits and also compensates for the resistance of the probe connecting cables. The latter ensures a high degree of linearity of measurement over a very wide dynamic range of probe conductivity.

Simultaneous water surface elevations at the locations of the probes were obtained using an ultra-violet recorder and in digital form using an analog-digital converter together with a micro-computer. In the latter case the data was stored on disks in a format suitable for subsequent numerical analysis. Fig. 4.2 illustrates the experimental set-up used for the study.

For the wave generator a calibration curve was obtained between wave period and dial setting on the variator over the full range of operation. This enabled any wave period to be selected by interpolation. Independent verification of the calibration was made by analysing data collected by two probes placed at a known distance apart. It was observed that the agreement was very satisfactory.

4.3.8. Calibration of wave probes and precautionary measures adopted

The calibration of the wave probes is a critical factor in the measurement of wave heights. An overall calibration from wave height to output voltage was performed using the ultra violet recorder and the data logger. This was achieved by noting the change in output voltage which occurs when the probes were raised or lowered by a known amount in still water.

An important requirement was that the calibration of each wave probe should be linear over the full range required for wave measurements. This was found valid for all positions of the probes used for this study. Because a linear calibration is influenced by the physical state of the wave probes, such as its uniformity, care has to be taken when handling them to ensure that no distortion occurs. Although this type of probe is fairly insensitive to the electrical effect of deposits on wires, the probes were regularly cleaned to prevent any large accumulation of material. It should be noted that films of oil or grease on the wires have a serious detrimental effect and must be removed thoroughly. It is recommended that probes should not be used in water having a film of oil on the surface.

The conductivity of the water changes with temperature by approximately 2 % per deg C and is also dependent on the concentration of dissolved salts in the hydraulic model. Both of these factors should be borne in mind during calibration

and when tests are in progress with sufficient care being exercised to minimise their influence. When new models are being used it is advisable to allow some time before measurements are taken to ensure uniform distribution of dissolved salt concentration. This necessitates regular probe calibration and in this study it was performed twice daily. This is necessary, particularly when using long probes, to ensure that there exist no changes in concentration along the length of the probe, which may result in relatively poor performance. When probes are used in close proximity to each other it is necessary for them to be energised at different frequencies to avoid mutual interaction.

During this investigation, linear calibration curves were obtained over the full depth range on all occasions. Calibration tests were performed before and after each test. A special test was also carried out with the probe placed close to the glass panels of the flume and with its bottom just above the channel bed. It was found that this position did not influence the linearity of the calibration. However such positions were not employed in this study. The closest proximity of a probe to a solid surface was in the measurement of run-up on sloping structures using long probes for which calibration tests were performed more frequently to ensure that the proximity had no significant effect on the performance of the probe.

4.4. Unidirectional acceleration tests

4.4.1. Details of apparatus

The unidirectional acceleration tests were performed in the 55 cm wide flume of length 13 m. In this test twenty-seven hollow block armour units were assembled into a cubic pack consisting of three layers and accelerated in initially still water while monitoring the force acting on the centre unit. Considerations which led to the selection of this method of experimentation have already been presented.

In order to achieve the required experimental conditions it was necessary to make use of a moving carriage. Onto this carriage were initially attached all except the centremost hollow block armour unit by means of a system of vertical bars and two horizontal porous plates which support the units at the top and bottom. A certain spacing had to be maintained between the units to permit a slight movement of the centremost unit which was independently attached to the carriage via a force transducer. The latter consisted of a 7.94 mm diameter bar, acting as a cantilever which was strain-gauged to provide a measure of force on

the unit.

The carriage was made of aluminium angle with wheels attached to both sides, rolling along two rails positioned on the top of the glass sides of the flume. This arrangement was considered to be suitable to monitor the force acting on the instrumented unit. The unit just above the instrumented unit was kept in position by making use of porous spacers. There was sufficient room for the transducer support to pass through the block in order to reach the innermost unit; Fig. 4.3 illustrates the relevant details of the apparatus.

When accelerating a body in initially still water it will naturally disturb the flow in its neighbourhood. If the fluid body is accommodated within an appreciably large boundary these disturbances will propagate until they are damped. However it was not possible to obtain such a facility for these experiments and it was decided to use a 55 cm wide flume in preference to one with a width of 30 cm. The block of units was a cube of approximately 12.5 cm side and comparing with the width of the flume, the side clearance between the outermost unit and the glass side is in the region of 20 to 22 cm. The bottom of the block assembly was maintained at a distance 8 cm from the flume bed.

It should be noted that sufficient clearance should be available on the sides and from the channel bed. If not, as the body accelerates, the flow field within the confined space will introduce unexpected surface profiles characterized by irregular oscillations and influenced by reflection from the flume sides leading to inaccuracy in the measured forces. It was appreciated that kinematics of a flow field in a confined space may be completely different from that of a relatively unconfined space. However, in this investigation it was observed that the clearance selected did not generate adverse surface profiles under the conditions in which the experiments were performed.

Furthermore as the velocity of the carriage increases the block of units tends to push a certain mass of water in front of it thus producing a free–surface gradient in the direction of the motion. This is a limitation of the experimental set–up and necessary precautions had to be taken at the design stage to account for these developments to ensure they exerted minimum influence on the measurements taken.

4.4.2. Force transducer

The force transducer is illustrated in Fig. 4.4 and consists of a cantilever beam ABCDEF bent at a 90° angle at point B. The portion ABCDE is of rectangular section whereas the protion EF is of circular section. The length CD is reduced in width to exhibit better bending properties and instrumented with two pairs of strain gauges located on either sides to produce a full bridge connection. The width of the rectangular section was mainly dictated by the dimensions of the strain gauges. The sectional geometry of the beam, which is characterized by the thickness and the longitudinal dimensions in the vertical direction, were a compromise between a transducer with a high natural frequency and one such that the stresses induced by the resistance against the motion were in the required range of measurement. This had to be achieved within the overall boundaries imposed by the external geometry of the flume which governed the positioning of the carriage. The portion AB was firmly attached to the centre of the carriage. The entire hollow block assembly was symmetrical about the longitudinal axis of the flume.

Calibration of the force transducer was performed by loading the unit at its centre by weights hung over a pulley system. This was done before and after each run. It was observed that on all occasions the transducer responded in a linear manner to an applied force in either direction and no variations were observed in the calibration coefficients.

4.4.3. Measurement of velocity-time profile

It was decided to measure the velocity-time profile by using a series of microswitches attached to the side of the flume, beside the rail, at constant intervals of 20 cm. As the carriage passes over them the D.C. circuit is broken and a signal is obtained. By monitoring the time between successive switches it was possible to compute the mean velocity which was assumed to be representative of the value corresponding to the mid-point between two switches.

4.4.4. Method adopted to obtain constant acceleration

The principle behind this experiment was to accelerate the carriage and block assembly by a suitable mechanism. In order to obtain acceleration of constant or very nearly constant magnitude it was decided to use a conical pulley coupled to a motor. A pulley of length 10.2 cm with extreme diameters 12.7 cm and 20.3 cm was used for this purpose. However, it was observed that in spite

of using specially selected towing cable, the acceleration measured over the full length of the flume was very small. Hence it was evident that the concept of a conical pulley by itself was not sufficient for this purpose. One of the reasons which account for this is that the difference in end diameters of the pulley was not large enough to obtain the desired change in velocity, noting that the choice of maximum diameter was restricted by weight and inertia considerations. The extension of the towing cable under an increasing load also contributed to this deficiency.

In order to overcome this problem, a regulator was attached to the motor and on increasing the rotational speed of the motor from zero to its maximum value, it was observed that a nearly constant acceleration could be achieved. This procedure was first done manually and in order to eliminate any human error and to obtain justifiable repetitive results a control motor (with D.C. supply) with gear box was attached to the regulator. By this method it was possible to increase uniformly the speed of the motor which drives the pulley. By varying the D.C. input voltage of the control motor it was possible to obtain different values of constant acceleration for the carriage. For this study, by using D.C. supplies of 4v and 6v, it was possible to obtain two values of constant acceleration with averages of 0.2 m/sec^2 and 0.4 m/sec^2 respectively.

The facility also permitted tests to be performed under constant velocity. For a constant position of regulator it was observed that the carriage moved at constant velocity for more than half the distance and accelerated very slightly towards the end of the flume. By varying the position of the regulator it was possible to obtain at least four different test conditions of constant velocity.

4.4.5. Initial stages of motion

Since the carriage was moving on metal rails it offered hardly any resistance and the initial forward thrust at the commencement of a run produced sufficient momentum to create a sag in the cable thus establishing a discontinuity in the towing concept. In effect the carriage was moving faster than the towing cable. This phenomenon was observed in the early stages of the movement. In order to eliminate this effect, weights were placed symmetrically on the carriage to increase the weight of the system. In addition the carriage was held with the cable taut at the commencement of each run. This ensured that the carriage was always towed throughout the experimental run with the towing cable in tension.

However, in spite of these precautions it was not possible to ensure a

region of constant acceleration at the very beginning of the motion. Allowing for the time taken for the cable to relieve itself of any minor sag, it is not surprising that a non-linear relationship exists during the initial phase. This problem was also encountered by Gibson and Wang (1977) when towing a model of pile clusters. Therefore it was decided not to incorporate measurements taken in that region into the computational process, attention being restricted to that portion of each test for which uniform acceleration was proved to exist.

4.4.6. Final stages of motion

It was observed that as the carriage accelerated, the block of units, although having an overall porosity of approximately 0.6, produced a water surface gradient in front of it similar to a bow-wave. However, this effect was only observed towards the end of the run when the speed was relatively high. To reduce this effect a series of honeycomb filters was placed close to the end of the flume. Although this reduced the phenomenon to a great extent it was decided not to include measurements taken in this region in the subsequent analysis because of the unreliability associated with it. However it should be appreciated that even under normal conditions a surface gradient would exist across the porous block structure (having the length of three hollow block units) due to the head loss caused by the motion of the assembly in initially still water. The influence of this effect on the present study will be considered in the next section when discussing the selection of the initial water level for the experiment.

4.4.7. Determination of still water depth

The determination of the still water depth for this experiment had to be given much consideration. If the water level was maintained at the top surface of the instrumented unit it was observed that surface distortion caused by the motion completely submerged the unit and the force recorded would include a component due to the immersed cylindrical section of the transducer.

Although the motion of the carriage produces an increase in water surface level at the forward interface, the relative motion between water and the assembly of units causes a head loss opposite to the direction of motion. The build up of head in front of the block structure is induced by its own motion. If this phenomenon is viewed from another frame of reference relative to the hollow block units, it is equivalent to accelerated flow through a porous block structure.

By performing several experimental runs with varying water depth it was

possible to select a suitable depth in which most of the unit was immersed but not completely submerged, to ensure that the fluid was not in contact with the cylindrical portion of the transducer. Furthermore it was also observed that as the carriage moved forward the build up of head in front of the structure was not excessive for a considerable length along the flume.

These considerations were also applied to the selection of appropriate lengths of an individual 'run' for subsequent analysis. It should be stressed that considerable time had to be spent with the aid of video equipment to obtain the required state of motion within each 'run'. Before the commencement of each experimental series several trial runs were performed for this purpose.

Goring and Raichlen (1979) in their study on drag forces on block bodies used an independently supported hollow tube with a streamlined cross–section to shield the transducer from major hydrodynamic forces. Their tests were conducted under submerged conditions. Although a similar shielding member could have been adopted for the present study it was not necessary to do so because the precautions taken proved to be very effective.

4.4.8. Vibrations in the apparatus

It became apparent early in the experimental programme that the carriage motion caused vibrations of the force transducer that precluded a simple analysis of the recorded signal. Appropriate modifications were made to the assembly which supported the units in order to minimize this effect. These modifications in some way or other increased the rigidity of the whole structural unit. It should be recognized that a moving body in general introduces vibrations and sufficient care should be exercised not only in the design of apparatus but also when analyzing the results obtained. Further discussion on this subject will be given in the analysis of results.

4.4.9. Experimental procedure

Constant acceleration and constant velocity tests were performed on block assemblies of Cobs, Sheds, Hobos and the Cylat. In the case of the latter a small cylindrical structure with approximately same dimensions as those of the other block structures was assembled using wooden dowels of diameter 20 mm and the Cylat unit was placed in position inside it. In effect the Cylat was in motion in an environment of a cylindrical lattice structure.

For each medium constant velocity tests were performed for at least five different magnitudes and constant acceleration tests were carried out for two different magnitudes. Several tests were duplicated to assess the repeatability of the results and to evaluate the performance of the experimental set-up with regard to its application to investigate this type of phenomenon. In each run the force acting on the unit and the motion of the carriage were recorded simultaneously via force transducer and microswitches. This was achieved by using an analog-digital converter in conjunction with a micro-computer and the measurements, which were collected at a sampling rate of 50 per second, were channelled to floppy disc storage. Fig. 4.5 illustrates the details of the experimental set-up used for the study.

4.5. Tests on a model breakwater section

4.5.1. Reflection, run-up and run-down tests

The tests on a model breakwater section were also performed in the 55 cm wide flume and the structure was assembled at the opposite end to that of the wave generator which is also a plunger type, very similar to that in the 30 cm wide flume.

The procedure adopted to measure the reflection was the same as that utilized for the oscillatory flow tests in the second phase of the project. It should be noted that the standing wave system produced due to reflection from a sloping surface is very similar to that from a vertical face (Fig. 4.6) but sufficient time should be given for this system to be developed. For steep slopes similar to that used in this study the standing wave continues to be very well-defined. However if the slope is shallow it could be difficult to monitor the incident/reflection wave system and the results may not be very reliable.

Apart from reflection coefficients, an additional wave probe was used to monitor run-up and run-down. For different armour layers these parameters were measured for varying heights at selected wave periods of 1.0, 1.5 and 2.0 secs. In all cases the underlayer and the core remained unchanged.

This technique was previously used by Stickland (1969) for tests performed on Cobs during their evolution. The model unit was of side length 5.93 cm and various combinations of slopes were investigated. Stickland's study included a breakwater slope, as well as a completed trapezoidal breakwater structure. The results of these tests were re-analyzed to extract further information.

Gunbak (1979) also used this technique for measurements on model breakwaters.

4.5.2. Measurement of lift and along-slope force

These tests were limited to Shed armour units and were performed on the model breakwater section used for reflection, run-up and run-down tests. The measurements were made on a centrally located armour unit positioned in the region where the still water level meets the breakwater at a water depth of approximately 25 cm. The experimental set up is illustrated in Figs. 4.7 and 4.8. Under these conditions the instrumented armour unit will be subjected to wave impact forces.

There are several important observations to be made in relation to the experimental set-up and its simulation of prototype conditions.

In reality the hollow block armour units are placed in contact with each other on all four sides. The bottom of the armour unit rests on the underlayer. Thus the lifting force on a given unit will be resisted by its weight and frictional forces acting between the contact surfaces of the units. The along-slope force will be resisted by its weight, the frictional forces acting between the bottom surface of the armour unit and the underlayer and by both shear and direct forces between adjacent units. The most critical case corresponding to lifting will occur in the absence of these frictional forces, that is when the unit is not in contact with its neighbours. It was decided to measure the wave forces, both lift and along-slope, corresponding to this situation. It should be noted that it is extremely difficult to model accurately the frictional forces acting between the units and the forces considered in this study relate to those acting on the unit in the absence of both side and bottom friction.

From the foregoing discussion it is evident that a certain amount of space had to be left around the instrumented armour unit in order to simulate the conditions specified. There were two alternatives available for this purpose.

The first was to reduce the size, on all sides, of an existing armour unit to ensure the required clearance. However, if this procedure was adopted it would have, to a certain extent, affected the geometry of the unit, particularly the two dimensional porosity of the interface and thus the projected area of the surfaces. Since Sheds possess high overall porosity, this method will cause an appreciable reduction in the percentage of solid material in the armour unit.

The second alternative was to introduce spacer material which would provide required spacing on all four sides. This method was adopted for the investigation and to ensure that spacer material did not interfere with the flow inside the armour units, porous frames made of perspex were used for this purpose. As illustrated in Fig. 4.8, eight such porous frames were used for the experimental set-up.

There were two other conditions to be satisfied in relation to the positioning of the instrumented armour unit. It was necessary to ensure both that the bottom surface of the armour unit was not in contact with the underlayer and that the top surface of the same was not protruding above that of the other armour units of the breakwater slope.

Failure to satisfy the first condition would have resulted in the armour unit striking the underlayer under the action of waves. If the second condition is not satisfied, the recorded along-slope force will have an additional component due to forces acting on the exposed surface area. This component will depend on the projected area of the exposed surface. If these two conditions are not satisfied the forces recorded will be different to that acting on a typical armour unit free to move perpendicular to the slope but contained within the armour assembly.

The forces on the unit were measured by using a strain gauged cantilever beam of square section with its fixed end firmly attached to a steel plate placed on the side of the flume. It was enclosed in a brass tube which was independently attached to the steel plate and this tube passed through the opening of the hollow block armour units. The transducer was very slightly longer than the tube and the armour unit on which the forces were to be measured was firmly attached to its end. The space between the tube and the cantilever beam was filled with grease.

The geometry of the underlayer was slightly modified beneath the instrumented unit in order to provide sufficient space between the bottom surface of the unit and the underlayer. This arrangement also ensured that the top surface of the instrumented armour unit was aligned with the corresponding surfaces of the other units in the armour assembly.

It should also be noted that the external diameter of the brass tube was smaller than that of the internal opening of Shed model units and as a consequence, it did not cause total obstruction of flow through the armour units during wave action.

Apart from the lift and along-slope forces, measurements were also made of the run-up and run-down on the breakwater slope and of the wave height at the toe of the structure. These measurements were made using the technique described earlier in Sections 4.3.7, 4.3.8 and 4.5.1.

4.5.3. Force transducer

The force transducer is illustrated in more detail in Fig. 4.9. It consists of a cantilever beam ABCD. The portions AB and CD are of section 6 x 6 mm. The cross-section corresponding to the length BC was uniformly reduced on all four sides to exhibit better bending properties. The reduced section was instrumented with pairs of strain gauges on each side to produce two full bridges for the measurement of lift and along-slope forces.

Since the transducer was to be submerged during the experiment, it was necessary to use an efficient water-proofing technique to ensure that the strain gauges remain well protected. In addition, a protective sleeve was shrunk along the entire length of the transducer. It was also ensured that the water-proofing surface was well clear of the internal surface of the brass tube.

For reasons explained in the previous section, the external diameter of the brass tube was restricted and as a consequence it was necessary to use a very small cross-section for the cantilever beam. It was also essential that the cantilever beam was centrally located inside the brass tube and that it did not strike the inside surface of the tube under wave loading.

The cross-section of the cantilever beam was mainly governed by the width of the strain gauges used for the study and by considerations presented in Section 4.4.2 in relation to the transducer used for the constant acceleration tests.

To ensure the rigidity of the entire experimental set-up, the fixed end of the cantilever beam was firmly attached to a vertical steel plate which was part of a rigidly attached steel frame, loaded for stability. Under these conditions no movement of the frame was possible and it remained so during wave action on the breakwater.

Calibration of the force transducer was performed by loading the armour unit at its centre by weights hung over a pulley system. This was done before and after each series of experimental runs for both lift and along-slope forces. It was observed that on all occasions the transducer responds in a linear manner to

an applied force in either direction and no variations were observed in the calibration coefficients for both lift and along-slope forces.

Another important aspect of the experiment relates to the positioning of the transducer and the instrumented armour unit in relation to the breakwater slope 1:1 1/3 (36.87 deg). This aspect is further illustrated in Fig. 4.10.

In fixing the armour unit on to the cantilever beam it was necessary to ensure that the surfaces corresponding to those of the transducer and the armour unit, indicated by lines PQ and RS, were parallel. When placing the transducer on the breakwater slope it was necessary to ensure that PQ (and RS) was parallel to the breakwater slope indicated by line XY. In addition, the top surface of the instrumented unit (RS) had to be aligned with the corresponding surfaces of the other armour units in the assembly. This required precise positioning of the transducer when attaching it to the steel side plate. It is only if these conditions are met that the measured force will correspond to the lift and along-slope forces.

4.5.4. Experimental procedure

The experimental procedure adopted for these tests was very similar to that of reflection, run-up and run-down tests described in Section 4.5.1. Simultaneous recordings of wave run-up and run-down, wave height at the toe of the structure, lift force and along-slope force were obtained for wave periods of 1.0, 1.5 and 2.0 seconds. At a given period, wave height was varied to obtain values of different wave steepness.

All measurements were made after the flow had stabilized. The force transducer and the wave gauges were connected to an analog-digital converter in conjunction with a micro-computer. A sampling rate of 200 per second was used for all four channels and data was stored on floppy discs. Fig. 4.11 illustrates the details of the experimental set-up and the instrumentation used for the study.

When performing reflection tests on breakwater slopes a wave filter was placed in front of the wave generator. Although this reduced the wave height, it produced a well-defined wave record which was desirable for analysis when using the loop-node technique. However in this phase of the project the emphasis was to obtain the maximum possible wave height which would generate greater impact forces on the instrumented armour unit. Hence a wave filter was not used and as a consequence the wave record at the toe of the structure was not expected to be as smooth as those observed in the earlier phase of the project.

Prior to any readings being taken an inspection was made to ensure that the instrumented armour unit did not strike the underlayer or neighbouring armour units during wave action. For the experimental conditions used for the study, the movement of the force transducer was very small and there was no possibility of the transducer making any contact with the inside surface of the brass tube.

During the experimental programme it was observed that the brass tube did not contribute towards a change in the flow pattern in its vicinity. There was sufficient space left between the tube and the armour units for water to move freely and as a consequence no visible build-up of water mass was observed in that locality. The water surface profile along the row of armour units containing the instrumented unit remained approximately constant.

4.6. Measurement of physical properties for random porous media

4.6.1. Porosity

Porosity had to be measured only in the case of randomly packed media. In all other cases it could be determined either by volumetric calculations or by knowing the specific gravity of the material. This was because the media consisted of well-defined assemblies generated by repetitive placing of the basic element. Thus actual measurement of porosity had to be made on randomly packed glass spheres and rounded stones. The porosity of these media was not measured in place inside the flume due to experimental difficulties. Instead the related properties namely, porosity, specific gravity and equivalent spherical diameter - which is applicable to rounded stones only - were measured by filling a box of rectangular dimensions with material packed in a similar fashion to that used in the preparation of experimental media. This method has been previously adopted by Keulegan (1973) for a study on rockfill media.

The porosity was obtained by weighing the media dry and submerged to the top surface, and subtracting the two quantities to determine the weight of water occupying the pores. Dividing the pore water weight by the weight of water occupying the same gross volume as that of the media yields the required value of porosity. The rectangular container used for this exercise had dimensions of the same order as that of the porous media used for the experiments.

Thus if W_w is the net weight of the container filled with water, W_s is the net weight of the container filled with media and W is the net weight of the container filled with media and water, the porosity is given by

$$n = \frac{W - W_s}{W_w} \tag{4.16}$$

Porosity measurements were also made on the interlocking type of armour units namely Dolos and Stabits. Although the units were packed in a predetermined manner, the resulting void matrix was rather complex. These measurements confirmed the values of porosity given by previous investigators who used the same placing arrangement.

4.6.2. Relative density

With the porosity known, the relative density is determined directly by dividing the dry weight of the assembled media by the weight of water occupying the same volume as that of the solids in the media.

$$R.D. = \frac{W_s}{(1-n)W_w} \tag{4.17}$$

4.6.3. Equivalent spherical diameter

The equivalent spherical diameter for the rounded stones is calculated by dividing the volume of solids by the number of particles in the sample and equating this to the volume of a sphere of unknown diameter. This simply requires that the equivalent sphere has the same volume as the mean particle volume. Thus if γ_w is the relative density of water, N is the number of particles in the sample, then the equivalent spherical diameter, d_s, is given by

$$\frac{\pi}{6} d_s^3 = \frac{W_s}{N(R.D).\gamma_w} \tag{4.18}$$

It should be noted that sufficient care should be taken to remove air bubbles from the pores before submerged weight measurements are performed. No corrections were made for wall effects and it is assumed that the use of a large container to accommodate more material reduced its influence on the measurement.

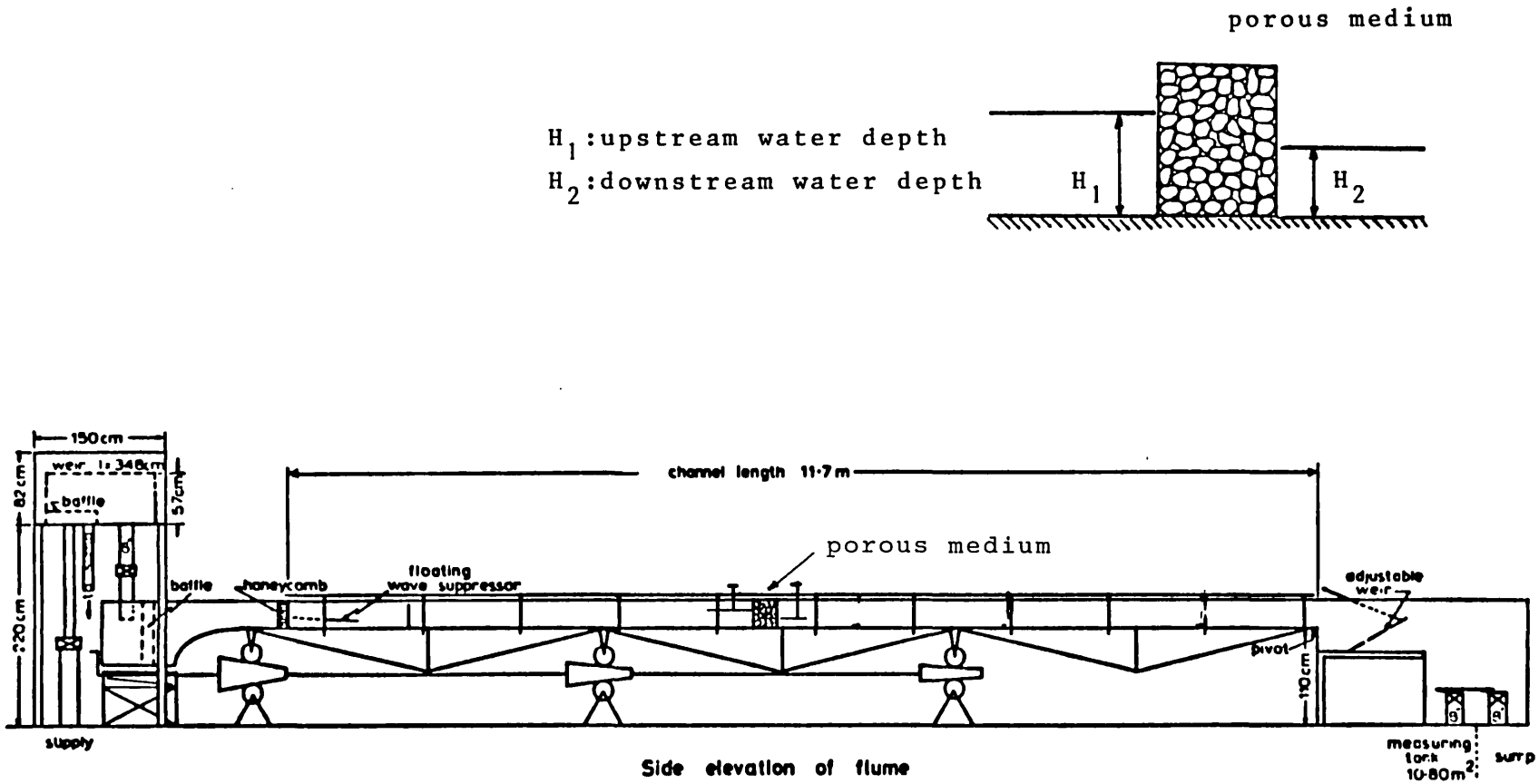


FIG.4.1 EXPERIMENTAL EQUIPMENT FOR STEADY FLOW PERMEABILITY TESTS

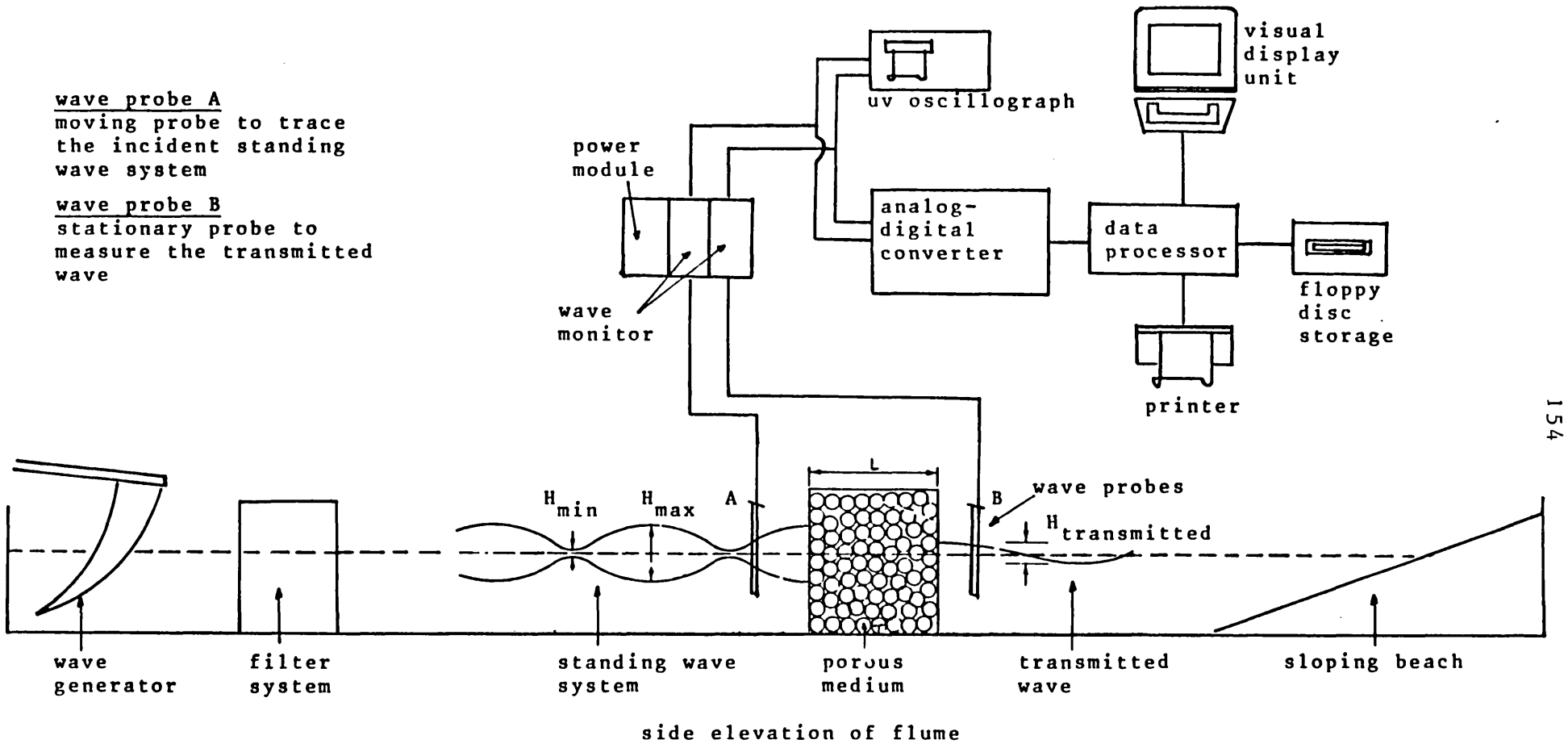


FIG.4.2 EXPERIMENTAL EQUIPMENT FOR OSCILLATORY FLOW TESTS

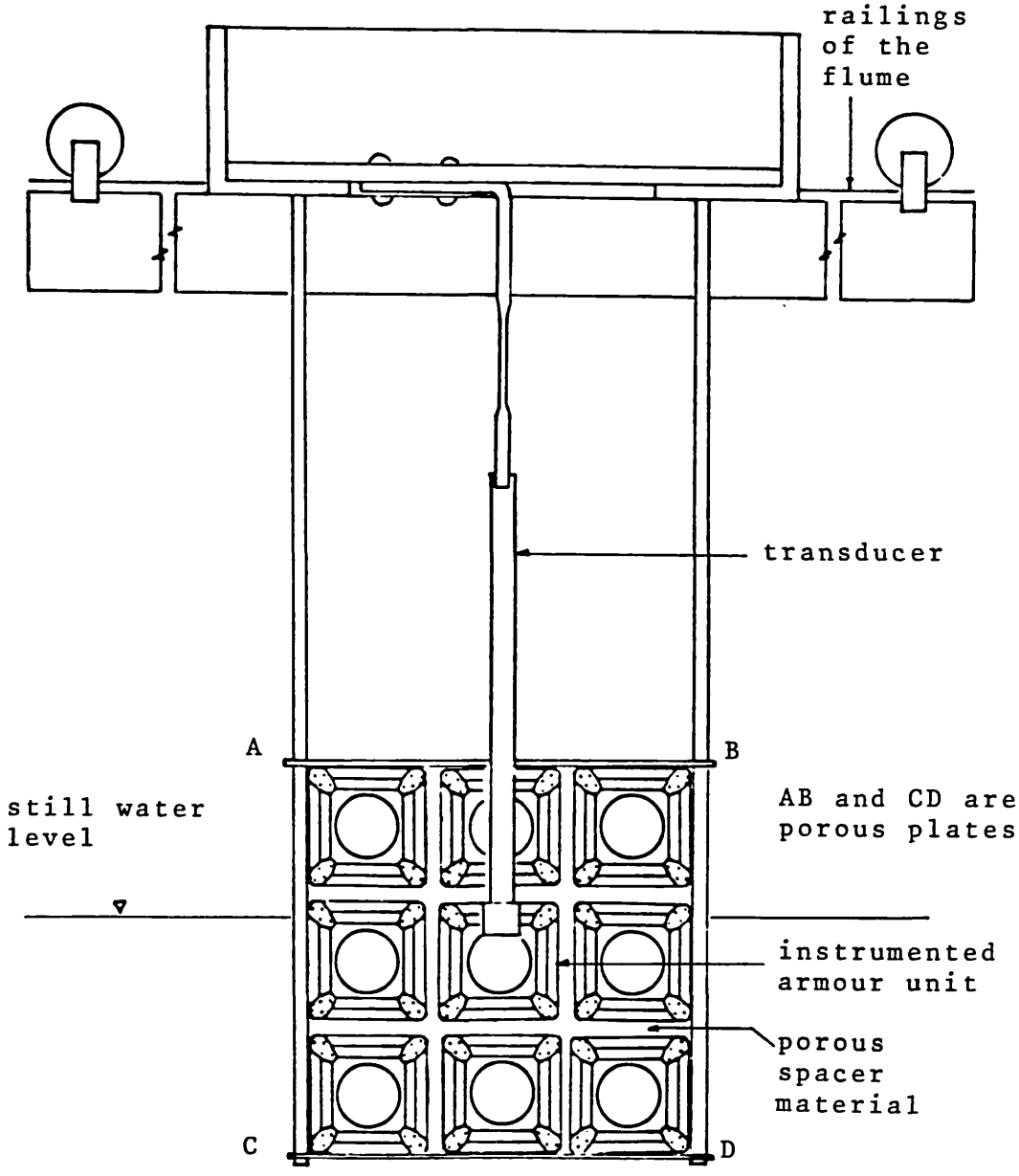


FIG.4.3 CROSS-SECTIONAL ELEVATION OF THE MOVING POROUS BLOCK FOR UNIDIRECTIONAL CONSTANT ACCELERATION TESTS

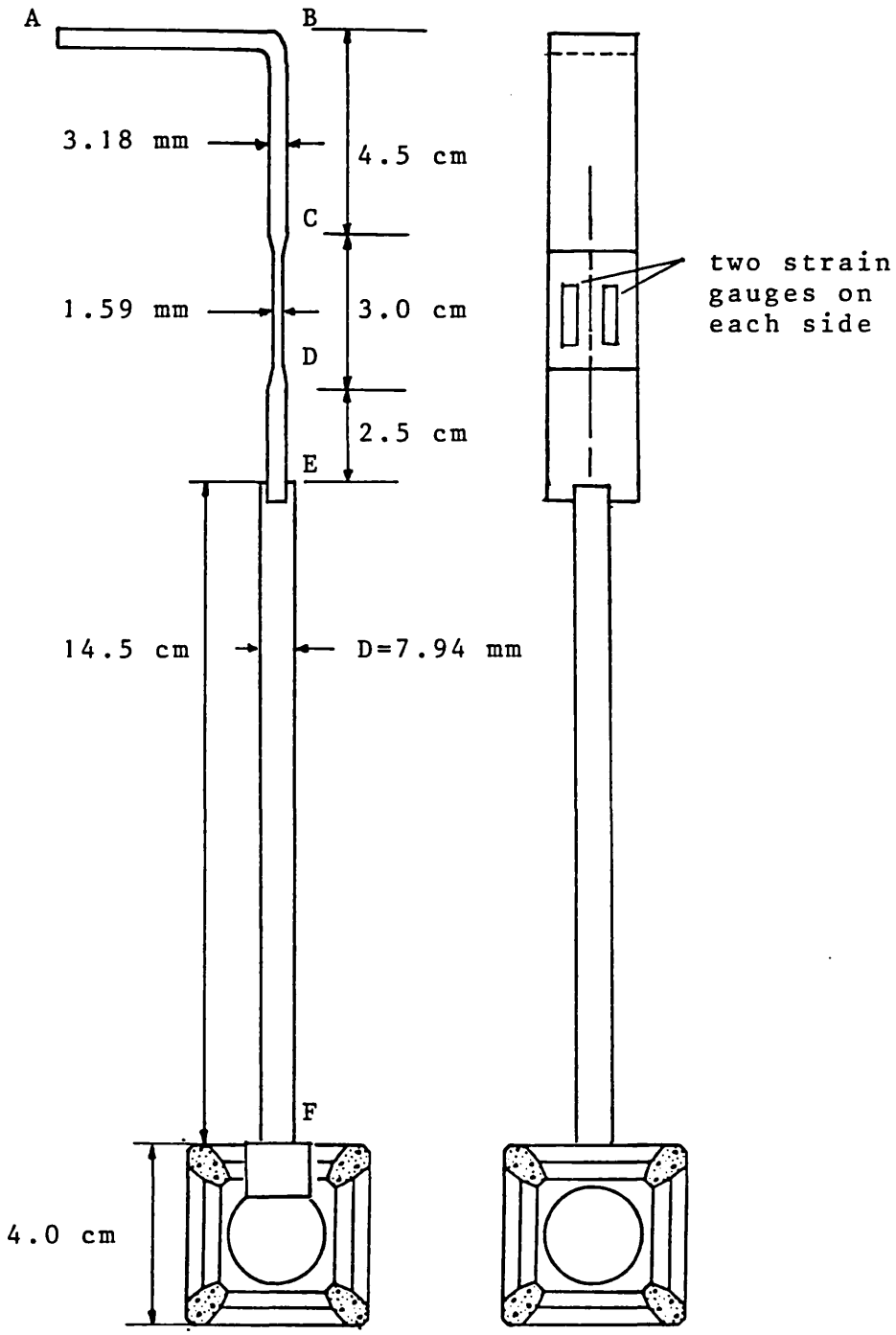


FIG.4.4 DETAILS OF THE FORCE TRANSDUCER USED FOR THE ACCELERATION TESTS

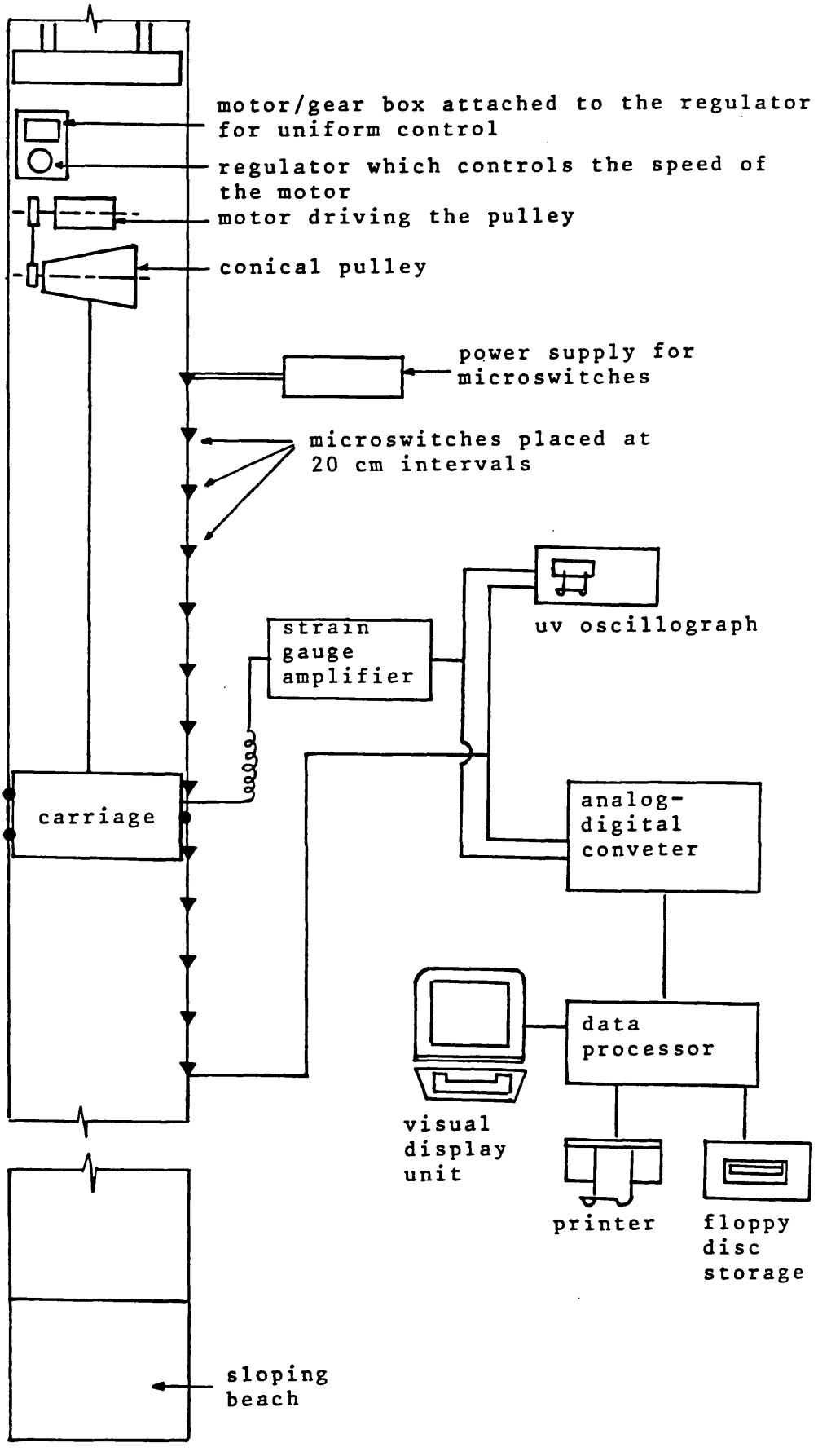


FIG.4.5 EXPERIMENTAL EQUIPMENT FOR UNIDIRECTIONAL ACCELERATION TESTS

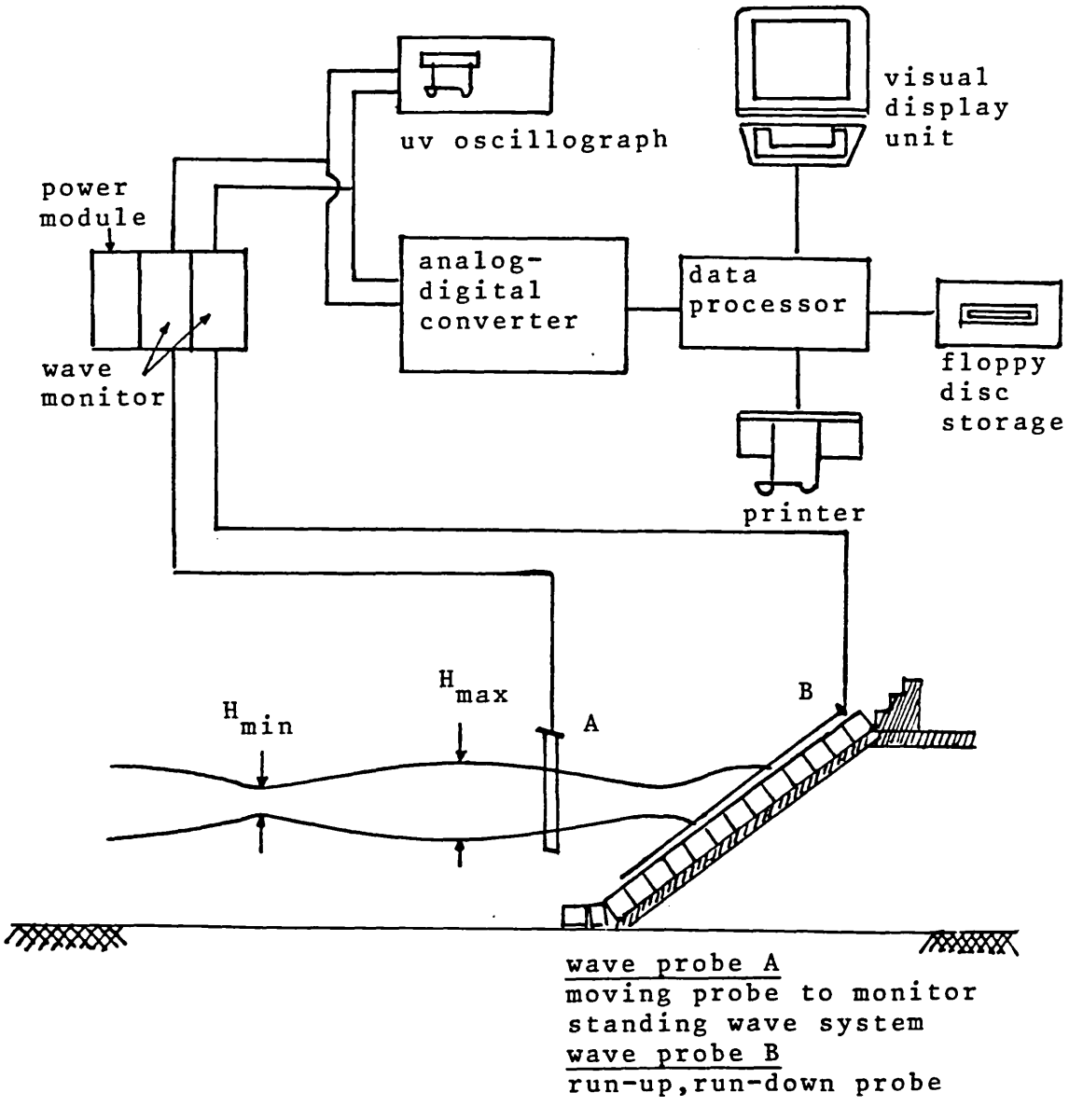


FIG.4.6 EXPERIMENTAL EQUIPMENT FOR REFLECTION,RUN-UP AND RUN-DOWN TESTS ON THE BREAKWATER SECTION

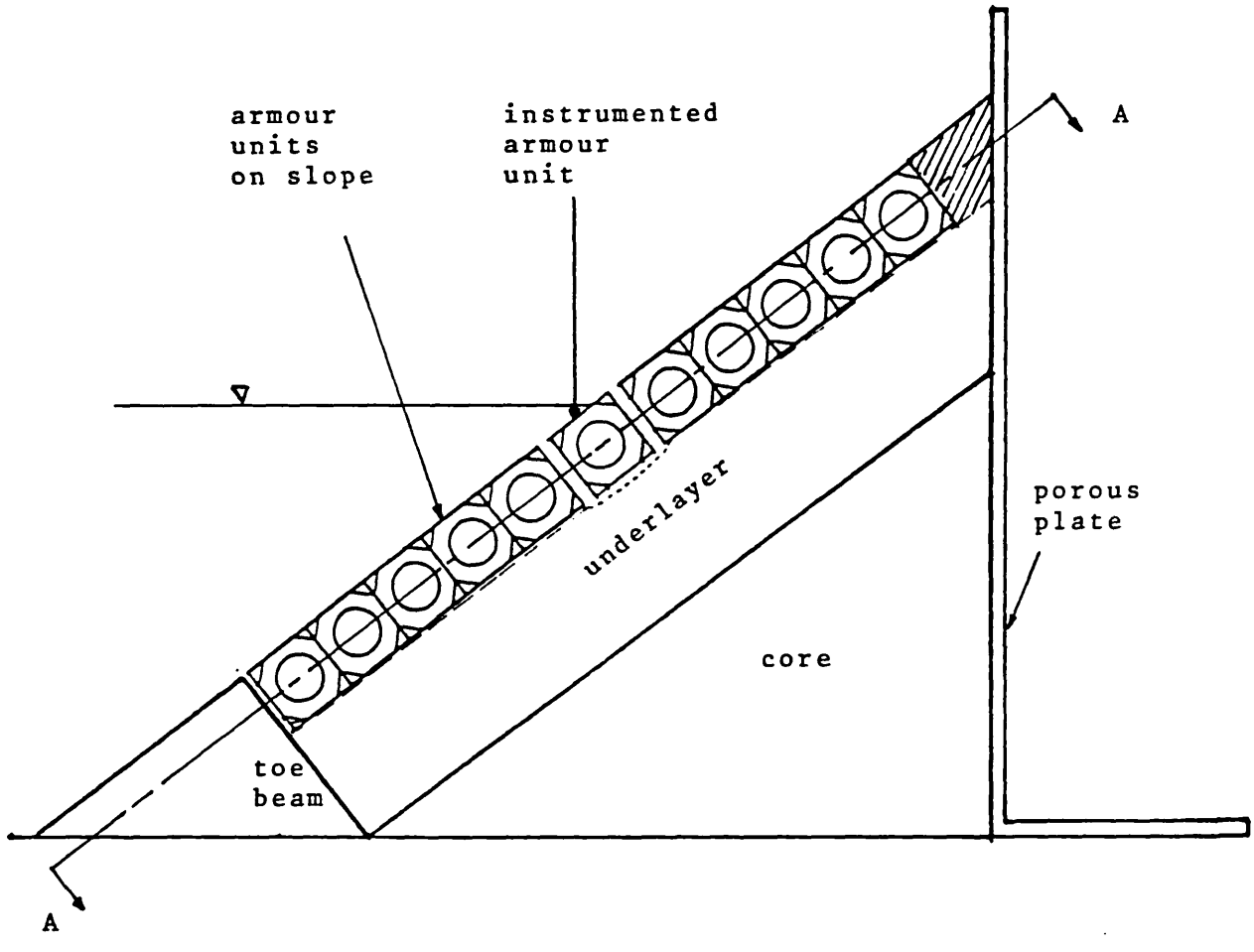


FIG.4.7 CROSS-SECTIONAL ELEVATION OF THE MODEL BREAKWATER

X:instrumented armour unit
1,2,3,4,5,6,7,8:porous spacer material

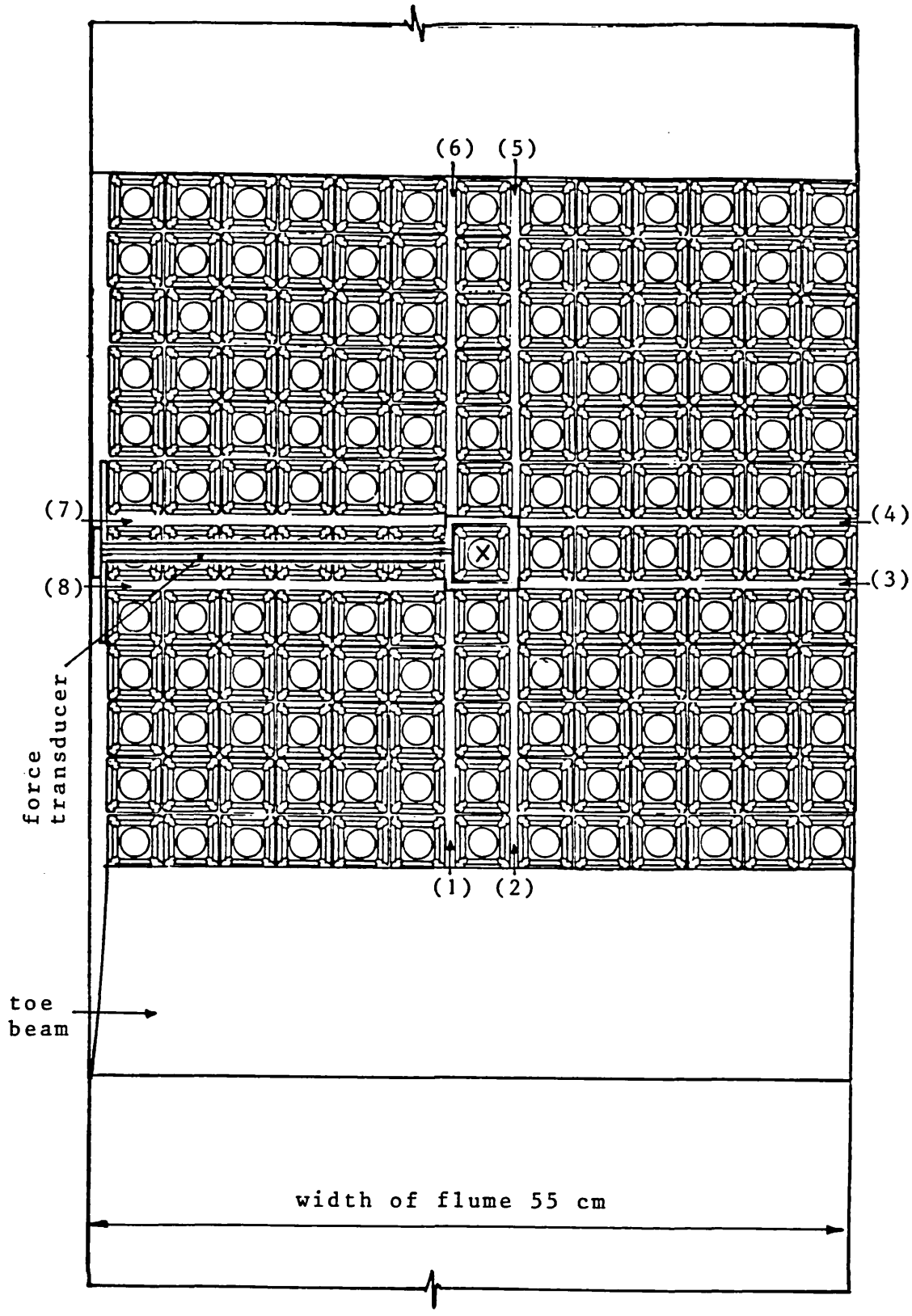


FIG.4.8 PLAN VIEW OF THE MODEL BREAKWATER -SECTION A-A ,FIG.4.7

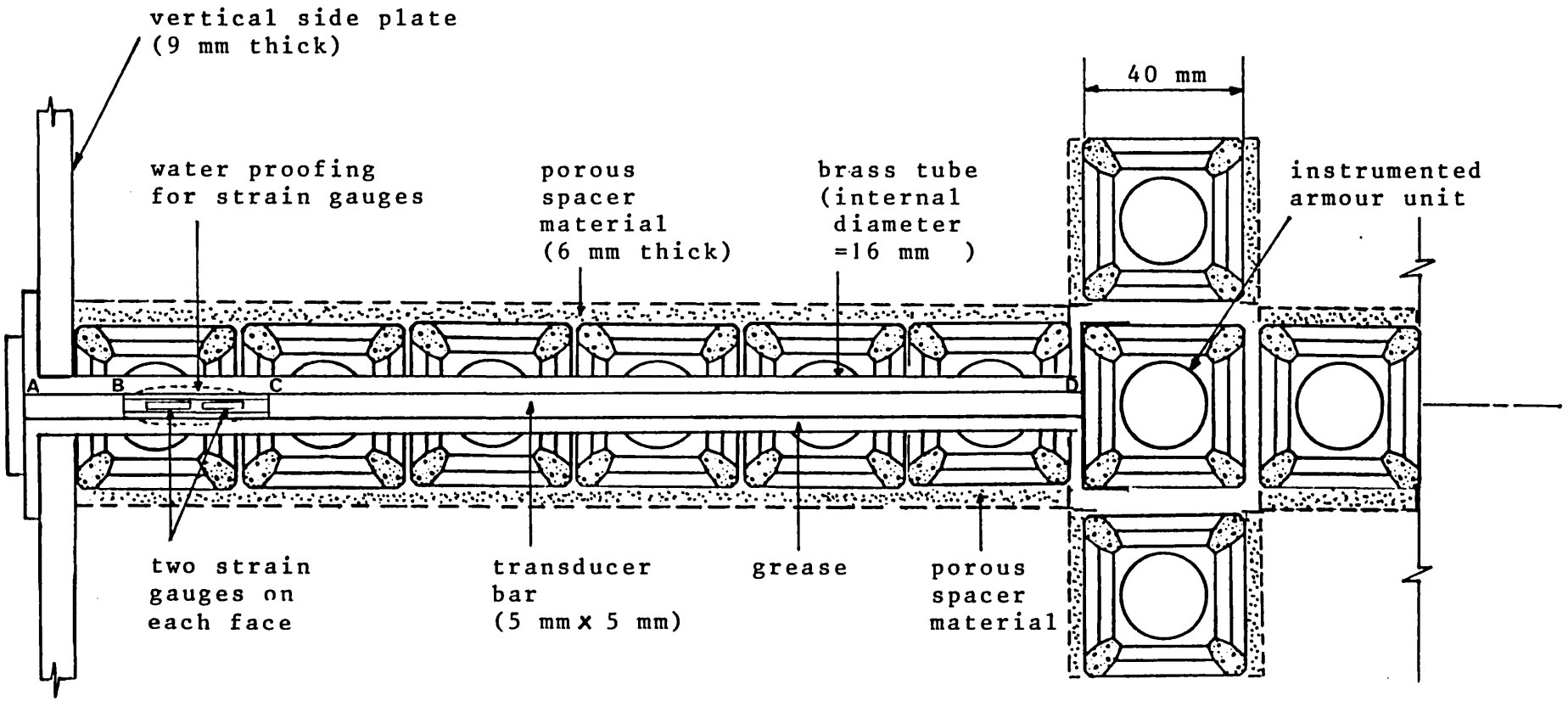
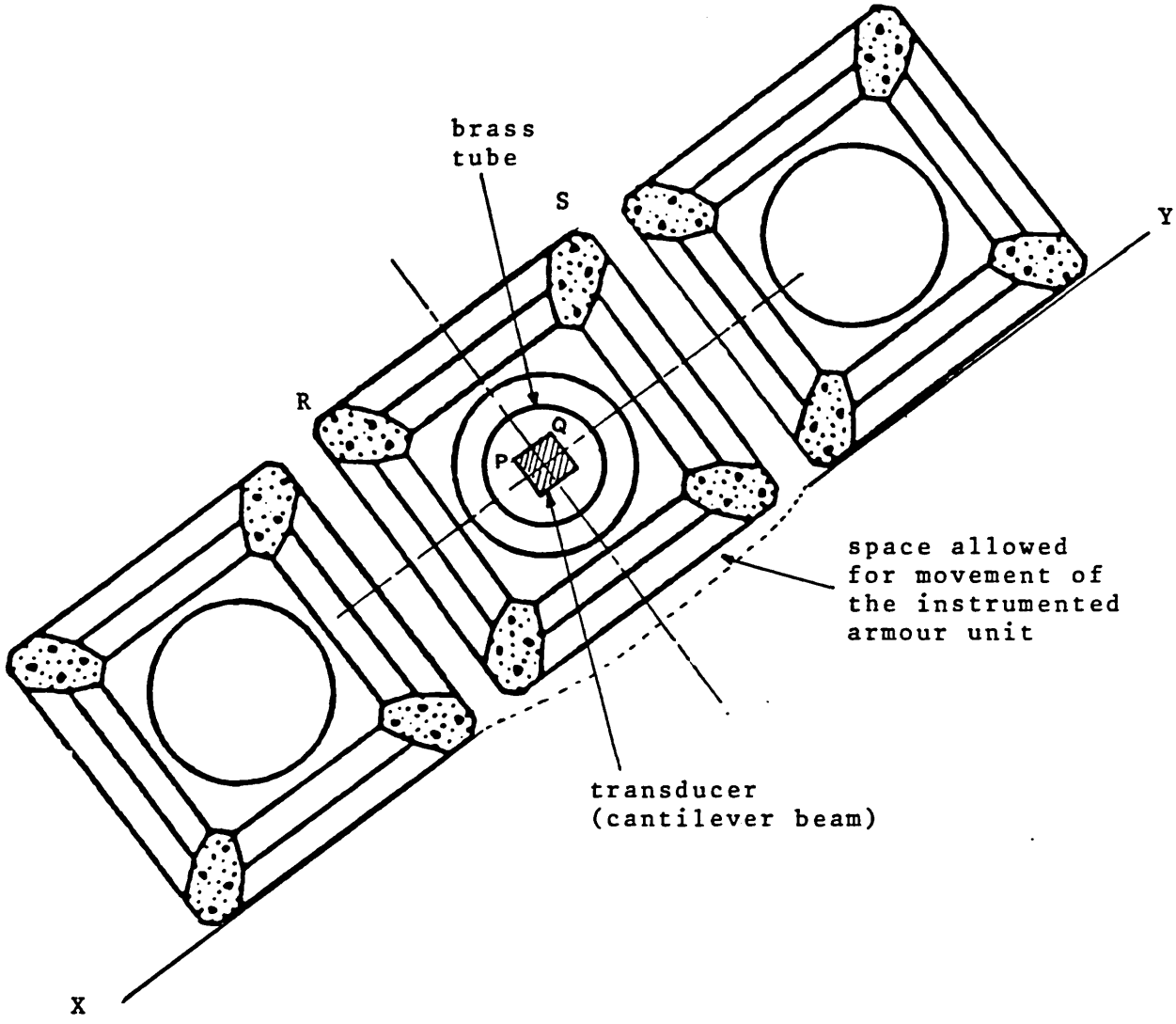


FIG.4.9 DETAILS OF THE FORCE TRANSDUCER



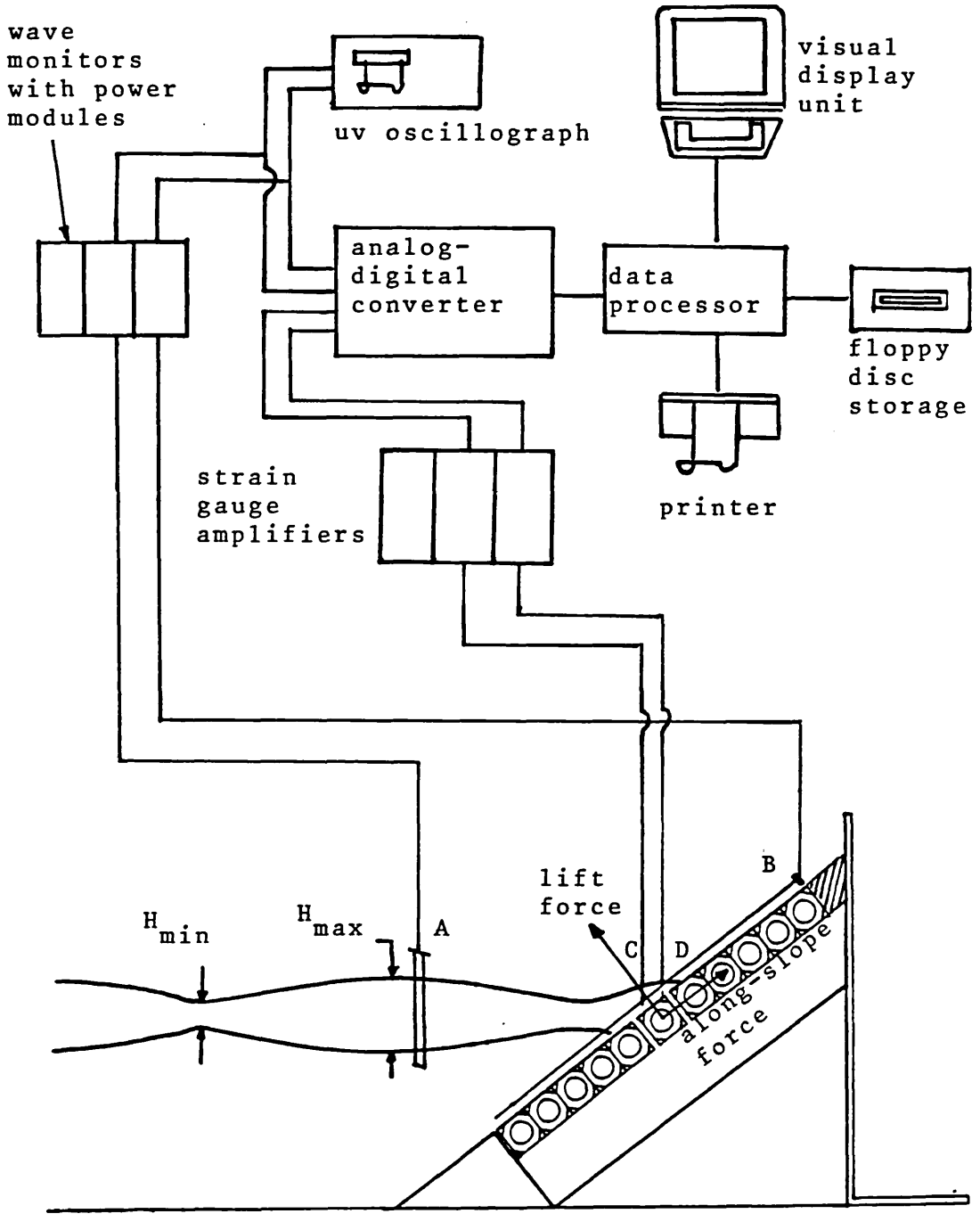
PQ surface of the transducer bar

RS top surface of the armour unit

XY slope of the underlayer (1:1 1/3)

For correct simulation,PQ,RS and XY should be parallel to each other.

FIG.4.10 DETAILED VIEW OF THE INSTRUMENTED ARMOUR UNIT



A:probe to measure wave height at the toe
B:probe to measure run-up and run-down
C:measurement of lift force
D:measurement of along-slope force

FIG.4.11 EXPERIMENTAL EQUIPMENT FOR MEASUREMENT OF LIFT AND ALONG-SLOPE FORCE ON THE BREAKWATER SECTION

CHAPTER 5 - THEORETICAL DEVELOPMENTS

5.1. Introduction

This chapter presents the theoretical developments relating to wave transmission and reflection through porous structures. Initial analysis will be limited to rectangular structures with and without a vertical impermeable face at the back (closed block and open block structures). Both analytical and numerical methods will be developed to analyse the problem. At a later stage modifications required for the inclusion of sloping sections will be discussed.

The basic structural forms considered in the analysis are illustrated below. They are considered to be homogeneous and isotropic porous structures with a horizontal bottom and are of length l located between x = 0 and x = l. The incident regular waves are assumed to be linear shallow water waves which do not break at the interface.

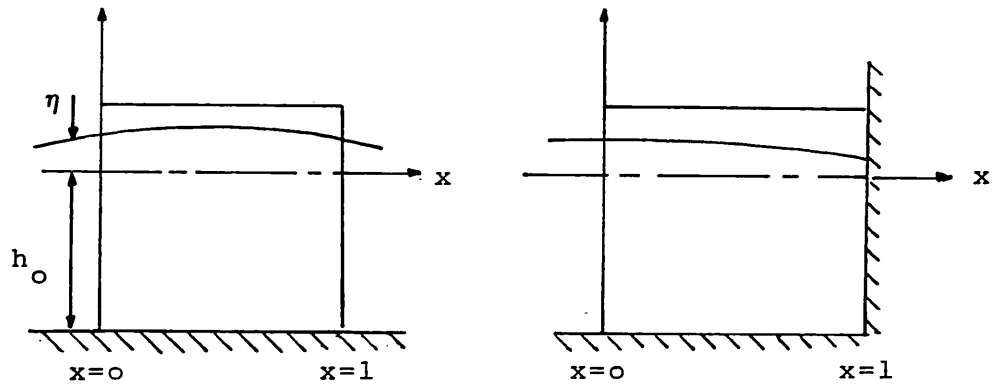


Fig. 5.1. Structural configurations used for analyses.

5.2. Governing equations

Continuity and momentum equations governing the motion outside the structure are expressed as,

$$\frac{\partial \eta}{\partial t} + \frac{\partial}{\partial x}\left\{u(h_o + \eta)\right\} = 0 \qquad (5.1)$$

$$\frac{\partial u}{\partial t} + u\frac{\partial u}{\partial x} + g\frac{\partial \eta}{\partial x} + \frac{1}{2}\frac{f_w|u|u}{(h_o + \eta)} = 0 \qquad (5.2)$$

where η is the free surface elevation relative to still water level.

h_o is the constant depth outside the structure.

u is the horizontal water particle velocity.

f_w is the wave friction factor which relates the bed shear stress, τ_b, to the kinematics of flow and expressed as,

$$\tau_b = \tfrac{1}{2}\rho f_w|u|u \qquad (5.3)$$

$|u|$ is the absolute value of velocity.

Continuity and momentum equations governing the motion inside the structure are expressed as,

$$n\frac{\partial \eta}{\partial t} + \frac{\partial}{\partial x}\left\{u(h_o + \eta)\right\} = 0 \qquad (5.4)$$

$$s\frac{\partial u}{\partial t} + s\frac{u}{n}\frac{\partial u}{\partial x} + gn\frac{\partial \eta}{\partial x} + gnFu = 0 \qquad (5.5)$$

where u is the horizontal component of the macroscopic velocity (discharge velocity).

n is the porosity.

F is the non-Darcy friction term. The Forchheimer equation is used to estimate this term and is expressed as,

$$F = a + b|u| \qquad (5.6)$$

a and b are steady, laminar and turbulent flow coefficients related to the hydraulic gradient by the expression,

$$I = au + bu^2 \qquad (5.7)$$

s is a factor expressing the effect of unsteady motion and is given by,

$$s = 1 + k_a(1 - n) \tag{5.8}$$

where k_a is an added mass coefficient.
k_a is expected to have a value between 0 and 0.5, which implies that s will vary in the region 1 to 1.5 for typical cases. In this study s will be taken as unity.

The influence of the inertia term is only significant if the constituent elements of the porous medium are widely separated. In the case of a compacted medium the flow pattern around each element interferes with that in adjoining pores and this contributes to the reduction of acceleration effects.

For flow through porous media it is important to note that the discharge velocity (u) and pore fluid velocity (u_p) are related by the expression,

$$u = nu_p \tag{5.9}$$

where n is the porosity, and that both u and u_p are velocities averaged over a flow area which is large compared with the size of an individual component of the porous medium.

5.3. Analytical developments

5.3.1. Simplifications for analytical developments

As discussed in the literature review, several investigators have considered analytical solutions to the problem of wave transmission through porous media. Although various mathematical techniques have been adopted the final expressions for transmission and reflection coefficients are very similar. The methods developed here are based on the work of Madsen (1974). However instead of obtaining a simplified explicit solution based on additional assumptions for the linearized friction factor, transmission and reflection coefficients, a more rigorous method of analysis is used to avoid such assumptions. Thus the results will be applicable over a wider range with less restrictions imposed upon their applications.

In order to obtain a closed-form analytical solution it is necessary to linearize the governing equations. For the equation of motion outside the structure it is necessary to impose the conditions that $|\eta| << h_o$ in which case $(h_o + \eta)$ will be replaced by h_o. It can be shown that under these conditions the term $u\frac{\partial u}{\partial x}$ may also be omitted.

Since the problem relates to a periodic solution, the bottom friction term is linearized by adopting the following relationship,

$$f_b\omega = \frac{1}{2}\frac{f_w|u|}{h_o} \tag{5.10}$$

where ω $(= \frac{2\pi}{T})$ is the radian frequency of the motion.

The governing equations for flow outside the structure then reduce to

$$\frac{\partial \eta}{\partial t} + h_o \frac{\partial u}{\partial x} = 0 \tag{5.11}$$

$$\frac{\partial u}{\partial t} + g \frac{\partial \eta}{\partial x} + f_b\omega u = 0 \tag{5.12}$$

The value of f_b is regarded as constant, independent of x and t. In the present analysis the influence of f_b will be neglected for flow outside the structure.

By adopting similar simplifications the equations of motion inside the structure can be linearized. The flow resistance term is represented by

$$f \frac{\omega}{n} = (a + b|u|)g \tag{5.13}$$

The value of f is regarded as constant, independent of x and t.

Consequently the governing equations are expressed as follows,

$$n \frac{\partial \eta}{\partial t} + h_o \frac{\partial u}{\partial x} = 0 \tag{5.14}$$

$$\frac{s}{n} \frac{\partial u}{\partial t} + g \frac{\partial \eta}{\partial x} + f \frac{\omega}{n} u = 0 \tag{5.15}$$

Although s is retained in the equation, it will be considered to assume a value of unity for computational purpose.

It is observed that both sets of equations relating to flow outside (eq. 5.11 and eq. 5.12) and inside (eq. 5.14 and eq. 5.15) the structure are very similar and the main differences are related to the friction factors for the two cases and the presence of porosity (n) for the latter.

In applying these equations to a particular problem it is important to note the assumptions which have been made in their derivation. For the equations which are applicable to incompressible fluid and media, it is assumed that the incident waves are long and that the pressure distribution both inside and outside the medium is nearly hydrostatic. Vertical accelerations have been neglected and the water surface is open to the atmosphere. Air entrainment and inertia effects are not considered in the analysis. Furthermore an appropriate method has to be used to evaluate the linearized friction factor (f) from the relationship given in eq. 5.13.

5.3.2. General solution of the simplified equations

In order to arrive at a periodic solution of radian frequency ω, it is convenient to express η and u in complex notation:

$$\eta = \mathrm{Re}[\xi(x)\exp(I\omega t)] \tag{5.16}$$

$$u = \mathrm{Re}[v(x)\exp(I\omega t)] \tag{5.17}$$

where $\xi(x)$ and $v(x)$ are complex functions of x only.

$\exp(I\omega t) = e^{I\omega t}$

$I = \sqrt{-1}$

The physical solution is given by the real part of the solution as indicated.

The solution for the flow outside the structure is obtained by substituting eq. 5.16 and eq. 5.17 into eq. 5.11 and eq. 5.12. The equation for ξ is found to be

$$\frac{\partial^2 \xi}{\partial x^2} + \frac{\omega^2}{gh_o}(1 - If_b)\xi = 0 \tag{5.18}$$

and v is given by,

$$v = \frac{-g}{I\omega(1 - If_b)} \frac{\partial \xi}{\partial x} \tag{5.19}$$

From the general solution η and u can be expressed as,

$$\eta = \text{Re}\left[\left\{a_1 \exp(-Ikx) + a_2 \exp(Ikx)\right\}\exp(I\omega t)\right] \tag{5.20}$$

$$u = \left[\sqrt{\frac{g}{h_o}}\frac{1}{\sqrt{1-If_b}}\left\{a_1 \exp(-Ikx) - a_2 \exp(Ikx)\right\}\exp(I\omega t)\right] \tag{5.21}$$

where a_1 and a_2 are complex amplitudes whose magnitudes give the physical wave amplitude.

k is the wave number given by

$$k = k_o \sqrt{1 - If_b} = k_o \sqrt[4]{1 + f_b^2}\exp(-I\varphi_b) \tag{5.22}$$

$$\text{in which } k_o = \frac{\omega}{\sqrt{gh_o}} \tag{5.23}$$

$$\tan 2\varphi_b = f_b \tag{5.24}$$

When the bottom friction is neglected, f_b is assumed to be zero and $k = k_o$.

The solution for the flow inside the structure is obtained by substituting eq. 5.16 and eq. 5.17 into eq. 5.14 and eq. 5.15. The equation for ξ is found to be,

$$\frac{\partial^2\xi}{\partial x^2} + \frac{\omega^2}{gh_o}(s - If)\xi = 0 \tag{5.25}$$

and v is given by,

$$v = \frac{-gn}{I\omega(s - If)}\frac{\partial\xi}{\partial x} \tag{5.26}$$

From the general solution η and u can be expressed as

$$\eta = \mathrm{Re}\left[\left\{a_1 \exp(-Ikx) + a_2 \exp(Ikx)\right\}\exp(I\omega t)\right] \tag{5.27}$$

$$u = \mathrm{Re}\left[\sqrt{\frac{g}{h_o}}\,\frac{n}{\sqrt{s-If}}\left\{a_1 \exp(-Ikx) - a_2 \exp(Ikx)\right\}\exp(I\omega t)\right] \tag{5.28}$$

where a_1 and a_2 are complex amplitudes whose magnitudes give the physical wave amplitude.
k is the wave number given by

$$k = k_o\sqrt{s - If} = k_o\sqrt[4]{s^2 + f^2}\,\exp(-I\varphi) \tag{5.29}$$

$$\text{in which} \quad k_o = \frac{\omega}{\sqrt{gh_o}} \tag{5.30}$$

$$\tan 2\varphi = \frac{f}{s} \tag{5.31}$$

5.3.3. Application to open block structures

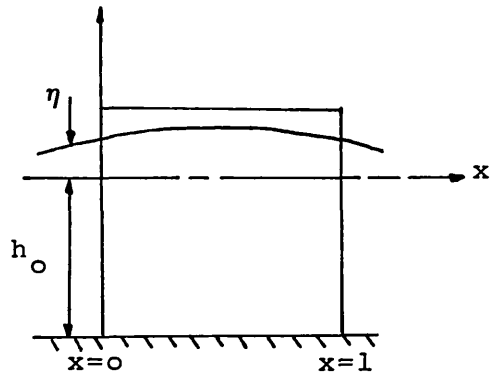


Fig. 5.2. Open block structure.

In analysing the above structure the governing equations have to be applied to three regions, namely, that occupied by the structure and the two regions outside it.

The general solution for the motion outside the porous structure is as

follows,

for $x \leqslant 0$,

$$\xi = a_i \exp(-Ik_o x) + a_r \exp(Ik_o x) \tag{5.32}$$

$$v = \sqrt{\frac{g}{h_o}} \left\{ a_i \exp(-Ik_o x) - a_r \exp(Ik_o x) \right\} \tag{5.33}$$

for $x \geqslant 1$,

$$\xi = a_t \exp(-Ik_o(x - 1)) \tag{5.34}$$

$$v = \sqrt{\frac{g}{h_o}}\, a_t \exp(-Ik_o(x - 1)) \tag{5.35}$$

where a_i, a_r and a_t are the incident, reflected and transmitted wave amplitudes. a_i is taken as real whereas a_r and a_t are complex. The magnitudes of a_r and a_t express the values of the physical wave amplitudes.

The general solution for the flow within the structure is as follows,

for $1 \geqslant x \geqslant 0$,

$$\xi = a_1 \exp(-Ikx) + a_2 \exp(Ik(x - 1)) \tag{5.36}$$

$$v = \sqrt{\frac{g}{h_o}} \frac{n}{\sqrt{s - If}} \left\{ a_1 \exp(-Ikx) - a_2 \exp(Ik(x - 1)) \right\} \tag{5.37}$$

In the above equations the unknown complex wave amplitudes are a_r, a_t, a_1 and a_2. They are determined by considering the continuity of surface elevation and velocity at the boundary interfaces.

at $x = 0$

$$a_i + a_r = a_1 + a_2 \exp(-Ikl) \tag{5.38}$$

$$a_i - a_r = \epsilon(a_1 - a_2 \exp(-Ikl)) \tag{5.39}$$

at $x = 1$

$$a_t = a_1 \exp(-Ikl) + a_2 \tag{5.40}$$

$$a_t = \epsilon[a_1 \exp(-Ikl) - a_2] \tag{5.41}$$

where $$\epsilon = \frac{n}{\sqrt{s - If}} \tag{5.42}$$

From these equations, expressions for the complex amplitude of the transmitted and reflected waves are obtained as,

$$\frac{a_t}{a_i} = \left[\frac{4\epsilon}{(1+\epsilon)^2 \exp(Ikl) - (1-\epsilon)^2 \exp(-Ikl)}\right] \tag{5.43}$$

$$\frac{a_r}{a_i} = \left[\frac{(1-\epsilon^2)\left\{\exp(Ikl) - \exp(-Ikl)\right\}}{(1+\epsilon)^2 \exp(Ikl) - (1-\epsilon)^2 \exp(-Ikl)}\right] \tag{5.44}$$

The velocity inside the structure is given by,

$$v = a_i \sqrt{\frac{g}{h_o}}\, 2\epsilon \left[\frac{(\epsilon+1)\exp(-Ikx) - (\epsilon-1)\exp(Ik(x-2l))}{(\epsilon+1)^2 - \exp(-2Ikl).(\epsilon-1)^2}\right] \tag{5.45}$$

and $$u = \mathrm{Re}\left\{v(x)\exp(I\omega t)\right\} \tag{5.46}$$

According to eqs. 5.34 and 5.32, the transmitted and reflected waves can be expressed as,

$$\eta_t = |a_t| \cos\left\{\omega t + k_o(1-x) + \varphi_t\right\} \tag{5.47}$$

$$\eta_r = |a_r| \cos\left\{\omega t + k_o x + \varphi_r\right\} \tag{5.48}$$

where a_t, a_r, φ_t and φ_r are independent of x and t.
Hence the transmission and reflection coefficients are determined from the modulus of the complex amplitudes of eqs. 5.43 and 5.44 and are expressed as,

$$K_t = \frac{|a_t|}{a_i} \tag{5.49}$$

$$K_r = \frac{|a_r|}{a_i} \tag{5.50}$$

5.3.4. Application to closed block structures (wave obsorbers)

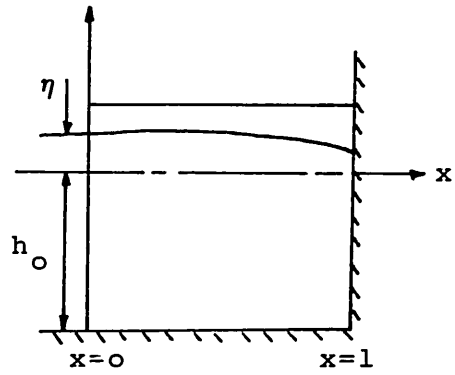


Fig. 5.3. Closed block structure.

In analysing closed block structures the governing equations have to be applied to two regions, one outside and the other inside the structure.

The general solution for the motion outside the porous structure is as follows,

for $x \leqslant 0$

$$\xi = a_i \exp(-Ik_o x) + a_r \exp(Ik_o x) \tag{5.51}$$

$$v = \sqrt{\frac{g}{h_o}} \left\{ a_i \exp(-Ik_o x) - a_r \exp(Ik_o x) \right\} \tag{5.52}$$

where a_i and a_r are the incident and reflected wave amplitudes. a_i is taken as real whereas a_r is complex.

The general solution for the flow within the structure is,

for $1 \geqslant x \geqslant 0$

$$\xi = a_1 \exp(-Ikx) + a_2 \exp(Ikx) \tag{5.53}$$

$$v = \sqrt{\frac{g}{h_o}}\,\epsilon\left\{a_1 \exp(-Ikx) - a_2 \exp(Ikx)\right\} \tag{5.54}$$

In these expressions the unknown complex wave amplitudes are a_r, a_1 and a_2. As before, the boundary conditions at the interfaces will be used to determine them.

At x = l, the velocity is zero on the impervious vertical boundary and from eq. 5.54

$$a_2 = a_1 \exp\left[-I2kl\right] \tag{5.55}$$

At x = 0, continuity of surface elevation and of velocity yields,

$$a_i + a_r = a_1 + a_2 \tag{5.56}$$

$$a_i - a_r = \epsilon(a_1 - a_2) \tag{5.57}$$

Hence the complex amplitude of the reflected wave is

$$\frac{a_r}{a_i} = \frac{(1 - \epsilon)\exp(I2kl) + (1 + \epsilon)}{(1 + \epsilon)\exp(I2kl) + (1 - \epsilon)} \tag{5.58}$$

The velocity inside the structure is given by,

$$v = a_i \sqrt{\frac{g}{h_o}}\, 2\epsilon\left[\frac{\exp(-Ikx) - \exp(Ik(x - 2l))}{(1 + \epsilon) + (1 - \epsilon)\exp(-I2kl)}\right] \tag{5.59}$$

$$\text{and} \quad u = \mathrm{Re}\left\{v(x)\exp(I\omega t)\right\} \tag{5.60}$$

According to eq. 5.51 the reflected wave can be expressed as,

$$\eta_r = |a_r| \cos\left[\omega t + k_o x + \varphi_r\right] \tag{5.61}$$

where a_r and φ_r are independent of x and t. Hence the reflection coefficient can be determined from the complex amplitude of eq. 5.58 and is given by :

$$K_r = \frac{|a_r|}{a_i} \tag{5.62}$$

It is noted that the general expressions for reflection and transmission coefficients obtained using different analytical techniques based on the long wave approximation are very similar. However two factors will have a significant influence on the final result. The first is the method of solution including the estimation of the linearized friction factor. The second is the way in which external losses and other phenomena which are not explicitly represented in the governing equations are incorporated in the solution. The range of applicability of the models with respect to both wave environment and type of structure will depend on these factors. For satisfactory agreement between experimental and predicted values due care should also be exercised in the determination of the relevant hydraulic properties of the porous medium that are included in the governing equations.

5.3.5. Determination of friction factor

In previous sections, transmission and reflection coefficients have been expressed in terms of the wave environment and the characteristics of the porous media. However, in order to arrive at a predictive solution for the types of structures considered it is necessary to evaluate the linearized friction factor represented by eq. 5.13 (i.e., $f\frac{\omega}{n} = (a + b|u|)g$).

This is achieved by invoking Lorentz principle of equivalent work which states that the average rate of energy dissipation should be the same whether evaluated using the non-linear resistance law or its linearized equivalent, and this yields :

$$\int_0^l \int_0^T f\frac{\omega}{n} u^2 \, dt \, dx = \int_0^l \int_0^T (a + b|u|)gu^2 \, dt \, dx \qquad (5.63)$$

where l is the length of structure.
T is the wave period.

Simplifying equation 5.63, f can be expressed as,

$$f - \frac{nagT}{2\pi} - \frac{nbgT}{2\pi}\Omega = 0 \qquad (5.64)$$

$$\text{where} \quad \Omega = \frac{\int_0^l \int_0^T |u|\, u^2 \, dt \, dx}{\int_0^l \int_0^T u^2 \, dt \, dx} \tag{5.65}$$

In these equations u can be determined from eqs. 5.45 and 5.59 for the type of structure considered taking the real part of the solution. However it is observed that u, and therefore Ω, is dependent of the friction factor. From this it is evident that f cannot be found explicitly from eq. 5.64 and an iterative procedure has to be adopted. Within this procedure Ω has to be determined by an appropriate numerical integration scheme. If it is assumed that the velocity inside the porous structure is independent of x, the double integral in eq. 5.65 is determined analytically to be :

$$\Omega = \frac{8}{3\pi} |u| \tag{5.66}$$

and f can be evaluated by an iterative procedure but with less computational effort. For this purpose it is appropriate to use the values of velocity at the centre of the structure. Thus f can be determined from the equation,

$$R = f - \frac{nagT}{2\pi} - \frac{nbgT}{2\pi} \frac{8}{3\pi} |u|_{\text{at } x=l/2} = 0 \tag{5.67}$$

5.3.6. Interface losses

In the analytical solutions the transmission and reflection coefficients are expressed in terms of the hydraulic characteristics (a,b), porosity (n), length of structure (l), water depth (h_o), wave period (T) and the incident wave amplitude (a_i).

It was pointed out earlier that in most laboratory flumes, the distance from the wave generator to the model is of limited length and the incident wave height cannot be measured without being disturbed by the influence of the reflected wave. With regard to porous structures the composite wave in front of the structure consists of a partial standing wave whose characteristics have already been discussed. The analytical models account for this wave system and it is seen from eq. 5.32 and eq. 5.51 that both incident and reflected wave components are

included. Hence the input wave amplitude corresponds to that of the incident wave (a_i).

With reference to the standing wave system it should be noted that in laboratory experiments the wave height at the open boundary will not strictly correspond to the height of the anti-node observed further away from the structure. Surface distortions occur in the immediate vicinity of the structure due to run-up and run-down on the vertical permeable interface. The problem is further complicated by the possible effect of air entrainment. The analytical model does not account for energy losses which occur at the interface. Since the calculation of the input wave amplitude (a_i) is based on anti-node and node heights (H_{max} and H_{min}) measured away from the structure it is necessary to include a correction factor to compensate for these effects. In the absence of such a factor the model will over-predict wave transmission.

An estimation of the interface losses can be obtained by performing a series of oscillatory flow tests on structures of negligible length but accurately representing the interface. The values of transmission and reflection coefficients from these tests can be used to evaluate a correction factor to account for these interface effects. Reference to this aspect will be made in the discussion of experimental results.

In the case of open block structures similar effects are also present at the rear interface. However their influence will be relatively small because the wave height closer to the end of the structure is reduced due to internal wave decay. In addition there is no equivalent to run-up and run-down at this interface. For the types of porous media used for this study and their geometry it was not considered necessary to include a correction factor for this effect at the rear face.

5.4. Numerical developments

5.4.1. Application to closed block structures (wave absorbers)

The primary objective of developing a numerical model for the present study is to simulate the internal non-Darcy flow in a porous structure. This would permit a detailed analysis of the influence of hydraulic and geometric characteristics of the porous matrix with regard to internal wave decay in a wave absorber.

The phenomenon to be modelled is shown in the figure below.

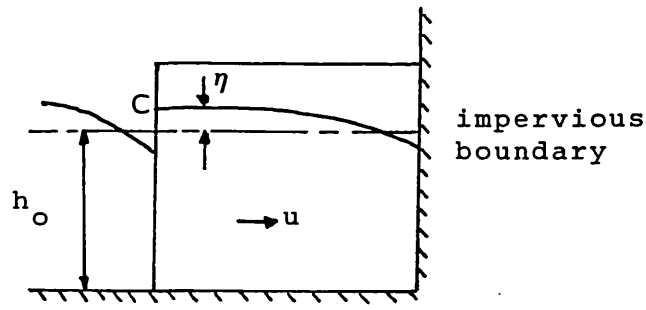


Fig. 5.4. Closed block structure (wave absorber)

The governing equations for the flow inside the structure correspond to eqs. 5.4 and 5.5.

Equations for horizontal momentum, continuity and the total differentials for u and η are expressed as,

$$\frac{u}{n}\frac{\partial u}{\partial x} + \frac{\partial u}{\partial t} + gn\frac{\partial \eta}{\partial x} = -gnFu \qquad (5.68)$$

$$\left(\frac{h_o + \eta}{n}\right)\frac{\partial u}{\partial x} + \frac{u}{n}\frac{\partial \eta}{\partial x} + \frac{\partial \eta}{\partial t} = 0 \qquad (5.69)$$

$$du = \frac{\partial u}{\partial x}dx + \frac{\partial u}{\partial t}dt \qquad (5.70)$$

$$d\eta = \frac{\partial \eta}{\partial x}dx + \frac{\partial \eta}{\partial t}dt \qquad (5.71)$$

The Forchheimer equation is used to estimate the non-Darcy term :

$$F = a + b\,|u| \qquad (5.6)$$

Hence the following hyperbolic system of differential equations will govern the flow (Abbott 1966).

$$\begin{bmatrix} \frac{h_o + \eta}{n} & 0 & \frac{u}{n} & 1 \\ \frac{u}{n} & 1 & gn & 0 \\ dx & dt & 0 & 0 \\ 0 & 0 & dx & dt \end{bmatrix} \begin{bmatrix} \frac{\partial u}{\partial x} \\ \frac{\partial u}{\partial t} \\ \frac{\partial \eta}{\partial x} \\ \frac{\partial \eta}{\partial t} \end{bmatrix} = \begin{bmatrix} 0 \\ -gnFu \\ du \\ d\eta \end{bmatrix} \qquad (5.72)$$

At this stage it is convenient to make the dependent variables u and η dimensionally identical through the transformation,

$$c = \sqrt{g(h_o + \eta)} \qquad (5.73)$$

where c represents wave celerity as obtained from the long wave approximation.

The equations of motion and continuity can now be expressed in terms of u and c as follows,

$$\frac{\partial u}{\partial t} + \frac{u}{n}\frac{\partial u}{\partial x} + 2cn\frac{\partial c}{\partial x} = -gnFu \qquad (5.74)$$

$$2\frac{\partial c}{\partial t} + \frac{c}{n}\frac{\partial u}{\partial x} + 2\frac{u}{n}\frac{\partial c}{\partial x} = 0 \qquad (5.75)$$

Of the several methods available for the numerical solution of the above set of equations, it was decided to use the finite differences.

5.4.2. Finite difference formulation and the method of solution

In using finite difference methods the objective is to solve the equations of motion and continuity for unsteady one dimensional non-Darcy flow at a finite number of grid points in the (x,t) plane. There are two basic types of fixed grid finite difference schemes namely, explicit and implicit schemes.

In an explicit method the unknown value is expressed directly in terms of the known values. For time dependent one dimensional problems such as the governing equations of the present study, this means that an unknown value at the advanced time level $(j + 1)\ \Delta t$ is calculated directly from the values at the known present time level $j\ \Delta t$ and from the values already calculated at $(j + 1)\Delta t$.

An implicit scheme, on the other hand, solves for a group of advance points through the use of simultaneous equations which include the unknowns at all points in the group. The value of the computed solution at any particular grid point depends on the solution at the adjacent grid points for the same time level.

Although the conservation of mass and momentum for any confined velocity field may be represented by a set of partial differential equations, these equations can be written in many finite difference forms. Approximation, truncation error, consistency, discretization error, convergence, stability and accuracy are the important numerical properties of any selected finite difference scheme and it is important to consider these properties to develop an acceptable predictive model.

In the present problem wave decay within a porous structure is considered and it is intended to study this decay at close intervals in order to monitor the wave propagation. For this purpose small values of Δt have to be chosen. In general, implicit methods result in higher computational cost per grid point per time step and it would be more economical to use an explicit method for this study. It should be noted that stability plays a decisive role with regard to explicit methods and it is important to ensure that the stability criteria are met without undue restrictions on Δt and Δx.

Finite difference formulations of the governing equations are presented in the next section followed by the analysis of relevant properties of the scheme adopted.

An explicit scheme with central differences in space and forward differences in time is used to discretize eqs. 5.74 and 5.75. In finite difference form the equations are expressed as,

$$u(i,\ j+1) = u(i,j) - \frac{\Delta t}{2\Delta x}\left[\frac{u(i,j)}{n}\left\{u(i+1,j) - u(i-1,j)\right\} + 2n\ c(i,j)\left\{c(i+1,j) - c(i-1,j)\right\}\right.$$

contd..

$$+ gn2\Delta x\ F(i,j)\ u(i,j)\Big] \tag{5.76}$$

$$c(i,\ j+1) = c(i,j) - \frac{\Delta t}{2\Delta xn}\left[u(i,j)\{c(i+1,j) - c(i-1,j)\}\right.$$

$$\left. + \frac{c(i,j)}{2}\{u(i+1,j) - u(i-1,j)\}\right] \tag{5.77}$$

The critical $\Delta t/\Delta x$ ratio that should ensure convergence and stability at all times is based on the maximum possible values of u and c and generalized over the entire solution domain. This aspect will be considered in the next section.

Eqs. 5.76 and 5.77 are then solved to advance the values of u and c at all the mesh points, exclusive of boundaries, from the initially still water level. Boundary conditions are then incorporated in order to obtain the complete solution.

5.4.3. Boundary conditions

With reference to Fig. 5.4 the right hand boundary condition indicates a zero normal velocity at the impervious vertical boundary. The left hand boundary condition represents the experimentally–determined movement of the outcrop point.

It should be noted that the left hand boundary (open boundary) may require special attention under certain conditions. It represents the prescribed time dependent movement of the outcrop point relative to the external wave. This concept was analysed in detail by Dracos (1969) for Darcy flow and was modified by Nasser (1977) for non–Darcy flow regimes by making appropriate alterations to the resistance term. When water enters the porous medium (during the rising stage), the outcrop point, C, in Fig. 5.4, coincides approximately with the free, external water level. However the inside and outside water levels may or may not coincide at the interface when the water is flowing out from the porous media. For the latter case a seepage face will be formed.

It should be noted that the above phenomena has been observed for materials such as crushed rock having a comparatively low value of porosity. Low permeability of the porous medium facilitates the development of a seepage face.

However the effectiveness of this phenomenon for various types of porous media has not been subjected to detailed investigation. From the experimental programme conducted for this project it was observed that for media with a relatively high value of porosity, the outcrop point coincides with the free water level. Small wave amplitudes and a uniform distribution of the voids in all three dimensions favour this coincident water level condition.

For the present the following boundary conditions will be used :

(i) The right hand boundary condition at the impervious boundary is u = 0 for all values of t.

(ii) The left hand boundary condition is a sine function representing the external wave assuming that the outcrop point coincides with the free water level.

From the foregoing discussion it is evident that only one of the two dependent variables (u and c) is known at each boundary. Although the discretized equations of motion and continuity (eqs. 5.76 and 5.77) may be used to evaluate the unknown variables, this does not make use of all the information available. A refined approximation is adopted in which the unknown dependent variable at one boundary is evaluated by incorporating the other dependent variable, known at time (j + 1). This is easily achieved by a combination of the momentum and continuity equations.

Subtracting the continuity equation from the momentum equation and using a forward finite difference scheme yields the left hand boundary condition at i = 1.

$$\frac{\partial u}{\partial t} - 2\frac{\partial c}{\partial t} + \frac{(u-c)}{n}\frac{\partial u}{\partial x} + 2\left(cn - \frac{u}{n}\right)\frac{\partial c}{\partial x} = -gnFu \qquad (5.78)$$

$$u(1, j+1) = u(1,j) + 2\left\{c(1,j+1) - c(1,j)\right\}$$

$$-\frac{\Delta t}{\Delta x}\left[\left\{\frac{u(1,j) - c(1,j)}{n}\right\}\left\{u(2,j) - u(1,j)\right\}\right.$$

$$\left. + 2\left\{n\,c(1,j) - \frac{u(1,j)}{n}\right\}\left\{c(2,j) - c(1,j)\right\}\right]$$

contd..

$$+ \text{gnF}(1,j)\ u(1,j)\ \Delta x\Big] \tag{5.79}$$

Adding the continuity and momentum equations and using a forward finite difference scheme yields the right hand boundary condition at i = N.

$$2\frac{\partial c}{\partial t} + \frac{\partial u}{\partial t} + \frac{(u+c)}{n}\frac{\partial u}{\partial x} + 2\left(cn + \frac{u}{n}\right)\frac{\partial c}{\partial x} = -\text{gnF}u \tag{5.80}$$

$$c(N,j+1) = c(N,j) - \tfrac{1}{2}\left\{u(N,j+1) - u(N,j)\right\}$$

$$- \frac{\Delta t}{\Delta x}\left[\frac{\left\{u(N,j) + c(N,j)\right\}\left\{u(N,j) - u(N-1,j)\right\}}{2n}\right.$$

$$+ \left\{nc(N,j) + \frac{1}{n}u(N,j)\right\}\left\{c(N,j) - c(N-1,j)\right\}$$

$$\left. + \frac{\Delta x\ \text{gnF}(N,j)\ u(N,j)}{2}\right] \tag{5.81}$$

On substituting u = 0 for all t at i = N eq. 5.81 is reduced to

$$c(N,j+1) = c(N,j) - \frac{\Delta t}{\Delta x}\left[\frac{-c(N,j)\ u(N-1,j)}{2n}\right.$$

$$\left. + n\ c(N,j)\left\{c(N,j) - c(N-1,j)\right\}\right] \tag{5.82}$$

5.4.4. Initial conditions

The external wave input at the left hand boundary (open boundary) is expressed as a sine function of the form.

$$\eta = A_o \sin 2\pi\frac{t}{T} \tag{5.83}$$

where A_o is the amplitude of the input wave.

T is the period of the input wave.

Care should be exercised when considering A_o because it corresponds to the amplitude of movement of the outcrop point. This aspect will be discussed at the end of this section.

Wave celerity is given by

$$c = \sqrt{g(h_o + \eta)} \tag{5.73}$$

and in more general form as applicable to the model,

$$c(1, j + 1) = \sqrt{g(h_o + A_o \sin \frac{2\pi(j)\Delta t}{T})} \tag{5.84}$$

for all j, is used for the program

Initial conditions for the problem are as follows,
$u = 0$ and $\eta = 0$ at all grid points at the start of the time interval (at $t = 0$).

$$\eta = 0 \text{ yields that } c(i,1) = \sqrt{gh_o} \tag{5.85}$$

$$u = 0 \text{ results in } u(i, 1) = 0 \tag{5.86}$$

In computing the u(i, j + 1) term, the friction term is evaluated from u(i,j) i.e. F(i,j). However it would be more appropriate if this is based on the values of velocity corresponding to both (i, j + 1) and (i,j). In the numerical scheme adopted an iterative procedure is employed to adjust the non-linear friction term, F, velocities, u, and celerities, c, at all mesh points by averaging the values between two successive time increments until a specific tolerance is reached. The iteration was carried out for five cycles and it was observed that the solution converges and only a difference in the fourth decimal place was observed when comparing with the original values.

Some aspects of the flow environment in the immediate vicinity of the left hand boundary have been presented in the previous section relating to the analytical model. In its present form the numerical model does not account for possible interface losses identified earlier. The input wave amplitude of the numerical model corresponds to the movement of the outcrop point which is considered (in this work, for the conditions studied) to coincide with the free water level. Hence A_o in eq. 5.83 refers to water level fluctuation at the interface and not the anti-node heights (H_{max}) observed further away, although they may be approximately equal. When using this parameter for computation it is important

to include the effect of interface losses by methods described earlier. Results of tests performed for this purpose will be discussed later in the application of the model.

5.5. Properties of the finite difference scheme

5.5.1. Equations used for the analysis

This section is concerned with the conditions that must be satisfied if the solution of the finite-difference equations is to be a sufficiently accurate approximation to the solution of the partial differential equations.

The horizontal momentum and continuity equations which govern the phenomena for one dimensional non-Darcy flow (eqs. 5.74 and 5.75) can be expressed as,

$$\frac{\partial}{\partial t} u_p + u_p \frac{\partial u_p}{\partial x} + c \frac{\partial}{\partial x} (2c) = -gnFu_p \tag{5.87}$$

$$\frac{\partial}{\partial t} (2c) + u_p \frac{\partial}{\partial x} (2c) + c \frac{\partial}{\partial x} u_p = 0 \tag{5.88}$$

where u_p is the pore fluid velocity ($u_p = \frac{u}{n}$).

The governing equations in finite difference form are as follows,

$$u_p(i,j+1) - u_p(i,j) + \frac{\Delta t}{2\Delta x} \left[u_p(i,j)\left\{u_p(i+1,j) - u_p(i-1,j)\right\} + 2\, c(i,j)\left\{c(i+1,j) - c(i-1,j)\right\} \right] = -gFn\, u_p(i,j)\, \Delta t \tag{5.89}$$

$$2\left\{c(i,j+1) - c(i,j)\right\} + \frac{\Delta t}{2\Delta x} \left[2u_p(i,j)\left\{c(i+1,j) - c(i-1,j)\right\} + c(i,j)\left\{u_p(i+1,j) - u_p(i-1,j)\right\} \right] = 0 \tag{5.90}$$

5.5.2 Approximation and truncation error

A numerical evaluation of approximation errors require a mathematical method to determine the extent to which the finite difference equations approximate the differential equations.

Taylor series expansion of the derivatives of the differential equations are adopted for this purpose. Any finite difference scheme will only consider a limited number of the terms of the Taylor expansion thereby introducing a truncation error. If the finite difference equation is subtracted from the series expansion then an order of magnitude estimate of the leading truncation error can be made.

Let U represent the exact solution of a partial differential equation with independent variables x and t, and u the exact solution of the difference equations used to approximate the partial differential equation. Furthermore let $\varphi_{i,j}(u) = 0$ represent the difference equation at the (i,j)th grid point. If u is replaced by U at the grid points of the difference equation then the value of $\varphi_{i,j}(U)$ is called the local truncation error at the grid point (i,j).

If a function f(x) has single-valued, finite and continuous derivatives with respect to x, then Taylor's theorem gives,

$$f(x + \Delta x) = f(x) + (\Delta x)\, f'(x) + \frac{(\Delta x)^2}{L^2} f''(x) + \frac{(\Delta x)^3}{L^3} f'''(x) \ldots \tag{5.91}$$

and

$$f(x - \Delta x) = f(x) - (\Delta x)\, f'(x) + \frac{(\Delta x)^2}{L^2} f''(x) - \frac{(\Delta x)^3}{L} f'''(x) \ldots \tag{5.92}$$

Three simple approximations of the first derivative are possible, the forward difference, the backward difference and the central difference.

The forward difference formula can be written as

$$f'(x) = \frac{d}{dx} f(x) = \frac{1}{\Delta x} \left[f(x + \Delta x) - f(x) \right] + 0 \left[\Delta x \right] \tag{5.93}$$

The backward difference formula can be written as

$$f'(x) = \frac{d}{dx} f(x) = \frac{1}{\Delta x} \left[f(x) - f(x - \Delta x) \right] + 0 \left[\Delta x \right] \qquad (5.94)$$

The central difference formula can be written as

$$f'(x) = \frac{d}{dx} f(x) = \frac{1}{2(\Delta x)} \left[f(x + \Delta x) - f(x - \Delta x) \right] + 0 \left[(\Delta x)^2 \right] \qquad (5.95)$$

in which formulae $0[\ ]$ represents the order of the leading error.

By using weighted combinations of these three difference formulae it is possible to derive other, more complicated difference approximations. Because of the leading error of $0[(\Delta x)^2]$, finite difference schemes with central differences are preferable due to the associated smaller truncation errors.

5.5.3. Consistency

For any finite difference scheme with a centre point i,j, it is usually desirable that in the limit as Δx, $\Delta t \to 0$, the difference equation should contract, about the centre point, to the original differential equation with the disappearance of the truncation error terms. If this requirement is satisfied the difference scheme is said to be consistent with the differential equation or unconditionally consistent should the error term tend to zero regardless of how Δx, $\Delta t \to 0$. If the error terms do not disappear as Δx, $\Delta t \to 0$, then the solution to the inconsistent difference scheme will be the solution to some different differential equation and not to the original.

Using the Taylor's series expansion and substituting those values in eqs. 5.87 and 5.88, the momentum and continuity equations can be expressed as follows,

$$\left[\frac{\partial u_p}{\partial t} + u_p \frac{\partial u_p}{\partial x} + 2c \frac{\partial c}{\partial x} + gnFu_p \right]$$

$$+ \left[\frac{\Delta t}{2} \frac{\partial^2 u_p}{\partial t^2} + \frac{\Delta t^2}{6} \frac{\partial^3 u_p}{\partial t^3} + \ldots\ldots \right.$$

contd..

$$+ u \frac{\Delta x^2}{6} \frac{\partial^3 u_p}{\partial x^3} + u_p \frac{\Delta x^4}{120} \frac{\partial^5 u_p}{\partial x^5} + \ldots$$

$$+ c \frac{\Delta x^2}{3} \frac{\partial^3 c}{\partial x^3} + c \frac{\Delta x^4}{60} \frac{\partial^5 c}{\partial x^5} + \ldots\ldots \Bigg] = 0 \text{ at } (i,j) \qquad (5.96)$$

$$\left[2 \frac{\partial c}{\partial t} + 2u_p \frac{\partial c}{\partial x} + c \frac{\partial u_p}{\partial x} \right]$$

$$+ \left[\Delta t \frac{\partial^2 c}{\partial t^2} + \frac{\Delta t^2}{3} \frac{\partial^3 c}{\partial t^3} + \ldots \right.$$

$$+ u_p \frac{\Delta x^2}{3} \frac{\partial^3 c}{\partial x^3} + u_p \frac{\Delta x^4}{60} \frac{\partial^5 c}{\partial x^5} + \ldots.$$

$$\left. + c \frac{\Delta x^2}{6} \frac{\partial^3 u_p}{\partial x^3} + c \frac{\Delta x^4}{120} \frac{\partial^5 u_p}{\partial x^5} + \ldots. \right] = 0 \text{ at } (i,j)$$

(5.97)

The above equations are an alternative way of writing eqs. 5.87 and 5.88 with the second square bracketed term being the truncation error. In the limit as Δx, $\Delta t \to 0$, regardless of the manner in which they do so, the truncation error will also tend to zero. Consequently, as the truncation error tends to zero the difference equations converge about the centre point (i,j), to the original differential equations. With both of these difference equations converging to their corresponding differential equations, this difference scheme satisfies the requirement of being unconditionally consistent with the original equations. Thus, from the standpoint of consistency, the above finite difference scheme may be used to represent the governing equations without any residual terms arising through the truncation errors.

5.5.4. Discretization error

Let U and C be exact solutions of a partial differential equation having x,t as independent variables and u and c be exact solutions of the finite difference equation approximating the partial differential equation. Then the differences

between the analytical and the numerical solution, (U−u) and (C−c) are called discretization errors. If the discretization errors decay with time as Δx, $\Delta t \to 0$, then the numerical solution (u,c) converges to the analytical solution provided certain conditions are satisfied.

5.5.5. Convergence

Although a difference scheme may be consistent with the corresponding differential equations, the solution to the former need not necessarily converge to that of the latter as Δx, $\Delta t \to 0$. It is possible, for certain values of the time step Δt and the grid size Δx, that the numerical solution will either become unstable or may even converge to an incorrect analytical solution. To ensure that this does not occur the proposed numerical scheme must be analytically tested such that in the limit as Δx, $\Delta t \to 0$, the convergence properties of its solution are known. A finite difference scheme is said to be convergent if u,c tends to U,C as Δt and Δx both tend to zero.

It is difficult directly to develop convergence conditions. Standard methods of estimating convergence could be used with ease to analyse the simplified wave equations. However if the same methods are applied to the governing equations of this study, the analysis is extremely tedious. Procedures have been developed to investigate convergence through stability and consistency conditions. Use is made of the Equivalence theorem which states that if the difference scheme is stable and consistent with the differential equation then its solution will converge to that of the differential equation.

5.5.6. Stability

When solving finite difference equations, an exact solution will only be obtained if computations were performed to an infinite number of significant figures or decimal places. However, since the calculations are carried out to a finite number of decimal places, round−off errors are introduced at each step. This results in the computed solution being different from the exact numerical solution and it is this difference that gives rise to the study of the stability of finite difference schemes. A set of difference equations will be stable if the cumulative effect of all the rounding errors is negligible. The amplification of the round−off error should remain bounded for all sections i as j tends to infinity. If the difference scheme is such that these errors are amplified during the computation process then the correct solution to the unstable scheme will be affected by the exponential growth of these errors.

For analytical investigations of the stability of finite difference schemes, one of two standard methods can be used (Smith 1979). The first method involves expressing the equations of motion in matrix form and examining the eigenvalues of the associated amplification matrix. In the second method, the eigenvalues are determined by using a finite Fourier series. Of the two methods the second is much simpler and will be used to test the stability of the present model.

Application of the Fourier stability method introduced by von Neumann (Smith 1979) can be illustrated as follows. The first step in determining whether and under which conditions a given scheme is stable is to assume that there exist an initial error for both c and u at every grid point between x = 0 and x = 1 at time t = 0. These error lines c' and u' can be resolved into finite, complex exponential Fourier series as follows,

$$c'(i,j) = \sum_{i=0}^{N} A_i \exp(I\sigma i\Delta x) \qquad i = 0, 1, 2 \ldots N \qquad (5.98)$$

where N is the total number of grid points.
A_i is the coefficient of the Fourier series.
σ is the wave number ($\sigma = \frac{2\pi}{L}$)
$I = \sqrt{-1}$

and $i\Delta x$ gives the coordinates of each point as i = 0, 1, 2 .... N. A similar series relationship can be developed for u'(i,j).

For a linear set of difference equations, their separate solutions are additive and consideration need only be given to the propagation of the error due to a single term as given by $A_i \exp(I\sigma i\Delta x)$. If the constant coefficient is written purely in terms of the corresponding error that governs its value, then c'(i,j) can be expressed as,

$$c'(i,j) = c' \exp(I\sigma i\Delta x) \qquad (5.99)$$

To investigate the propagation of this error function as t increases, it is necessary to develop another finite Fourier series such that when t = 0, the solution reduces to that of the above. Adopting the same procedure as before, the final time and space dependent error function c'(i,j) can be expressed as,

$$c'(i,j) = c' \exp(I\sigma i\Delta x) \exp(I\beta j\Delta t) \qquad (5.100)$$

where β is the wave frequency ($\beta = 2\pi/T$)
and $j\Delta t$ gives the time level at j = 0, 1,2 ..... etc.

The line of errors c'(i,j) defined by the earlier equation, and u'(i,j), will decay with time only if the modulus of the amplification factor $\exp(I\beta\Delta t)$ is always less than or equal to unity. Thus the von Neumann condition for stability states that a difference scheme will only be stable if

$$|\lambda| = |\exp(I\beta\Delta t)| \leqslant 1 \qquad (5.101)$$

As the error functions c'(i,j) and u'(i,j) will satisfy the same difference equations as c(i,j) and u(i,j) then substituting the former in the governing difference equations will enable λ to be evaluated.

5.5.6. Non-linear stability

To determine the influence of the non-linear terms on the stability of a finite difference scheme, it is not correct to consider the propagation of only one Fourier component as before. This is because different components of the Fourier series will interact with one another through the non-linear terms. However it is possible to investigate the stability of a non-linear difference scheme by considering a linearised version of the equation. This is achieved by resolving the non-linear terms into linear components with constant coefficients (Liggett and Cunge 1975).

For the governing equations used in the present study, the corresponding quasi-linearised momentum and continuity equations can be written as follows,

$$\frac{\partial u_p}{\partial t} + u_{po}\frac{\partial u_p}{\partial x} + c_o\frac{\partial}{\partial x}(2c) = -gn(a + bn|u_{po}|)u_p \qquad (5.102)$$

$$\frac{\partial}{\partial t}(2c) + u_{po}\frac{\partial}{\partial x}(2c) + c_o\frac{\partial(u_p)}{\partial x} = 0 \qquad (5.103)$$

where $u_p = \frac{u}{n}$ (5.104)

$$F = a + bn|u_{po}| \qquad (5.105)$$

and u_{po}, c_o are constant local values of the velocity and celerity. In substituting u_{po} and c_o in the investigation of stability $u_p(i,j)$ and $c(i,j)$ are considered to be slowly varying functions of x and t so that they can be considered constants. Therefore, only the linearized equations are investigated with $u_p(i,j) = u_{po}$ and $c(i,j) = c_o$.

The finite difference form of the linearized governing equations (eqs. 5.102 and 5.103) can be deduced from eqs. 5.89 and 5.90 with the required modifications made.

Substituting the error functions for c and u as given by eq. 5.100 into the finite difference equations and simplifying yields the following two equations,

$$\left\{(\lambda - 1) + \varphi u_{po} + gFn\Delta t\right\}u'_p + \left\{2\varphi c_o\right\}c' = 0 \qquad (5.106)$$

$$\left\{\varphi c_o\right\} u'_p + \left\{2(\lambda - 1) + 2\varphi u_{po}\right\}c' = 0 \qquad (5.107)$$

where $\lambda = \exp(I\beta\Delta t)$ (5.108)

$\varphi = \frac{\Delta t}{\Delta x} I\sin(\sigma\Delta x)$ (5.109)

$\sigma = 2\pi/L$ (5.110)

$\beta = 2\pi/T$ (5.111)

$F = a + b\, n|u_{po}|$ (5.105)

From the above equations in order that $u'_p \neq 0$ and $c' \neq 0$, the coefficient determinant of these quantities must be equal to zero.

$$\begin{vmatrix} (\lambda - 1) + \varphi u_{po} + gFn\Delta t & 2\varphi c_o \\ \varphi c_o & 2(\lambda - 1) + 2\varphi u_{po} \end{vmatrix} = 0 \qquad (5.112)$$

Solving for λ yields,

$$\lambda = (1 - \frac{gFn\Delta t}{2}) \pm I\left\{\frac{\Delta t}{\Delta x}(c_o \mp u_{po})\sin(\sigma\Delta x)\right\} \qquad (5.113)$$

The above solution was arrived at by neglecting the terms containing products of Δt.

$$|\exp(I\beta\Delta t)|^2 = \left(1 - \frac{gFn\Delta t}{2}\right)^2 + \left\{\frac{\Delta t}{\Delta x}\,(c_o \mp u_{po})\,\sin(\sigma\Delta x)\right\}^2 \leqslant 1 \tag{5.114}$$

For certain wave numbers $\sin(\sigma\Delta x)$ could be as large as unity. Setting it equal to unity, the above equation results in the necessary condition that

$$|(c_o \mp u_{po})\,\frac{\Delta t}{\Delta x}| \leqslant 1 \tag{5.115}$$

together with a lower limit of Δt in order that eq. 5.114 is satisfied.

From eq. 5.114, the general stability condition is found to be,

$$\Delta t \leqslant \left[\frac{gFn}{\frac{g^2F^2n^2}{4} + \left(\frac{c_o \mp u_{po}}{\Delta x}\right)^2 \sin^2(\sigma\Delta x)}\right] \tag{5.116}$$

It is evident from eq. 5.114 that the finite difference scheme is computationally satisfactory only in the presence of friction. High damping or friction coefficients (F) aid the stability of the scheme.

CHAPTER 6 - STEADY FLOW PERMEABILITY TESTS AND OSCILLATORY FLOW TESTS

6.1. Introduction

The principal objective of the extensive experimental programme conducted for the present study is to provide an understanding of the influence of voids and geometry of armour on energy dissipation for commonly used coastal structures. Porous media selected for the study were representative of a wide range of such structures.

For analysis and discussion the experimental programmes are classified under the following sections.

1. (a) Tests to determine physical properties.
   (b) Steady flow permeability tests.
   (c) Oscillatory flow tests.
   (d) Interface losses due to fluid–structure interaction at the open boundary.

2. Unidirectional constant acceleration and constant velocity tests for a moving porous block.

3. Additional tests under oscillatory flow conditions to study the following :
   (a) Performance of closed block structures (wave absorbers) and comparison with corresponding open block structures.
   (b) Influence of submerged porous media.
   (c) Response to the introduction of a front slope to an existing open block structure.
   (d) Performance of trapezoidal porous block structures and equivalent rectangular blocks.
   (e) Influence of the length of structure for open and closed block structures.

4. Tests on a breakwater slope.
   (a) Reflection, run–up and run–down studies on a breakwater section.
   (b) Measurement of lift and along–slope force acting on a single hollow block armour unit of a breakwater section.

5. Studies of scale effects on wave transmission and reflection associated with porous media.

The purpose of this chapter and the next four is to present the results from experimental programmes performed during the various phases of the project. Each of the above sections is discussed in a separate chapter and reference is made to its relationship to the overall project. At the end of each chapter an evaluation is made of the theoretical analysis presented in Chapter 5 by comparing it with experimental results.

A summary of the experimental programme is given in Table 6.1. It identifies the type of test performed for each of the individual experimental media investigated. For convenience, the numbering system which was used at the beginning of this section to classify the experimental programme is adopted in the table. It also identifies the chapters in which the different experimental programmes are discussed.

6.2. Physical properties of porous media

Results from tests pertaining to physical properties relate to overall porosity, characteristic dimension and relative density. The measurement of these parameters for randomly packed spheres and stones was outlined in Chapter 4.

One of the preliminary observations made in the analysis of steady flow and oscillatory flow test results relates to the definition of the physical property of characteristic dimension which is used as one of the parameters to identify a porous medium. This parameter is particularly important in the definition of Reynolds number and as a consequence in the analyses of steady flow test results.

For porous media there are two criteria adopted in the definition of the characteristic dimension. The first is based on the voids and the second on the solid material.

Rockfill is normally characterized by an equivalent diameter for which the geometric mean diameter and the equivalent spherical diameter are two popular definitions. The latter was used for this study. Randomly packed spheres and spherical lattice structures were also identified by their diameters with no reference to the voids.

For hollow block armour units the characteristic dimension was based on the internal voids. Table 6.2 summarises the physical properties of the porous media used for this study together with figures illustrating which dimension has been used in the definition. Porous blocks consisting of Dolos and Stabit units were

identified by a characteristic dimension related to the length of the armour block (ref. Table 6.2). This was necessary because the voids matrix generated in the packing of these units is complex.

The cylindrical lattice structures used in this investigation were selected such that the characteristic dimension remains the same whether it is based on solids or voids. For example, the central void of the repetitive unit of the cylindrical lattice structure has a projected area d x d where d is the diameter of the cylinder. The two vertical pile structures used for the study were also designed on this concept. The spacing in longitudinal and lateral directions was 15 mm, equal to the diameter of the cylinder.

Tests were also performed to determine the porosity of porous blocks consisting of Dolos and Stabits, of randomly packed spheres and stones, and the equivalent spherical diameter of rounded stones (ref. Section 4.6). For other porous media direct measurements were made to determine the characteristic dimension.

6.3. Steady flow permeability tests

6.3.1. Method of analysis

The objective of the steady flow test programme was to obtain an understanding of the resistance equation under free surface conditions for different porous structures. For this purpose it was necessary to examine which type of resistance equation will most closely represent the phenomenon under investigation.

The two equations for the hydraulic gradient–velocity relationship considered for analyses (ref. Section 2.2.2) were as follows,

(1) The Forchheimer form $I = au + bu^2$ (6.1)

(2) The exponential form $I = cu^m$ (6.2)

Of these two equations the Forchheimer form is more illustrative due to the fact that laminar and turbulent components are expressed by separate terms. This permits the evaluation of the degree of turbulence (ref. Section 2.2.2) by computing the ratio

$$\xi = \frac{I_T}{I_L} = \frac{b}{a} u \qquad (6.3)$$

In addition to eqs. 6.1 and 6.2, a Friction factor – Reynolds number relationship (ref. Section 2.2.2) of the form

$$I = c_1 \frac{1}{d} \frac{u^2}{2g} \tag{6.4}$$

where

$$c_1 = \frac{c_2}{Re} + c_3 \tag{6.5}$$

and

$$Re = ud/\gamma \tag{6.6}$$

where d = characteristic dimension was also examined.

The respective coefficients in these equations were determined by using linear regression analysis based on a least squares technique. The goodness of fit is represented by the linear correlation coefficient.

It should be noted that the Friction factor – Reynolds number relationship given by eq. 6.4 can be developed from the Forchheimer equation and as a consequence it will have the same linear correlation coefficient. However, computations involving Reynolds number, c_2 and c_3 will depend on the characteristic dimension (d) of the porous media. This relationship is consistent with the form normally used for head loss – velocity relationships for pipe flow.

6.3.2. Discussion of experimental results

Table 6.3 presents a summary of the results from steady flow tests. In addition to the respective equations, the table also illustrates the relevant physical properties, maximum and minimum values of mean velocity and hydraulic gradient, an estimation of the linear correlation coefficient and the value of velocity at which laminar and turbulent terms in the Forchheimer equation are equal in magnitude ($u = a/b$). The latter, together with eq. 6.3, will be used to assess the degree of turbulence.

Clearly at full-scale Reynolds number will be an order of magnitude greater than those attainable in laboratory models. However, it is considered that the flow regime in the present test was turbulent, thus minimising the possible scale effects.

From the results it is clearly evident that both Forchheimer and Exponential form of resistance equation can be used for hydraulic gradient – velocity relationship for steady flow through porous media. This conclusion is strengthened by the fact that results have been obtained covering a wide range of porous media. As discussed in the literature review, most of the previous investigations were limited to three or four types of porous media and as a consequence it was previously difficult to confirm this conclusion for different media.

It is observed that the Exponential form exhibits a better correlation than the Forchheimer form. This can be explained by the fact that in the latter case, the experimental values are used to determine the coefficients of an equation of which the exponents of the velocity terms are predetermined, in contrast to the Exponential form where this is determined by regression analysis. In effect the Exponential form has more flexibility correlating variables. The exponent of the velocity term varies between 1.2 and 1.6 for the porous media used in this study. Both equations more or less coincide with each other for lower values of velocity and significant deviations are observed only for higher values.

When considering the results for hollow block units and cylindrical lattice structures, which constitute well–defined porous media, it is evident that Cobs and Sheds have flow coefficients which are approximately the same.

For cylindrical lattice structures, as the diameter increases the turbulent flow coefficient b in the Forchheimer equation and c and m in the Exponential equation decrease indicating that for a given velocity the hydraulic gradient decreases. A similar observation – with the exception of the value of m – is made with respect to the increase in diameter of the two Hobo units.

The results for randomly packed spheres and rounded stones show that the constants a, b, c and m decrease with increase in diameter from 19 mm to 25 mm. All three media classified under this section display similar characteristics.

Figs. 6.1.a and b to Figs. 6.10.a and b illustrate the results from steady flow tests. For each medium two plots are presented. In the first, experimental values of I versus u are plotted together with the fitted curves of Forchheimer and Exponential form. In the second, experimental values of c_1 versus Reynolds number are plotted together with the fitted curve $c_1 = c_2/Re + c_3$. From these curves it is evident that experimental values have been obtained at very close intervals of velocity over a wide range whose limits were determined by the practical limitations of the experimental set–up.

From Table 6.3 the maximum values of mean velocity and hydraulic gradient recorded in the experimental programme are approximately 0.37 m/sec and 0.70 m/m respectively.

In order to compare the performance of different structures, the fitted curves for the Forchheimer, Exponential and Friction factor – Reynolds number relationships are presented in separate figures. For this purpose the structures consisting of hollow block units and cylindrical lattices are classified into one group. Randomly packed spheres and rounded stones are classified into a second group. This allows a differentiation between structures having a well–defined porous matrix and those having a randomly oriented porous matrix.

Figs. 6.11.a and b refer to the Forchheimer relationship for the two groups of structures. Fig. 6.11.a clearly illustrates the efficiency of structures consisting of hollow block units compared with the cylindrical lattice structures. This figure also illustrates that as the characteristic dimension of the cylindrical lattice structure increases, the hydraulic gradient for a given velocity decreases. In the case of randomly packed media, the curve for rounded stones lies between those corresponding to the spheres. The hydraulic gradient for the larger diameter spheres is less than that for the smaller diameter spheres. For randomly packed media the hydraulic gradient decreases for increase in porosity.

Figs. 6.12.a and b refer to the Exponential relationship and the results are very similar to those presented in Figs. 6.11.a and b.

The friction factor – Reynolds number relationship for experimental media are presented in Figs. 6.13.a and 6.13.b. The curves for hollow block units are placed close to each other and in fact those for Cobs, Sheds and Hobo (25) can be represented by a single curve. In the case of cylindrical lattice structures, the curves are widely spaced for low values of Reynolds number, converging only at high values.

Plots of $\xi = I_T / I_L$ versus velocity (u) for the experimental media are given in Figs. 6.14.a and b. These curves can be used to investigate the on–set of turbulence based on the ratio of turbulent and laminar components of the hydraulic gradient.

Fig. 6.14.a illustrates that under steady flow conditions, the performances of hollow block units are very similar to each other. For cylindrical lattice structures, as the diameter is increased the value of velocity corresponding to the

on-set of turbulence is increased. As an example, the values of the velocity at which the laminar and turbulent terms become equal to each other for the 15 mm, 20 mm and 30 mm structures are 0.20, 0.51 and 0.85 m/sec respectively. These results clearly indicate the importance of the dimension of the void in relation to the on-set of turbulence. This trend is also observed for the assembly of spheres.

With reference to the governing parameters identified for porous media, all geometric parameters except the dimension of the void (d) are constant for the three cylindrical lattice structures. A plot of turbulent flow coefficient (b) versus void dimension (d) is given in Fig. 6.15. Using the above property it can be assumed that b is proportional to a certain power (m) of the dimension of the void (i.e., $b \propto d^m$). From the regression analysis on the three sets of values of b and d it was found that m equals -1.983 with a correlation coefficient of 0.96.

Although this observation is based on only three points, a high correlation coefficient supports the presence of an inverse square law. It should be noted that lattice structures of this nature provide an excellent opportunity of varying a single geometric parameter at a time, while maintaining all other parameters constant.

The results from the three cylindrical lattice structures, two Hobo units and two assemblies of randomly packed spheres illustrate the sensitivity of the flow coefficients in the resistance equation to changes in the characteristic dimension of the void and the interface properties.

An overall view of the results of this section of the experimental programme clearly indicates the importance of the hydraulic parameters a and b in the Forchheimer equation and of the geometric parameters in characterizing different porous media.

6.3.3. Comparison with previous investigations

In the literature review (ref. Section 2.5.1), reference was made to previous studies on cylindrical lattice structures performed by Kondo and Toma (1972). In the results of that study presented in Fig. 2.1.d, the authors fitted a single curve given by

$$c_1 = \frac{2gdn^5 I}{u^2} = \frac{0.54}{Re^{1/6}} \qquad (6.7)$$

This applied to results obtained from three structures of diameters 4, 11 and 34 mm with approximately eight experimental values for each medium. The results from the present investigation do not support this finding. Perhaps if more readings had been obtained by Kondo and Toma over a wider range of Reynolds number it would have been noticed that the results could not have been presented by a single curve.

It was also noted in the literature review that previous investigators had used enclosed permeameters to determine the steady flow coefficients. Results from selected investigations are given in Table 6.4 which refer to the work of Nasser and McCorquodale (1974), Sollitt and Cross (1972) and Volker (1969). These tests were performed on different types of rock media using vertical permeameters. The permeameter used by Nasser and McCorquodale had a rectangular section (29.5 cm x 30.5 cm), whereas that used by Sollitt and Cross had a circular section (diameter = 20.3 cm). Velocities up to a maximum of 0.17 m/sec were used in these studies.

From these results it is evident that the values of both a and b in $I = au + bu^2$ decrease with increasing diameter. They also indicate the sensitivity of the two parameters to variations in the diameter of the rock. In general the values obtained by the different investigators are consistent with each other and are of the same order of magnitude.

The present study included an investigation on rockfill media consisting of rounded stone having an equivalent spherical diameter of 3.48 cm. A comparison with previous investigations indicates that for the present study the observed value of the laminar flow coefficient is higher and the turbulent flow coefficient lower, the respective coefficients being 1.12 sec/m and 14.085 sec/m^2. This difference is attributed to the use of a different experimental set-up, namely, a horizontal bed flume in which the porous medium is subjected to free-surface flow conditions. The reasons for the use of this apparatus were discussed in Chapter 3. Although the porous medium consisting of rounded stone used in the present study is not the same as those listed in Table 6.4, the above cross-comparison, to a certain extent, illustrates the variability of laminar and turbulent flow coefficients determined by the use of different experimental apparatus.

6.4. Oscillatory flow tests

6.4.1. Method of analysis

The objectives of the oscillatory flow tests were to determine reflection, transmission and loss coefficients for rectangular, porous, block structures. The majority of these were previously tested under steady flow conditions.

For each porous structure the reflection, transmission and energy loss coefficients are defined as

$$K_r = \frac{H_r}{H_i} \tag{6.8}$$

$$K_t = \frac{H_t}{H_i} \tag{6.9}$$

$$K_d = (1 - (K_r^2 + K_t^2))^{\frac{1}{2}} \tag{6.10}$$

In defining the loss coefficient, wave energy losses have been made equivalent to a wave of height H_d of the same period as the incident wave and in the same water depth. Eq. 6.10 is obtained by the conservation of energy.

Each porous medium was tested for two or more wave periods under different wave heights. By considering the variation of the coefficients K_t, K_r and K_d with wave steepness it is possible to assess the performance of each porous block. From an engineering point of view a porous medium exhibiting high loss coefficients with minimum reflection and transmission will be efficient in relation to wave energy dissipation. High reflection coefficients are not favourable in relation to scour at the base of a structure whereas high transmission coefficients increase wave activity in the area protected by the structure. On this basis a comparative study is made of all porous media used for this investigation. The most frequently used wave periods were 1.0 and 1.5 secs.

6.4.2. Discussion of experimental results

Figs. 6.16 to 6.33 illustrate the results from oscillatory flow tests on different media in which transmission (K_t), reflection (K_r) and loss (K_d) coefficients have been plotted against wave steepness (H_i/L). Discussion of these results

includes brief comments on individual plots, comparison of groups of structures such as cylindrical lattices and an overall comparison of porous media used in the study.

Cob units

Fig. 6.16 refers to a porous block consisting of Cob armour units. Transmission coefficients decrease with increasing wave steepness whereas reflection coefficients do not indicate any definite variation with steepness. The loss coefficient increases with steepness and remains approximately constant at higher values. This figure clearly illustrates that low amplitude waves of longer period are effectively transmitted through the porous structure whereas high amplitude waves of a shorter period are dissipated. The change of the transmission coefficient from 0.45 to 0.10 over the steepness range is comparatively high with respect to the variations of other coefficients.

Shed units

Fig. 6.17 refers to a porous block of Shed armour units and is very similar to that obtained for Cob armour units. This plot also indicates that for a given steepness, waves with longer period exhibit increased transmission. In comparison with the Cob unit, the reflection coefficients tend to decrease very slightly with increasing steepness. A close similarity exists between the plots for Cob and Shed armour units with respect to all three coefficients.

Hobo units

Figs. 6.18 to 6.20 relate to three hollow block units (Hobo) of surface openings 16, 20 and 25 mm respectively. The observations on transmission, reflection and loss coefficients are similar to those described earlier. However, it is clear that for the longer wave period transmission and reflection coefficients are greater thus yielding a lower loss coefficient. The reflection coefficient again displays no definite dependence on steepness.

A comparison of the three figures provides information on the influence of the external surface opening while maintaining other geometric parameters constant. As the diameter of the surface opening increases the transmission coefficient increases and the reflection coefficient decreases for both wave periods. The change in the loss coefficient is not significant as it is counter-balanced by the opposing variation of transmission and reflection coefficients. For the structure consisting of Hobo units having the largest opening (25 mm) the reflection and

transmission coefficients are similar in value.

The reflection coefficients are very much influenced by the two dimensional porosity of the vertical interface. It can be expected that Hobo units with minimum surface opening (16 mm) would exhibit highest reflection and as the surface opening increases the reflection coefficient should decrease with increased transmission. The two dimensional porosity of the vertical interfaces for the three units is 9.93, 15.5 and 24.4 percent respectively and these values give an indication of the effective area of the reflecting surface at the interface.

Dolos and Stabit units

The results from tests on block structures consisting of Dolos and Stabit units packed in a predetermined manner as described in Section 3.4.6 are given in Figs. 6.21 and 6.22. Although the results from the Dolos follow the same trend as those described previously, the transmission coefficient at a period 1.5 secs is very much higher than that at 1.0 sec. This significant difference was not observed previously and is also not present in the case of the Stabits. It also contributes to lower loss coefficients at longer periods. The results from Stabits are consistent with those presented above.

When considering relative magnitudes of transmission, reflection and loss coefficients for the porous structures discussed so far, the transmission coefficients are observed to be the lowest and the loss coefficients the highest. The reflection coefficients are placed in-between and on some occasions are in the same range as the transmission coefficients.

Cylindrical lattice structures

The results for cylindrical lattice structures are given in Figs. 6.23 and 6.25. Structures consisting of 15 and 20 mm diameter members show similar characteristics to each other, with transmission decreasing and energy losses increasing with increasing steepness. However, considerable scatter is present in the reflection coefficients particularly for the structure with 15 mm diameter members. The transmission coefficients of these two structures are higher than those observed for porous structures consisting of hollow blocks, and are also greater than the reflection coefficients. The former lie in the same range as the loss coefficients for small values of steepness. It is evident that the voids matrix of this type of structure transmits more energy than it reflects. Previous investigations have also indicated that cylindrical surfaces exhibit low reflection

coefficients.

The performance of the cylindrical lattice structure consisting of 30 mm members is different to that of the first two. The transmission and reflection characteristics are in the same range but the transmission coefficient increases with increasing steepness for both wave periods tested. Hitherto all structures displayed similar characteristics with regard to transmission in that it decreases with increasing steepness. This observation is consistent because of the increase in frictional losses. However, the behaviour of the 30 mm cylindrical lattice structure cannot be explained on this basis.

In analysing wave action on porous media there exist two basic cases which can be identified depending on the ratio of wave height to particle diameter (H_i/d_p).

If this ratio is small the waves will begin to interact with individual components of the breakwater material, leading to a partial reflection directly off the element surface. In this case the theoretical assumption of a continuum no longer applies and the description of the porous flow by eqs. 5.4 and 5.5 is not valid. The equations are best applicable when the incident wave height exceeds the element diameter of the medium.

A closer inspection of the 30 mm cylindrical lattice structure revealed that for small wave amplitudes at the given water depth the waves are reflected from one of the horizontally placed cylindrical members in the first row of the structure. This accounts for the high values of reflection coefficient observed for this structure. As the steepness increases the waves overtop this horizontal member resulting in increased transmission within the steepness range tested.

At the lower period it is observed that reflection coefficients are larger than transmission coefficients whereas at the higher period the opposite is observed. The transmission coefficient for the higher wave period is greater than at the lower period. This indicates that as the period increases the transmission increases with a slight reduction in reflection.

The variation of transmission coefficients with wave height to water depth ratio (H_i/d) is given in Fig. 6.26. Since depth remains constant, in effect it illustrates the variation of transmission coefficient versus incident wave height. It is evident that the 20 mm structure transmitted more energy than the 15 mm structure and it is also clear that waves of longer period result in greater

transmission coefficients.

This discussion establishes that the behaviour of a given structural form is very much dependent on its characteristic dimension. In the present experimental programme three different structures were tested in the same wave environment. From another frame of reference this is equivalent to considering a particular structure in a varying wave environment on the basis of values of the parameter H_i/d_p. From this it can be concluded that the performance of a given structure will depend both on the void dimension and wave environment.

Pile structures

The performance of two pile structures is illustrated in Figs. 6.27 and 6.28. In the case of the structure whose members are aligned in both directions very high transmission coefficients are observed together with low reflection coefficients. The loss coefficients are even smaller than the transmission coefficients. It is evident that this type of structural form is not effective as an energy dissipator. In comparison with the structures discussed so far this configuration represents a porous medium with minimum tortuosity. The performance of the same structure is greatly improved when alternate rows are staggered. As illustrated in Fig. 6.28, the transmission coefficients are considerably reduced with a very small increase in the reflection coefficient. The loss coefficients are greater than the transmission coefficients and are between 0.75 and 0.80.

The results from these two pile structures consisting of cylindrical members of 15 mm diameter clearly indicate the influence of tortuosity. Both structures are of approximately the same porosity ($\approx$ 0.785) with all parameters except tortuosity remaining constant. Hence it is concluded that when pile structures are used it is always best to adopt a staggered layout for efficient performance.

As a point of interest, it is relevant to compare the performance of the 15 mm cylindrical lattice structure having a porosity of 0.607 (Fig. 6.23) with that of the previous two pile structures. The latter constitutes a particular form of pile structure with additional horizontal members, reducing the porosity of the total structure by approximately 0.2. In comparison with the pile structures the lattice structure exhibits reduced transmission, increased reflection and increased loss coefficients. The presence of the horizontal members and the resulting voids matrix account for these observations.

Spherical lattice structures

Figs. 6.29 and 6.30 refer to the results from spherical lattice structures. In comparing these two structures it is observed that the one consisting of larger spheres (diameter = 51 mm) reflects less energy for both wave periods. Transmission coefficients are also slightly lower particularly at the higher wave period, thus contributing to higher loss coefficients. All geometric parameters, except the dimension of the voids, remain constant and it is evident that the larger void matrix corresponding to a diameter of 51 mm is more efficient than that of the smaller one corresponding to diameter 38 mm for the test conditions used for this study, noting that the porosities are identical.

Randomly packed spheres and rounded stones

The results from tests on randomly packed spheres of diameter 19 mm and 25 mm are given in Figs. 6.31 and 6.32 and it is observed that they are very similar to each other in performance. In the case of these two media the transmission coefficient for both periods can be represented by a single curve. Closer examination reveals that the reflection coefficients for the structure consisting of the larger spheres are slightly less than those for the smaller spheres, thus contributing to higher loss coefficients.

The performance of porous media consisting of rounded stones is illustrated in Fig. 6.33; the results follow a trend similar to those of randomly packed spheres but with increased transmission. The reflection coefficients are in the same range as those of the 25 mm spheres.

In the case of spherical lattice structures and randomly packed spheres, lower reflection coefficients are observed for media with larger constituent elements. Although reflection from a vertical-faced porous structure is heavily dependent on the two-dimensional porosity and roughness of the vertical interface, it also depends on the dissipation characteristics of voids within the structure. The results from the tests indicate that larger spherical elements generate an interface and a voids structure which is more efficient in relation to energy dissipation.

The variation of transmission coefficients versus wave height to water depth (H_i/d) ratio for these structures is given in Fig. 6.34. A similar plot is given in Fig. 6.26 for cylindrical lattice structures. From this plot it is evident that the 38 mm spherical lattice transmits more energy than the 51 mm spherical lattice particularly at high periods. The performance of randomly packed spheres

is very similar although they exhibit lower transmission characteristics in comparison with spherical lattice structures. This can be explained by the increase in tortuosity which occurs when regularly placed elements are displaced to generate a random media. For all media the transmission coefficients were greater for the higher period than the lower period.

6.4.3. Observations on transmission and reflection coefficients

From the results obtained from different porous media it is observed that transmission coefficients follow a consistent pattern with regard to variation with wave steepness. Provided the wave height exceeds the element diameter or the characteristic dimension of the media, transmission coefficients decrease with increasing steepness. As the wave period increased, more wave energy is transmitted through the porous medium. As the steepness increases, frictional losses which depend on velocity and as a consequence on wave height and wave period, increase resulting in lower amplitudes for the transmitted wave. However, if the wave height is small in comparison to the element diameter, waves interact with individual components of the structure in contrast to effective flow through a porous medium. This leads to partial reflection directly off the element surface and variation of transmission coefficient is different – as observed and discussed in this case of the 30 mm cylindrical lattice structure.

Unlike the transmission coefficients, the reflection coefficients do not display a definite reliance on wave steepness. Reflection coefficients also displayed more scatter compared with transmission coefficients. The observed behaviour is probably due to experimental error in the determination of the minimum and maximum amplitudes of the wave envelope in the reflected region. In spite of the precautionary measures adopted (ref. Section 4.3.4), it is very difficult to determine the exact position of the loops and nodes in a physical model. In some experiments two-dimensional porosity, shape and roughness of the reflecting surface may have contributed to the scatter in the data.

This problem has been encountered by all those who have adopted the loop-node technique for the measurement of reflection coefficients. Some of the difficulties associated with this technique were discussed by Nasser and McCorquodale (1974) in the analysis of their results. Even recent contributions on the subject (Madsen, P.A. and Warren 1984) focus attention on this problem. It has been shown that the expressions for the reflection coefficient are very sensitive to erroneous results in node height (H_{min}).

In Section 4.3.3, it was proved that the first order approximation for the reflection coefficient can be expressed as,

$$K_r = \frac{A - B}{A + B} \tag{6.11}$$

where $A = H_{max}$ (loop height)

$B = H_{min}$ (node height)

and $A > B$.

Using this formulae it can be shown that the change ΔK_R in the reflection coefficient (K_r) for small changes δB in B and δA in A are given by,

$$\Delta K_r = \frac{-2A}{(A + B)^2} \delta B \qquad \text{due to } \delta B \tag{6.12}$$

$$\Delta K_r = \frac{2B}{(A + B)^2} \delta A \qquad \text{due to } \delta A \tag{6.13}$$

provided δA, $\delta B << (A + B)$.

These expressions illustrate that an error in the measurement of node height will have a greater influence on the final result than when the same error occurs in the loop height. It is also evident that this technique is sensitive for small values of the node height, B, which will always be less than the corresponding loop height, A.

Nasser and McCorquodale (1974) state that in the presence of non-linear waves which do not follow the principle of superposition there may be a tendency for the measured loop height to be reduced relative to the maximum superposition height or the node height to be increased relative to the minimum superposition height or both. From eq. 6.11 it is evident that the application of the loop-node technique could then result in an underestimation of the reflection coefficient.

The foregoing discussion illustrates the limitations of this technique and the importance of careful experimentation when it is adopted. It demands that every wave record be checked and carefully sorted so that cases where serious instability occurs be eliminated from the subsequent analysis. In the present study

this method was found to give repeatable results. On repeating a particular test series perfect agreement was obtained for the transmission wave height whereas the incident and reflected wave heights varied very slightly. However the reflection coefficients were found to be in the same range and from an experimental point of view this proved to be very satisfactory. Although no significant dependence on steepness is observed, the results clearly represent the range in which the reflection coefficients lie for different media tested.

6.4.4. Comparison with previous investigations

Some of the results from previous experimental investigations on wave transmission and reflection from coastal structures are presented in Fig. 6.35. They illustrate typical variations of the coefficients with steepness. It is noted that these results show considerable scatter with regard to both transmission and reflection coefficients. Results of investigations conducted by Sollitt and Cross (1972), Nasser and McCorquodale (1974) and Madsen, Shusang and Hanson (1978) indicate the presence of scatter for both coefficients particularly for reflection, not withstanding the fact that on some occasions the variables have been plotted on logarithmic scale. Even transmission coefficients for randomly placed rockfill observed by Nasser and McCorquodale (1974) exhibit considerable scatter although the general trend indicates higher transmission for media with larger diameter having increased porosity.

The results of the present study are consistent with those presented by previous investigators. However, the scatter in results, particularly in transmission coefficients are found to be very much less in the present work.

6.4.5. Concluding remarks

A comparison of the results obtained in the entire experimental programme can be made by considering the relative magnitude of the transmission, reflection and loss coefficients. Table 6.5 classifies the different porous media on this basis. This table can be used to evaluate the importance of a given coefficient for the two different wave periods used for the study. For example, on one hand it clearly illustrates the ineffectiveness of a uniformly aligned pile structure which transmits most of the incident energy. On the other hand it shows that a structural configuration consisting of Hobo units and having greater overall porosity can be used to obtain reduced transmission with increased loss coefficients. The influence of staggering of piles in increasing the efficiency of the overall structure is also clearly observed.

It should be noted that the observations made in Table 6.5 are only valid for the experimental conditions used for this study and any interpretation made should be within this range of wave steepness. However this type of broad classification is effective in comparing the performance of a wide range of porous media.

One of the main conclusions from the oscillatory flow tests is a recognition of the importance of the governing parameters particularly those related to the geometry, identified in Section 3.3 in the classification of porous media. It is established that a porous media cannot be identified only by a single parameter such as overall porosity or characteristic dimension but other parameters have also to be stated. The porous media used in the experimental programme were selected such that geometric parameters could be varied in a systematic way for the purpose of comparison.

From the present experimental programme, the three cylindrical lattice structures provide information on the characteristic dimension of the void as do the spherical lattice structures. The influence of tortuosity is evident from the two pile structures and the cylindrical lattice structure made with members having the same diameter. The family of Hobo units illustrates the importance of the external opening of the voids matrix for constant shape and size of voids. Behaviour of various armour units when packed into rectangular block structures is illustrated by the tests on both hollow block and interlocking type of armour.

It is also noted that rectangular block structures consisting of Cob, Shed, Cylindrical lattice structures (20 mm) and Hobo (20 mm) represent structures having approximately the same characteristic dimension of the void and for the first three structures even the porosity is approximately the same. However it is observed that they do not perform in a similar fashion. For the first three structures this is due to the variation in the shape of the void whereas the variation in porosity also contributes to the latter.

From the preceding discussion and the discussion of results presented in Section 6.4.2, it is evident that a considerable degree of cross-comparison can be made between the different types of porous media used for oscillatory flow tests. Table 6.6 summarises the different cross-comparison studies discussed so far. This table consists of two columns, the first identifies the particular study and the second identifies the different porous media used for that study. It illustrates the advantages of using the experimental media selected for this study to perform oscillatory flow tests.

The results from steady flow permeability tests and oscillatory flow tests for a wide range of porous structures have clearly established the importance of governing parameters, both geometric and hydraulic, in relation to flow through porous media identified in Section 3.3. In previous investigations not more than three different types of porous structural forms have been used and as a consequence sufficient information was not available to comment on the parameters required to characterise porous media.

6.5. Tests to determine interface losses

The objectives of these tests were to determine the losses which occurred at the frontal fluid–structure interface. The importance of this phenomenon was discussed under theoretical developments in Section 5.3.6. An estimate of the interface losses are best obtained by performing a series of oscillatory flow tests on a structure of negligible length but representing accurately the fluid–structure interface. These losses are closely related to the two–dimensional porosity of the interface and it is for this reason that the tests were performed on the accurately reproduced interface having negligible length in the direction of wave propagation.

To perform these tests on randomly packed porous media is difficult because of the practical limitations associated in creating the structural configuration required for the experiment. However this could be easily achieved in the case of rectangular porous structures consisting of Cob and Shed model armour units. Since these units are produced in two equal halves pinned together, it is possible to assemble a vertical structure which produced the interface accurately while limiting its length to that of half a unit.

The results from the two tests on Cob and Shed interfaces are presented in Figs. 6.36 and 6.37. It is noticed that the transmission coefficients for both structures lie between 0.65 and 0.85 which is quite low when considering the very short length of the structure. The recorded reflection coefficients are also very low varying between 0.2 and 0.3. It is clearly evident that loss coefficients which occur at the interface can be as large as 0.7, particularly for higher values of steepness. The results from these tests will be incorporated in the mathematical models in order to account for the interface losses. From an experimental point of view, these results are subjected to the same limitations as for those discussed in the previous section under oscillatory flow tests.

It is interesting to compare the results of interface losses (Figs. 6.36 and 6.37) with the oscillatory flow tests on pile structures (Figs. 6.27 and 6.28). The

main observation is that the performance of the Cob and Shed interfaces is very similar to that of the pile structure with its members aligned in both directions (Fig. 6.27). All three coefficients are in the same range and the variation with steepness indicates the same trend. In effect, the performance of a pile structure of length 28.5 cm is equivalent to that of the Cob or Shed interface of length approximately 2 cm corresponding to that of half a unit.

Of the two interfaces, that consisting of Cobs exhibits slightly higher loss coefficients and lower transmission coefficients, for the experimental conditions adopted for this study. In fact, the performance of the Cob interface (Fig. 6.36) is even comparable to that of the pile structure with alternate rows staggered (Fig. 6.28). From a viewpoint of two-dimensional porosity of interfaces - "blockage", - the Cob and Shed interfaces have values of 20.9 and 22.8 percent respectively. These are based on the dimension of the innermost opening of each unit. The corresponding interfaces of the two pile structures have values of 47.4 percent.

The foregoing discussion clearly illustrates the effectiveness of the void structure in both Cob and Shed units.

6.6. Evaluation of the theoretical analyses

Theoretical developments pertaining to wave transmission through and reflection by rectangular porous block structures were presented in Chapter 5. An analytical model was developed to predict the transmission, reflection and energy loss coefficients for open block structures, of the type used for oscillatory flow tests. The input data required were the incident wave conditions and the properties of the porous media.

The analytical model considers the interaction of non-breaking, linear, shallow-water waves with a porous structure characterised by its length, the overall porosity (n) and the laminar and turbulent flow coefficients (a and b in the equation $I = au + bu^2$) determined under steady flow conditions. The wave climate is identified by the wave height, period and still water depth.

An important observation which arose in relation to wave action on porous structures was the presence of interface losses, investigated by a series of tests, the results of which were presented in Figs. 6.36 and 6.37. If these losses were not taken into account, the theoretically predicted values of transmission and reflection coefficients will be higher, resulting in an overestimation of the coefficients.

Due to interface losses, the amplitude of the wave transmitted into the structure at the front face is smaller and this reduces the transmission coefficients of the overall structure for given incident wave conditions.

There are two components of wave height which contribute towards wave reflection from an open block structure. The first corresponds to direct wave reflection from the front face and the second corresponds to internal reflection of the wave transmitted into the structure. Both components are to a certain extent affected by interface losses.

Direct wave reflection from the front face is very much dependent on the two-dimensional porosity of the vertical interface. The reflection coefficients measured in the tests to determine interface losses correspond to this case. Internal reflections while being dependent on the overall porosity are also influenced by the wave height transmitted into the structure at the front interface as the latter constitutes the energy available for both internal reflections and external transmission. This wave height is very much dependent on interface losses which reduce its magnitude. Unsteady flow effects and air entrainment are two other phenomena which influence wave motion inside a porous structure.

The results from tests to determine interface losses provide wave transmission and reflection coefficients for the front interface in the absence of reflection from the interior of the structure.

The transmission coefficients decrease with increasing steepness and the results from both Cob (Fig. 6.36) and Shed (Fig. 6.37) interfaces in the range $0.010 < H_i/L < 0.035$

$$K_{tf} = -8.712 \frac{H_i}{L} + 0.909 \qquad (6.14)$$

where

$$K_{tf} = \frac{H_t}{H_i} \qquad (6.15)$$

H_t is the transmitted wave height

H_i is the incident wave height.

This was derived by linear regression analysis with a correlation coefficient of 0.85. The reflection coefficients were approximately constant around 0.225.

The influence of interface losses were only determined for Cob and Shed units. For the theoretical analysis the results from these tests were also applied for Hobo units and randomly packed spheres and stones. However, these losses were not considered in the analysis of cylindrical lattice structures because it was observed that their influence was comparatively small mainly due to the cylindrical shape of the members and the relatively large two-dimensional porosity of the vertical interface. If eq. 6.14 is applied it would overestimate this effect. Further reference to this aspect will be made later in this chapter.

A rectangular porous structure has two vertical interfaces, one at the front and the other at the rear. The overall transmission coefficient (K_t) is defined with respect to the wave height transmitted at the back (H_{tb}) and the incident wave height at the front face (H_{if}). Similarly, transmission coefficients can also be defined for the front and rear interfaces based on the transmitted and incident wave heights at those interfaces.

Thus the following transmission coefficients are defined.

$$K_t = \frac{H_{tb}}{H_{if}} \quad \text{for the overall structure} \tag{6.16}$$

$$K_{tf} = \frac{H_{tf}}{H_{if}} \quad \text{for the front interface} \tag{6.17}$$

$$K_{tb} = \frac{H_{tb}}{H_{ib}} \quad \text{for the rear interface} \tag{6.18}$$

where H_{tb} - wave height transmitted at the back of the structure
H_{ib} - incident wave height at the rear interface
H_{tf} - wave height transmitted at the front interface
H_{if} - incident wave height at the front interface.

From these expressions, the following relationship can be obtained

$$\frac{H_{ib}}{H_{tf}} \cdot K_{tf} \cdot K_{tb} = K_t \tag{6.19}$$

The analytical model as described in Section 5.3.3 computes the overall transmission coefficient on the basis that both K_{tf} and K_{tb} are equal to unity. In effect, the transmission coefficient computed by the model corresponds to the ratio H_{ib}/H_{tf}. This value has to be multiplied by both K_{tf} and K_{tb} in order to account for interface losses. The value thus obtained will be compared with experimental data.

The expression for the transmission coefficient obtained from the tests performed in relation to interface losses was used to estimate K_{tf} (eq. 6.14). This gives K_{tf} as a function of wave steepness and is considered to be the best approximation for this purpose.

K_{tb} is assumed to be equal to unity. For the types of porous structures used for this study the height of the waves towards the rear of the structure is greatly reduced and there were no disturbances visible in the flow pattern at the rear interface. Measurements confirmed that wave heights on either side of this interface were approximately equal to each other. In addition, there is no equivalent to run-up and run-down at this interface. Under these conditions, neglecting rear interface losses would not have any critical influence on the final result.

The modification required for the reflection coefficient cannot be analysed on the same basis as that for the transmission coefficients.

The reflection coefficient can be defined on a more physical basis by using the following expression.

$$K_r = \frac{H_r}{H_{if}} = \frac{H_{r\,ff} + H_{r\,rr}}{H_{if}} \qquad (6.20)$$

where H_r = reflected wave height.

$H_{r\,ff}$ = component of H_r which is directly reflected from the front face.

$H_{r\,rr}$ = component of H_r which is reflected from the interior of the porous structure.

H_{if} = incident wave height at the front face.

From eq. 6.20 reflection coefficients are defined for the two components

of the reflected wave height as follows.

$$K_{r\ ff} = \frac{H_{r\ ff}}{H_{if}} \tag{6.21}$$

$$K_{r\ rr} = \frac{H_{r\ rr}}{H_{if}} \tag{6.22}$$

Although $K_{r\ ff}$ may be approximated by the reflection coefficients obtained from tests relating to interface losses, it is not possible to estimate the influence of interface losses on the magnitude of the reflected wave height within a porous structure. The reduction in $H_{r\ rr}$ due to losses at the interface cannot be estimated from the experimental investigations. The main difference in the experimental and predicted values of the reflection coefficient is due to this reason.

From the preceding discussion, it is evident that the predicted values of reflection coefficients have to be multiplied by a modification factor to account for the differences explained. Using eq. 6.20 it can be shown that the modified value of the reflection coefficient is of the form

$$K_r = K_r^* \cdot K_m \tag{6.23}$$

in which K_r^* = predicted value

K_m = modification factor.

It can also be shown from eq. 6.20 that K_m can be expressed as follows,

$$K_m = \left[1 - \left(\frac{\Delta H_{r\ rr}}{H_{if}}\right)/K_r^*\right] \tag{6.24}$$

in which $\Delta H_{r\ rr}$ accounts for the difference in the reflected wave height due to the presence of interface losses.

K_m was evaluated by performing a series of oscillatory flow tests for calibration of eq. 6.23. These tests were performed on porous structures consisting of hollow blocks and cylindrical lattice structures. For structures consisting of hollow blocks, K_m was found to be approximately 0.9 and this value was used for

computations. For cylindrical lattice structures K_m was close to unity.

Figs. 6.38 to 6.44 show the comparison between the predicted and observed values of transmission, reflection and loss coefficients for the structures consisting of hollow block units and cylindrical lattices.

The agreement for the structures consisting of Cobs (Fig. 6.38) and Sheds (Fig. 6.39) is very satisfactory. Closer examination of the results indicated that the theoretical predictions of wave transmission at higher values of steepness were greater than the measured values. It should be noted that as the steepness increases the influence of air entrainment is greater, resulting in reduced transmission.

The results from the two structures consisting of Hobo units (Fig. 6.40 and 6.41) indicate that although satisfactory agreement is obtained for the units having the larger opening (25 mm), the theoretically predicted wave transmission coefficients for the other units having smaller opening (20 mm) are comparatively higher.

In comparison with Cobs and Sheds, the Hobo units have a different internal structure. The dimensions of the internal surface opening and the central void of Cobs and Sheds were approximately the same whereas a significant difference exist between these two parameters for Hobo units having small external openings. This difference contributes to the development of two-phase flow under wave action for porous block structures consisting of Hobo units.

As the diameter of the surface opening decreases the degree of air entrainment increases and the resulting internal flow is very much different to that described by the governing equations used for the theoretical study. In fact, when the openings are very small, the internal flow is characterised by jets of water released through these openings as the wave moves along the structure. Under these conditions the overall resistance of the porous structure is very much greater than estimated by laminar and turbulent flow coefficients determined under steady, single-phase flow. Hence both unsteady flow effects and two-phase flow account for the higher values predicted by the analytical model for the Hobo units with 20 mm opening. For the unit having a diameter of 25 mm the agreement is very satisfactory, confirming the arguments presented earlier. As the diameter of the surface opening increases, the agreement between experimental and predicted values improves and under these conditions the flow within the structure is well represented by the governing equations.

The influence of the surface opening manifests itself clearly in the two-dimensional porosity of the surface, the values of which for Cob, Shed, Hobo (25 mm) and Hobo (20 mm) are 20.9, 22.8, 24.4 and 15.5 percent respectively.

It should also be noted that deviations in the theoretically predicted values are greater for waves with a smaller period. Apart from the fact that long wave approximations are not strictly valid under the wave conditions used in the study, it has been pointed out by previous investigators that air entrainment is more crucial for breaking waves having a short period in contrast to non-breaking waves of long period.

The results for the three cylindrical lattice structures are presented in Figs. 6.42 to 6.44. The agreement is satisfactory for transmission, reflection and energy loss coefficients for all three structures. This confirms that no serious error is introduced by neglecting interface losses for these types of structures. In comparison, the scatter for the 15 mm lattice is greater than that for the other two lattices. If the dimensions of the voids were further reduced, for example, to values below 10 mm, there is a greater likelihood that interface losses will have a significant influence on the results.

It was pointed out in Section 6.5 that the overall performance of the Cob and Shed interfaces under oscillatory flow conditions was similar to that of structures consisting of vertical piles with alternate rows staggered and having an overall length fifteen times greater than the former. This gives an indication of the relative magnitude of losses encountered by both structures and the importance of interface losses in relation to the Cob and Shed units.

Figs. 6.45, 6.46 and 6.47 illustrate the results from randomly packed spheres and stones. The agreement is very satisfactory particularly for low values of steepness. As pointed out earlier, interface losses determined for Cob and Shed interfaces were incorporated into the solution.

There are several important observations to be made in comparing the results of the present study with those undertaken previously.

Firstly, the laminar and turblent flow coefficients used for the analyses were determined under steady, single phase, free-surface flow conditions as part of this study. It was pointed out in Chapter 2 that most investigators made use of empirical formulae to determine these properties.

Secondly, previous studies have concentrated mostly on rockfill media whereas a variety of porous media were included in this investigation. This study thus exposes in greater detail some of the differences which are present when the same structure is subjected to conditions of steady and unsteady flow. The use of porous hollow blocks and lattice structures permits visual observation of flow inside the structure. This opportunity is not available when using randomly packed porous media. The occurrence of air entrainment and complex two-phase flow patterns through pores during the rising and falling stages of wave motion were clearly observed. These observations highlight the limitations of using laminar and turbulent flow coefficients determined under steady, single-phase flow conditions in the equations of motion relating to unsteady flow.

The concept of interface losses in its present form has not been considered in previous investigations. The use of cuboid units in rectangular porous block form enabled these losses to be investigated in detail.

Another point of interest which arises in the comparison relates to the method of solution adopted in this study. It should be noted that no further simplifying assumptions were made to the expressions derived for transmission and reflection coefficients (eqs. 5.43 and 5.44). The friction factor was determined by an iterative procedure based on eq. 5.63. In using the same governing equations Madsen (1974) made several assumptions to obtain a relatively simplified expression for the transmission and reflection coefficients for structures of small length. These assumptions enabled the derivation of an explicit solution for the linearized friction factor in terms of the breakwater geometry, incident wave characteristics and the hydraulic properties of the porous media. Madsen's solutions for the transmission coefficient, reflection coefficient and the friction factor are summarized below,

$$K_t = \frac{1}{1 + \lambda} \tag{6.25}$$

$$K_r = \frac{\lambda}{1 + \lambda} \tag{6.26}$$

where
$$\lambda = \frac{k_o l f}{2n} = \tfrac{1}{2}\left[-\left(1 - \frac{k_o l \alpha}{2\omega}\right) + \sqrt{\left(1 + \frac{k_o l \alpha}{2\omega}\right)^2 + \frac{16\beta}{3\pi} a_i \frac{1}{h_o}}\right] \tag{6.27}$$

in which f = friction factor

k_o = wave number ($= \frac{2\pi}{L}$)

ω = wave frequency ($= 2\pi/T$)

a_i = incident wave height

h_o = still water depth

l = length of structure

n = porosity

α, β = flow coefficients in Engelund's equation for the hydraulic gradient.

Madsen further simplified the expression for the friction factor, f, to the form

$$\lambda = \frac{k_o l f}{2n} = \tfrac{1}{2}\left\{\sqrt{1 + \frac{16\beta a_i}{3\pi}\frac{1}{h_o}\left(1 + \frac{R_c}{R_d}\right)} - 1\right\} \tag{6.28}$$

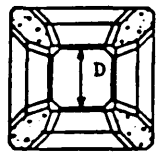
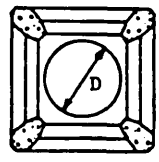
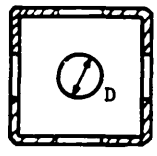
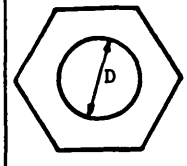
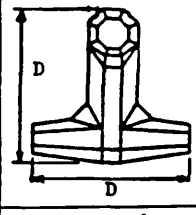
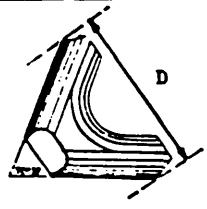
in which R_c and R_d are Reynolds numbers characterizing the flow in the porous structure. The first referred to a critical value and the second referred to the actual value for a given situation.

The solution obtained in the present study is based on the evaluation of the complex functions and their modulii for transmission and reflection coefficients (eqs. 5.43 and 5.44) without further assumptions. The friction factor is determined by an iterative procedure (eq. 5.63) to an accuracy of 1×10^{-3}, i.e., 0.1%.

TABLE 6.1 SUMMARY OF THE EXPERIMENTAL PROGRAMME

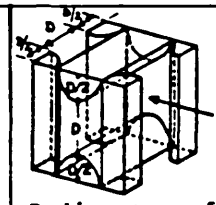
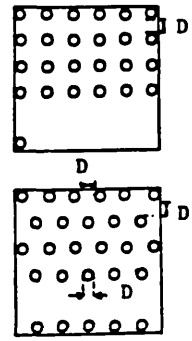
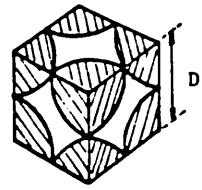
Relevant chapter ⟩	Chapter 6			Chapter 7	Chapter 8	Chapter 9		Chapter 10
The numbers which identify the type of test, correspond to those given in the detailed classification presented in section 6.1 ⟩	1.a tests to determine physical properties	1.b steady flow permeability tests	1.c oscillatory flow tests 1.d tests to determine interface losses	2 unidireectional constant acceleration and velocity tests	3 additional tests under oscillatory flow conditions	4 tests on a breakwater slope 4a Reflection, run-up and run-down studies	4b Measurement of lift and onslope force	5 Scale effect studies on wave transmission and reflection
Experimental media								
Cob		1.b	1.c 1.d	2	3a,3b,3d,3e	4a		
Shed (uniform placing) (staggered placing)		1.b	1.c 1.d	2	3a,3e	4a 4a	4b	
Hollow block								
Hobo 1 (16 mm)			1.c			4a		
Hobo 2 (20 mm)		1.b	1.c	2		4a		
Hobo 3 (25 mm)		1.b	1.c			4a		
Hexagonal unit (Hexo)						4a		
Dolos	1.a		1.c					
Stabit	1.a		1.c					
Cylindrical lattice								
Lattice 1 (15 mm)		1.b	1.c					5
Lattice 2 (20 mm)		1.b	1.c	2				5
Lattice 3 (30 mm)		1.b	1.c					5
Pile structures								
Structure 1 (members aligned)			1.c					
Structure 2 (alternate rows staggered)			1.c					
Spherical lattices								
Lattice 1 (38 mm)			1.c					5
Lattice 2 (51 mm)			1.c					5
Randomly packed spheres								
Spheres (19 mm)	1.a	1.b	1.c					
Spheres (25 mm)	1.a	1.b	1.c					
Randomly packed stones								
Rounded stones	1.a	1.b	1.c		3c,3e			

TABLE 6.2 PHYSICAL PROPERTIES OF EXPERIMENTAL MEDIA

Experimental media and Characteristic dimension (D)		Overall porosity (%) ref.note 1	Two-dimensional porosity (%) ref.note 2
Cob D=19.0 mm		62.72	20.90
Shed D=21.54 mm		61.43	22.80
Hollow Block (Hobo) Hobo 1 (D=16.0 mm) Hobo 2 (D=20.0 mm) Hobo 3 (D=25.0 mm)		79.00 80.30 82.30	9.93 15.50 24.40
Hexagonal unit Hexo D=35.0 mm		36.16	36.16
Dolos D=43.0 mm		50.00	
Stabit D=35.0 mm		52.00	

continued overleaf

TABLE 6.2 continued

Experimental media and Characteristic dimension (D)		Overall porosity (%) ref.note 1	Two-dimensional porosity(%) ref.note 2
Cylindrical lattice Lattice 1 (D=15mm) Lattice 2 (D=20mm) Lattice 3 (D=30mm)	 D=diameter of cylinder	 60.70 60.70 60.70	 25.00 25.00 25.00
Pile structure Structure 1 D=15 mm Structure 2 D=15 mm	D=diameter of cylinder 	 78.50 78.50	 47.40 47.40
Spherical lattice Lattice 1 (D=38mm) Lattice 2 (D=51mm)	D=diameter of sphere 	 47.64 47.64	
Randomly packed spheres Spheres 1 (D=19mm) Spheres 2 (D=25mm)	D=diameter of sphere	 35.00 39.40	
Randomly packed rounded stones Stones (D=34.8 mm)	D=equivalent spherical diameter	 36.20	

Note: 1) Overall porosity refers to the three-dimensional porosity of the rectangular block structure.
2) Two-dimensional porosity refers to that of the vertical interface of the rectangular block structure.

TABLE 6.3 RESULTS FROM STEADY FLOW PERMEABILITY TESTS

Porous media	Properties	Maximum and minimum velocities measured (m/s)		Maximum and minimum hydraulic gradients observed (m/m)		Fitted curves $I = au + bu^2$ ($I_L = au$ $I_T = bu^2$) $I = au^m$	Correlation coefficient r	Velocity (u^*) at which $I_L = I_T$ $u^* = a/b$ m/s	Fitted curves $I = C_1(1/d)(u^2/2g)$ $C_1 = (C_2/Re) + C_3$
		V_{min}	V_{max}	I_{min}	I_{max}				
Rectangular block of SHED units	P = 0.614 D = 21.54 mm	0.049	0.255	0.030	0.560	$I = 0.703u + 5.802u^2$ $I = 4.434u^{1.538}$	0.991 0.997	0.121	$C_1 = (5743.9/Re) + 2.452$
Rectangular block of COB units	P = 0.627 D = 19.00 mm	0.048	0.236	0.042	0.561	$I = 0.917u + 6.407u^2$ $I = 4.872u^{1.496}$	0.993 0.999	0.143	$C_1 = (5826.9/Re) + 2.384$
Rectangular block of HOBO units	P = 0.803 D = 20.00 mm	0.050	0.230	0.055	0.630	$I = 1.051u + 7.188u^2$ $I = 5.394u^{1.484}$	0.988 0.998	0.146	$C_1 = (7396.9/Re) + 2.821$
Rectangular block of HOBO units	P = 0.823 D = 25.00 mm	0.078	0.261	0.055	0.476	$I = 0.566u + 4.683u^2$ $I = 3.894u^{1.588}$	0.989 0.998	0.121	$C_1 = (6320.4/Re) + 2.297$
Cylindrical lattice structure	P = 0.607 D = 15.00 mm	0.015	0.311	0.013	0.494	$I = 0.612u + 3.051u^2$ $I = 2.176u^{1.352}$	0.974 0.997	0.200	$C_1 = (2422.4/Re) + 0.910$
Cylindrical lattice structure	P = 0.607 D = 20.00 mm	0.048	0.331	0.044	0.363	$I = 0.682u + 1.338u^2$ $I = 1.497u^{1.274}$	0.952 0.998	0.510	$C_1 = (4801.3/Re) + 0.522$
Cylindrical lattice structure	P = 0.607 D = 30.00 mm	0.055	0.370	0.059	0.331	$I = 0.642u + 0.751u^2$ $I = 1.143u^{1.226}$	0.939 0.999	0.855	$C_1 = (10169.3/Re) + 0.437$
Randomly packed spheres	P = 0.350 D = 19.00 mm	0.040	0.173	0.080	0.705	$I = 1.707u + 14.632u^2$ $I = 9.460u^{1.465}$	0.979 0.999	0.117	$C_1 = (10843.1/Re) + 5.522$
Randomly packed spheres	P = 0.394 D = 25.00 mm	0.031	0.197	0.049	0.700	$I = 1.454u + 11.558u^2$ $I = 7.406u^{1.441}$	0.987 0.999	0.126	$C_1 = (15994.2/Re) + 5.687$
Randomly packed rounded stone	P = 0.362 D = 34.80 mm	0.022	0.184	0.030	0.657	$I = 1.120u + 14.085u^2$ $I = 8.606u^{1.518}$	0.970 0.998	0.080	$C_1 = (23868.9/Re) + 9.652$

Note: P - Porosity

D - Characteristic dimension

- Length of structure kept constant at 30 cm

- Correlation coefficient for the relationship $C_1 = C_2/Re + C_3$ is the same as that for the relationship $I = au + bu^2$

TABLE.6.4 RESULTS OF STEADY FLOW PERMEABILITY TESTS FROM PREVIOUS INVESTIGATIONS

Investigator(s)	Porous medium	Characteristic dimension (cm)	Porosity	$I = au + bu^2$		Velocity (u^*) at which $I_L = I_T$ $u^* = a/b$ (m/sec)
				a (sec/m)	b $(sec/m)^2$	
Nasser and McCorquodale (1974b)	Crushed rock characterized by the geometric mean diameter	4.4	0.49	0.40	50.0	8.00×10^{-3}
		1.7	0.43 - 0.443	0.90	150.0	6.00×10^{-3}
		1.6	0.372 - 0.377	1.00	210.0	4.76×10^{-3}
		0.7	0.482 - 0.486	1.70	330.0	5.15×10^{-3}
Sollit and Cross (1972)	Gravel, mostly igneous rock characterised by the equivalent spherical diameter	3.48	0.434	0.14	44.4	3.15×10^{-3}
		1.97	0.439	1.08	92.5	11.68×10^{-3}
		0.83	0.430	3.27	220.0	14.86×10^{-3}
Volker (1969)	Crushed aggregate characterized by the geometric mean diameter	1.37	-----	1.05	127.2	8.25×10^{-3}

TABLE.6.5 RESULTS FROM OSCILLATORY FLOW TESTS
RELATIVE MAGNITUDE OF TRANSMISSION (K_t), REFLECTION (K_r) AND ENERGY LOSS (K_d) COEFFICIENTS

Relative magnitude	Wave period (sec)	Porous medium
$K_d > K_r > K_t$	1.0 and 1.5	Cob
	1.0 and 1.5	Shed
	1.0 and 1.5	Hobo (16 mm)
	1.0 and 1.5	Hobo (20 mm)
	1.0	Hobo (25 mm)
	1.0	Dolos
	1.0	Stabits
	1.0	Cylindrical lattice structure (30 mm)
	1.0	Spherical lattice structure (38 mm)
	1.0 and 1.5	Randomly packed spheres (25 mm)
	1.0 and 1.5	Randomly packed spheres (19 mm)
$K_d > K_r \geqslant K_t$	1.5	Dolos
	1.5	Stabits
	1.0	Randomly packed stones
$K_d > K_r \approx K_t$	1.0 and 1.5	Spherical lattice structure (51 mm)
	1.5	Randomly packed stones
$K_d > K_t \geqslant K_r$	1.5	Hobo (25 mm)
$K_d > K_t > K_r$	1.0	Cylindrical lattice structure (15 mm)
	1.0	Cylindrical lattice structure (20 mm)
	1.0 and 1.5	Pile structure (staggered)
$K_d \geqslant K_t > K_r$	1.5	Cylindrical lattice structure (15 mm)
	1.5	Cylindrical lattice structure (20 mm)
	1.5	Cylindrical lattice structure (30 mm)
$K_d \geqslant K_t \approx K_r$	1.5	Spherical lattice structure (38 mm)
$K_t > K_d > K_r$	1.0 and 1.5	Pile structure (uniform)

TABLE.6.6 CROSS-COMPARISON STUDIES WITH EXPERIMENTAL MEDIA

Type of cross-comparison study	Experimental media used
1. Performance of porous blocks consisting of different types of hollow block armour units	Cobs, Sheds, Hobo 1, Hobo 2, Hobo 3
2. Performance of porous blocks consisting of different types of interlocking armour units and comparison with (1)	Dolos and Stabits
3. Performance of porous blocks having approximately the same porosity and characteristic dimension (of void) but of different void shape	Cobs, Sheds and Cylindrical lattice 2
4. Influence of external opening of a hollow block armour unit while maintaining overall porosity approximately the same	Hobo 1, Hobo 2, Hobo 3
5. Influence of characteristic dimension while maintaining all other parameters constant	A) Cylindirical lattices 1,2 and 3 B) Spherical lattices 1 and 2
6. Performance of pile structures with and without horizontal members	Pile structures 1,2 and Cylindrical lattice 2
7. Influence of tortuosity while maintaining all the other parameters constant	Pile structures 1 and 2

continued overleaf

TABLE.6.6 continued

Type of cross-comparison study	Experimental media used
8. Performance of randomly packed media	Spheres 1,2 and rounded stones
9. The performance of spherical elements in a randomly packed medium and in a spherical lattice	Randomly packed spheres 1,2 and spherical lattices 1,2
10. The influence of diameter of the constituent element in randomly packed media while maintaining other parameters approximately the same	Spheres 1 and 2
11. The performance of a spherical lattice and randomly packed stones, both having approximately the same diameter	Spherical lattice 1 and rounded stones

FIG.6.1.A HYDRAULIC GRADIENT vs MEAN VELOCITY

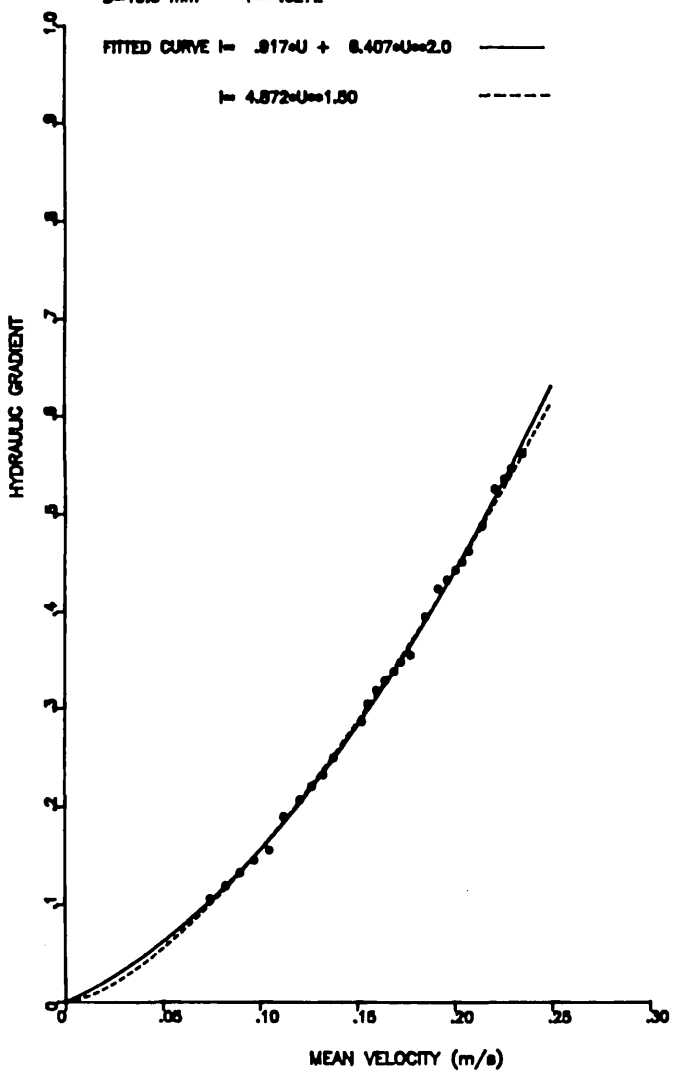


FIG.6.1.B LOSS COEFFICIENT vs REYNOLDS NUMBER

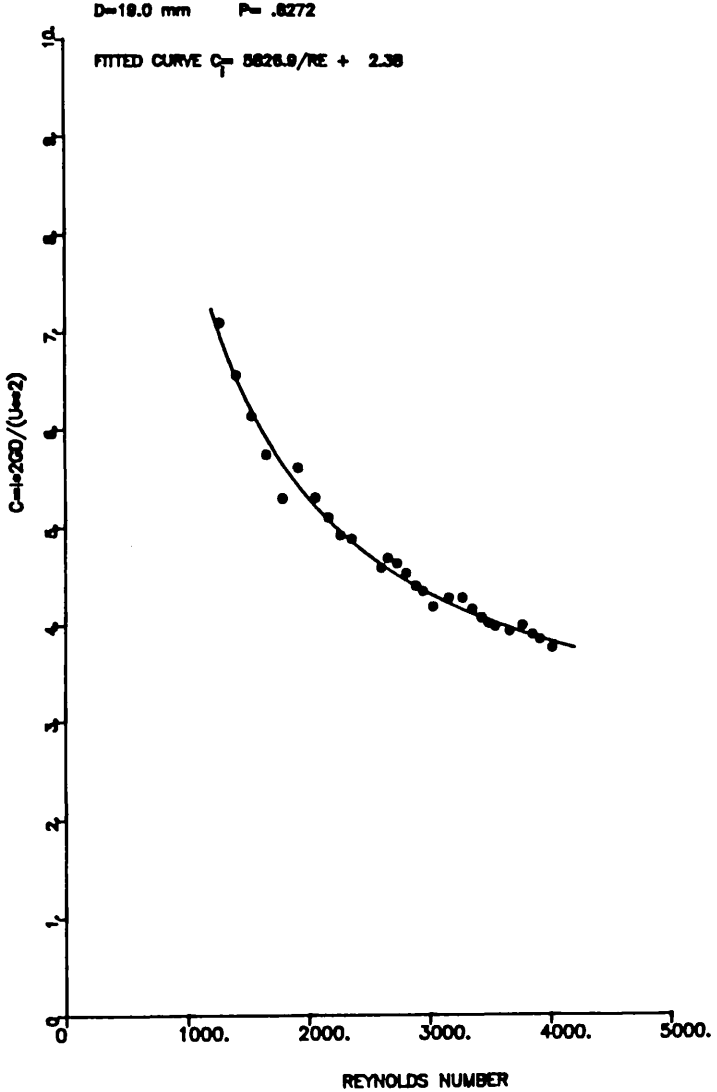


FIG.6.2.A HYDRAULIC GRADIENT vs MEAN VELOCITY

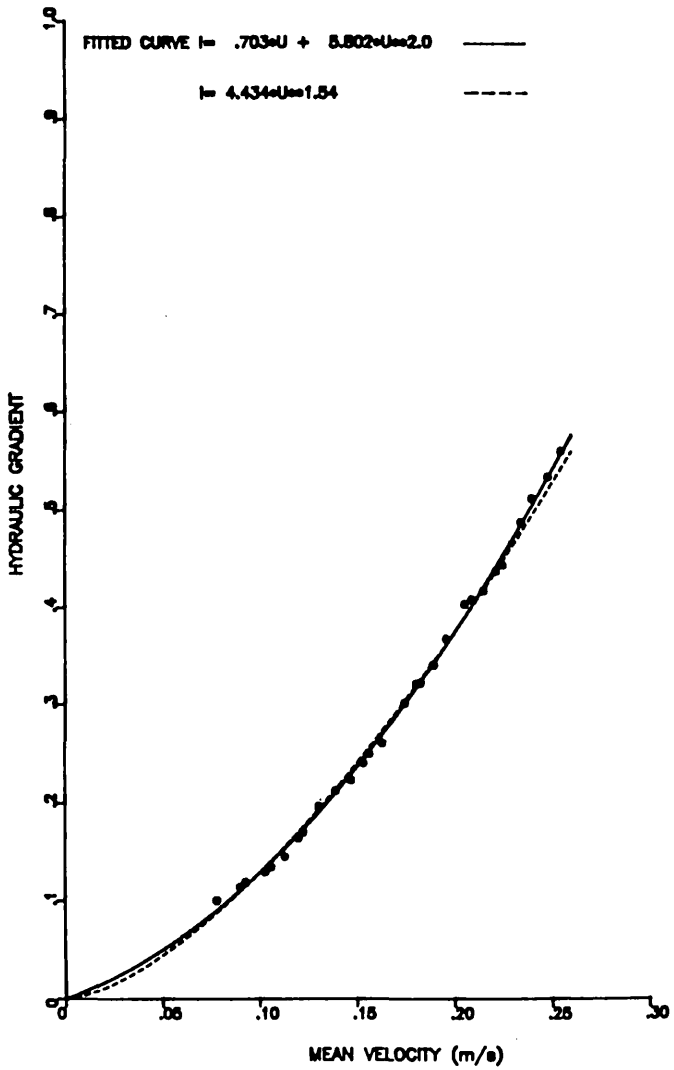


FIG.6.2.B LOSS COEFFICIENT vs REYNOLDS NUMBER

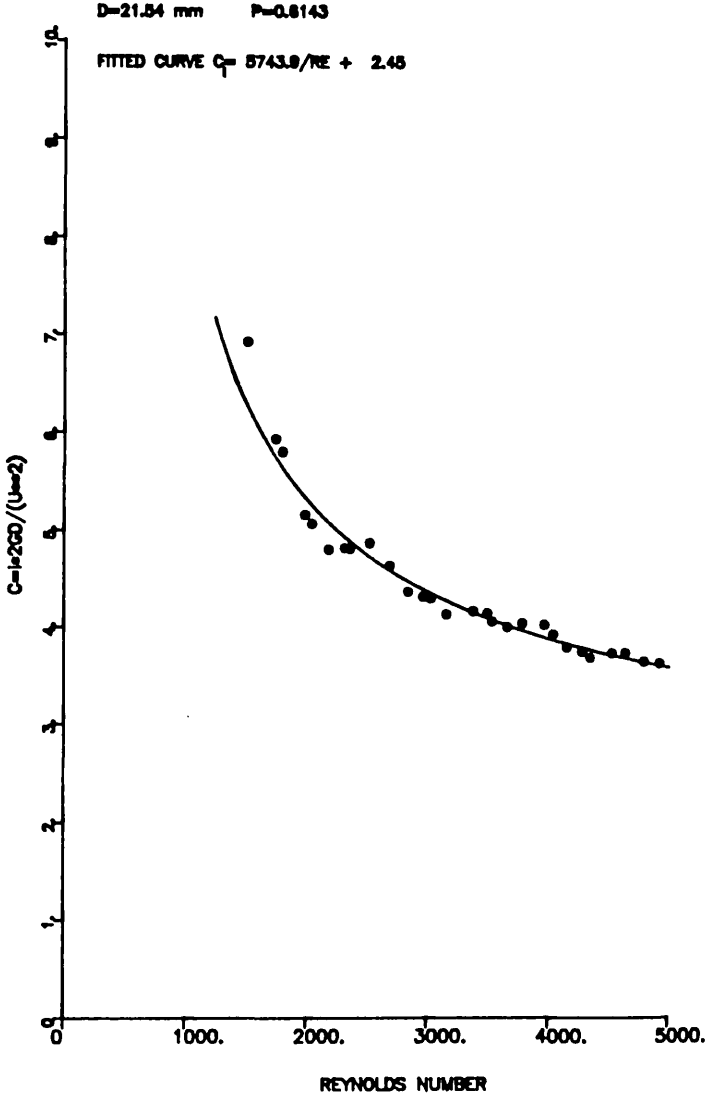


FIG.6.3.A HYDRAULIC GRADIENT vs MEAN VELOCITY

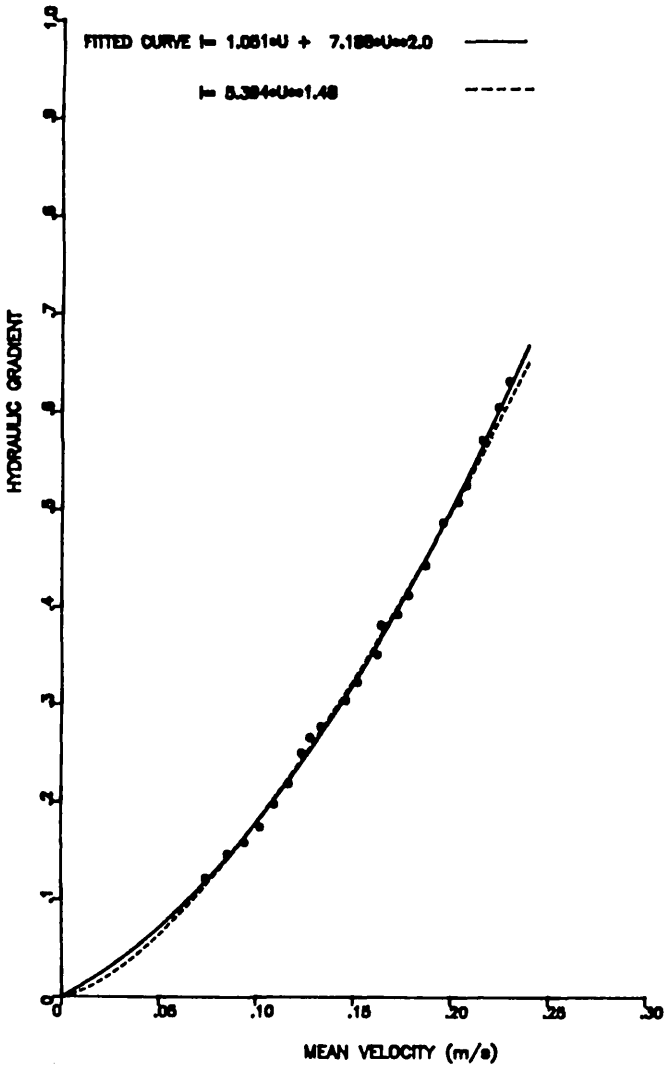


FIG.6.3.B LOSS COEFFICIENT vs REYNOLDS NUMBER

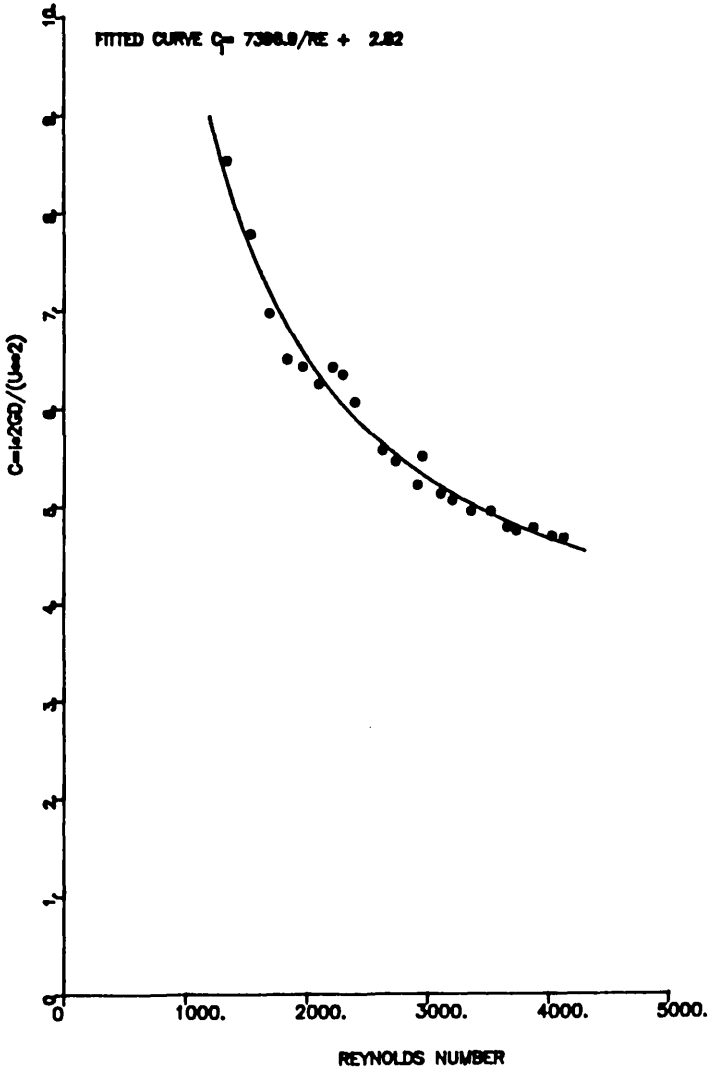


FIG.6.4.A HYDRAULIC GRADIENT vs MEAN VELOCITY

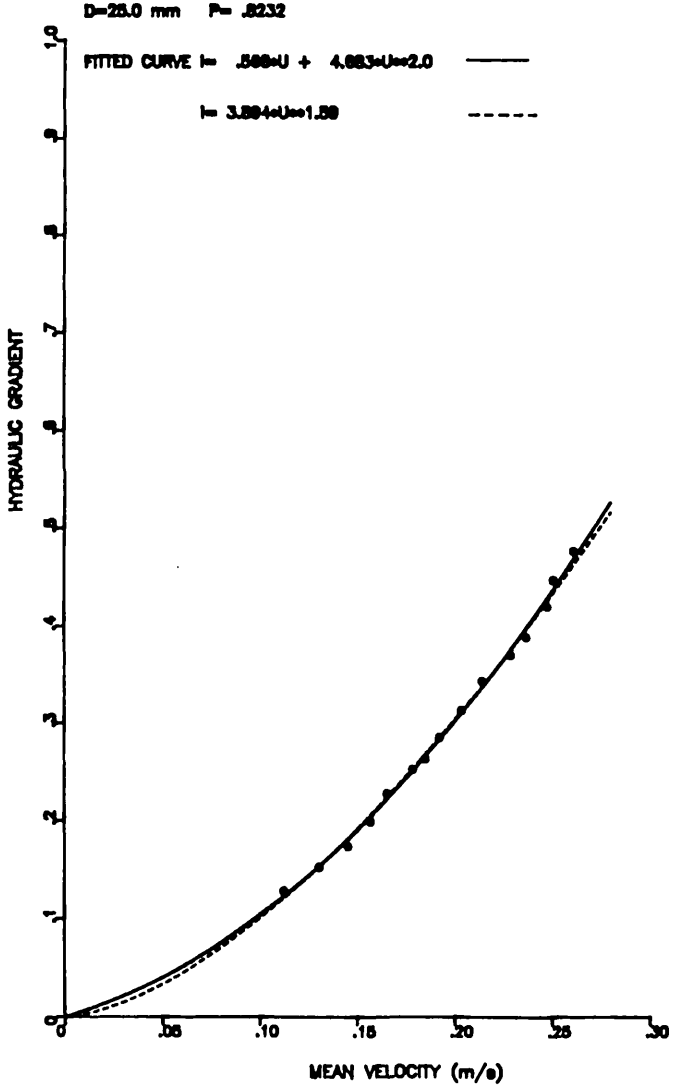


FIG.6.4.B LOSS COEFFICIENT vs REYNOLDS NUMBER

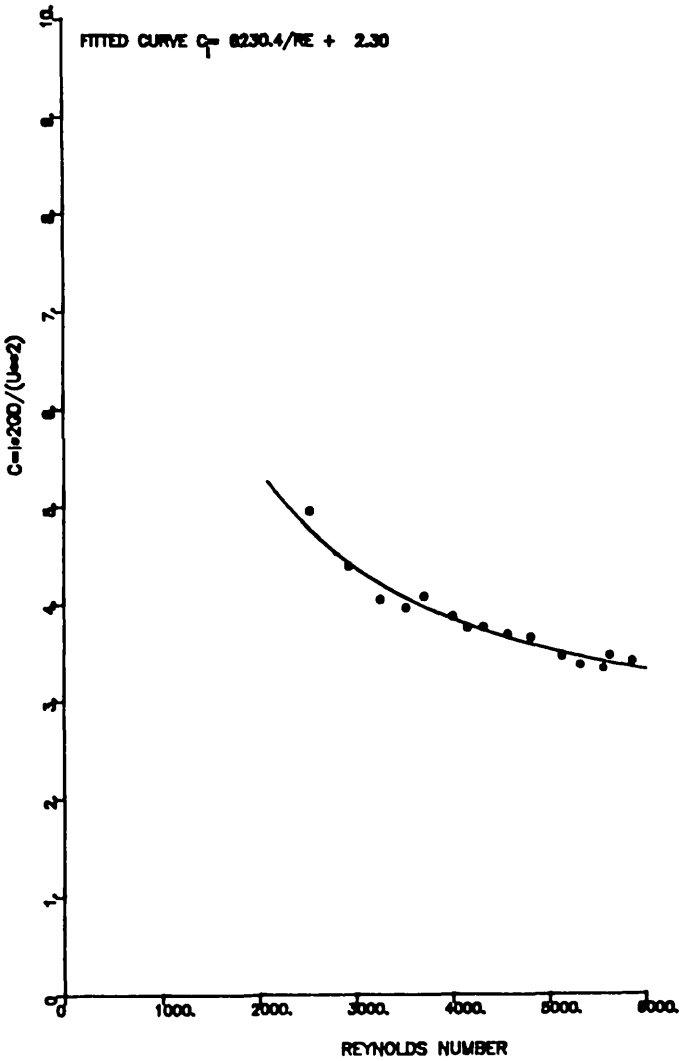


FIG.6.5.A HYDRAULIC GRADIENT vs MEAN VELOCITY

CYLINDRICAL LATTICE STRUCTURE

D=15.0 mm P= .8070

FITTED CURVE I= .812*U + 3.051*U**2.0 ——

I= 2.178*U**1.35 - - - - -

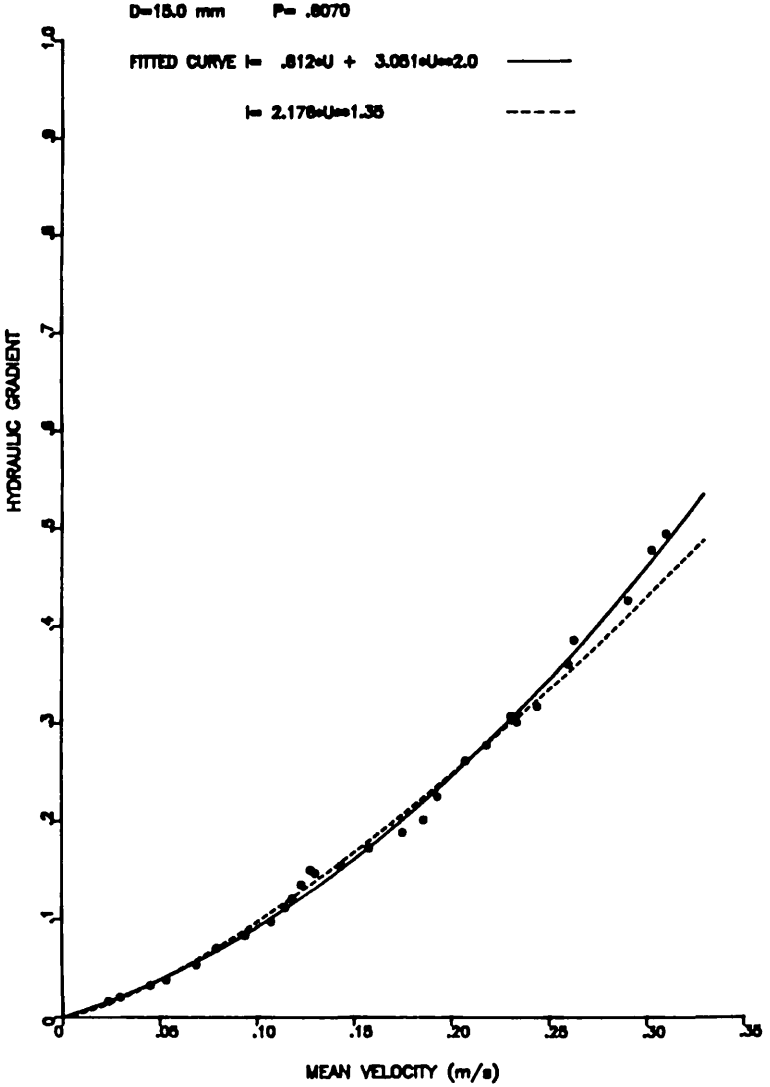


FIG.6.5.B LOSS COEFFICIENT vs REYNOLDS NUMBER

CYLINDRICAL LATTICE STRUCTURE

D=15.0 mm P= .8070

FITTED CURVE C_f= 2422.4/RE + .91

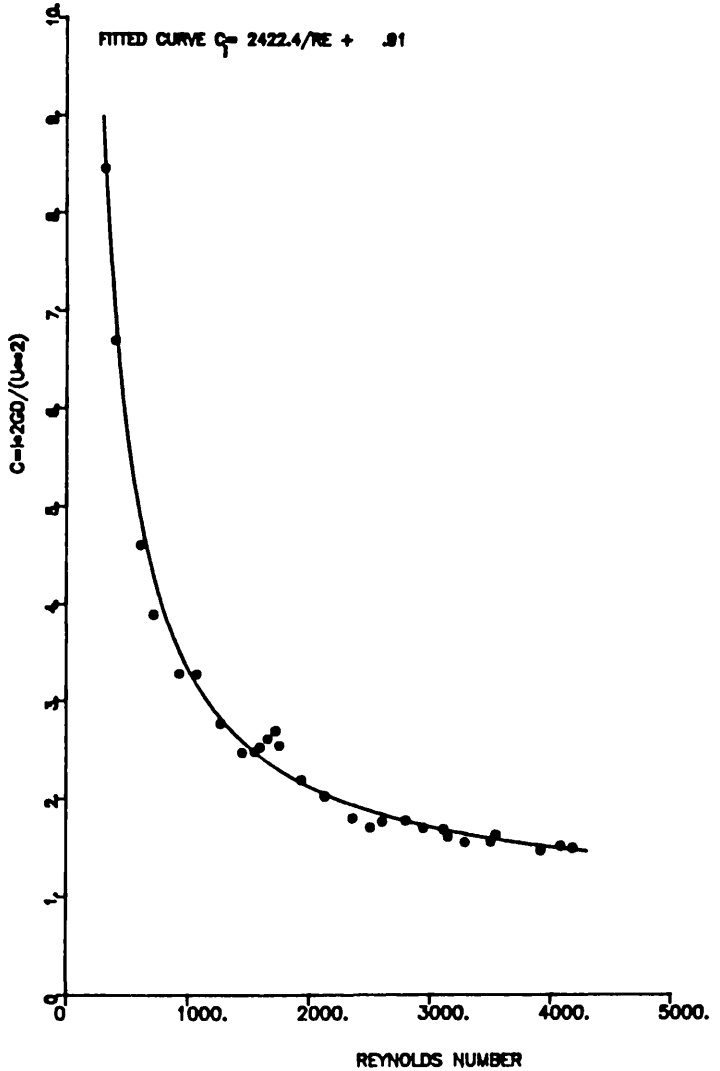


FIG.6.6.A HYDRAULIC GRADIENT vs MEAN VELOCITY

CYLINDRICAL LATTICE STRUCTURE

D=20.0 mm P= .6070

FITTED CURVE I= .662*U + 1.338*U**2.0 ———

I= 1.487*U**1.27 - - - - -

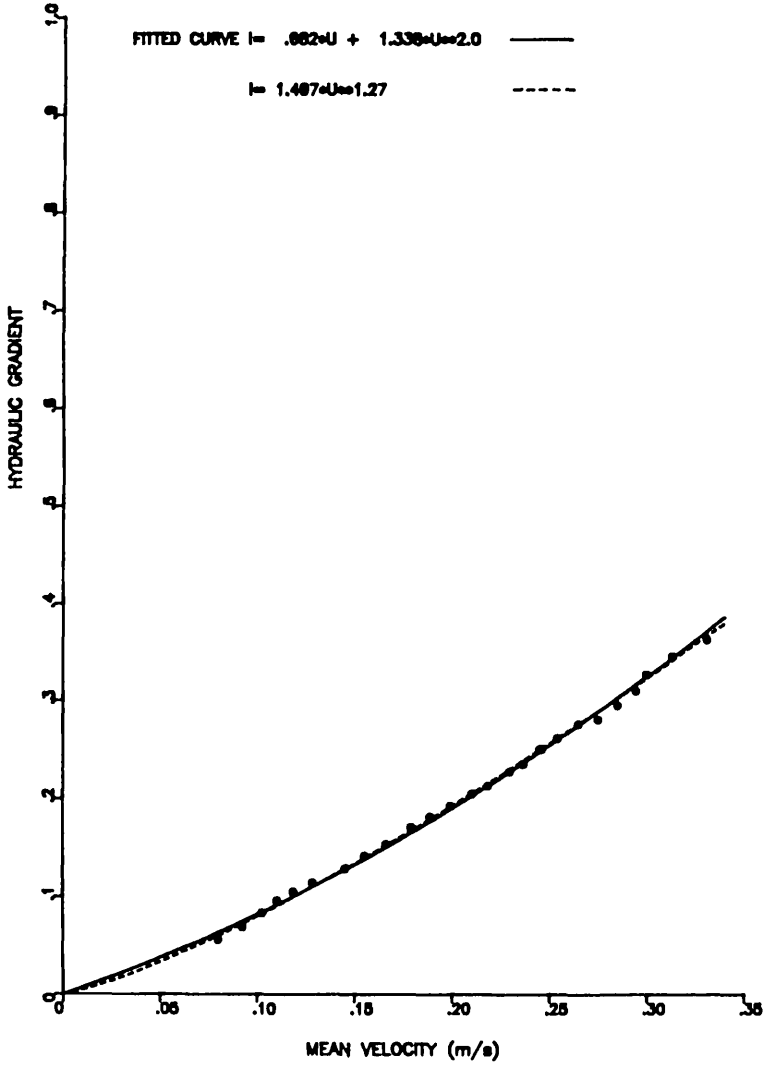


FIG.6.6.B LOSS COEFFICIENT vs REYNOLDS NUMBER

CYLINDRICAL LATTICE STRUCTURE

D=20.0 mm P= .6070

FITTED CURVE C_f= 4801.3/RE + .52

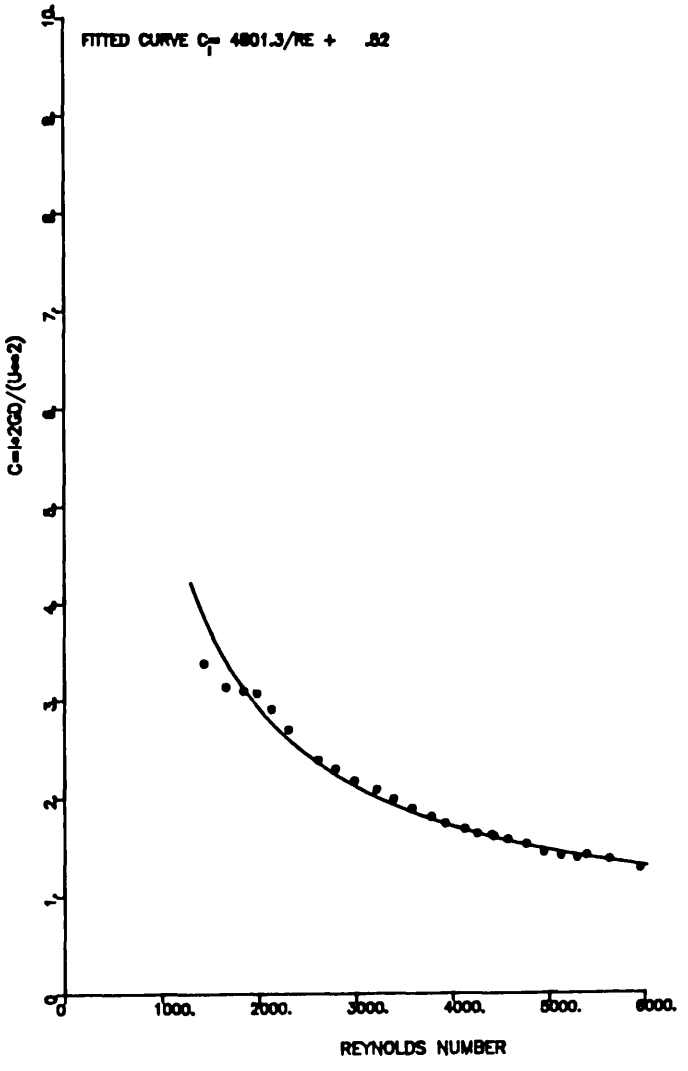


FIG.6.7.A HYDRAULIC GRADIENT vs MEAN VELOCITY

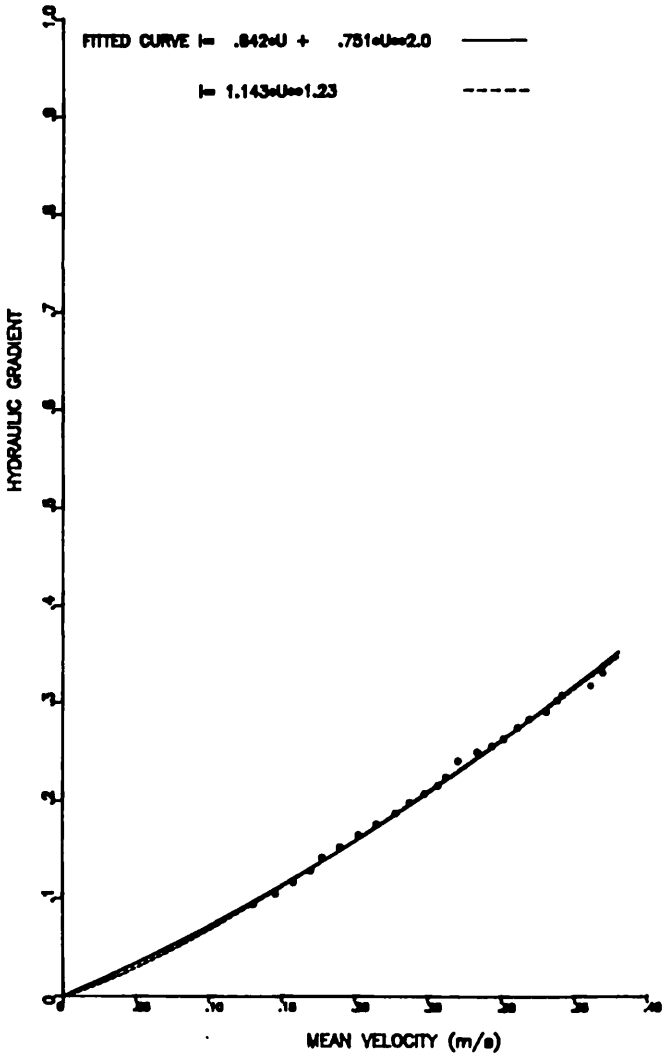


FIG.6.7.B LOSS COEFFICIENT vs REYNOLDS NUMBER

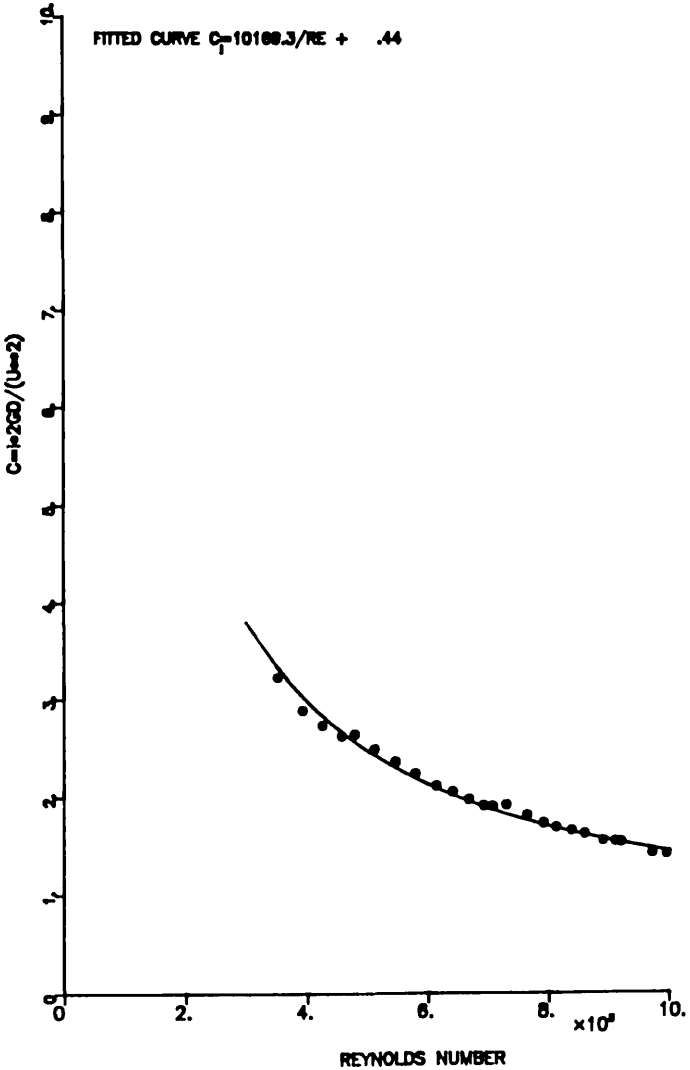


FIG.6.8.A HYDRAULIC GRADIENT vs MEAN VELOCITY

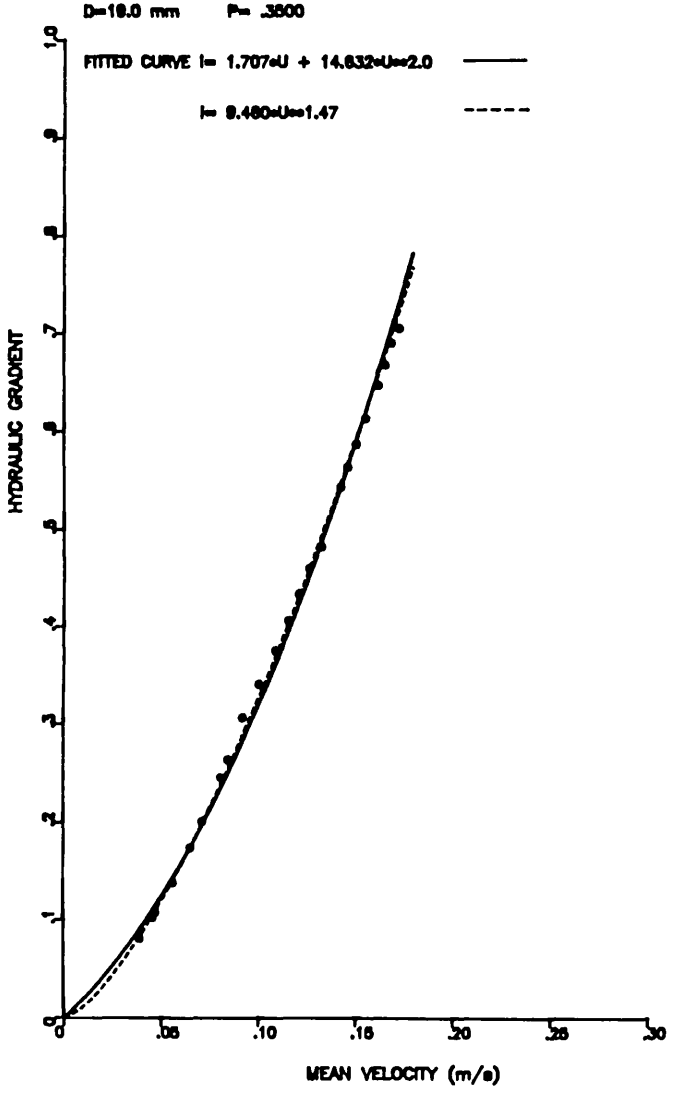


FIG.6.8.B LOSS COEFFICIENT vs REYNOLDS NUMBER

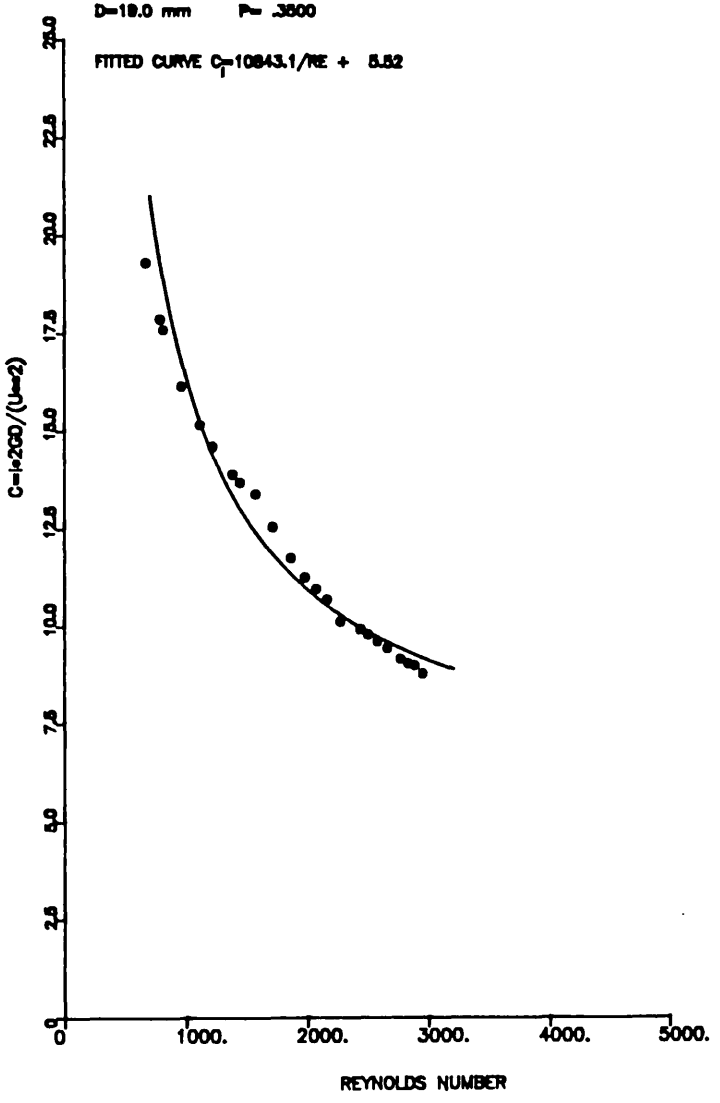


FIG.6.9.A HYDRAULIC GRADIENT vs MEAN VELOCITY

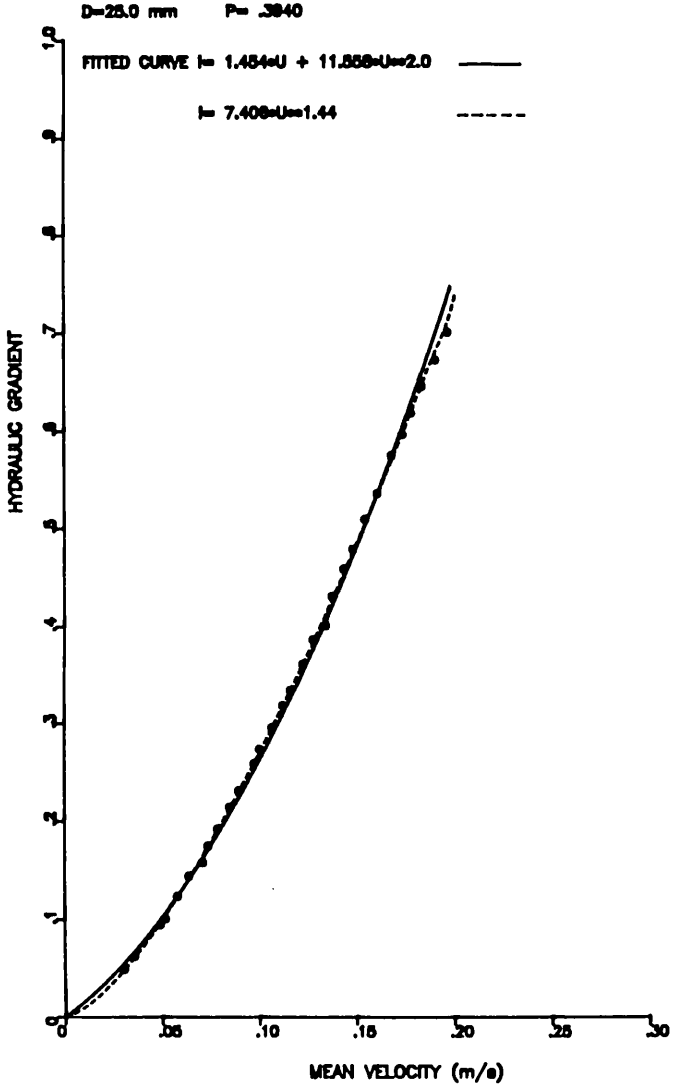


FIG.6.9.B LOSS COEFFICIENT vs REYNOLDS NUMBER

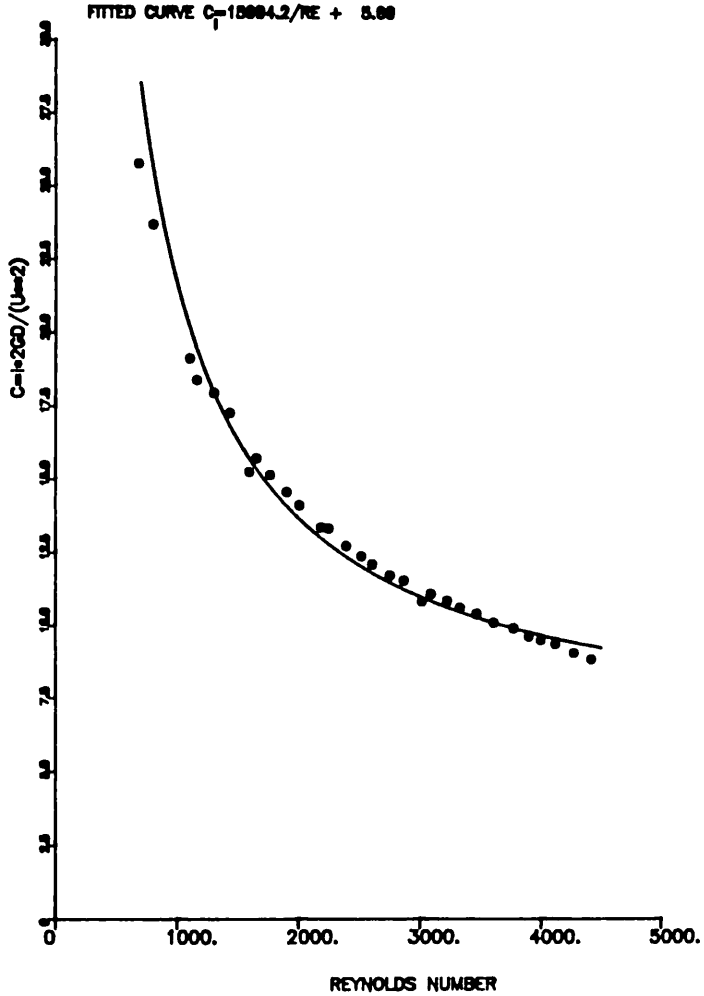


FIG.6.10.A HYDRAULIC GRADIENT vs MEAN VELOCITY

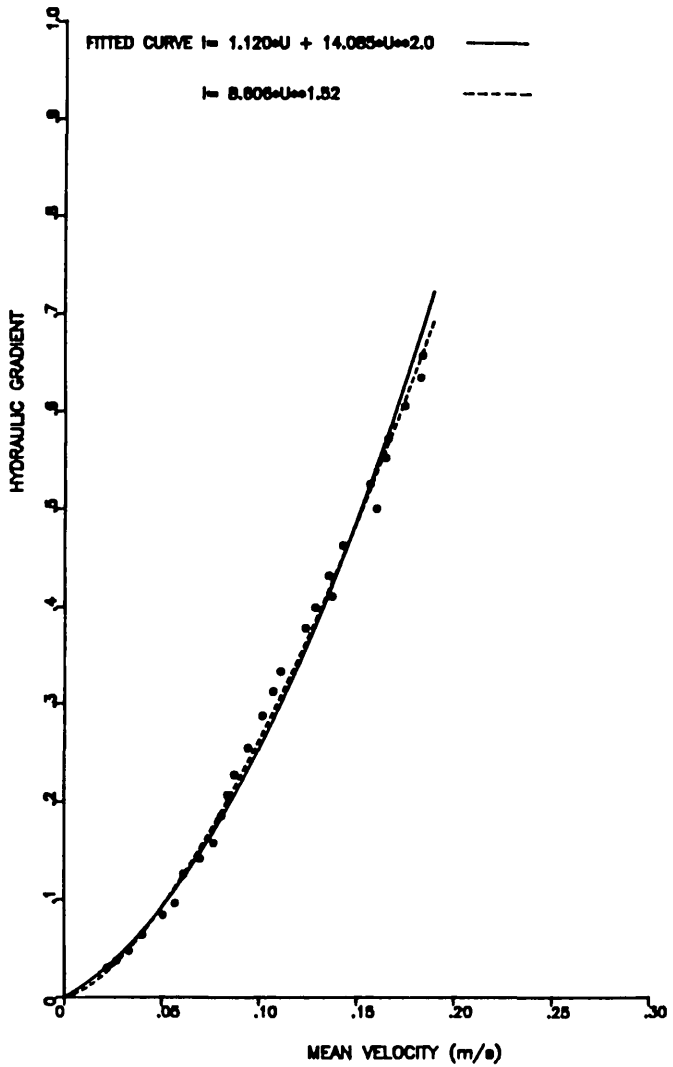


FIG.6.10.B LOSS COEFFICIENT vs REYNOLDS NUMBER

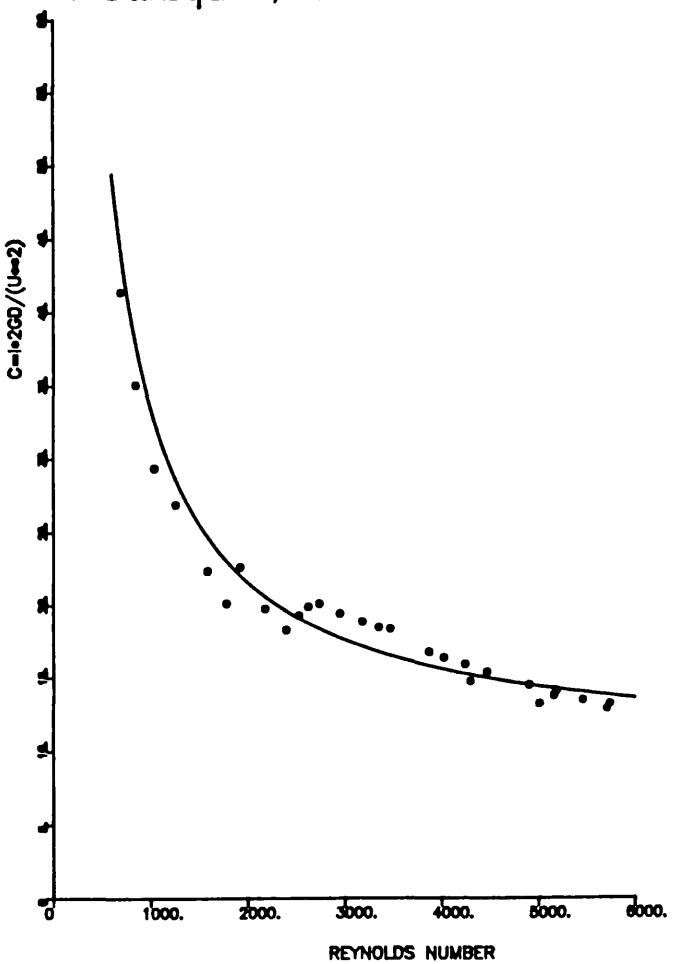


FIG.6.11.A HYDRAULIC GRADIENT vs MEAN VELOCITY

FITTED CURVES $I = A \cdot U + B \cdot U^{**}2$

HOLLOW BLOCK UNITS AND CYLINDRICAL LATTICE STRUCTURES

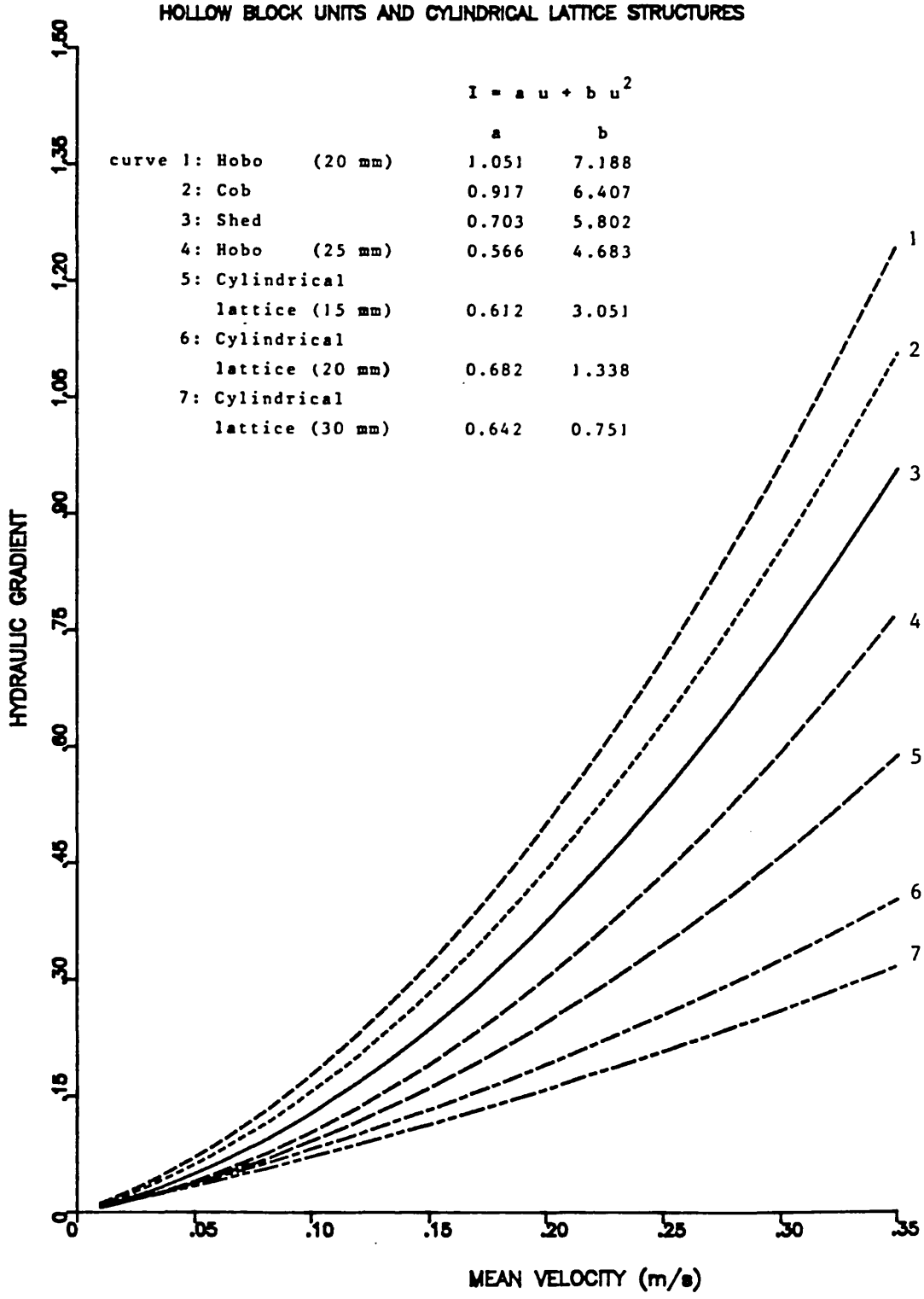


FIG.6.11.B HYDRAULIC GRADIENT vs MEAN VELOCITY

FITTED CURVES $I = A \cdot U + B \cdot U^{**}2$

RANDOMLY PACKED SPHERES AND ROUNDED STONES

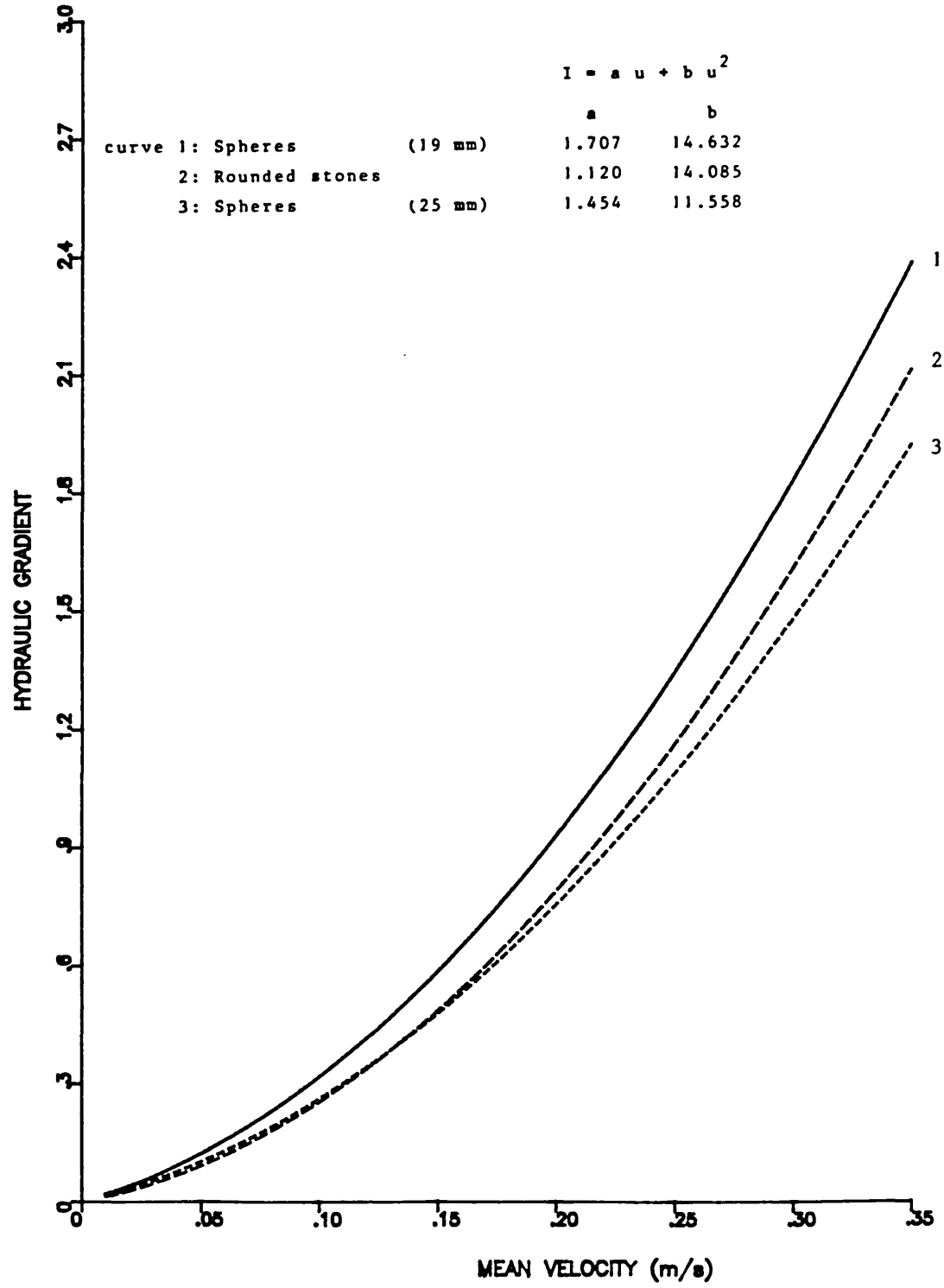
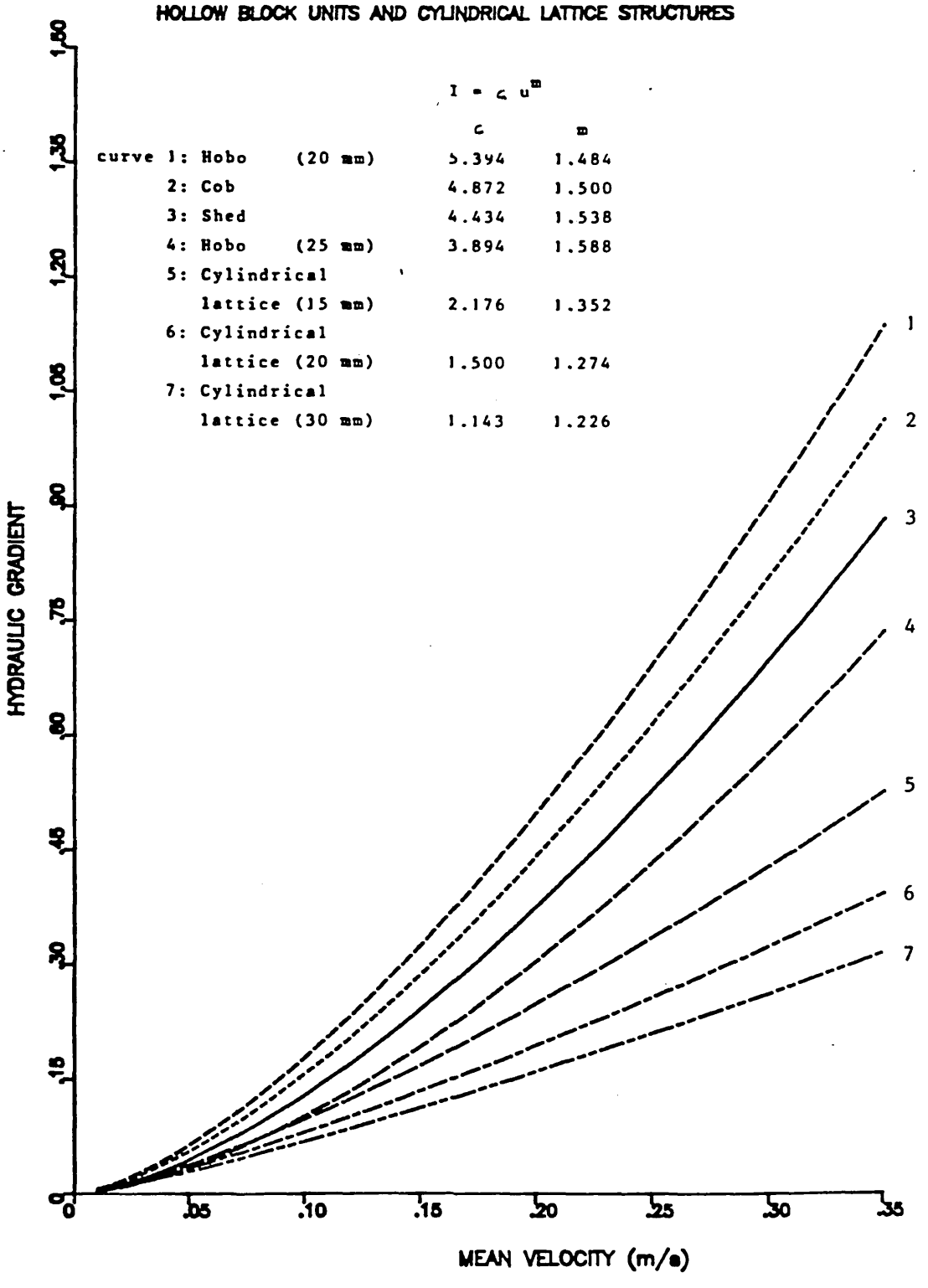


FIG.6.12.A HYDRAULIC GRADIENT vs MEAN VELOCITY

FITTED CURVES $I = c\,U^{m}$

HOLLOW BLOCK UNITS AND CYLINDRICAL LATTICE STRUCTURES



$I = c\,u^{m}$

		c	m
curve 1: Hobo	(20 mm)	5.394	1.484
2: Cob		4.872	1.500
3: Shed		4.434	1.538
4: Hobo	(25 mm)	3.894	1.588
5: Cylindrical lattice	(15 mm)	2.176	1.352
6: Cylindrical lattice	(20 mm)	1.500	1.274
7: Cylindrical lattice	(30 mm)	1.143	1.226

FIG.6.12.B HYDRAULIC GRADIENT vs MEAN VELOCITY

FITTED CURVES $I = c \cdot U^{m}$

RANDOMLY PACKED SPHERES AND ROUNDED STONES

$I = c\, u^{m}$

			c	m
curve 1:	Spheres	(19 mm)	9.460	1.465
	2: Rounded stones		8.606	1.518
	3: Spheres	(25 mm)	7.406	1.441

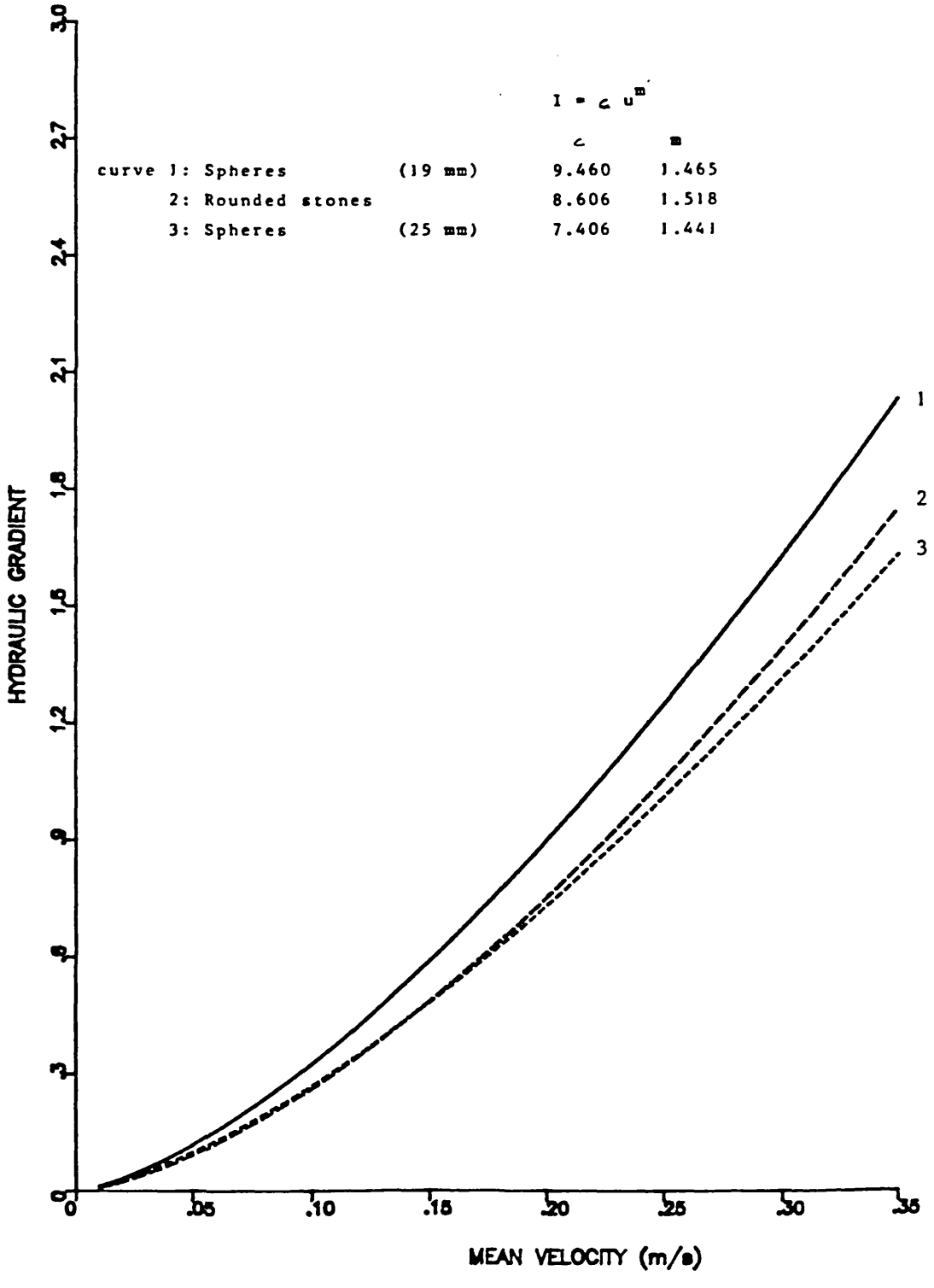


FIG.6.13.A LOSS COEFFICIENT vs REYNOLDS NUMBER

FITTED CURVES $C1=C2/RE + C3$

HOLLOW BLOCK UNITS AND CYLINDRICAL LATTICE STRUCTURES

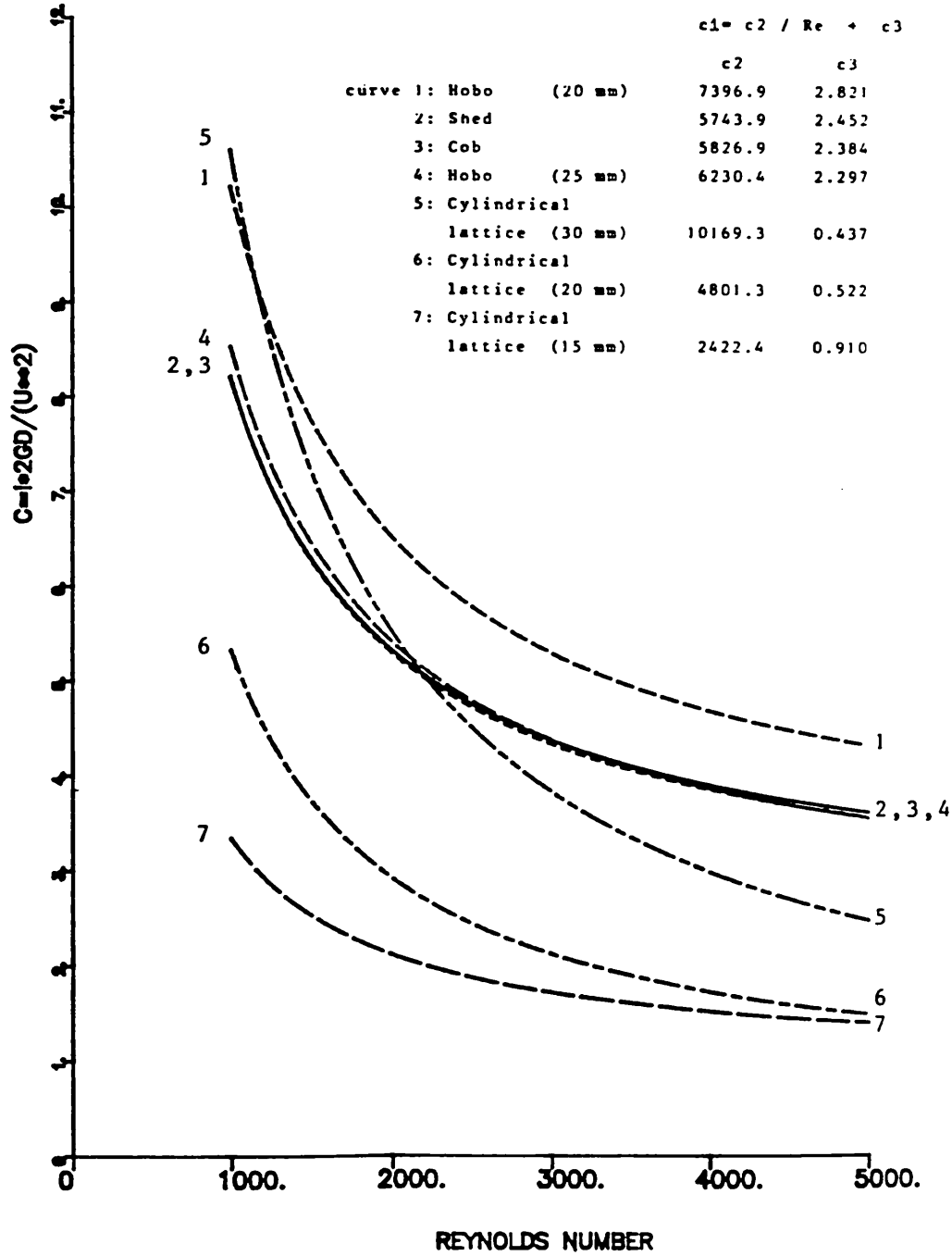


FIG.6.13.B LOSS COEFFICIENT vs REYNOLDS NUMBER

FITTED CURVES $C1 = C2/RE + C3$

RANDOMLY PACKED SPHERES AND ROUNDED STONES

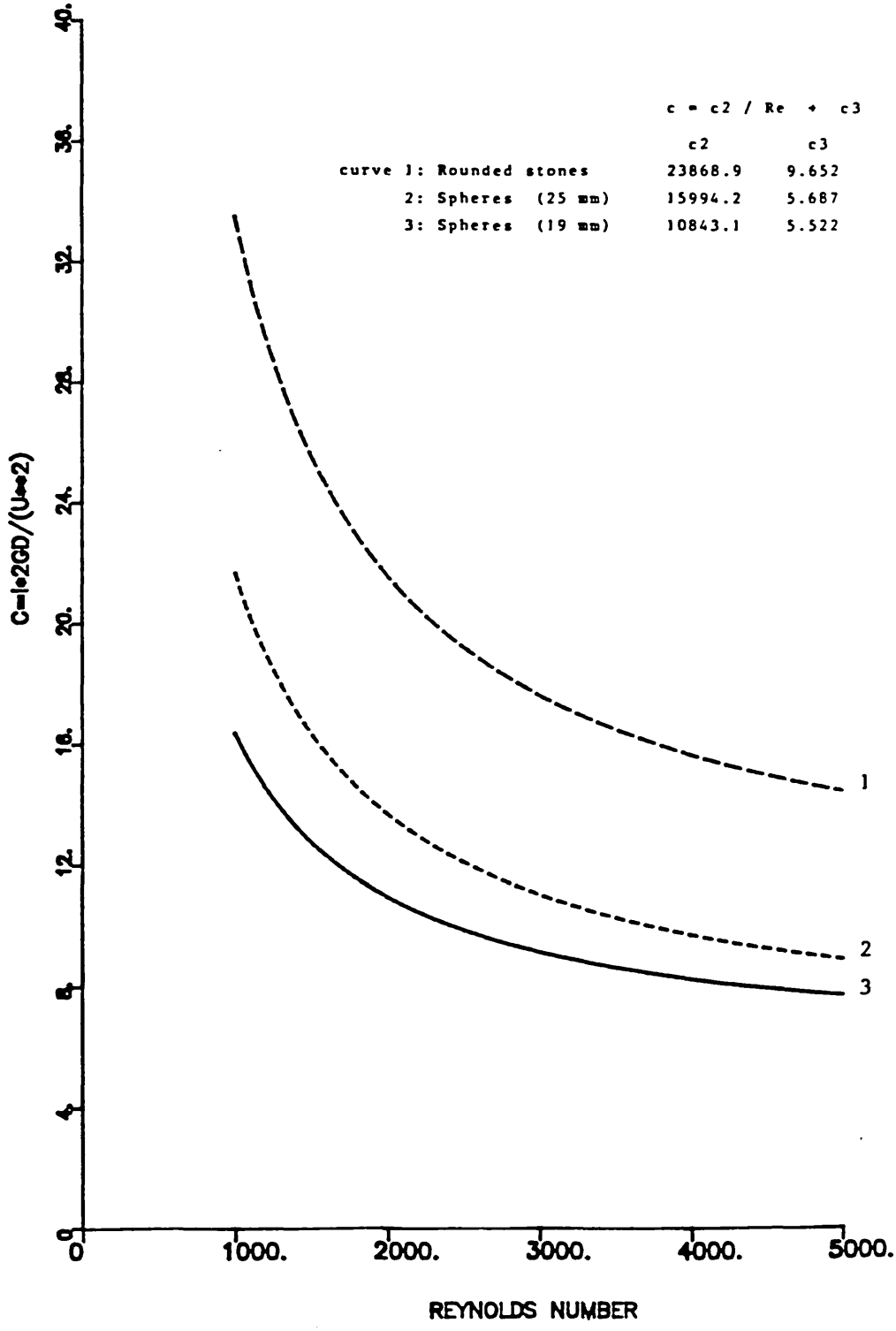


FIG.6.14.A I_T / I_L vs VELOCITY

$I=I_L + I_T$ WHERE $I_L=A*U$ AND $I_T=B*U**2$

FOR HOLLOW BLOCK UNITS AND CYLINDRICAL LATTICE STRUCTURES

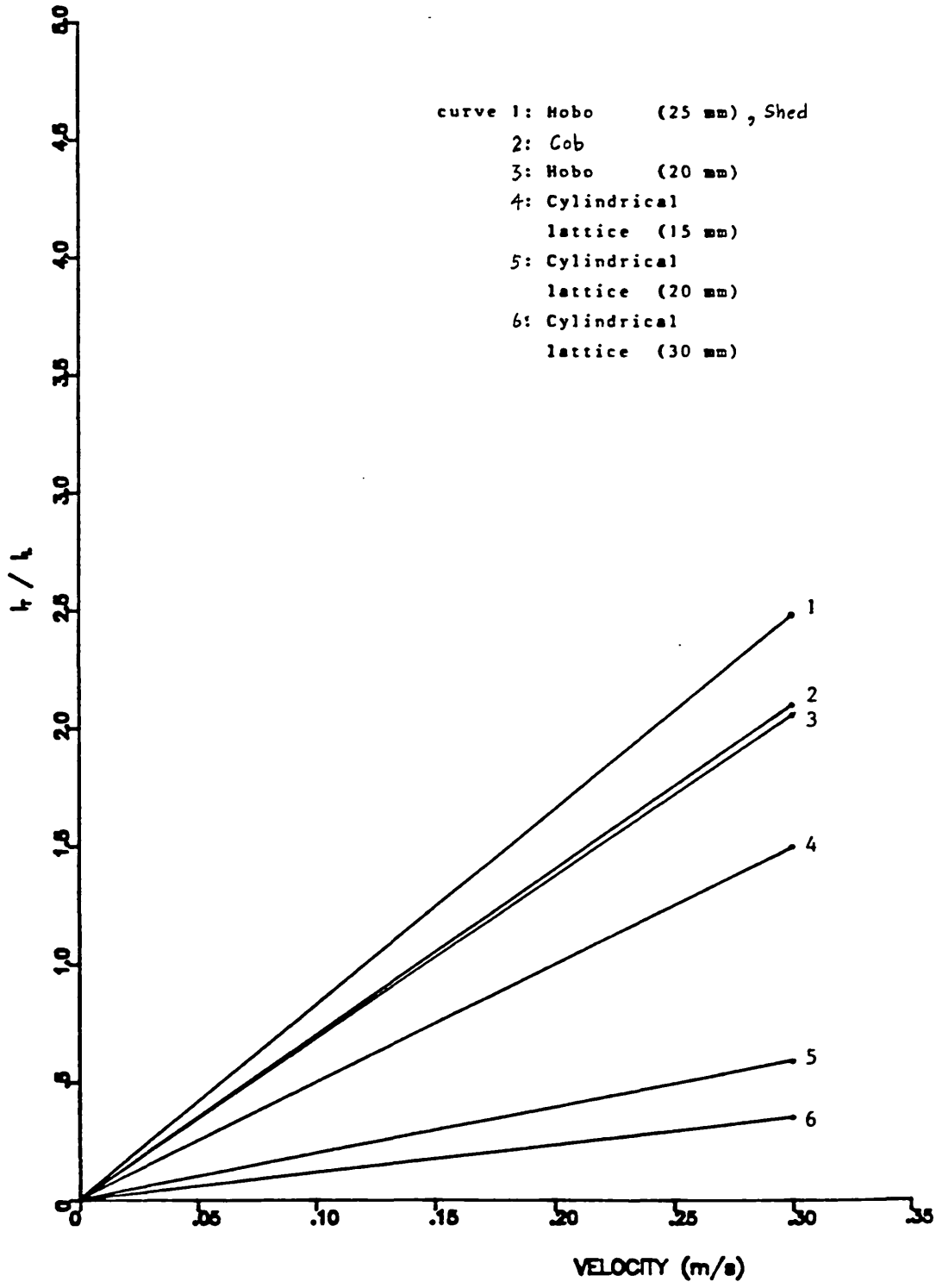


FIG.6.14.B h_T / h_L vs VELOCITY

$I=I_L + I_T$ WHERE $I_L=A*U$ AND $I_T=B*U**2$

FOR RANDOMLY PACKED SPHERES AND ROUNDED STONES

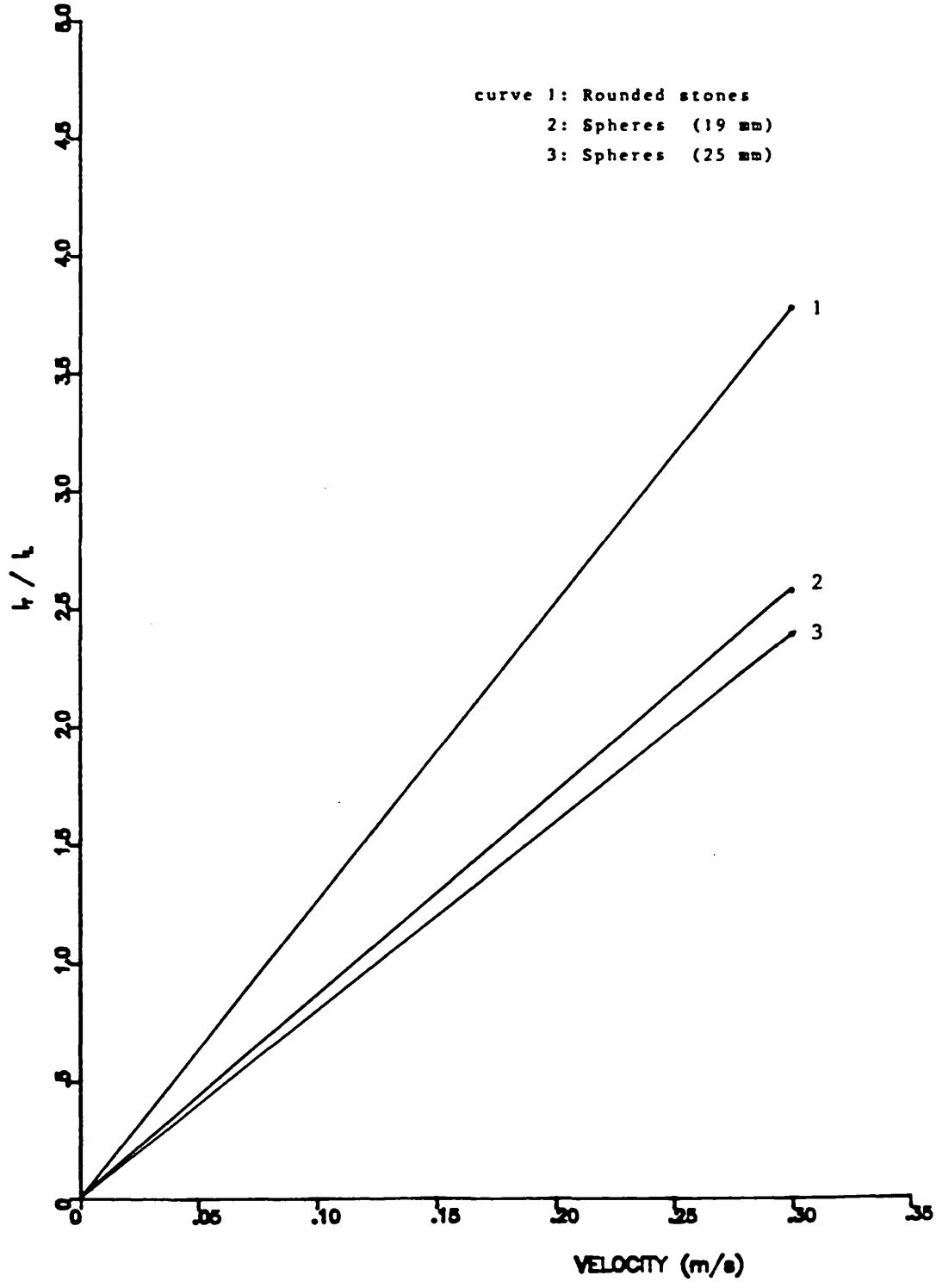


FIG.6.15 TURBULENT COEFFICIENT vs DIAMETER

B IN I=A*U + B*U**2

FOR CYLINDRICAL LATTICE STRUCTURES

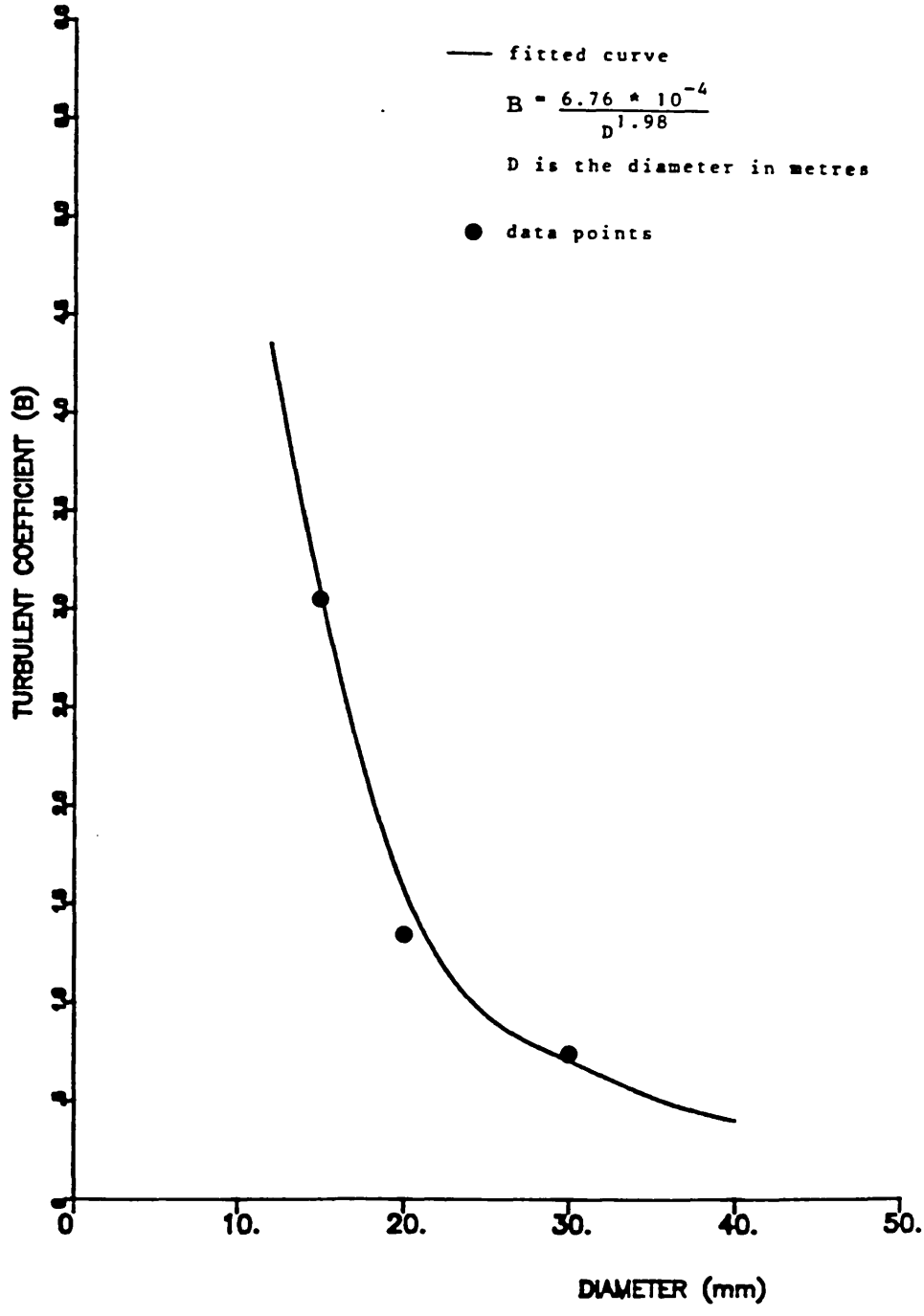


FIG.6.16 KT,KR and KD vs STEEPNESS

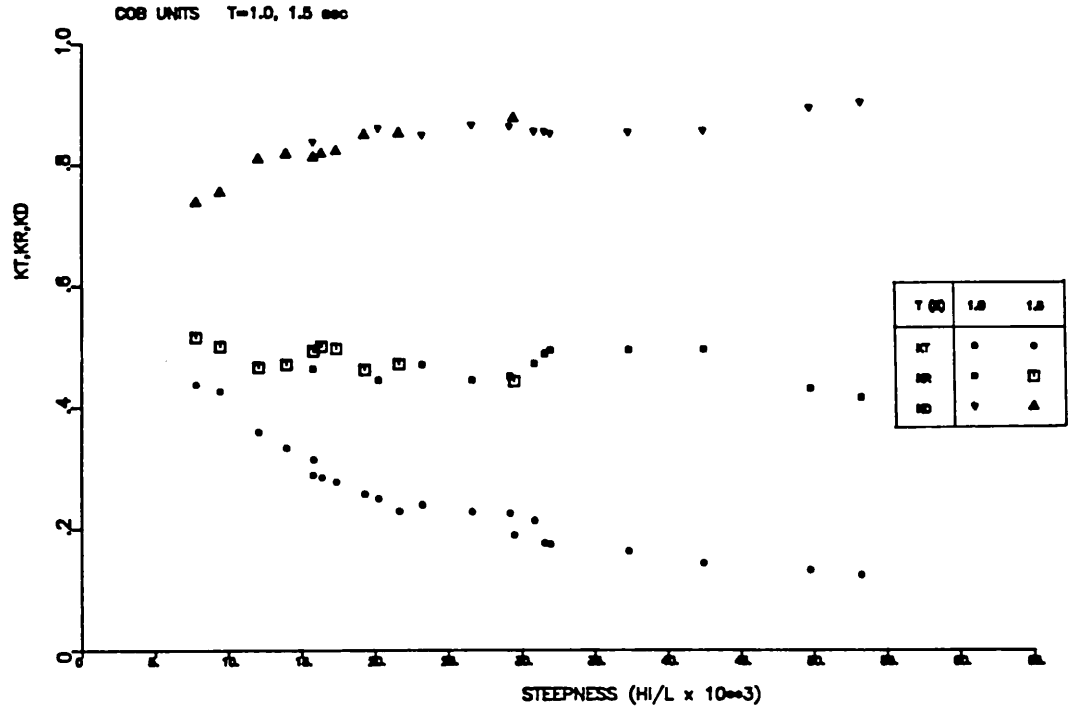


FIG.6.17 KT,KR and KD vs STEEPNESS

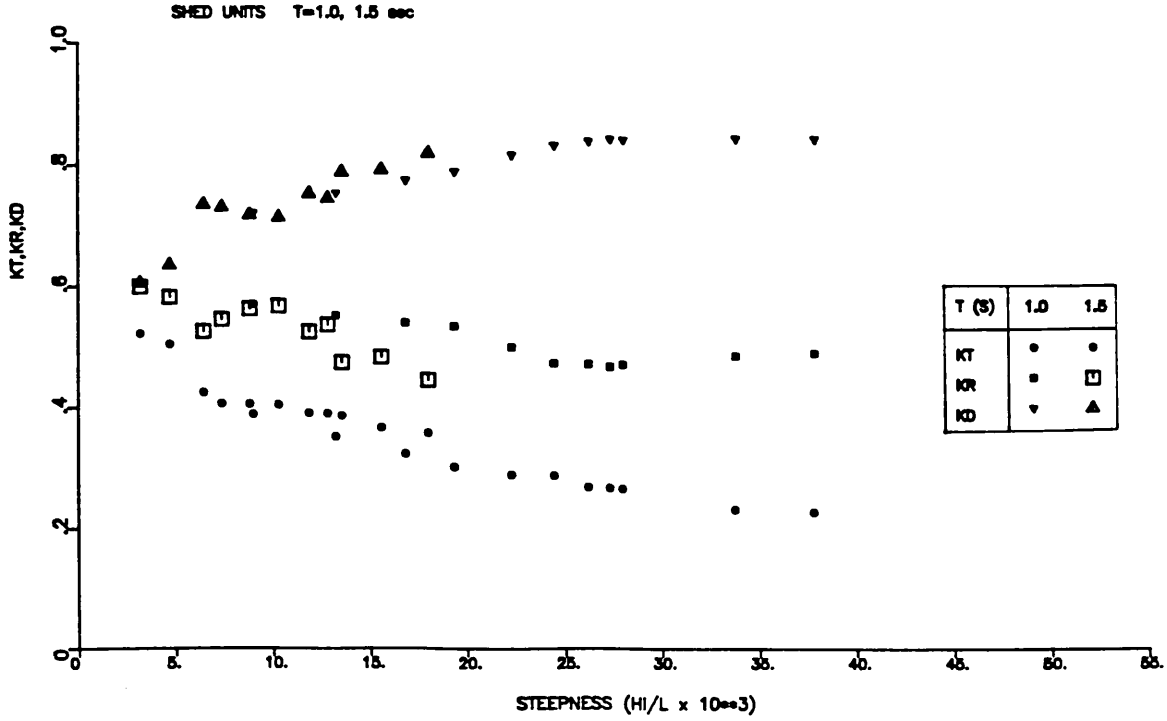


FIG.6.18 KT,KR and KD vs STEEPNESS

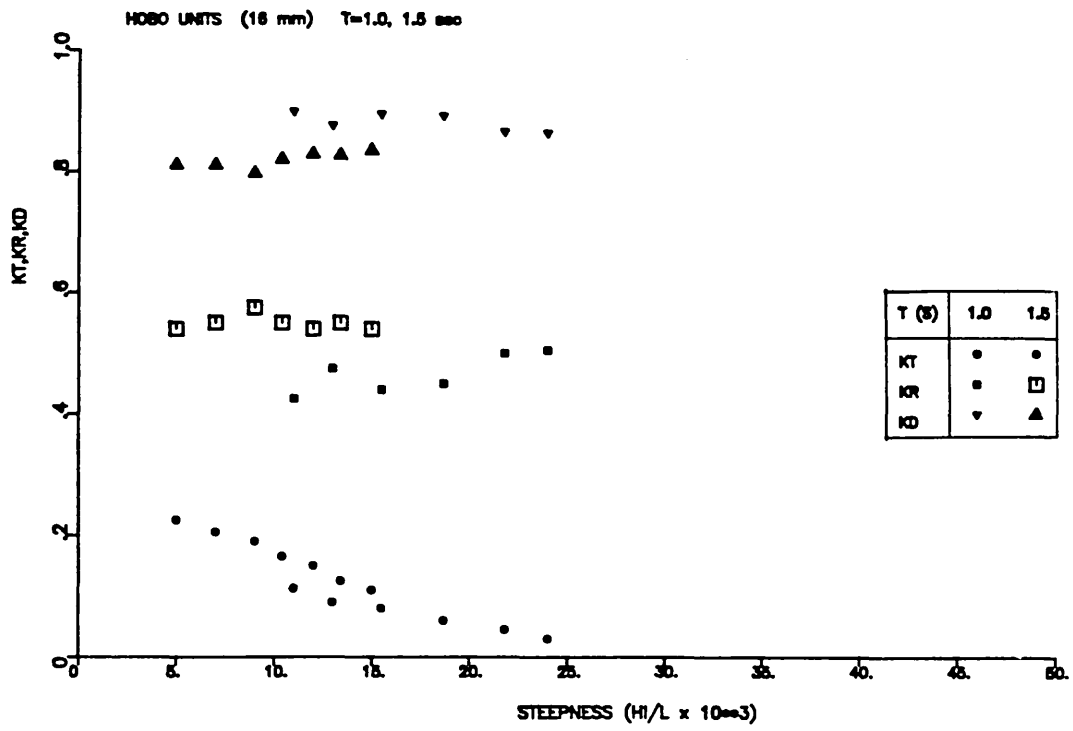


FIG.6.19 KT,KR and KD vs STEEPNESS

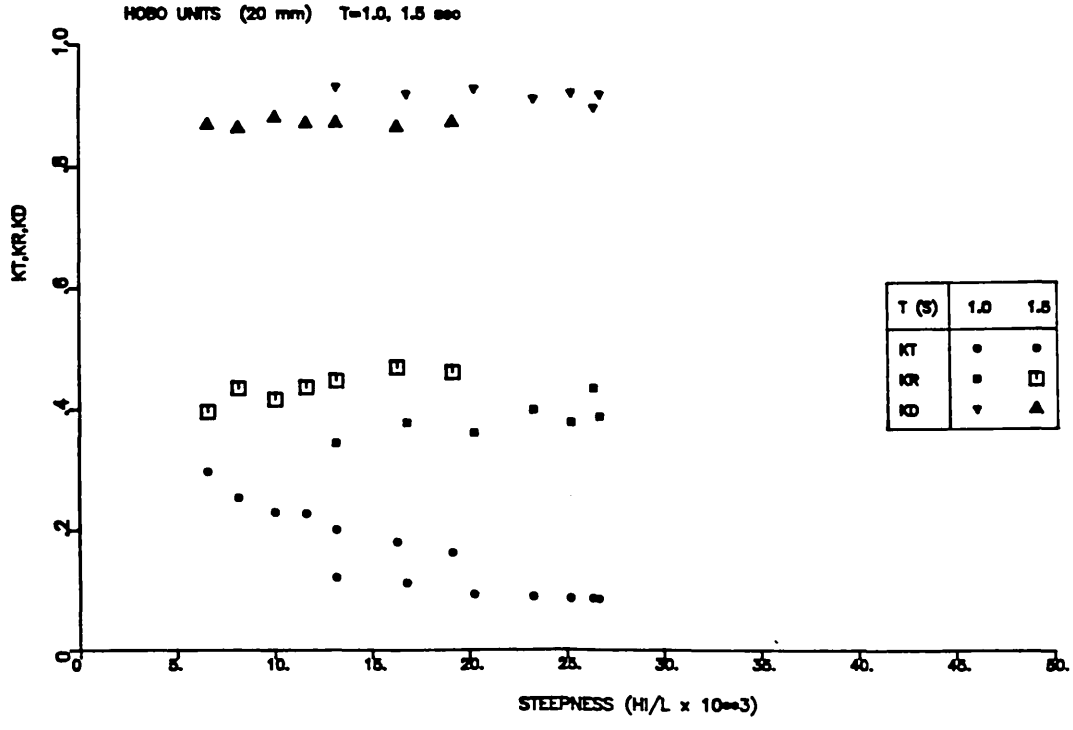


FIG.6.20 KT,KR and KD vs STEEPNESS

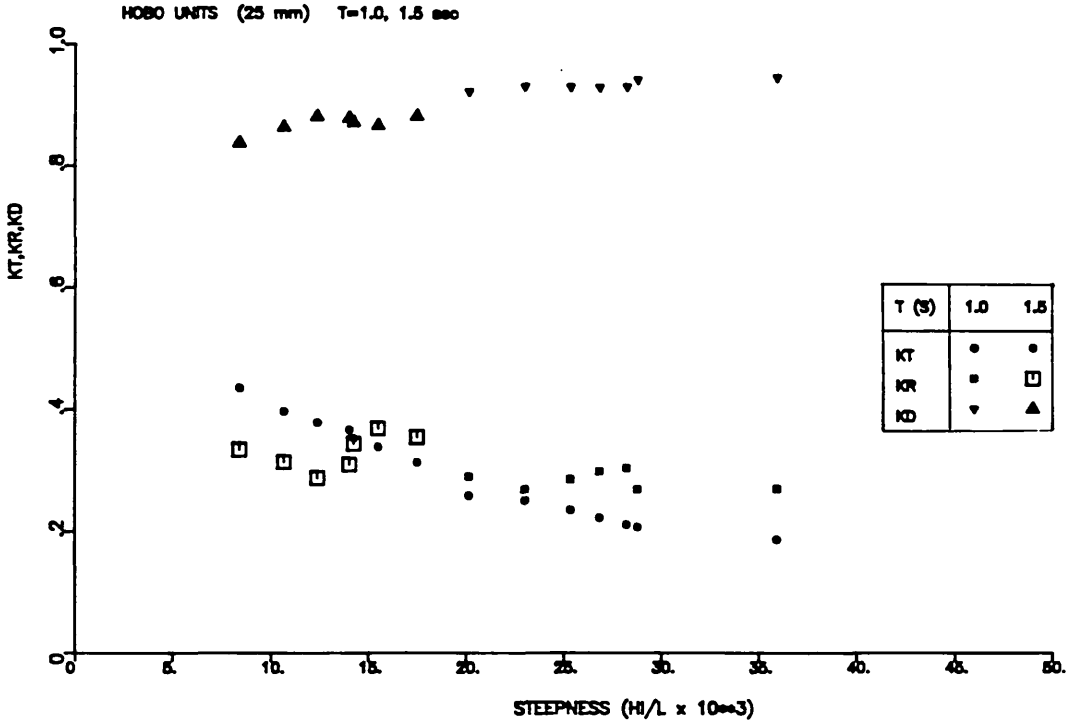


FIG.6.21 KT,KR and KD vs STEEPNESS

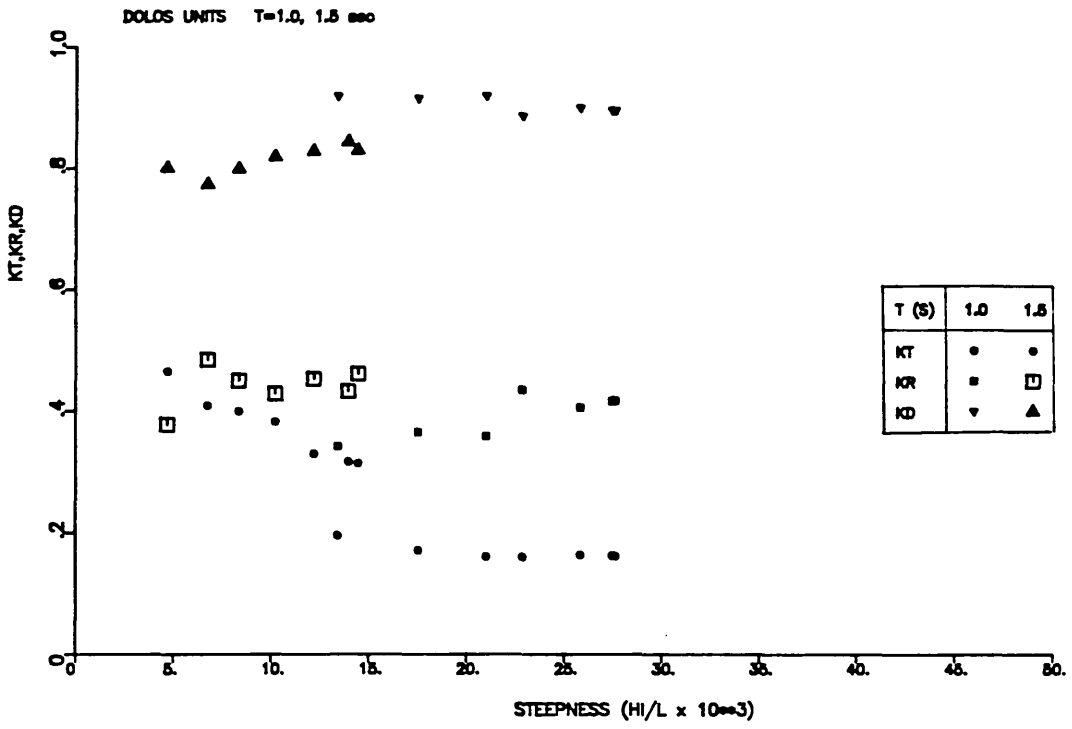


FIG.6.22 KT,KR and KD vs STEEPNESS

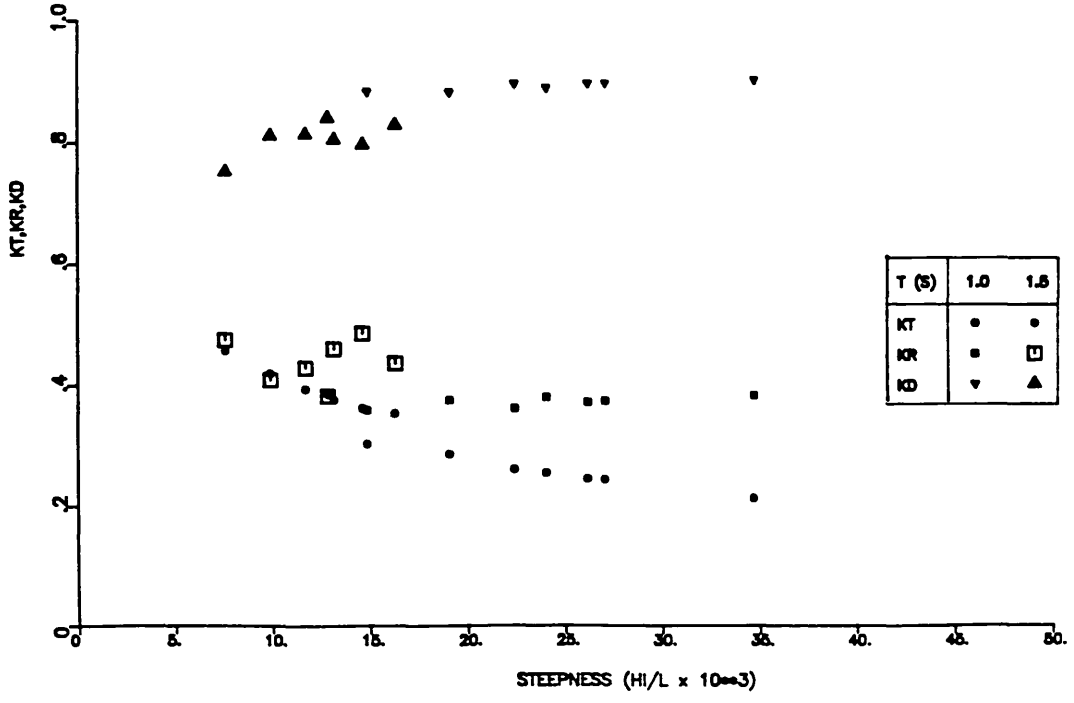


FIG.6.23 KT,KR and KD vs STEEPNESS

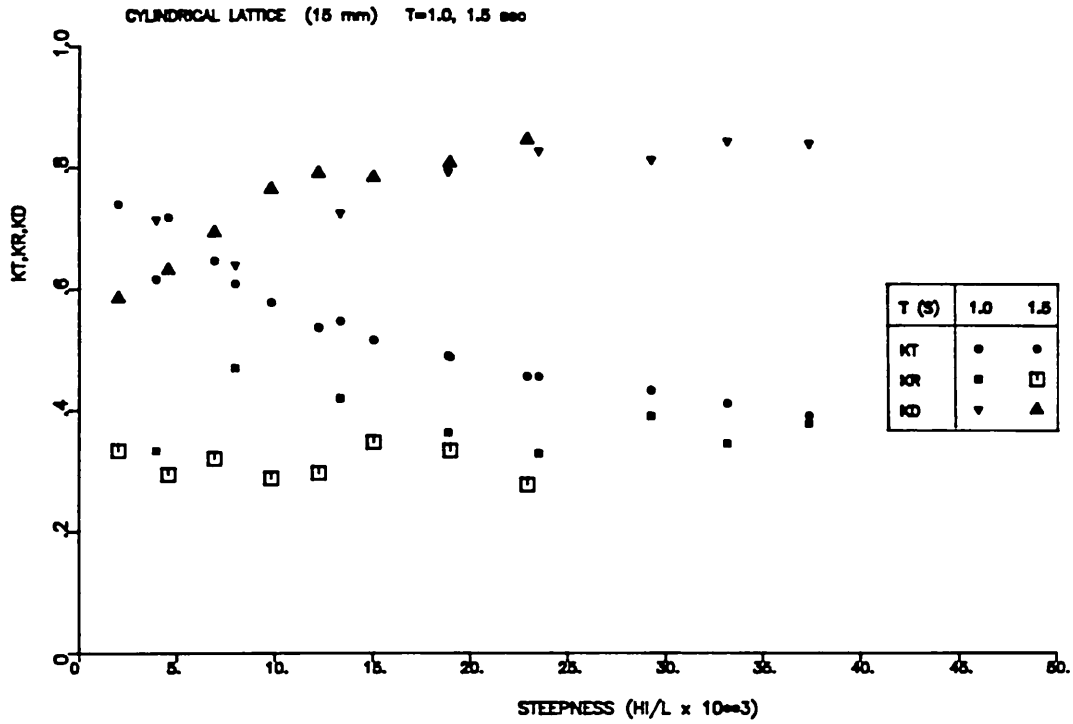


FIG.6.24 KT,KR and KD vs STEEPNESS

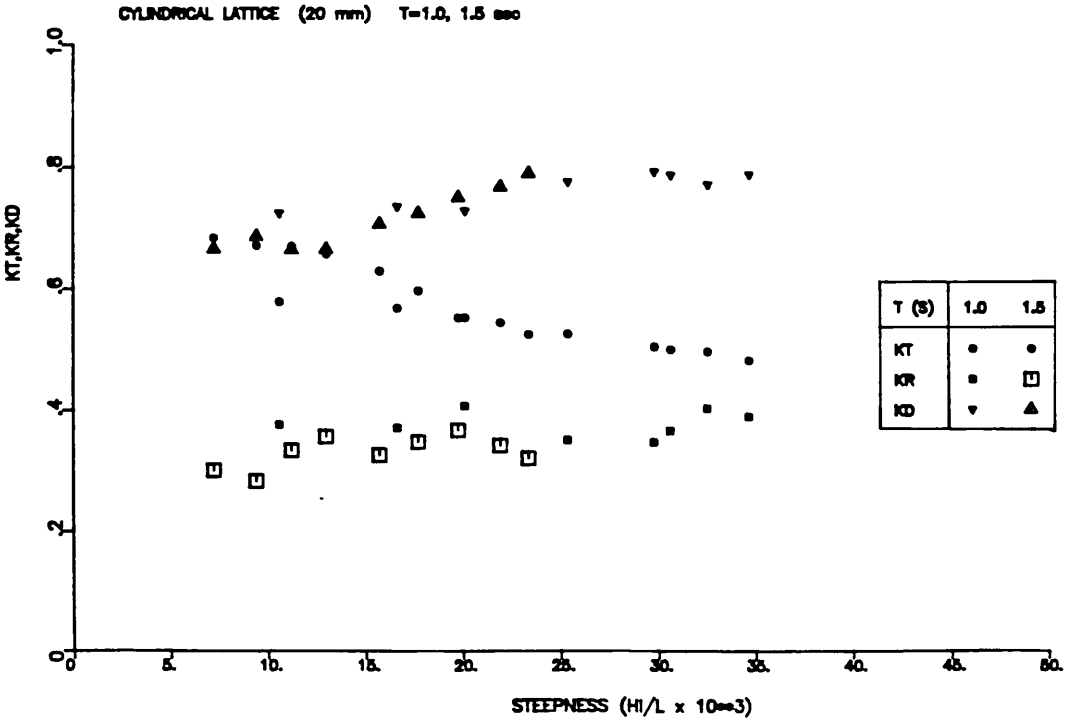


FIG.6.25 KT,KR and KD vs STEEPNESS

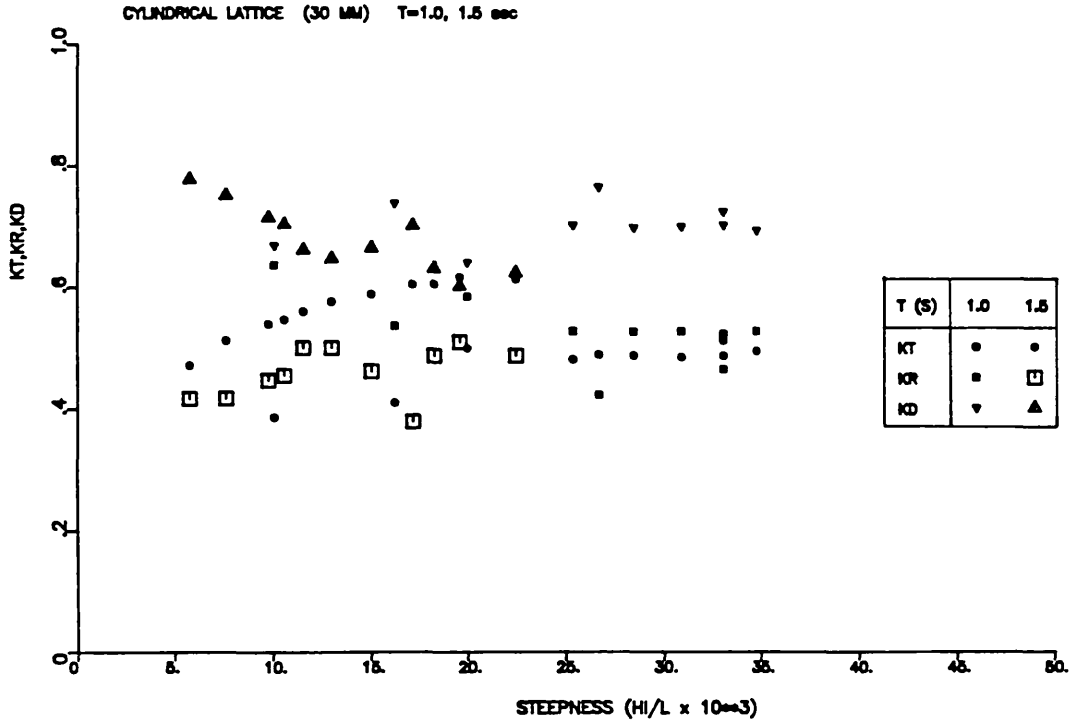


FIG 6.26 K_T VS H_I/D

FOR CYLINDRICAL LATTICE STRUCTURES

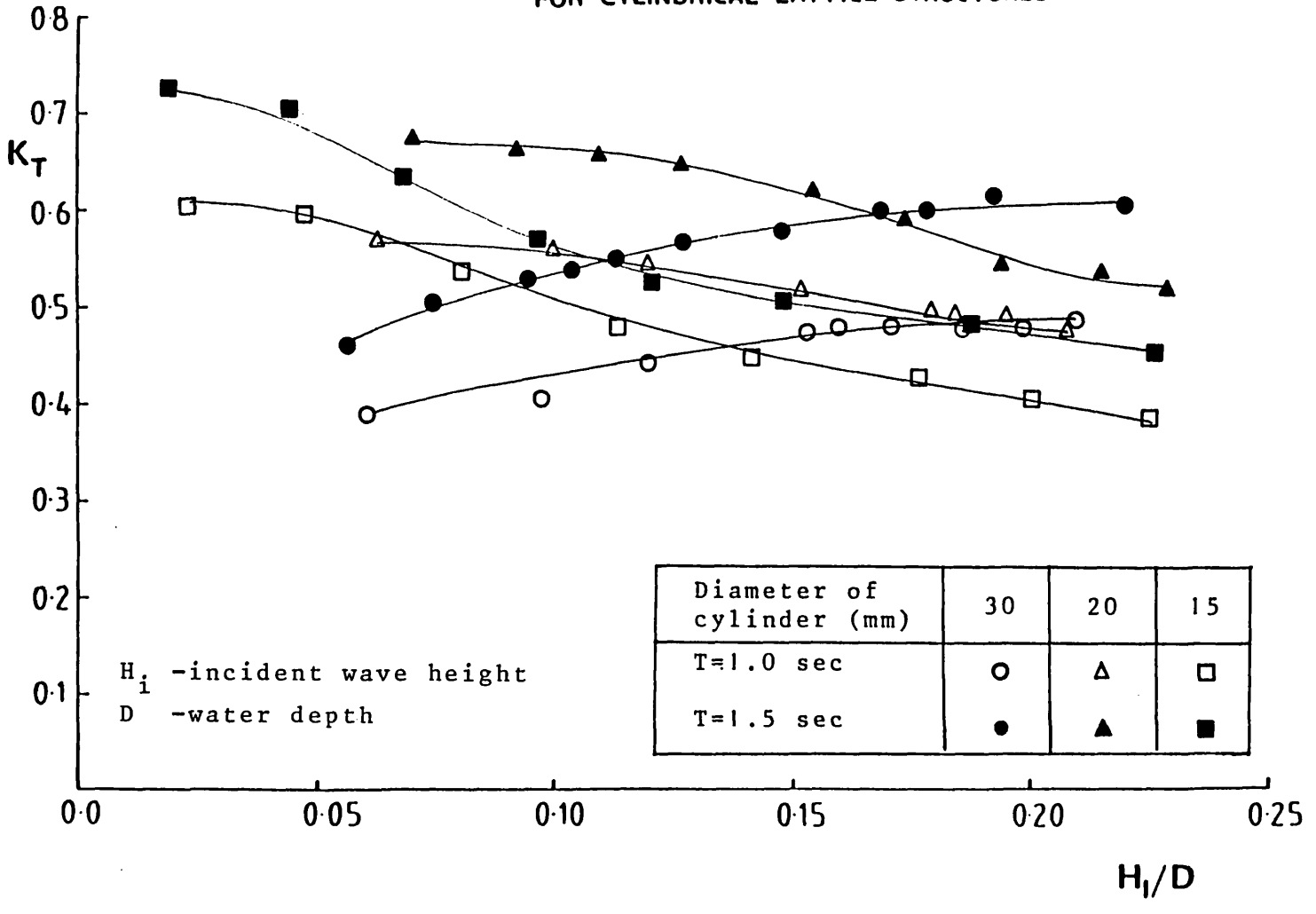


FIG.6.27 KT,KR and KD vs STEEPNESS

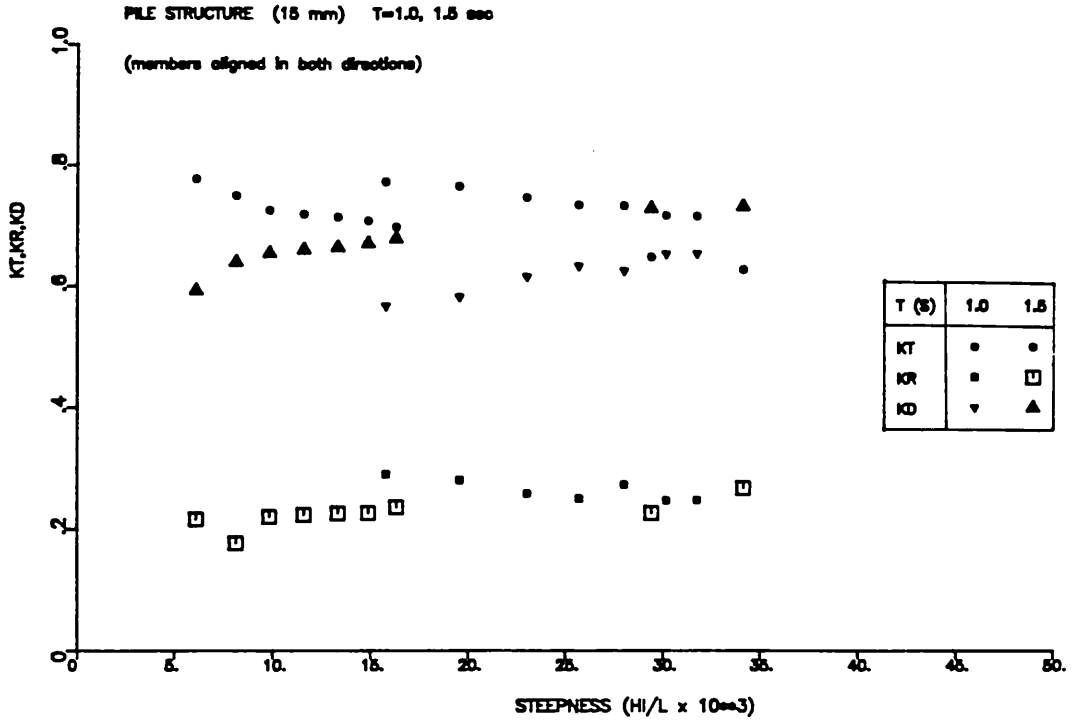


FIG.6.28 KT,KR and KD vs STEEPNESS

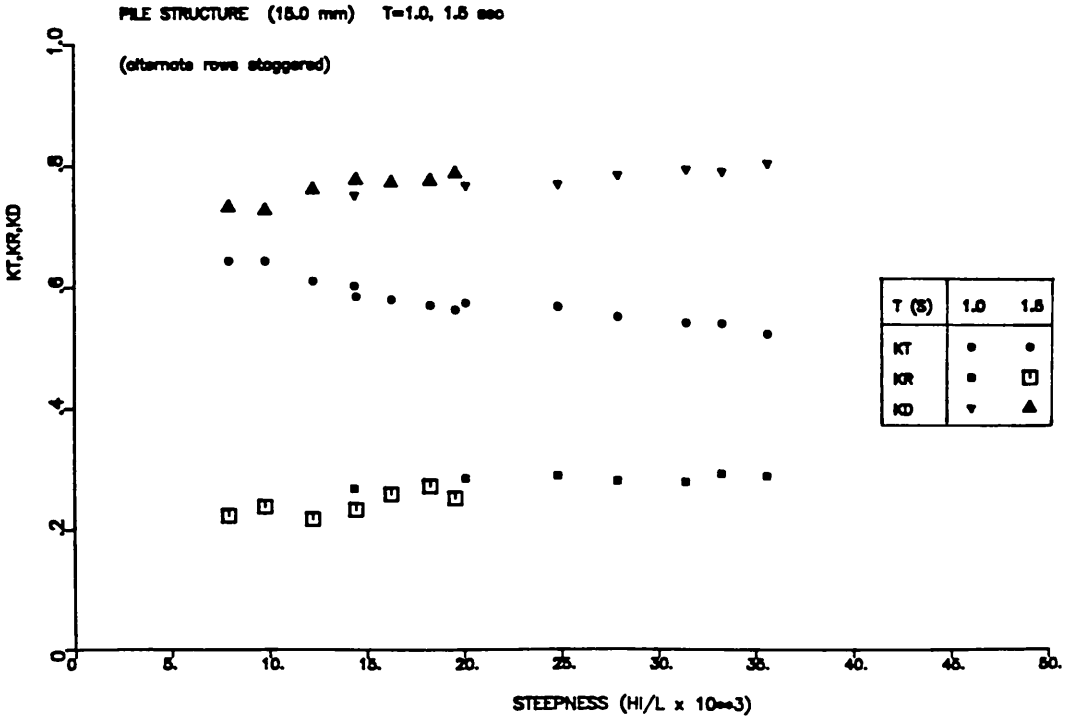


FIG.6.29 KT,KR and KD vs STEEPNESS

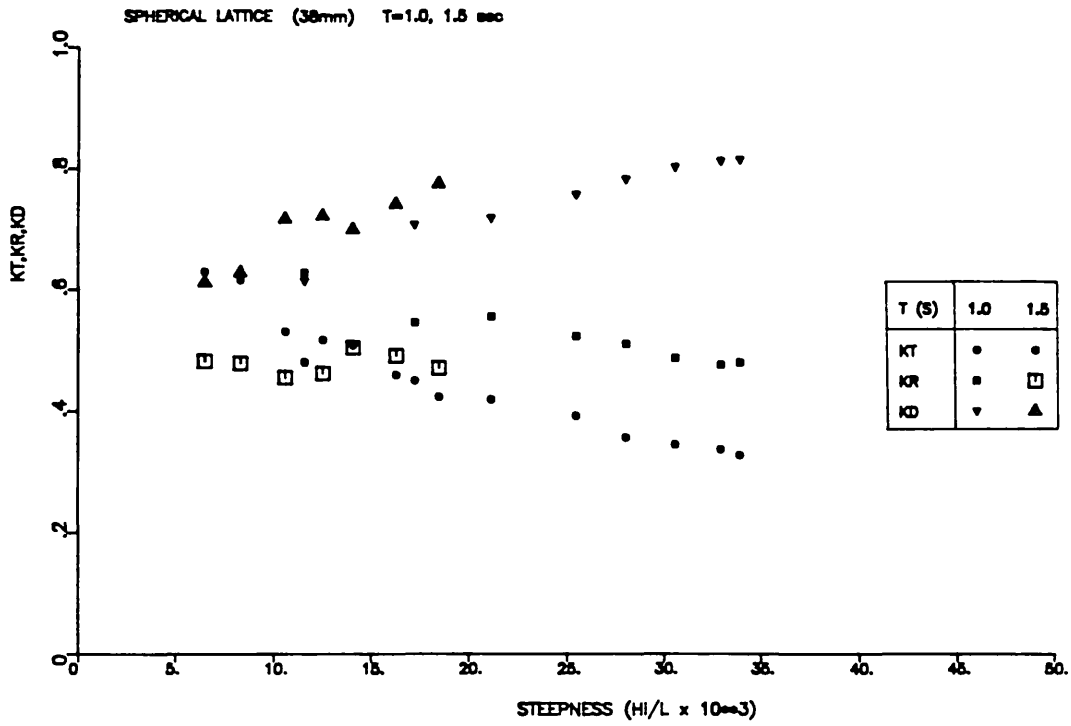


FIG.6.30 KT,KR and KD vs STEEPNESS

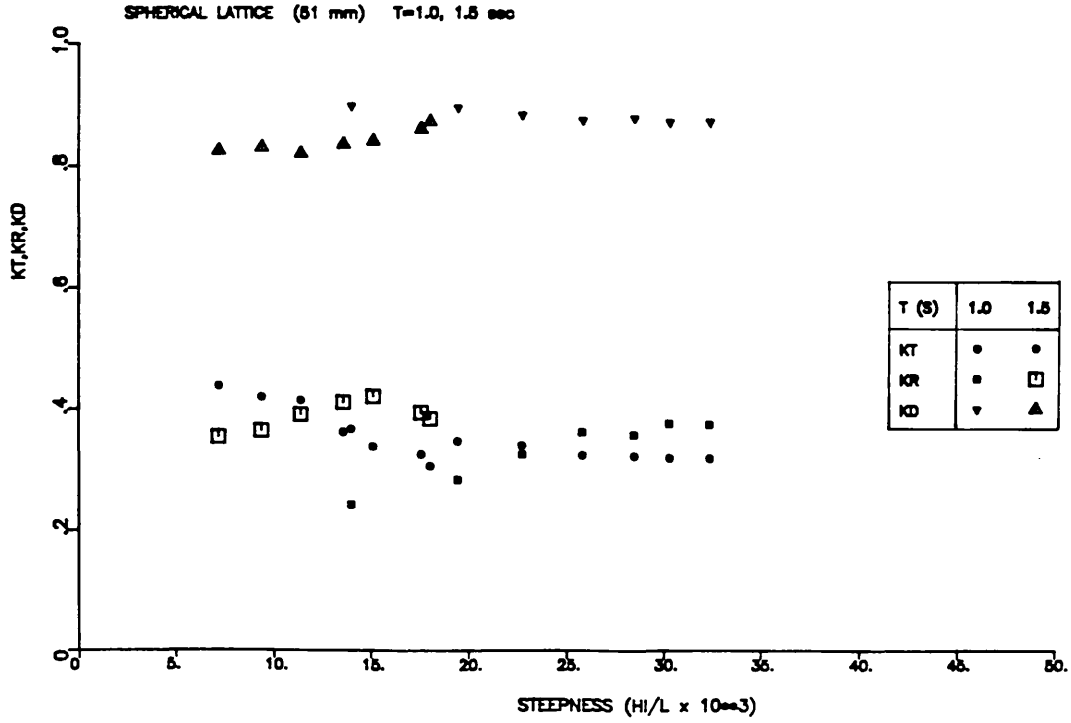


FIG.6.31 KT,KR and KD vs STEEPNESS

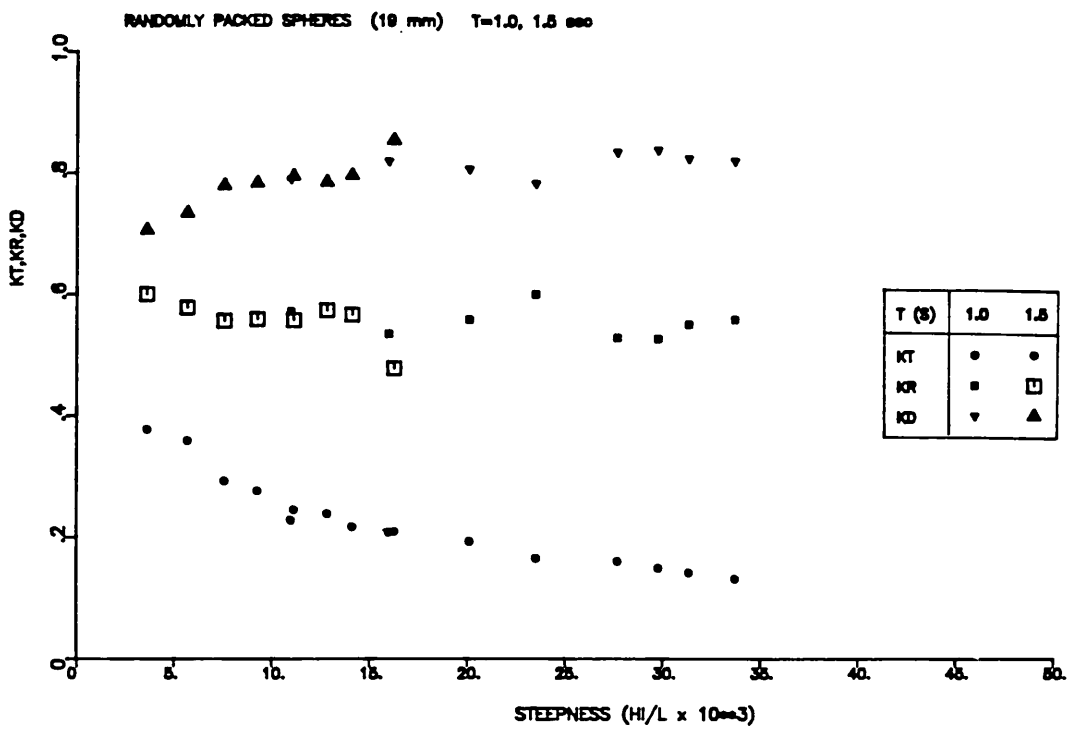


FIG.6.32 KT,KR and KD vs STEEPNESS

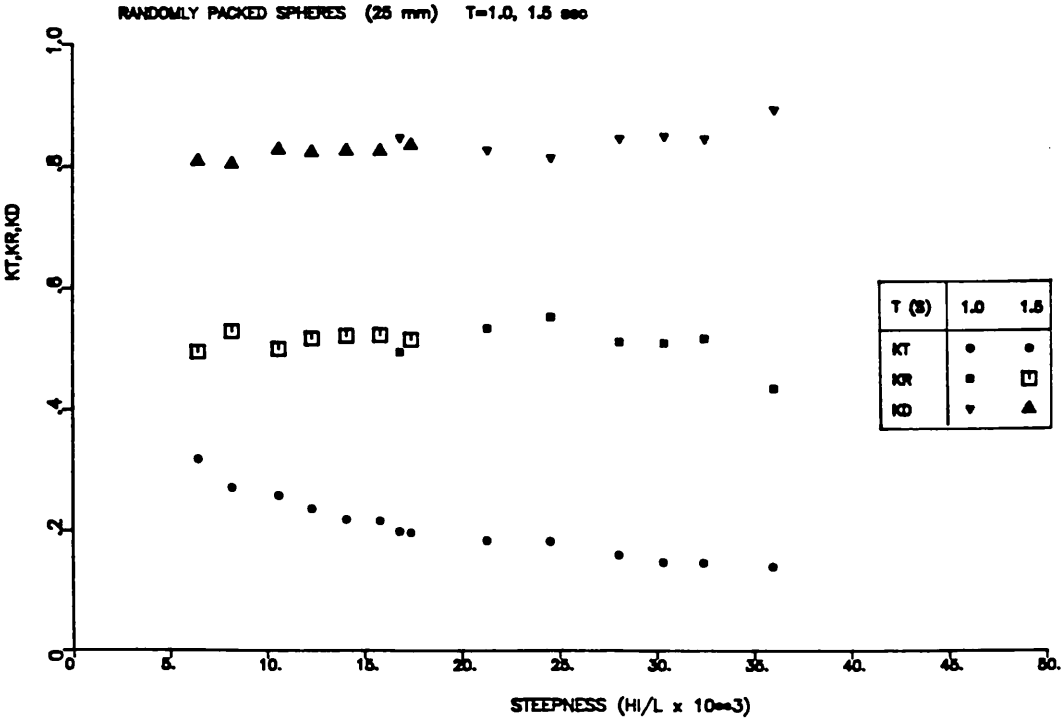


FIG.6.33 KT,KR and KD vs STEEPNESS

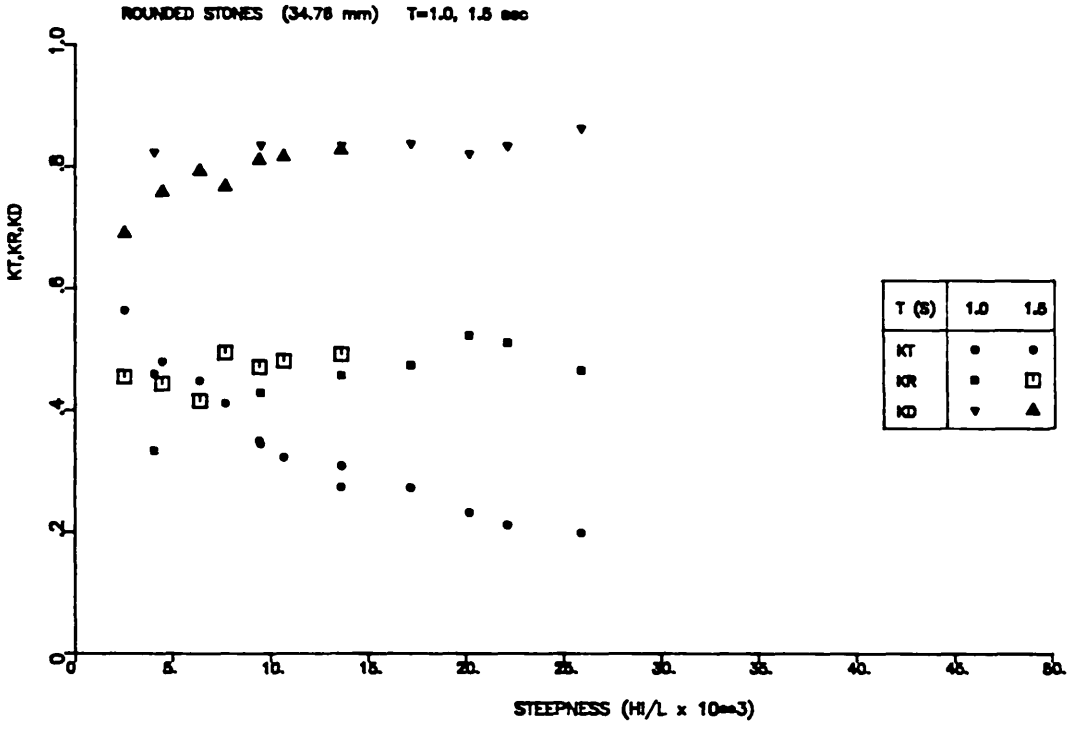
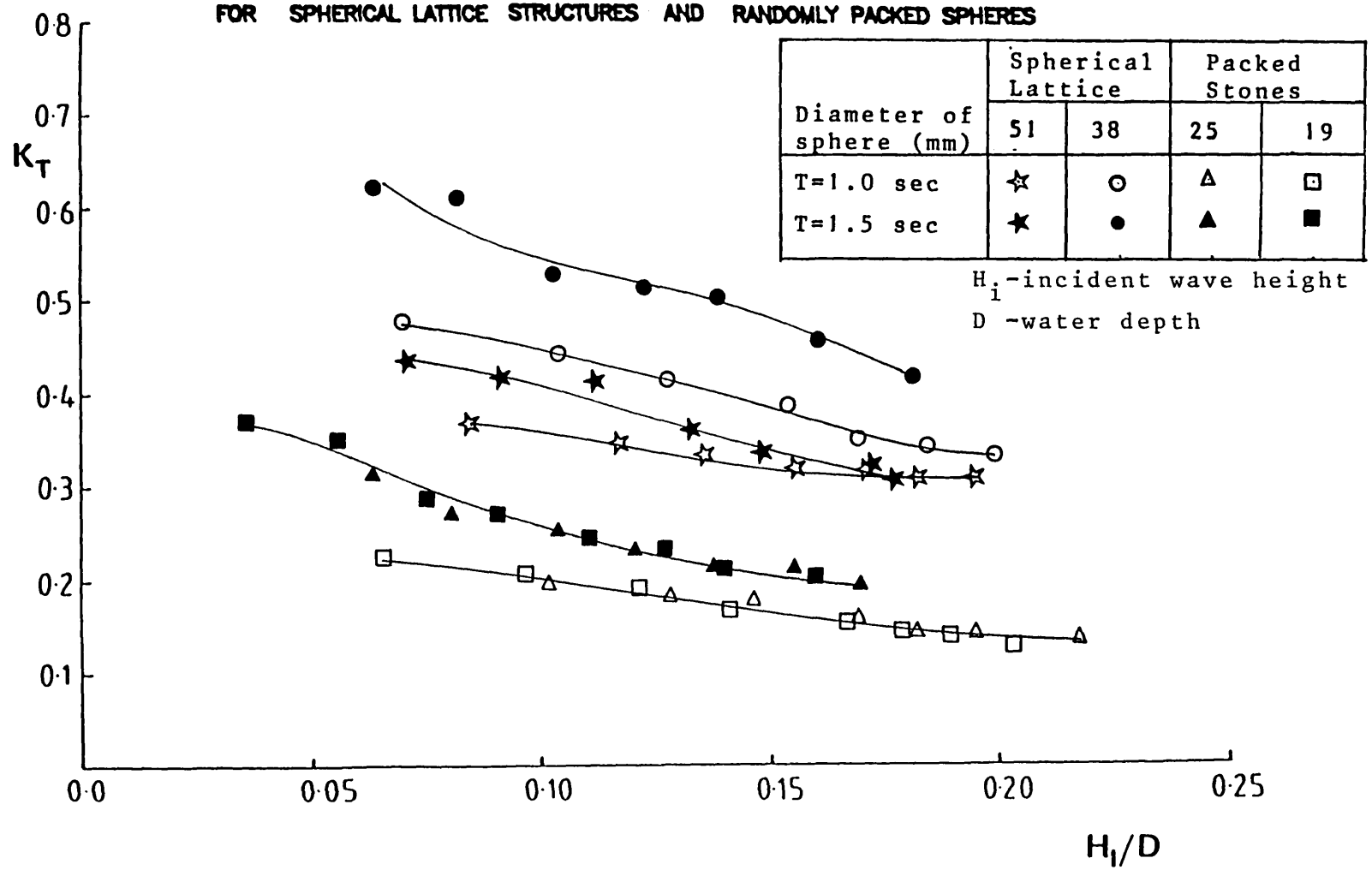


FIG 6.34 K_T VS H_I/D

FOR SPHERICAL LATTICE STRUCTURES AND RANDOMLY PACKED SPHERES



Diameter of sphere (mm)	Spherical Lattice		Packed Stones	
	51	38	25	19
T=1.0 sec	☆	○	△	□
T=1.5 sec	★	●	▲	■

H_i -incident wave height

D -water depth

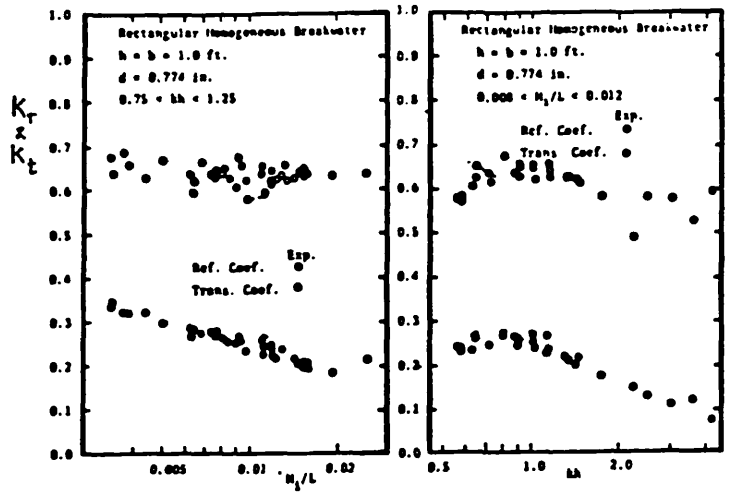
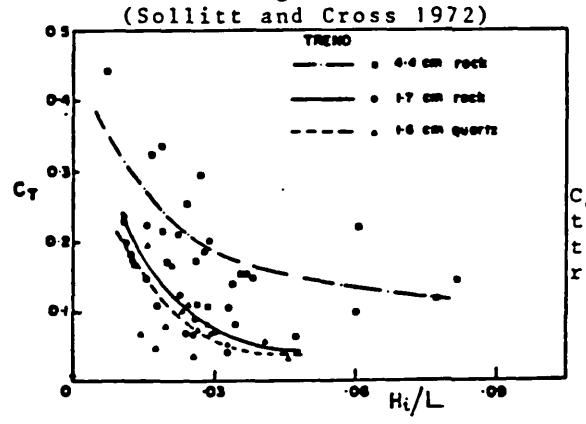


Fig.6.35.a Reflection and transmission coefficients for rectangular breakwaters (Sollitt and Cross 1972)



C_T refers to the transmission at the impervious rear face

Fig.6.35.b Transmission coefficients for rectangular absorber with impervious rear face (Nasser and McCorquodale 1974b)

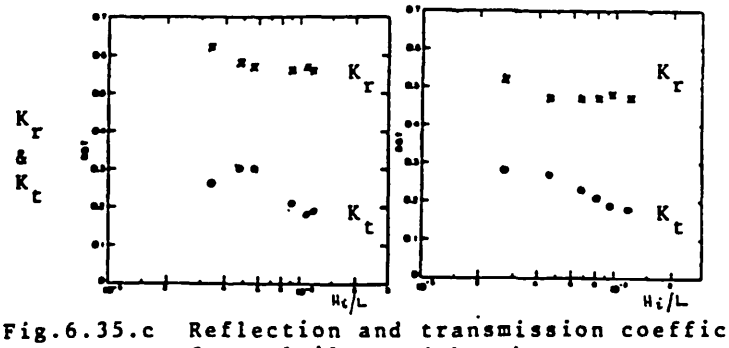


Fig.6.35.c Reflection and transmission coefficients for multilayered breakwater (Madsen, Shusang and Hanson 1978)

FIG.6.35 RESULTS FROM SELECTED INVESTIGATIONS ON WAVE REFLECTION AND TRANSMISSION THROUGH POROUS STRUCTURES

FIG.6.36 KT,KR AND KD vs STEEPNESS

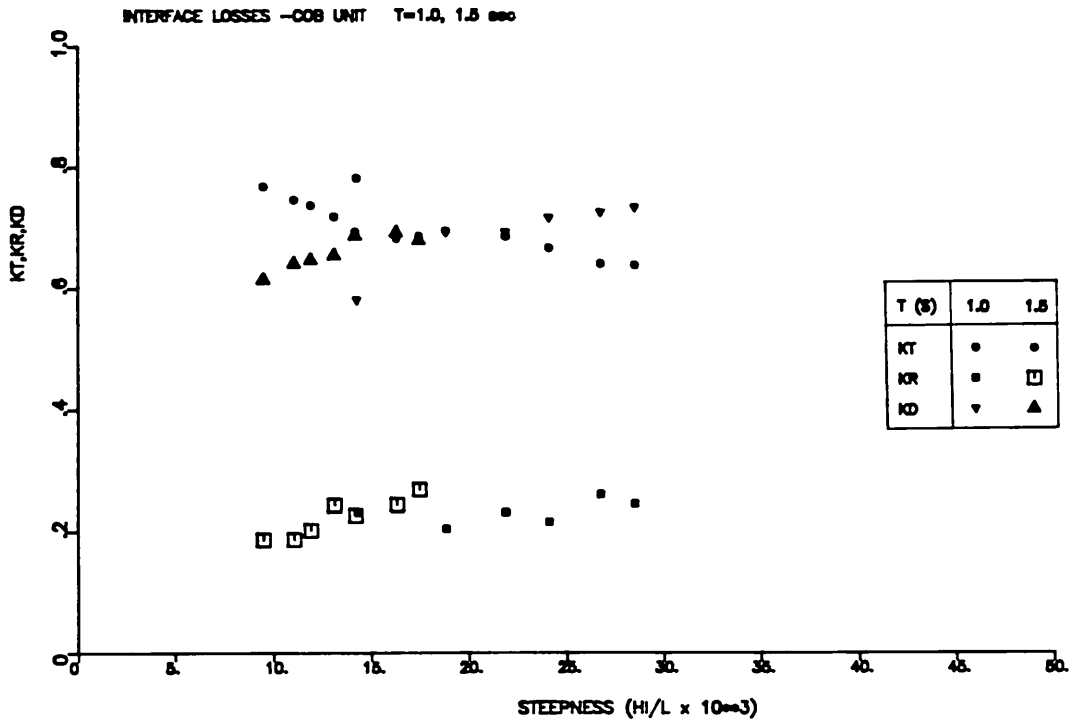


FIG.6.37 KT,KR and KD vs STEEPNESS

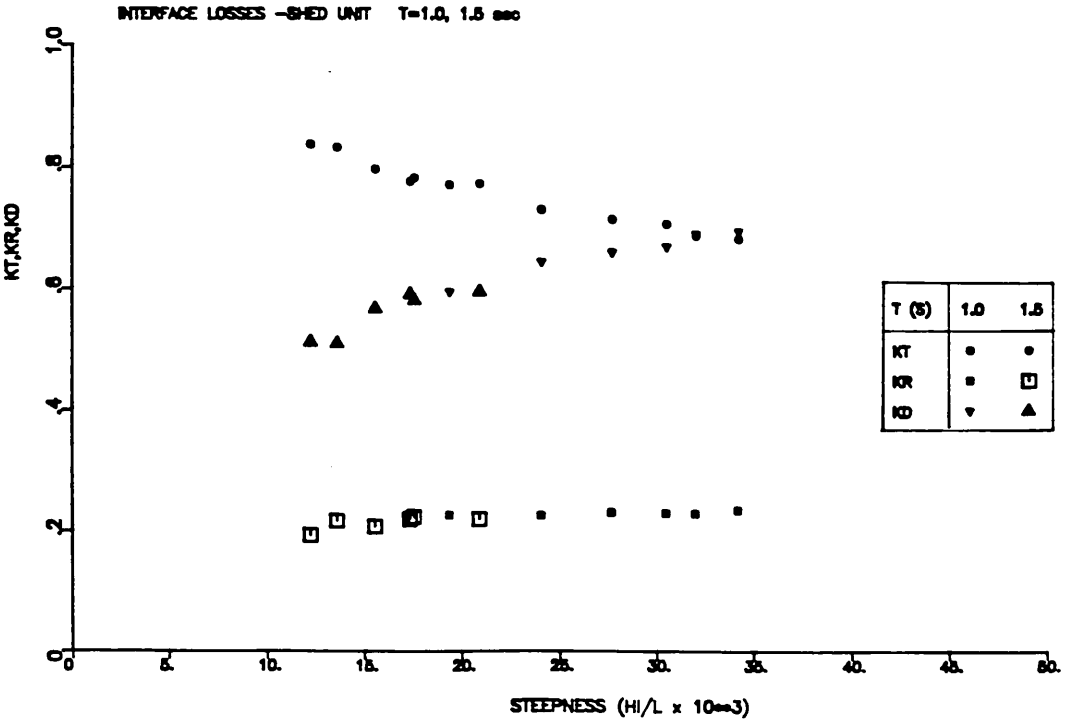


FIG.6.38 COMPARISON OF EXPERIMENTAL AND THEORETICAL VALUES

TRANSMISSION , REFLECTION AND LOSS COEFFICIENTS

POROUS BLOCK CONSISTING OF COB UNITS

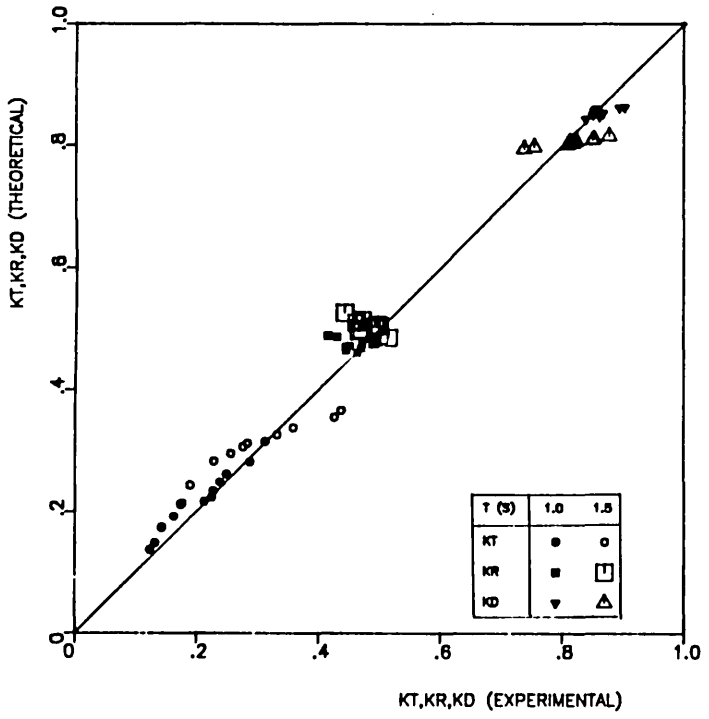


FIG.6.39 COMPARISON OF EXPERIMENTAL AND THEORETICAL VALUES

TRANSMISSION , REFLECTION AND LOSS COEFFICIENTS

POROUS BLOCK CONSISTING OF SHED UNITS

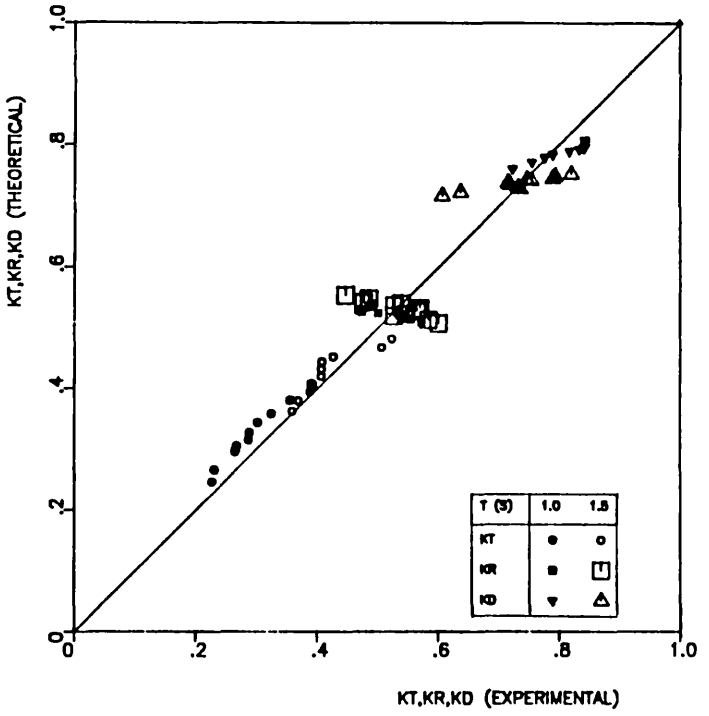


FIG.6.40 COMPARISON OF EXPERIMENTAL AND THEORETICAL VALUES

TRANSMISSION , REFLECTION AND LOSS COEFFICIENTS

POROUS BLOCK CONSISTING OF HOBO (20 MM) UNITS

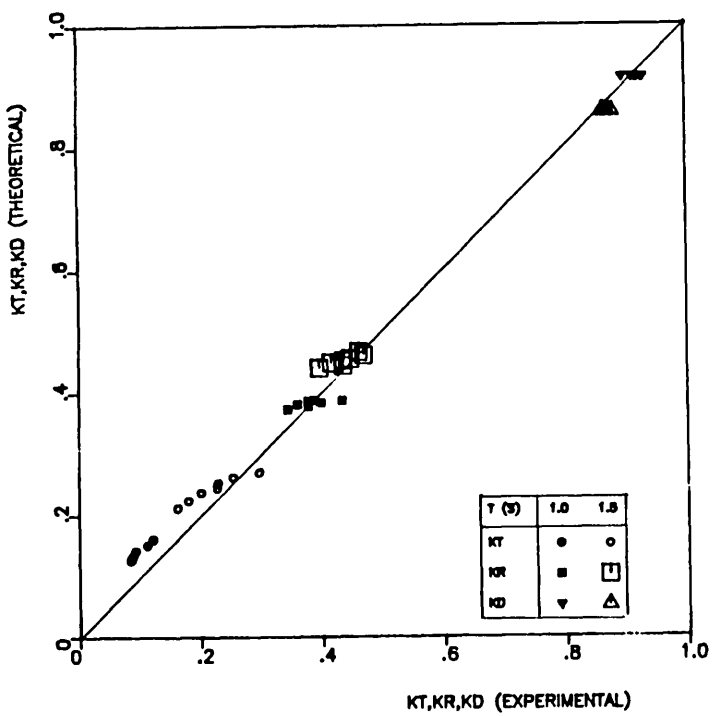


FIG.6.41 COMPARISON OF EXPERIMENTAL AND THEORETICAL VALUES

TRANSMISSION , REFLECTION AND LOSS COEFFICIENTS

POROUS BLOCK CONSISTING OF HOBO (25 MM) UNITS

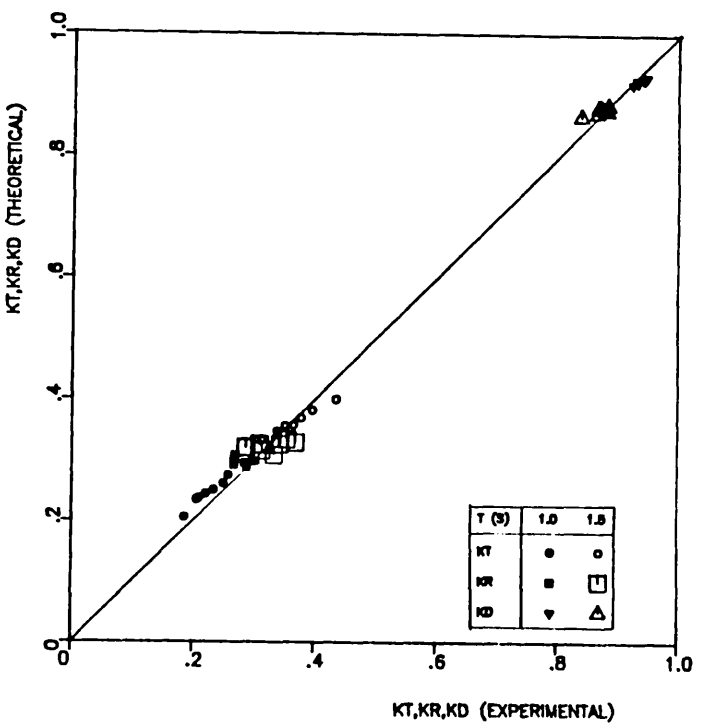


FIG.6.42 COMPARISON OF EXPERIMENTAL AND THEORETICAL VALUES

TRANSMISSION , REFLECTION AND LOSS COEFFICIENTS

CYLINDRICAL LATTICE STRUCTURE (15 MM)

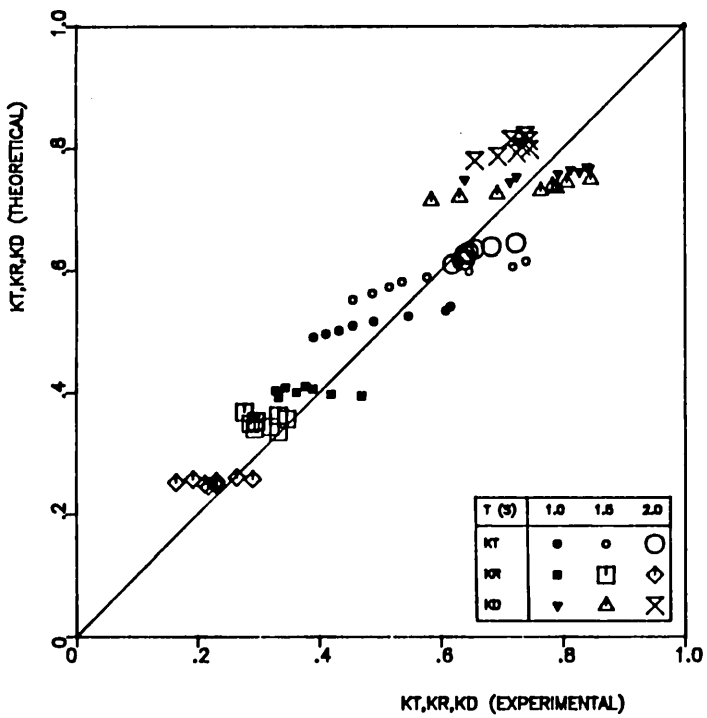


FIG.6.43 COMPARISON OF EXPERIMENTAL AND THEORETICAL VALUES

TRANSMISSION , REFLECTION AND LOSS COEFFICIENTS

CYLINDRICAL LATTICE STRUCTURE (20 MM)

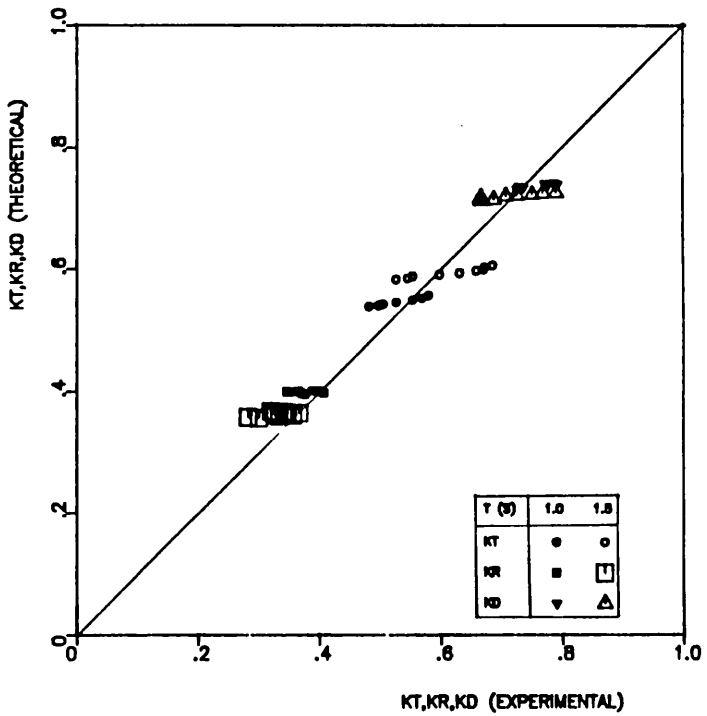


FIG.6.44 COMPARISON OF EXPERIMENTAL AND THEORETICAL VALUES

TRANSMISSION , REFLECTION AND LOSS COEFFICIENTS

CYLINDRICAL LATTICE STRUCTURE (30 MM)

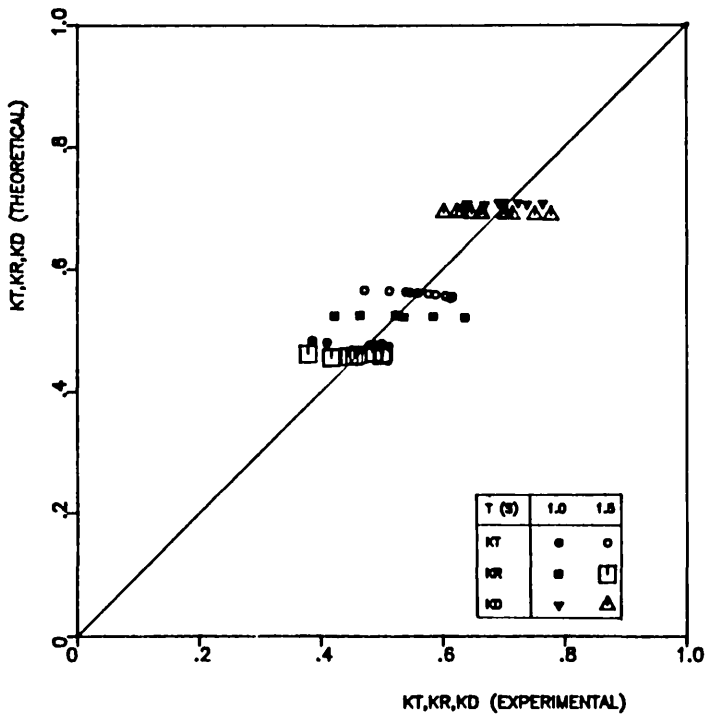


FIG.6.45 COMPARISON OF EXPERIMENTAL AND THEORETICAL VALUES

TRANSMISSION , REFLECTION AND LOSS COEFFICIENTS

RANDOMLY PACKED SPHERES (19 MM)

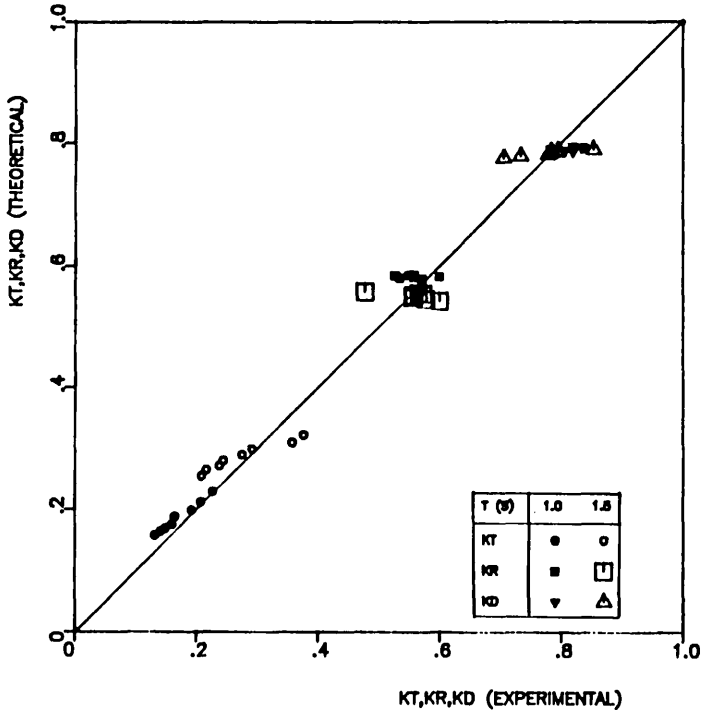


FIG.6.46 COMPARISON OF EXPERIMENTAL AND THEORETICAL VALUES

TRANSMISSION , REFLECTION AND LOSS COEFFICIENTS

RANDOMLY PACKED SPHERES (25 MM)

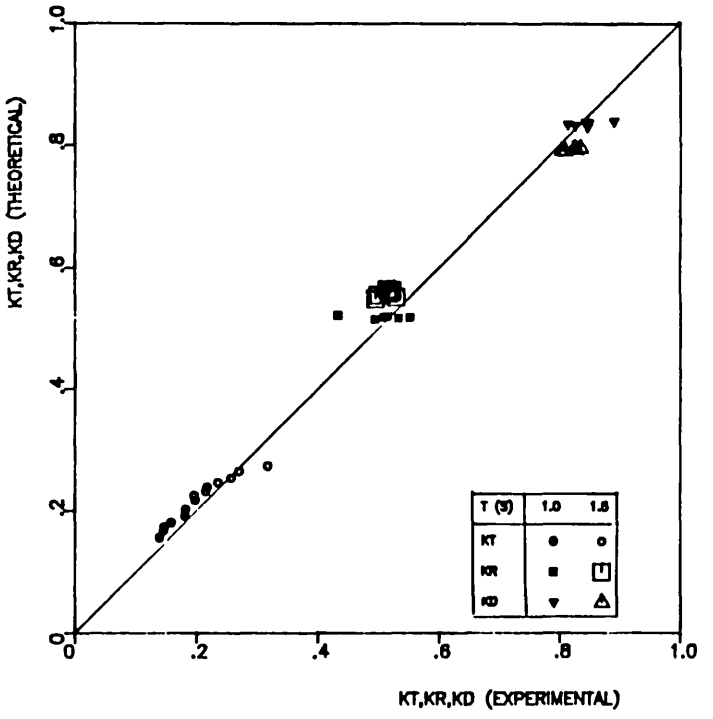
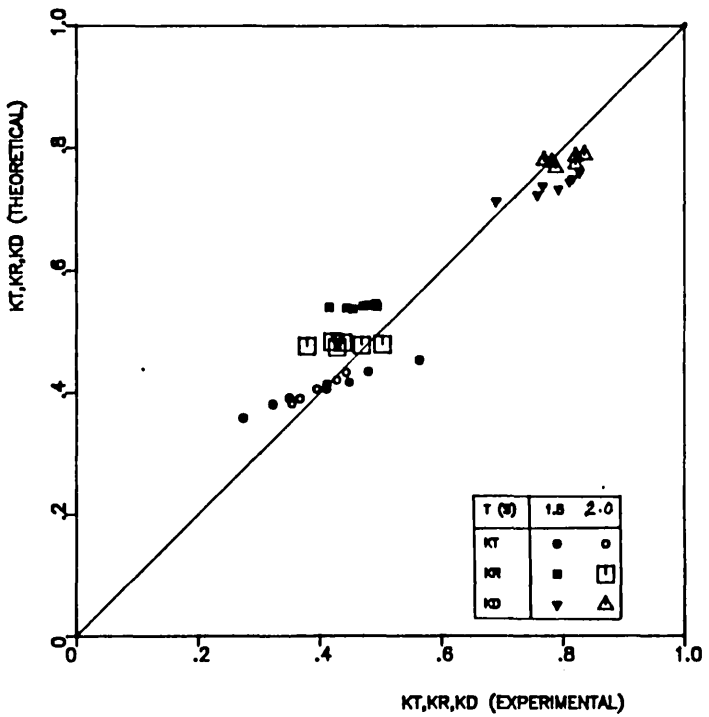


FIG.6.47 COMPARISON OF EXPERIMENTAL AND THEORETICAL VALUES

TRANSMISSION , REFLECTION AND LOSS COEFFICIENTS

RANDOMLY PACKED STONES (34.8 MM)



CHAPTER 7 - CONSTANT ACCELERATION AND VELOCITY TESTS FOR MOVING POROUS BLOCK

7.1. Introduction

From the results of steady flow tests it was established that the hydraulic gradient - velocity relationship can be expressed in the form,

$$I = au + bu^2 \qquad (7.1.)$$

This was found to be valid for widely varying types of porous media used in the present study.

It was pointed out that very few tests have been performed on porous media under unsteady flow conditions. Of these studies the most relevant contribution was made by Hannoura and McCorquodale (1978a) who used a U-tube oscillator for their investigation. It was assumed that one-dimensional unsteady flow in porous media can be expressed in the form,

$$I = (a + b|u|)\, u + \frac{(1 + c)}{g} \frac{du}{dt} \qquad (7.2)$$

where

$c = \frac{(1 - n)}{n} c_n$ = acceleration coefficient

c_n = inertia coefficient

n = porosity

and the value of c was determined by assuming that laminar and turbulent flow coefficients (a and b) under steady flow conditions remain same for unsteady flow.

A similar approach was made by Gibson and Wang (1977) in analysing the results of force measurements on a pile cluster accelerated in initially still water. Information on drag force was determined by towing the model at a constant speed and when accelerating it was ensured that the model passed that speed at approximately constant acceleration.

When an inviscid fluid accelerates past a stationary object, the object experiences a resistance force which is equal to the sum, around the body of the

object, of the pressure components in the direction of acceleration. This force consists of two parts. The first part is derived from the pressure gradient to accelerate the ambient flow and the second part accounts for the resistance resulting from the acceleration of the fluid particles induced by the body, as would be the case if the body was accelerated through an inviscid fluid at rest.

When a viscous fluid is accelerated past a stationary object the motion which starts from rest is initially irrotational and attached. As the velocity increases separation occurs, a wake forms and develops. The formation of the wake results not only in a 'form drag' which would be present if the motion was steady but also in changes in inertial forces. The effects of unsteady flow depend upon the intensity and duration of the acceleration, the time required for the formation of a wake, the shape of the body and the extent to which the body is streamlined.

From the foregoing discussion it is observed that the form drag under unsteady flow need not be the same as for steady flow and viscous, unsteady flow, inertial resistance need not be the same as that of an inviscid fluid. In effect the drag and inertia forces are interdependent and time-dependent. Both are also influenced by the preceding history of fluid motion. In view of these factors it is evident that a purely theoretical description of drag and inertial forces is not possible.

Some of the essential features of the influence of unsteady flow can be investigated experimentally under two-dimensional conditions, in which either the body or the fluid is subjected to predetermined motion along a straight line. Although this type of study can be performed within a well-defined flow environment on structural elements such as cylindrical members, similar studies cannot be extended to porous media because they generate a much more complex flow environment not amenable to simple analysis. It should also be noted that under these conditions it is not possible to extend arguments valid for single bodies to study the behaviour of porous media under the same conditions of flow.

The objective of the present study is to obtain an insight into the influence of time-dependent motion by considering a relatively manageable case : that of the motion of a porous block under unidirectional constant acceleration and constant velocity. The consequence of using the above conditions is that the governing equations describing the motion are reduced to a workable form dependent only on a single parameter and experimental results can be correlated more effectively.

7.2. Method of analysis

On the basis of the findings from the steady flow tests and from the foregoing discussion, the forces acting on a single hollow block armour unit within a porous media composed of the same units can be assumed to have a form,

$$F = au + bu^2 + c\dot{u} \qquad (7.3.a)$$

or

$$F = b_o u^2 + c_o \dot{u} \qquad (7.3.b)$$

where

$\dot{u}$ = value of constant acceleration.

In the above equations $c\dot{u}$ and $c_o\dot{u}$ are the additional terms which account for the effects of constant acceleration.

If the force, velocity and acceleration are known, the coefficients in eq. 7.3 can be determined by the method of least squares. In this method the objective is to correlate the measured force with the theoretical force and the respective coefficients are determined for the best fit values of the predicted and observed forces for the selected time period.

A residual force is defined as

$$R(t) = F_t(t) - F_m(t) \qquad (7.4)$$

in which

F_t is the theoretical force given by eq. 7.3

and F_m is the measured force.

The coefficients are then determined such that the value of the function $\int R^2 dt$ is a minimum.

This function can also be expressed in the form,

$$\varphi = \sum R^2 . \Delta t = \sum_{i=1}^{ND} [F_t(t) - F_m(t)]^2 \, \Delta t \qquad (7.5)$$

ND = number of data points used for the analysis

Δt = sampling rate

TM = ND.Δt

= time duration of measurements used for analysis

The method for minimising R is to partially differentiate with respect to each of the coefficients in turn and equate each of the partial derivatives to zero. Minimisation with respect to the coefficients a, b and c yields,

$$\int R \frac{\partial R}{\partial a} dt = 0$$

$$\int R \frac{\partial R}{\partial b} dt = 0 \qquad (7.6)$$

$$\int R \frac{\partial R}{\partial c} dt = 0$$

The results from the above three simultaneous equations can be expressed in the form

$$\begin{bmatrix} A_{11} & A_{12} & A_{13} \\ A_{21} & A_{22} & A_{23} \\ A_{31} & A_{32} & A_{33} \end{bmatrix} \begin{bmatrix} a \\ b \\ c \end{bmatrix} = \begin{bmatrix} B_1 \\ B_2 \\ B_3 \end{bmatrix} \qquad (7.7)$$

in which the coefficients are given by

$$A_{11} = \int u^2 dt$$

$$A_{12} = \int u^3 dt$$

$$A_{13} = \int u\,\dot{u} dt$$

$$A_{21} = A_{12}$$

$$A_{22} = \int u^4 dt$$

$$A_{23} = \int u^2 \dot{u} dt \qquad (7.8.a)$$

$$A_{31} = A_{13}$$

$$A_{32} = A_{23}$$

$$A_{33} = \int \dot{u}^2 dt$$

and $$B_1 = \int F_m u dt$$

$$B_2 = \int F_m u^2 dt \qquad (7.8.b)$$

$$B_3 = \int F_m \dot{u} dt$$

The force acting on a hollow block armour unit under constant acceleration can be represented by either eq. 7.3.a or eq. 7.3.b, the most suitable form being judged by an estimation of the goodness of fit.

In the present investigation it was found that the force under constant acceleration flow conditions was best described by the relationship,

$$F = bu^2 + c\dot{u} \qquad (7.9)$$

in which

b = drag coefficient under constant acceleration
c = acceleration coefficient
$\dot{u}$ = value of constant acceleration

For the tests under constant velocity corresponding to that of steady flow the experimental values of force were fitted to the curve

$$F = b'u^m \qquad (7.10)$$

in which

b' = drag coefficient under steady flow
m = power of velocity ≈ 2.0

For the experimental conditions adopted for the present study, best correlations for constant acceleration and constant velocity tests were obtained when using eq. 7.9 and 7.10 respectively.

In any experimental technique relating to moving objects, vibrations are likely to develop which could distort the results. From the initial stages of this experimental programme, it was apparent that the carriage motion introduced vibrations which prevented a simple analysis of force data (ref. Section 4.4.8).

Hence care had to be exercised in adopting data reduction methods depending on the relative influence of vibration. This aspect was critically evaluated by Sarpkaya and Collins (1978) in relation to the test apparatus used by Garrison, Field and May (1977) to study the influence of drag and inertia forces on a cylinder in periodic flow. With reference to the force traces, concern was expressed over the presence of large amplitude vibrations scattered unevenly. Sarpkaya and Collins were of the opinion that under such circumstances it would be difficult to extract reliable information without appropriate analysis.

The natural frequencies of the force transducer in air and water were 11.5 Hz and 10.0 Hz respectively. Initial tests indicated that a signal having a frequency approximately equal to 10 Hz was present in the force signal and as the velocity increased the magnitude of this signal increased. After modifications were made to the apparatus to increase its overall rigidity, the magnitude of the signal was greatly reduced. Considering the expected frequency range, the force signal was recorded at a sampling rate of 50 Hz.

The measured force data from constant acceleration tests $F_m(t)$ was subjected to a multi-point smoothing procedure in order to compute the smoothed force $F_s(t)$. The force coefficients b and c in eq. 7.9 were determined from this force time - history. A frequency analysis was performed on the residual force,

$$F_r(t) = F_m(t) - F_s(t) \qquad (7.11)$$

which was obtained after trend removal.

7.3. Discussion of experimental results

The results from constant acceleration tests are summarized in Table 7.1. For each armour unit tests were performed for two values of constant acceleration and for a series of values of constant velocity. The lower value of constant acceleration lies in the range 0.15 - 0.24 m/sec^2 and the higher value lies in the range 0.35 - 0.47 m/sec^2. Both velocity - time relationship for the motion of the carriage and force - velocity relationship for the measured force have a very high correlation coefficient. Hence there exists good agreement between the experimental and fitted curve.

In the presentation of results a non-conventional unit 'gm force' was used for force measurements. This has been adopted mainly because of the comparatively small values of force measured in this study (1 gm force = 980.665

x 10^{-5} N).

For three of the armour units, results from two experimental runs are presented for the higher value of constant acceleration to assess the repeatability of the experiment. The variation in acceleration did not exceed 0.01 m/sec^2. With regard to the force coefficient, the variation in drag coefficient is very small whereas the variation in the acceleration coefficient is much greater. This aspect will be considered in detail at a later stage when considering the relative magnitudes of the force components.

The results from constant velocity tests are given in Table 7.2 together with the velocity and mean force which were used. The velocity exponent in eq. 7.10 lies in the range 1.76 to 1.91 which is somewhat less than the expected 2.0. The correlation coefficient is very high indicating good agreement between the experimental and fitted curves. It is noticed that velocities as high as 2.25 m/sec were reached during the experiments.

In order to investigate the validity of a square law relating force and velocity ($F \propto u^2$), data from constant velocity tests were re-analysed to obtain the drag coefficient b' in eq. 7.10 maintaining the velocity exponent at 2.0. The values thus obtained are also given in Table 7.2. They do not differ significantly from the earlier values but the corresponding correlation coefficients are lower indicating that the goodness of the fit was lower than previously.

Since the main objective was to investigate the physics of the phenomenon, curves with best correlation coefficients were used to simulate a given set of experimental observations.

Figs. 7.1 to 7.5 show the results from the test programme performed on Cob, Shed, Hobo and Cylat units respectively. In each case a porous medium consisting of these units was accelerated or moved at constant velocity while measuring the force acting on the centremost unit. Details of the apparatus and the experimental procedures were presented in Chapter 4.

For each unit tested the results are presented in a set of six figures illustrating the following,

(a) variation of measured force (F_m) versus time;
(b) variation of smoothed force (F_s) versus time;
(c) spectral analysis of the residual force (F_r);

(d) variation of the measured force (F_m) versus velocity together with the fitted curve;

(e) velocity–time plot for the motion of the carriage;

(f) force versus velocity plots for constant velocity tests together with the fitted curve.

The results presented in Figs. 7.1 to 7.5 generally refer to the higher value of acceleration. However for comparison a set corresponding to a lower value of acceleration is presented for Hobo units (Figs. 7.4.a to 7.4.e).

For all media the corresponding plots indicate a similar trend in the behaviour of the variable parameters.

The variation of measured force versus time illustrates the signal recorded by the force transducer. A signal having a frequency approximately equal to 10 Hz is present and it is evident that the signal is more pronounced towards the latter part of the time history. This phenomenon is common to any moving apparatus. As the velocity of the carriage increases, the amplitude of the vibration increases uniformly as seen in the record.

The plots of smoothed force versus time clearly illustrate the increase of force with time. The influence of magnitude of acceleration on force is seen when comparing Figs. 7.3.b and 7.4.b. These two refer to the Hobo unit but with higher and lower value of acceleration respectively (0.414 m/sec^2 and 0.151 m/sec^2). The force recorded for the latter is comparatively small.

The objective of performing spectral analysis on the residual force is to obtain information on the frequencies present in the recorded signal. The analysis on all records reveal a single peak corresponding to the natural frequency of the transducer in water. Hence it is evident that there are no other flow-induced vibrations present in the records.

The variation of measured force versus velocity is similar to the variation with time because velocity and time are linearly related ($\Delta u = \alpha \Delta t$). The fitted curve is also represented on the same plot.

The velocity–time plot for the motion of the carriage illustrates the extent to which constant acceleration is achieved by using the present experimental arrangement.

Velocity measured in this experiment represents the mean value of velocity between two microswitches all of which are placed at 20 cm intervals. As the carriage gathers speed the time taken to pass the switches decreases. Hence the value of velocity has not been sampled at constant time intervals but at constant length intervals along the flume. It is for this reason that the spacing between the points in the velocity–time plot decreases with increasing time. At the commencement of the experiment the carriage is kept well behind the first switch in order to allow for the time taken for the string to relieve itself from any minor sag and related instabilities in the initial period of motion. In effect, when the carriage reaches the first switch it is under constant acceleration. This method of analysis has its limitation due to the reduced number of points in the early stages of the motion. However, high correlation coefficients indicate that the fitted straight lines are true representations of the experimental values.

Force versus velocity plots for constant velocity tests illustrate the variation of the mean force against the respective values of the constant velocity at which the carriage moved. The fitted curve is also given in the same plot. It is assumed that four to five data points evenly distributed over a wide velocity range are sufficient to obtain a representative curve and this is further strengthened by the high correlation coefficient observed in all four cases. Hence these curves will be used in conjunction with those under constant acceleration to study and compare the differences between steady and unsteady flow conditions.

Figs. 7.6 to 7.9 illustrate the force–velocity relationships obtained under both constant acceleration and constant velocity for the different units investigated. For each unit the respective curves are presented in a single plot and a close similarity exists in the results obtained for the four porous units. The family of curves obtained for each unit indicates the same trend. The magnitudes of the forces are approximately same for the Cob, Shed and Hobo units. The Cylat experiences higher forces.

The curves obtained from the two values of constant acceleration and from constant velocity tests clearly indicate that as the value of acceleration increases from zero the measured force increases. The curves for Shed, Hobo and Cylat units, for the higher value of acceleration, are presented for two experimental runs, mainly to illustrate the repeatability of the results. The two curves are very close to each other and the drag force coefficients in the equations are also approximately the same.

If ΔF_{TF} is defined as the difference between the total force under

constant acceleration and constant velocity, at any given velocity, with reference to eqs. 7.9 and 7.10 ΔF_{TF} can be expressed as

$$\Delta F_{TF} = bu^2 + c\dot{u} - b'u^m \qquad (7.12)$$

From Figs. 7.6 to 7.9 the value of ΔF_{TF} increases with increasing velocity, particularly for the higher value of acceleration.

Since the inertia force component due to constant acceleration is assumed to be constant, the above observation is due to the increase in the drag force component. In effect the drag force corresponding to a given instantaneous velocity within a flow with constant acceleration differs from that for the same constant velocity in a flow with zero acceleration; the former is greater than the latter. From the two values of constant acceleration which were used in this investigation, it is evident that as the value of acceleration increases the corresponding increase in the drag force is greater.

This aspect is further illustrated in Figs. 7.10 to 7.13 in which both the difference in drag force (ΔF_{DF}) and total force (ΔF_{TF}) are plotted against velocity.

$$\Delta F_{TF} = bu^2 + c\dot{u} - b'u^m \qquad (7.12)$$

$$\Delta F_{DF} = bu^2 - b'u^m \qquad (7.13)$$

$$(\text{i.e. } \Delta F_{TF} = \Delta F_{DF} + c\dot{u})$$

For each unit two graphs are presented. The first corresponding to constant velocity and the lower value of acceleration. The second is similar to the first but with reference to the higher value of acceleration. These curves represent the relative magnitude of two force components. The first is the difference between the drag force in steady flow and that in an unsteady flow domain. The second is the constant inertia force. Together these two components constitute the difference in total force (ΔF_{TF}).

From these plots it is evident that the influence of the acceleration component is comparatively small and, as observed in Table 7.1, the velocity at which the drag force component equals the acceleration component is in the range 0.04 – 0.25 m/sec. Beyond this region the drag force dominates as it increases with square of velocity.

From a comparison of the lower and higher values of constant acceleration used for the study, the increase in drag force at the higher value is much more than the corresponding increase at the lower value. The same cannot be stated for the acceleration component which does not indicate a specific reliance on the magnitude of acceleration. However the results from two values of constant acceleration are not sufficient to study this aspect in detail. From the results on four types of porous media used in this study the force component due to acceleration is small in magnitude compared with the increase in drag force in the presence of an accelerating flow.

Fig. 7.14 is a plot of b in $F = bu^2 + c\dot{u}$ (eq. 7.9) versus acceleration ($\dot{u}$). The steady flow coefficient b' in $F = b'u^2$ (eq. 7.10) corresponding to zero acceleration is also marked. The general trend of the relationship between b and $\dot{u}$ for each of the units tested is also indicated in the figure. These curves are based on three values namely zero, lower and higher values of acceleration. For values of acceleration up to 0.2 m/sec^2 the variation in b is very small but for values beyond that an increase in b is evident. Although this conclusion is based on limited data, it is supported by the fact that all units indicate the same trend.

Fig. 7.15 illustrates the force versus velocity relationships under constant velocity for all four units used in the investigation. It is clearly evident that forces experienced by Cob, Shed and Hobo are approximately the same whereas the forces on the Cylat unit are much higher. A cross-comparison between Figs. 7.6 to 7.9 indicates that the same trend is present under constant acceleration. It was pointed out earlier in Section 3.4 that Cob, Shed and Hobo units are very similar in relation to external shape and size with differences present in the internal voids structure. However, the structure of the Cylat unit is quite different to that of the previous three although it has approximately the same overall porosity and external dimensions. The difference in external structural form accounts for the higher forces experienced by this unit.

7.4. Concluding remarks

Previous studies on accelerated flow conditions have been based on the assumption that drag coefficients obtained under steady flow conditions remain the same for accelerated flow conditions. In order to examine this concept more closely, four porous media – mainly consisting of hollow block armour units – were subjected to constant acceleration and velocity tests. In the case of the former, two values of acceleration were used.

The study reveals that the total force under constant acceleration can be expressed as

$$F_{TF(CA)} = F_{DF(CA)} + F_{IF(CA)} \tag{7.14}$$

in which

$$F_{DF(CA)} = F_{DF(CV)} + \Delta F_{DF(CA)} \tag{7.15}$$

where

$F_{TF(CA)}$ - total force under constant acceleration
$F_{DF(CA)}$ - drag force under constant acceleration
$F_{IF(CA)}$ - inertia force under constant acceleration
$F_{DF(CV)}$ - drag force under constant velocity
$\Delta F_{DF(CA)}$ - difference in drag force under constant acceleration and constant velocity

Measurements of drag force under constant velocity, $F_{DF(CV)}$, were obtained by performing a series of tests at constant velocity and fitting a curve to the force versus velocity data. On all occasions more than four experimental values of the force versus velocity were used for this purpose. It is assumed that the fitted curve is representative of the phenomenon under investigation, an assumption supported by the high correlation coefficients obtained (Table 7.2 and Fig. 7.15).

The relative magnitude of the drag force under constant velocity ($F_{DF(CV)}$) and the total force under constant acceleration ($F_{TF(CA)}$) are presented in Figs. 7.6 to 7.9.

From this study it is observed that the difference in drag force identified by $\Delta F_{DF(CA)}$ can be quite significant. At constant acceleration, $\Delta F_{DF(CA)}$ increases with increasing velocity. At a given velocity $\Delta F_{DF(CA)}$ increases with increasing acceleration (Figs. 7.10 to 7.13).

The constant inertia force ($F_{IF(CA)}$), due to constant acceleration, is small in comparison with the increase in drag force. Its magnitude did not always increase with an increase in the magnitude of acceleration. Only two values of constant acceleration were used for this study and as a consequence it is not possible to study this aspect in detail. The relative magnitudes of $\Delta F_{DF(CA)}$ and $F_{IF(CA)}$ are presented in Figs. 7.10 to 7.13.

The apparatus used for the study proved to be successful for this investigation. When an experiment was repeated the variation in acceleration did not exceed 0.01 m/sec^2, i.e., less than 5%, and the measured parameters were very similar.

TABLE 7.1 RESULTS FROM UNIDIRECTIONAL CONSTANT ACCELERATION TESTS

	LV and HV refer to lower and higher value of acceleration	Time and velocity at the start and end of experiment		Motion of carriage $u = \alpha t + \beta$ (m/sec) r = correlation coefficient			Force - velocity relationship $F = bu^2 + c\dot{u}$ (gm force) r = correlation coefficient (1 gm force = 980.665 x 10^{-5} N)				$u^* = (c\dot{u}/b)^{1/2}$ (m/sec)
		TS (s) TE	US (m/s) UE	α	β	r	b	c	$c\dot{u}$	r	
COB units	LV	0.8 2.78	0.304 0.734	0.226	0.123	0.989	33.23	3.82	0.87	0.981	0.161
	HV	0.58 2.56	0.455 1.157	0.354	0.250	0.983	41.00	5.39	1.91	0.989	0.216
SHED units	LV	0.70 2.68	0.308 0.779	0.238	0.141	0.992	31.00	3.69	0.88	0.989	0.168
	HV	0.98 2.96	0.371 1.121	0.379	0.000	0.976	42.01	0.88	0.33	0.991	0.089
		0.74 2.72	0.416 1.153	0.373	0.140	0.980	42.99	0.21	0.08	0.994	0.043
HOBO units	LV	0.28 2.26	0.312 0.611	0.151	0.27	0.973	31.53	8.99	1.36	0.953	0.207
	HV	0.14 2.12	0.395 1.244	0.429	0.335	0.965	38.29	5.46	2.34	0.994	0.247
		0.02 2.00	0.511 1.330	0.414	0.503	0.982	37.98	2.25	0.93	0.991	0.156
CYLAT units	LV	0.52 2.5	0.276 0.589	0.158	0.194	0.979	42.83	9.97	1.57	0.878	0.192
	HV	0.02 2.0	0.279 1.21	0.469	0.270	0.980	50.07	1.03	0.48	0.996	0.098
		0.02 2.0	0.294 1.22	0.467	0.285	0.972	47.18	5.25	2.45	0.990	0.228

u^* is the velocity at which the drag force component equals the acceleration component.

Characteristic Dimension (D) of the units

Cob D=19.0 mm
Shed D=21.5 mm
Hobo D=25.0 mm
Cylat D=20.0 mm

TABLE.7.2 RESULTS FROM CONSTANT VELOCITY TESTS

	Values of constant velocity (m/s)	Mean force (gm force)	Fitted curve $F = b'u^m$ r = correlation coefficient b'	m	r
COB units	0.247	2.50	31.17	1.84	0.995
	0.769	17.02			
	1.338	54.01	32.76	2.00	0.872
	1.500	70.03			
SHED units	0.247	2.06	30.47	1.91	0.998
	0.769	19.43			
	1.338	51.36	30.76	2.00	0.850
	2.250	140.00			
HOBO units	0.417	4.64	29.95	1.89	0.979
	0.588	12.20			
	0.784	22.41	30.75	2.00	0.863
	1.154	41.11			
	2.308	130.31			
CYLAT units	0.625	17.43	41.93	1.76	0.997
	0.769	27.84			
	1.020	43.96	40.63	2.00	0.853
	1.429	71.17			
	2.157	159.83			

Characteristic Dimension (D) of the units

Cob D=19.0 mm
Shed D=21.5 mm
Hobo D=25.0 mm
Cylat D=20.0 mm

1 gm force = 980.665×10^{-5} N

FIG.7.1.A FORCE vs TIME PLOT

FOR COB UNITS UNDER ACCELERATION

MOTION OF TROLLEY U=0.364*T + 0.250 m/s

1 gm force = 980.665 x 10^{-5} N

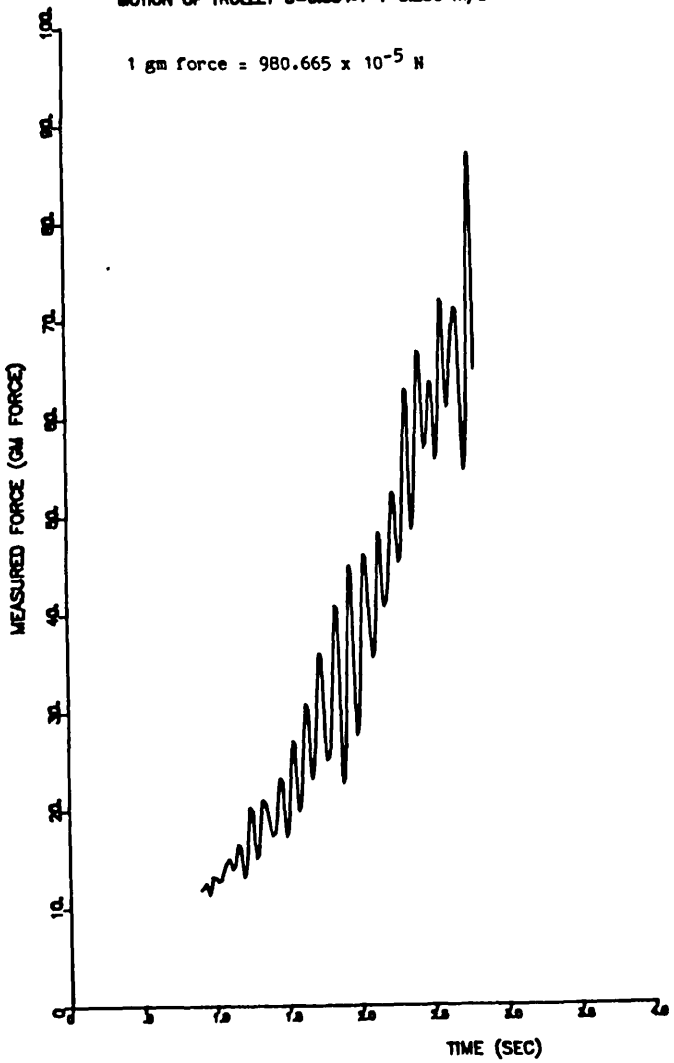


FIG.7.1.B FORCE vs TIME PLOT

FOR COB UNITS UNDER ACCELERATION

MOTION OF TROLLEY U=0.364*T + 0.250 m/s

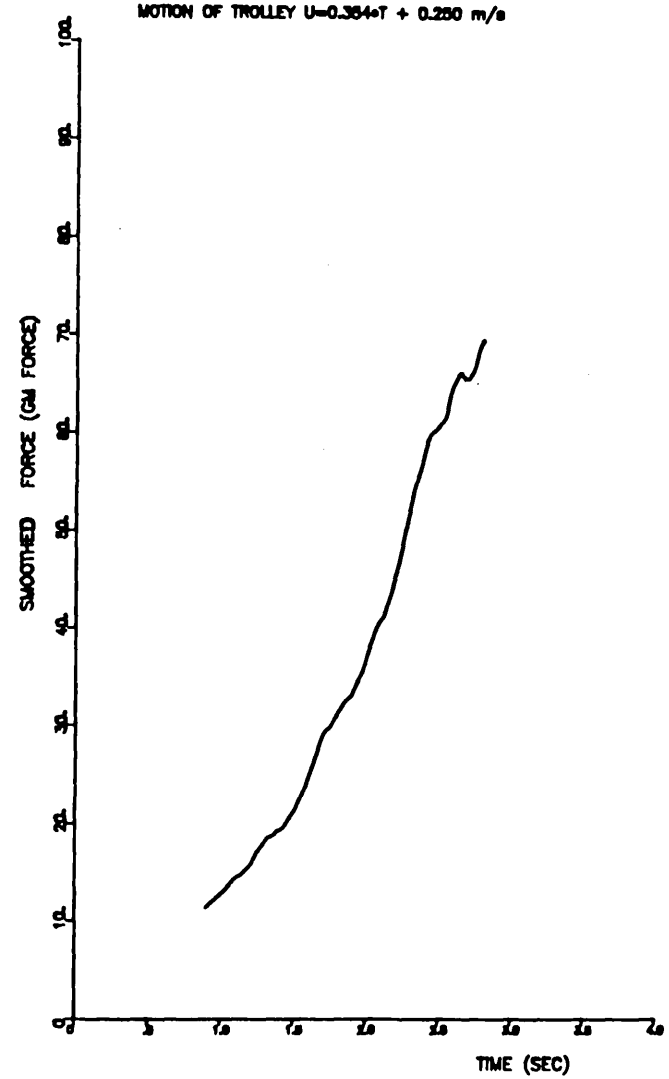


FIG.7.1.C SPECTRAL ANALYSIS OF RESIDUAL FORCE

FOR COB UNITS UNDER ACCELERATION

MOTION OF TROLLEY U=0.354eT + 0.250 m/s

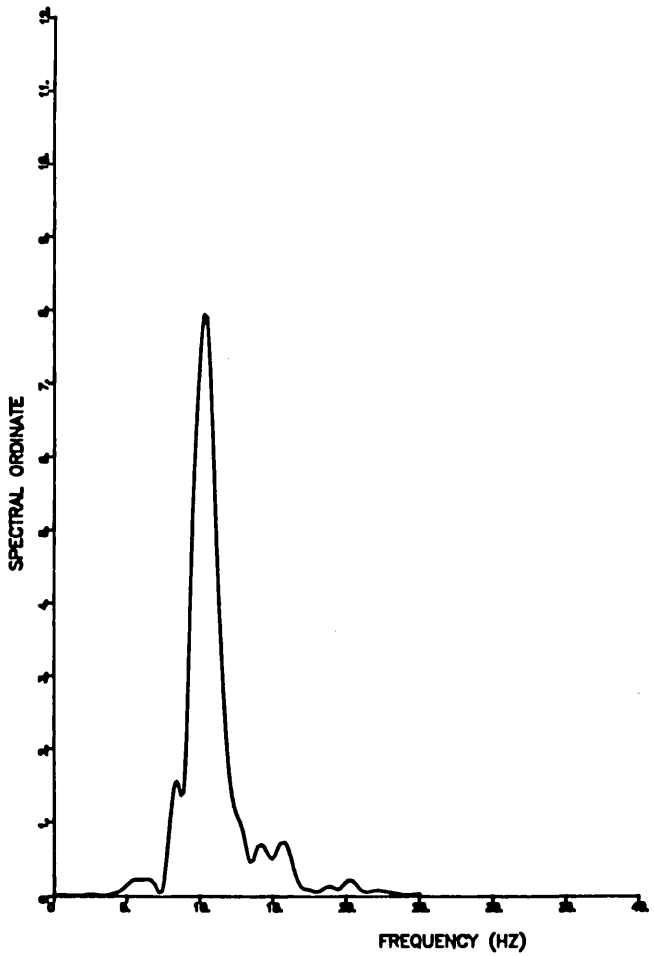


FIG.7.1.D FORCE vs VELOCITY PLOT

FOR COB UNITS UNDER ACCELERATION

MOTION OF TROLLEY U= .354eT + .250 m/s

----- $F = 41.00\ u^2 + 5.39\ \dot{u}$ gm force

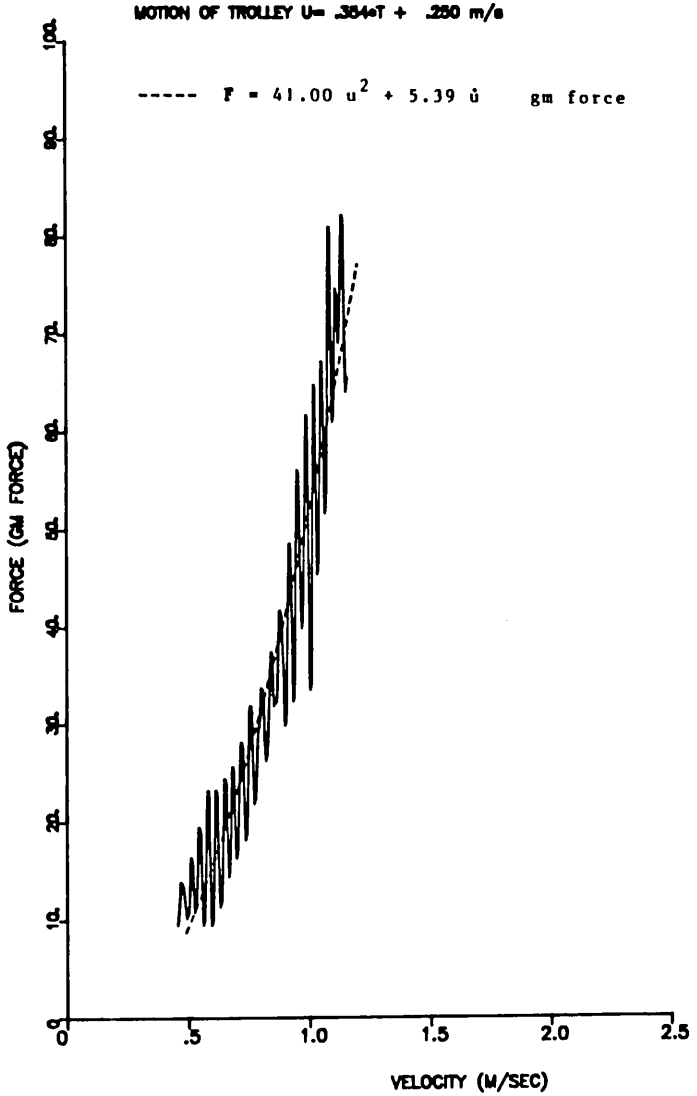


FIG.7.1.E VELOCITY TIME PROFILE FOR THE TROLLEY

BLOCK OF COB ARMOUR UNITS

U=0.354eT + 0.250 m/sec

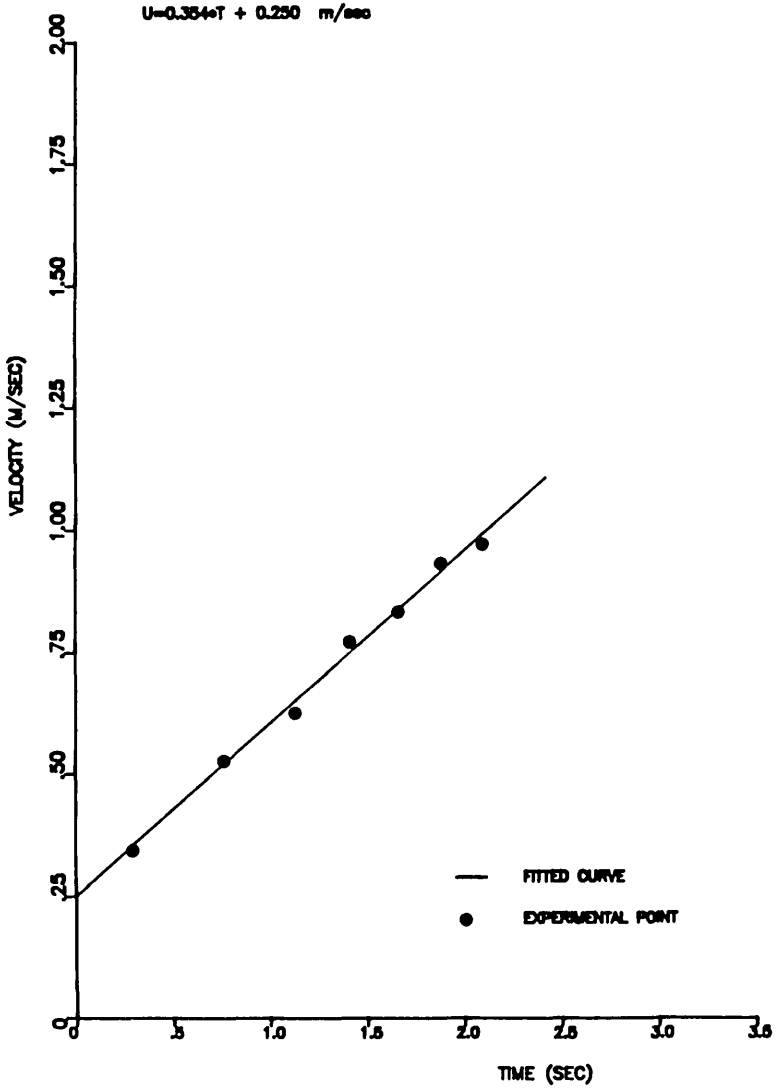


FIG.7.1.F FORCE vs VELOCITY PLOT

FOR COB UNITS UNDER UNIFORM VELOCITY

U=0.247/0.769/1.338/1.50 m/s

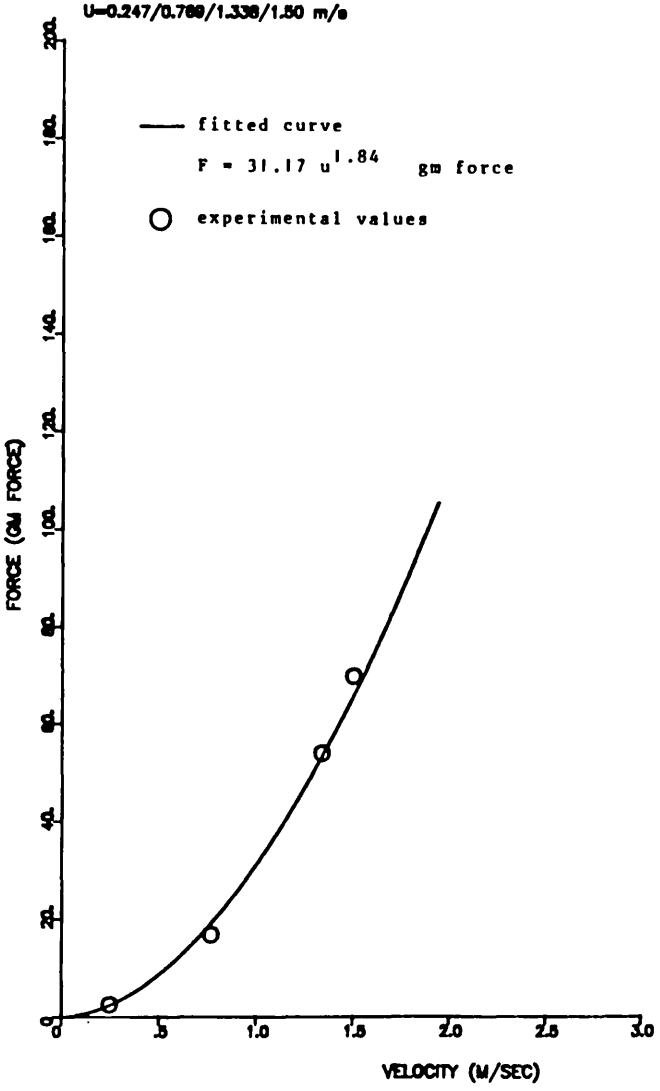


FIG.7.2.A FORCE vs TIME PLOT

FOR SHED UNITS UNDER ACCELERATION

MOTION OF TROLLEY U=0.373*T + 0.140 m/s

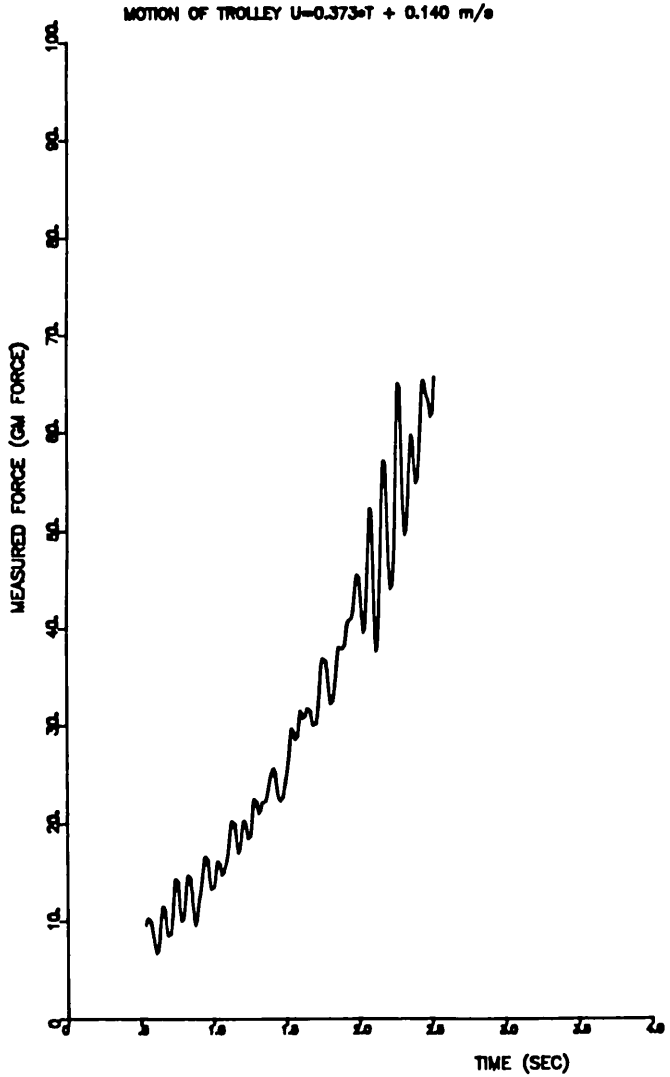


FIG.7.2.B FORCE vs TIME PLOT

FOR SHED UNITS UNDER ACCELERATION

MOTION OF TROLLEY U=0.373*T + 0.140 m/s

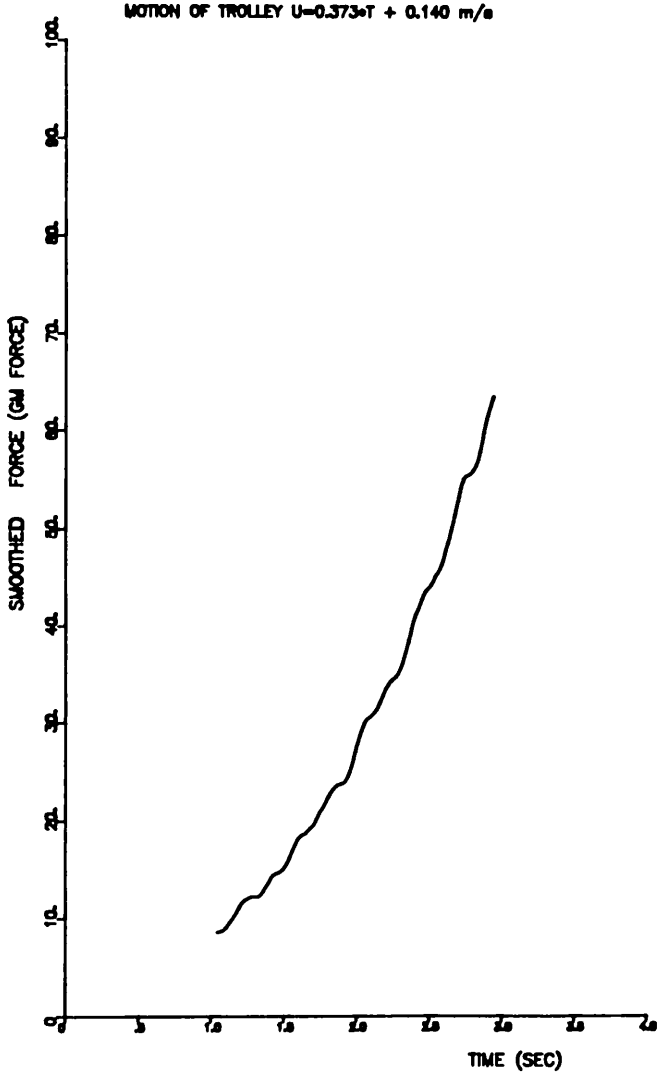


FIG.7.2.C SPECTRAL ANALYSIS OF RESIDUAL FORCE

FOR SHED UNITS UNDER ACCELERATION

MOTION OF TROLLEY U=0.373*T + 0.140 m/s

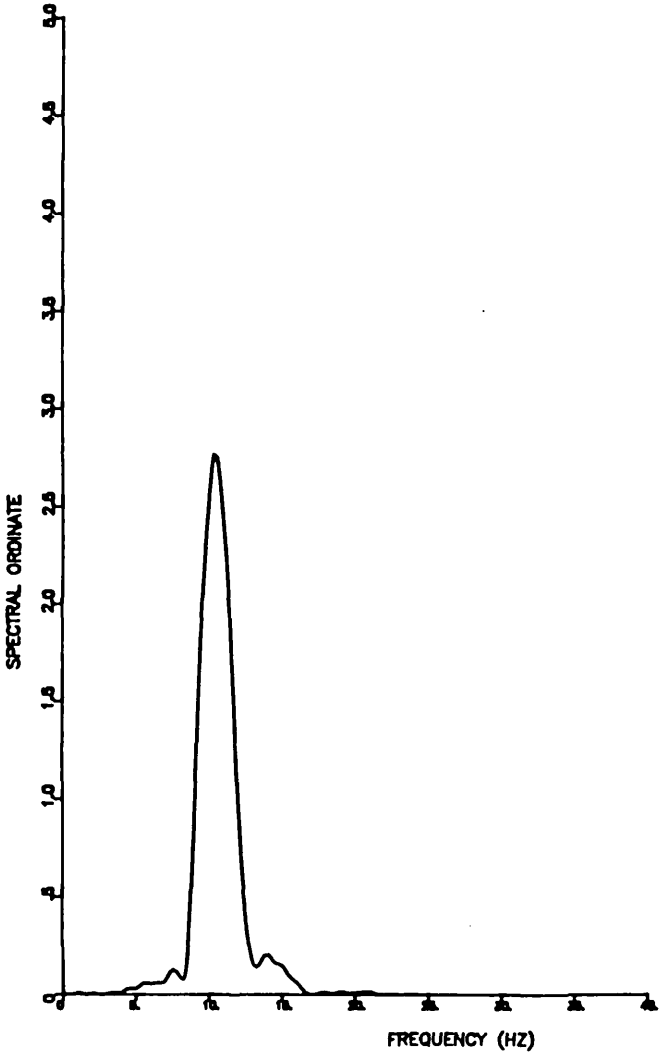


FIG.7.2.D FORCE vs VELOCITY PLOT

FOR SHED UNITS UNDER ACCELERATION

MOTION OF TROLLEY U= .373*T + .140 m/s

----- $F = 42.99\ u^2 + 0.21\ \dot{u}$ gm force

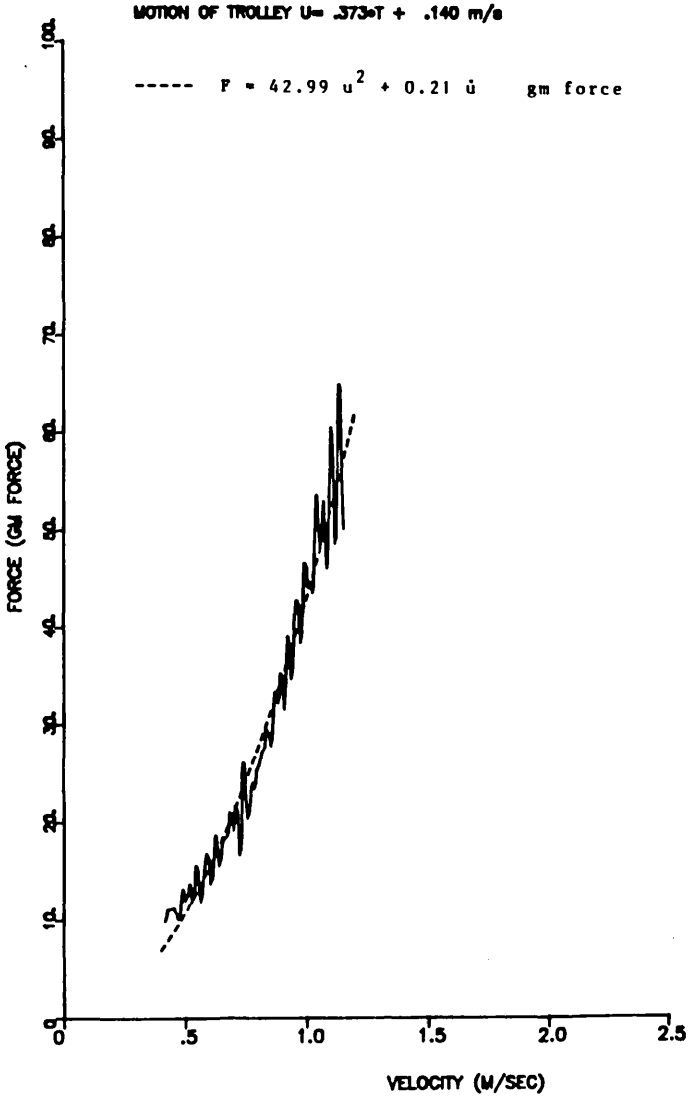


FIG.7.2.E VELOCITY TIME PROFILE FOR THE TROLLEY

BLOCK OF SHED ARMOUR UNITS

U=0.373*T + 0.140 m/sec

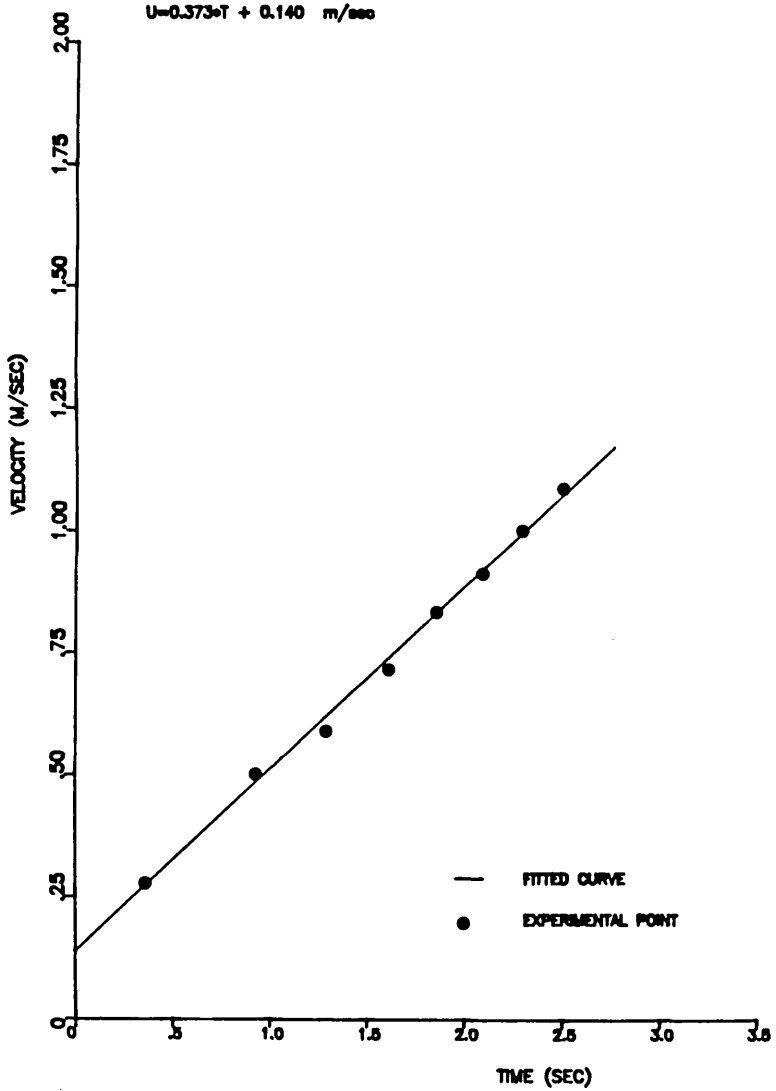


FIG.7.2.F FORCE vs VELOCITY PLOT

FOR SHED UNITS UNDER UNIFORM VELOCITY

U=0.247/0.769/1.338/2.25 m/s

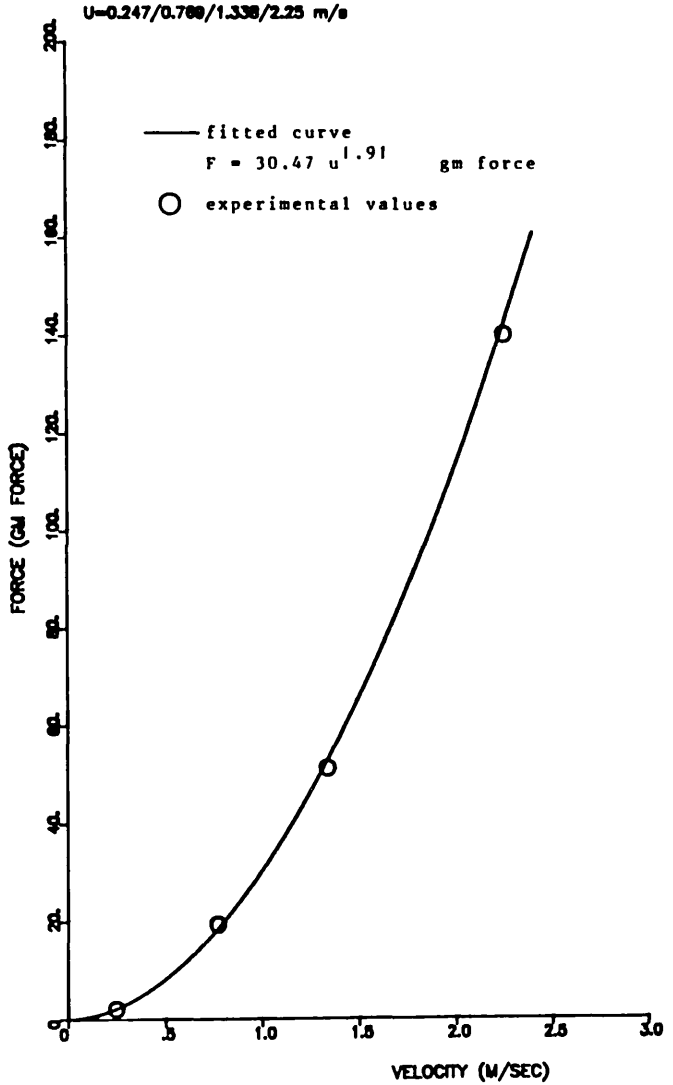


FIG.7.3.A FORCE vs TIME PLOT

FOR HOBO UNITS UNDER ACCELERATION

MOTION OF TROLLEY U=0.414*T + 0.503 m/s

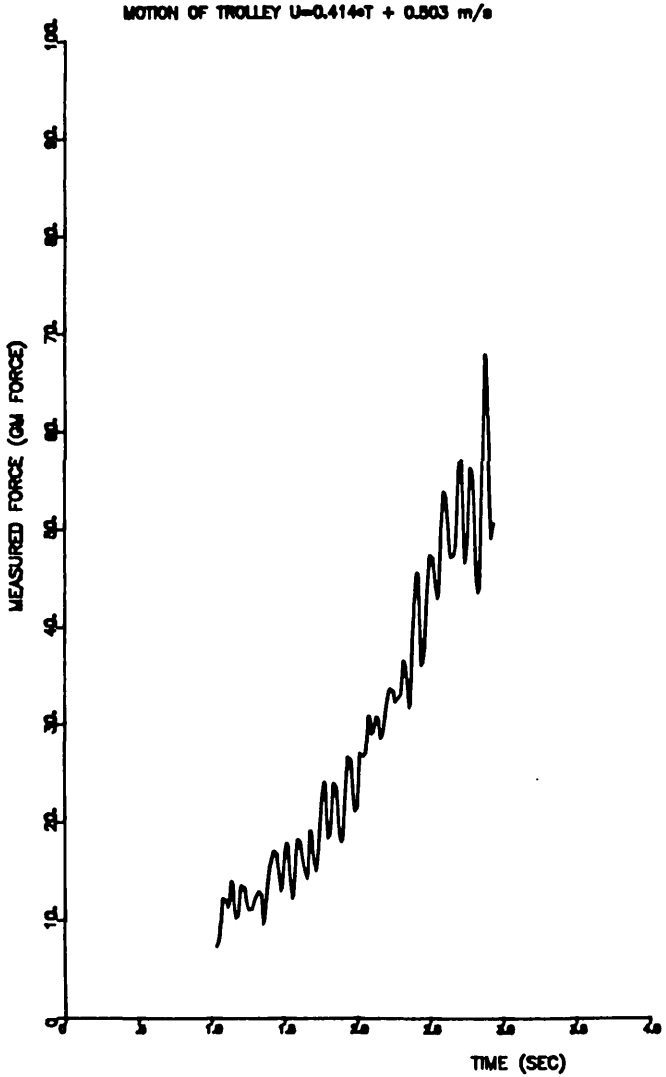


FIG.7.3.B FORCE vs TIME PLOT

FOR HOBO UNITS UNDER ACCELERATION

MOTION OF TROLLEY U=0.414*T + 0.503 m/s

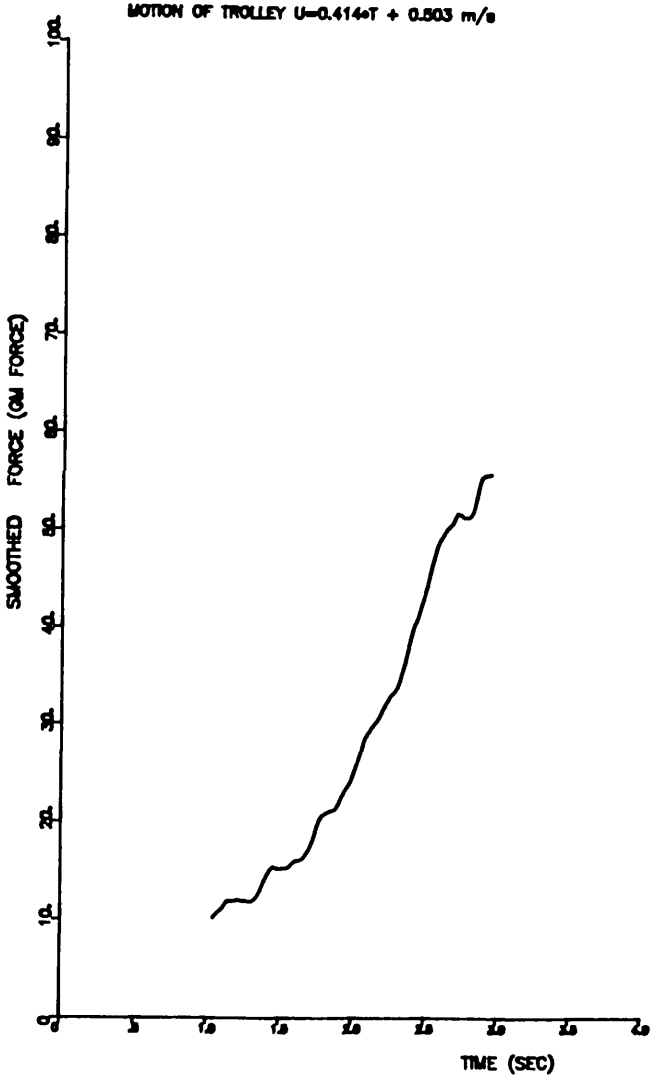


FIG.7.3.C SPECTRAL ANALYSIS OF RESIDUAL FORCE

FOR HOBO UNITS UNDER ACCELERATION

MOTION OF TROLLEY U=0.414eT + 0.503 m/s

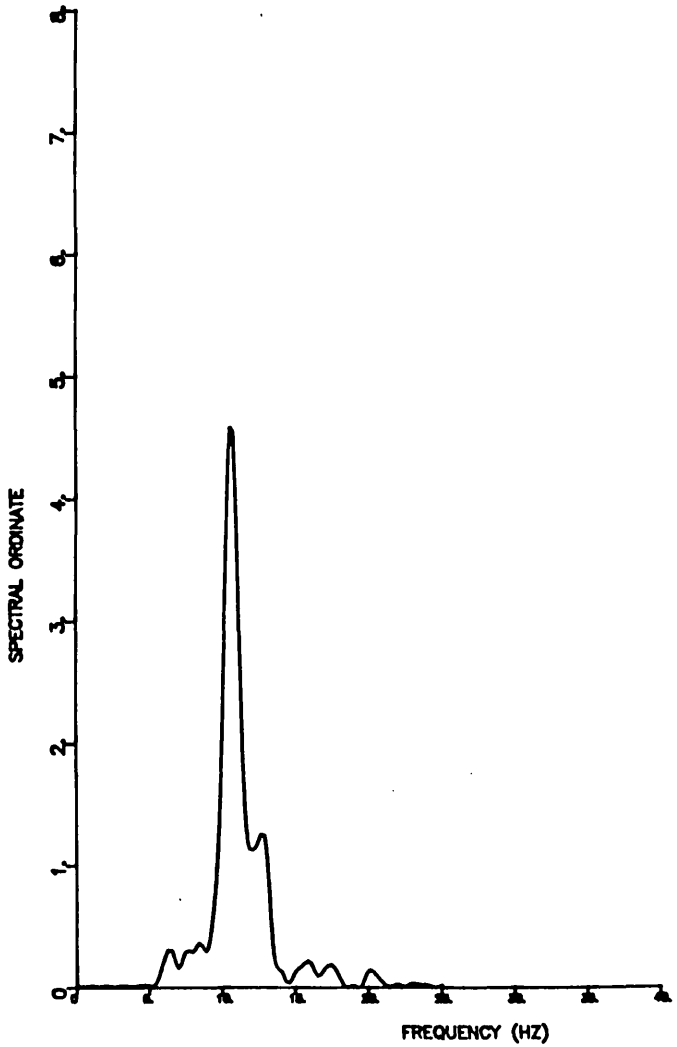


FIG.7.3.D FORCE vs VELOCITY PLOT

FOR HOBO UNITS UNDER ACCELERATION

MOTION OF TROLLEY U= .414eT + .503 m/s

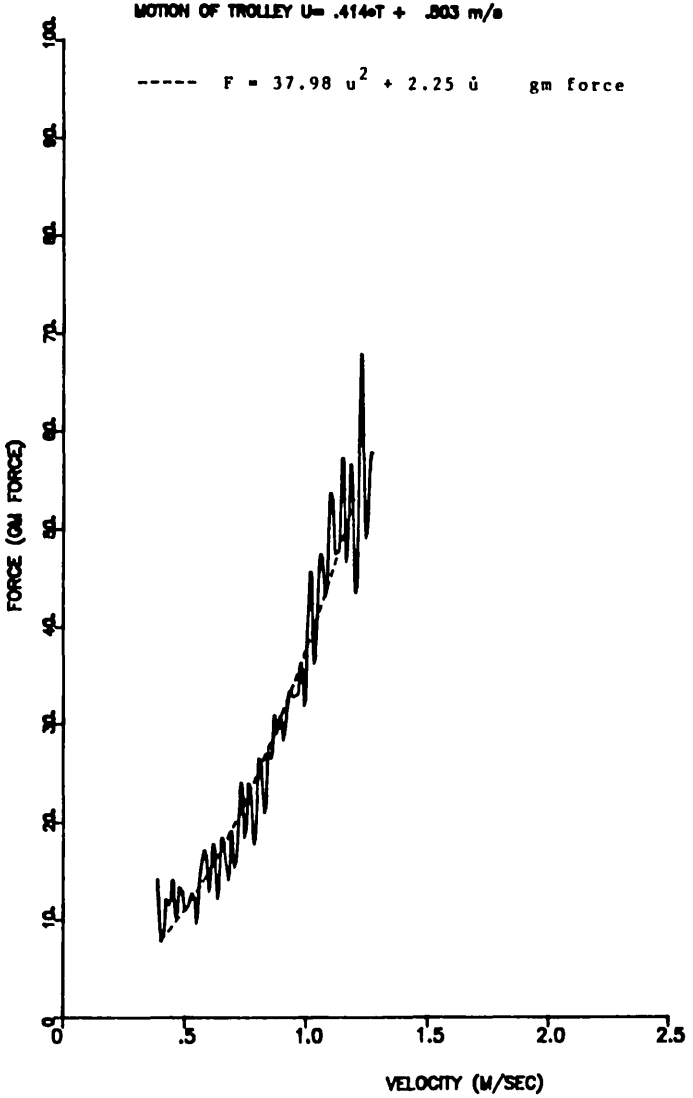


FIG.7.3.E VELOCITY TIME PROFILE FOR THE TROLLEY

BLOCK OF HOBO ARMOUR UNITS

U=0.414eT + 0.503 m/sec

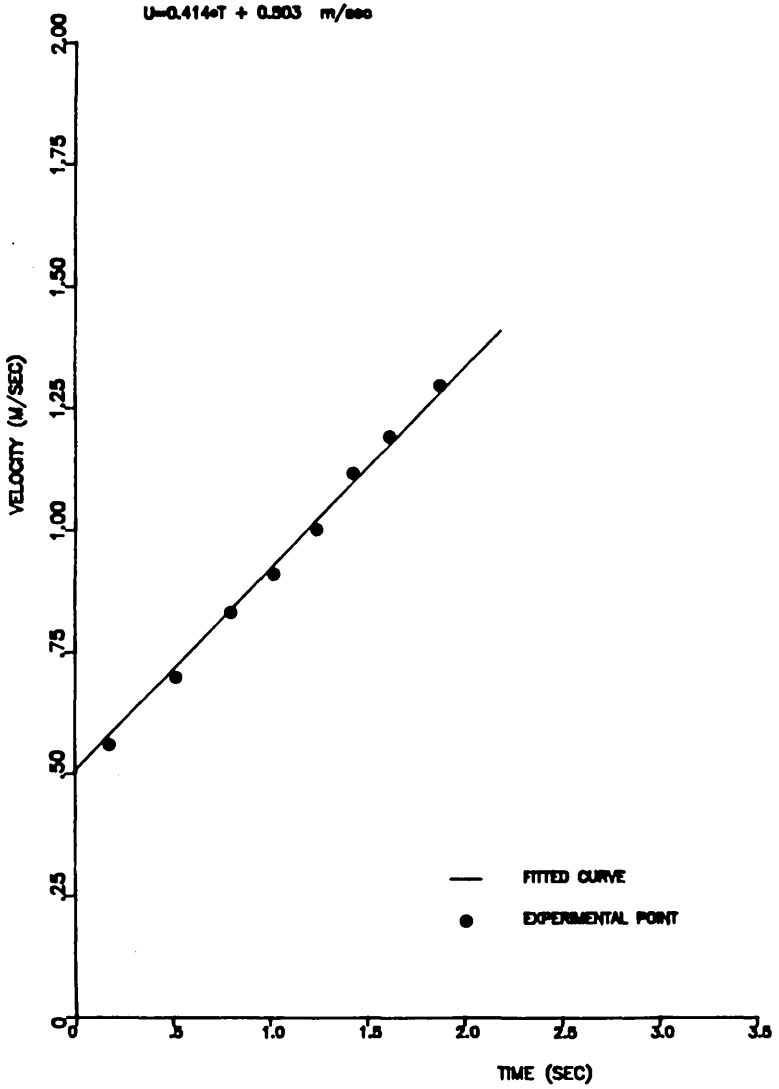


FIG.7.3.F FORCE vs VELOCITY PLOT

FOR HOBO UNITS UNDER UNIFORM VELOCITY

U=0.417/0.588/0.784/1.154/1.538/2.308 m/s

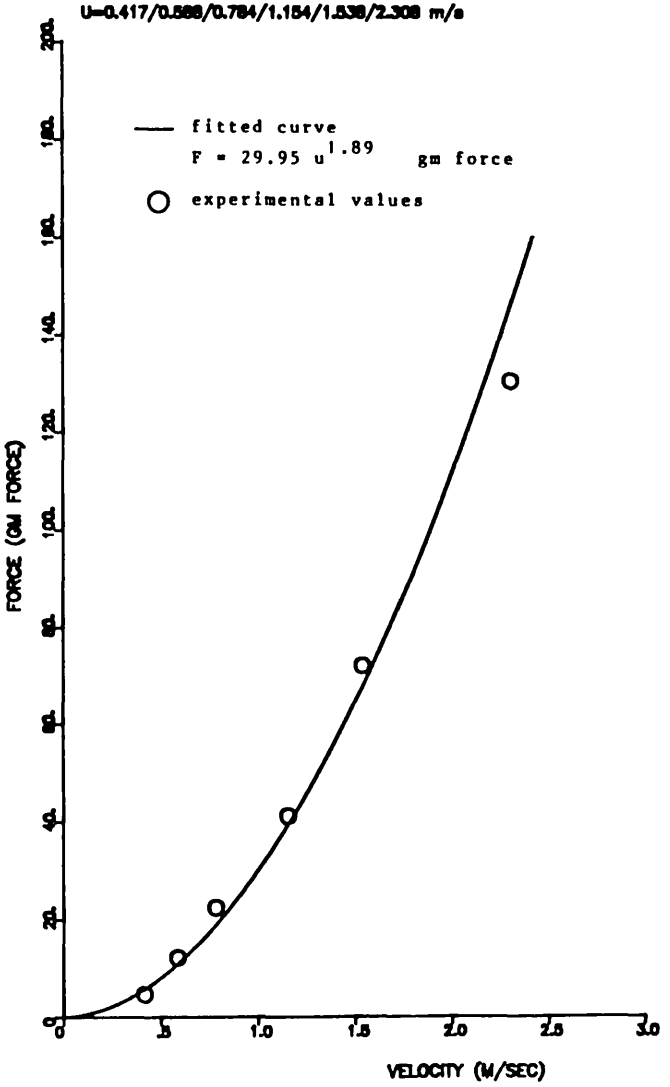


FIG.7.4.A FORCE vs TIME PLOT

FOR HOBO UNITS UNDER ACCELERATION

MOTION OF TROLLEY U=0.151•T + 0.270 m/s

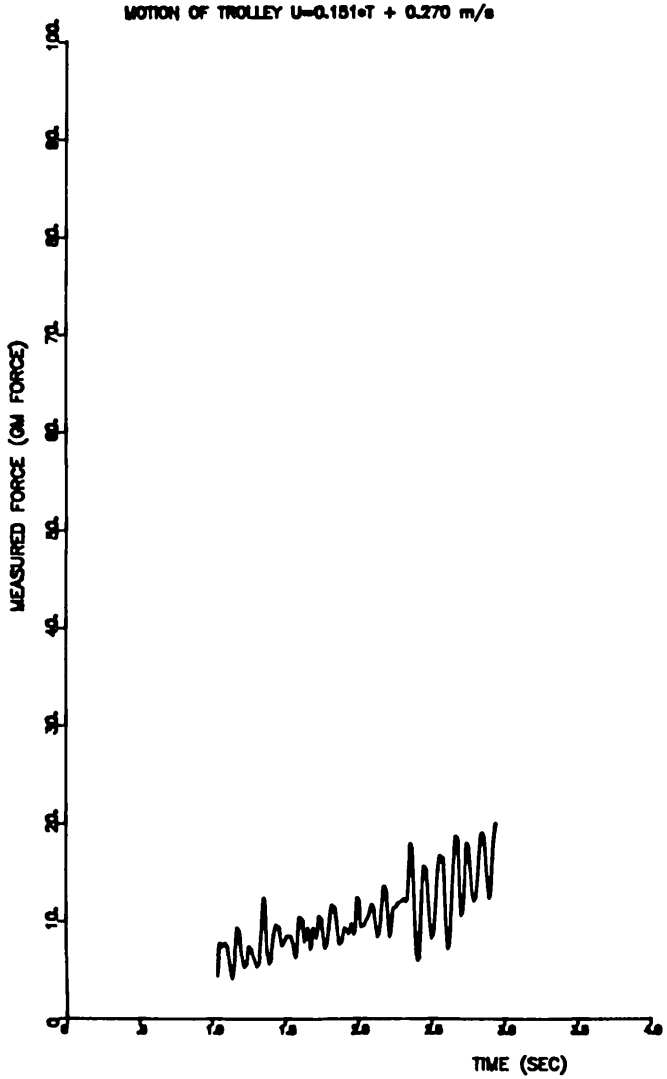


FIG.7.4.B FORCE vs TIME PLOT

FOR HOBO UNITS UNDER ACCELERATION

MOTION OF TROLLEY U=0.151•T + 0.270 m/s

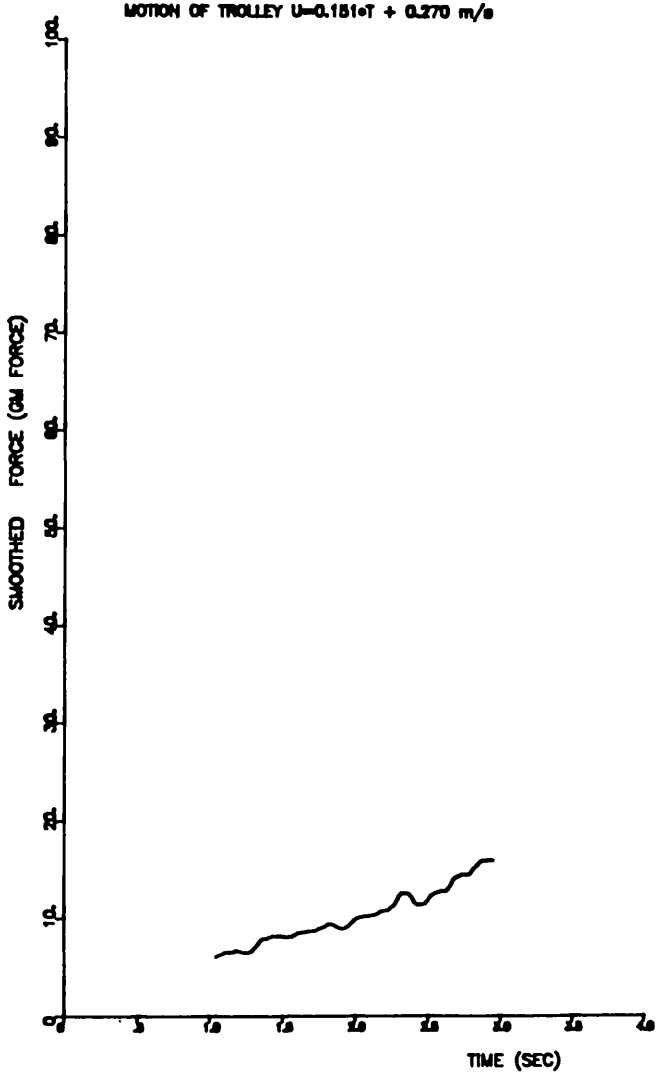


FIG.7.4.C SPECTRAL ANALYSIS OF RESIDUAL FORCE

FOR HOBO UNITS UNDER ACCELERATION

MOTION OF TROLLEY U=0.151*T + 0.270 m/s

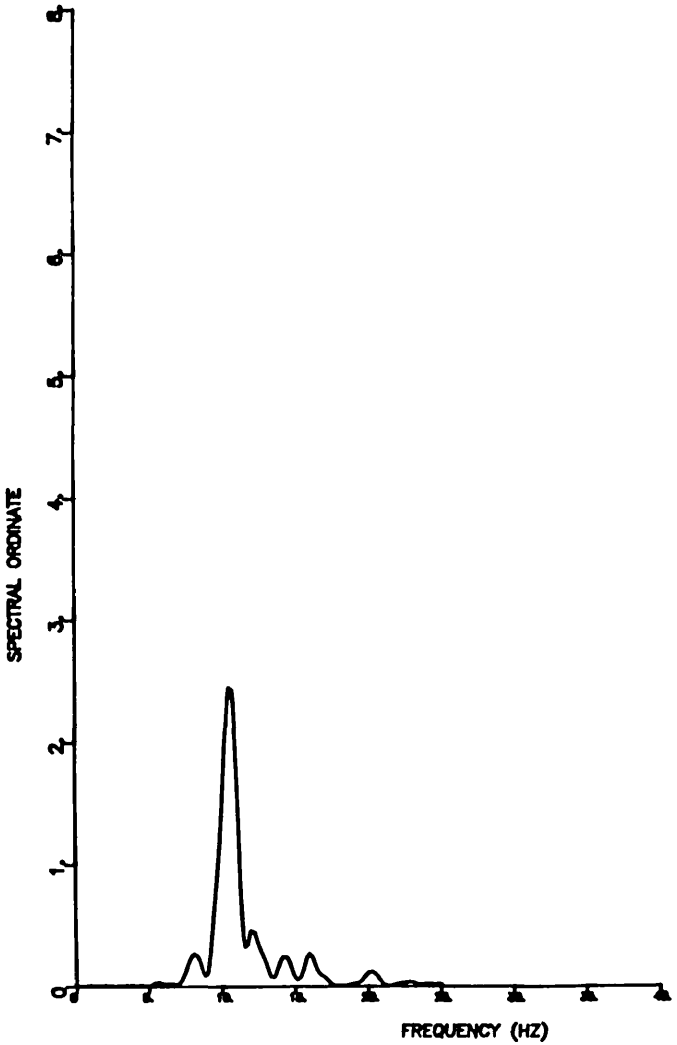


FIG.7.4.D FORCE vs VELOCITY PLOT

FOR HOBO UNITS UNDER ACCELERATION

MOTION OF TROLLEY U= .151*T + .270 m/s

----- $F = 31.53\ u^2 + 8.99\ \dot{u}$ gm force

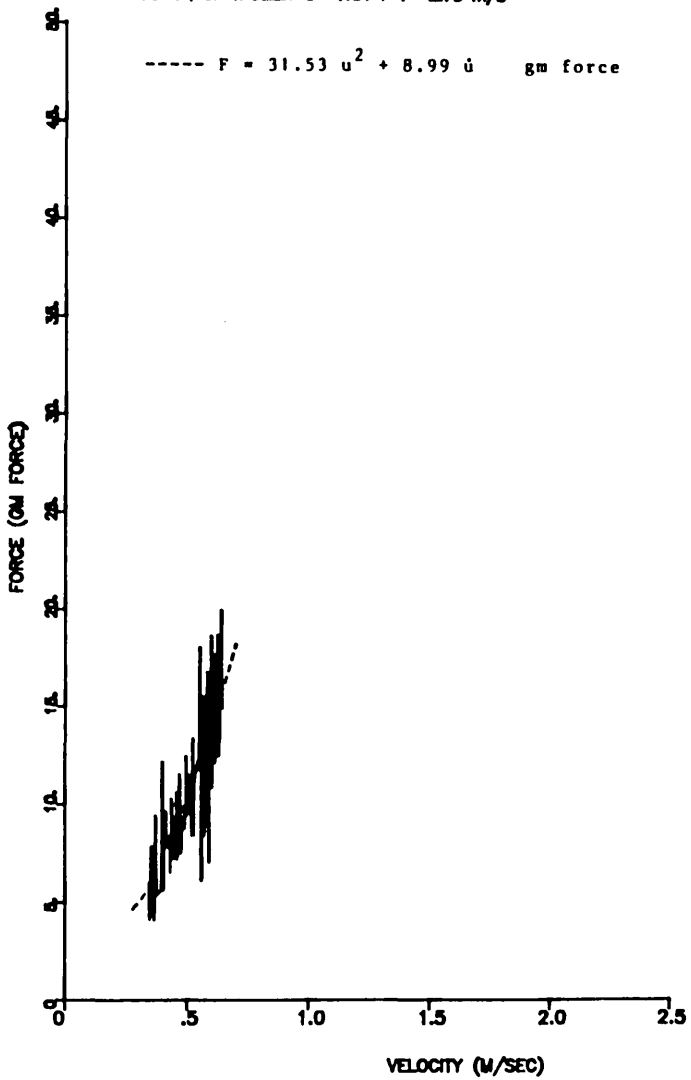


FIG.7.4.E VELOCITY TIME PROFILE FOR THE TROLLEY

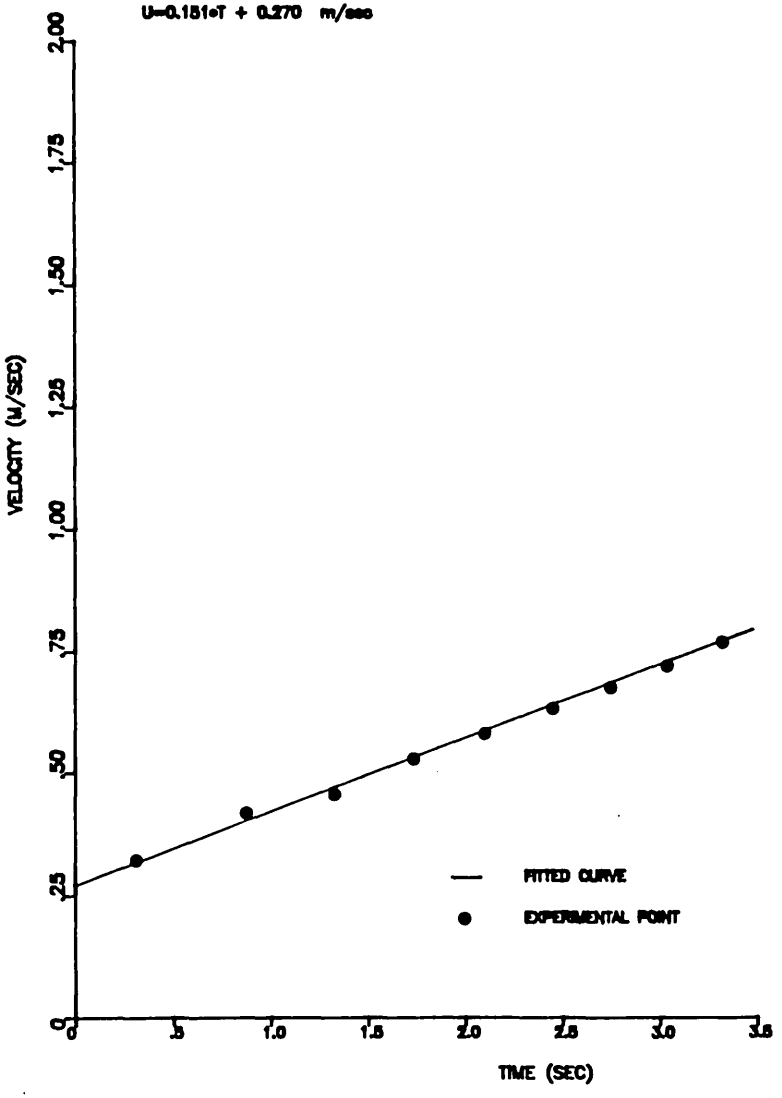


FIG.7.5.A FORCE vs TIME PLOT

FOR CYLAT UNDER ACCELERATION

MOTION OF TROLLEY U=0.469*T + 0.270 m/s

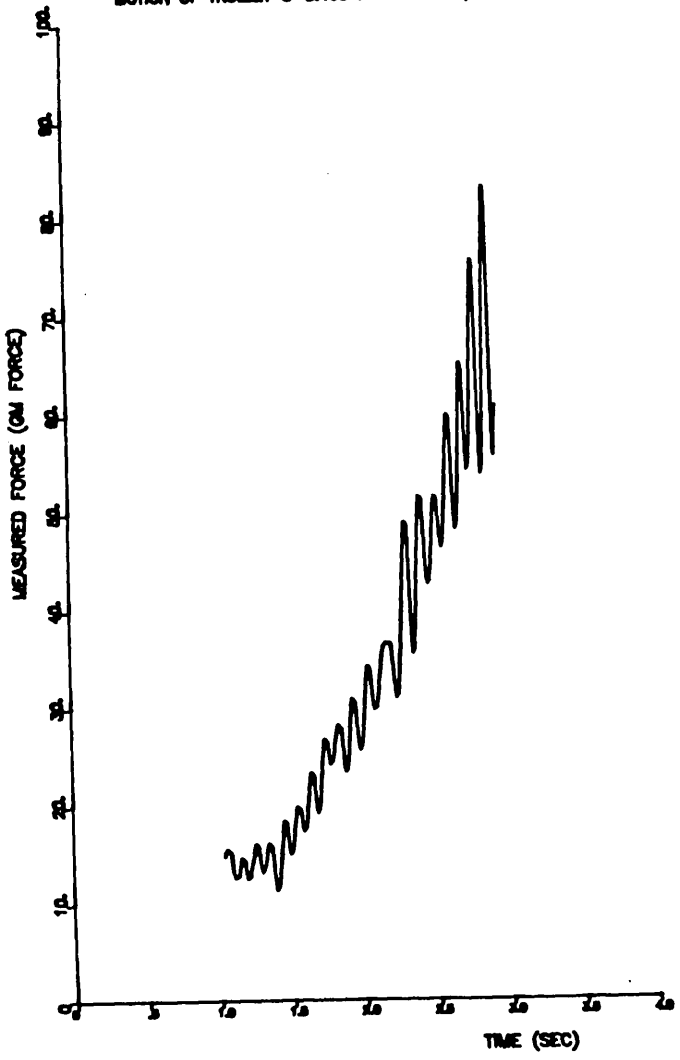


FIG.7.5.B FORCE vs TIME PLOT

FOR CYLAT UNDER ACCELERATION

MOTION OF TROLLEY U=0.469*T + 0.270 m/s

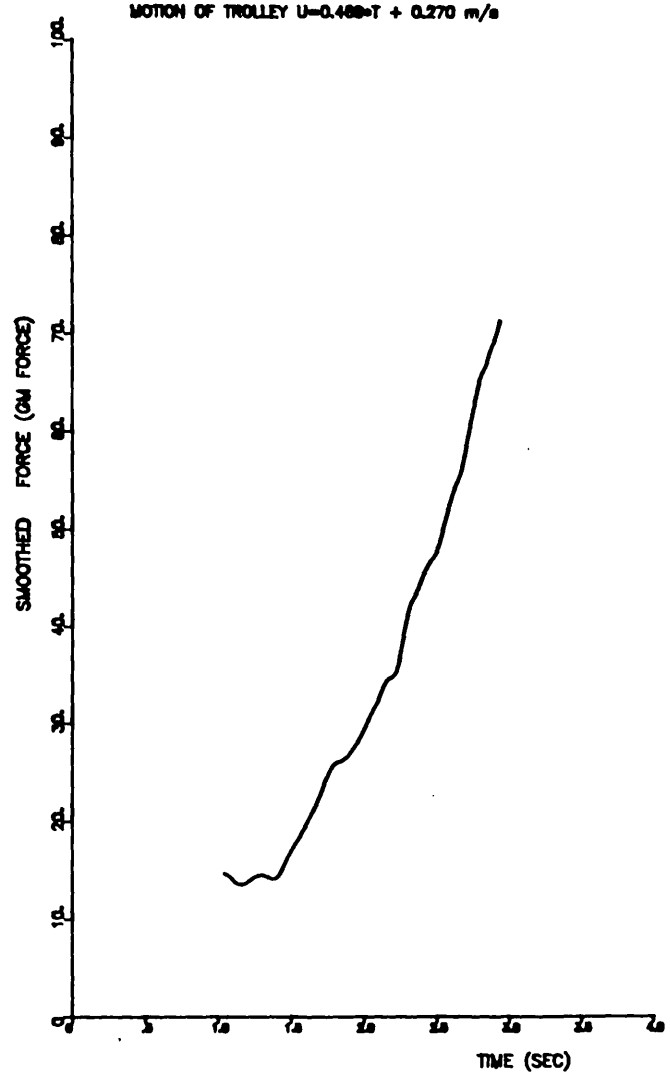


FIG.7.5.C SPECTRAL ANALYSIS OF RESIDUAL FORCE

FOR CYLAT UNITS UNDER ACCELERATION

MOTION OF TROLLEY U=0.469*T + 0.270 m/s

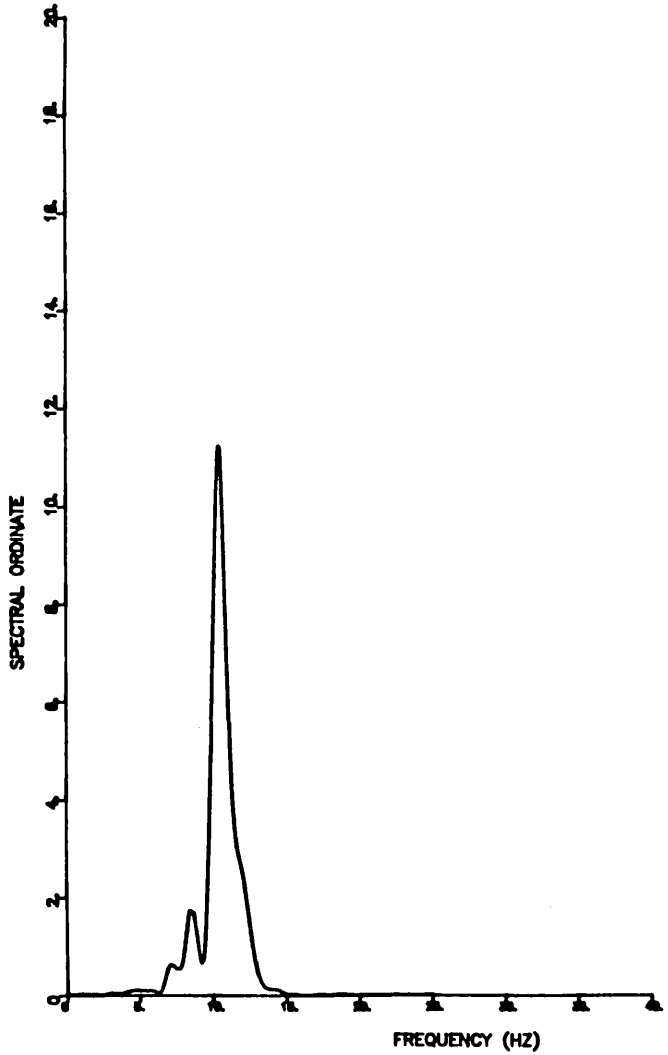


FIG.7.5.D FORCE vs VELOCITY PLOT

FOR CYLAT UNITS UNDER ACCELERATION

MOTION OF TROLLEY U= .469*T + .270 m/s

----- $F = 50.07\ u^2 + 1.03\ \dot{u}$ gm force

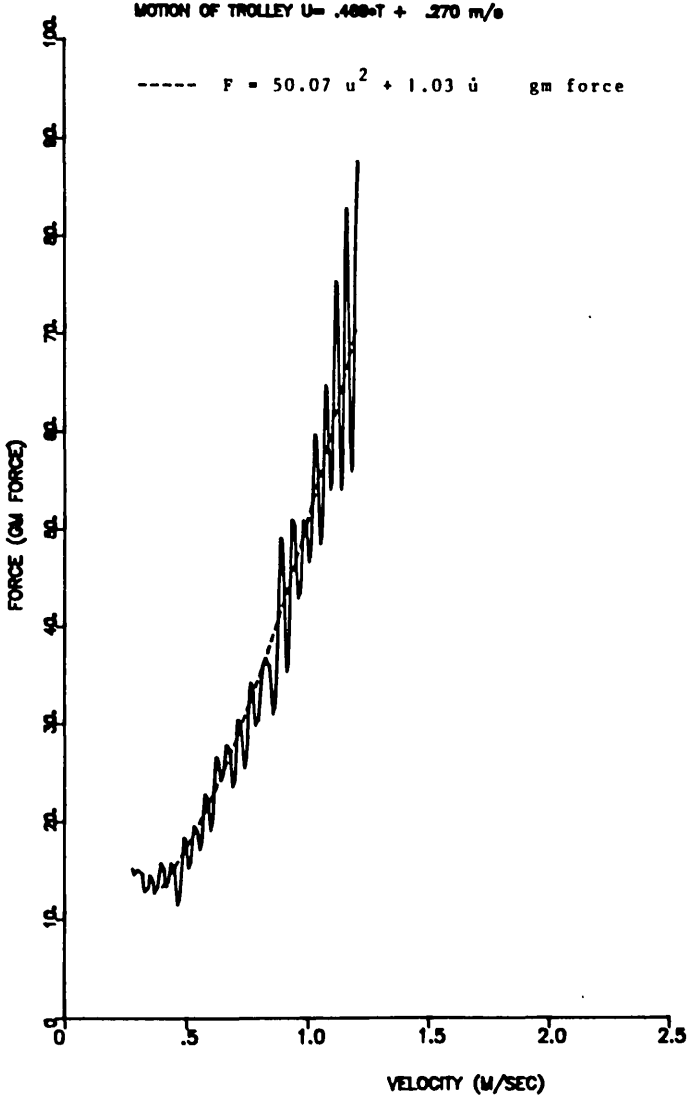


FIG.7.5.E VELOCITY TIME PROFILE FOR THE TROLLEY

BLOCK OF CYLAT ARMOUR UNITS

U=0.469*T + 0.270 m/sec

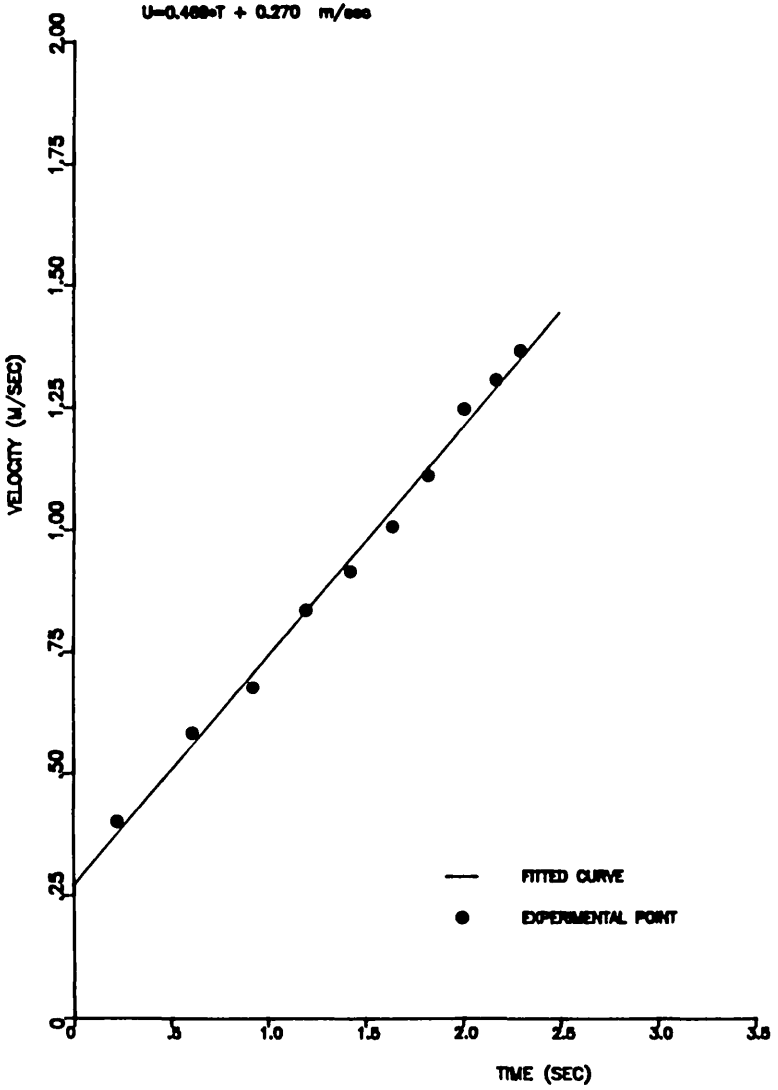


FIG.7.5.F FORCE vs VELOCITY PLOT

FOR CYLAT UNITS UNDER UNIFORM VELOCITY

U=0.625/0.769/1.020/1.429/2.157 m/s

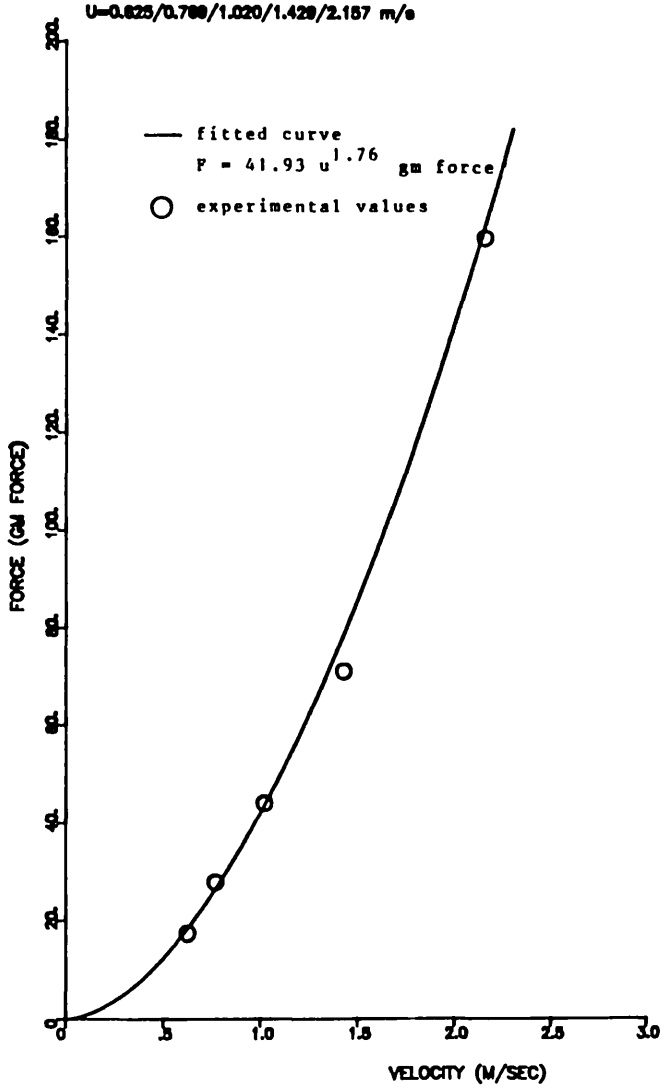


FIG.7.6 FORCE vs VELOCITY FOR COB UNITS

FITTED CURVES FOR EXPERIMENTAL OBSERVATIONS

Equation of curve $F = b\,u^{k} + c\,\dot{u}$

	b	k	c	$\dot{u}$
curve 3	41.00	2.00	5.39	0.354
curve 2	33.23	2.00	3.82	0.226
curve 1	31.17	1.84	——	0.000

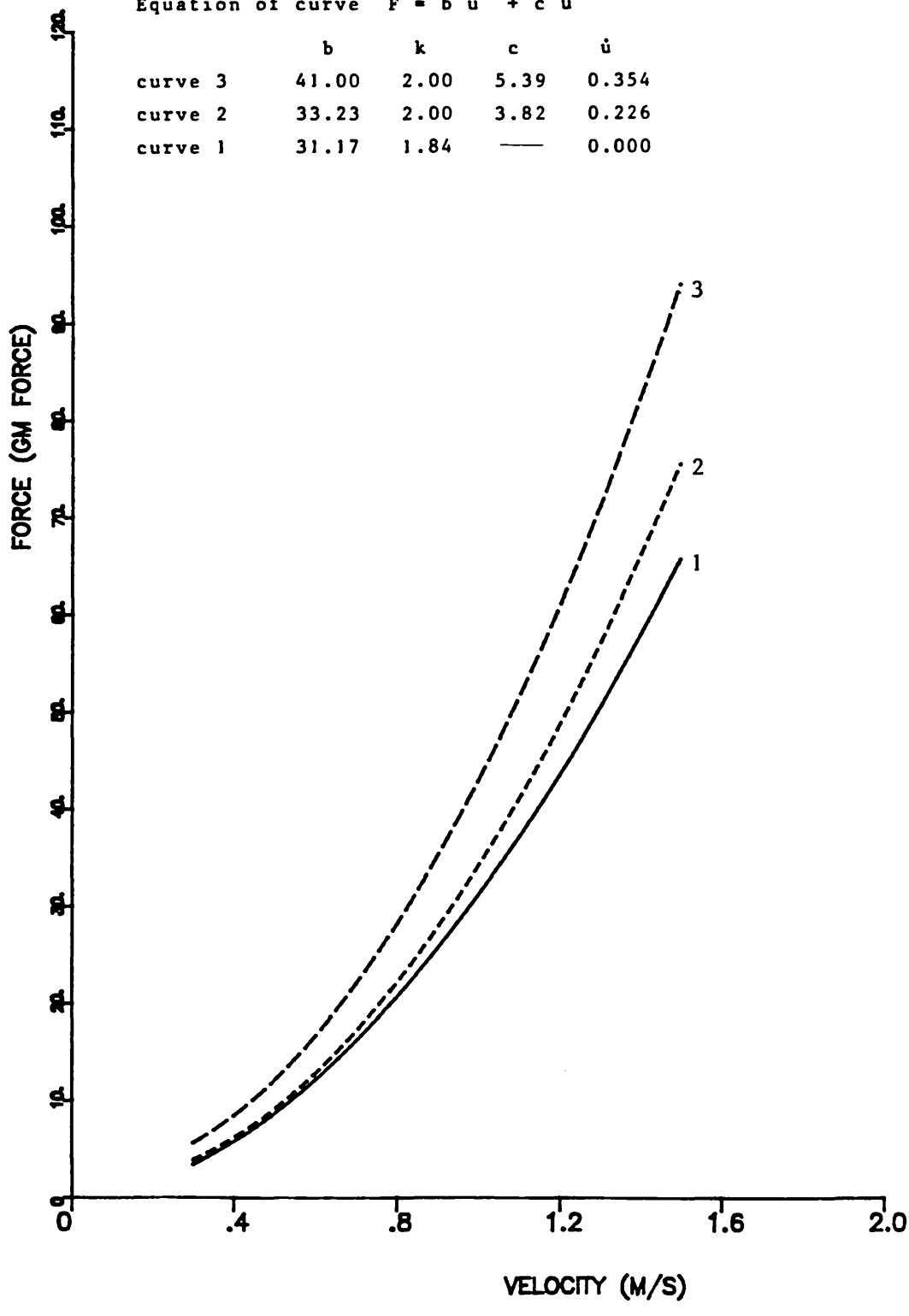


FIG.7.7 FORCE vs VELOCITY FOR SHED UNITS

FITTED CURVES FOR EXPERIMENTAL OBSERVATIONS

Equation of curve $F = b\,u^{k} + c\,\dot{u}$

	b	k	c	$\dot{u}$
curve 4	42.99	2.00	0.21	0.373
curve 3	42.01	2.00	0.88	0.379
curve 2	31.00	2.00	3.69	0.238
curve 1	30.47	1.91	——	0.000

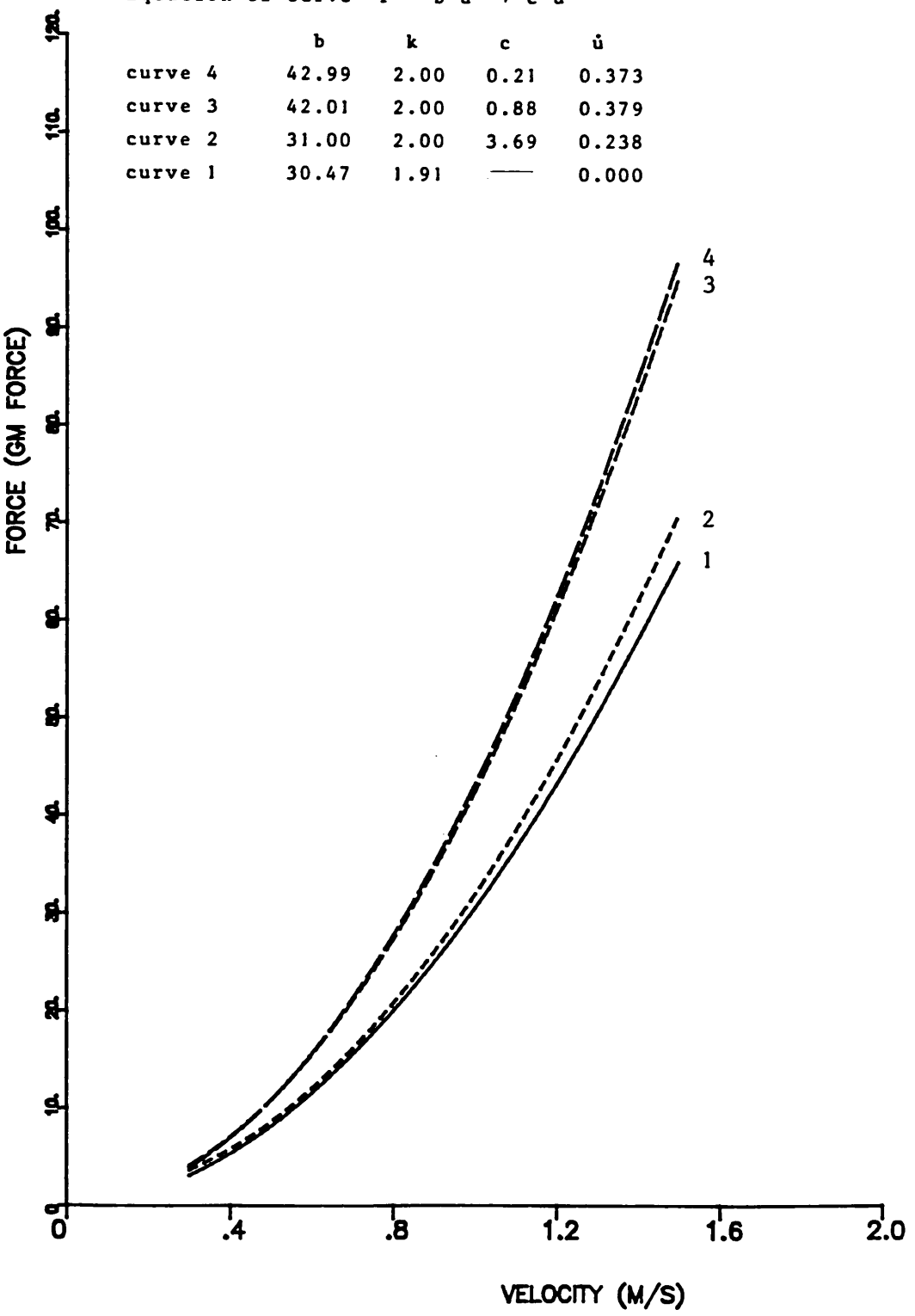


FIG.7.8 FORCE vs VELOCITY FOR HOBO UNITS

FITTED CURVES FOR EXPERIMENTAL OBSERVATIONS

Equation of curve $F = b\,u^{k} + c\,\dot{u}$

	b	k	c	$\dot{u}$
curve 4	38.29	2.00	5.46	0.429
curve 3	37.98	2.00	2.25	0.414
curve 2	31.53	2.00	8.99	0.151
curve 1	29.95	1.89	——	0.000

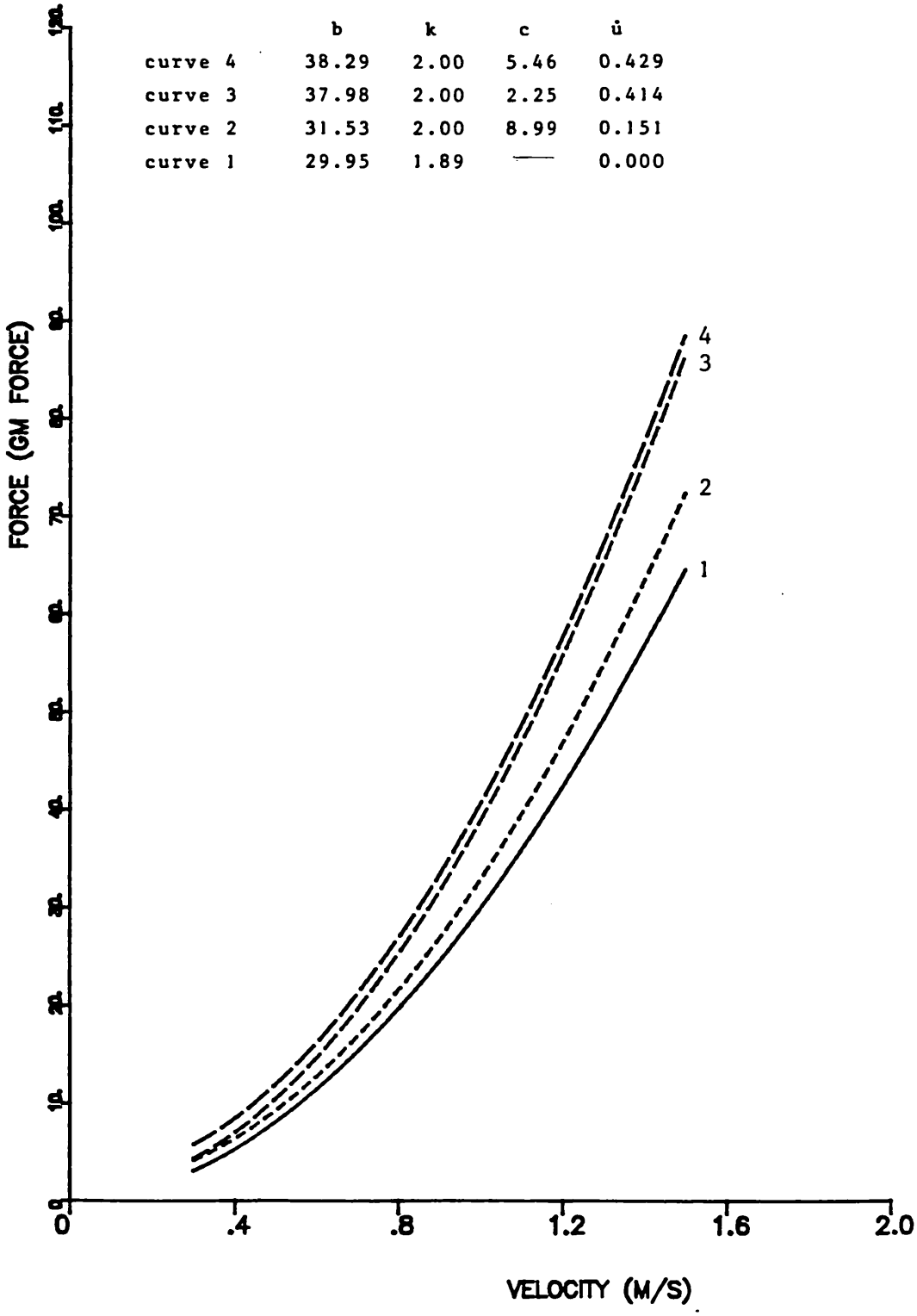


FIG.7.9 FORCE vs VELOCITY FOR CYLAT UNITS

FITTED CURVES FOR EXPERIMENTAL OBSERVATIONS

Equation of curve $F = b\,u^{k} + c\,\dot{u}$

	b	k	c	$\dot{u}$
curve 4	50.07	2.00	1.03	0.469
curve 3	47.18	2.00	5.25	0.467
curve 2	42.83	2.00	9.97	0.158
curve 1	41.93	1.76	——	0.000

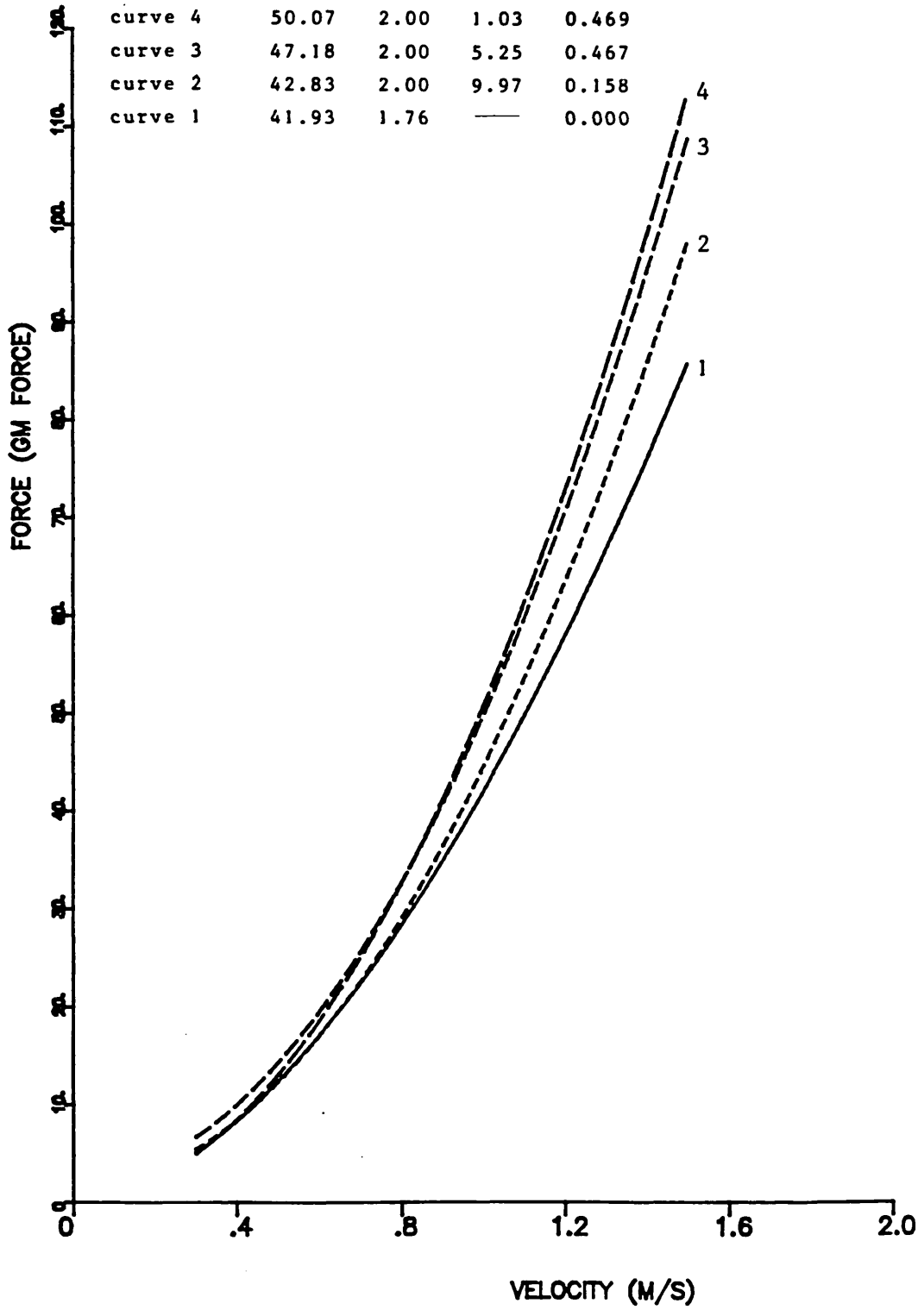


FIG.7.10.A DIFFERENCE IN FORCE vs VELOCITY

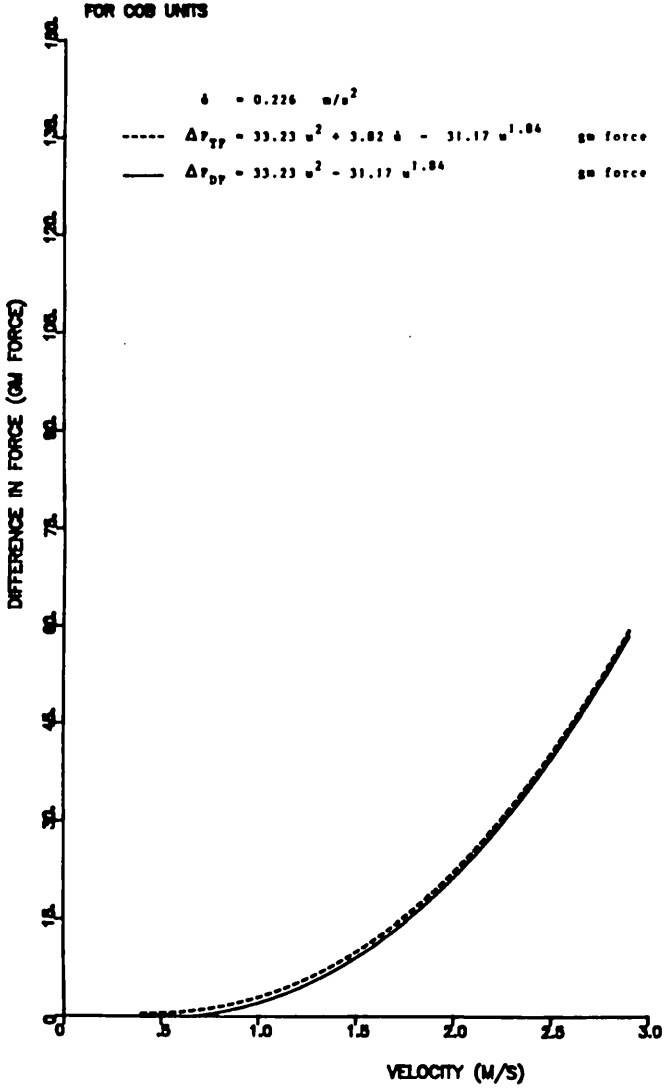


FIG.7.10.B DIFFERENCE IN FORCE vs VELOCITY

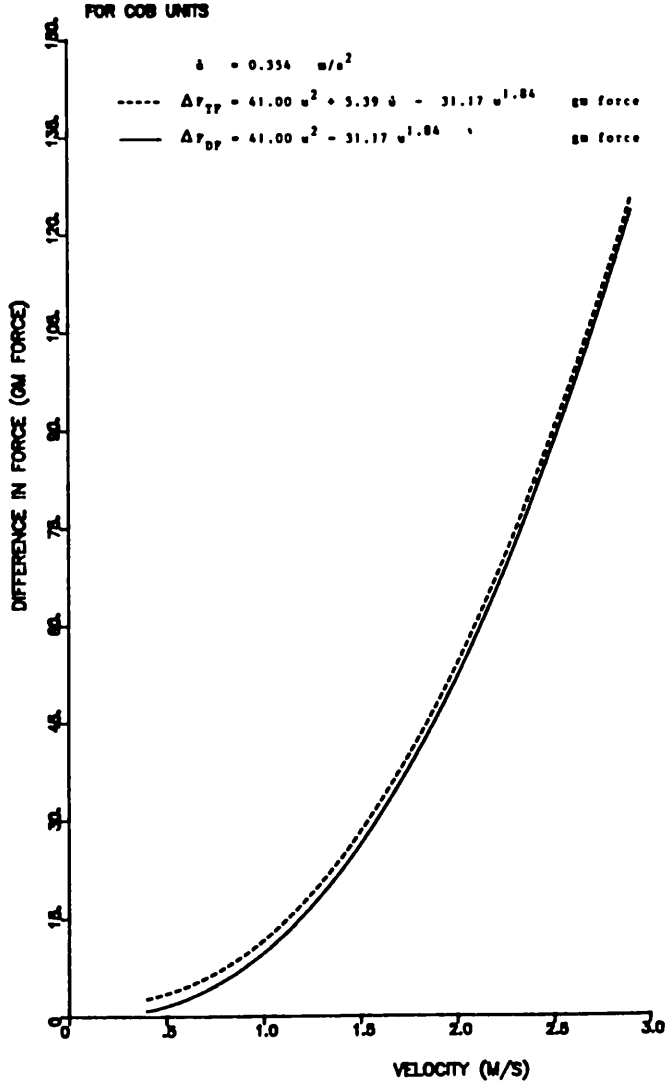


FIG.7.11.A DIFFERENCE IN FORCE vs VELOCITY

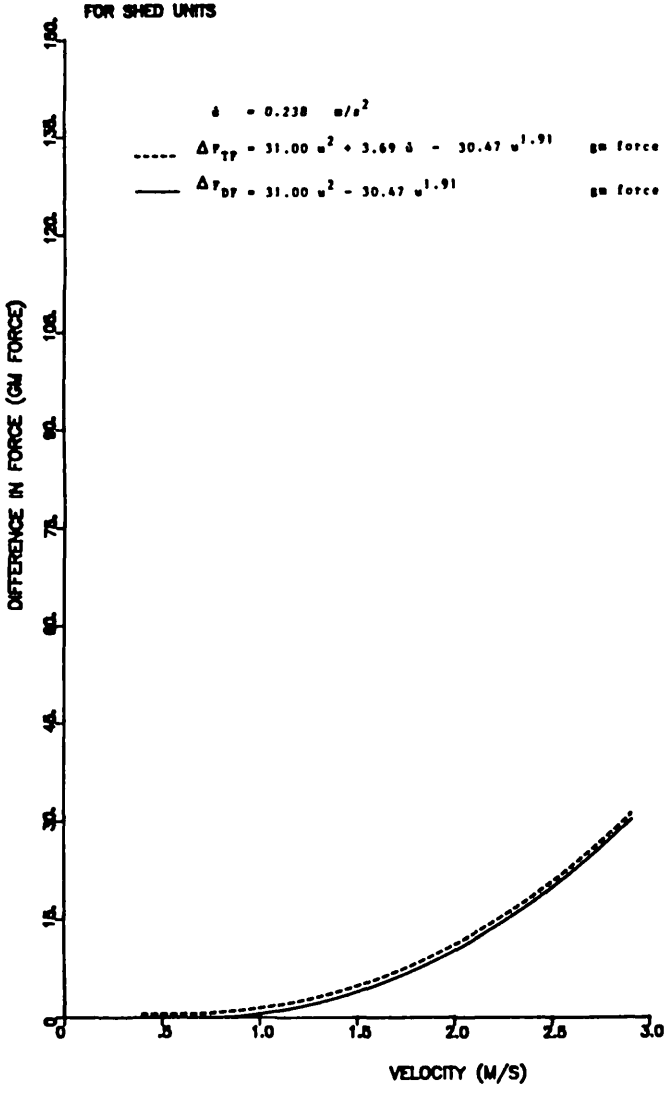


FIG.7.11.B DIFFERENCE IN FORCE vs VELOCITY

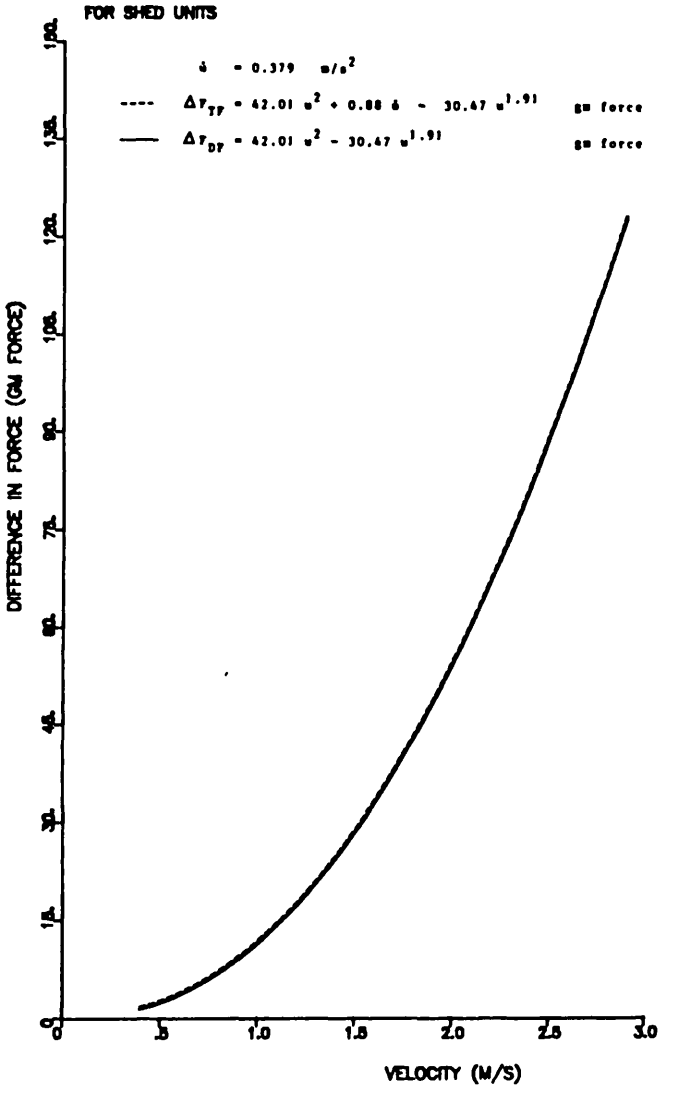


FIG.7.12.A DIFFERENCE IN FORCE vs VELOCITY

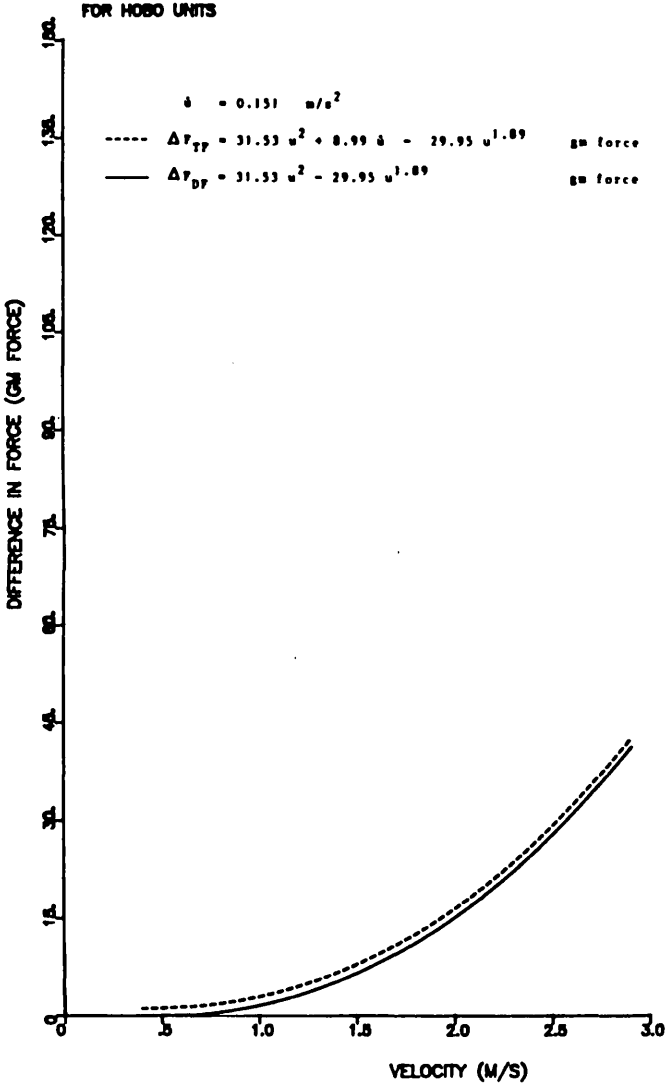


FIG.7.12.B DIFFERENCE IN FORCE vs VELOCITY

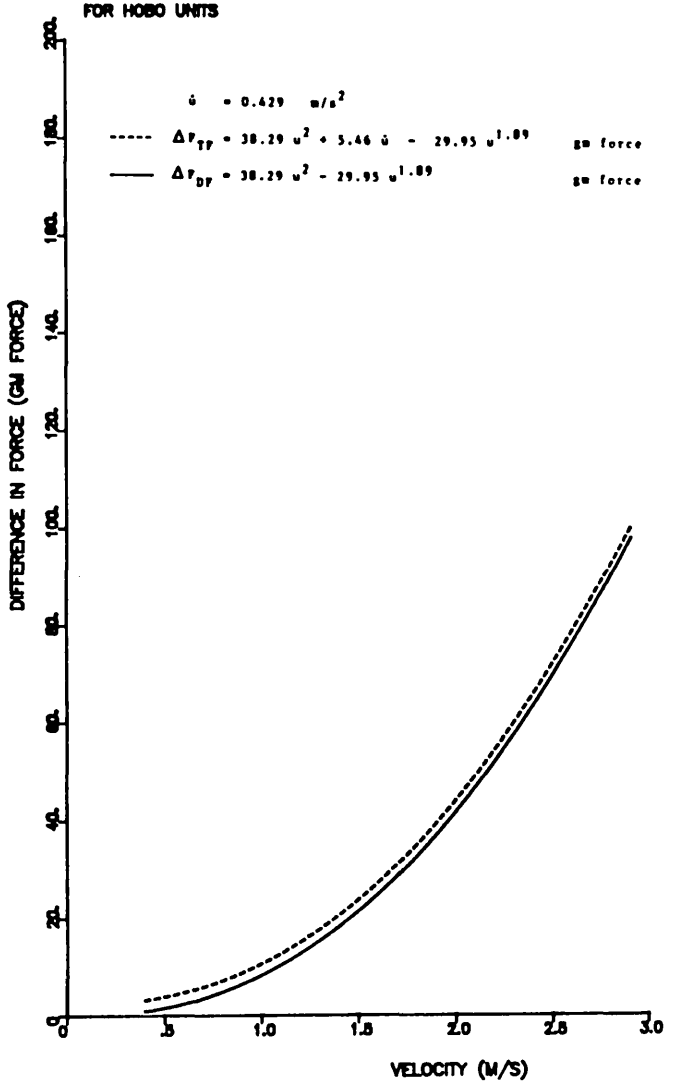


FIG.7.13.A DIFFERENCE IN FORCE vs VELOCITY

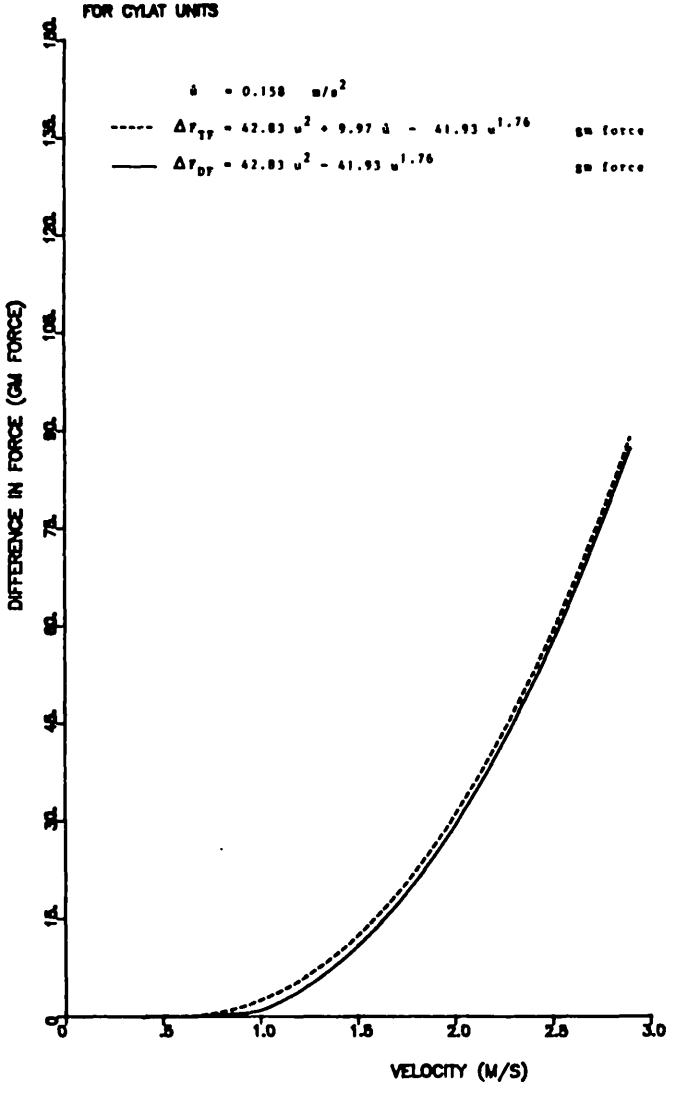


FIG.7.13.B DIFFERENCE IN FORCE vs VELOCITY

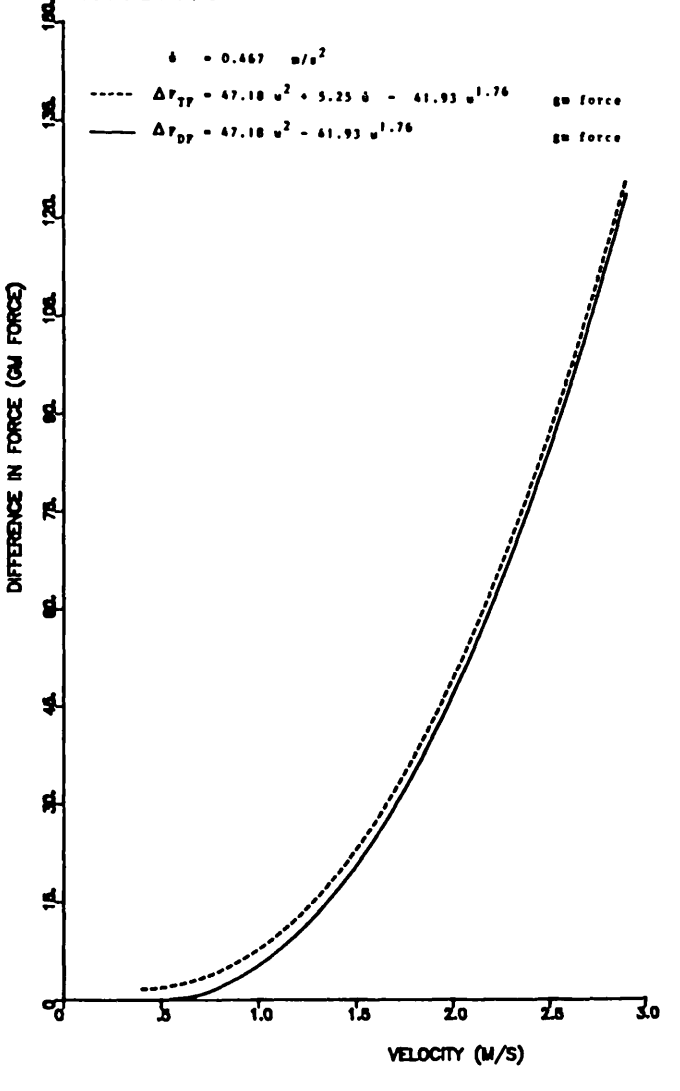


FIG.7.14 DRAG FORCE COEFFICIENT vs ACCELERATION

B in $F = B*u^2 + c*\dot{u}$ (const acc)

$F = B'*u^2$ (const vel)

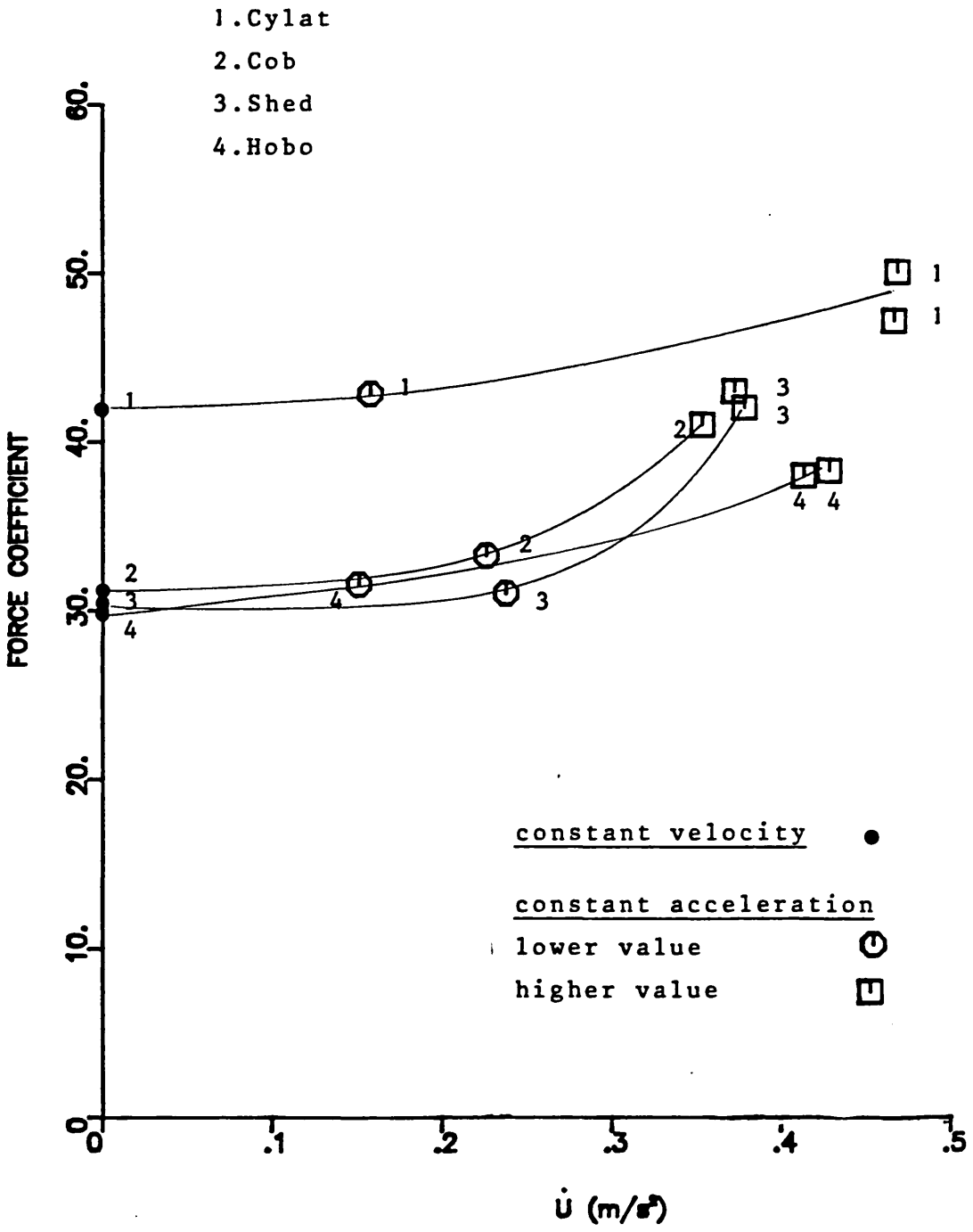


FIG.7.15 FORCE vs VELOCITY

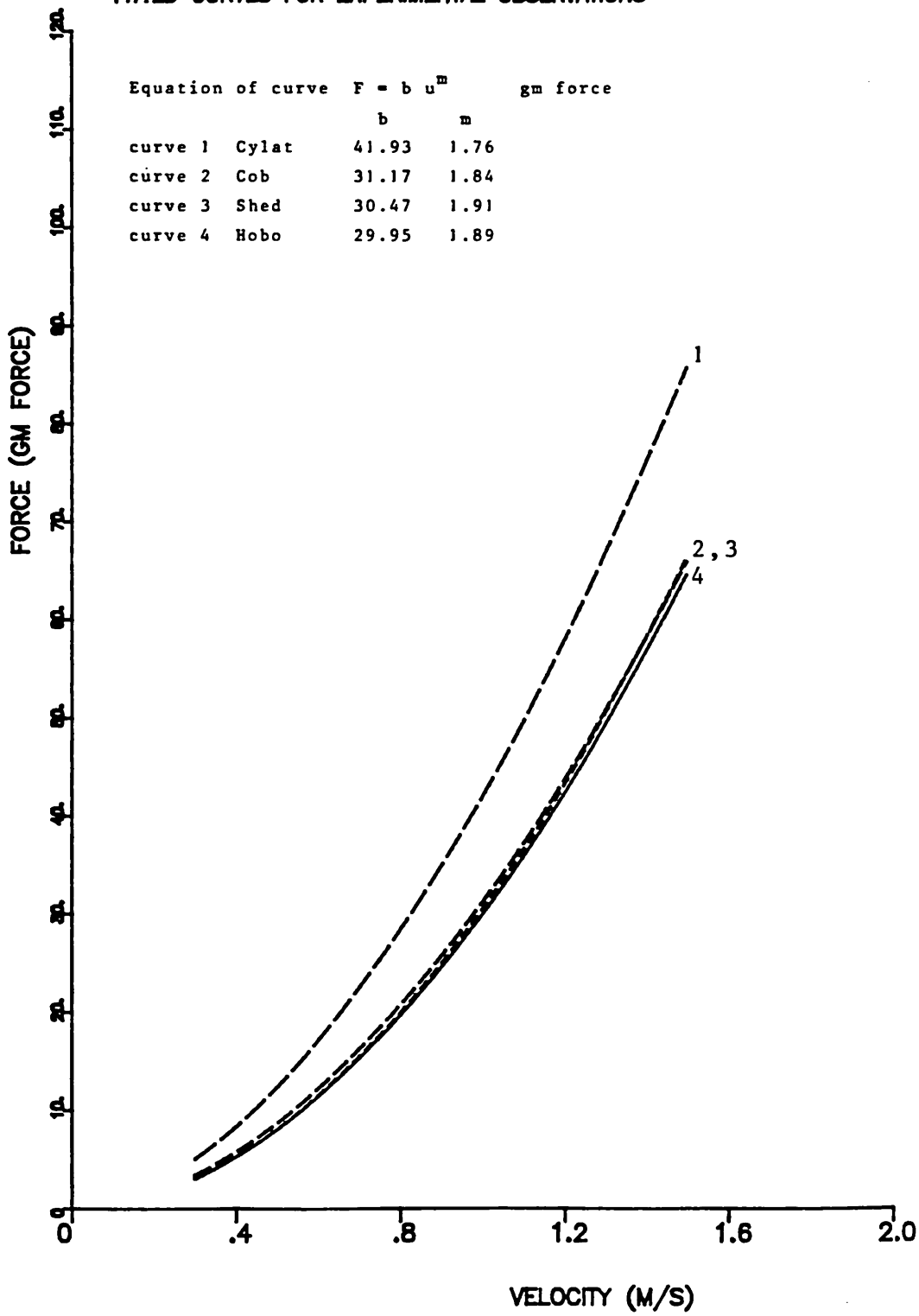
UNDER CONSTANT VELOCITY

FOR COB, SHED, HOBO AND CYLAT UNITS

FITTED CURVES FOR EXPERIMENTAL OBSERVATIONS

Equation of curve $F = b\,u^m$ gm force

		b	m
curve 1	Cylat	41.93	1.76
curve 2	Cob	31.17	1.84
curve 3	Shed	30.47	1.91
curve 4	Hobo	29.95	1.89



CHAPTER 8 - ADDITIONAL TESTS UNDER OSCILLATORY FLOW CONDITIONS

8.1. Introduction

The main test programme under oscillatory flow conditions involved the measurement of transmission, reflection and energy loss coefficients for a wide range of porous, open block, non-submerged structures of rectangular section. The results of this study were presented in Chapter 6. In addition to those tests it was necessary to perform a series of tests for different structural configurations and wave conditions. The results of these tests are presented in this chapter. The type of tests which were performed in this phase of the project were identified in Section 6.1 when presenting the summary of the experimental programme.

8.2. Performance of closed block structures (porous wave absorbers)

8.2.1. Method of analysis

The main difference between open block and closed block porous structures of rectangular shape is the presence of a vertical impermeable face at the rear of the latter, Fig. 8.1. A solid impermeable rectangular block structure is effectively a vertical wall with very high reflection coefficients. A porous structure of the same type having a vertical impermeable face at the back can be effectively used as an energy absorber exhibiting low reflection coefficients and not permitting external transmission on the lee side. As pointed out by Madsen, P.A. (1983) experimental investigations for these types of structure are of very limited extent. For the purpose of theoretical analysis several previous investigators made use of vertical-faced closed block porous structures to simulate sloping rubble mound structures with an impermeable core.

In the present study a variety of open block structures was experimentally investigated under oscillatory flow tests. To supplement these studies, closed block structures consisting of both Cob and Shed armour units were investigated. In the case of the latter a comparison was made with the corresponding open block structure. Closed block structures are also referred to as porous wave absorbers.

To assess the overall performance of both types of structure, the parameters defined below were used to study internal and external wave action.

Reference is also made to Fig. 8.1.

As discussed in Section 4.3.3, the composite wave system in front of the structure consists of a partial standing wave, characterised by loop and node height, expressed as H_{max} and H_{min} respectively. The incident and reflected wave heights for both types of structure are given by

$$H_i = \frac{H_{max} + H_{min}}{2} \tag{8.1}$$

$$H_r = \frac{H_{max} - H_{min}}{2} \tag{8.2}$$

Hence the reflection coefficient is given by,

$$K_r = \frac{H_{max} - H_{min}}{H_{max} + H_{min}} \tag{8.3}$$

For the open block structure the external transmission coefficient is given by, $K_t = \frac{H_t}{H_i}$ (8.4)

where H_t is the transmitted wave height at the lee of the structure and H_i is the incident wave height.

To study wave attenuation inside the structure it is necessary to identify an internal transmission coefficient. This coefficient, which varies with location along the length of the structure, is defined at any given point x ($0 < x < l$), by

$$K'_{t\ \text{at } x} = \frac{H_x}{H_o} \tag{8.5}$$

where H_x is the measured wave height within the structure at a distance x from the front interface.

H_o is the loop height at the front interface.

l is the length of the structure.

The energy loss coefficients (K_d) for both open and closed block structures are defined below.

For open block structures $K_d = \sqrt{1 - (K_t^2 + K_r^2)}$ (8.6)

For closed block structures $K_d = \sqrt{1 - K_r^2}$ (8.7)

In eqs. 8.6 and 8.7, K_r and K_t are given by eqs. 8.3 and 8.4 respectively. The basis on which the energy loss coefficient is defined was presented earlier in Section 6.4.1.

It should be pointed out that in the case of rectangular block structures consisting of Cobs and Sheds it is possible to measure internal wave decay directly because wave probes can be inserted through the relatively large openings of both armour units provided the columns of units are aligned in the vertical direction. This advantage is not available for other types of porous media such as rounded stones.

8.2.2. Discussion of experimental results

Figs. 8.2 to 8.6 illustrate the results of tests performed on a closed block structure of length 160 cm consisting of Cob armour units. Due to the limited number of armour units available, the lateral width of the structure was limited to four armour units and experimental conditions were achieved by partitioning an existing flume to accommodate the narrow structure.

In the test programme the structure was subjected to wave periods of 1.0, 1.5 and 2.0 secs. For each period the amplitude was varied and reflection coefficients determined. In addition for selected wave amplitudes, at least two for each period, wave height attenuation was monitored along the length of the structure. The water depth was maintained constant at 23 cm.

In the presentation of results attention is focused on two main areas of interest. The first relates to the monitoring of wave decay inside the structure for different wave periods and amplitudes. This is illustrated by plotting the internal transmission coefficient, K_t' given by eq. 8.5, against the distance along the length of the structure, Figs. 8.2 to 8.5. The second relates to the reflection characteristics of the structure. This is illustrated by plotting the reflection coefficient, K_r, given by eq. 8.3, against wave steepness and the ratio of wave height to water depth, Fig. 8.6.a and b.

Fig. 8.2 illustrates the influence of wave period in relation to wave

decay in the structure. In each case the wave amplitude is approximately the same and the water depth constant. It is evident that waves of higher period are more effectively transmitted through the structure exhibiting higher transmission coefficients whereas those with a lower period are damped. At a distance of 30 cm inside the structure the transmission coefficients corresponding to wave period of 1 sec is only 0.2 in comparison with wave periods of 1.5 and 2.0 secs which exhibit corresponding coefficients in the region of 0.47. The influence of the rear vertical face is evident in the form of increased transmission coefficients near to it due to the presence of the standing wave at that end.

Figs. 8.3 to 8.5 illustrate the influence of wave height for a given period. For wave period of 2.0 secs it is clear that waves with higher amplitude are damped more effectively than those with lower amplitude. The same trend is observed for the other two wave periods although the difference is not evident as in the first case. This is mainly due to the fact that the difference in wave amplitudes at the given periods was small.

Figs. 8.6.a and 8.6.b refer to the variation of the reflection coefficient of the structure with wave steepness (H_i/L) and wave height to depth ratio (H_i/d). For all three wave periods the reflection coefficients lie in the range 0.3 to 0.4. Although the scatter in experimental results is not appreciable, they do not indicate a specific dependence on wave steepness or incident wave height.

The second closed block structure investigated in the present programme consisted of Shed units and was of overall length 32 cm, a fifth of the length of the previous structure consisting of Cobs. For this structure tests were also performed on the corresponding open block configuration. As before, three wave periods were used with varying amplitude. The depth was kept constant at 20 cm.

As in the previous case the results from these tests covered both internal and external wave characteristics. Internal wave decay of both open and closed block structures is illustrated for different incident wave conditions by plotting the internal transmission coefficient, K_t', given by eq. 8.5, against the distance along the length of the structure, Figs. 8.7 to 8.10. The external wave characteristics are illustrated by plotting the reflection coefficient, K_r, given by eq. 8.3, and the external transmission coefficient, K_t, given by eq. 8.4 against wave steepness, Fig. 8.11. Obviously external transmission coefficients are only applicable to open block structures.

Figs. 8.7 and 8.8 illustrate the influence of wave height on internal

damping at constant period of 1.5 secs. In the case of the open block structure, Fig. 8.7, the wave height decreases along the length of the structure and waves with small amplitude are transmitted more effectively, as indicated by the higher internal transmission coefficients.

The performance of the corresponding closed block structure (Fig. 8.8) indicates that the transmission coefficient decreases within the length of the first few armour units and then increases, reaching approximately unity at the rear vertical face. Again in this case small amplitude waves were transmitted more effectively.

Figs. 8.9 and 8.10 illustrate to a certain extent the influence of wave period. The results refer to the internal wave decay at three different periods but the wave amplitudes also differ and hence it is not possible to comment on wave period in isolation. The amplitude of waves used in the plot increases with decreasing wave period. These two plots present a similar trend to that of Figs. 8.7 and 8.8 discussed previously. For the open block structure, Fig. 8.9, waves having a period of 2.0 secs are more effectively transmitted than the other two wave periods.

In the case of the closed block structure, Fig. 8.10, it is evident that waves with a period of 2.0 secs and having the least amplitude exhibit high internal transmission coefficients whereas waves with a period of 1.0 sec and having the highest amplitude exhibit lower coefficients. The results for waves with period 1.5 secs lie in between but closer to the former than the latter.

Fig. 8.11 illustrates the reflection coefficients for both closed and open block structures and the external transmission coefficients for the latter. The external transmission coefficients lie in the range 0.28 to 0.48 and these values are consistent with those observed earlier when performing oscillatory flow tests on a similar structure (ref. Section 6.4.2). These results confirm that small amplitude waves with longer periods exhibit high external transmission coefficients. The reflection coefficients for the closed block structure are less than those for the open block structure except at a wave period of 2 secs.

Similar observations were also made by Benassai, Ragone and Sciortino (1983) when testing a vertical porous modular breakwater constructed entirely from pre-cast concrete units. The presence of the rear impermeable wall reduced wave reflection for both regular and random waves.

The performance of the open block structure is very similar to that

discussed in Section 6.4.2 when analysing the results of oscillatory flow tests. However the results for closed block structures demand closer examination.

8.2.3. Remarks on the overall performance of closed block structures (porous wave absorbers)

The discussion on closed block structures encompasses two areas of interest, the first on the performance of these types of structure, particularly the influence of the length of structure. For this purpose a comparison will be made between the two closed block structures, the first consisting of Cobs having an overall length of 160 cm and the second consisting of Sheds having an overall length of 32 cm. The second area of discussion considers the relative merits of open and closed block structures consisting of Sheds.

From the results of tests on the two closed block structures used for the present study, it is evident that their performance is heavily dependent on the location of the impermeable vertical face and, as a consequence, on the length of the structure.

From Figs. 8.8 and 8.10 it is observed that although there is an initial reduction in wave height due to internal losses, this effect is masked by the influence of the standing wave generated by wave reflection from the rear face. For a given wave period, internal transmission coefficients are higher for waves with small amplitudes. However, if the influence of wave period is considered the initial reduction in wave height is greater for waves of shorter period having high amplitudes. This is clearly illustrated in Fig. 8.10 which shows that for waves having a period of 1 sec, the minimum transmission coefficient observed is 0.5 occurring at a distance 8.5 cm away from the interface. Thereafter the influence of the standing wave increases the coefficient to 0.66. If the same parameters are considered for waves having a period of 1.5 secs (Fig. 8.8), the minimum transmission coefficient recorded is 0.72 at a distance 7.5 cm away from the interface. The subsequent increase in the transmission coefficient is very high, reaching values approximately equal to unity with maximum values registered by waves having the smallest amplitude.

In comparison, the results of the closed block structure consisting of Cob units and of greater overall length (Figs. 8.2 to 8.5) is different to the above. By the time the wave reaches the rear face most of the energy is dissipated and the influence of the standing wave generated at the reflective wall is a minimum. For example, from Fig. 8.2, for waves having period of 1.5 secs the minimum

transmission coefficient recorded is 0.07 at a distance 130 cm away from the interface and the subsequent increase in its value is very small, reaching only 0.14. Hence if an absorber is of sufficient length the wave height attenuation within the structure is high, resulting in a very small increase in transmission coefficient at the rear vertical impermeable face.

From a view point of reflection coefficients, both structures exhibit similar characteristics with values lying between 0.3 and 0.4. The single exception is for a 2 secs wave period for the shorter closed block structure which exhibits a reflection coefficient of 0.5 (Fig. 8.11).

A comparison of a closed block structure with its corresponding open block structure is made with reference to the two structures consisting of Shed armour units. With respect to internal wave action it is evident that an open block structure reduces the wave height progressively along the length of the structure in contrast to closed block structures whose behaviour has been already discussed. However, the former would contribute to external transmission in the lee of the structure. Reflection coefficients for both structures and the external transmission coefficients for the open block structure are given in Fig. 8.11. Except for waves having a period of 2 secs, the reflection coefficients for the open structure are higher.

From the above analysis of results it is observed that as the length of a closed block structure increases for a given wave environment its internal wave motion becomes very similar to that of its corresponding open block structure. This is particularly so for high amplitude waves with small period.

The energy loss coefficients, defined by eqs. 8.6 and 8.7, for the structures described in this section are given in Figs. 8.12.a and b. Fig. 8.12.a relates to the open and closed block structures consisting of Shed armour units and of overall length 32 cm. It indicates that energy losses for the closed block structure to be greater than that of the corresponding open block structure. Although the number of data points is limited, losses increase with increasing steepness. Fig. 8.12.b relates to the closed block structure consisting of Cob armour units and of overall length 160 cm. The energy loss coefficients for the three different wave periods remain approximately constant, just above 0.9. These results illustrate the relative merits of open and closed block structures and also provide information on the energy absorbing capability of different structures under varying wave period and wave height.

8.2.4. Practical applications of closed block structures (porous wave absorbers)

The results from tests on closed block structures can be effectively applied in relation to the performance of perforated caisson type breakwaters. In some situations conventional rubble mound breakwaters may prove to be an expensive solution when armour stones are not freely available. A similar solution may be impractical when ships have to be accommodated along the harbour side of the breakwater and when the deck of the breakwater has to be used for handling and storage of goods. In such situations vertical breakwaters may be used. Although these are more economical with respect to materials, they reflect a large proportion of the incident wave energy. This may be reduced by incorporating perforations and a voids chamber in the structure.

Basically a perforated breakwater consists of a porous wall (screen) having openings - which may be in the form of a series of slots or holes - placed at a distance in front of a solid vertical face. Waves incident on the screen are partially reflected and transmitted into the voids chamber with energy being lost mainly due to turbulence in the flow through the openings. The transmitted wave is reflected from the rear impermeable face with further losses and reflections in its passage through the porous wall. The superposition of these waves contributes to the formation of standing waves in the voids chamber and in front of the structure. The amplitude of these waves will be dependent on the losses due to the porous wall and on the length of the voids chamber. If the reflection coefficient for the structure is K_r, the maximum height of the standing wave outside the structure will be $(1 + K_r)H_i$ in which H_i is the incident wave height.

The wave forces on a perforated breakwater are somewhat less than those on a solid faced breakwater, but due to lack of sand fill in certain areas of the structure stability of the breakwater becomes an important consideration.

Fig. 8.13.a illustrates a structure in which the voids chamber is only a part of a very wide structure having rock-fill compartments thus ensuring stability.

For caisson type breakwaters the configuration in the horizontal plane (cross-sectional plan view) plays an important role. Graveson (1979) pointed out that forces experienced by a breakwater with a solid rectangular section (plan view) are approximately 40% more than those experienced by a similar structure consisting of a cylindrical section with cylinders kept vertical adjacent to each other. It would seem appropriate to combine the principles of perforated breakwaters and cylindrical caissons to produce a structure as illustrated in Fig. 8.13.b. It is a slotted

breakwater having an internal permeable wall. The main purpose of this design is to produce a breakwater with minimum wave reflection and high energy losses for all wave directions and periods of practical interest while maintaining the economic advantage of thin-walled shell caissons.

The foregoing discussion illustrates the importance of the two-dimensional porosity of the porous wall and the structure of the voids chamber in relation to reflection and energy dissipation from wave absorbers.

It should be noted that for a fixed length of void chamber the performance of the wave absorber in suppressing reflections will be sensitive to wave length (or period) of the incident wave. This is due to the formation of standing waves inside the chamber and as a consequence these structures are susceptible to seiche motion. Furthermore, the reflection coefficient for the absorber will also depend on the resistance of the porous wall (screen). If the screen is very resistive, the incident waves will be completely reflected from it with minimum wave transmission into the voids chamber and, conversely, if the screen is highly porous almost complete reflection will occur from the rear impermeable face with the porous screen proving to be ineffective. Reflection coefficients corresponding to both these extreme cases will be high. This implies the existence of an optimum porosity for the porous wall which will give minimum values of reflection coefficients for a given incident wave condition. It should be noted that the resistance of the screen is proportional to the square of velocity through the openings while the orbital velocity is proportional to wave height thus relating optimum porosity to wave height.

Weckmann, Bigham and Dixon (1983) presented results from a study on a wave absorbing structure consisting of a solid leeward wall fronted by a multi-baffled timber pile system, Fig. 8.13.c. The performance of the structure was very much dependent on the number of baffles and the porosity. The results indicated that a three row baffle system with 30% porosity was most effective for the given test conditions with a maximum reflection coefficient of 0.42.

An alternative to this type of structure is to replace the porous wall and voids chamber by a porous medium similar to the closed block structures investigated in this study. This type of structure has an added advantage of contributing to the overall stability because of the increase in solid material in the region otherwise occupied by the voids chamber. Such structures, built with pre-cast concrete units, have been widely used in Japan (Shiraishi, Palmer and Okamoto 1976, Ijima, Tanaka and Okuzono 1976 and Shimada, Yuasa and Iwasa

1981).

From previous investigations and from this study it is evident that wave absorbing structures perform at their best for wave breaking conditions with relatively short waves having high amplitudes rather than non-breaking long waves of small amplitude.

8.3. Performance of porous submerged structures

As a part of the present investigation two submerged open block structures consisting of Cob armour units were investigated in order to compare their performance with non-submerged structures of the same type. With the non-submerged case, a group of three structures was thus available for comparison. The ratios of the heights of the structures to still water depth (H_{st}/d) for the three structures under investigation were 1.456, 1.04 and 0.832 respectively. The range of wave amplitudes generated were such that the first remains emerged, the second is just emerged and overtopped by the waves ($H_{st}/d \approx 1.0$) and the third is fully submerged.

Figs. 8.14 to 8.16 illustrate the performances of these three structures. In comparing the first two (Figs. 8.14 and 8.15), it is observed that the reflection coefficients of the latter are reduced due to overtopping whereas the transmission coefficients remain unchanged. It should be noted that the second structure represents a critical stage in which the height of the structure is approximately equal to the water depth and the overtopping waves are absorbed by the structure within a short distance from the front interface.

In comparing the second and third structures (Figs. 8.15 and 8.16) the transmission coefficients of the latter have increased to values greater than 0.7 whereas the reflection coefficients have reduced to values less than 0.25. The energy loss coefficients for the third structure are very low and in some circumstances are less than the transmission coefficients. From these results it can be stated that as the degree of submergence increases, the efficiency of the structure decreases with increased wave transmission. However, as evident from the results of the second structure, Fig. 8.15, marginal overtopping did not reduce the efficiency of the structure.

The results of these tests are also applicable in the analysis of overtopping of an otherwise non-submerged structure particularly in relation to the extent of overtopping. The performance of these three structures illustrates the

influence of the degree of submergence on transmission, reflection and energy loss coefficients.

8.4. Performance of an open block structure with a sloping front

8.4.1. References to previous investigations

Hitherto the open and closed block porous structures considered have vertical faces on both sides. These structures would thus exhibit high reflection coefficients in comparison with a sloping structure. To investigate the influence of a sloping interface, a slope consisting of the same material was introduced to the open block structure consisting of rounded stones, Fig. 3.12. Before considering the results of the present study, reference is made to previous investigations in order to highlight the main developments in this field.

Wave breaking occurs when the steepness of a wave exceeds a critical value. In defining critical steepness there are two distinct groups of breaking processes. One occurs in deep water (or constant water depth) due to superposition of waves or due to the effects of a forcing function on waves such as wind or opposing currents. The other is wave breaking in shallow water due to limited depth. It is this category which is of interest in relation to energy dissipation and reflection from coastal structures.

On a smooth slope, the parameters which govern wave breaking are the wave steepness (H/L) and slope (s). For sufficiently steep slopes or sufficiently low amplitudes an incident wave does not break and is completely reflected. When the slope decreases or steepness increases, a threshold is reached where breaking commences.

Wave breaking due to limited depth was investigated by Miche (1949) using periodic standing waves on a plane slope extending to deep water. Linear wave theory was used to transform the maximum near-shore wave steepness to deepwater and to define a critical deepwater wave steepness

$$\left(\frac{H_o}{L_o}\right)_{crit} = \left(\frac{2\alpha}{\pi}\right)^{\frac{1}{2}} \frac{\sin^2\alpha}{\pi} \qquad (8.8)$$

where α is the surface slope.

This breaking criterion is based on the hypothesis that the maximum water surface slope attainable without breaking on a reflecting surface is equal to the slope of the reflecting surface itself.

Miche states that because $(H_o/L_o)_{crit}$ is the maximum steepness at which the wave remains stable on the slope, any deepwater wave steepness (H_o/L_o) which exceeds this will break and be reflected at the critical steepness. For non-breaking waves the reflection coefficient is set equal to unity.

The definition of a reflection coefficient follows directly as,

$$K_r = \frac{(H_o/L_o)_{crit}}{(H_o/L_o)} \quad \text{if the ratio is less than 1}$$

$$= 1 \quad \text{otherwise} \qquad (8.9)$$

It should be noted that these reflection coefficients represent a theoretical value. The actual value will be smaller due to effects of viscosity, roughness and permeability. Miche recommends a multiplication factor of 0.8 for smooth slopes.

Iribarren and Nogales (1949) studied the problem using trochoidal theory for uniform progressive waves and presented a semi-empirical solution given by

$$\left(\frac{H}{L_o}\right)_{crit} = 0.19 \tan^2\alpha \qquad (8.10)$$

From their work it was evident that the single dimensionless parameter defined by

$$\xi = \frac{s}{\left(\frac{H}{L_o}\right)^{\frac{1}{2}}} \qquad (8.11)$$

in which s = the slope = $\tan\alpha$

H = total height of the breaking wave

plays an important role.

Using eqs. 8.10 and 8.11, the critical value approximately corresponds to

$$\xi_{o\ crit} \approx 2.3 \qquad (8.12)$$

If ξ < 2.3 waves break and the reflection coefficient is less than unity.

Miche's expression for reflection coefficient can be expressed in terms of ξ and ξ'_{crit} as follows

$$\left.\begin{aligned} K_r &= \left(\frac{\xi}{\xi'_{crit}}\right) \text{ if the ratio is less than 1} \\ &= 1 \qquad \text{otherwise.} \end{aligned}\right\} \qquad (8.13)$$

in which ξ'_{crit} is the critical value of ξ for the onset of breaking.

Battjes (1974) presented a synthesis of wave breaking on slopes introducing the parameter $\xi = \tan\alpha/\sqrt{H/L_o}$ for defining the critical steepness. The importance of this parameter in defining flow characteristics on slopes is now widely accepted. Battjes calibrated the previous equation for smooth slopes using observations made by Hunt (1959) and expressed K_r as,

$$K_r = 0.1\ \xi^2 \qquad (8.14)$$

Fig. 8.17.a is reproduced from Battjes (1974) and shows the above equation compared with data obtained from tests conducted by Moraes (1970) on smooth slopes. The experimental points for the four slopes more or less coincide with each other and with eq. 8.14 for ξ < 2.5. Hence for breaking waves the agreement is satisfactory. For ξ > 2.5 they diverge with gentler slopes giving less reflection than steeper slopes at the same value of ξ.

Mattsson (1963) performed experiments on smooth, rough and permeable slopes with regular waves and measured wave reflection. Fig. 8.17.b relates to his work, illustrating the variation of reflection coefficient versus steepness on 1 in 3.0 slope. The equation $K_r = 0.1\ \xi^2$ is also plotted on the same graph for comparison. This figure illustrates the influence of permeability and roughness in reducing the reflection coefficient, particularly for low values of steepness. As steepness increases the reflection coefficient remains constant and it can be stated that for low values of ξ, for which plunging breakers occur, permeability characteristics are not as effective in reducing wave reflection. This may be due to phenomena such as air entrainment in the porous media which will contribute towards decrease in transmission and increase in reflection, particularly at high steepness. It is also noticed that the reflection coefficients given by the curve

$K_r = 0.1\ \xi^2$ are higher than those observed, particularly for rough and permeable slopes.

Gunbak (1979) measured wave reflection when conducting stability tests with regular waves. The test structures were composed of W_{50} = 100 gm. armour rocks with slopes of 1 in 2.5 and 1.5 with the depth maintained at 1 m. The results of these measurements are shown in Figs. 8.17.c and d. The equation $K_r = 0.1\ \xi^2$ has also been plotted in Fig. 8.17.c but multiplied by a modification factor for permeability and roughness. In this case a factor of 0.45 has been used. Results presented in Fig. 8.17.d demonstrate that at high values of ξ with a 1 in 1.5 slope the reflection stabilizes around a constant value of 0.46. It is noticed that comparatively large scatter exists for the experimental data.

Except for the work of Mattsson, little information is available on wave reflection on permeable slopes. It is for this reason that a sloping beach consisting of the same material was added to the vertical-faced, open-block structure made of rounded stones in this work.

8.4.2. Discussion of experimental results

Fig. 8.18 presents a comparison between the two structures with and without a sloping face. The tests were performed for a wave period of 1.5 secs and slope angle of 13.24 degrees. The introduction of the sloping surface reduced both transmission and reflection coefficients with the reduction in the latter very much greater than the former. This clearly illustrates the influence of a sloping structure on wave reflection. In this case, which relates to a very mild slope, the reduction in the reflection coefficient is approximately 0.35. The corresponding variation in the transmission coefficient is less than 0.1. Under these conditions the sloping structure exhibits high energy loss coefficients.

The results presented in Fig. 8.18 referred to a structure with a fixed slope. In order to study the effects due to the variation of slope angle, a series of tests was performed for five different slope angles at a wave period of 1 sec. The results of these tests together with those presented in Fig. 8.18 are given in Fig. 8.19. In this plot the reflection coefficient (K_r) is plotted against ξ^* (= $\sin\alpha/\sqrt{H_i/L_o}$). The independent variable ξ^* is very similar to the surf similarity parameter $\xi = \tan\alpha/\sqrt{H_i/L_o}$ with the difference being the use of sine of the slope instead of the tangent. This change has been made to accommodate the experimental values relating to structures with a vertical face ($\sin\alpha = 1.0$).

From Fig. 8.19 it is observed that for vertical-faced structures the reflection coefficient lies in the range 0.45 to 0.55 for values of ξ^* greater than 7. Sloping structures exhibit low reflection coefficients which increase with increasing values of ξ^* (and slope angle).

The reflection coefficients obtained are well below the values given by the equation $K_r = 0.1\ \xi^{*2}$. These results clearly illustrate the influence of porosity on the reflection coefficient for both sloping and vertical-faced structures. The reflection coefficients of the porous structures are found to be low in comparison with those corresponding to smooth or rough faced impermeable structures. It should be noted that this reduction is obtained at the expense of a certain amount of wave transmission which is observed in the lee of the structure.

The reflection coefficients presented in Fig. 8.19 relate to six slopes, ranging between 8 and 41 degrees. Although the transmission coefficients corresponding to these conditions are not presented, it was observed that in the wave steepness range 0.02 to 0.025 the variation in the transmission coefficients was only 0.06 around a mean value of 0.10. The corresponding variations in the reflection coefficients exceeded 0.23. These results together with those presented in Fig. 8.18 establish that reflection coefficients are more sensitive to variations in slope than are transmission coefficients.

This subject will be further considered in the analysis of results of reflection from a porous trapezoid, Section 8.5, as well as from a breakwater section of hollow block armour, Section 9.2.1.

8.5. Performance of a porous trapezoidal structure

In the previous section, results pertaining to a rectangular porous block structure with and without a sloping front face were discussed. Tests on porous trapezoidal structures provide information in two areas of interest. Firstly, they enable the comparison of a trapezoidal form with its equivalent rectangular form. The structural configuration of the latter was extensively investigated under oscillatory flow tests. Secondly, most investigators who have performed theoretical studies on porous structures adopted an equivalent rectangular form when analyzing complex trapezoidal structures (Madsen and White 1976b, Sollitt and Cross 1972, Nasser and McCorquodale 1975).

In the present investigation a trapezoidal porous structure consisting of Cob armour units was used for the tests. The slopes on either sides were

maintained at 1:1. Two equivalent rectangular structures were also considered. The dimensions of the first were based such that both structures have the same submerged volume at the still water depth of 20 cm used for the study. The dimensions of the second were such that the vertical interfaces of the rectangular form were located at the points where the still water level met the sloping faces of the trapezoid. It is evident that the first structure is longer than the second by a distance d.cotα where d is the still water depth and α the angle of slope.

The results from the test series are given in Figs. 8.20 to 8.22. The trapezoidal structure exhibits the lowest transmission and reflection coefficients with very high loss coefficients. The first equivalent rectangular structure – based on equal submerged volume – exhibits increased transmission and reflection coefficients. These coefficients are further increased by a very small amount for the second equivalent structure which is shorter in length than the first. The general trends of the results are similar to those observed in the oscillatory flow tests (Section 6.4.2). These results clearly indicate the advantage of using a trapezoidal porous structure in preference to a similar one of rectangular form from the viewpoint of reflection and transmission of energy.

It is also noted that in comparing the length of the three structures at still water level, the first equivalent rectangular structure is longer than the other two which are of equal length. This dimension is closely associated with the amount of energy transmitted. Although this dimension for the trapezoidal structure is less than or equal to its equivalent rectangular form, the former transmits less energy proving it to be an efficient configuration. Reduction in reflection coefficients were expected in the trapezoid due to the sloping front face.

Further reference to this structure will be made when discussing the results of the tests on a breakwater sloping section, Section 9.2.1.

8.6. Influence of length of open and closed block structures in relation to their overall performance

From the results already presented, it is possible to obtain information on the influence of length of structures in relation to their performance. Hitherto this subject was discussed in detail in relation to the performance of closed block structures (wave absorbers) consisting of Cob and Shed armour units, Section 8.2.3.

With respect to open block structures, the performance of the two equivalent rectangular sections consisting of Cob units provide an opportunity for

comparison. The two structures were of length 33.28 and 52.00 cm respectively (1:1.56 ratio). From Figs. 8.21 and 8.22 it is observed that the transmission coefficients of the former is slightly greater than the latter. The reflection coefficients for both structures lie in the same range.

The results from tests to determine interface losses can be compared with those performed on open block structures for oscillatory flow tests. The length of the structure used for the latter is sixteen times the former with values of 32.0 and 2.0 cm respectively. In the case of Cob armour units a comparison is made between Figs. 6.36 and 6.16. The corresponding figures for Shed armour units are Figs. 6.37 and 6.17 respectively. The general trend in the comparison is the same for both Cob and Shed armour units. As the length of the structure increases from 2.0 to 32.0 cm, transmission coefficients decreases and reflection coefficients increase. The magnitude of the reduction in transmission is greater than the corresponding increase in reflection, thus contributing to greater loss coefficients. Transmission coefficients are more sensitive to length than reflection coefficients, as was also evident from the comparison presented in the previous paragraph for the Cob structure.

In addition to the above tests, this aspect was further investigated by using two open-block rectangular structures consisting of rounded stones and of overall length 45.0 and 55.0 cm respectively (1:1.22 ratio). Fig. 8.23 shows the results from these tests. They indicate a reduction in the transmission coefficient for the longer structure. The reflection coefficients for both cases are in the same range but the scatter is too large to predict a trend in the results.

In this section, and in Section 8.2.3, the influence of length of structure in relation to overall performance has been assessed for both open and closed block structures by considering pairs of structures consisting of the same material but of different length. The length ratio for the pairs of open block structures varied from 1:1.22, 1:1.56 and 1:16.0. The ratio for the closed block structure was 1:5.0. From these tests it is clear that internal wave decay and external transmission are more sensitive than reflection coefficients to variations in the length of the structure.

Fig. 8.24 presents the variation of the transmission coefficient with steepness for three structures of different geometry. The overall performance of the above structures are presented separately in Figs. 6.33, 8.23 and 8.18 respectively. Figure 8.24 illustrates to a certain extent the sensitivity of the transmission coefficients to length of structure and to the introduction of a front

slope.

The highest transmission coefficients are observed for the structure having a length of 45 cm. As the length of the structure is increased to 55 cm, a reduction in transmission is observed. The lowest transmission coefficients are obtained when a front slope is added to the first structure, and the maximum reduction observed for the transmission coefficient is around 0.1. With reference to wave transmission through a structure, these results illustrate the relative influence of extending the length of an existing open block structure or the introduction of a sloping front.

8.7. Evaluation of the theoretical analyses

Theoretical developments pertaining to wave action on porous closed block structures were presented in Chapter 5. Two methods of approach were used for this purpose. An analytical model was developed to predict the reflection coefficient and a numerical model was developed to predict the internal wave decay. The latter simulates the internal non-Darcy flow in a porous structure.

Results from the experiments performed on the porous absorber consisting of Cob armour units and of overall length 160 cm were used to evaluate the theoretical developments.

Some of the important aspects in the application of the analytical model to predict transmission and reflection coefficients for open block structures were presented in Section 6.6. The main difference between open and closed block structures is the presence of the rear vertical impermeable face in the case of the latter. The development and solution technique of the analytical model for both these structures are very similar with the only difference being with regard to the rear boundary condition. Hence the underlying concepts and comments presented in Section 6.6 on reflection and transmission coefficients for open block structures are also applicable for closed block structures. In this respect it is obvious that K_t, eq. 6.16, and K_{tb}, eq. 6.18, are both equal to zero due to the absence of wave transmission on the lee side of closed block structures. In relation to the reflection coefficients for the overall structure it was necessary to use a modification factor as described in Section 6.6 and expressed by eqs. 6.23 and 6.24.

The results of the comparison for reflection coefficients are presented in Fig. 8.25 and it is observed that satisfactory agreement exists for all three periods used for the study. It should be noted that while interface losses contribute

towards a reduction in the reflection coefficient, air entrainment increases the same, with reduced transmission. From oscillatory flow tests it was observed that the degree of air entrainment in rectangular blocks consisting of Cob and Shed armour units was not as high as that observed in Hobo units, particularly for those with a smaller opening. Hence the comparison is not significantly influenced by air entrainment which was not accounted for in the theoretical development.

Results from the application of the numerical model to the same absorber are presented in Figs. 8.26 to 8.29. These plots refer to wave periods of 1.0, 1.5 and 2.0 secs at a mean water depth of 23 cm. Figs. 8.26 and 8.27 refer to wave period 2.0 secs but with different incident wave heights. For wave periods 1.5 and 1.0 secs, comparisons are presented for one value of incident wave height.

In applying the model, interface losses were accommodated by introducing the expression for K_{tf} given by eq. 6.14. It should be noted that the internal transmission coefficient defined by eq. 8.5 can also be expressed as,

$$K_t' = \frac{H_{tf}}{H_o} \cdot \frac{H_x}{H_{tf}} \qquad (8.15)$$

where H_x is the measured wave height within the structure at a distance x from the interface.

H_o is the loop height at the interface.

H_{tf} is the wave height transmitted at the front interface.

and $K_{tf} = \frac{H_{tf}}{H_o}$ is the transmission coefficient at the front interface.

The results from experiments on interface losses were used to estimate the ratio H_{tf}/H_o in eq. 8.15. If this term is not included the predicted transmission coefficients are comparatively higher than those observed in the experiments.

The restriction of the ratio between time and space increments imposed by eq. 5.115 produced solutions satisfying conditions for numerical convergence and stability. The influence of the grid size used in discretizing the x–t plane was investigated by applying the model for the 160 cm long absorber with values of Δx ranging from 16 to 40 cm. The finer grid produced better agreement and the results presented refer to the 16 cm grid size.

The input data for the numerical model is the same as that for the analytical model. However the non-linear resistance term in the equation $I = au + bu^2$ is retained in contrast to the linearized version adopted for the analytical model.

It is noted that the variation of the surface elevation at the front interface is an input boundary condition. In the present study experimental investigations were limited to small amplitude waves and the longest wave period that could be generated was 2.0 secs. However, any time-dependent function describing the movement of the outcrop point can be used as the input boundary condition.

In its present form the numerical model is applicable to porous absorbers with vertical faces at the front and at the rear with the latter being impervious. In relation to sloping structures it is necessary to adopt an equivalent rectangular form to account for the sloping front face. It is evident that this model is applicable for structures which do not permit external transmission, and in reality corresponds to those having an impermeable core. Usually the core is built at a slope for construction purpose but its inclination will influence the final result only marginally because most of the energy is dissipated by the time the wave reaches the central core.

A closer look at the internal transmission coefficients indicates that its values increase in the region of the rear impervious wall due to the effects of the standing wave. The water level fluctuation obtained by the assumption of a vertical core will represent a marginal overestimation than that determined by an inclined core.

Apart from the verification of the numerical model by comparison with experimental data, it was necessary to investigate certain features of the same in relation to its applicability for different porous structures and varying conditions. For this purpose three approaches were adopted.

In the first approach the model was applied to investigate flow through five rectangular absorbers each of length 150 cm, consisting of Cob and Shed armour units and cylindrical lattice structures of 15, 20 and 30 mm diameter. In each case it was assumed that the structure was located in a water depth of 38 cm and subjected to waves of period 2.0 secs and an incident wave amplitude of 18 cm at the front interface. The laminar and turbulent flow coefficients obtained from steady flow tests were used for the study. The results from this exercise are

presented in Table 8.1 and represent the variation of internal transmission coefficient given by eq. 8.5 versus distance along the length of the structure. Modifications for interface losses have not been included for any of the media.

This table clearly illustrates that as the turbulent flow coefficient increases, the wave amplitude decreases more rapidly as the wave propagates within the structure. This observation is consistent with the physics of flow through porous media. In this context it should be noted that under steady flow conditions the hydraulic gradient was expressed by the Forchheimer relationship (i.e. $I = au + bu^2$) from which it was deduced that for $I_{turbulent} \gtrless I_{laminar}$ the macroscopic velocity, u, should satisfy $u \gtrless a/b$ respectively. For the incident wave system adopted in this study, the horizontal orbital velocity at the free surface corresponding to wave heights at the front and rear interfaces are approximately equal to 1.00 and 0.35 m/sec respectively. The values of the critical velocity $u_c = a/b$ for different media are also given in Table 8.1 and it is seen that the minimum orbital velocity exceeds the critical value for three of the structures. This gives an indication of the degree of turbulence associated with the respective structures and the importance of the turbulent term in relation to energy dissipation.

If interface losses were included in the analysis it would have increased the damping characteristics of the media particularly for the absorbers consisting of Shed and Cob armour units.

The second approach was to examine the sensitivity of the flow coefficients by analysing the response of the solution to an increment (± 25%) in both laminar and turbulent flow coefficients. This study was limited to the absorber consisting of Shed armour units used in the first approach. The results from this exercise are presented in Table 8.2 and indicate the percentage variation in the wave height along the length of the structure due to positive and negative increments in a and b. The results illustrate that the turbulent flow coefficient (b) has a greater influence on the damping characteristics of the wave absorber.

The third approach was to study the sensitivity in relation to variation with wave period. This study was also limited to the absorber consisting of Shed armour units but under a different wave environment to that of the previous two cases. The structure was of length 150 cm but was in a still water depth of 20 cm and subjected to waves having an amplitude of 5.0 cm at the front interface. These conditions were consistent with those adopted for the experimental investigation of the present study. Five wave periods 1.0, 2.0, 3.0, 4.0 and 5.0 secs were used for the study.

The results from this exercise are presented in Table 8.3 and represent the variation of the internal transmission coefficient defined by eq. 8.5 along the length of the structure. Effects due to interface losses have not been included in the analyses. The results illustrate that waves having a higher period are more effectively transmitted through the structure in comparison with those having a lower period.

Investigations of interface losses indicated that losses corresponding to waves of lower steepness were less than those corresponding to higher steepness. Thus, if interface losses were accounted for, the difference between the internal transmission coefficients for two different wave periods at a given location of the structure will be greater than those obtained by using the values given in Table 8.3.

Another aspect which was investigated in this study was the concept of equivalent rectangular sections used to simulate trapezoidal structures. The experimental investigations were limited to three structures consisting of Cob armour units and the results were presented in Section 8.5.

The analytical model was used to predict the reflection, transmission and energy loss coefficients for the trapezoidal structure and the two equivalent rectangular structures, Fig. 8.30. The application of the model to the latter two was very similar to that presented earlier in Section 6.6 relating to oscillatory flow tests. The results are presented in Figs. 8.31 and 8.32 and they indicate satisfactory agreement between experimental and predicted values.

For the analysis of the trapezoidal structure, it was possible either to adopt an equivalent rectangular structure based on equal submerged volume or one having equal length at the mean water level, Fig. 8.30. Of these two structures the first is longer by $d.\cot\alpha$ where d is the still water depth and α is the slope angle.

It should be noted that reflection coefficients corresponding to sloping structures are very much smaller in magnitude than those corresponding to vertical structures. This aspect was discussed in Section 8.4 in relation to the experimental investigations performed as part of this study. It was observed that sloping structures displayed better energy dissipation characteristics.

A trapezoidal structure has an inclined interface and the resulting losses at that surface will be different from that of a vertical interface which was investigated as a part of this study. Transmission coefficients of a sloping interface will be lower mainly due to the reduction, on the vertical plane, of the

projected area of the voids matrix. For example, in the case of an interface consisting of Cob armour units placed at an angle of 45 degrees the projected area of the square opening is reduced by a factor of 0.71 in comparison with a vertical interface of the same units. Although the reduction in the transmission coefficients will be small, there is a greater likelihood that the reflection coefficients corresponding to a sloping interface being very much smaller than those corresponding to a vertical interface.

This aspect was illustrated to a certain extent in the experimental investigation of the trapezoidal porous structure and its equivalent rectangular structures. The lowest transmission coefficients were observed for the trapezoidal structure. In the case of the second equivalent rectangular structure which was based on the concept of both structures having equal length at still water depth, the observed transmission coefficients were approximately 0.15 more than the trapezoidal structure.

Although significant wave action takes place in the vicinity of the mean water level, the reduced transmission coefficients for the trapezoidal structure is mainly due to the presence of the sloping interface which increases interface losses. The relative magnitude of these losses can be assessed by comparing the experimental values of transmission coefficients.

It was also observed that the first equivalent structure which was longer at still water depth exhibits transmission coefficients approximately 0.10 greater than that for the trapezoidal structure. This indicates that the increase in the interface losses had a greater influence in reducing transmission coefficients than that of increased length, which in this case was $d.\cot\alpha$ where d is the still water depth and α the slope angle. These observations justify the arguments presented on the importance of interface losses in relation to performance of porous structures.

From the preceding discussion on experimental observations, it was concluded that from a viewpoint of transmission coefficients it would be appropriate to use an equivalent rectangular structure based on submerged volume. The increase in length of the structure at the still water depth will account for increased losses at the interface of the sloping structure. However, it should be noted as the wave period increases the relative influence of interface losses decreases and as a consequence the rectangular structure based on submerged volume may overestimate the overall internal resistance, thereby underestimating transmission characteristics.

When the analytical model was used to predict the transmission coefficients of the trapezoidal structure, it was found that for wave periods of 1.0 and 1.5 seconds, satisfactory agreement was obtained when the sloping surface was transformed to an equivalent rectangular section based on equal submerged volume. The interface losses corresponding to a vertical face and expressed by eq. 6.14 were incorporated in the model. However for the wave period of 2.0 secs satisfactory agreement was obtained when the transformation of the sloping surface was based on equal length at still water depth. In effect the first equivalent rectangular structure (length 525.0 cm) overestimated the overall internal resistance.

Reflection coefficients for the equivalent rectangular structures predicted by the model were greater than those observed experimentally for the trapezoidal structure. This is mainly due to the relatively high reflection coefficients exhibited by a vertical face in contrast to those of the sloping surface, although in this case the slope was comparatively steep, 45 deg. Analysis of the results indicate that theoretically predicted values have to be multiplied by a factor of 0.7 for satisfactory agreement. This factor is similar to that used in Section 6.6 in the analyses of porous rectangular open block structures. In that case the modification factor only accounted for interface losses from a vertical face. However in this situation the modification factor not only accounts for similar losses from a sloping interface but also accounts for the reduction in the reflection coefficient due to the sloping boundary of the structure.

The results from the comparison for the trapezoidal structure are presented in Fig. 8.33 and it is noticed that satisfactory agreement is observed for both transmission and reflection coefficients.

	Porous blocks consisting of hollow block armour		Cylindrical lattice structures		
	Cob	Shed	D =15mm	D =20mm	D =30mm
In $I = au + bu^2$					
a (sec/m)	0.917	0.703	0.612	0.682	0.642
b $(sec/m)^2$	6.407	5.802	3.051	1.338	0.751
$u^* = a/b$ (m/sec)	0.143	0.121	0.200	0.510	0.855
n (porosity)	0.627	0.614	0.607	0.607	0.607
Distance along the length of structure (cm)	Internal transmission coefficients				
0.0	1.000	1.000	1.000	1.000	1.000
15.0	0.780	0.798	0.850	0.861	0.875
30.0	0.665	0.665	0.745	0.757	0.779
45.0	0.509	0.543	0.641	0.656	0.690
60.0	0.421	0.458	0.564	0.581	0.625
75.0	0.344	0.382	0.475	0.508	0.559
90.0	0.298	0.339	0.452	0.458	0.509
105.0	0.271	0.321	0.470	0.472	0.540
120.0	0.279	0.340	0.521	0.522	0.595
135.0	0.287	0.353	0.543	0.548	0.632
150.0	0.292	0.359	0.548	0.555	0.647

Incident wave amplitude A_0 = 18 cm
Wave period = 2 sec
Still water depth = 38 cm

TABLE.8.1 NUMERICAL SOLUTION FOR THE INTERNAL TRANSMISSION COEFFICIENTS FOR DIFFERENT POROUS MEDIA

Rectangular porous absorber consisting of Shed armour units

Distance along the length of structure (cm)	1 a = 0.7034 b = 5.8022 Values obtained from steady flow tests	2 a = 0.7034 b = 7.2528 increase of b by 25%	3 a = 0.8793 b = 5.8022 increase of a by 25%	4 a = 0.7034 b = 4.3517 decrease of b by 25%	5 a = 0.5276 b = 5.8022 decrease of a by 25%
	Wave amplitude	- Wave amplitude (cm) and - Percentage reduction in wave amplitude with respect to values given in column 1 Percentage reduction in wave height = $(A - A_1)/A_1$ % A is the wave amplitude A_1 is the corresponding wave amplitude in column 1			
0.0	18.00	18.00	18.00	18.00	18.00
15.0	14.40	14.14 -1.81%	14.26 -0.96%	14.69 +2.03%	14.54 +0.96%
30.0	12.01	11.64 -3.03%	11.79 -1.83%	12.41 +3.39%	12.23 +1.84%
45.0	9.82	9.40 -4.29%	9.54 -2.87%	10.31 +4.98%	10.11 +2.91%
60.0	8.28	7.85 -5.16%	7.96 -3.82%	8.79 +6.19%	8.60 +3.9%
75.0	6.91	6.50 -6.00%	6.57 -4.96%	7.42 +7.32%	7.27 +5.19%
90.0	6.12	5.72 -6.49%	5.72 -6.47%	6.61 -7.96%	6.55 +7.00%
105.0	5.78	5.37 -7.24%	5.26 -9.01%	6.32 +9.22%	6.39 +10.48%
120.0	6.14	5.65 -8.08%	5.50 -10.47%	6.78 +10.45%	6.89 +12.11%
135.0	6.39	5.86 -8.20%	5.68 -11.08%	7.07 +10.60%	7.20 +12.63%
150.0	6.51	6.00 -8.13%	5.79 -11.07%	7.19 +10.44%	7.32 +12.57%

Incident wave amplitude A_0 = 18 cm

Wave period = 2 sec

Still water depth = 38 cm

TABLE.8.2 RESPONSE OF THE NUMERICAL SOLUTION TO VARIATIONS IN LAMINAR AND TURBULENT FLOW COEFFICIENTS

Rectangular porous absorber consisting of Shed armour units

Distance along the length of structure (cm)	- Internal transmission coefficients and - Percentage reduction in wave amplitude with respect to the incident wave amplitude (A_0). i.e. $100(A_0 - A_x)/A_0$ for varying periods.				
	T = 1.0 sec	T = 2.0 sec	T = 3.0 sec	T = 4.0 sec	T = 5.0 sec
0.0	1.0	1.0	1.0	1.0	1.0
15.0	0.633 36.72%	0.758 24.16%	0.802 19.78%	0.830 17.00%	0.848 15.16%
30.0	0.483 51.72%	0.618 38.20%	0.672 32.76%	0.710 28.98%	0.737 26.32%
45.0	0.337 66.34%	0.484 51.64%	0.550 44.98%	0.597 40.30%	0.632 36.76%
60.0	0.264 73.60%	0.399 60.08%	0.466 53.40%	0.517 48.28%	0.561 43.94%
75.0	0.195 80.54%	0.319 68.06%	0.389 61.14%	0.448 55.22%	0.503 49.66%
90.0	0.157 84.26%	0.270 73.04%	0.346 65.40%	0.419 58.12%	0.484 51.62%
105.0	0.121 87.86%	0.230 77.04%	0.322 67.76%	0.404 59.56%	0.474 52.62%
120.0	0.113 88.68%	0.236 76.40%	0.335 66.46%	0.416 58.36%	0.485 51.52%
135.0	0.117 88.26%	0.247 75.26%	0.343 65.74%	0.422 57.82%	0.489 51.12%
150.0	0.126 87.40%	0.256 74.42%	0.349 65.10%	0.427 57.30%	0.493 50.68%

Incident wave amplitude A_0 = 5 cm

Still water depth = 20 cm

TABLE.8.3 SENSITIVITY OF THE NUMERICAL SOLUTION TO VARIATIONS IN WAVE PERIOD

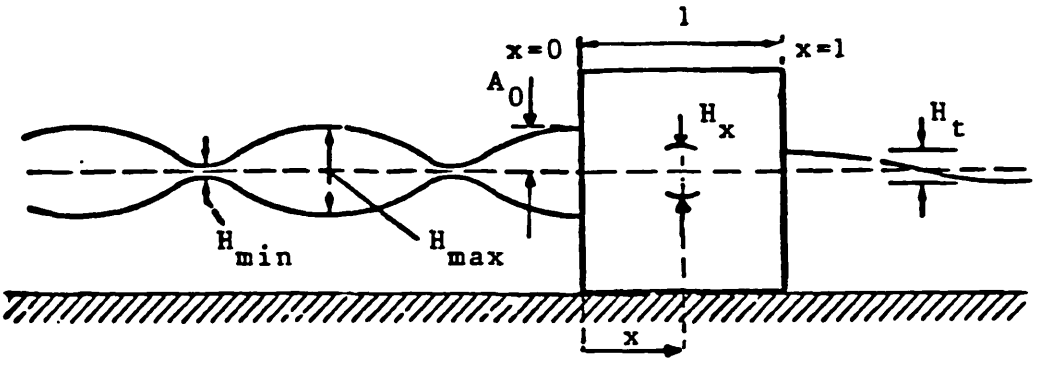


Fig.8.1.a Open block structure

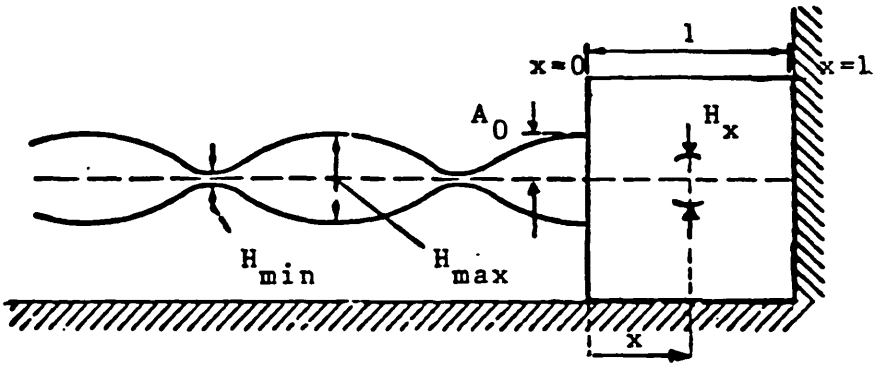


Fig.8.1.b Closed block structure

Reflection coefficients

for both open and closed block structures

$H_i = \frac{H_{max} + H_{min}}{2}$ and $H_r = \frac{H_{max} - H_{min}}{2}$

$K_r = H_r / H_i$

Internal transmission coefficients

for both open and closed block structures

$K'_t = H_x / H_0$ at a distance x from the front interface

H_x is the measured wave height within the structure at a distance x from the interface

H_o is the loop height at the front interface $(=2*A_o)$

External transmission coefficients

for open block structure

$K_t = H_t / H_i$

H_t is the transmitted wave height at the lee of the structure

H_i is the incident wave height

FIG.8.1 OPEN AND CLOSED BLOCK STRUCTURES

FIG.8.2 WAVE DECAY IN A POROUS ABSORBER

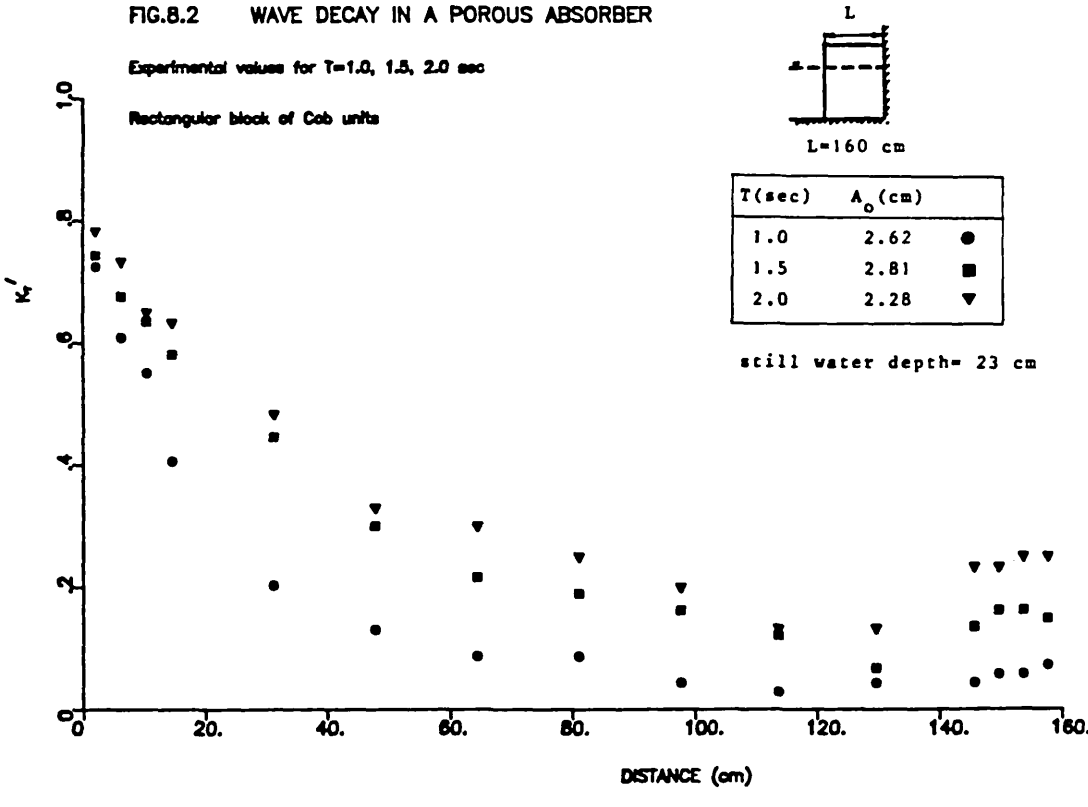


FIG.8.3 WAVE DECAY IN A POROUS ABSORBER

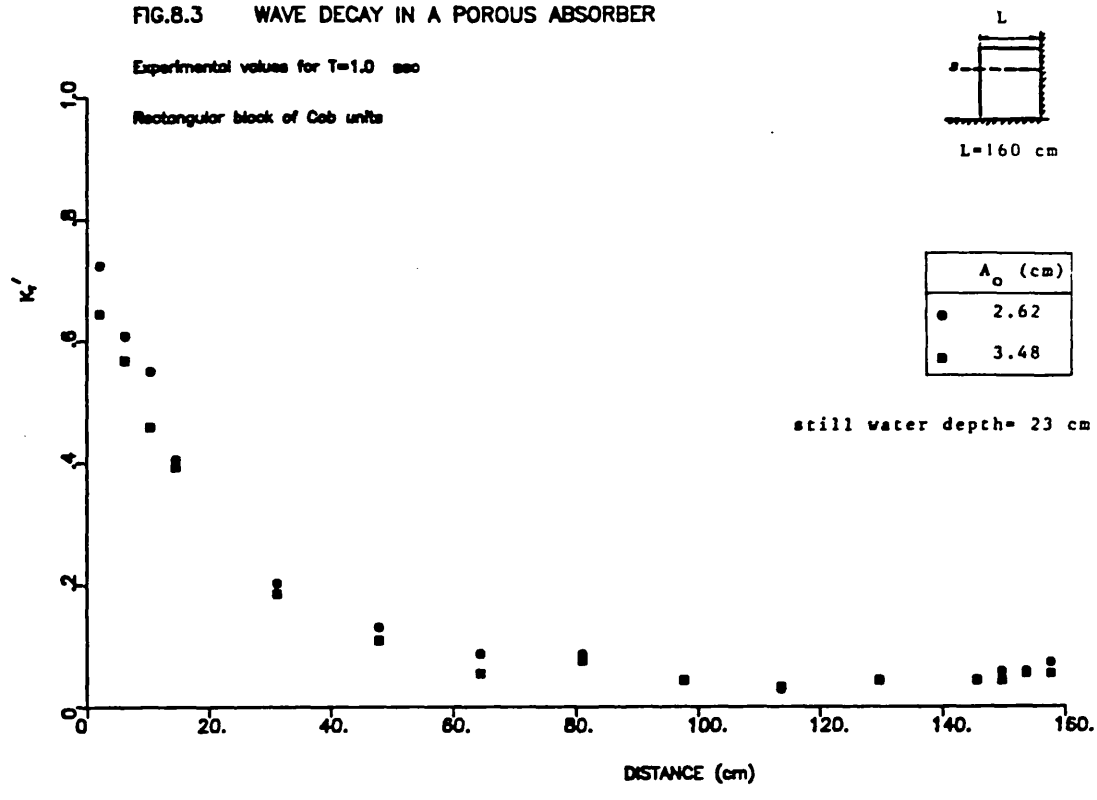


FIG.8.4 WAVE DECAY IN A POROUS ABSORBER

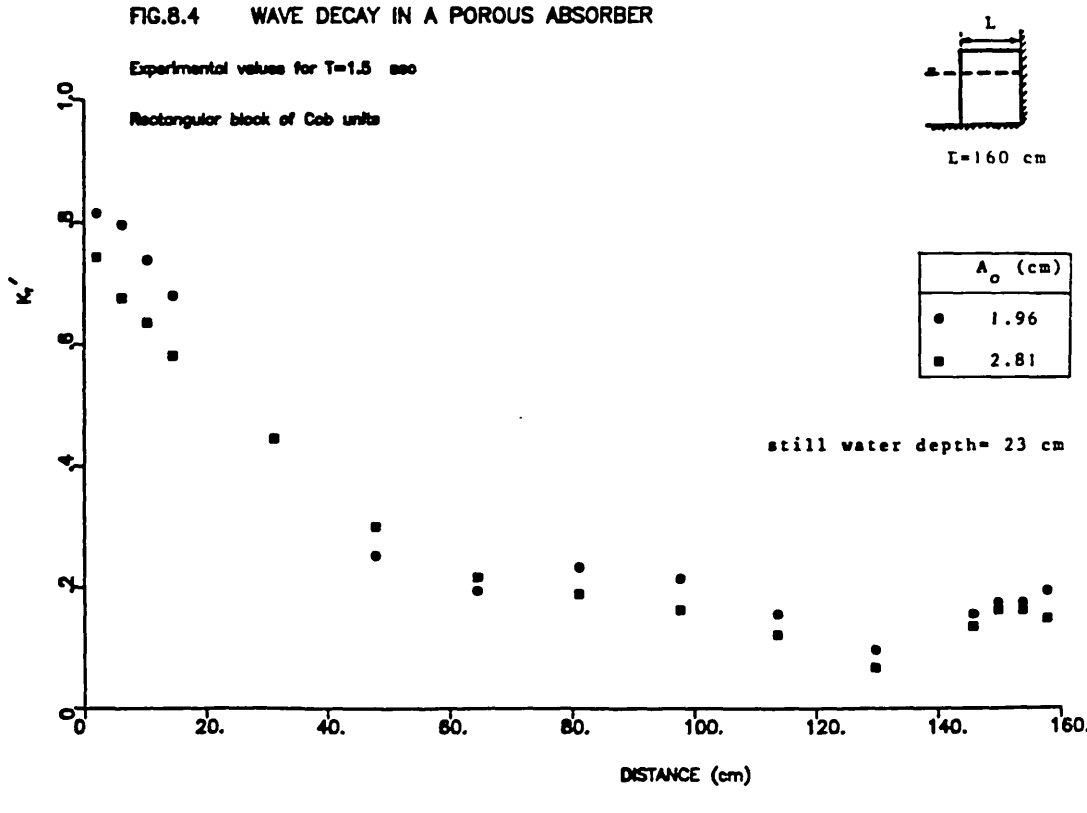


FIG.8.5 WAVE DECAY IN A POROUS ABSORBER

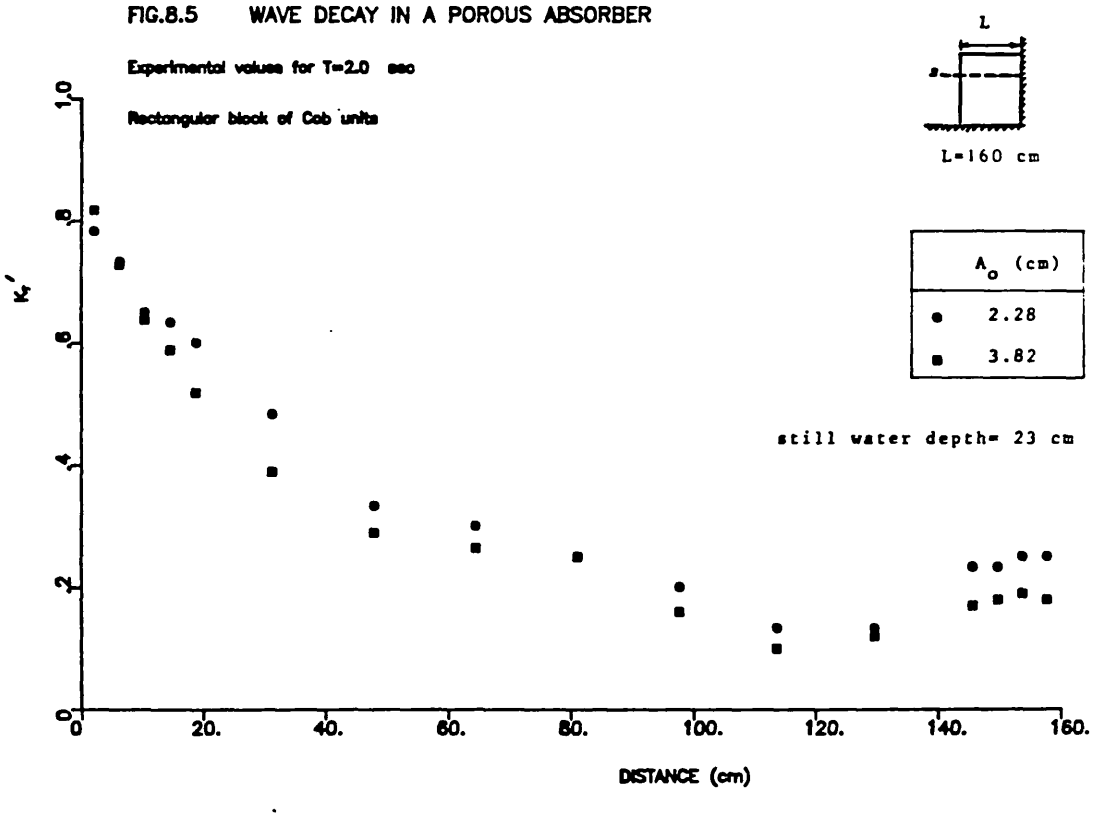


FIG.8.6.A REFLECTION COEFFICIENT (KR) vs STEEPNESS

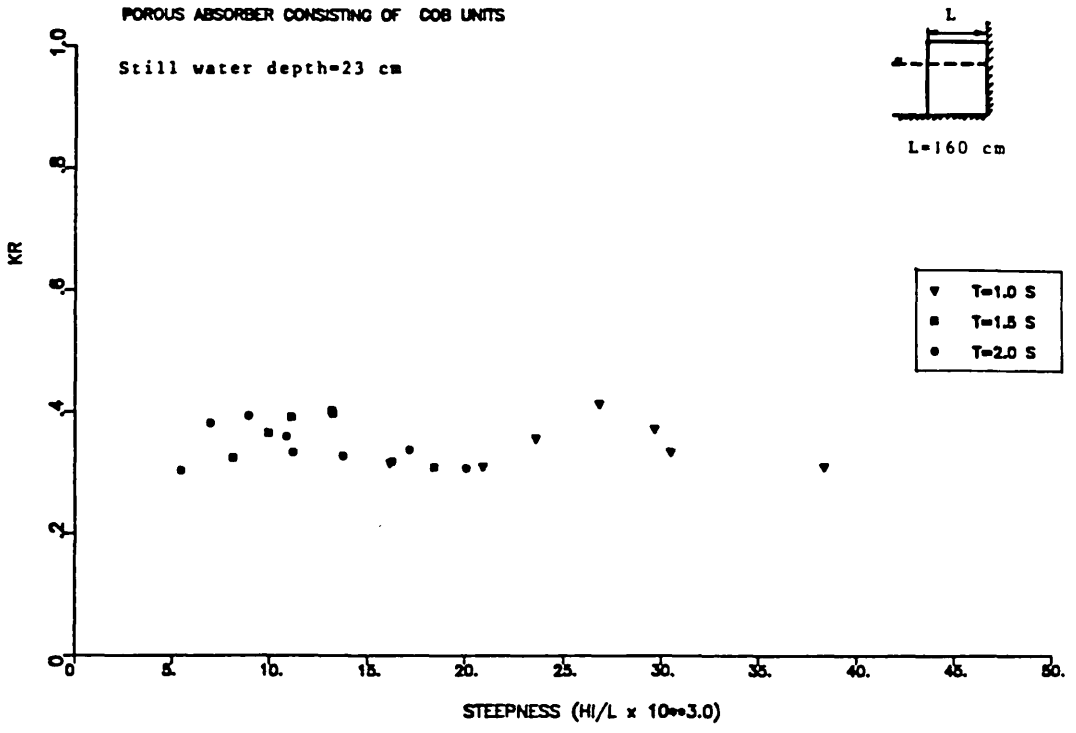


FIG.8.6.B KR vs WAVE HEIGHT/DEPTH (HI/D) RATIO

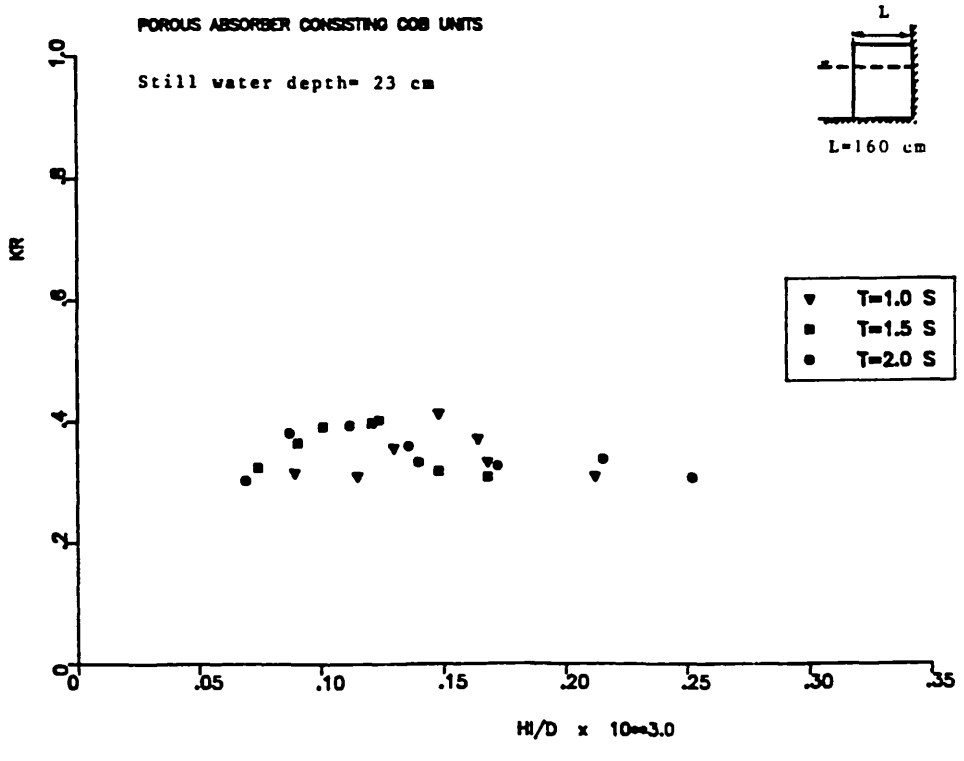


FIG.8.7 WAVE DECAY IN AN OPEN BLOCK STRUCTURE

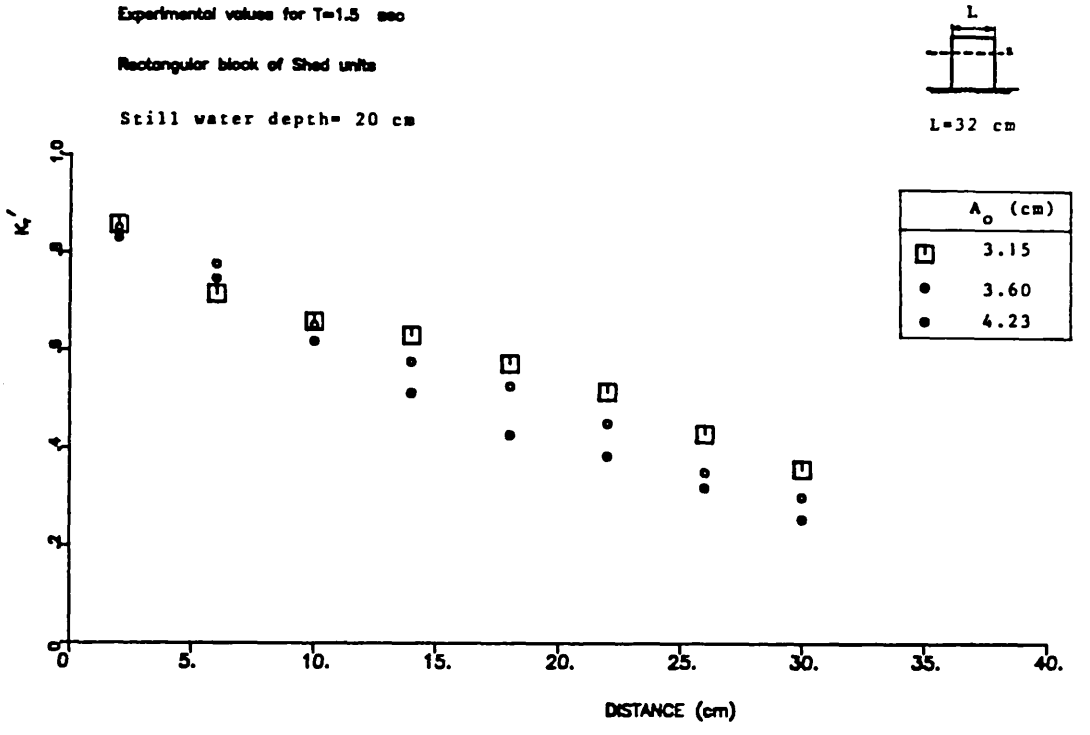


FIG.8.8 WAVE DECAY IN AN ABSORBER (CLOSED BLOCK STRUCTURE)

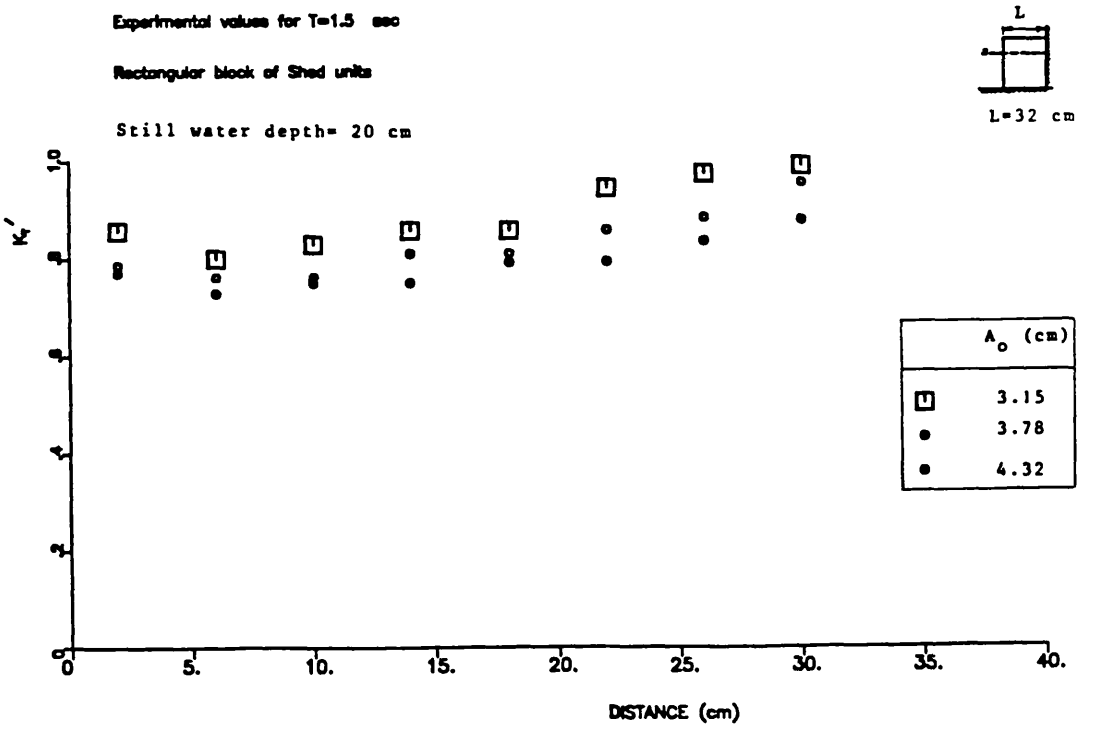


FIG.8.9 WAVE DECAY IN AN OPEN BLOCK STRUCTURE

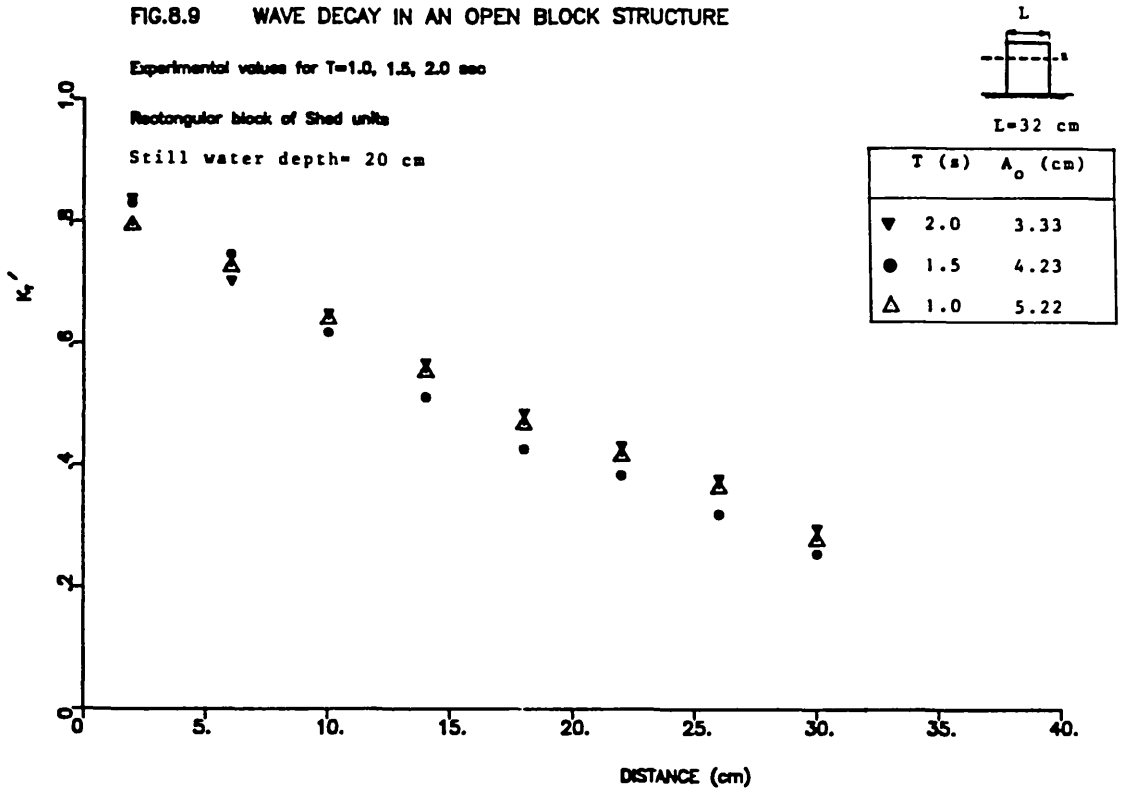


FIG.8.10 WAVE DECAY IN A ABSORBER (CLOSED BLOCK STRUCTURE)

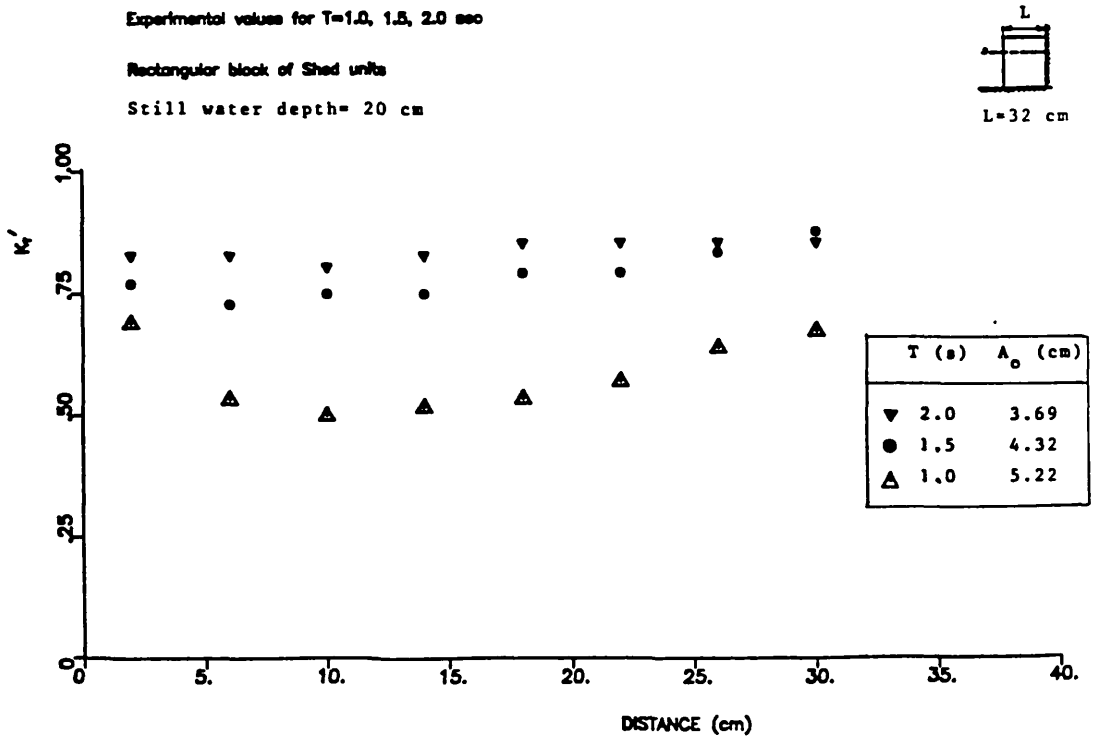
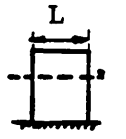


FIG.8.11 KT,KR vs STEEPNESS

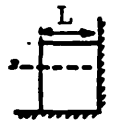
COMPARISON OF PERFORMANCE OF A RECTANGULAR BLOCK OF SHED UNITS WITH AND WITHOUT AN IMPERMEABLE FACE AT THE BACK

wave period	open block		closed block
	KT	KR	KR
T=1.0 S	*	●	O
T=1.5 S	●	■	□
T=2.0 S	★	▲	△

Still water depth= 20 cm



open block



closed block

L=32 cm

FIG.8.12.A KD vs STEEPNESS

COMPARISON OF PERFORMANCE OF A RECTANGULAR BLOCK OF SHED UNITS WITH AND WITHOUT AN IMPERMEABLE FACE AT THE BACK

Still water depth= 20 cm

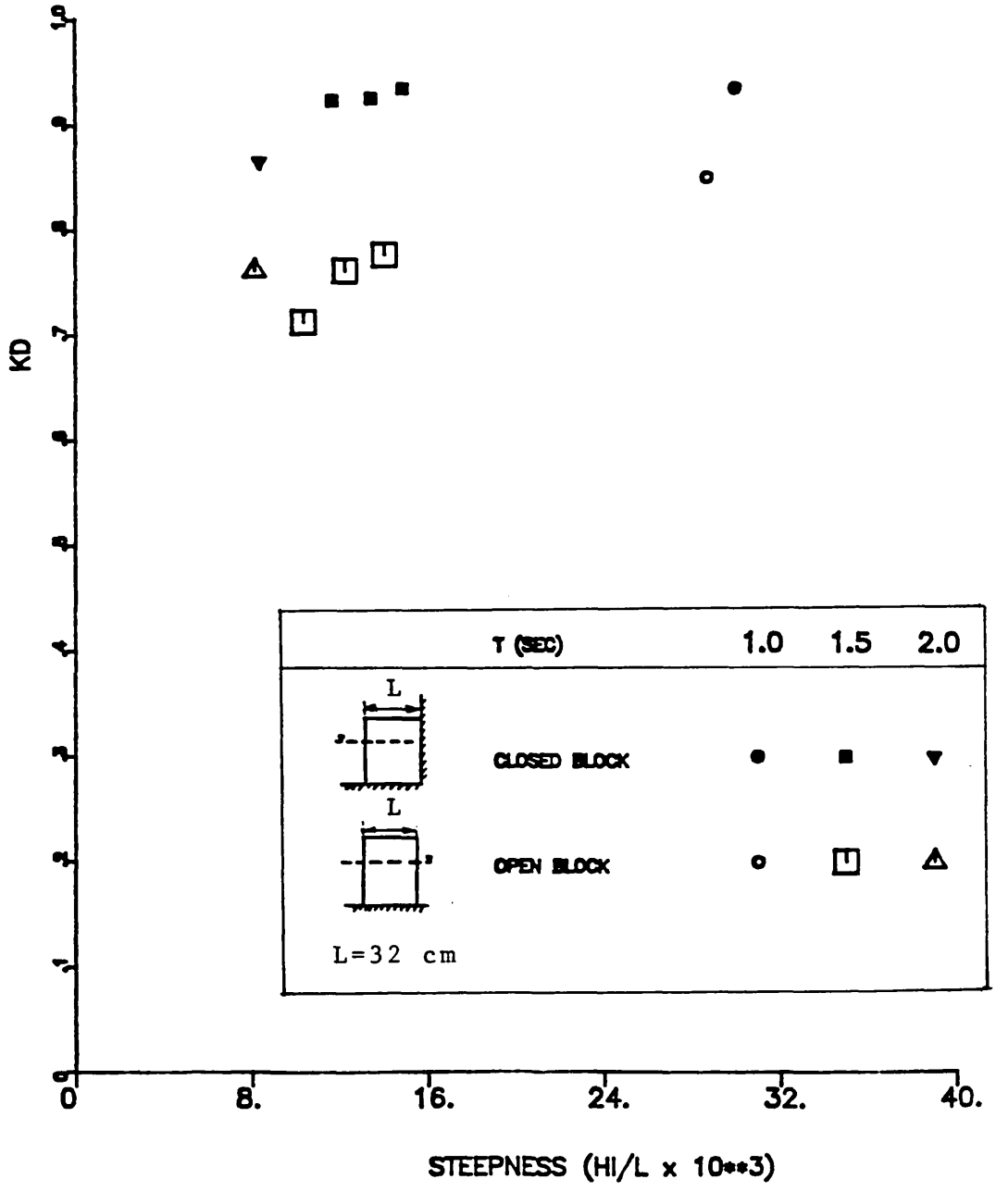
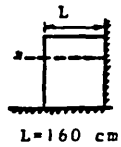


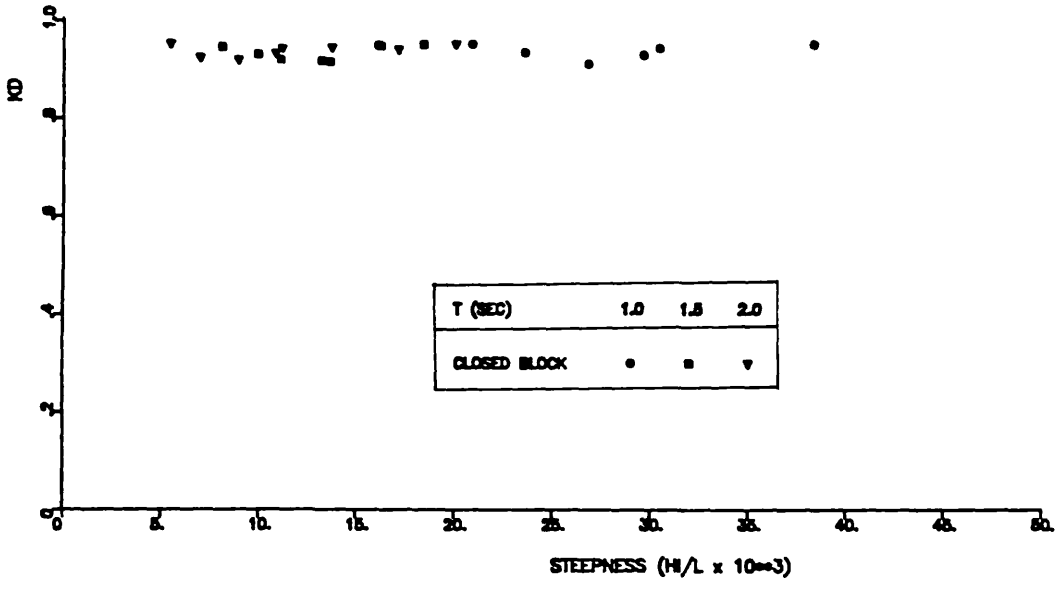
FIG.8.12.B KD vs STEEPNESS

PERFORMANCE OF A RECTANGULAR ABSORBER

CONSISTING OF COB UNITS

Still water depth= 23 cm





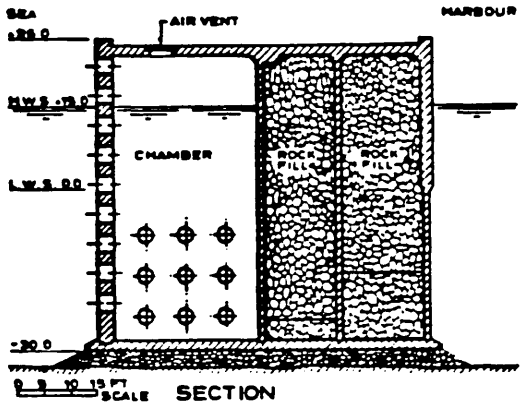


Fig.8.13.a Baie Comeau Breakwater
(Agerschou,et.al 1984)

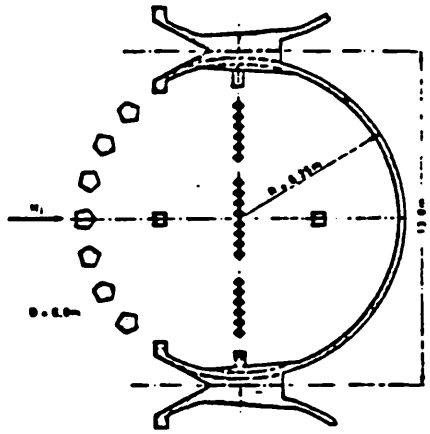


Fig.8.13.b Slotted breakwater with internal permeable wall
(Gravesen 1979)

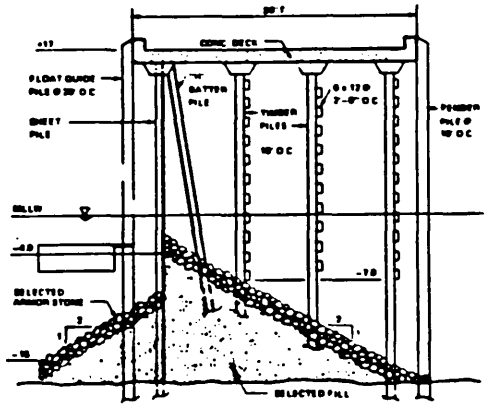


Fig.8.13.c Wave absorbing pier
(Weckmann,Bigham and Dixon 1983)

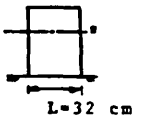
FIG.8.13 DIFFERENT TYPES OF WAVE ABSORBERS

FIG.8.14 KT,KR AND KD vs STEEPNESS

RECTANGULAR BLOCK OF COB UNITS T=1.0, 1.5 sec

HEIGHT OF STRUCTURE/WATER DEPTH =1.456 (NON SUBMERGED)

Still water depth= 20 cm



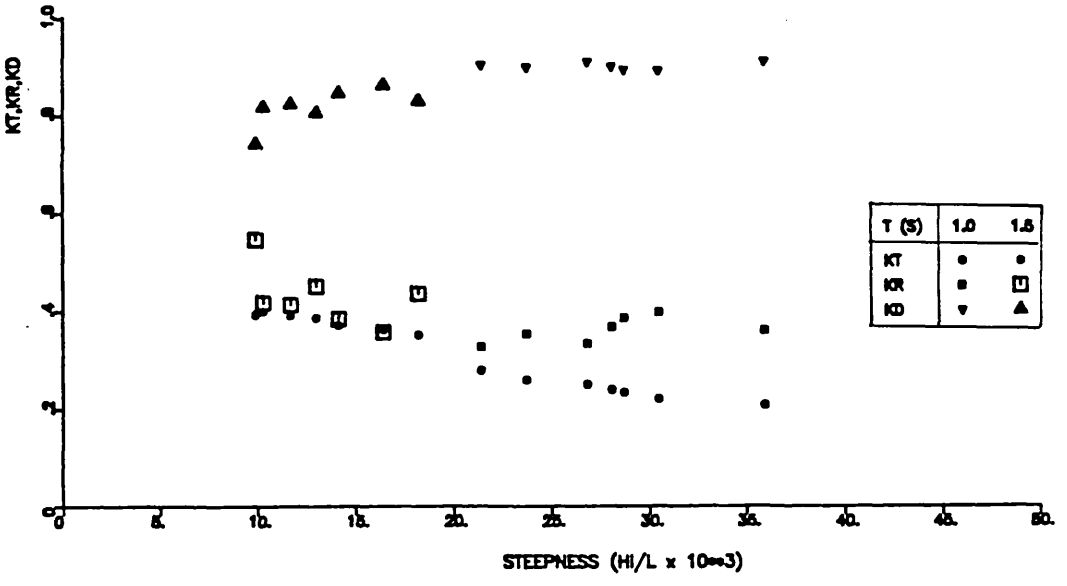
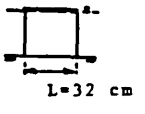


FIG.8.15 KT,KR AND KD vs STEEPNESS

RECTANGULAR BLOCK OF COB UNITS T=1.0, 1.5 sec

HEIGHT OF STRUCTURE/WATER DEPTH =1.040 (JUST SUBMERGED)

Still water depth= 20 cm



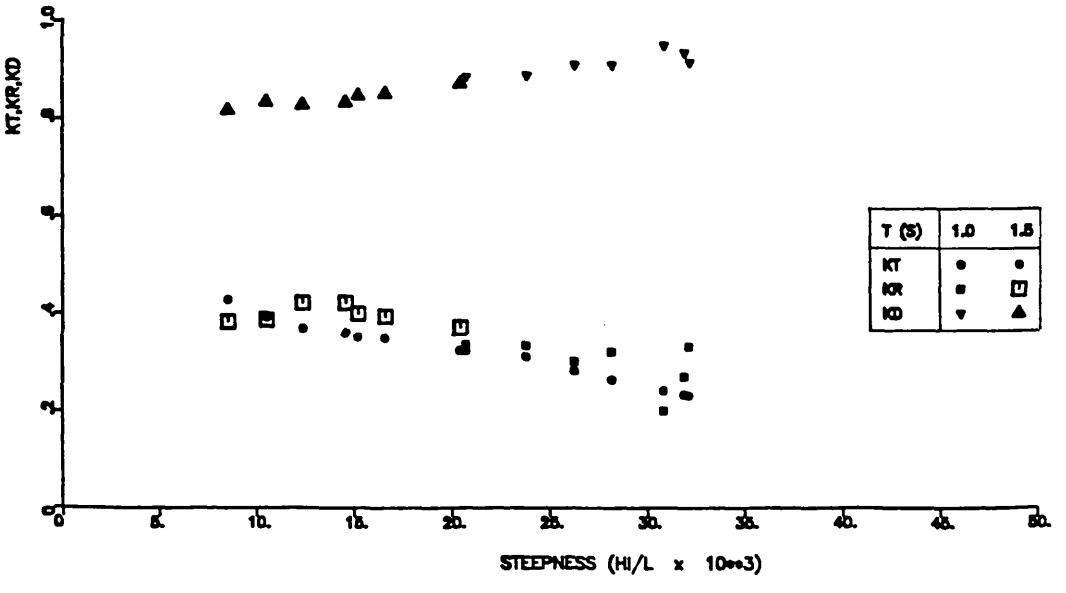


FIG.8.16 KT,KR AND KD vs STEEPNESS

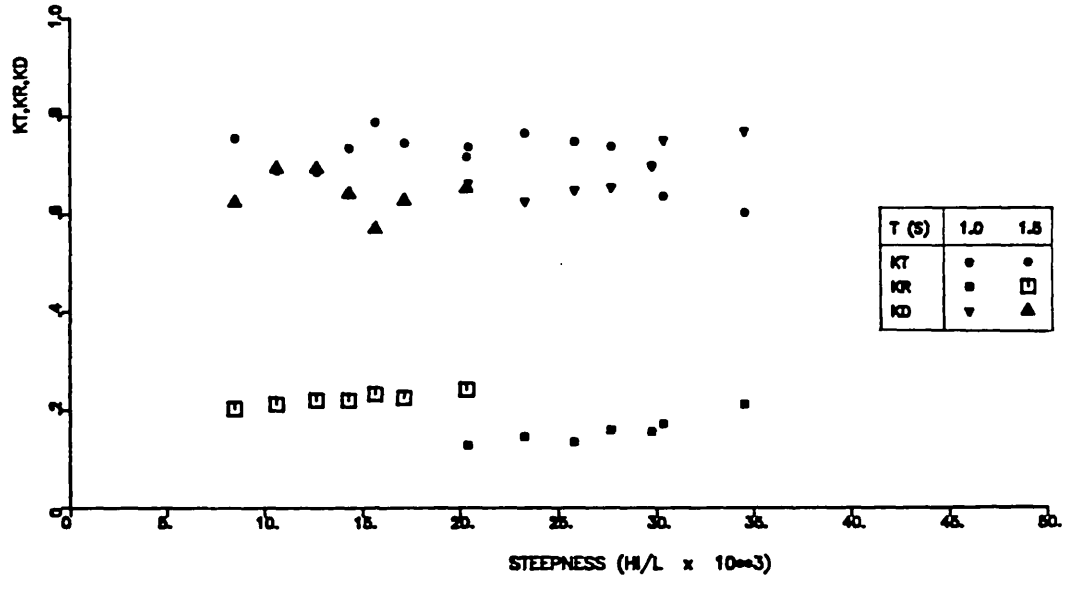
RECTANGULAR BLOCK OF COB UNITS T=1.0, 1.5 sec

HEIGHT OF STRUCTURE/WATER DEPTH =0.832 (FULLY SUBMERGED)

Still water depth= 20 cm



L=32 cm



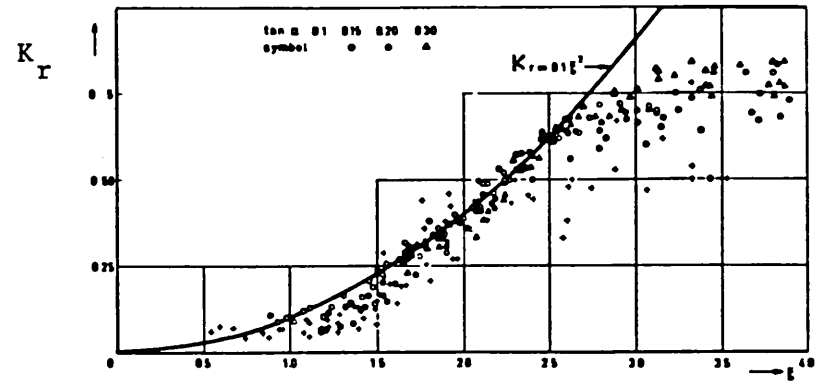


Fig.8.17.a Reflection coefficient vs surf similarity parameter
(Battjes 1974)

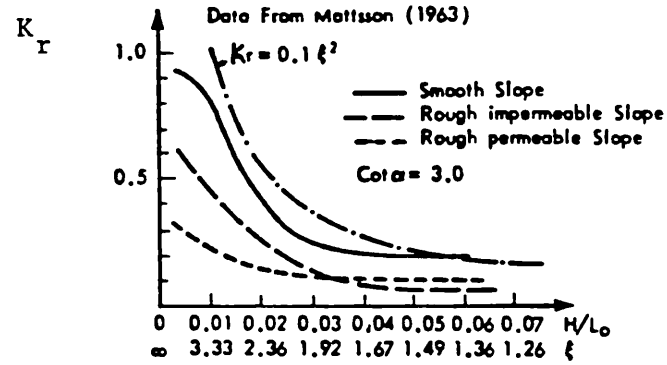


Fig.8.17.b Effect of roughness and permeability on reflection coefficient
(Gunbak 1979 based on data from Mattsson 1963)

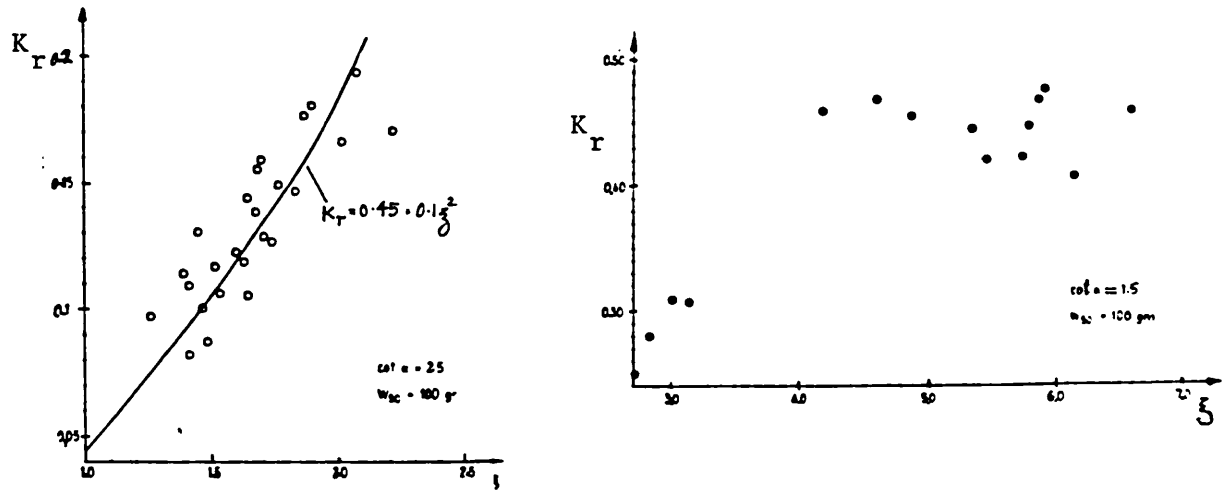


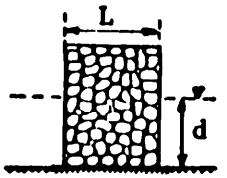
Fig.8.17.c and 8.17.d Wave reflection from a rubble mound breakwater
(Gunbak 1979)

FIG.8.17 RESULTS FROM SELECTED INVESTIGATIONS ON WAVE REFLECTION FROM SLOPING SURFACES

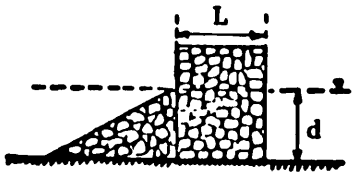
FIG.8.18 KT,KR AND KD vs STEEPNESS

INFLUENCE OF A SLOPING FRONT FACE AT T=1.5 SEC

FOR STRUCTURES CONSISTING OF ROUNDED STONES



structure A



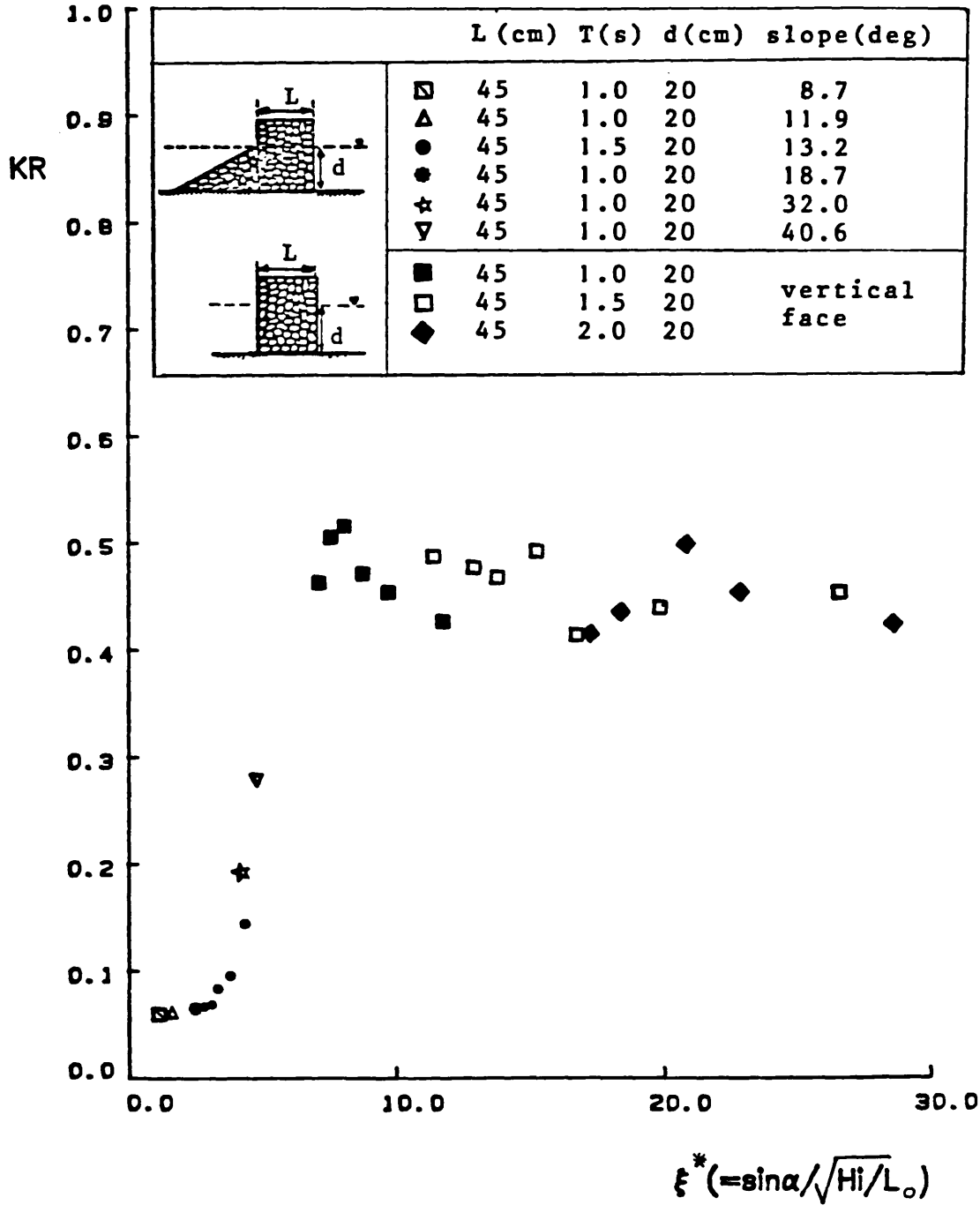
structure B

slope=13.2 deg
L=45 cm
d=20 cm

	structure	
	A	B
T (S)	1.5	1.5
KT	●	○
KR	■	□
KD	▼	△

FIG.8.19 KR vs $\xi^*(=\sin\alpha/\sqrt{Hi/L_o})$

FOR SLOPING AND VERTICAL FACED STRUCTURES CONSISTING OF ROUNDED STONES



	L (cm)	T(s)	d(cm)	slope(deg)
▨	45	1.0	20	8.7
△	45	1.0	20	11.9
●	45	1.5	20	13.2
●	45	1.0	20	18.7
☆	45	1.0	20	32.0
▽	45	1.0	20	40.6
■	45	1.0	20	vertical face
□	45	1.5	20	
◆	45	2.0	20	

FIG.8.20 K_T, K_R AND K_D VS STEEPNESS

Porous trapezoidal structure
consisting of Cob armour units

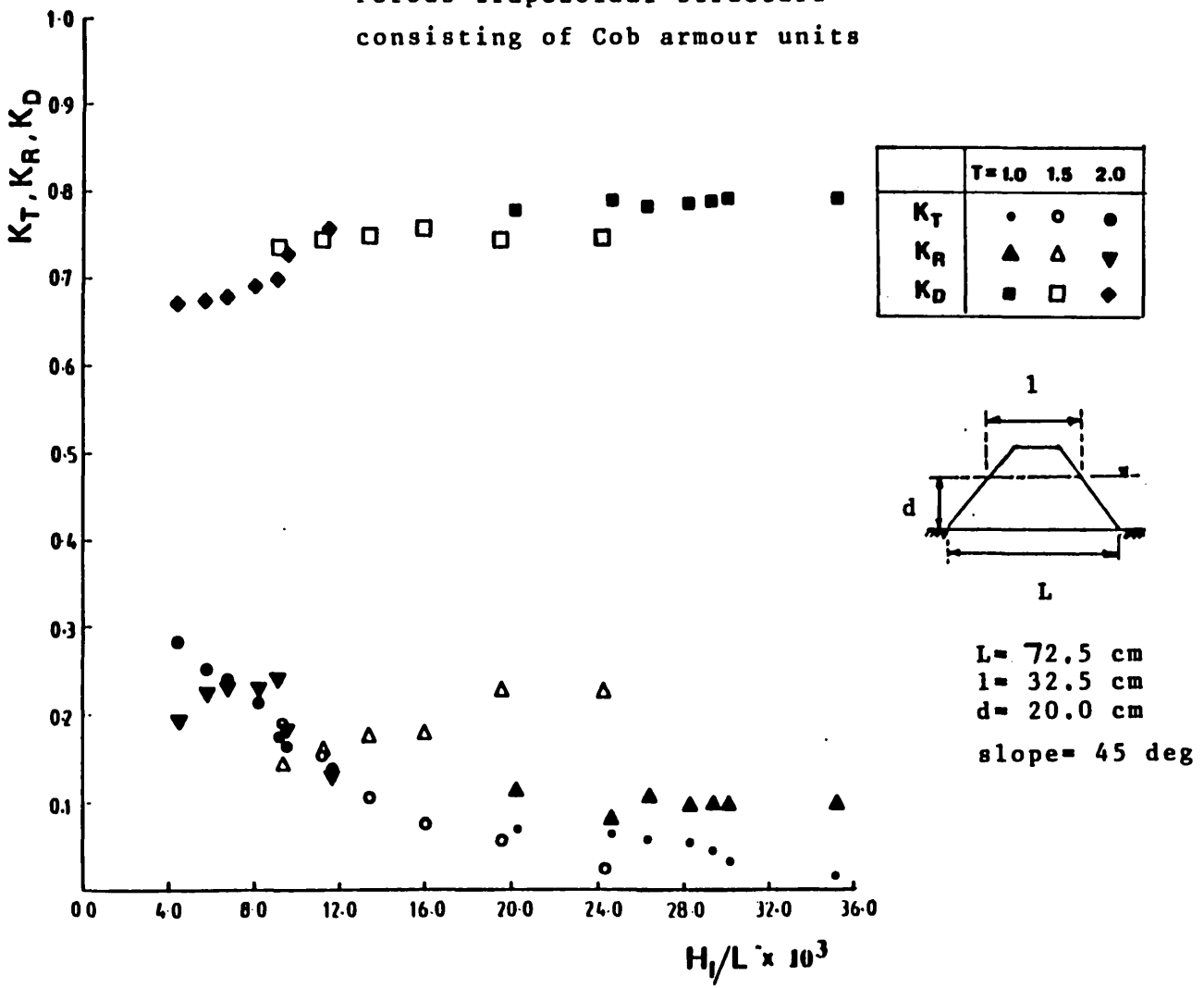


FIG.8.21 K_T, K_R AND K_D VS STEEPNESS

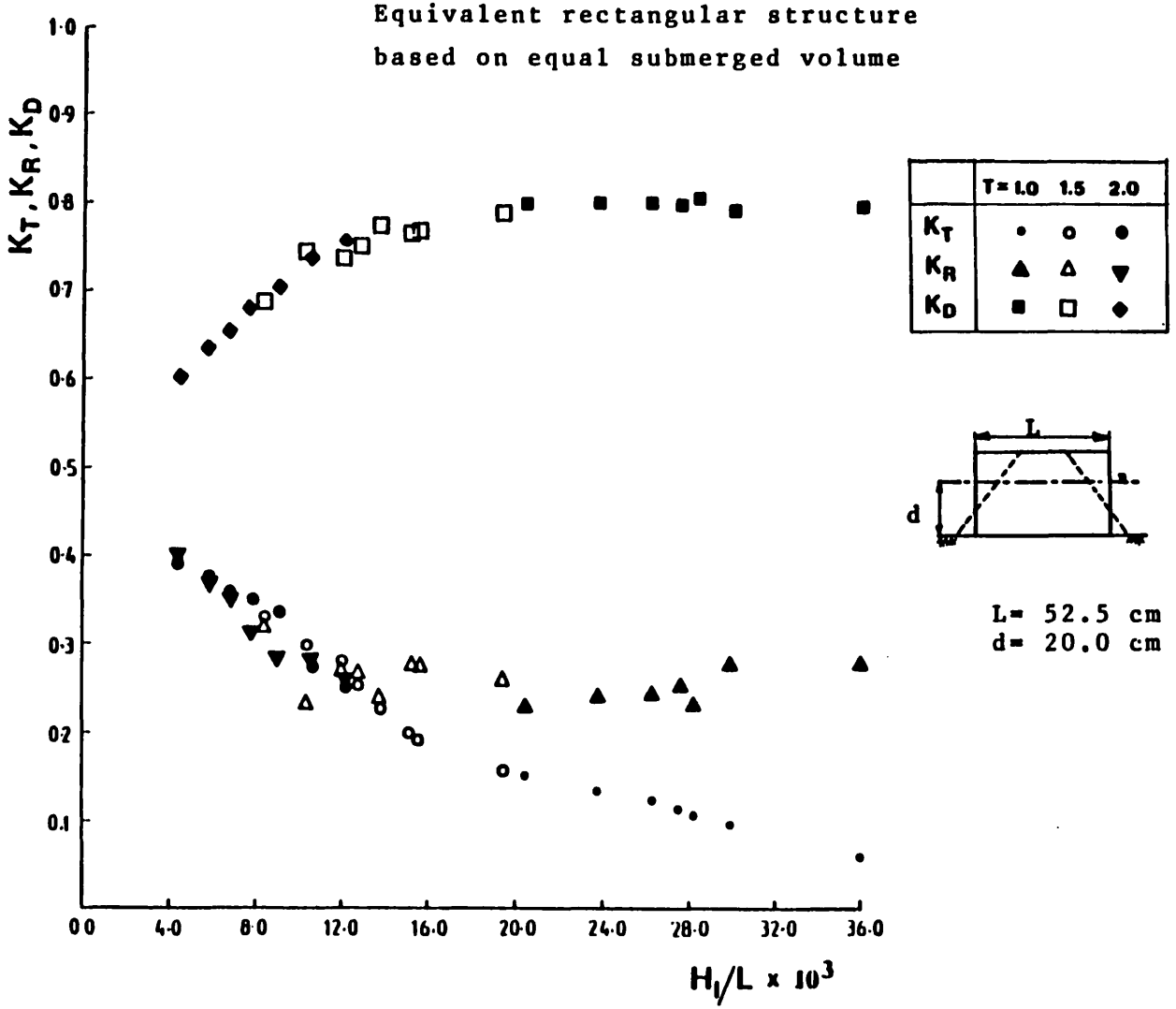


FIG.8.22 K_T, K_R AND K_D VS STEEPNESS

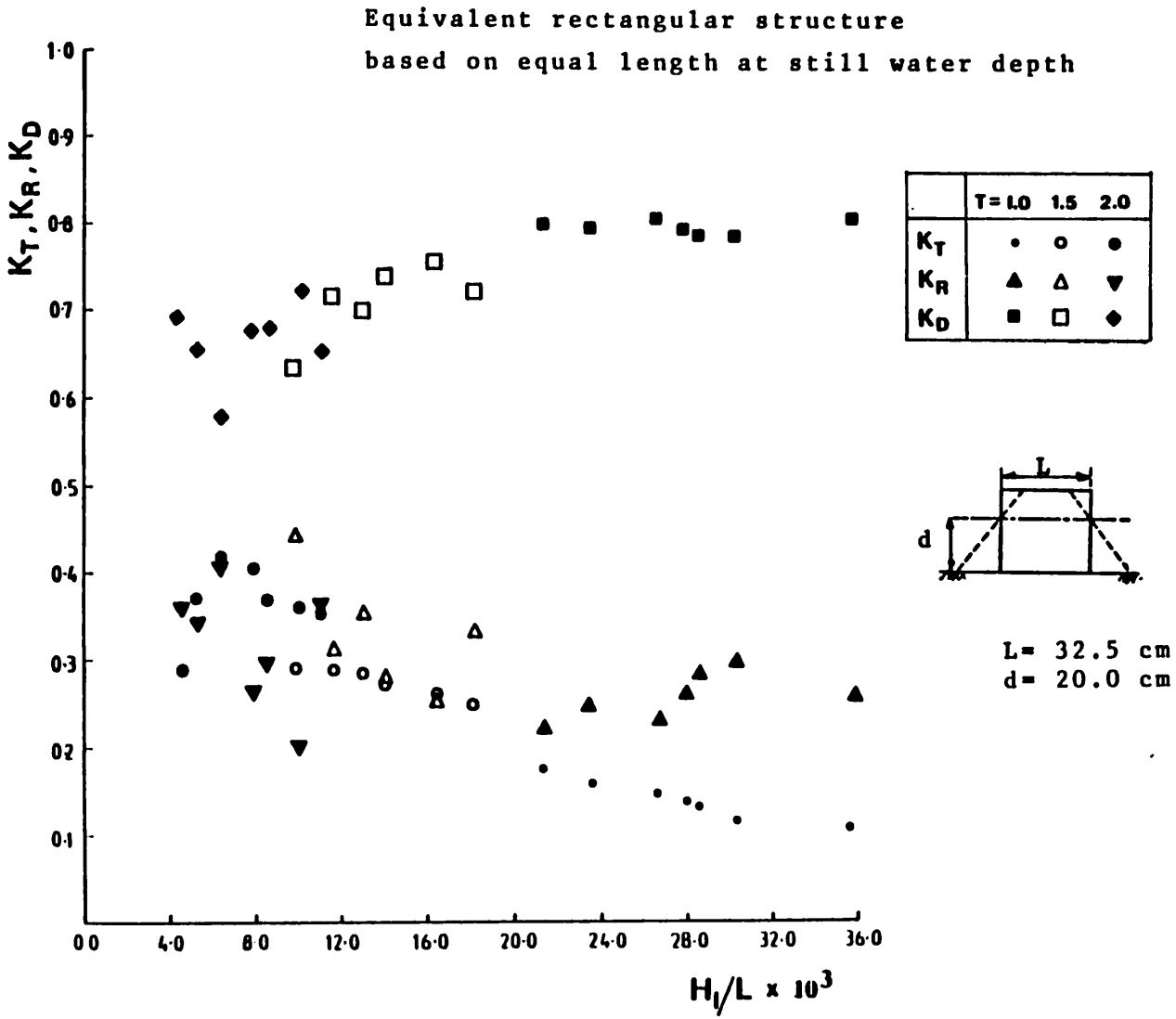
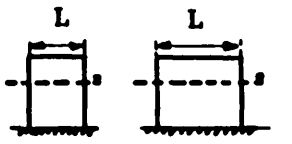
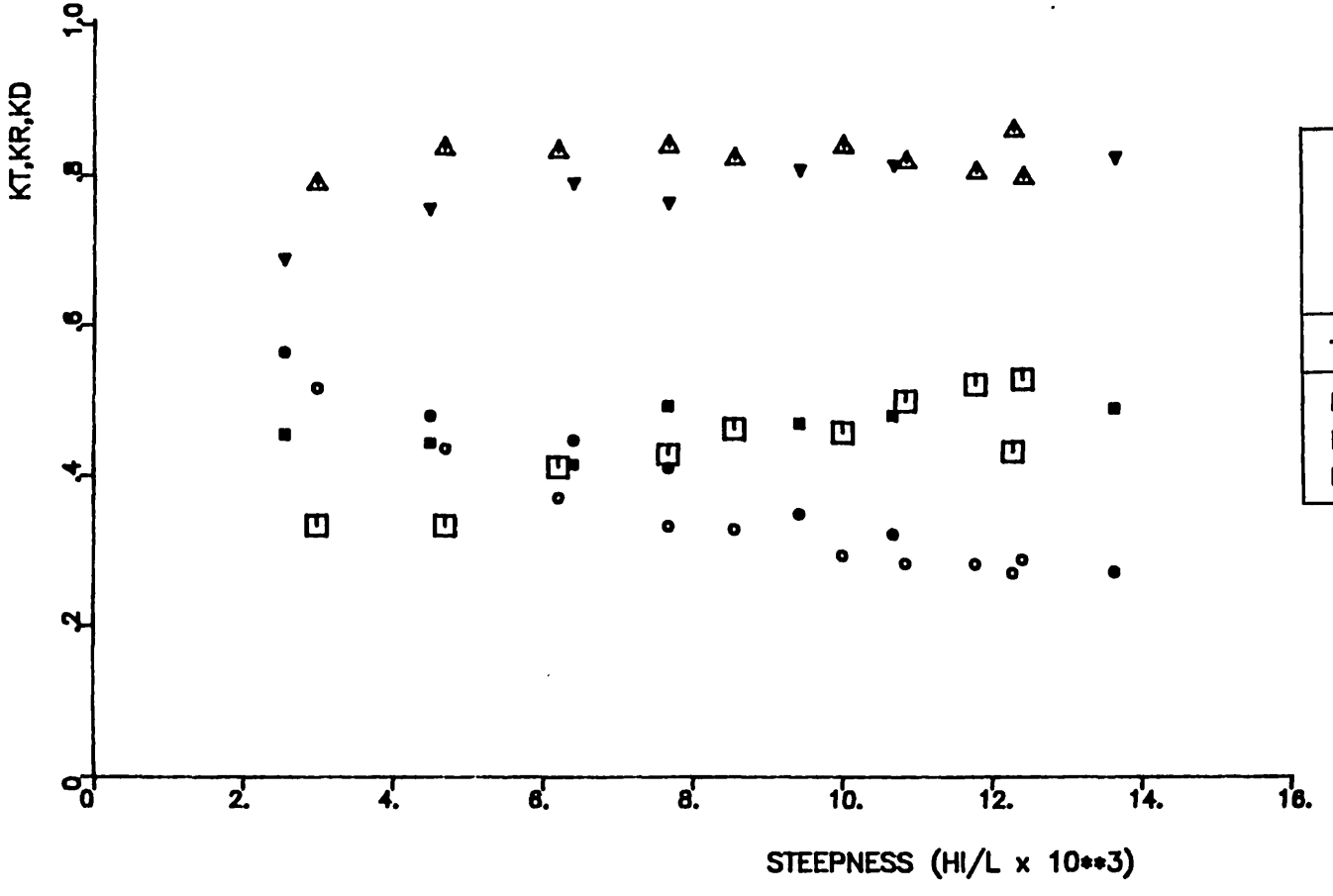


FIG.8.23 KT,KR AND KD vs STEEPNESS

INFLUENCE OF LENGTH OF STRUCTURE AT T=1.5 SEC

CONSISTING OF ROUNDED STONES L=45.0 AND 55.0 CM





	Structure length (cm) L=45	L=55
T (S)	1.5	1.5
KT	●	○
KR	■	□
KD	▼	△

FIG.8.24 KT vs STEEPNESS

FOR VARYING STRUCTURAL GEOMETRY

(POROUS MEDIA CONSISTING OF ROUNDED STONES)

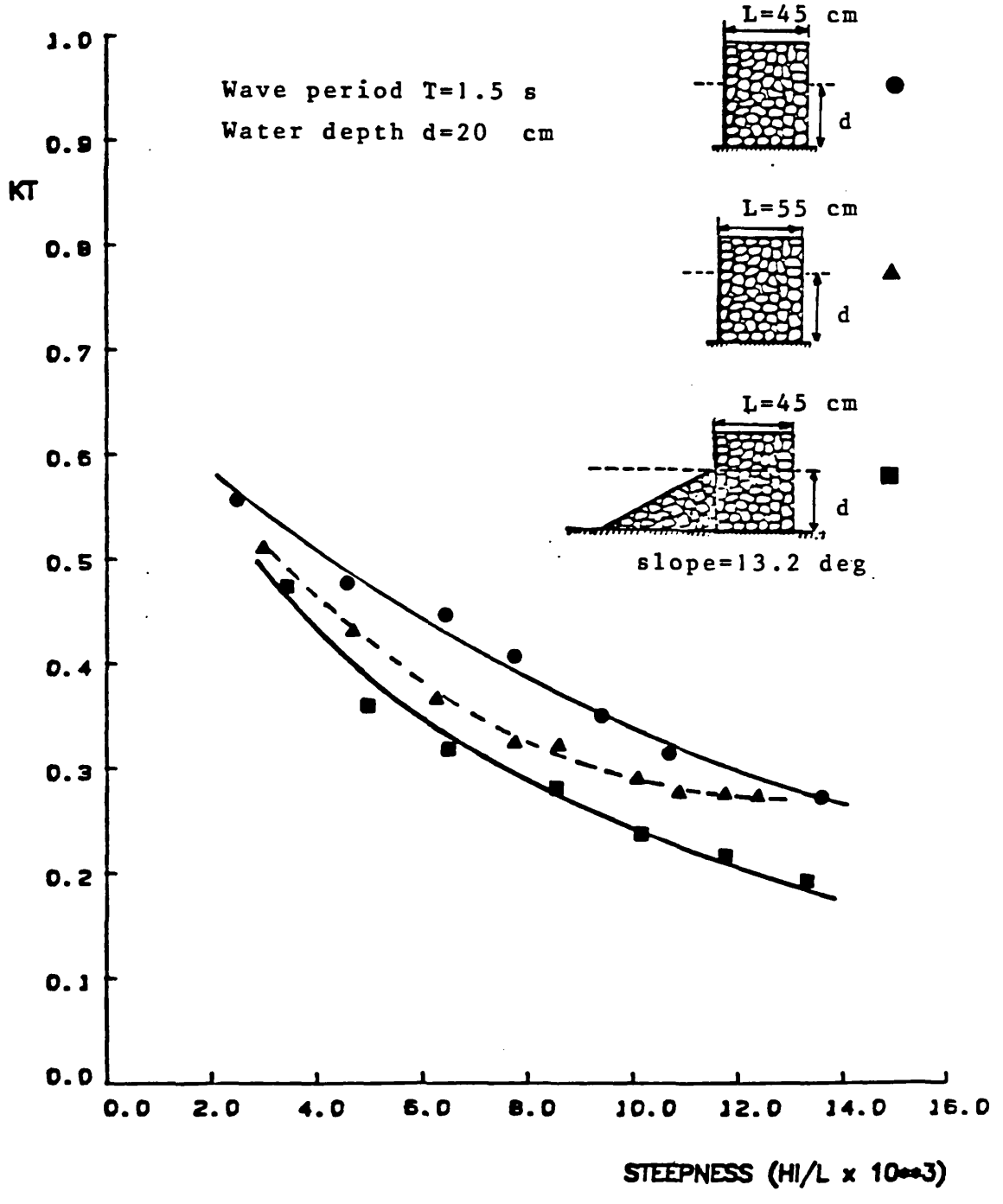


FIG.8.25 COMPARISON OF EXPERIMENTAL AND THEORETICAL VALUES

REFLECTION COEFFICIENTS

POROUS ABSORBER CONSISTING OF COBS

LENGTH OF ABSORBER =160 cm

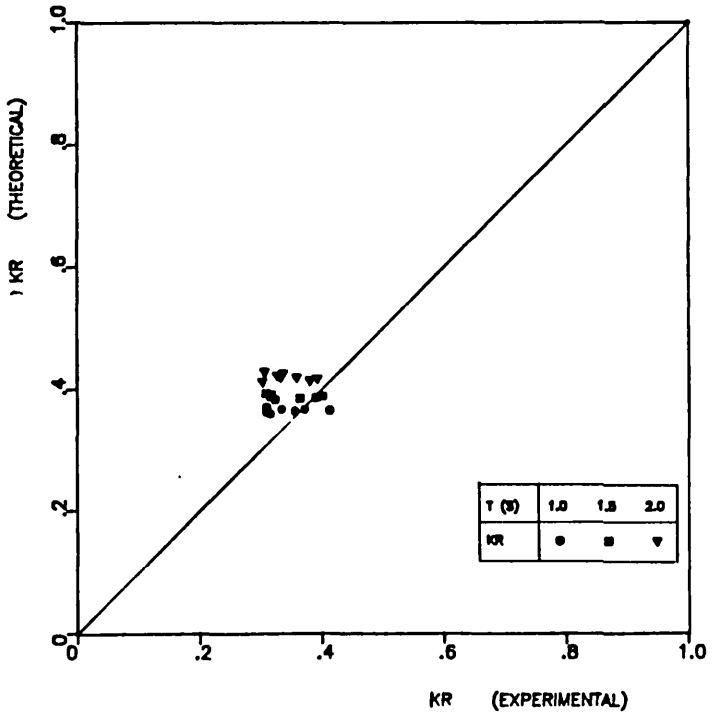


FIG.8.26 WAVE DECAY IN A POROUS ABSORBER

Comparison of experimental and theoretical values

Length of structure =160 cm and T =2.0 sec

Still water depth= 23 cm

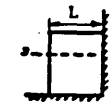


FIG.8.27 WAVE DECAY IN A POROUS ABSORBER

Comparison of experimental and theoretical values

Length of structure =160 cm and T =2.0 sec

Still water depth =23 cm

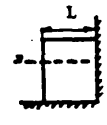
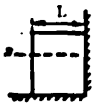


FIG.8.28 WAVE DECAY IN A POROUS ABSORBER

Comparison of experimental and theoretical values

Length of structure =160 cm and T =1.5 sec

Still water depth =23 cm



A_0= 2.81 cm

■ experimental values

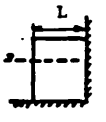
○ predicted values

FIG.8.29 WAVE DECAY IN A POROUS ABSORBER

Comparison of experimental and theoretical values

Length of structure =160 cm and T =1.0 sec

Still water depth =23 cm



A_0= 2.62 cm

■ experimental values

○ predicted values

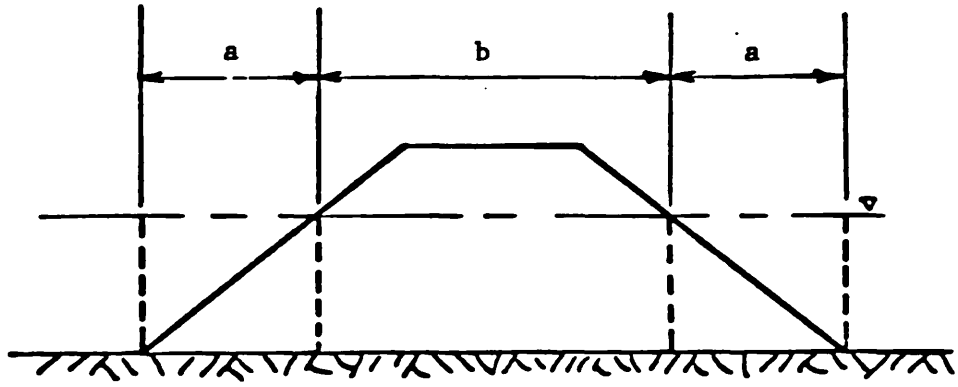


Fig.8.30.a Porous trapezoidal structure

Note: a=20 cm and b=32.5 cm for the structure used in this investigation.

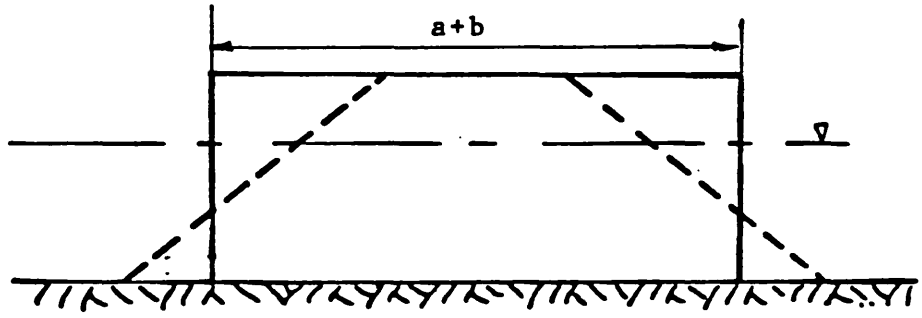


Fig.8.30.b Equivalent rectangular structure based on equal submerged volume

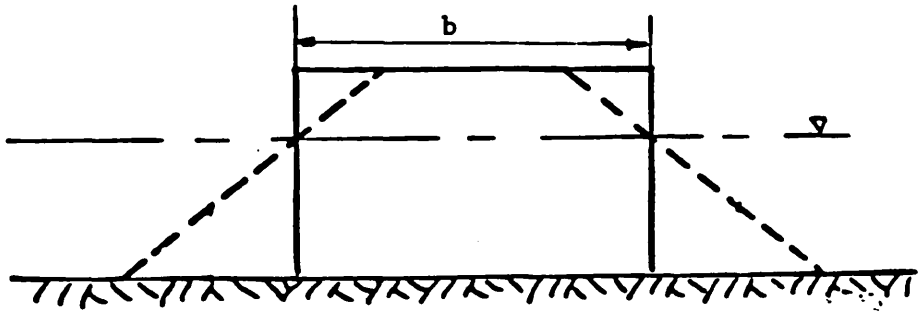


Fig.8.30.c Equivalent rectangular structure based on equal length at still water depth

FIG.8.30 POROUS TRAPEZOID AND ITS EQUIVALENT RECTANGULAR STRUCTURES

FIG.8.31 COMPARISON OF EXPERIMENTAL AND THEORETICAL VALUES

TRANSMISSION , REFLECTION AND LOSS COEFFICIENTS

POROUS RECTANGULAR BLOCK CONSISTING OF COBS

LENGTH OF STRUCTURE =52.0 cm

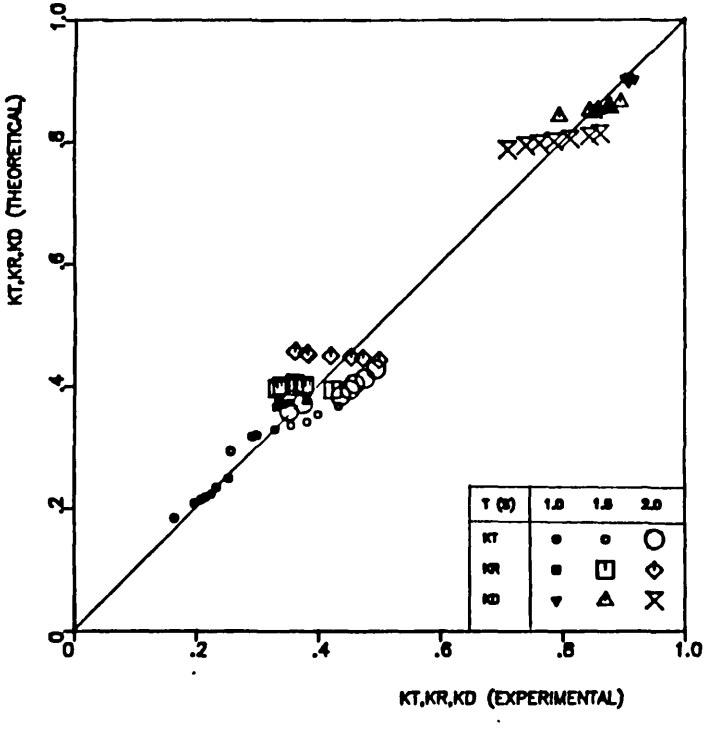


FIG.8.32 COMPARISON OF EXPERIMENTAL AND THEORETICAL VALUES

TRANSMISSION , REFLECTION AND LOSS COEFFICIENTS

POROUS RECTANGULAR BLOCK CONSISTING OF COBS

LENGTH OF STRUCTURE =33.3 cm

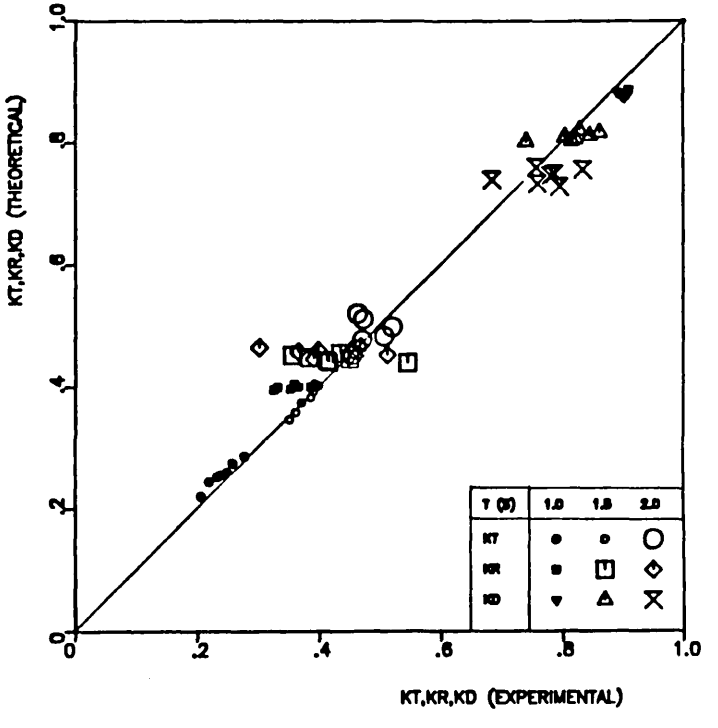
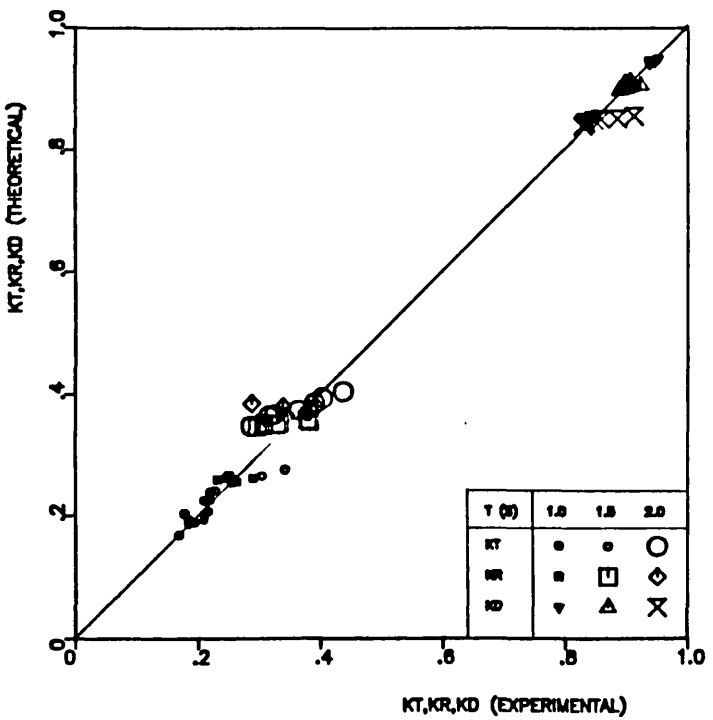


FIG.8.33 COMPARISON OF EXPERIMENTAL AND THEORETICAL VALUES

TRANSMISSION , REFLECTION AND LOSS COEFFICIENTS

POROUS TRAPEZOIDAL BLOCK CONSISTING OF COBS



CHAPTER 9 - TESTS ON A BREAKWATER SLOPING SECTION

9.1. Introduction

Results of experimental programmes discussed so far relate to porous structures constructed with a single material. Performance of structures with both vertical and sloping faces were discussed. This chapter relates to the tests performed on a three-layered breakwater section of slope 1:1 1/3. Two types of tests were performed in this phase of the project. The first was the measurement of reflection, run-up and run-down on different hollow block armour units. The second was the measurement of lift and along-slope force acting on a single armour unit. In addition, reference will be made to previous investigations of similar units and results from selected studies will be re-analysed for comparison with those of the present study.

9.2. Reflection, run-up and run-down studies

9.2.1. Discussion of results

The objective of this programme was to obtain information on reflection, run-up and run-down on a breakwater sloping section for seven different armour layer arrangements. For a constant slope of 1:1 1/3, reflection, run-up and run-down coefficients were determined for wave periods of 1.0, 1.5 and 2.0 secs. For each period the wave height was varied in order to vary the steepness. The depth was kept constant at 25 cm for all tests.

The slope of 1:1 1/3 used in this study represents the steepest slope on which hollow block armour units have been previously tested. It is known that steep slopes reflect more energy and thus the results from this investigation will relate to higher values of reflection.

In this study run-up and run-down are defined as the maximum and minimum vertical excursions with respect to the still water level. The corresponding coefficients are defined with respect to the incident wave height.

Some of the main developments in the study of reflection from sloping surfaces were presented in Sections 8.4.1 and 8.4.2 in relation to wave action on a sloping structure consisting of rounded stones.

Figs. 9.1 to 9.7 illustrate the behaviour of reflection (H_r/H_i), run-up (R_u/H_i) and run-down (R_d/H_i) coefficients for different armour layer arrangements used for this study. In each case the coefficients are plotted against wave steepness (H_i/L). Since the breakwater slope was maintained constant it was not necessary to use the parameter $\xi = \tan\alpha/\sqrt{H_i/L}$ as the dependent variable. A similar plot is also presented for the results of the trapezoidal structure consisting of Cob armour units (Fig. 9.8). The performance of this structure was discussed in Section 8.5 and is presented in this chapter for cross-comparison. It should be noted that for each wave period a minimum of six readings were taken for different values of steepness. In most of the previous studies such as Stickland (1969) the number of points was limited to three.

From the results presented in Figs. 9.1 to 9.7 it is evident that waves with longer period reflect more energy than those of shorter period. At constant wave period the reflection coefficients do not indicate a specific dependence on steepness although limited scatter is present in the results. Under these test conditions the variation of the reflection coefficient at a given period does not exceed 0.15.

Run-up and run-down coefficients exhibit more scatter and an overall comparison indicates that, in general both coefficients decrease with increasing wave steepness. For each armour layer arrangement the results are contained within a range which can be identified by its upper and lower bound values.

The performances of Cob and Shed armour units when placed in a regular pattern (Figs. 9.1 and 9.2) are very similar and the respective coefficients lie in the same range. No significant difference is observed for the Shed armour when placed in a staggered pattern (Fig. 9.3). Although the latter generates an assembly of porous armour units with same porosity but with increased tortuosity, it has not contributed towards increased energy losses. The hexagonal unit which does not possess lateral porosity exhibits slightly higher reflection coefficients (Fig. 9.7) than Cobs and Sheds, particularly for waves with small period. The run-up coefficients are also much higher in comparison. These results thus indicate the advantage of introducing lateral porosity for single layer armour units and it was previously noticed that increasing tortuosity may not necessarily increase energy losses by a significant amount. In relation to the armour layer this highlights the importance of an interconnected voids matrix with continuous and unobstructed flow paths for increased energy dissipation.

Figs. 9.4 to 9.6 relate to the performance of Hobo units having circular

openings of diameter 16, 20 and 25 mm respectively. Close examination of the results indicates that the reflection coefficient increases with decreasing diameter of the circular opening of the armour unit. This is particularly evident in the comparison of first and second plots (Figs. 9.4 and 9.5). The run-up coefficients for the first and third units (i.e. with openings of 16 and 25 mm) are greater than those for the second unit, although there is considerable scatter in the results obtained for the 25 mm unit.

In discussing the performance of the Hobo units there are two extreme cases which have to be considered. On one hand, if the diameter of the opening is gradually reduced to zero the armour layer would represent a smooth surface for which reflection coefficients will be very high, with values in the region of 0.6 or greater. These values were observed by Hydraulics Research Station (1983) in tests on smooth slopes. The corresponding run-up coefficients would also be higher and may lead to overtopping of the structure. On the other hand, if the diameter is gradually increased, it would reach a stage at which the opening would be so large that waves will be reflected directly from the underlayer. In this event the armour layer is reduced to an assembly of thin-walled hollow cubes with very large surface openings on all sides, placed on the underlayer. For this situation the reflection coefficient will correspond to that of a slope consisting of rockfill but its magnitude slightly reduced due to the presence of the skeleton armour layer. Under these conditions the underlayer will be fully exposed to incident wave action.

Reflection and run-up coefficients for the above two extreme cases discussed will be higher than those corresponding to an intermediate value of the surface opening. It is evident that there will exist an optimum diameter at which maximum energy dissipation would occur with minimum energy reflection. However the magnitude of this diameter of the surface opening of the armour unit and the resulting reflection coefficient will depend on wave steepness and slope of the structure. The problem is further aggravated if directionality of the incident wave is considered. Hence it is not possible to identify an optimum diameter for the surface opening in the absence of further investigations. In practice this diameter will be a representative value from a range of diameters. It should correspond to low reflection coefficients in relation to a wide range of values of wave steepness to be encountered by the structure when in service.

The results from the present investigation on the three Hobo units correspond to three cases within the two extreme boundaries identified earlier. They clearly illustrate the influence of the diameter of the surface opening in

relation to energy dissipation. Of these three armour units, that having a surface opening of 16 mm performs less efficiently than the other two. From a viewpoint of both wave reflection and run-up, the second unit having a surface opening of 20 mm performs best for the wave conditions used in the present test programme. The performance of this unit is very similar to that of the Cob and Shed armour units.

Fig. 9.8 illustrates the results of the porous trapezoidal structure consisting of Cob units. In comparing it with the breakwater section of Cob armour units (Fig. 9.1), it exhibits high reflection coefficients even though wave energy is transmitted through the structure. The reason for this is the increased slope of 1:1 of the porous trapezoid in comparison with $1:1\,^1/_3$ of the breakwater section.

These results demonstrate that the front slope continues to play a critical role with respect to reflection even in the presence of a continuous voids matrix within the structure allowing wave transmission. In this case the overall porosity of the structure is 0.63. The observed run-up coefficients are comparatively low for the porous trapezoid and this is mainly due to the internal transmission through the porous structure. As illustrated in Fig. 8.20, the external transmission coefficient (H_t/H_i) based on the transmitted wave height in the lee of the structure varied from 0.5 to 0.15 in the steepness range used for the study.

Hitherto the results from this investigation on different hollow block armour units have been represented on an individual basis. In order to obtain an overall view of the results of the complete experimental programme, reflection, run-up and run-down coefficients for all armour units were plotted against the surf similarity parameters $\xi = \tan\alpha/\sqrt{H_i/L}$. The plots for each coefficient are presented in Figs. 9.9 to 9.11.

Although a certain amount of scatter is observed in these figures, the results identify a certain domain in which the respective coefficients lie. There are two important observations to be made in relation to these figures.

Firstly, each plot contains results corresponding to six different hollow block units. In one case the same unit has been used in a different laying arrangement. In addition, the results of a porous trapezoid are also included. Thus the domain identified for each of the coefficients is representative of a wide range of hollow block armour units.

Secondly, the results for each armour unit were based on wave records from three different wave periods and for each such period results corresponding to six different wave heights are included. In effect for a given breakwater slope and wave period the maximum variation of the surf similarity parameter has been obtained within experimental limits by considering a wide range of wave heights. Although the increased number of points has contributed towards the overall scatter, results have been obtained over a wider range of the independent variables.

From the foregoing discussion, it is established that the respective domains identified for the reflection, run-up and run-down coefficients cover wide ranges of both type of hollow block armour and incident wave conditions.

With regard to the relative magnitude of the three coefficients it is noticed that for reflection, run-up and run-down, the maximum values observed are approximately 0.42, 1.4 and 1.25 respectively. In the case of run-down coefficients most of the values are below 1.0.

9.2.2. Re-analysis of test results of Stickland (1969) on Cob units

Results of previous investigations on Cob and Shed armour units have been presented by Stickland (1969), Hydraulics Research Station (1983) and Wilkinson and Allsop (1983). Of these the first refers to the Cob unit, the second to the Shed unit and the third presents an overall view of the hollow block concept in relation to armour units placed in a single layer.

Stickland (1969) reports extensive model studies on the Cob armour unit performed with regular waves prior to its adoption in a design. The side length of the model unit used for the study was 5.93 cm. The results of these tests were presented only in tabular form illustrating the variation of reflection, run-up and run-down coefficients with incident wave height. Since the present study on hollow block armour units was performed with regular waves using a model of side length 4.0 cm, it is appropriate to re-analyse the results of Stickland (1969) using the same method of approach adopted for the present study.

The basic two-dimensional test programme performed by Stickland (1969) encompassed two types of structures.

The first type was a breakwater section of varying slope. This facility permitted the investigation of slopes 1:2½ (21.80°), 1:2 (26.57°), 1:1½ (33.69°) and 1:1 1/3 (36.87°). It is relevant to note that this breakwater section was

constructed without a central core and the underlayer was laid on an impermeable timber frame. In order to avoid re-constructing a rubble mound for each angle of slope, the test frame was hinged at the lower end to enable the required slopes to be obtained. The length of the slope used for this phase of the investigation was carried well above the maximum anticipated level of run-up to ensure that no overtopping took place.

The second type of structure investigated by Stickland was a complete breakwater structure having a central core in addition to the underlayer. The structure had a front slope of 1:1 1/3 and rear slope 1:1. It simulated an actual prototype breakwater cross-section to be constructed with Cob armour units.

For both types of structure, Stickland measured reflection, run-up and run-down coefficients for varying incident wave conditions. In each case four wave periods namely, 1.2, 1.4, 1.6 and 1.8 secs were used and for each period three values of wave height were considered. The water depth was kept constant at 38.1 cm.

Since the tests performed by Stickland dealt with varying slopes and steepness, they provide an opportunity to investigate the variation of the reflection coefficient with the surf similarity parameter $\xi = \tan\alpha/\sqrt{H_i/L}$.

Fig. 9.12.a illustrates the variation of reflection coefficient (K_r) versus surf similarity parameter (ξ) for varying breakwater slopes. This can be used to investigate the influence of slope for given period or vice versa. For a given period the reflection coefficient decreases with decreasing slope and, for a given slope, it also decreases with decreasing wave period. These observations apply to all slopes and wave periods. It establishes that long period waves acting on a steep slope produce high reflection coefficients, whereas short period waves acting on a mild slope produce low reflection coefficients.

Fig. 9.12.b presents a comparison of the performance of the breakwater sloping section having a slope of 1:1 1/3 with that of the complete breakwater structure. The latter has a front slope of 1:1 1/3 and a rear slope of 1:1 and for this trapezoidal structure readings were obtained for seven different wave periods.

The scatter in the plotted values is greater for the trapezoidal structure. It is also observed that the reflection coefficients corresponding to this structure are slightly higher than those of the breakwater sloping section. At a given period the wave heights measured during the testing of the trapezoidal structure were

higher than those observed for the breakwater sloping section. In most cases the trapezoidal structure was subjected to overtopping waves. Under these extreme conditions, it is quite possible that the wave records obtained by using the loop-node technique were not well-defined in comparison with those obtained under mild incident wave conditions. Hence it is inevitable that a greater degree of scatter will be present in the results for the trapezoidal structure.

Figs. 9.13 and 9.14 refer to the run-up and run-down coefficients observed for the breakwater sloping section. Although a particular trend is not observed in relation to variation of slope, the plots illustrate the range in which the respective coefficients lie. The scatter for the run-down coefficients is comparatively low. Also marked in Fig. 9.14 are the run-down coefficients obtained for the trapezoidal breakwater structure. The corresponding run-up coefficients were not identified because on most of the occasions the structure was overtopped.

With regard to the relative magnitude of the three coefficients investigated, it is noted that in the case of the breakwater sloping section the maximum values of reflection, run-up and run-down recorded were approximately 0.42, 1.6 and 0.9 respectively.

9.2.3. Empirical equations for the prediction of reflection coefficients

Empirical equations for the prediction of reflection coefficients from sloping structures have been presented by several investigators. Of these, two of the more recent contributions pertaining to rubble mound breakwaters have been made by Losada and Gimenez-Curto (1981) and Seelig (1983). In both studies the reflection coefficient was related to the surf similarity parameter (ξ) by using two constant coefficients evaluated from experimental data. The surf similarity parameter was defined with respect to the incident wave height and deep water wave length (L_o).

Losada and Gimenez-Curto (1981) used the following relationship for the prediction of the reflection coefficient.

$$K_r = a\,(1 - \exp(-\xi b)) \qquad (9.1)$$

where

$$\xi = \frac{\tan\alpha}{\sqrt{H_i/L_o}} \qquad (9.2)$$

H_i = incident wave height
L_o = deep water wave length
a,b = constants to be evaluated from experimental data.

This exponential relationship was also used to correlate run-up, run-down and transmission coefficients for rough, permeable slopes and breakwater structures under the action of regular waves.

The studies of Seelig (1983) included reflection from both smooth and rough slopes and the following relationships were examined,

$$K_r = \tanh (a\xi^b) \tag{9.3}$$

and

$$K_r = \frac{a\xi^2}{\xi^2 + b} \tag{9.4}$$

where ξ is defined by eq. 9.2
a,b = constants to be evaluated from experimental data.

Eq. 9.3 is based on the equation proposed by Battjes (1974) whereas eq. 9.4 was developed using data from several laboratory studies.

In the case of smooth slopes the values of a and b in eq. 9.3 were taken as 0.1 and 2.0 respectively for conservative results. The recommended values of a and b in eq. 9.4 were 1.0 and 5.5 respectively.

For sloping revetments faced with armour units, Seelig recommends that the parameter a in eq. 9.4 be multiplied by a reduction factor. In effect the relative influence of roughness in reducing reflection coefficients has been incorporated into this parameter which has a value of 1.0 for smooth slopes.

Seelig also points out that in breakwaters there is complex inter-relationship between reflection, transmission and dissipation (internal and external) and as a consequence it is difficult to predict wave reflection coefficients for rubble mound breakwaters. For a quick conservative estimate for design purpose it is recommended that values of a and b in eq. 9.4 be taken as 0.6 and 6.6. Designers are also referred to laboratory data under similar conditions.

In the present study both eqs. 9.1 and 9.4 were used to obtain a correlation between flow characteristics and surf similarity. The flow characteristics considered were the reflection, run-up and run-down coefficients. The surf similarity parameter was based on the incident wave height and wave length in contrast to eq. 9.2 which was based on deep water wave length.

Experimental results from this study as well as those of Stickland (1969) were used for the analysis. It should be pointed out that wave heights used by Stickland (1969) were comparatively larger than those used for the present study and as a consequence the ranges of the surf similarity parameter in the two studies were different.

In the case of the present study results from reflection, run-up and run-down tests on all hollow block armour units (Figs. 9.9, 9.10 and 9.11) were used to determine the coefficients of eqs. 9.2 and 9.4. However, the results pertaining to the Cob trapezoid were excluded because it represented a different structural configuration to that of the others. Table 9.1 summarises the results from this analysis, giving the respective coefficients - calculated by the least squares method - and a generalized correlation coefficient to assess the "goodness of fit".

In each case more than 125 experimental values have been used for the computation of these coefficients and, as was pointed out earlier, the experimental data covered a wide range of incident wave conditions for a constant slope of $1:1\,^1/_3$.

In analysing Stickland's data, results from the breakwater section of varying slope (Figs. 9.12.a, 9.13 and 9.14) were used to determine the respective coefficients of eqs. 9.2 and 9.4. The results from the complete breakwater section were not used because of its different structural configuration. The results of the analysis are presented in Table 9.2 on the same basis to that of Table 9.1.

In each case more than 50 experimental values have been used for the computation of these coefficients and they cover a wide range of incident wave conditions for varying slopes.

In analysing the results presented in Table 9.1 and 9.2, it is observed that the "goodness of fit" of the reflection coefficient is higher than that of run-up and run-down coefficients, mainly due to the scatter in the results of run-up and run-down data.

There are several important observations to be made in a comparison of the results from Tables 9.1 and 9.2. Firstly, the surf similarity parameter corresponding to the experimental values of this study was in the range 4–13 whereas the corresponding range for Stickland's data was between 1.4–3.5. Secondly, the model armour units tested by Stickland were larger than those used for the present study. Thirdly, Stickland's data were limited to Cob armour units whereas six different hollow block armour units were used in the present study.

An important point which arises from the comparison of the results from Tables 9.1 and 9.2 relates to the predicted values of the reflection coefficient. Given below are two expressions for the reflection coefficient, the first (eq. 9.5) is based on the data from this study and the second (eq. 9.6) is based on data from Stickland's tests.

$$K_r = \frac{0.41\xi^2}{\xi^2 + 22.2} \qquad (9.5)$$

$$K_r = \frac{0.51\ \xi^2}{\xi^2 + 5.0} \qquad (9.6)$$

On one hand it is noticed that for values of ξ greater than 4 the reflection coefficients predicted by eq. 9.6 are comparatively higher than those predicted by eq. 9.5. For example, when using eq. 9.6 reflection coefficients as high as 0.49 are predicted for values of ξ in the region of 10 whereas the values determined experimentally are less than 0.4.

On the other hand it is noticed that if eq. 9.5 is used to predict reflection coefficients for values of ξ less than 4 the predicted values are less than those observed by Stickland.

It is known that reflection coefficients are comparatively higher for small amplitude long waves acting on steep slopes, i.e., for high values of ξ. For hollow block armour units the results from the present study indicate that reflection coefficients do not exceed 0.4, although higher values are predicted by eq. 9.6. Similarly for high amplitude short waves acting on mild slopes – wave conditions corresponding to low values of ξ – the reflection coefficients observed are not as low than those predicted by eq. 9.5.

These observations clearly show that the expressions given by eqs. 9.5 and 9.6 should only be used to predict the reflection coefficients for values of ξ which lie within a certain range, defined by the maximum and minimum values of ξ used to determine the respective constants in eqs. 9.5 and 9.6. Thus sufficient care should be exercised when extrapolating in either direction. The same argument holds for run-up and run-down coefficients.

The foregoing discussion also recognises the importance of obtaining experimental data over a wider range so that more generalized formulae can be obtained.

Some of the differences observed in the two expressions for the reflection coefficient (eqs. 9.5 and 9.6) may also be due to scale effects. The side lengths of the Cob armour units used in this study and those used by Stickland were 4.2 and 5.9 cm respectively.

Attention is also focused on the results of Losada and Gimenez-Curto which are summarized in Table 9.3. These results are of the same order of magnitude and consistent with those presented in Tables 9.1 and 9.2. However the number of experimental values used by Losada and Gimenez-Curto for the different cases are fewer than those used for the present study. The results, to a certain extent, illustrate the variations in the coefficients a and b in eq. 9.1 when determined from different sets of experimental data obtained using various types of armour units.

The correlation coefficients corresponding to the results of Losada and Gimenez-Curto are comparatively higher. This is mainly due to the fact that the equations presented in Table 9.3 have been obtained from tests performed on a particular type of armour unit. However, if a general relationship was to be obtained for a group of armour units such as that performed in this study (Table 9.1), the correlation coefficient will be lower mainly due to the increase in the overall scatter.

For cross-comparison purpose the results from reflection tests on Dolos units (HRS 1970) using regular waves were re-analysed to determine the respective coefficients in eq. 9.4. For $1.5 < \xi < 3.5$ the expression obtained for the reflection coefficient was

$$K_r = \frac{0.94\ \xi^2}{\xi^2 + 20.2} \qquad (9.7)$$

with a correlation coefficient of 0.847.

Fig. 9.12.c is a plot of K_r vs ξ, illustrating the scatter in the experimental results for different slopes and incident wave conditions.

For $\xi < 3.5$ the values of K_r given by eq. 9.7 are less than those predicted by eq. 9.6. The latter refers to the Cob armour unit based on Stickland's data.

Apart from eqs. 9.1 and 9.4 which were used to analyse the results from this study and that of Stickland (1969), the following relationships were also examined to correlate reflection, run-up and run-down data.

$$Y = a\xi + b \qquad (9.8)$$

$$Y = a\xi^b \qquad (9.9)$$

$$Y = a\xi/(\xi + b) \qquad (9.10)$$

In these equations, Y refers to the dependant variable and ξ is, again, the surf similarity parameter. Although a good fit was obtained for certain coefficients, from an overall point of view in relation to reflection, run-up and run-down coefficients, it was observed that eqs. 9.1 and 9.4 represented the best correlation between the variables.

9.3. Measurement of lift and along-slope forces

9.3.1. Types of loads acting on armour units

The importance of both lift and along-slope forces in relation to the performance of single layer hollow block armour units was introduced in Section 3.5.7 in justifying the measurement of these two force components as part of the present study.

Until very recently, forces acting on armour units and the resulting stresses have been given very little consideration. Since then it has been found (Ligteringen 1983) that in the case of interlocking type of units the phenomenon of rocking and the resulting collision between blocks which occurred under certain conditions caused impact loads several times greater than the expected hydraulic loads. Some aspects of material and structural design of concrete armour units were presented by Burcharth (1983) and Ligteringen, Mol and Groeneveld (1985).

Before analysing the results of the present study attention is focused on typical load conditions relevant to concrete armour units.

For a given armour unit there are three important phases that can be identified in the construction process :

(1) Casting and transportation for storage
(2) Transportation to the site and placing
(3) Service state

The load conditions corresponding to the first and second phases are well-defined and mainly concern the static weight of a unit. Adequate support should be provided during handling, transport and placing and under normal circumstances these two phases do not produce critical conditions resulting purely from static loads.

In the case of hollow block armour units a certain amount of abrasion and impact may occur when placing one unit beside another to a predetermined layout and sufficient care should be exercised in doing so.

The load conditions corresponding to the service state are rather complex and demand closer examination. The types of load encountered in this phase include static, dynamic, abrasive, thermal and chemical loads (Burcharth 1983).

The static load mainly consists of the weight of units and stresses due to settlement of underlayers. Sometimes armour units, particularly those of an interlocking type, may get wedged between other units due to wave action resulting in an additional static load.

Unlike interlocking units, the in-situ static loads due to overlying hollow block units are well-defined because they are placed in a regular pattern. It is observed that these loads may be critical for armour units located at the bottom end of the armour slope. An integral part of a breakwater constructed with hollow block units is the toe beam and for its design it is necessary to assess accurately the overall static load. It should be noted that the settlement of underlayers generally contributes to an increase of this load. Although static loads are not critical when considered in isolation, they may prove to be decisive when acting in combination with other types of loads.

Dynamic loads are essentially of two types. The first are oscillating

forces which are gradually varying or quasi–static loads due to wave action on a slope. These oscillating forces are normally exerted during uprush and downrush of waves.

For hollow block armour units the oscillatory nature of these forces will be reflected in the traces of both lift and along–slope force. Lift forces will be resisted by the weight of the unit and frictional forces acting between the contact surfaces. Hence if lift forces are sufficient to cause motion of the unit then abrasion will result.

The second type of dynamic loads are impact forces which may arise due to several reasons. Direct wave impact on the armour units, rocking, rolling and collisions between units, and parts of one broken unit striking another unit are some of the main causes of these loads.

In the case of single layer hollow block units, the placing arrangement is such that only forces due to direct wave impact play a vital role. Since a given unit is in contact with the neighbouring units such that the contact surfaces are well–defined in the vertical plane, the influence of rocking, rolling and collisions is reduced to a minimum. In addition, the slope corresponding to the upper surface of the armour units is aligned throughout the breakwater and it is very unlikely that parts of units will be removed and displaced over a considerable distance. This advantage is not present in the case of interlocking type of armour units in which the upper surface of the armour layer is uneven and characterized by protrusions from armour units. The contact surfaces are also randomly positioned.

The occurrence of impact forces on hollow block units will be reflected in the traces of both lift and along–slope forces in the form of sharp peaks superimposed on the gradually varying or quasi–static loads identified earlier.

The foregoing discussion clearly identifies certain characteristic features which can be expected in the traces of both wave induced lift and along–slope force acting on single layer hollow block armour units. It is evident that these features will be dependent on the incident wave conditions.

Apart from these forces, Burcharth (1983) identified thermal and chemical loads. The first results from stresses due to temperature differences during the hardening process and the second due to corrosion of reinforcement, sulphate reaction etc. Burcharth also points out that for slender interlocking units the dynamic and static forces are critical whereas for bulky units (generally cuboid),

dynamic and thermal loads are critical.

9.3.2. Methods of assessing loads on armour units

Theoretical, experimental and field studies have been used to study static and dynamic loads acting on armour units.

Theoretical approaches have been presented by Barends, Kogel, Uijttewaal and Hagenaar (1983) and Austin and Schlueter (1982). These models require the use of coefficients which have to be determined experimentally or found by the use of empirical formulae. Calibration against prototype data is also an important factor in verifying the applicability of the model.

A variety of experimental techniques is available to measure forces on armour units. In this study a force transducer using strain gauges was adopted to measure both lift and along-slope force. Similar techniques have been previously used to measure the forces acting on Tetrapods (Ligteringen 1983) and Dolosse (Van Hijum 1985). However, detailed results have not been presented. The use of strength-scaled models (Timco and Mansard 1982) has been recently introduced to give an indication whether the strength of an armour unit is sufficient to withstand a given wave climate.

Hitherto full-scale prototype measurement of wave forces acting on armour units have not been reported. However, in the near future Dolos units are to be tested for this purpose (Howell 1986).

Apart from these techniques similarity methods have been adopted by Burcharth (1981) to study the dynamic forces acting on Dolos units. Both drop tests and pendulum tests at prototype scale have been used to simulate rocking of units and impact from broken pieces of units displaced by the waves.

9.3.3. Method of analysis

In the present study measurements were made of lift and along-slope forces acting on a single hollow block armour unit not in contact with its neighbouring units or with the underlayer. Regular waves were used for the experimental programme.

In discussing wave induced forces on an armour unit it was pointed out that both oscillatory and impact forces will be exerted depending on the wave

environment.

In the experimental programme wave forces were measured for periods 1.0, 1.5 and 2.0 seconds. For a given period wave steepness was varied by generating waves of different heights. The still water depth was also varied from 23 cms to 28 cms in steps of 1 cm. At one extreme of this depth-range the armour unit was partially submerged and at the other extreme fully submerged.

In collecting data the datum for both force and wave height was maintained at still water level free from any disturbances due to waves. The readings obtained thus represents variations above and below the values corresponding to this initial state. In this respect it should be noted that when the instrumented armour unit is initially submerged in the absence of waves, a buoyant force will be acting on it. The recorded forces, both lift and along-slope, will thus correspond to those in excess or less than the respective components of the submerged weight. Hence the zero value of forces corresponding to the datum level in reality relates to the components of submerged weight. In the case of wave run-up, run-down and wave height at the toe of the structure, the records represent variations with respect to the still water level used for the particular experiment.

In analysing the force traces reference is made to studies by Stive (1984) and Fuhrboter (1986) on wave impact on uniform slopes at approximately prototype scale. Both authors measured pressures using a series of pressure gauges with a high frequency response to analyse the peak pressures.

A typical schematization of the time-dependent force record of either the lift or along slope is presented in Fig. 9.15. This is based on a similar illustration by Stive (1984) for wave impact pressures on a uniform slope.

At the time t=0 the force corresponds to that of the initial state. The time-dependent force trace is divided into two parts. The first corresponds to a gradually varying part of duration t_o, of the order of the wave period and having a maximum value of F_o. The second corresponds to the impact component of duration t_i and peak value of F_i in excess of F_o. The total peak force recorded will thus be the sum of F_o and F_i. The time t_r on Figure 9.15 relates to the rise time of force F_o.

Both Stive and Fuhrboter analysed the peak pressures which were evaluated visually from analog records. On-line evaluation by computer was not

adopted because of the very short impact duration in the total record. No analyses were performed on the impact duration.

The wave heights generated in the present study were comparatively smaller than those used by Stive and Fuhrboter. The wave impact load was thus not of great magnitude. The force traces were recorded both digitally (at a sampling rate of 200 per second) and on a UV recorder. The latter was included to ensure that all peak forces were correctly recorded. The records obtained by using these two methods were found to be identical.

The typical schematization of a force record presented in Fig. 9.15 refers to a general case. The characteristic features identified will vary according to the incident wave height, wave period and the still water depth. For example, in the case of small amplitude, long period waves the peak forces will be hardly noticeable particularly when the instrumented armour unit is initially submerged in still water conditions. In this case the dynamic load will consist only of the oscillatory, gradually varying component. On the other hand short waves having a comparatively large amplitude will exert impact forces for certain water depths depending on the degree of submergence of the instrumented armour unit.

In analysing force traces the important aspect was the determination of the peak force whenever it was found to be present. When waves impact on the armour unit, the force transducer records a peak value followed by damping of the recorded signal. Vibrations of the transducer are superimposed on the force record. Because of the presence of these vibrations it is quite likely that the recorded peak impact is slightly greater than the true value. However if a smoothing procedure similar to that adopted for the analysis of results from unidirectional constant acceleration tests was used, the peak value of the smoothed records will be lower than the true value. Hence the true value lies between the peak recorded in the measured force traces and the peak recorded in the smoothed force traces.

This aspect was not present in the analysis of force records from unidirectional constant acceleration tests because the forces exerted on the instrumented armour unit gradually increased from zero and were free from impact forces.

A moving point smoothing procedure was adopted for the analysis of force records. The number of data points contained per cycle of high frequency vibration can be calculated from the sampling rate of data and the natural

frequency of the force transducer in water. The number of points used for each operation of the moving point smoothing procedure was selected to be less than the number of data points contained per cycle.

It was expected that the smoothed values thus obtained would be representative of the original record and contain reduced peaks. If this condition is not satisfied the peak signals will be considerably reduced and most of the characteristic features of the original record will be lost.

9.3.4. Presentation of results and discussion

The measurement of forces on a hollow block armour unit were obtained for two different cases based on the characteristics of the underlayer. In the first case the primary armour rested on a permeable underlayer which consisted of a secondary layer and a central core. This corresponds to the breakwater section used for reflection, run-up and run-down studies. In the second case the primary armour layer rested on an impermeable underlayer. The objective of performing tests under different conditions was to assess the influence of the permeability of the underlayer on the forces acting on a hollow block armour unit. In these experiments the position of the instrumented armour unit remained constant at a depth of 23.5 cm (Fig. 9.16).

The results of the experimental programme are summarised in Tables 9.4 to 9.9. Of these, Tables 9.4, 9.5 and 9.6 relate to the results from the complete breakwater section, Tables 9.7 and 9.8 refer to the tests performed with an impermeable underlayer and Table 9.9 presents a comparison between the results for the two cases considered.

In all the tests performed repeatable records were obtained for both lift and along-slope forces. These records were also consistent with the typical schematization of a force record presented in Fig. 9.15. As identified earlier, the characteristic features of the force records were heavily dependent on the properties of the incident wave and the position of the instrumented armour unit relative to the still water depth.

Each table represents the important properties of the incident wave, wave motion along the armoured slope and the measured forces. Wave measurements corresponding to wave height at the toe, run-up and run-down are given for each case. The force measurements correspond to the maximum values of upward (positive) and downward (negative) components of lift and along-slope forces.

Values obtained from both measured and smoothed data are presented for completeness.

In the presentation of results a non-conventional unit 'gm force' was used for force measurements. This has been adopted mainly because of the comparatively small values of force measured in this study (1 gm force = 980.665 x 10^{-5} N).

The smoothing procedure did not have a significant influence on the wave height records. Since these records were well-defined and free from vibrations, the values corresponding to measured data are presented. However in the case of force measurements, a significant difference was observed in the peak values and hence those corresponding to both measured and smoothed data are presented.

The tabulated values of the variables represent the mean value ($\bar{x}$) from a set of ten observations. The standard deviation (σ_n) and the coefficient of variation ($\sigma_n/\bar{x}$) are also given to assess the spread of values about the mean. The latter is expressed as a percentage. In the case of lift (F_{lift}) and along-slope (F_{slope}) forces, the values are also presented in dimensionless form as a ratio of the respective components of the submerged weight. W_{sl} and W_{ss} are these two components in the direction of the lift and along-slope forces respectively. For wave measurements, additional information is presented in the form of wave steepness (H_t/L), run-up (R_u/H_t) and run-down (R_d/H_t) coefficients. These coefficients were based on the wave height at the toe of the structure, H_t.

An overall analysis of the results indicates that the smoothed values were more stable than the measured values. This was evident from the fact that on most occasions the standard deviation and the coefficient of variation were comparatively smaller for the smoothed values. The smoothing procedure had reduced the magnitude of the peak signals corresponding to impact forces. An analysis of the results indicated that for more than 75% of the experimental data the reduction in the magnitude of the peak signal was less than 35%.

In the analysis of wave measurements, values above and below the still water depth were considered positive and negative respectively. In the case of force measurements the upward along-slope force and the upward lift force were considered positive (Fig. 9.17). Based on this sign convention, force traces at the instant of wave impact on the armour unit are characterized by a positive

along-slope force and a negative lift force, the latter acting in the direction of the core.

The wave impact is followed by run-up during which the water level reaches a maximum above the still water depth. The next stage is the run-down during which the water level falls progressively. It passes the still water level and reaches a minimum value. The process is repeated by the commencement of run-up. For the wave conditions used in the experiments the run-up and run-down process was complete before the arrival of the succeeding wave.

For the experimental conditions used for this study it was observed that the upward normal force which tends to lift the armour unit from the primary armour assembly occurred during the run-down phase when the water level on the breakwater slope was between the maximum value of run-up and the still water depth. It was also observed that at the point of wave impact the run-up probe registered positive values indicating that it occurred when the water level on the slope was higher than the still water level.

In relation to the performance of a hollow block armour unit the critical aspects of the forces traces are the impact components of both lift and along-slope forces and the upward normal component of the lift force. To analyse the relative magnitude of these components they have been represented in dimensionless form with respect to the corresponding components of the submerged weight. These ratios thus represent the magnitude of wave induced dynamic forces in comparison with static forces which would otherwise be present.

The impact forces play a vital role with respect to the durability of the armour unit. Apart from imposing peak loads on the armour unit, these forces also cause collisions between armour units during wave impact, particularly in the upward direction. There is a greater likelihood of this occurring when the armour units are not properly laid out. Under these conditions long narrow crevices are produced between the units, thus allowing displacement. These crevices may also develop due to settlement of the underlayer. The downward normal component due to wave impact will introduce a certain amount of pressure on the underlayer and this may contribute to settlement.

The upward normal forces are resisted by the corresponding component of submerged weight and the frictional forces between the armour units. Removal of armour units by lifting is one of the possible failure modes for breakwaters consisting of hollow block armour units and as a consequence a proper estimate of

the lift forces is necessary. During the service state partial lifting of armour units will lead to abrasion of the contact surfaces.

Table 9.4 refers to six tests performed on the breakwater section at a constant depth of 24 cm for wave periods 1.0, 1.5 and 2.0 secs respectively. At this depth approximately 60% of the instrumented armour unit was submerged (Fig. 9.16). The purpose of these tests was to study the influence of varying wave height at a given period and the period-dependent characteristics of the force records.

There are two important observations to be made in relation to the results presented in Table 9.4. The first relates to the magnitude of the force components measured. Of these components the maximum values occur in the upward along-slope force. In some instances the relative magnitude of this component is of the order of 5 when based on measured data. The smoothed values are lower, approximately 3.5. The second relates to the positive lift force, a critical design aspect. It is observed that this force is equal to or less than the corresponding submerged weight component and on most occasions the relative magnitude is very much less than unity.

Tests 1, 2 and 3 refer to a wave period of 1.0 sec but with different wave heights. Results from all three tests indicated the presence of peak forces in the upward along-slope and downward normal (negative lift) directions corresponding to the instant of impact of the wave front. Of these two forces the upward along-slope component is found to be significantly greater than the other. As the wave height decreases the magnitude of the respective components decreases.

Tests 4 and 5 refer to wave periods of 1.5 secs. Although the results follow a similar trend in comparison with the first three tests, the magnitude of the impact force acting upward along-slope was reduced considerably. The reduction in the downward normal force is not very significant. However the records of lift force indicated that the sharp peaks were not evident as before and that, to a great extent, the records were characterised by the gradually varying type of dynamic forces identified earlier.

Test 6 refers to a wave period of 2.0 secs. The records of both along-slope and lift forces were free from impact loads and consist of only gradually varying or quasi-static loads.

Figs. 9.18 to 9.20 represent plots of the measured variables for wave

periods 1.0, 1.5 and 2.0 secs corresponding to tests 1, 4 and 6 respectively. The plots clearly illustrate the variation with time of the different variables and the repeatability of the force signals resulting from waves of regular period is good. Reference is made in particular to the characteristic features of the impact loads for waves of short period and purely oscillating loads for waves of longer period.

Fig. 9.21 represents a plot of the smoothed variables corresponding to Test 1. In comparison with the measured variables of the same test (Fig. 9.18), the smoothed force records are free of vibrations from the damping of the recorded signal and the magnitude of the peak impact load is lower.

Fig. 9.22 illustrates the variation of the along–slope force for different incident wave conditions at a constant depth of 24 cm. These records refer to Tests 1 to 6. The magnitude of the impact load reduces as the wave height decreases at constant period and when the period increases for similar wave heights. Significant changes in the force records are observed as the wave period varies from 1.0 to 2.0 secs.

The results from these tests indicated that at short periods corresponding to high values of wave steepness the force records were characterized by sharp peaks superimposed on gradually varying or oscillating forces. However as the wave period increased and the wave steepness decreased, the influence of the dynamic impact loads decreased resulting in force records characterized by gradually varying forces only.

Table 9.5 refers to three tests (test, 7, 8, 9) performed on the same breakwater section at a constant water depth of 25 cm for wave periods 1.0, 1.5 and 2.0 secs respectively. At this depth approximately 80% of the instrumented armour unit was submerged (Fig. 9.16).

The characteristic features of the force traces from these three tests were consistent with those presented earlier (Test 1–6). However in comparison with Test 6, the force traces of the along–slope force corresponding to Test 9 indicated the presence of a mild impact upward component at wave period of 2.0 secs. Apart from the relative influence of the still water depth, this may have been due to the greater magnitude of the incident wave height corresponding to Test 9.

In this context it is noted that when comparing Test 5 with Test 6, peak forces were observed for the former at wave period 1.5 secs, although a greater wave height produced only a gradually varying type of force at a wave

period of 2.0 secs, corresponding to the latter. This implies that the characteristics of the force records are dependent on both the wave height and wave period.

Table 9.6 refers to six tests (Tests 10–15) performed on the same breakwater section at constant wave period of 1.0 sec with the depth varying from 23 to 28 cm in steps of 1 cm. The objective of this test series was to determine the influence of the relative position of the instrumented armour unit on the recorded force traces. For water depths 23, 24 and 25 cm the armour unit was partially submerged whereas for the other depths – 26, 27 and 28 cm – it is fully submerged (Fig. 9.16).

The force records from these tests were consistent with those observed in the previous tests and the relative magnitude of the force components were of the same order of magnitude. As the degree of submergence increases, the intensity of the impact force reduces. This is mainly due to the fact that at greater levels of submergence most of the impact energy is absorbed by the row of armour units positioned above that of the row containing the instrumented armour unit. Hence under these conditions the instrumented armour unit is not fully exposed to direct wave impact forces.

Closer examination of force records indicated that at depths of 23 and 24 cm, peak forces were observed for both lift and along–slope force corresponding to the point of impact. As the depth increased the influence of sharp peak components was greatly reduced in the lift force traces. However the along–slope force continued to exhibit peak components although their magnitude was reduced in comparison with those corresponding to values at lower depths.

The upward normal force (positive lift) remains less than the corresponding component of the submerged weight for most of the tests and only in the data obtained at water depths of 23 and 24 cm was the magnitude greater than this component.

Wave action on the breakwater section with a permeable underlayer for a wave period of 1 sec is illustrated in Plate 1.

Tables 9.7 and 9.8 refer to the tests performed with the primary armour layer resting on an impermeable underlayer. For this purpose a thin perspex sheet was introduced between the armour layer and the underlayer of the existing breakwater section. This sheet was firmly attached to the sides of the flume.

Table 9.7 refers to two series of tests performed at depths of 24 and 25 cm respectively. In each case a minimum of two wave periods was investigated. Although the force traces had similar characteristic features and were consistent with those obtained from the tests on the permeable breakwater section, it was observed that the peak force components corresponding to wave impact were more significant. These components were also present in the traces corresponding to wave periods 1.5 and 2.0 secs.

Figs. 9.24 and 9.25 represent plots of the measured variables for wave periods 1.0 and 1.5 secs. These records refer to Tests 16 and 17 respectively. Fig. 9.26 illustrates the smoothed variables corresponding to Test 16. It is evident that a close similarity exists between these records for the breakwater section with an impermeable underlayer and those corresponding to the breakwater section with a permeable underlayer (Figs. 9.18 to 9.21).

Table 9.8 refers to six tests performed on the same test section at a constant period of 1 sec. with the depth varying from 23 to 28 cm in steps of 1 cm. The results of this test series were very similar to those from the corresponding test series performed on the breakwater section. The only different feature observed relates to the upward normal (positive lift) force corresponding to depths of 27 and 28 cm. The force traces indicated the presence of comparatively high values of the positive lift force which acted on the armour unit for a longer duration than observed previously.

Closer examination of the experimental conditions revealed that corresponding to those two situations, the impermeable underlayer which consisted of a perspex sheet moved very slightly in the direction perpendicular to the slope. This was mainly due to the effects of uplift pressure forces acting on it. It was quite possible that under these conditions the underlayer came in contact with the instrumented armour unit, thus accounting for the increased upward normal (positive lift) component.

The above observation was supported by the fact that increased lift forces occurred when the water level along the slope was always below the still water level. In effect a pressure gradient develops due to the difference in water levels on either side of the impermeable underlayer, with still water depth maintained on the leeward side and the run-down level maintained on the seaward side of the structure. The uplift pressure force which acts on the underlayer will depend on the difference between the still water depth and the run-down depth. This force may prove to be critical when high values of run-down occur at a

relatively greater still water depth.

In order to study this phenomenon in detail the experiments corresponding to these two depths were repeated. It was observed that after a certain duration movement of the underlayer caused some of the armour units to be displaced from their original positions. Although the armour units were partially lifted, none was extracted from the armour layer.

Although this observation is not directly relevant to the performance of hollow block armour units placed on rockfill, it highlights one of the critical design aspects when placing such armour units on geotextiles. It is important that materials used for this purpose be firmly attached to reduce the effects of movement due to uplift pressure forces acting on them. This phenomenon is identified as breathing of the underlayer and its consequences can be particularly important when placing comparatively lightweight porous armour blocks on geotextiles. It is important to ensure that the submerged weight component of the armour units perpendicular to the slope be large enough to resist the possible movement of the underlayer. These observations also focus attention on the importance of the permeability of geotextile materials used for this type of purpose. By having a porous material the pressure build-up can be reduced to a great extent.

Table 9.9 presents a comparison of the results obtained from tests performed with and without a permeable underlayer. The corresponding tests are presented one below the other for ease of comparison. The results are presented in three sets depending on the type of investigation.

One of the main observations is that the introduction of an impermeable underlayer has not caused a significant change in either the lift force or the along-slope force. Characteristic features of the force records remain the same for both structural configurations. The only difference relates to the effects due to the movement of the impermeable underlayer which occurred under certain circumstances, as was discussed earlier.

An overall comparison of the results indicates that there exists a slight increase in the upward normal (positive lift) force when adopting an impermeable underlayer. If the analysis is based on measured data, the relative magnitude of this force component (force/component of armour weight) can be as high as 1.5 under stable conditions of the underlayer. However values of up to 3.8 were observed with the movement of the underlayer. Under these circumstances the

primary armour layer was not stable.

Apart from the two tests (Tests 25 and 26) during which certain amount of instability was observed, the primary armour layer remained stable throughout the experimental programme. All the tests were repeated and both structural configurations were exposed to wave action for a longer duration than before to investigate the presence of any instability which may occur. However, the primary armour layer remained stable throughout these tests.

With reference to the impact force components of both lift and along–slope force, the introduction of an impermeable underlayer on most of the occasions reduced the upward along–slope force component and increased the downward normal (negative lift) component. The relative magnitude of the along–slope force component has a maximum value of just over 5 for the breakwater section. The maximum value of the downward normal (negative lift) is of the order of 2.5 for the structure having an impermeable underlayer. These values are based on measured data.

These values which are based on measured data may overestimate the maximum values due to the vibrations of the transducer being superimposed on the recorded signal. In this context the corresponding values based on smoothed data represent a lower bound and may even underestimate the same. However the results from both measured and smoothed data provide an assessment of the order of magnitude of the respective force components acting on a typical hollow block armour unit under different incident wave conditions.

In order to illustrate certain characteristic features of the force components given in Tables 9.4 to 9.9, the respective components were plotted against wave steepness and water depth, the two main variables.

Figs. 9.27.a and b refer to the measured values of the positive along–slope force component plotted against wave steepness and water depth respectively. From the results for water depths of 24 and 25 cm, for which a number of data points is available, for the breakwater section, BWS, it is evident that the force component increases with increasing steepness. The maxima of the recorded force components for water depths 24 and 25 cm correspond to a wave steepness of approximately 0.06, for which value only single readings are available for water depths of 23 and 26 cm. The magnitudes of the components were approximately equal. As the depth increases the recorded values are much lower even though the wave steepness is greater than 0.07. This is due to submergence

of the unit and as the degree of submergence increases the force components are lower even at increased steepness. Most of the energy is probably absorbed by the units placed in the vicinity of the still water level. Fig. 9.27.b presents the variation in the force components for different water depths. This plot provides a clear comparison between the respective force components for the breakwater section, BWS, and that with the impermeable underlayer, IUL.

The measured values of the positive lift force component are presented in Figs. 9.28.a and b. These plots follow a similar trend to that observed in the analysis of the positive along–slope force component and can similarly be used to interpret the influence of wave steepness and the relative position of the instrumented armour unit. However, in comparison with the positive along–slope force component the magnitude of the lift force component is much lower. The very high values recorded for water depths of 27 and 28 cm refer to the conditions under which the impermeable underlayer moved due to uplift pressure and they cannot be considered valid, but this effect demonstrates an important aspect of designs involving are impermeable underlayer.

It should also be noted that when waves act on the armoured slope, the instrumented armour unit may be fully exposed during certain phases, particularly during the run–down phase. This will cause a change in the force field due to the absence of the buoyant force. In the experiments performed the datum corresponds to the still water depth. Wave–induced dynamic forces in excess of the static forces corresponding to the datum level are presented in Tables 9.4 to 9.9. Thus if the instrumented armour unit was initially submerged, an error will be present in the recorded force measurements during the phase when the armour unit is exposed. However it was observed that none of the critical design forces were present in this phase and only the maximum value of the downward along–slope force would have been affected.

In this study the downward along–slope force was not considered a critical design aspect and the force traces confirmed that impact forces were not present for this component. In the absence of such components in that direction it was evident that minimum damage would occur from possible collisions between armour units. Table 9.9 indicates that the introduction of the impermeable underlayer increased the magnitude of this force component.

The downward along–slope force acting on a hollow block armour unit can be assessed in relation to the design of the toe beam of the breakwater. For a breakwater constructed with hollow block armour units, the toe structure should

be able to withstand the downward component of the static weight of the armour units and additional wave-induced forces. In comparison with the static weight corresponding to a typical breakwater section having 8 to 10 rows of armour units, the wave-induced forces in that direction are small. In Tables 9.4 to 9.9, the relative magnitudes of the force components are expressed in terms of the submerged weight. The same ratio based on the component of static weight is smaller (by a factor of 0.56) and in this case is more relevant for analyses because the buoyant force reduces the load on the toe beam. The influence of wave-induced downward forces can be incorporated in the estimation of the overall load acting on the toe beam. The results from this study provide information on the order of magnitude of this force component.

For still water depths 23, 24 and 25 cm the instrumented armour unit is partially submerged before the commencement of the experiment and this introduces an error in the recorded force measurements when the armour unit is fully submerged during wave action. Under these conditions the measured values of the upward along-slope and the upward normal (positive lift) forces will be slightly overestimated and those corresponding to the downward normal (negative lift) force will be slightly underestimated.

This error depends on the degree of exposure at still water depth. It was observed that the degree of submergence expressed as a volumetric ratio is less than 50% only in the case corresponding to a still water depth of 23 cm. Hence this error does not introduce a significant change and for still water depths of 24 and 25 cm the calculated difference in the relative magnitude of the force measurements is less than 0.3.

With reference to the values of recorded force measurements corresponding to these depths (Table 9.9), it is evident that the magnitude of this error will not cause a serious discrepancy in the interpretation of experimental results relating to critical design forces.

In relating the model measurements to the prototype, it must be noted that hydraulic modelling of wave impact on armoured slopes is strongly influenced by the presence of scale effects. Stive (1984) reviewed some of the previous studies which have been performed on this subject. It has been observed that surface tension in a model is too large resulting in lower air absorption during wave breaking. This contributes to increased impact pressures.

The overall conclusion drawn by Stive (1984) was that the only suitable

solution for avoiding scale effects was to perform tests at approximately prototype scale with wave heights exceeding 0.5 m. However, in most cases this is not possible due to laboratory limitations and economic consideration and hence the use of hydraulic models having a scale ratio of the order of 1:30 is inevitable. Thus in order to obtain reliable information from model studies due care should be given to the influence of scale effects. This is particularly important when a critical design aspect of the prototype is underestimated due to such effects.

The instrumentation system used for this study proved to be very successful. Throughout the experimental programme the force transducer performed with a high degree of reliability exhibiting a linear response that was repeatable. The water-proof coating used to protect the strain gauges remained intact for long durations under the most severe conditions encountered in the model tests. The sensitivity of the load transducer was extremely satisfactory in that it was able to measure very small forces accurately. This was confirmed by results from a series of calibration tests performed with different conditions of static loading. The repeatability of the peak signals corresponding to wave impact forces was excellent, as illustrated earlier, Figs. 9.18 to 9.20 and Figs. 9.24 to 9.25.

9.3.5. Comparison with previous investigations

Attention is now focused on the results from some of the previous studies on wave force measurements on armour units.

Figs. 9.29 and 9.30 refer to results presented by Ligteringen (1983) and Ligteringen and Heydra (1984) on Tetrapod units. Both bending moments and acceleration measurements were monitored. The first was achieved with strain gauges instrumented in one leg of the armour unit. For the second accelerometers were used. Fig. 9.29 illustrates the peak bending moments acting on the armour unit at three different positions. It is evident that the armour units located near the still water level are subjected to heavy impact forces. Fig. 9.30 illustrates the measured acceleration, but detailed analyses of the results were not given.

Figs. 9.31. refers to some recent tests performed by Scott, Turcke, Baird and Readshaw (1987) on Dolos armour units. Both bending and torsional moments were measured by using special internal strain gauge transducers. Fig. 9.31.b presents a typical plot of the moments measured at one location and Fig. 9.31.c illustrates the variation of this response profile with the position of the instrumented armour unit. As the degree of submergence increases, the response profile changes from sharp peaks to a gradually varying type of profile having

reduced peaks. These results are consistent with the observations made in the present study.

In addition to the tests described earlier, reference is made to two investigations performed by Sigurdsson (1962) and Sandstrom (1974b). In both studies forces were measured on idealized breakwater sections consisting of spherical elements as the primary armour layer.

Sigurdsson (1962) performed tests on 1 in 1 and 1 in 3 slopes. From the measurements the forces acting on armour units were categorised in relation to different flow conditions. Sigurdsson emphasised the importance of hydraulic forces which occur under the toe of an advancing breaker or when the water is flowing out of the breakwater. Attention was also focused on the lowest level of wave retreat as an important factor in determining the distribution of hydraulic forces with depth. It was also observed that considerable impact forces occur when the breaker front strikes the capstones in a rubble mound breakwater and that the forces were directed upward and parallel to the breakwater face. The magnitude of this component was greater for mild breakwater slopes.

Sandstrom (1974b) conducted a series of experiments similar to that of Sigurdsson. Tests were performed for constant wave height of 7 cm with wave periods 0.8 and 1.0 sec respectively. The steepest slope investigated was 1 in 1.5. Sandstrom identified critical normal forces on armour units below the still water level caused by the sudden change in direction of the flow due to the interaction of the run-down with the incoming breaker. For armour units above the still water level run-up was the dominant loading mechanism for slope gradients 1 in 3 and 1 in 4.

The observations made in the present study are consistent with those of the above-described investigations on spherical elements. In particular, Sigurdsson's comments on impact forces are relevant to this study and detailed analyses of these force components for different incident wave conditions are presented in Tables 9.4 to 9.9. It is noted that the layout pattern of the primary armour layer used in the present study was similar to that used by Sigurdsson (1962) and Sandstrom (1974b). The basic difference was that hollow block armour units of cubic shape were used in place of spheres.

Fitted equation	a	b	r
$K_r = a\xi^2/(\xi^2 + b)$	0.410	22.185	0.773
$R_u/H_i = a\xi^2/(\xi^2 + b)$	1.046	1.687	0.337
$R_d/H_i = a\xi^2/(\xi^2 + b)$	0.983	9.339	0.664
$K_r = a(1 - \exp(-\xi b))$	2.293	0.157	0.711
$R_u/H_i = a(1 - \exp(-\xi b))$	9.085	0.002	0.371
$R_d/H_i = a(1 - \exp(-\xi b))$	15.114	0.010	0.326

Note:- $\xi = \tan\alpha/\sqrt{H_i/L}$

where H_i = incident wave height

L = wave length

r is a generalized correlation coefficient to assess the goodness of fit.

TABLE.9.1 EQUATIONS FOR REFLECTION, RUN-UP AND RUN-DOWN COEFFICIENTS BASED ON DATA FROM THE PRESENT STUDY

Fitted equation	a	b	r
$K_r = a\xi^2/(\xi^2 + b)$	0.510	5.020	0.705
$R_u/H_i = a\xi^2/(\xi^2 + b)$	1.537	1.412	0.450
$R_d/H_i = a\xi^2/(\xi^2 + b)$	0.757	1.985	0.564
$K_r = a(1 - \exp(-\xi b))$	4.957	0.020	0.765
$R_u/H_i = a(1 - \exp(-\xi b))$	9.108	0.016	0.349
$R_d/H_i = a(1 - \exp(-\xi b))$	9.798	0.016	0.652

Note:- $\xi = \tan\alpha/\sqrt{H_i/L}$

where H_i = incident wave height

L = wave length

r is a generalized correlation coefficient to assess the goodness of fit.

TABLE.9.2 EQUATIONS FOR REFLECTION, RUN-UP AND RUN-DOWN COEFFICIENTS BASED ON DATA FROM TESTS PERFORMED BY STICKLAND(1969)

$K_r = a(1-\exp(-\xi^{*}b))$

$R_u/H_i = a(1-\exp(-\xi^{*}b))$

$R_d/H_i = a(1-\exp(-\xi^{*}b))$

$\xi = \tan\alpha / \sqrt{H_i/L_0}$

where H_i = incident wave height

L_0 = deep water wave length

r is a generalized correlation coefficient to assess the degree of fitness

Fit and generalized correlation coefficents of the model defined for the reflection coefficient on rough, permeable slopes

Type of armour unit	a	b	r
Dolos(Wallingford)	3.999	0.020	0.83
Rubble(Sollit and Cross)	0.503	0.125	0.70
Rip-rap(Gunbak)	1.351	0.071	0.97

Fit and generalized correlation coefficents of the model defined for run-up of water on rough, permeable slopes

Type of armour unit	a	b	r
Rip-rap(Ahrens and McCartney, 1975)	1.789	0.455	0.96
Rip-rap(Gunbak, 1976)	1.451	0.523	0.81
Rubble(Dai and Kamel, in Gunbak, 1979)	1.370	0.596	0.61
Tetrapods(Jakson, in Gunbak, 1979)	0.934	0.750	0.74
Dolos(Wallingford, in Gunbak, 1979)	1.216	0.567	0.74
Quadripods(Dai and Kamel, in Gunbak, 1979)	1.538	0.248	0.86

Fit and generalized correlation coefficients of the model defined for run-down of water on rough, permeable slopes

Type of armour unit	a	b	r
Rubble (Dai and Kamel)	0.852	0.426	0.60
Rip-rap(Gunbak)	6.220	0.040	0.93
Dolos(Wallingford)	1.061	0.266	0.83
Quadripods(Dai and Kamel)	0.795	0.448	0.70

TABLE.9.3 EQUATIONS FOR REFLECTION, RUN-UP AND RUN-DOWN COEFFICIENTS (Losada and Gimenez-Curto 1981)

TABLE 9.4 RESULTS FROM BREAKWATER SECTION WITH A PERMEABLE UNDERLAYER

1 gm force = 980.665 x 10^{-5} N

Test No.	T(sec) wave period	d(cm) water depth	KEY a)mean value b)standard deviation c)coeff of variation(%) d)dimensionless ratio (relative magnitude)	Wave environment			Maximum values of force components							
							Lift(gm f) -		Slope(gm f) +		Lift(gm f) +		Slope(gm f) -	
							measured	smoothed	measured	smoothed	measured	smoothed	measured	smoothed
				H_t(cm) wave height	R_u(cm) run-up	R_d(cm) run-down	F_{lift}/W_{sl}		F_{slope}/W_{ss}		F_{lift}/W_{sl}		F_{slope}/W_{ss}	
				H_t/L	R_u/H_t	R_d/H_t								
1	1.0	24	a)	8.04	9.73	4.03	24.46	21.23	98.76	63.92	27.92	13.38	16.61	16.00
			b)	0.54	0.72	0.60	7.65	6.85	5.14	4.32	4.27	1.53	2.26	1.44
			c)	6.7	7.4	15.0	31.3	32.2	5.2	6.8	15.3	11.4	13.6	8.5
			d)	0.063	1.21	0.50	0.96	0.84	5.18	3.35	1.10	0.53	0.87	0.84
2	1.0	24	a)	6.91	7.57	4.30	30.23	20.77	90.92	62.30	17.77	11.54	19.38	13.38
			b)	0.42	0.66	0.32	5.38	3.03	9.22	2.88	6.19	1.79	1.60	0.80
			c)	6.0	8.7	7.5	17.8	14.6	10.1	4.6	34.8	15.5	8.2	6.0
			d)	0.054	1.10	0.62	1.19	0.82	4.77	3.27	0.70	0.45	1.02	0.70
3	1.0	24	a)	5.72	6.19	3.72	19.85	14.77	77.99	59.07	19.85	11.54	18.46	12.23
			b)	0.00	0.09	0.07	2.22	0.00	4.00	0.00	3.16	0.80	1.85	0.89
			c)	0.00	1.5	1.7	11.2	0.0	5.1	0.0	15.9	6.9	10.0	7.3
			d)	0.045	1.08	0.65	0.78	0.58	4.09	4.00	0.78	0.45	0.97	0.64
4	1.5	24	a)	3.63	4.80	5.04	21.23	14.77	45.23	34.77	15.07	13.23	12.92	11.38
			b)	0.14	0.05	0.14	1.41	0.00	3.49	2.24	1.97	1.27	1.51	0.69
			c)	3.8	2.2	2.7	6.6	0.00	7.7	6.4	13.1	9.6	11.7	6.00
			d)	0.017	1.32	1.39	0.84	0.58	2.37	1.82	0.59	0.52	0.68	0.60
5	1.5	24	a)	3.41	4.37	3.97	18.15	14.77	37.23	31.38	14.46	12.00	13.54	11.08
			b)	0.14	0.09	0.09	1.27	0.00	3.44	1.85	1.66	0.92	0.87	0.00
			c)	4.1	2.0	2.3	7.0	0.00	9.2	5.9	11.5	7.7	6.4	0.0
			d)	0.016	1.28	1.16	0.71	0.58	1.95	1.65	0.57	0.47	0.71	0.58
6	2.0	24	a)	4.34	3.69	3.14	16.15	14.31	18.00	16.61	12.46	11.08	13.38	12.92
			b)	0.09	0.00	0.00	0.80	0.80	0.80	0.00	1.53	0.00	1.53	0.00
			c)	2.10	0.00	0.00	4.9	5.59	4.44	0.00	12.3	0.00	11.4	0.00
			d)	0.015	0.85	0.72	0.64	0.56	0.94	0.87	0.49	0.44	0.70	0.68

TABLE 9.5 RESULTS FROM BREAKWATER SECTION WITH A PERMEABLE UNDERLAYER

1 gm force = 980.665 x 10^{-5} N

				Wave environment			Maximum values of force components							
Test No.	T(sec) wave period	d(cm) water depth	KEY a)mean value b)standard deviation c)coeff of variation(%) d)dimensionless ratio (relative magnitude)	H_t(cm) wave height	R_u(cm) run-up	R_d(cm) run-down	Lift(gm f) -		Slope(gm f) +		Lift(gm f) +		Slope(gm f) -	
							measured	smoothed	measured	smoothed	measured	smoothed	measured	smoothed
				H_t/L	R_u/H_t	R_d/H_t	F_{lift}/W_{sl}		F_{slope}/W_{ss}		F_{lift}/W_{sl}		F_{slope}/W_{ss}	
7	1.0	25	a)	8.51	9.29	4.47	21.46	17.54	105.92	58.38	25.15	7.38	32.54	21.92
			b)	0.28	0.43	0.18	0.89	1.30	6.96	3.45	3.32	0.00	3.57	0.61
			c)	3.3	4.6	4.0	4.2	7.4	6.6	5.9	13.2	0.00	10.96	2.8
			d)	0.065	1.09	0.53	0.84	0.69	5.55	3.06	0.99	0.29	1.71	1.15
8	1.5	25	a)	6.09	7.49	5.50	22.52	20.31	50.21	37.29	12.18	8.86	21.04	17.72
			b)	0.26	0.28	0.07	0.74	0.00	2.71	1.81	2.22	0.74	0.91	0.91
			c)	4.3	3.7	1.3	3.3	0.00	5.4	4.9	18.2	8.3	4.3	5.1
			d)	0.028	1.23	0.90	0.89	0.80	2.63	1.96	0.48	0.35	1.10	0.93
9	2.0	25	a)	5.98	5.61	4.06	22.15	19.94	26.21	22.89	10.71	9.97	17.35	14.77
			b)	0.09	0.25	0.00	0.00	0.74	1.38	0.91	0.74	0.91	0.91	0.00
			c)	1.5	4.5	0.0	0.0	3.7	5.3	3.9	6.9	9.1	5.2	0.0
			d)	0.020	0.94	0.68	0.87	0.78	1.38	1.20	0.42	0.39	0.91	0.77

TABLE 9.6 RESULTS FROM BREAKWATER SECTION WITH A PERMEABLE UNDERLAYER

1 gm force = 980.665 x 10^{-5} N

				Wave environment			Maximum values of force components							
Test No.	T(sec) wave period	d(cm) water depth	KEY a)mean value b)standard deviation c)coeff of variation(%) d)dimensionless ratio (relative magnitude)	H_t(cm) wave height	R_u(cm) run-up	R_d(cm) run-down	Lift(gm f) -		Slope(gm f) +		Lift(gm f) +		Slope(gm f) -	
							measured	smoothed	measured	smoothed	measured	smoothed	measured	smoothed
				H_t/L	R_u/H_t	R_d/H_t	F_{lift}/W_{sl}		F_{slope}/W_{ss}		F_{lift}/W_{sl}		F_{slope}/W_{ss}	
10	1.0	23	a)	7.88	9.88	3.48	42.69	41.76	95.53	75.46	34.61	19.15	12.69	8.54
			b)	0.21	0.28	0.18	8.28	4.97	12.06	2.68	6.31	1.29	2.34	1.29
			c)	2.7	2.8	5.2	19.4	11.9	12.6	3.6	18.2	6.71	18.5	15.0
			d)	0.062	1.25	0.44	1.68	1.64	5.01	3.96	1.36	0.75	0.67	0.45
11	1.0	24	a)	8.04	9.73	4.03	24.46	21.23	98.76	63.92	27.92	13.38	16.61	16.00
			b)	0.54	0.72	0.60	7.65	6.84	5.14	4.32	4.27	1.53	2.26	1.44
			c)	6.7	7.4	15.0	31.3	32.2	5.2	6.8	15.3	11.4	13.6	8.5
			d)	0.063	1.21	0.50	0.96	0.84	5.18	3.35	1.10	0.53	0.87	0.84
12	1.0	25	a)	7.75	8.94	4.15	35.77	16.61	104.53	56.07	21.92	7.16	27.0	21.46
			b)	0.17	0.56	0.37	7.32	1.31	8.10	2.76	4.47	0.61	2.76	0.89
			c)	2.2	6.2	8.8	20.5	7.9	7.7	4.9	20.4	8.5	10.2	4.2
			d)	0.060	1.15	0.54	1.41	0.65	5.48	2.94	0.86	0.28	1.42	1.13
13	1.0	26	a)	7.93	9.38	4.48	37.45	16.35	98.89	45.89	22.41	5.01	31.91	25.84
			b)	0.24	0.21	0.43	5.97	1.18	21.82	3.03	4.67	1.29	1.62	0.00
			c)	3.0	2.2	9.5	16.0	7.2	22.1	6.6	20.8	25.8	5.1	0.0
			d)	0.060	1.18	0.57	1.47	0.64	5.19	2.41	0.88	0.20	1.67	1.36
14	1.0	27	a)	9.41	10.39	4.30	26.11	18.72	67.25	37.18	16.09	10.81	30.85	26.63
			b)	0.34	0.26	0.39	2.50	1.83	11.08	0.65	2.74	1.83	2.14	0.91
			c)	3.6	2.5	9.1	9.6	9.6	16.5	1.7	17.0	16.9	6.9	3.4
			d)	0.071	1.10	0.46	1.03	0.74	3.53	1.95	0.63	0.43	1.62	1.40
15	1.0	28	a)	9.75	10.25	4.51	24.53	18.72	47.73	37.71	18.20	16.61	29.27	25.05
			b)	0.82	0.49	0.33	2.91	2.50	6.43	2.39	0.65	1.40	1.83	0.91
			c)	8.4	4.8	7.2	11.9	13.4	13.5	6.3	3.5	8.4	6.2	3.6
			d)	0.072	1.05	0.46	0.97	0.74	2.50	1.98	0.72	0.65	1.54	1.31

TABLE 9.7 RESULTS FROM BREAKWATER SECTION WITH AN IMPERMEABLE UNDERLAYER

1 gm force = 980.665 x 10^{-5} N

				Wave environment			Maximum values of force components							
Test No.	T(sec) wave period	d(cm) water depth	KEY a)mean value b)standard deviation c)coeff of variation(%) d)dimensionless ratio (relative magnitude)	H_t(cm) wave height	R_u(cm) run-up	R_d(cm) run-down	Lift(gm f) -		Slope(gm f) +		Lift(gm f) +		Slope(gm f) -	
							measured	smoothed	measured	smoothed	measured	smoothed	measured	smoothed
				H_t/L	R_u/H_t	R_d/H_t	F_{lift}/W_{sl}		F_{slope}/W_{ss}		F_{lift}/W_{sl}		F_{slope}/W_{ss}	
16	1.0	24	a)	9.33	11.59	6.64	33.76	17.40	69.09	52.48	37.45	21.36	21.34	16.88
			b)	1.15	1.04	1.15	9.40	6.54	6.97	5.66	6.60	0.91	1.94	1.18
			c)	12.3	9.0	17.2	27.8	37.5	10.1	10.8	17.6	4.30	9.1	7.0
			d)	0.073	1.24	0.71	1.33	0.69	3.62	2.75	1.47	0.84	1.12	0.89
17	1.5	24	a)	3.23	5.57	5.50	12.29	9.23	39.69	35.07	21.54	18.46	13.23	10.45
			b)	0.23	0.33	0.25	1.38	0.00	2.06	2.13	0.87	0.00	1.27	0.87
			c)	7.2	5.9	4.5	11.2	0.0	5.2	6.1	4.0	0.0	9.6	8.3
			d)	0.015	1.72	1.70	0.48	0.36	2.08	1.84	0.85	0.73	0.69	0.55
18	1.0	25	a)	8.94	11.12	6.80	42.20	22.41	61.71	44.04	18.99	13.18	30.85	25.32
			b)	0.94	0.57	0.79	4.35	3.33	3.10	4.98	2.14	1.18	2.14	0.83
			c)	10.5	5.1	11.6	10.3	14.9	5.0	11.3	11.3	8.9	6.9	3.3
			d)	0.069	1.25	0.76	1.66	0.88	3.24	2.31	0.75	0.52	1.62	1.33
19	1.5	25	a)	6.40	10.82	8.06	45.84	15.69	71.07	40.61	19.38	15.07	28.92	25.54
			b)	0.20	0.41	0.09	4.45	1.77	4.86	1.07	2.32	0.69	0.87	0.69
			c)	3.2	3.8	1.1	9.7	11.3	6.8	2.6	12.0	4.6	3.0	2.7
			d)	0.029	1.69	1.26	1.80	0.62	3.73	2.13	0.76	0.59	1.52	1.34
20	2.0	25	a)	6.92	9.23	6.09	36.92	19.38	60.92	43.38	18.46	13.38	24.46	20.77
			b)	0.50	1.08	0.13	5.98	0.92	3.92	2.77	2.61	0.80	0.80	1.53
			c)	7.2	11.7	2.1	16.2	4.8	6.4	6.4	14.1	6.0	3.3	7.4
			d)	0.023	1.33	0.88	1.45	0.76	3.2	2.28	0.73	0.53	1.28	1.09

TABLE 9.8 RESULTS FROM BREAKWATER SECTION WITH AN IMPERMEABLE UNDERLAYER

1 gm force = 980.665 x 10^{-5} N

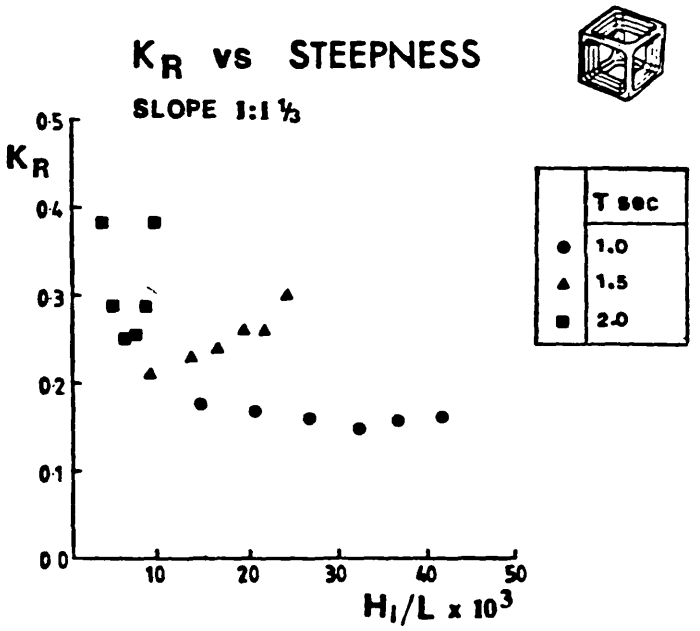
Test No.	T(sec) wave period	d(cm) water depth	KEY a)mean value b)standard deviation c)coeff of variation(%) d)dimensionless ratio (relative magnitude)	Wave environment			Maximum values of force components							
				H_t(cm) wave height	R_u(cm) run-up	R_d(cm) run-down	Lift(gm f) -		Slope(gm f) +		Lift(gm f) +		Slope(gm f) -	
							measured	smoothed	measured	smoothed	measured	smoothed	measured	smoothed
				H_t/L	R_u/H_t	R_d/H_t	F_{lift}/W_{sl}		F_{slope}/W_{ss}		F_{lift}/W_{sl}		F_{slope}/W_{ss}	
21	1.0	23	a)	7.61	10.62	6.51	22.68	18.46	75.42	60.13	29.54	24.00	16.88	13.71
			b)	0.43	0.52	0.42	3.66	5.22	4.78	3.40	0.99	1.40	0.65	1.34
			c)	5.6	4.9	6.4	16.1	28.3	6.3	5.7	3.3	5.8	3.8	9.8
			d)	0.060	1.39	0.85	0.89	0.73	3.96	3.15	1.16	0.94	0.89	0.72
22	1.0	24	a)	9.33	11.59	6.64	33.76	17.40	69.09	52.48	37.45	21.36	21.34	16.88
			b)	1.15	1.04	1.15	9.40	6.54	6.97	5.66	6.60	0.91	1.94	1.18
			c)	12.3	9.0	17.2	27.8	37.5	10.1	10.8	17.6	4.3	9.1	7.0
			d)	0.073	1.24	0.71	1.33	0.69	3.62	2.75	1.47	0.84	1.12	0.89
23	1.0	25	a)	8.94	11.12	6.80	42.20	22.41	61.71	44.04	18.99	13.18	30.85	25.32
			b)	0.94	0.57	0.79	4.35	3.33	3.10	4.98	2.14	1.18	2.14	0.83
			c)	10.5	5.1	11.6	10.3	14.9	5.0	11.3	11.3	8.9	6.9	3.3
			d)	0.069	1.25	0.76	1.66	0.88	3.24	2.31	0.75	0.52	1.62	1.33
24	1.0	26	a)	10.38	11.86	6.17	50.1	23.21	65.13	40.08	31.38	24.26	36.13	31.64
			b)	0.53	0.38	0.34	5.07	2.58	4.49	4.27	2.96	1.54	0.91	1.18
			c)	5.1	3.2	5.5	10.1	11.1	6.9	10.6	9.4	6.3	2.5	3.7
			d)	0.079	1.14	0.59	1.97	0.91	3.41	2.1	1.23	0.95	1.9	1.66
25	1.0	27	a)	11.49	12.73	6.80	63.54	23.21	56.44	30.85	57.75	54.32	46.94	37.45
			b)	0.64	0.39	0.75	5.30	3.40	5.02	2.56	3.91	2.58	2.77	0.83
			c)	5.5	3.1	11.1	8.3	14.6	8.9	8.3	6.8	4.7	5.9	2.2
			d)	0.086	1.11	0.59	2.50	0.91	2.96	1.62	2.27	2.14	2.46	1.96
26	1.0	28	a)	10.83	13.07	5.43	63.55	17.67	56.17	27.16	97.32	94.15	49.05	37.98
			b)	0.61	0.79	0.31	7.64	3.25	14.6	1.62	7.56	9.46	4.29	1.34
			c)	5.7	6.1	5.7	12.0	18.4	26.0	6.0	7.8	10.0	8.7	3.5
			d)	0.080	1.21	0.50	2.5	0.7	2.95	1.42	3.83	3.70	2.57	1.99

TABLE 9.9 COMPARISON OF RESULTS FROM BREAKWATER SECTIONS WITH AND WITHOUT A PERMEABLE UNDERLAYER

				Wave environment			Maximum values of force components							
Test No.	T(sec) wave period	d(cm) water depth	BWS-break water section IUL-impermeable underlayer	wave height H_t/L	run-up R_u/H_t	run-down R_d/H_t	Lift(gm f) -		Slope(gm f) +		Lift(gm f) +		Slope(gm f) -	
							measured	smoothed	measured	smoothed	measured	smoothed	measured	smoothed
							F_{lift}/W_{sl} (rel. mag.)		F_{slope}/W_{ss} (rel. mag.)		F_{lift}/W_{sl} (rel. mag.)		F_{slope}/W_{ss} (rel. mag.)	
GROUP (1)														
1	1.0	24	BWS	0.063	1.21	0.50	0.96	0.84	5.18	3.35	1.10	0.53	0.87	0.84
16	1.0	24	IUL	0.073	1.24	0.71	1.33	0.69	3.62	2.75	1.47	0.84	1.12	0.89
5	1.5	24	BWS	0.016	1.28	1.16	0.71	0.58	1.95	1.65	0.57	0.47	0.71	0.58
17	1.5	24	IUL	0.015	1.72	1.70	0.48	0.36	2.08	1.84	0.85	0.73	0.69	0.55
GROUP (2)														
7	1.0	25	BWS	0.065	1.09	0.53	0.84	0.69	5.55	3.06	0.99	0.29	1.71	1.15
18	1.0	25	IUL	0.069	1.25	0.76	1.66	0.88	3.24	2.31	0.75	0.52	1.62	1.33
8	1.5	25	BWS	0.028	1.23	0.90	0.89	0.80	2.63	1.96	0.48	0.35	1.10	0.93
19	1.5	25	IUL	0.029	1.69	1.26	1.80	0.62	3.73	2.13	0.76	0.59	1.52	1.34
9	2.0	25	BWS	0.020	0.94	0.68	0.87	0.78	1.38	1.20	0.42	0.39	0.91	0.77
20	2.0	25	IUL	0.023	1.33	0.88	1.45	0.76	3.20	2.28	0.73	0.53	1.28	1.09
GROUP (3)														
10	1.0	23	BWS	0.062	1.25	0.44	1.68	1.64	5.01	3.96	1.36	0.75	0.67	0.45
21	1.0	23	IUL	0.060	1.39	0.85	0.89	0.73	3.96	3.15	1.16	0.94	0.89	0.72
11	1.0	24	BWS	0.063	1.21	0.50	0.96	0.84	5.18	3.35	1.10	0.53	0.87	0.84
22	1.0	24	IUL	0.073	1.24	0.71	1.33	0.69	3.62	2.75	1.47	0.84	1.12	0.89
12	1.0	25	BWS	0.060	1.15	0.54	1.41	0.65	5.48	2.94	0.86	0.28	1.42	1.13
23	1.0	25	IUL	0.069	1.25	0.76	1.66	0.88	3.24	2.31	0.75	0.52	1.62	1.33
13	1.0	26	BWS	0.060	1.18	0.57	1.47	0.64	5.19	2.41	0.88	0.20	1.67	1.36
24	1.0	26	IUL	0.079	1.14	0.59	1.97	0.91	3.42	2.10	1.23	0.95	1.90	1.66
14	1.0	27	BWS	0.071	1.10	0.46	1.03	0.74	3.53	1.95	0.63	0.43	1.62	1.40
25	1.0	27	IUL	0.086	1.11	0.59	2.50	0.91	2.96	1.62	2.27	2.14	0.46	1.96
15	1.0	28	BWS	0.072	1.05	0.46	0.97	0.74	2.50	1.98	0.72	1.65	1.54	1.31
26	1.0	28	IUL	0.080	1.21	0.50	2.50	0.70	2.95	1.42	3.83	3.70	2.57	1.99

FIG.9.1 RESULTS FROM COB ARMOUR UNITS

(regular arrangement)



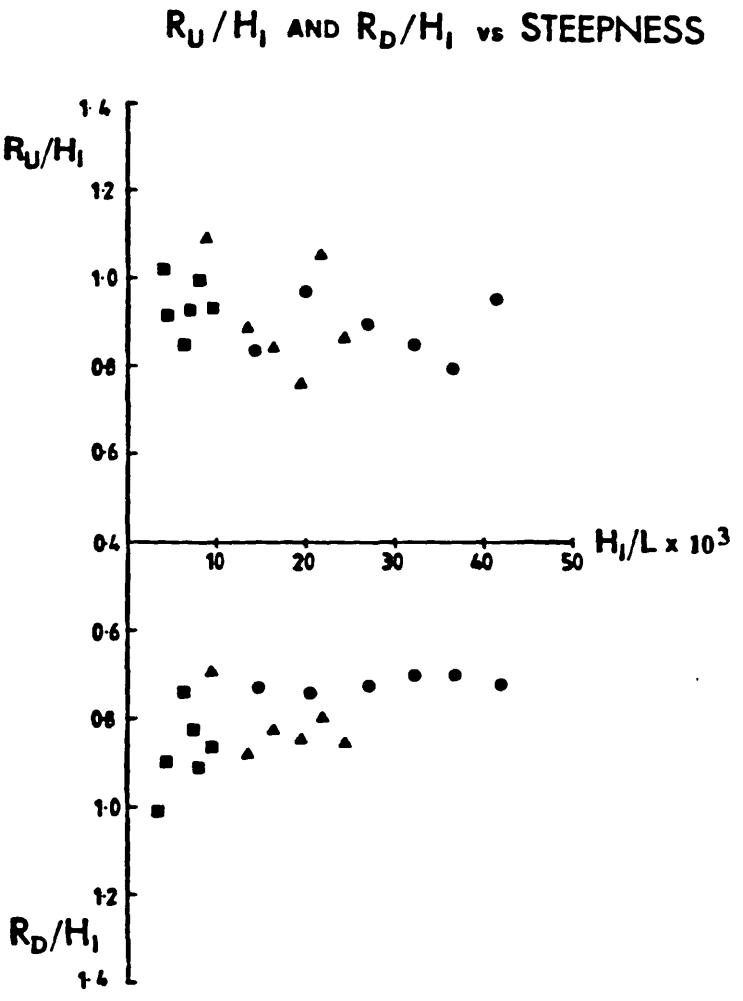
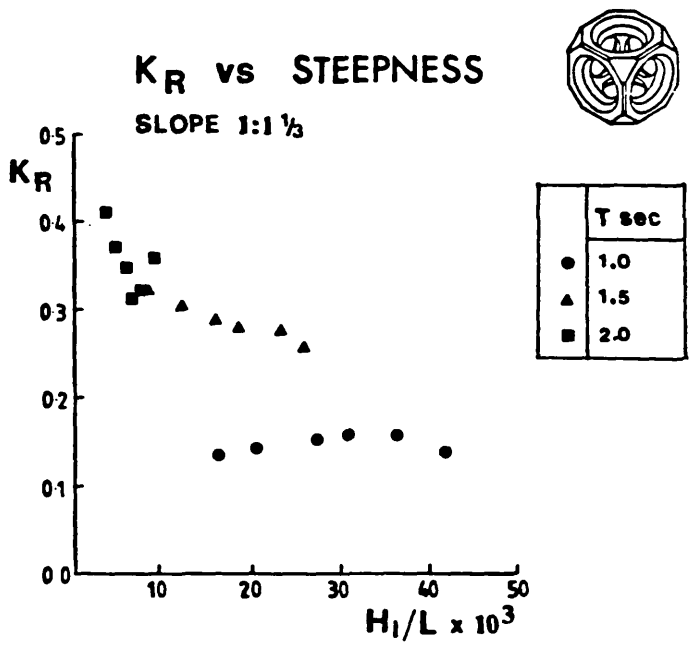


FIG.9.2 RESULTS FROM SHED ARMOUR UNITS

(regular arrangement)



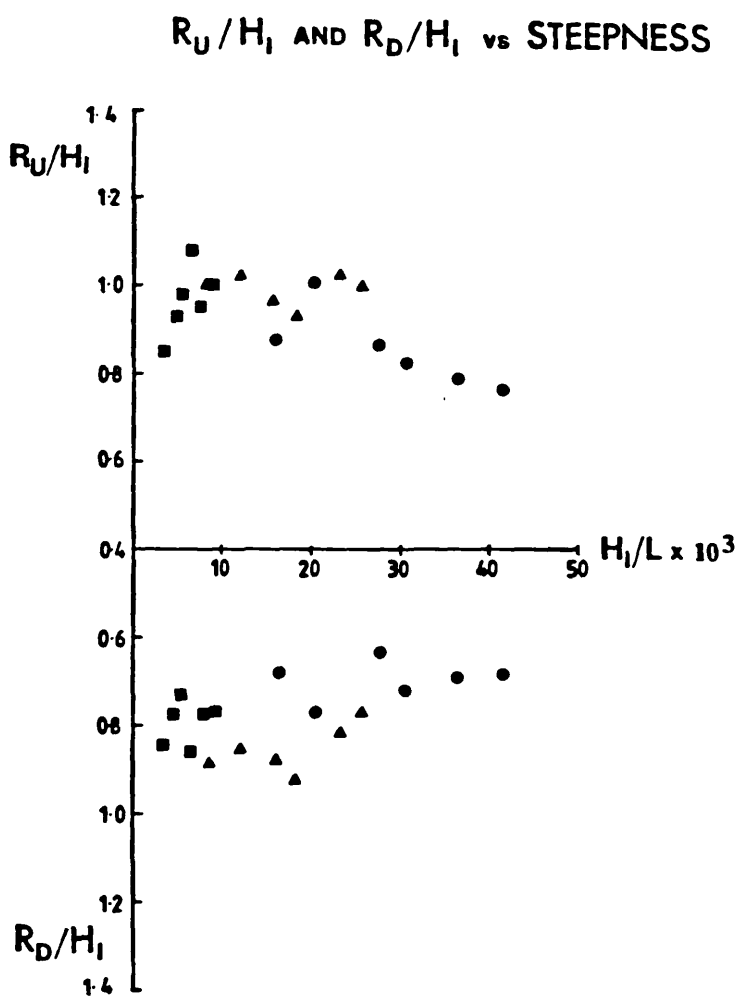
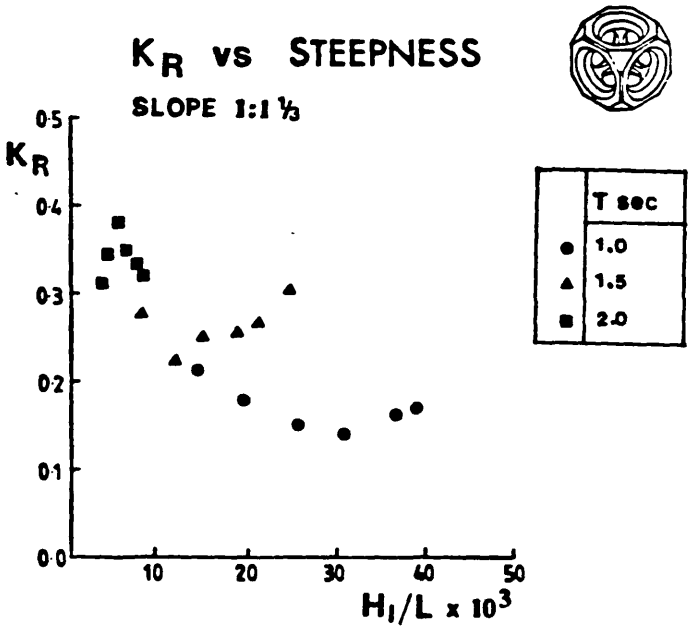


FIG.9.3 RESULTS FROM SHED ARMOUR UNITS

(staggered arrangement)



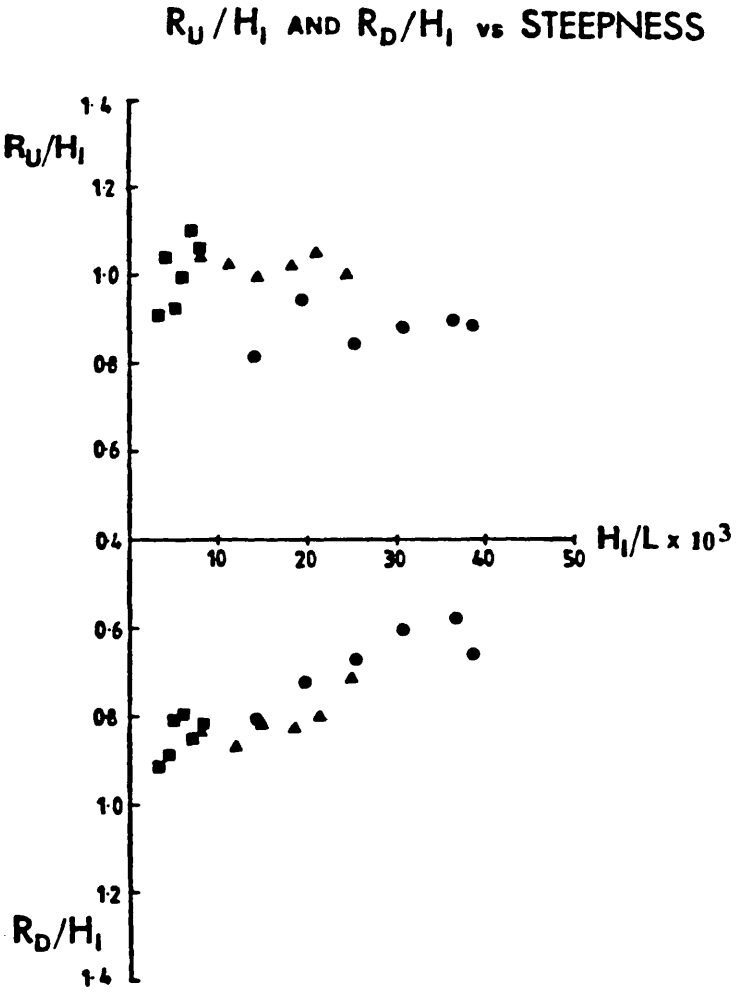
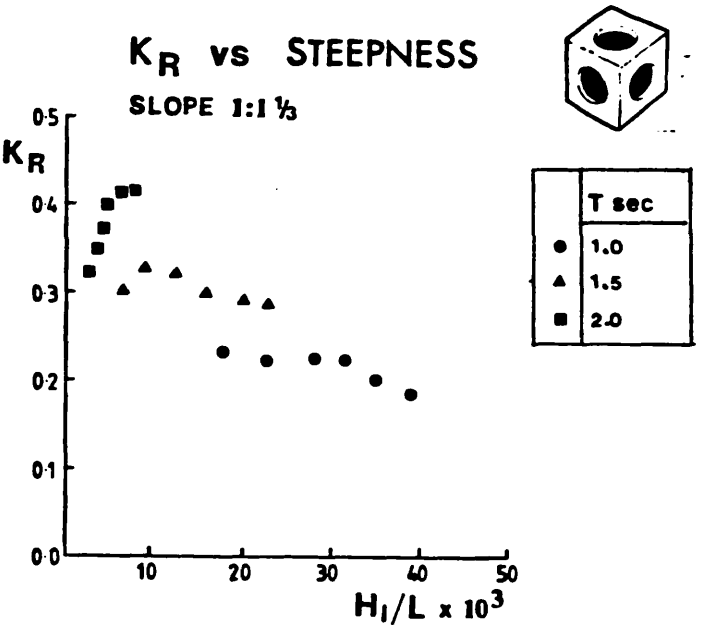


FIG.9.4 RESULTS FROM HOBO ARMOUR UNITS

HOBO (16 mm) UNITS (regular arrangement)



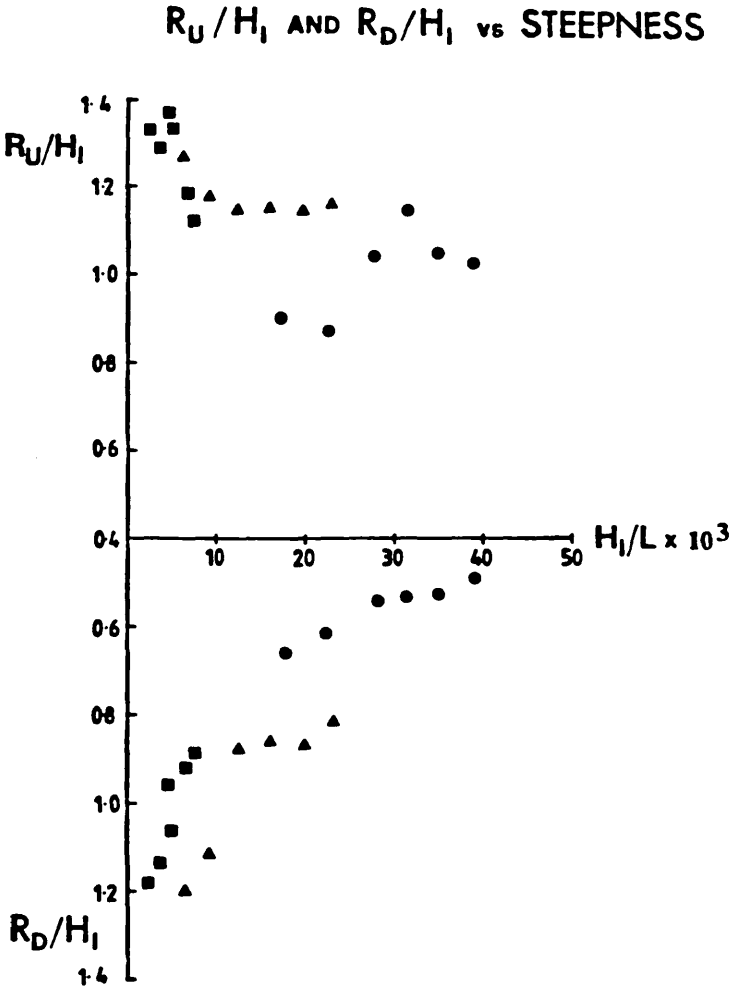


FIG.9.5 RESULTS FROM HOBO ARMOUR UNITS

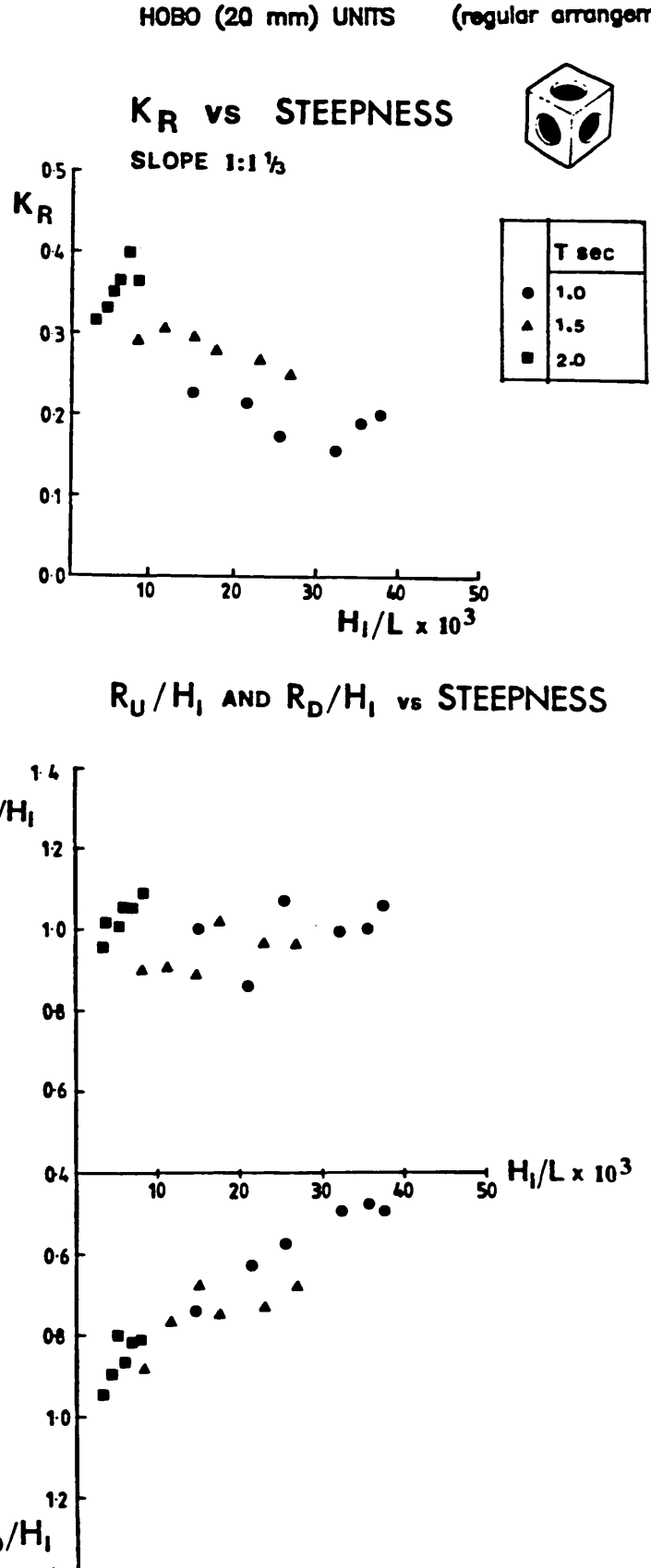
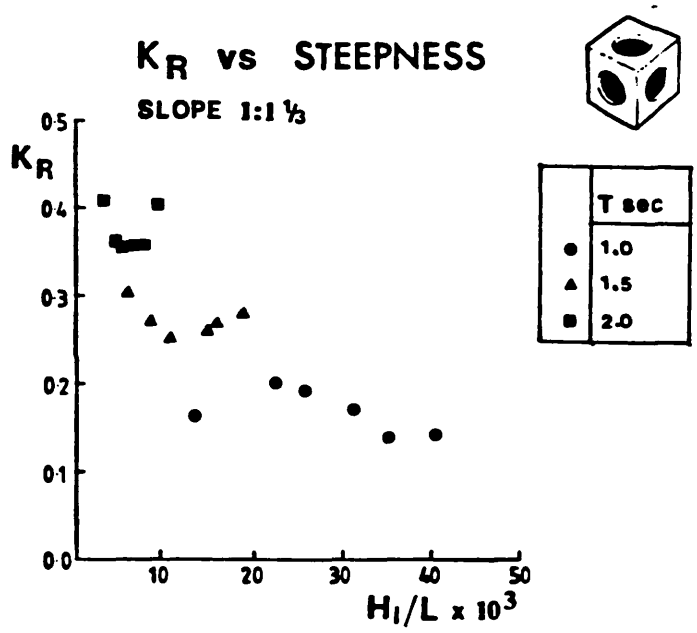


FIG.9.6 RESULTS FROM HOBO ARMOUR UNITS

HOBO (25 mm) UNITS (regular arrangement)



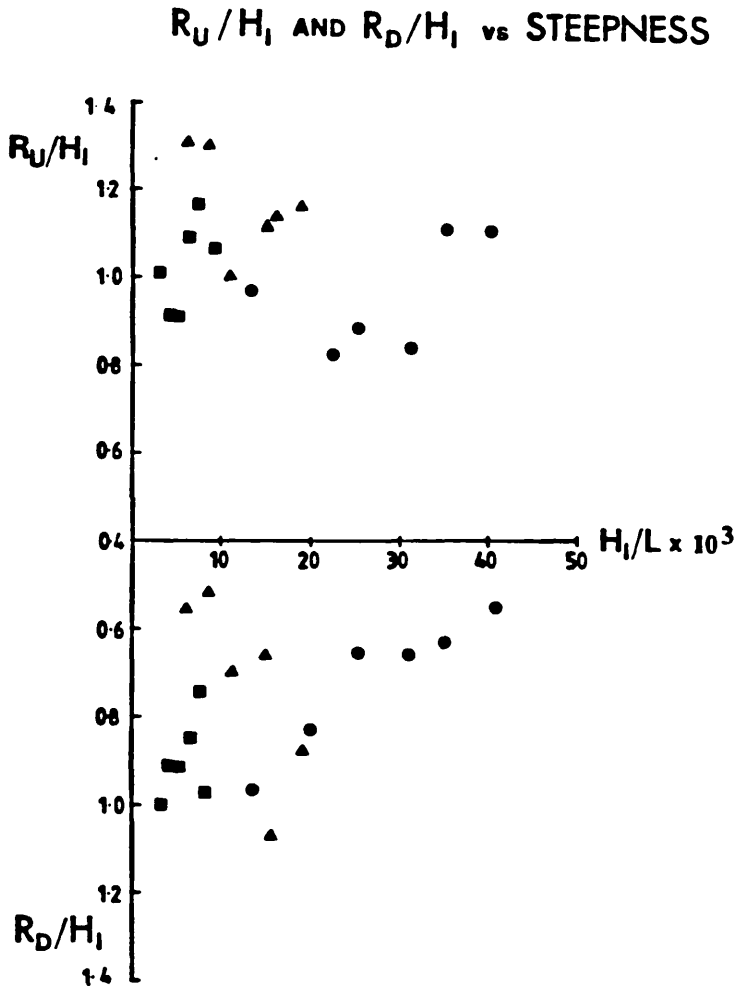
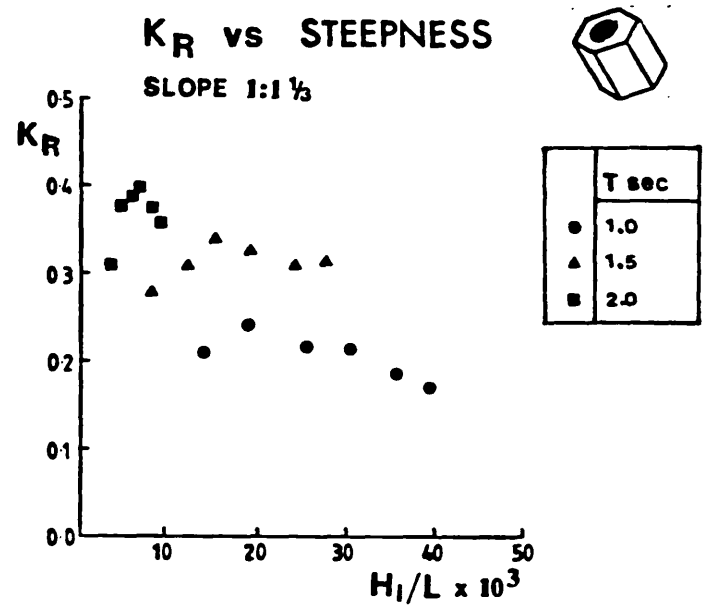


FIG.9.7 RESULTS FROM HEXO ARMOUR UNITS



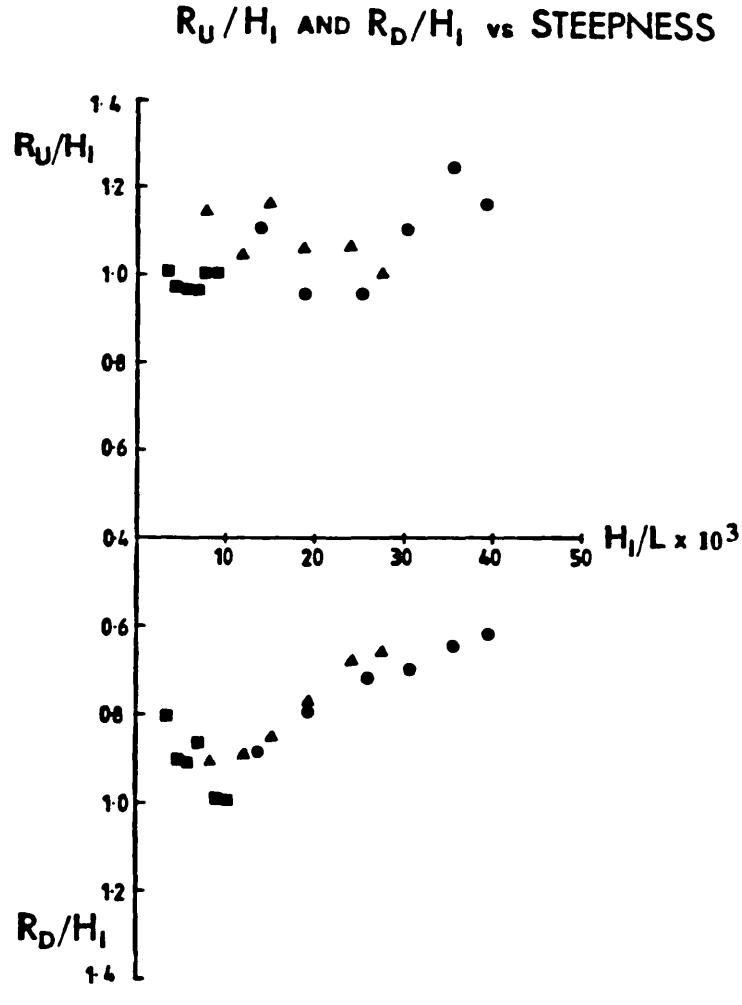
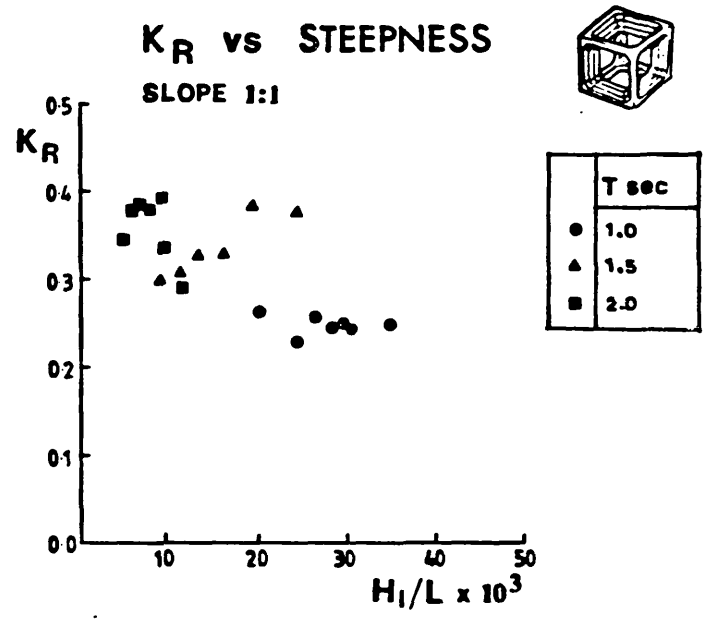


FIG.9.8 RESULTS FROM POROUS TRAPEZOID

CONSISTING OF COB UNITS



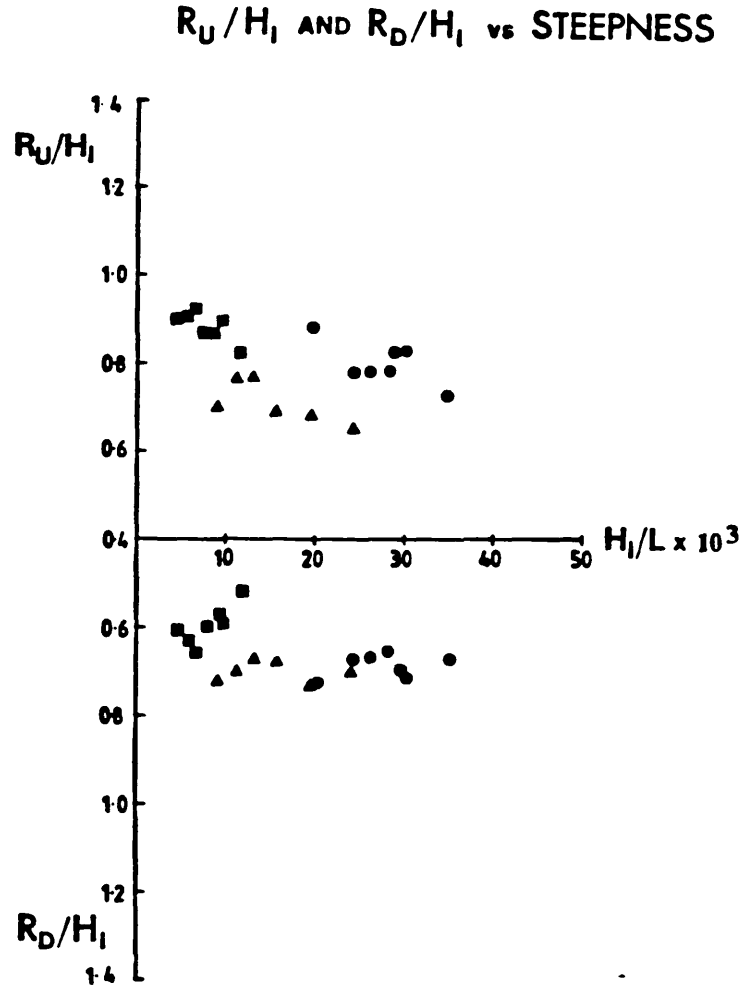


FIG.9.9 K_R vs tan α /(H_i/L)**0.5

FOR SLOPES (1:1 1/3) OF VARYING ARMOUR

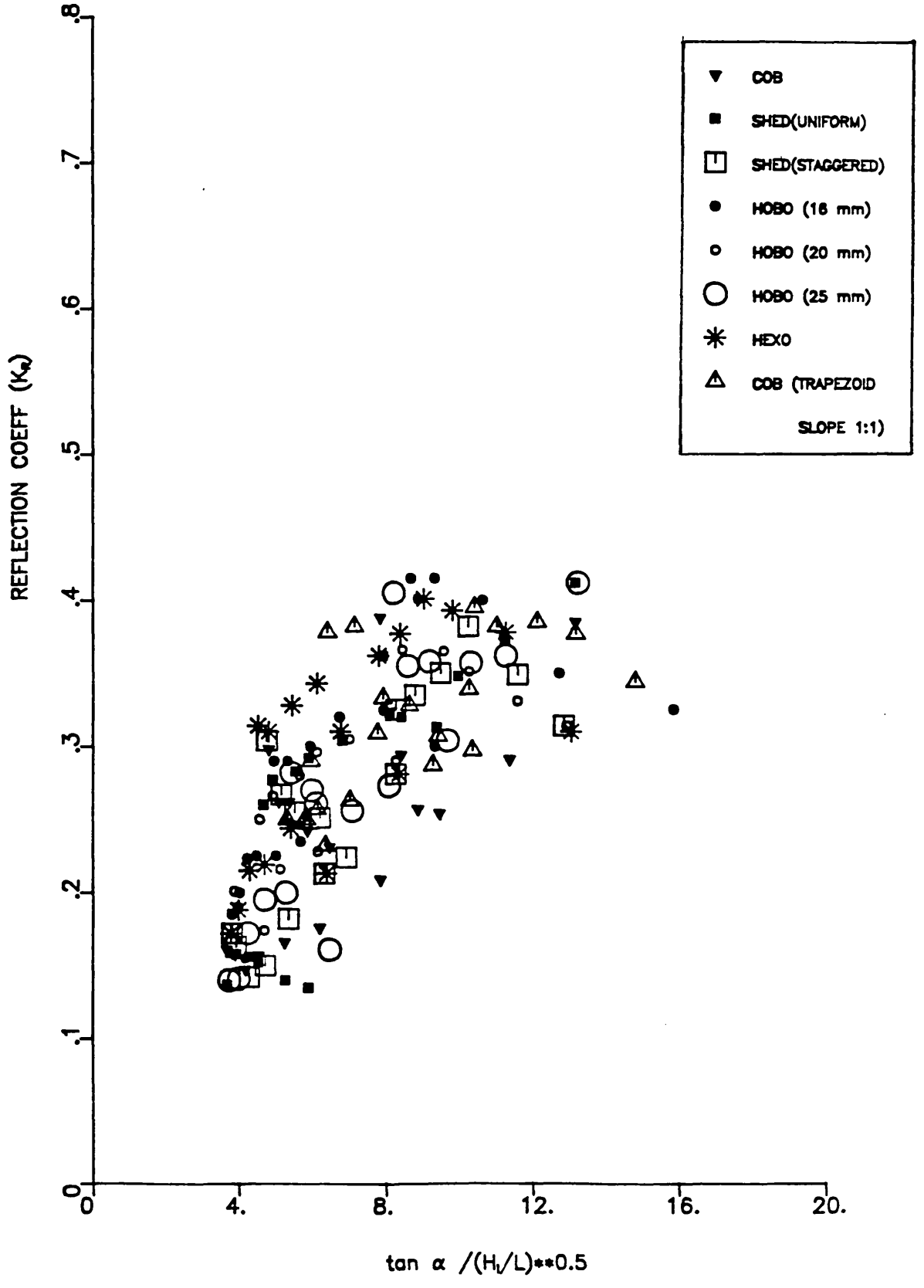


FIG.9.10 R_u/H_i vs $\tan\alpha/(H_i/L)^{**}0.5$

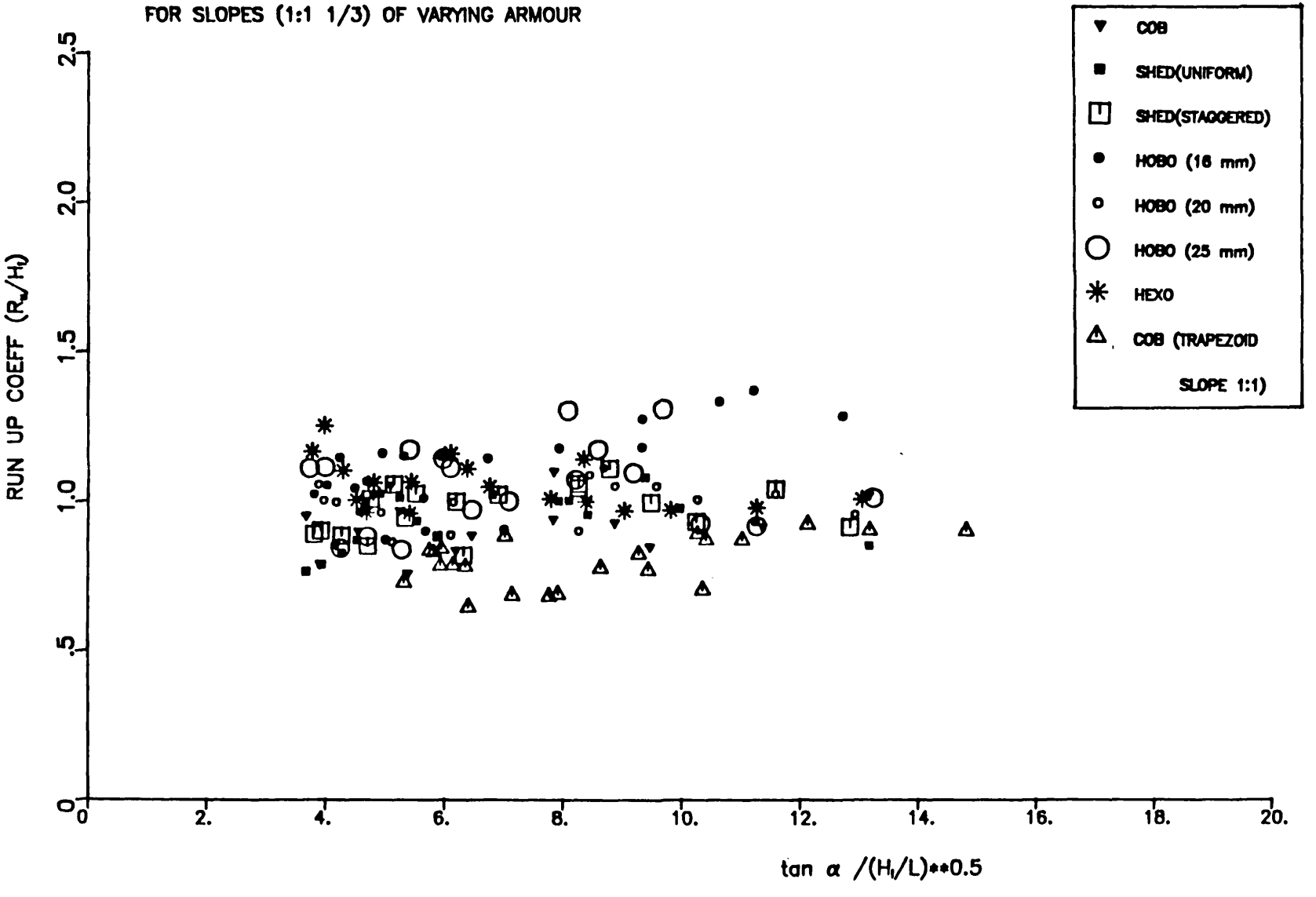


FIG.9.11 R_d/H_i vs tan α /(H_i/L)**0.5

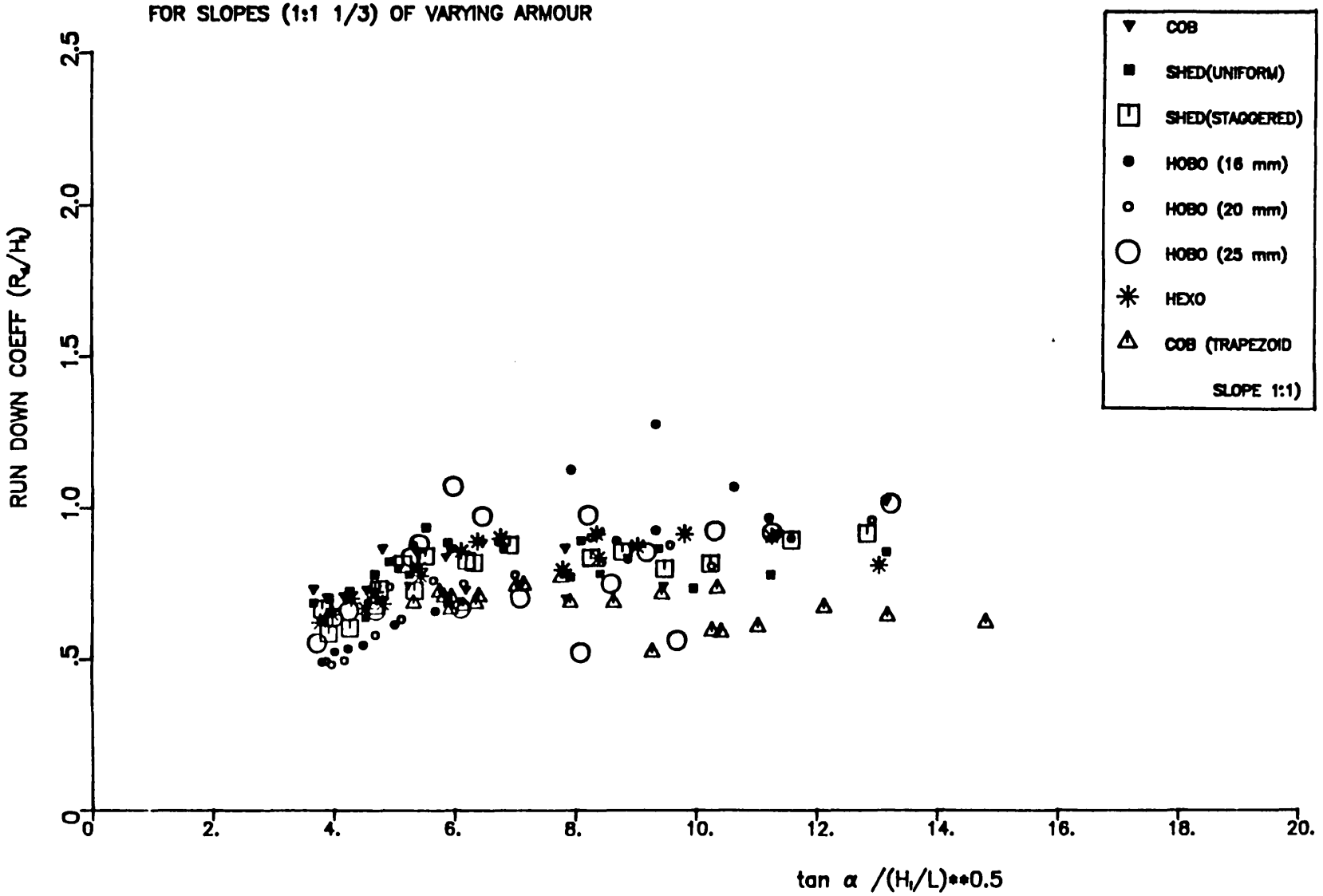


FIG.9.12.A K_R vs TAN α/ $(H_i/L)^{**}0.5$

FOR SLOPES CONSISTING OF COBS

SLOPES 1:1 1/3 , 1:1 1/2 , 1:2 , 1:2 1/2

Re-analysis of Stickland(1969)

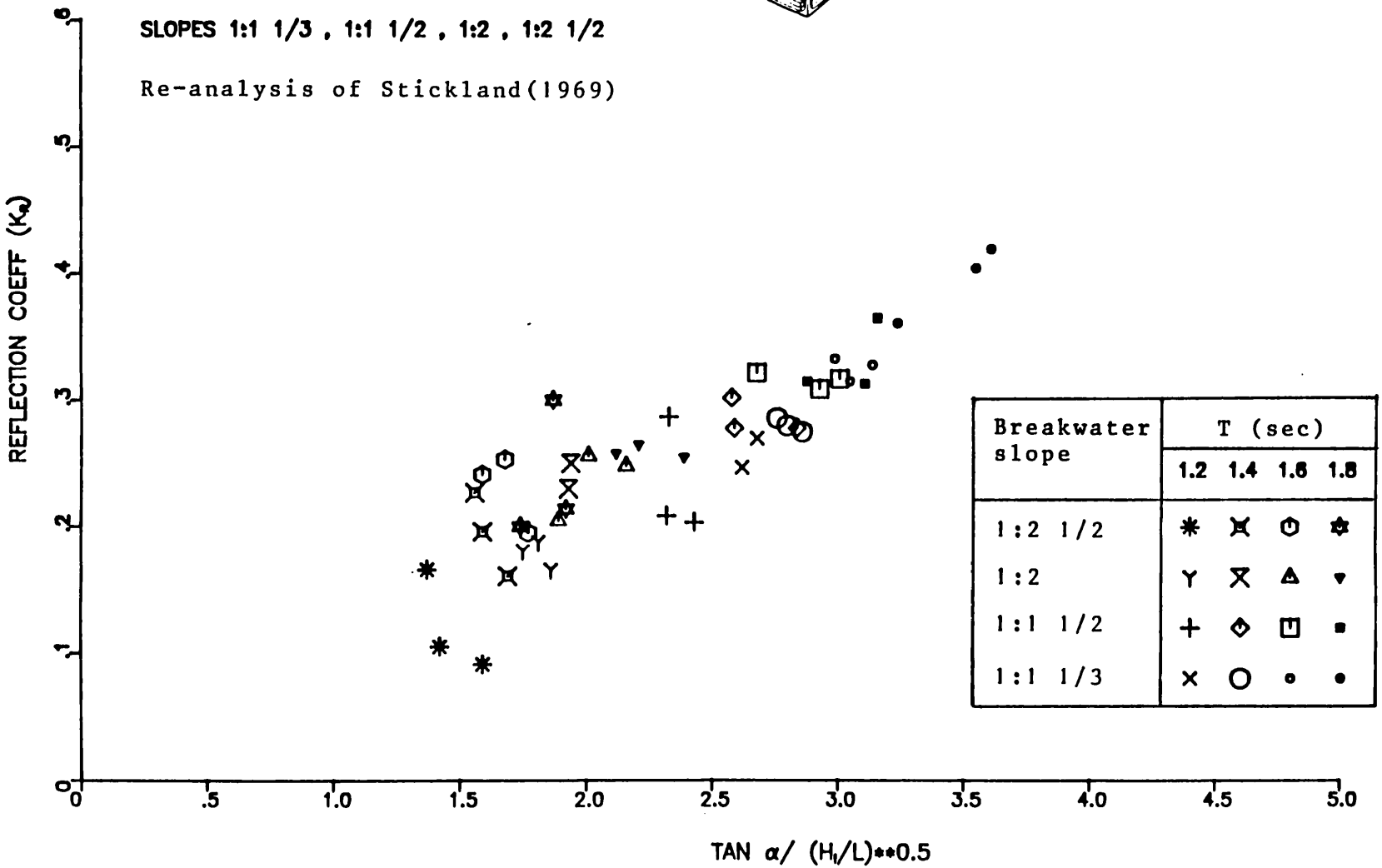


FIG.9.12.B K_r vs tan α /(H_i/L)**0.5

FOR BREAKWATER SLOPE AND COMPLETE SECTION (1:1 1/3)

Re-analysis of Stickland (1969)

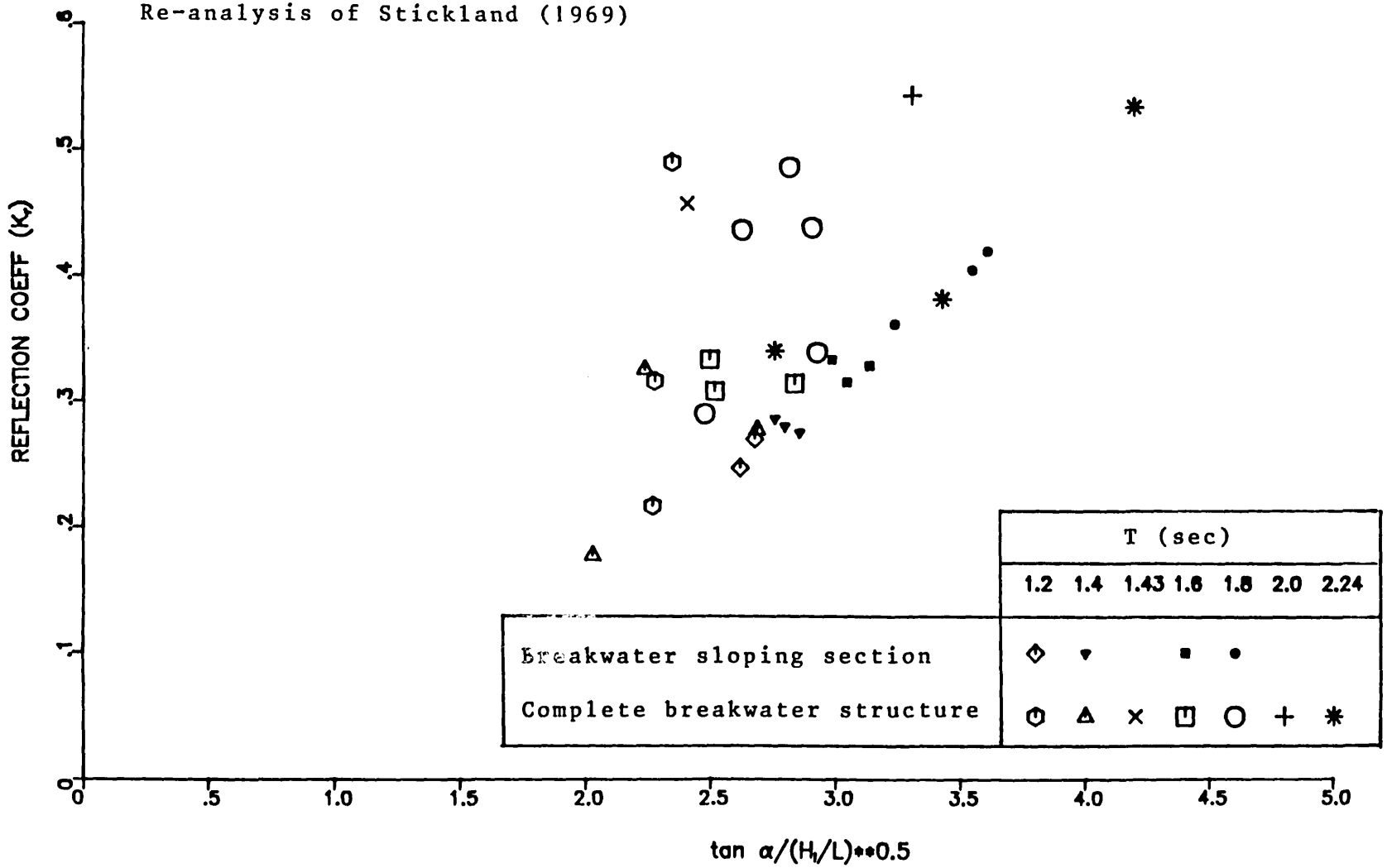


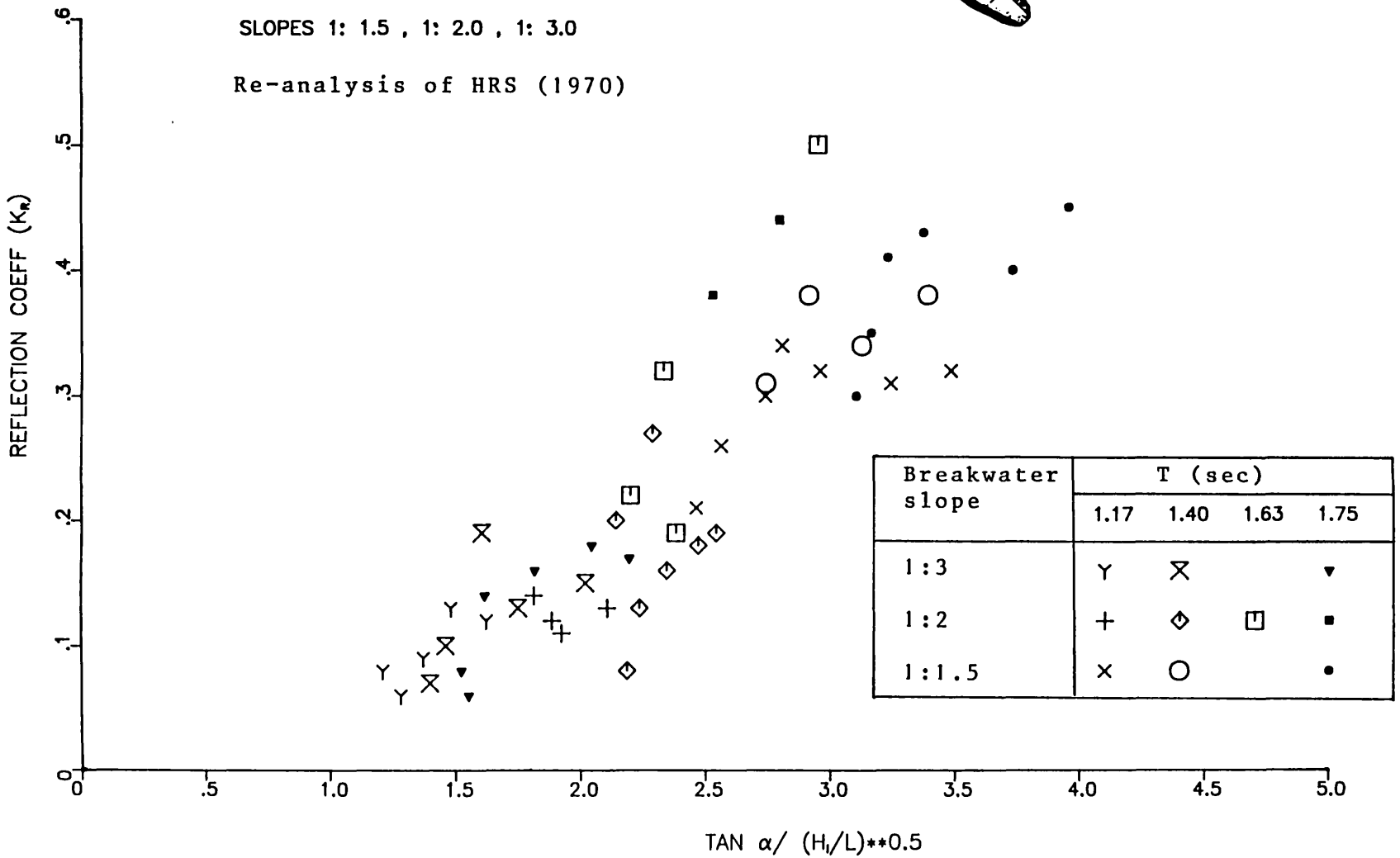
FIG.9.12.C K_R vs TAN α/ (H_I/L)**0.5

FOR SLOPES CONSISTING OF DOLOS ARMOUR UNITS

SLOPES 1: 1.5 , 1: 2.0 , 1: 3.0

Re-analysis of HRS (1970)





Breakwater slope	T (sec)			
	1.17	1.40	1.63	1.75
1:3	Y	⊠		▼
1:2	+	◇	□	■
1:1.5	×	○		●

FIG.9.13 R_u/H_1 vs tan α /(H_1/L)**0.5

FOR SLOPES CONSISTING OF COBS

SLOPES 1:1 1/3, 1:1 1/2, 1:2, 1:2 1/2

Re-analysis of Stickland (1969)

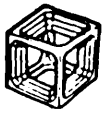


FIG.9.14 R_d/H_1 vs tan $\alpha/(H_1/L)^{**}0.5$

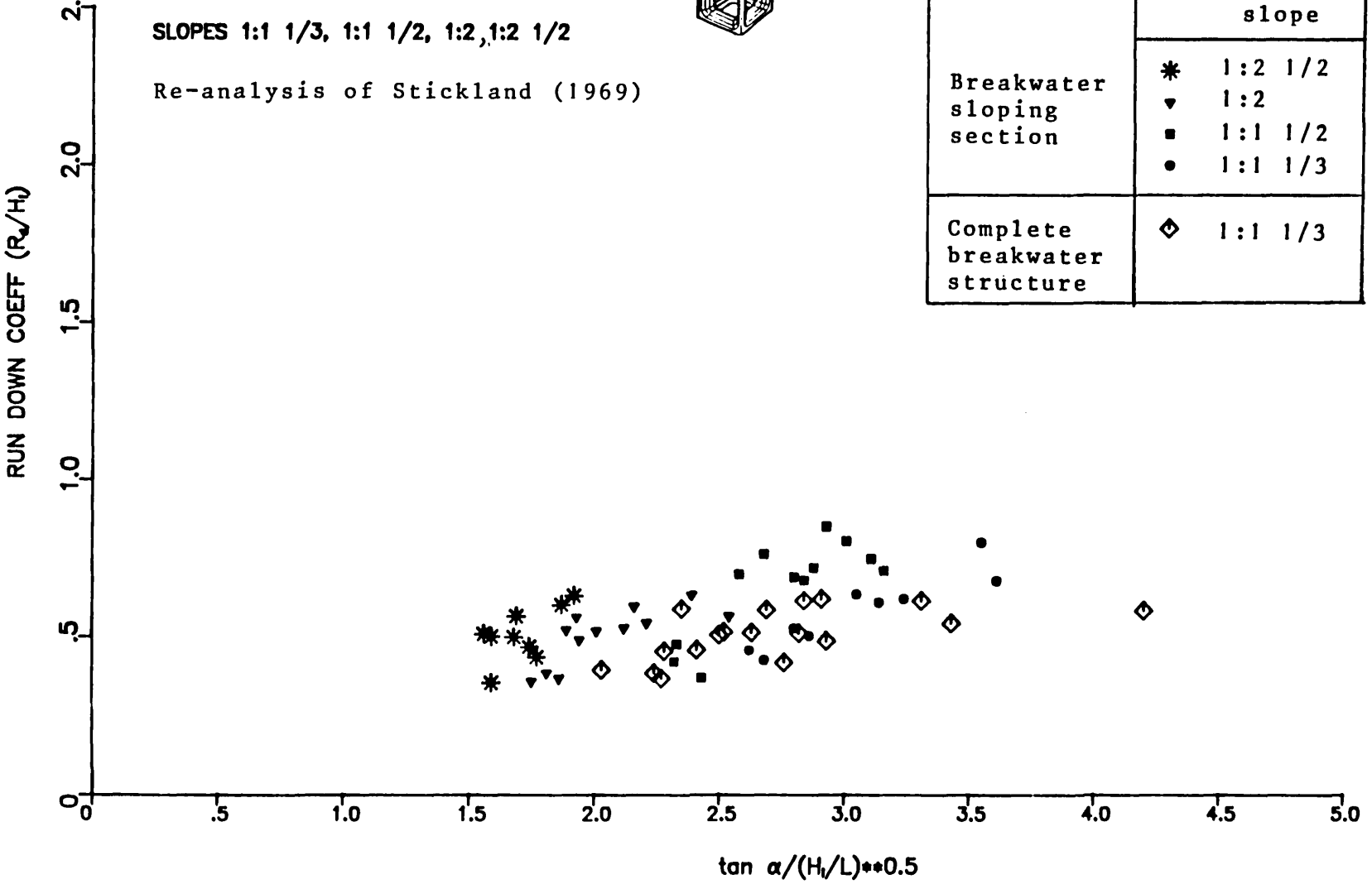
FOR SLOPES CONSISTING OF COBS

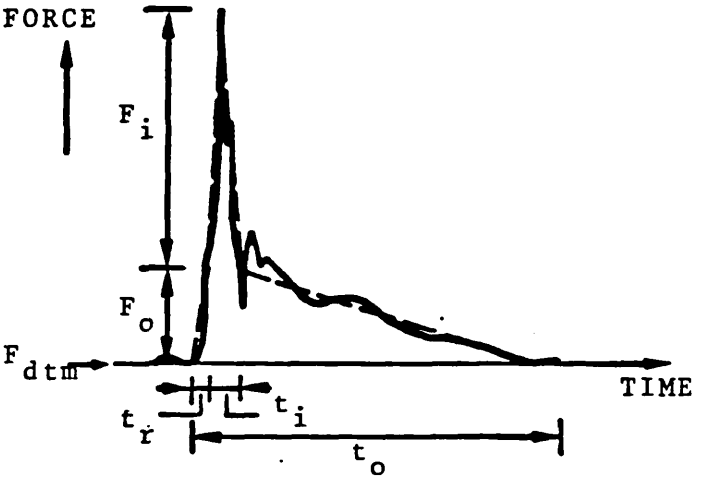
SLOPES 1:1 1/3, 1:1 1/2, 1:2, 1:2 1/2

Re-analysis of Stickland (1969)



	slope
Breakwater sloping section	✱ 1:2 1/2 ▼ 1:2 ■ 1:1 1/2 ● 1:1 1/3
Complete breakwater structure	◈ 1:1 1/3





F_{dtm} =force corresponding to still water depth (datum force)

F_o =gradually varying or quasi-static force

F_i =impact force (in excess of F_o)

t_r =rising time of F_o

t_i =impact duration

t_o =duration of gradually varying force

FIG.9.15 TYPICAL SCHEMATIZATION OF TIME-DEPENDENT WAVE IMPACT FORCES BY PERIODIC WATER WAVES (after Stive 1984)

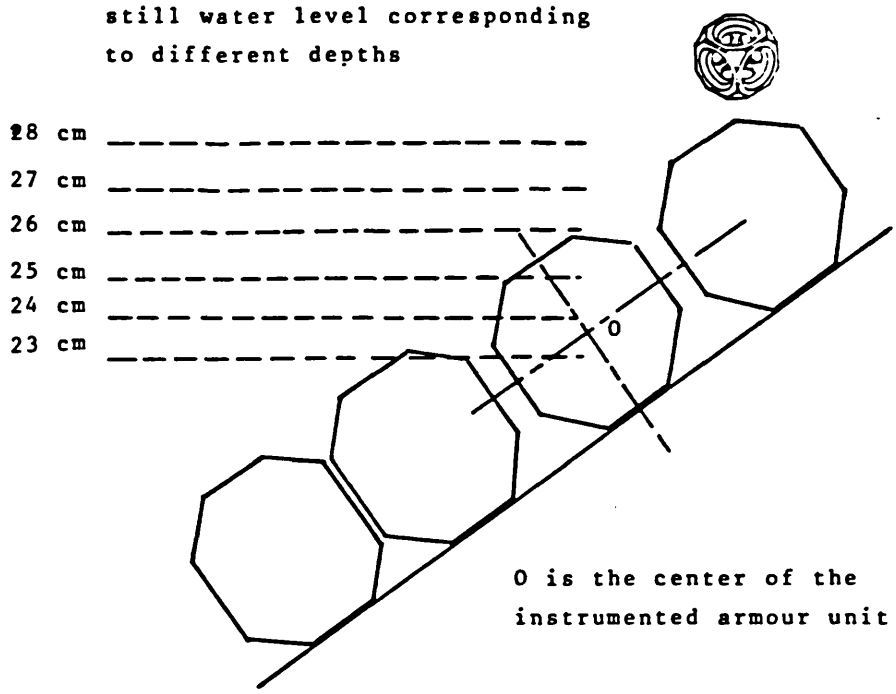


FIG.9.16 POSITION OF THE INSTRUMENTED ARMOUR UNIT FOR VARYING DEPTH

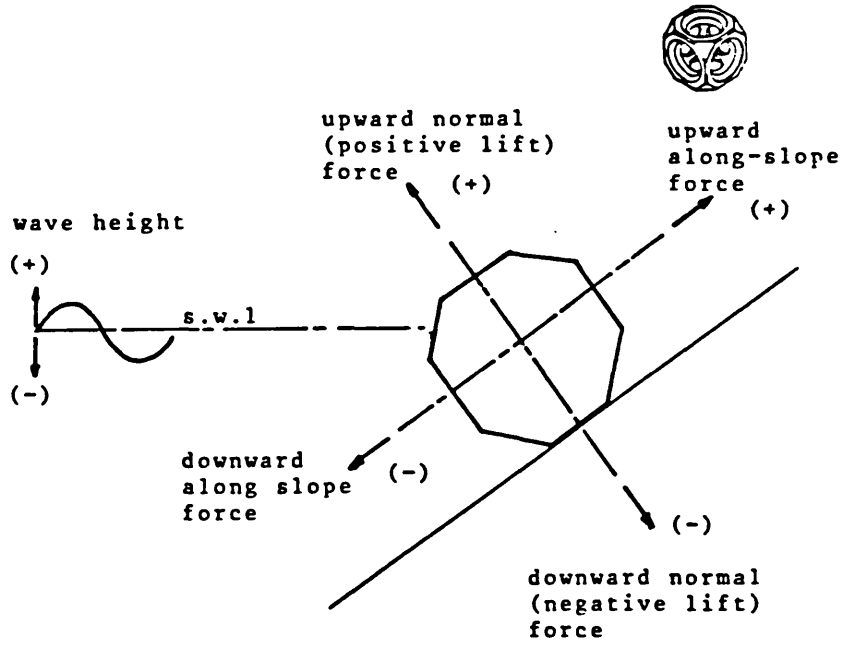
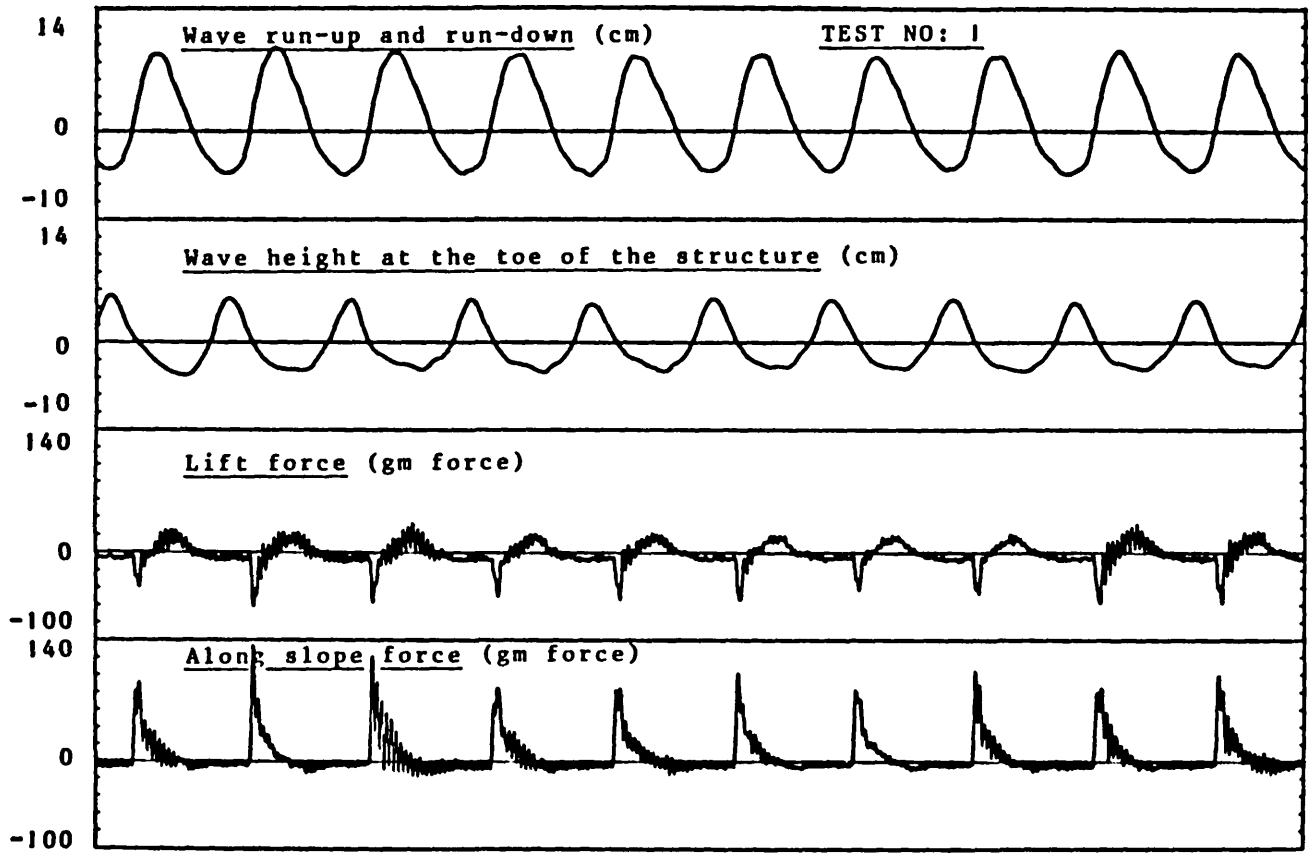


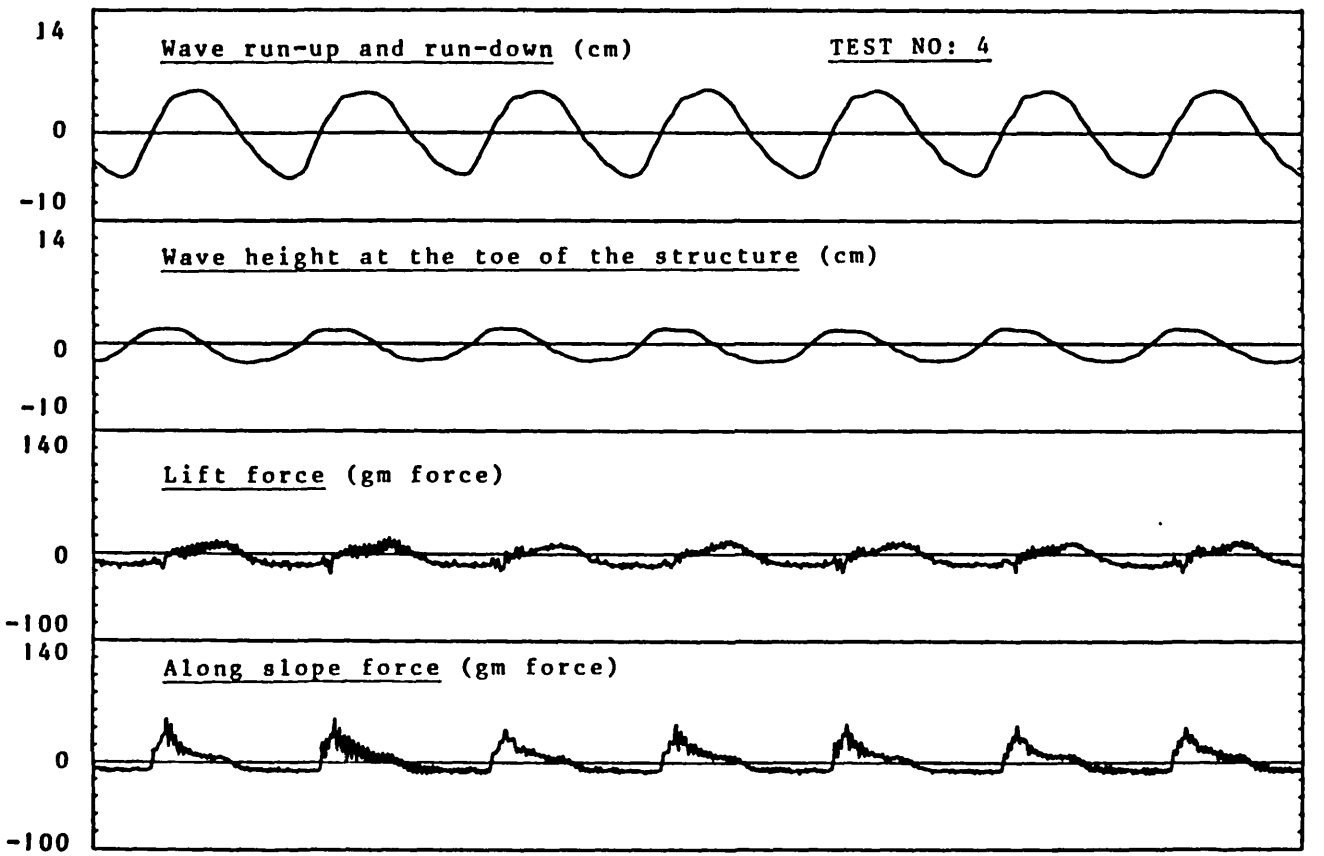
FIG.9.17. SIGN CONVENTION FOR WAVE HEIGHT AND FORCE MEASUREMENTS



For breakwater section with a permeable underlayer
T=1.0 sec , H_t=8.04 cm

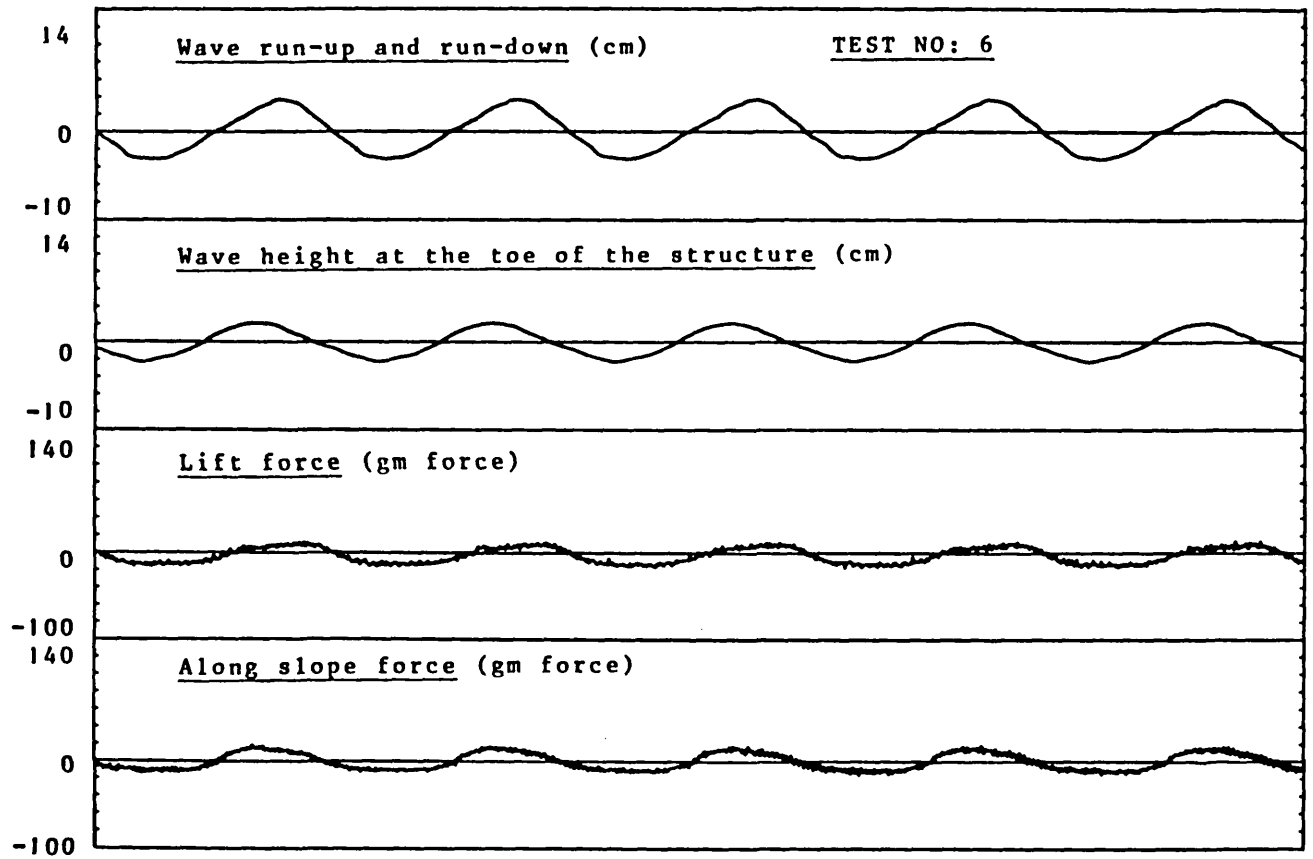
FIG.9.18 WAVE HEIGHT AND FORCE MEASUREMENTS (MEASURED VALUES)

1 gm force = 980.665 x 10^{-5} N



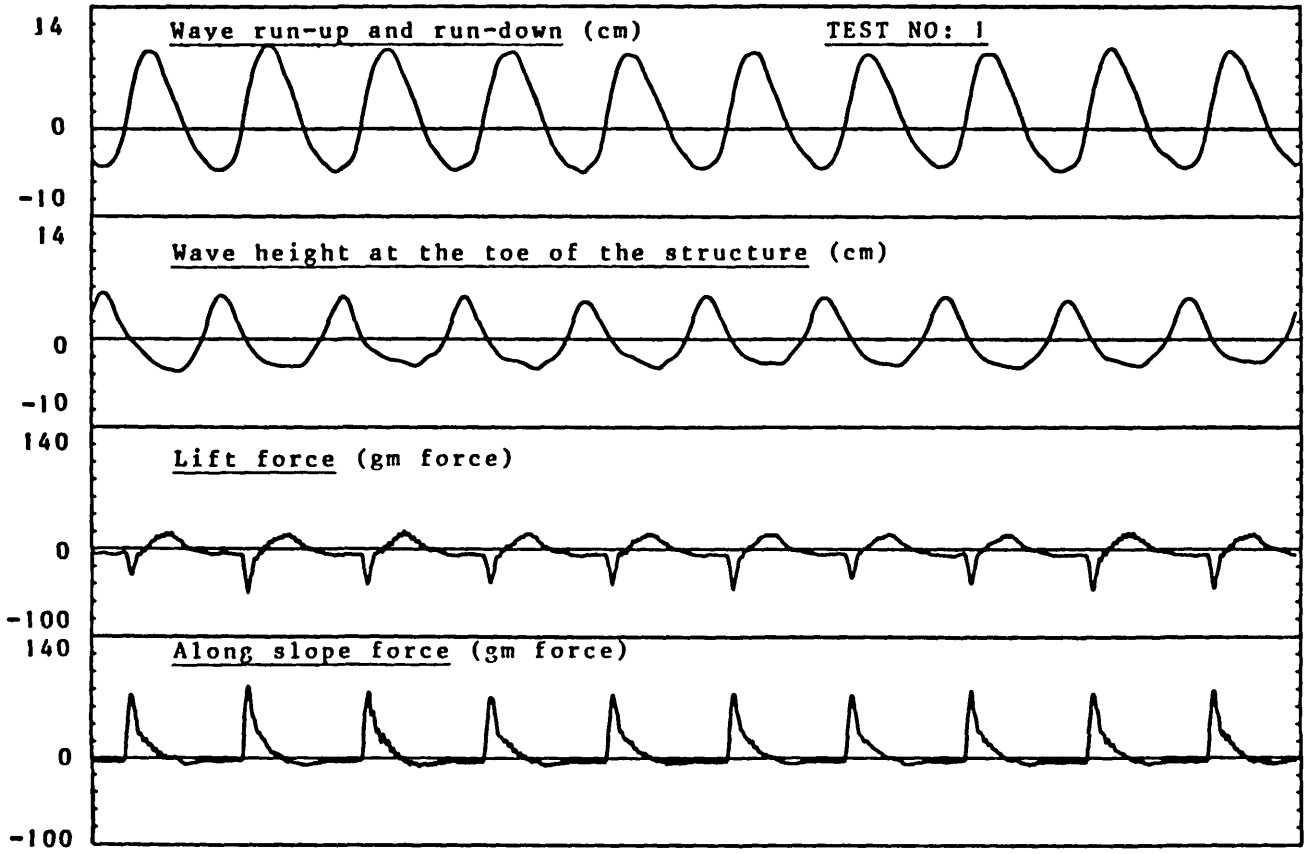
For breakwater section with a permeable underlayer
T=1.5 sec , H_t=3.63 cm

FIG.9.19 WAVE HEIGHT AND FORCE MEASUREMENTS (MEASURED VALUES)



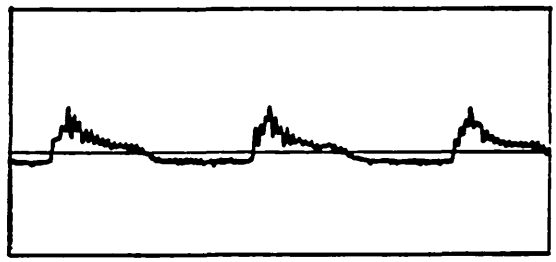
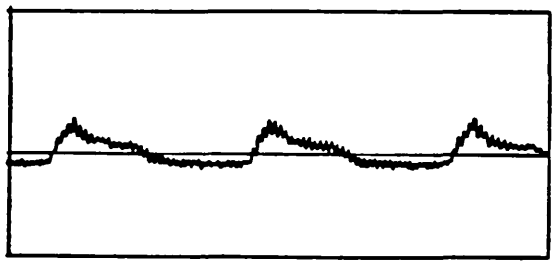
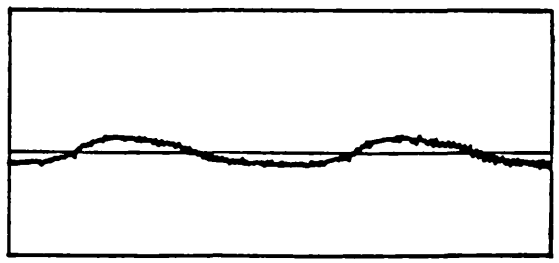
For breakwater section with a permeable underlayer
T=2.0 sec , H_t=4.34 cm

FIG.9.20 WAVE HEIGHT AND FORCE MEASUREMENTS (MEASURED VALUES)



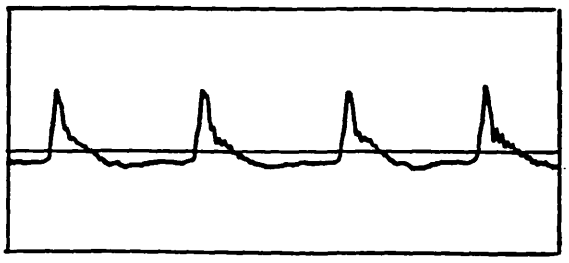
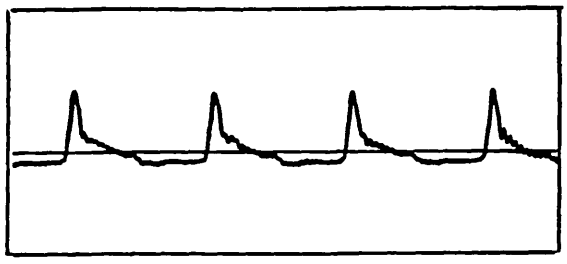
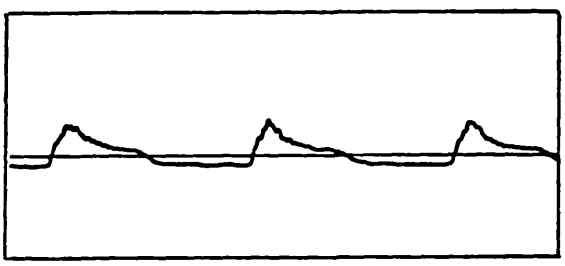
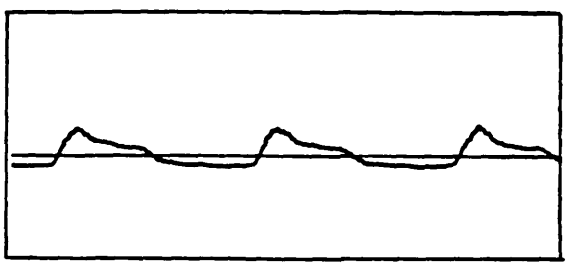
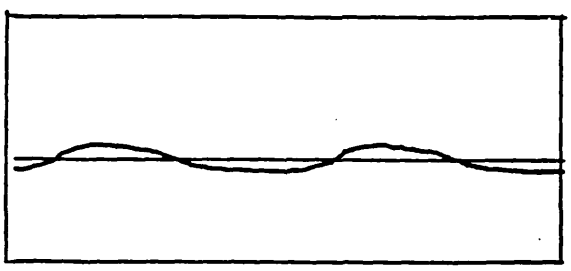
For breakwater section with a permeable underlayer
T=1.0 sec , H_t=8.04 cm

FIG.9.21 WAVE HEIGHT AND FORCE MEASUREMENTS (SMOOTHED VALUES)

Profiles of along slope force (measured values)	T (sec) wave period	H_t (cm) wave height at the toe
	1.0	8.04
	1.0	6.91
	1.0	5.72
	1.5	3.63
	1.5	3.41
	2.0	4.34

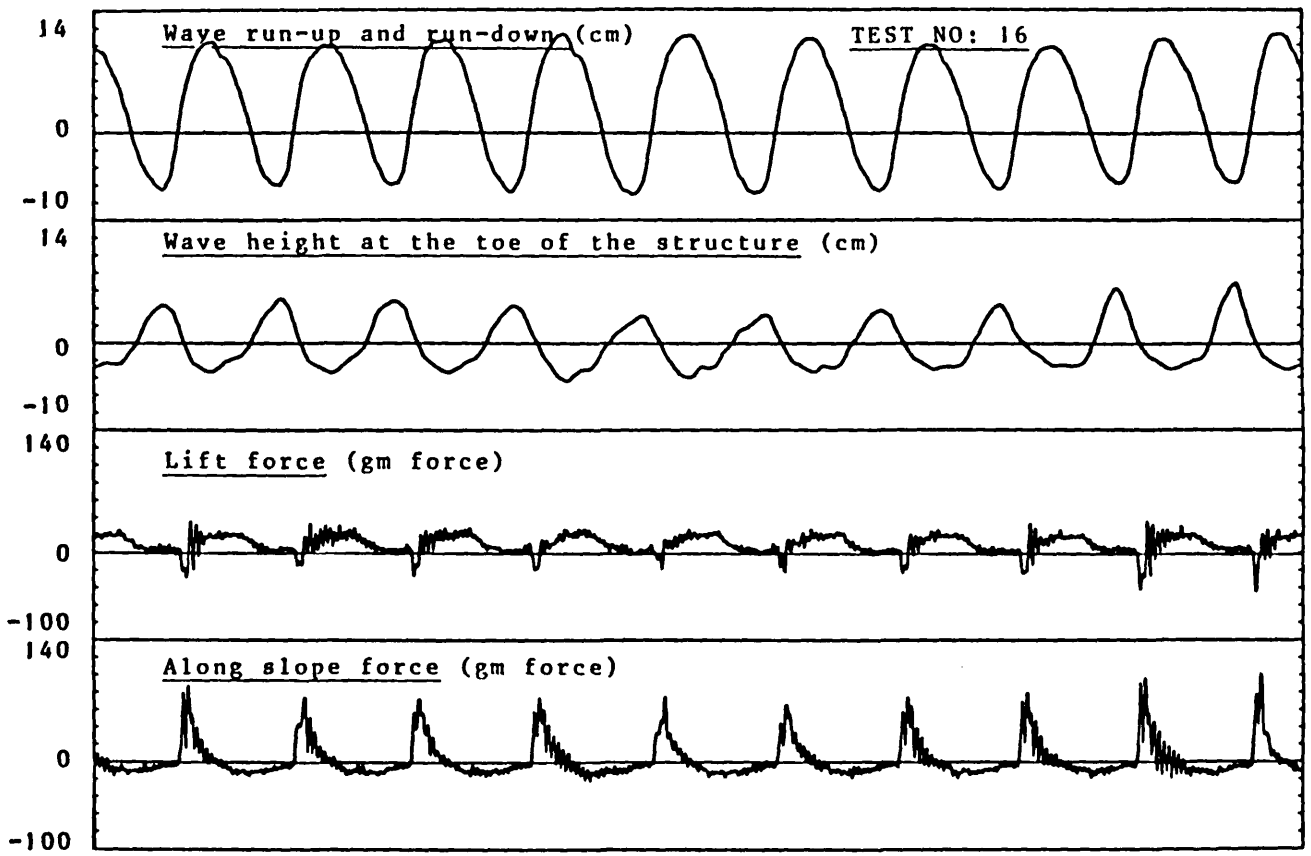
still water depth=24 cm

FIG.9.22 VARIATION OF ALONG SLOPE FORCE (MEASURED VALUES) FOR DIFFERENT INCIDENT WAVE CONDITIONS

Profiles of along slope force (smoothed values)	T (sec) wave period	H_t (cm) wave height at the toe
	1.0	8.04
	1.0	6.91
	1.0	5.72
	1.5	3.63
	1.5	3.41
	2.0	4.34

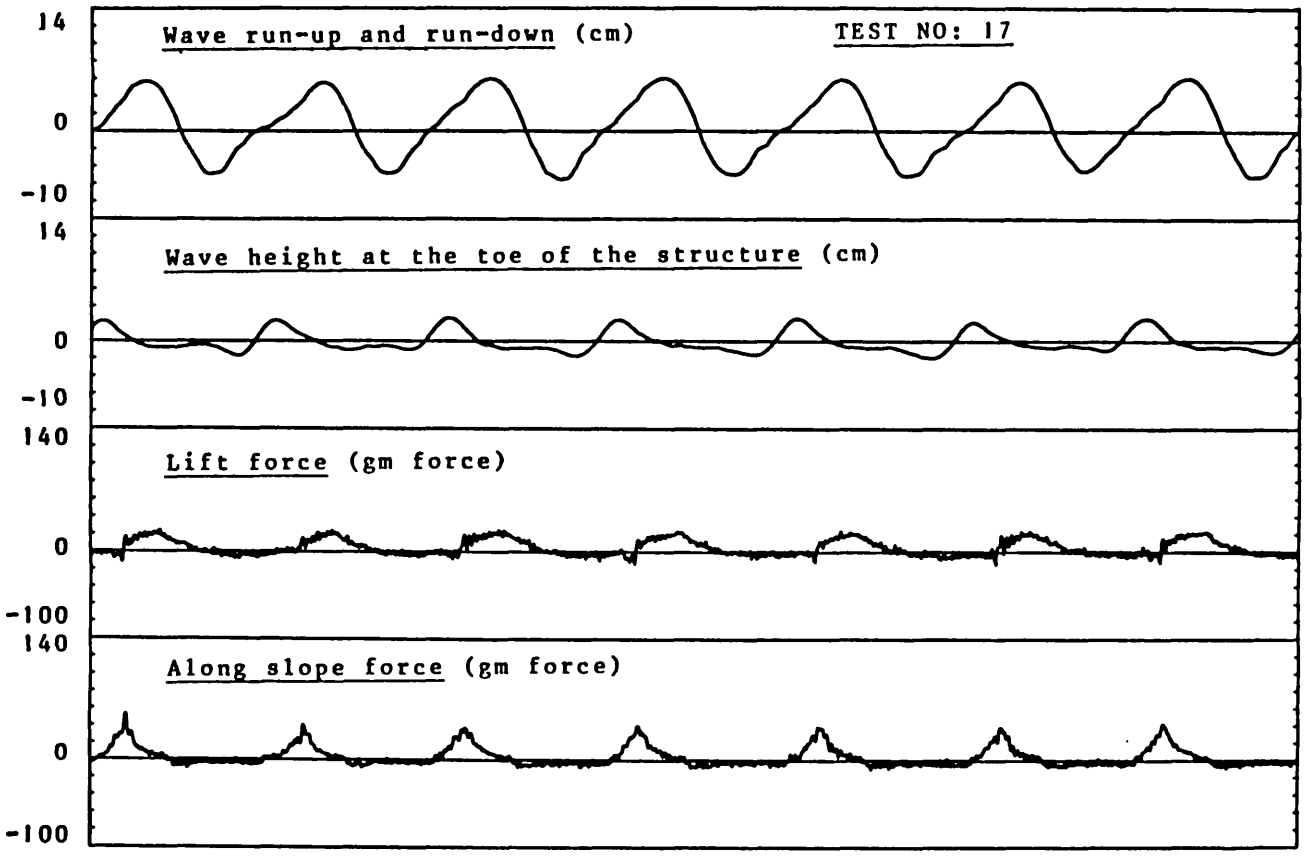
still water depth=24 cm

FIG.9.23 VARIATION OF ALONG SLOPE FORCE (SMOOTHED VALUES) FOR DIFFERENT INCIDENT WAVE CONDITIONS



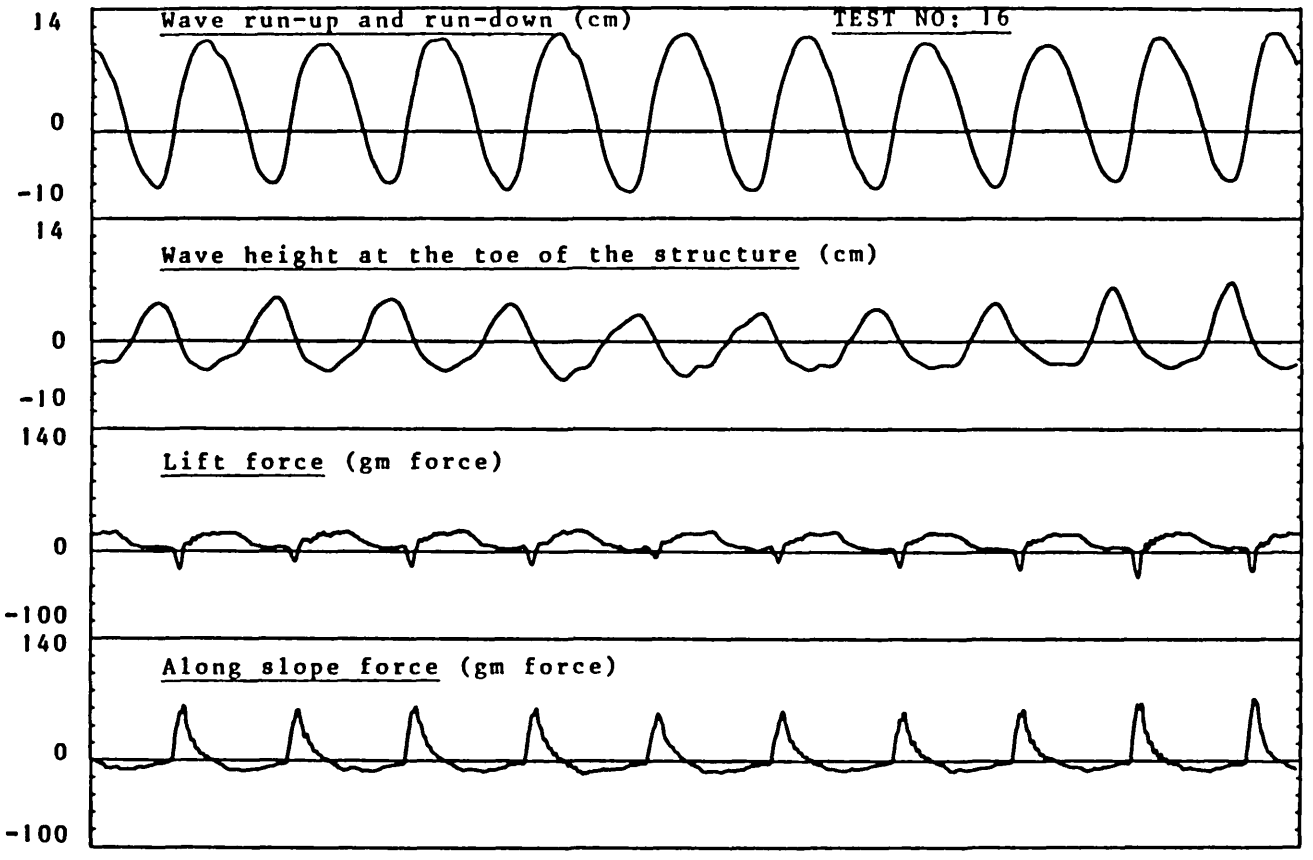
. For breakwater section with an impermeable underlayer
T=1.0 sec , H_t=9.34 cm

FIG.9.24 WAVE HEIGHT AND FORCE MEASUREMENTS (MEASURED VALUES)



For breakwater section with an impermeable underlayer
T=1.5 sec , H_t=3.23 cm

FIG.9.25 WAVE HEIGHT AND FORCE MEASUREMENTS (MEASURED VALUES)



For breakwater section with an impermeable underlayer
T=1.0 sec , H_t=9.34 cm

FIG.9.26 WAVE HEIGHT AND FORCE MEASUREMENTS (SMOOTHED VALUES)

FIG.9.27.A $F_{SLOPE(+)}$ / W_{SS} vs STEEPNESS

$F_{SLOPE(+)}$ – POSITIVE ALONG SLOPE FORCE (MEASURED FORCE)

W_{SS} – SUBMERGED WEIGHT COMPONENT

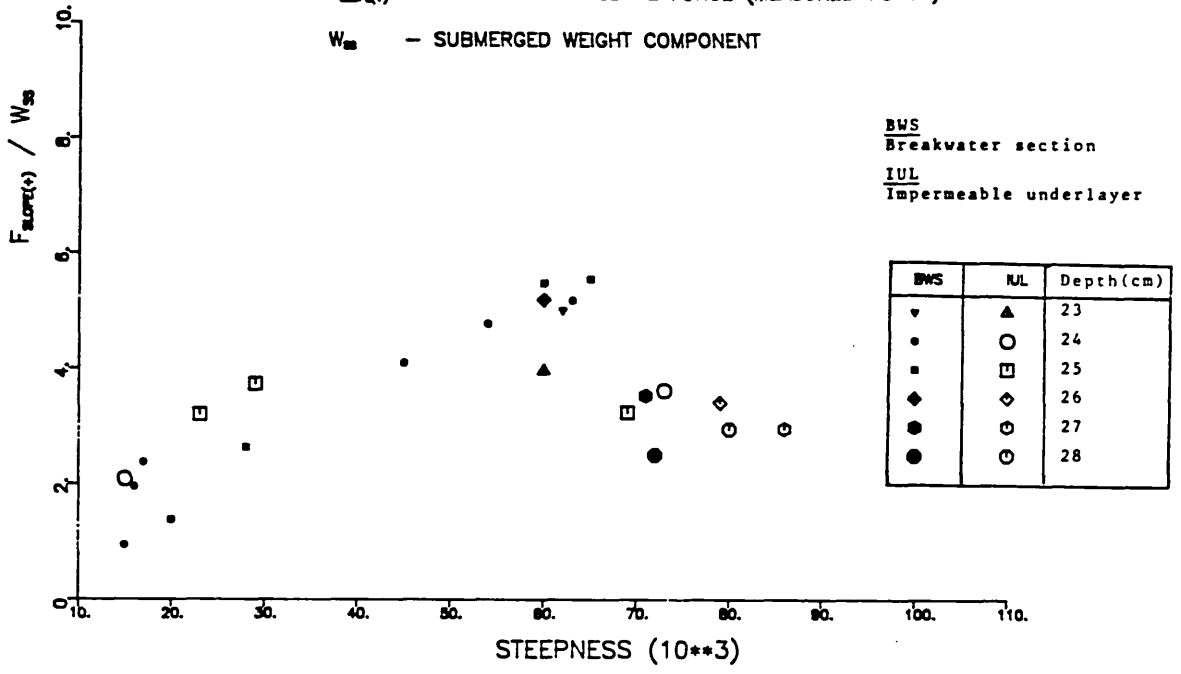


FIG.9.27.B $F_{SLOPE(+)}$ / W_{SS} vs WATER DEPTH

$F_{SLOPE(+)}$ – POSITIVE ALONG SLOPE FORCE (MEASURED FORCE)

W_{SS} – SUBMERGED WEIGHT COMPONENT

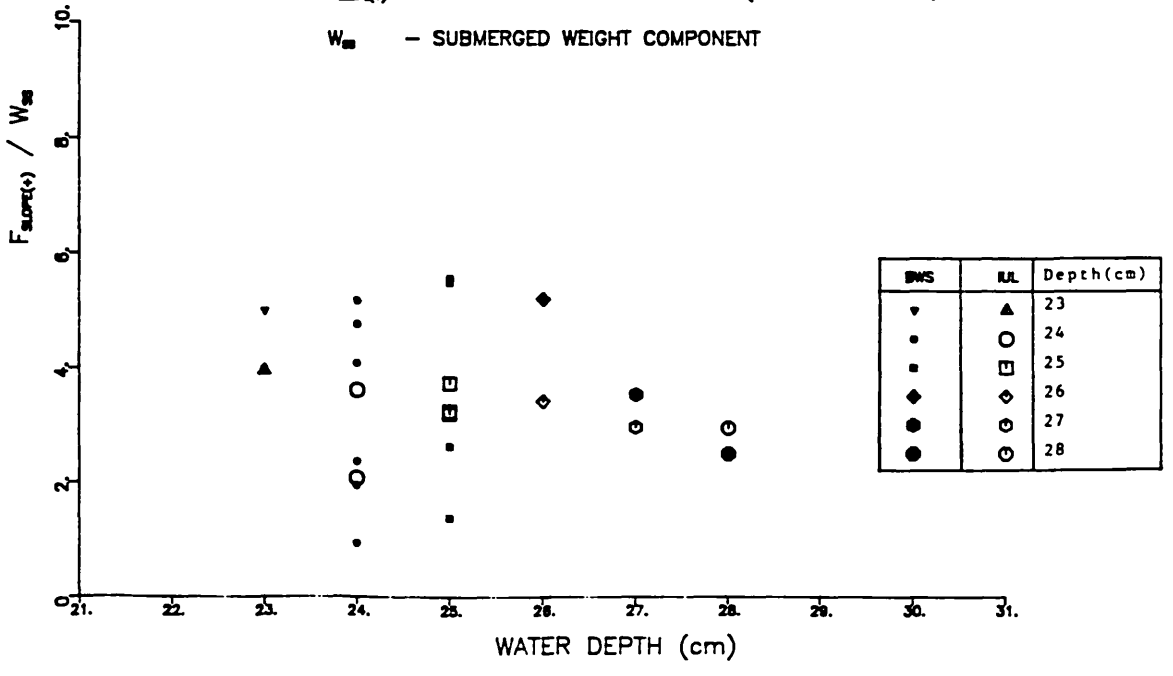


FIG.9.28.A $F_{LIFT(+)}$ / W_{SL} vs STEEPNESS

$F_{LIFT(+)}$ – POSITIVE LIFT FORCE (MEASURED FORCE)

W_{SL} – SUBMERGED WEIGHT COMPONENT

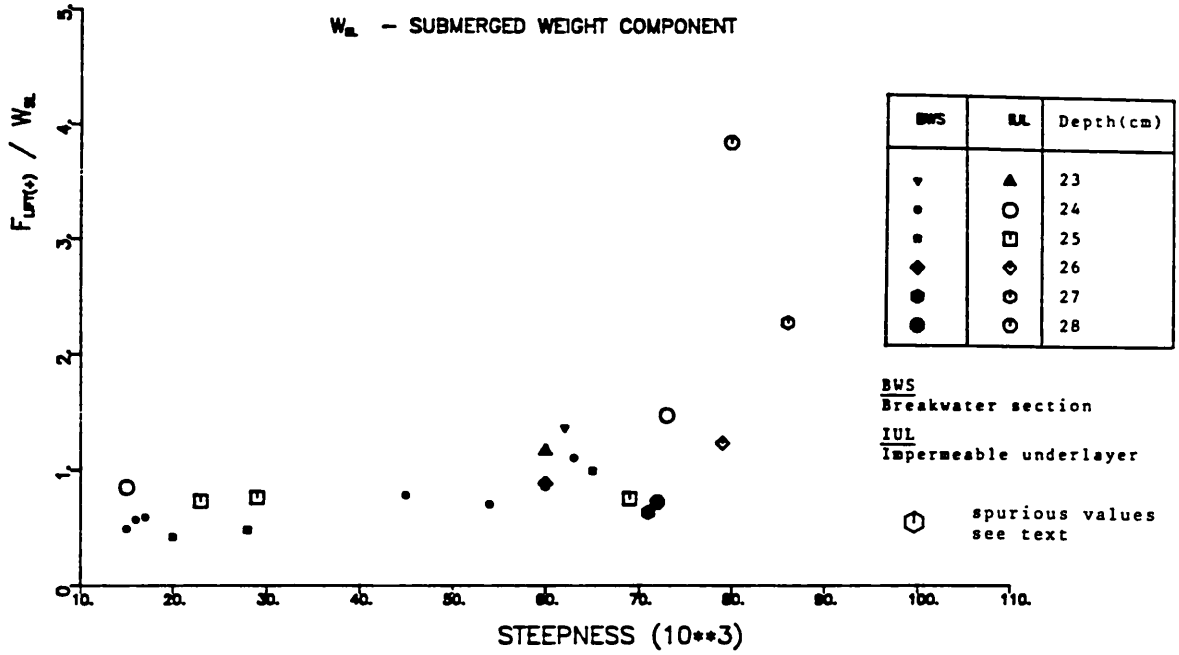
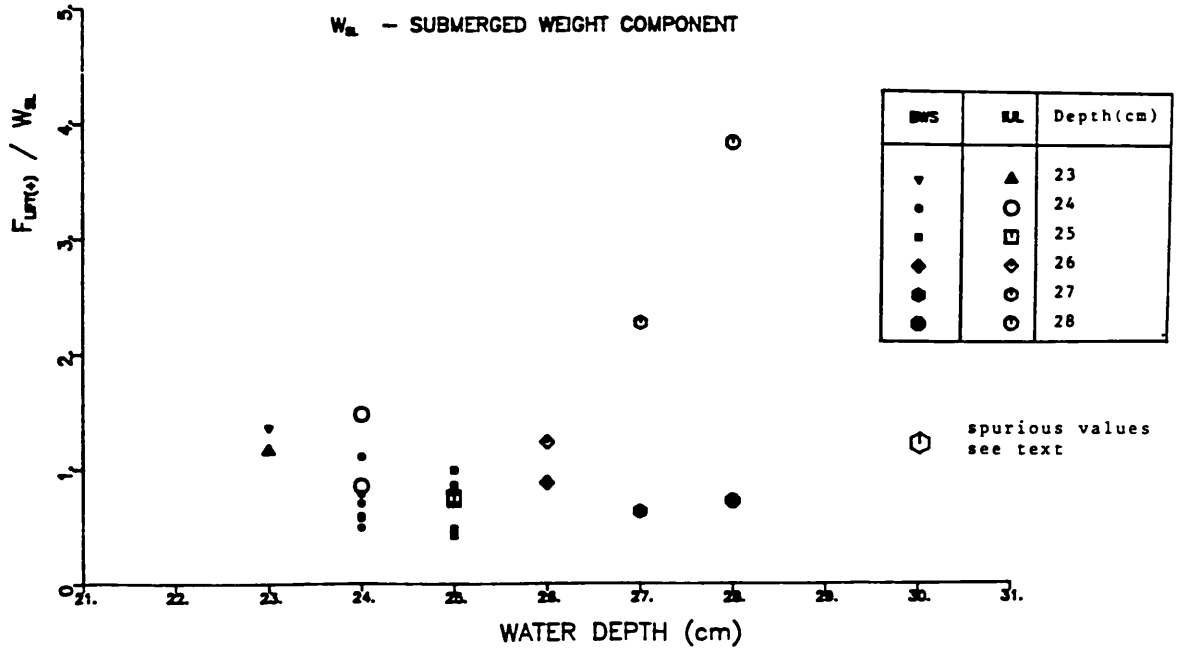


FIG.9.28.B $F_{LIFT(+)}$ / W_{SS} vs WATER DEPTH

$F_{LIFT(+)}$ – POSITIVE LIFT FORCE (MEASURED FORCE)

W_{SL} – SUBMERGED WEIGHT COMPONENT



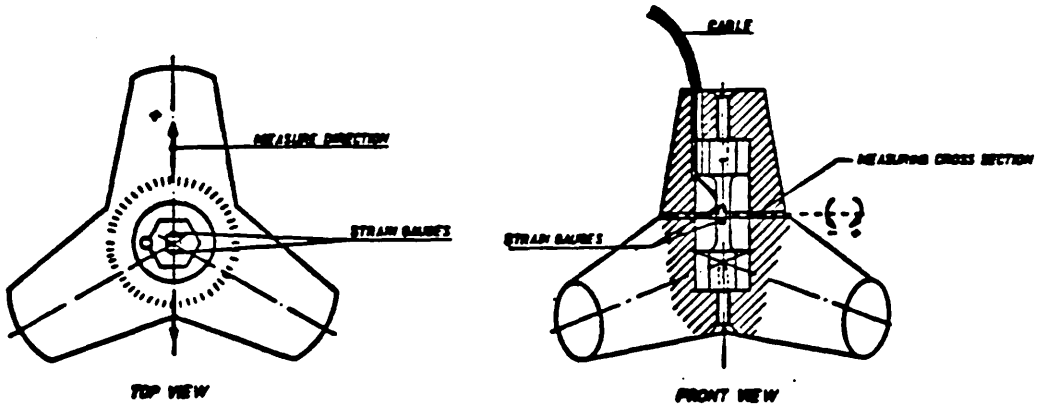


Fig.9.29.a Tetrapod armour unit instrumented with strain gauges in one leg for the measurement of bending moment

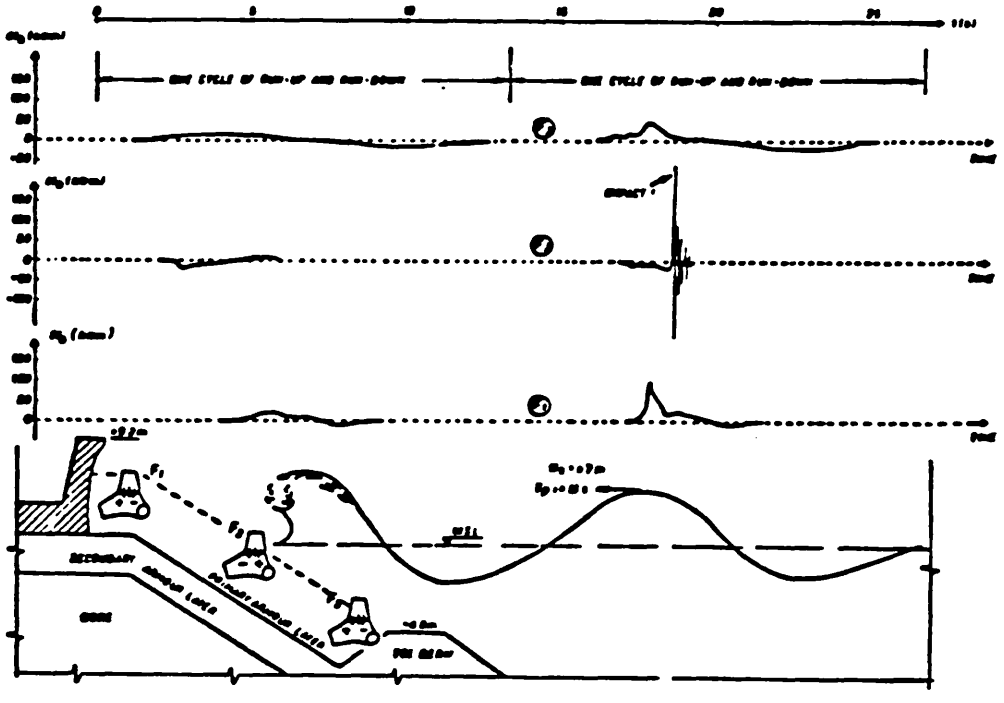


Fig.9.29.b The bending moments in the leg of a Tetrapod placed at various positions along the slope

FIG.9.29 MEASUREMENT OF BENDING MOMENTS IN MODEL TETRAPOD ARMOUR UNITS
(Ligteringen and Heydra 1984)

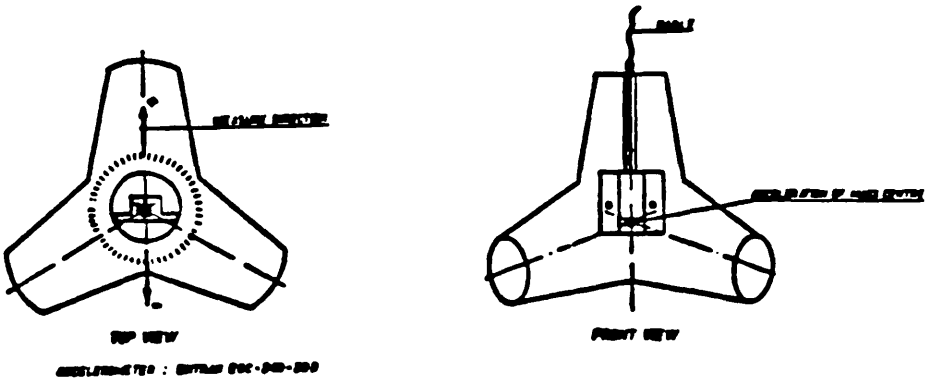


Fig.9.30.a Tetrapod armour unit instrumented with accelerometer for the measurement of acceleration

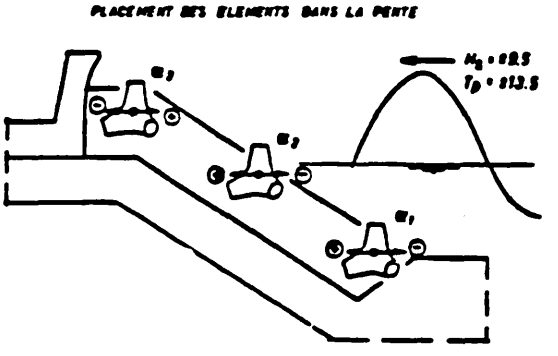


Fig.9.30.b Positions of the instrumentèd armour units

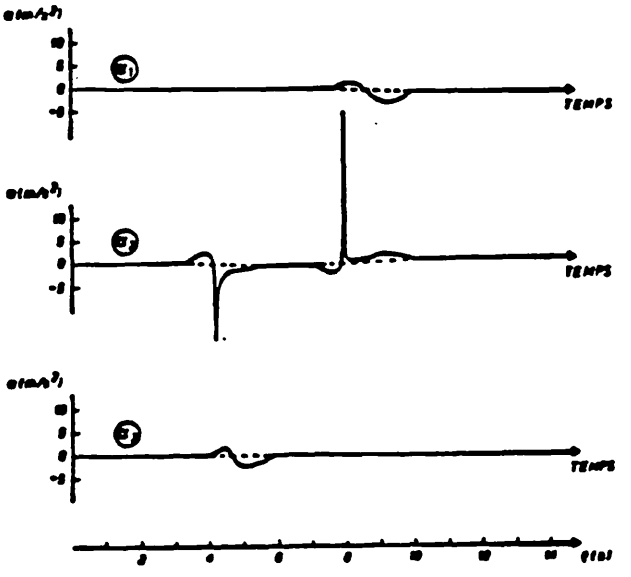


Fig.9.30.c Measured accelerations from model Tetrapod armour units

FIG.9.30 MEASUREMENT OF ACCELERATION IN MODEL TETRAPOD ARMOUR UNITS
(Ligteringen 1983)

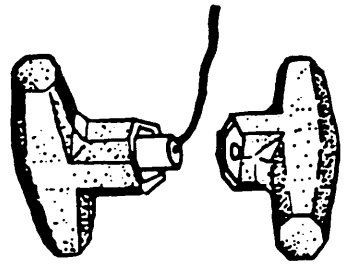


Fig.9.31.a Dolos armour unit instrumented with strain gauges for the measurement of internal bending moment and torsional moment

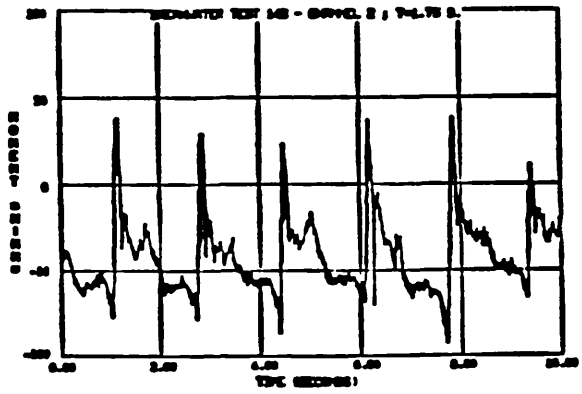


Fig.9.31.b Measured bending moments at a given location



Fig.9.31.c Variation of the structural response profile (bending moment) with position for a model wave height of 19.0 cm

FIG.9.31 MEASUREMENT OF BENDING MOMENTS IN MODEL DOLOS ARMOUR UNITS

(Scott,Turcke,Baird and Readshaw 1987)

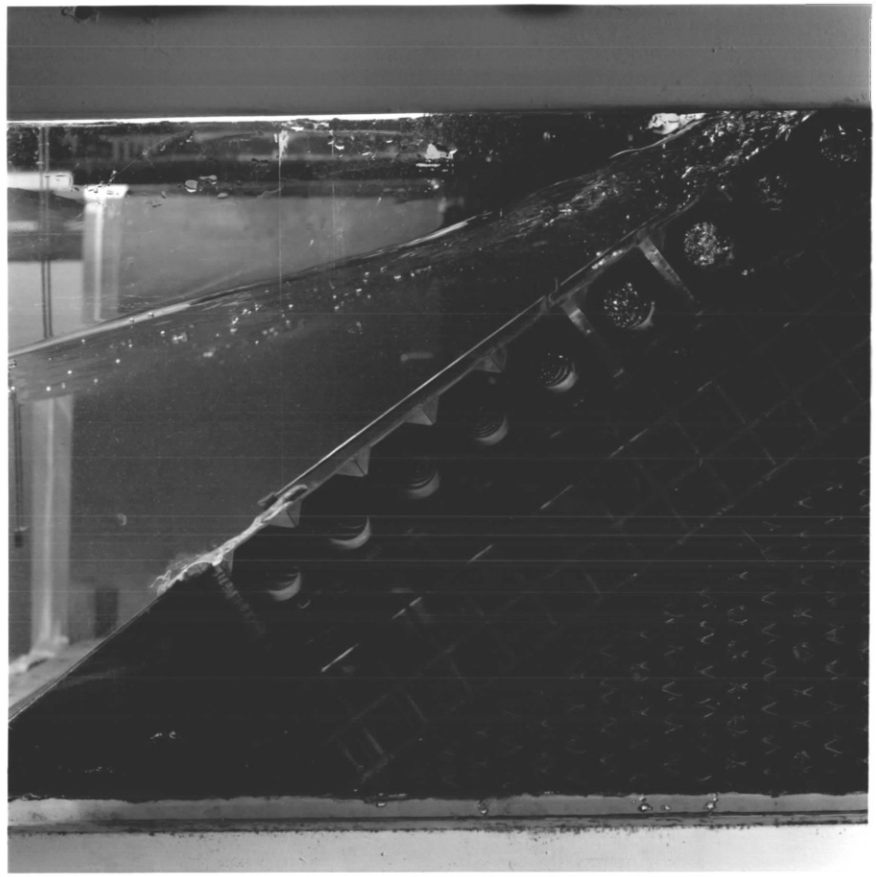




PLATE 1 WAVE ACTION ON THE MODEL BREAKWATER

CHAPTER 10 - SCALE EFFECTS IN MODELS OF POROUS COASTAL STRUCTURES

10.1 Introduction

Hydraulic modelling frequently involves the simulation of large systems at a substantially reduced scale which usually prevents the attainment of full similitude between model and prototype. Scale effects may be defined as any hydraulic inaccuracy in model performance caused by the reduced size of the model. Such effects may be present to some degree in any model smaller than its prototype.

The forces that may affect a flowing fluid are those of inertia, gravity, pressure, viscosity, elasticity and surface tension. To obtain dynamic similarity between two flow fields when all these forces act, all corresponding force ratios must be the same in model and prototype. In most engineering problems some of the forces may not be involved, may be of negligible magnitude or may oppose other forces in such a way that the effects of both are reduced. In each problem of similitude a proper understanding of the fluid phenomena is necessary to determine how the problem may be satisfactorily simplified by elimination of the irrelevant, negligible or compensating forces.

Most of the hydraulic phenomena that may be met in coastal engineering projects could be simulated with considerable accuracy if it were possible to satisfy both Froude and Reynolds laws simultaneously. Gravity and inertia being predominant, coastal hydraulic models are generally designed and operated in accordance with the Froude criterion. The other forces are assumed to be negligible. However, when the linear scale is too small, viscous forces may become significant and cause inaccuracies in model performance. Therefore, selection of scale for a model involving wave action usually requires a compromise between economy and the degree of accuracy required. In this chapter certain aspects related to modelling of wave transmission through a porous breakwater on a natural undistorted scale are presented.

10.2. Modelling for transmission and reflection on undistorted scale

Breakwaters are usually constructed of rubble with natural rock or concrete armour. In addition to the scale effects discussed earlier, porous structures exhibit further problems when modelling for reflection and transmission. The major problem is largely because of the probability that flow through the

structure may not be turbulent. Hudson (1979) observed that generally there is relatively more wave energy reflected and less transmitted in the model structure than in the prototype unless the model scale is large enough to ensure that motion is fully turbulent in the model. Using the Froude criterion and scaling the core material geometrically will result in a less permeable core in the model, leading to relatively higher down-rush pressures from inside the structure. In order to correct for this dissimilarity it is suggested that the sizes of the core material in the model should be larger than would be indicated by direct application of the linear scale.

Flow through porous media has to be correctly represented with due regard to the similitude of the hydraulic gradient in model and prototype. For example, hydraulic model tests on breakwaters are normally carried out at small scales such that the flow through various layers of the breakwater is not completely turbulent. Hence in breakwater model tests where transmission is considered critical, it is important to recognize the modelling requirements of both the armour layer and the underlayer. Model design must take these into account and appropriate modifications made in the construction of the model.

It is required that the flow through the main armour layers is properly scaled in order to obtain reliable results with respect to their stability and related factors. Hence for this region the emphasis is on stability and the weight of the armour unit or stone must be accurately reproduced and errors must be avoided in scaling these weights. Breakwater models are normally constructed at scales in the region 1:30 to 1:40. In such models the main armour layer is composed of units which have characteristic dimensions of the order of 5 cm. For typical flow conditions encountered in models the Reynolds number for the main armour will be approximately 5×10^4 which is an acceptable value for similitude.

However the condition nearer to the core of the structure is quite different; both the dimensions of the stone and the magnitude of velocities are relatively small. The Reynolds number characterizing the flow is below the critical value required for fully turbulent flow. This is of particular importance for wave transmission and will also influence the stability of the main armour layer and the reflection from the breakwater. In order to achieve a correct and more representative hydraulic gradient in the model, some of the interior layers and the core could be made of stones larger than the Froude criterion would demand, satisfying the requirement

$$d_m = k\, d_p \left(\frac{L_m}{L_p}\right) \qquad (10.1)$$

$k(\geq 1)$ is an enlargement factor which should be applied to the linear scale.

$\frac{L_m}{L_p}$ $(= L_r)$ is the linear scale.

d_m and d_p are characteristic dimensions of the stones in the cores of the model and prototype.

Hudson (1979) pointed out that reflection from rubble mound breakwaters does not usually lead to serious scale errors when using undistorted models. In three-dimensional studies i.e. those conducted to determine the wave condition near to and in the lee of the breakwater and those associated with stability of the round-head, excess wave reflection external to the breakwaters can be reduced satisfactorily by placing absorbers around the perimeter of the model basin and in front of the wave generator. However when reflected waves from breakwaters have an adverse effect Hudson (1979) recommends that the increase in wave reflection from the breakwater due to scale effects can be reduced by wire mesh screens placed on the seaward side of the structure. He also states that the proper value of the reflection coefficient would be best obtained by special two dimensional tests on a larger scale.

10.3. Methods of determining the scale ratio for particle size

Methods for calculating the enlargement factor k in eq. 10.1 have been presented by LeMehaute (1965), Keulegan (1973), Jensen and Klinting (1983). Of these studies the first and the last are similar to each other in that an expression for the hydraulic gradient – velocity relationship was assumed as the initial step. Jensen and Klinting (1983) used Engelund's (1953) formula given by eq. 2.12 whereas LeMehaute (1965) used the formula given by eq. 2.13 (LeMehaute 1957). Keulegan (1973) adopted equations arising from a limited experimental study. However in all these studies attention was not focused on the relative influence of laminar and turbulent flow coefficients for different media or the influence of porosity.

The first two methods were assessed by Hudson (1979) for a model and prototype of porosity 0.46. The linear scale used in the comparison was 1:100.

The water depth, wave environment and the stone sizes used represented the ranges of these variables commonly found in prototype structures. He was of the opinion that both porosity and size of the core material have an appreciable effect on wave transmission and that it is important to obtain accurate values of these variables for the core material used in the prototype structure. The ratio of the values of k as obtained by the methods of LeMehaute (1965) and Keulegan (1973) varied from 1.20 to 1.40 and in view of the uncertainty Hudson (1979) recommended the use of the average of the values obtained by the two methods. He also showed that under typical conditions the value of k can be as high as 6.

Although these calculations provide a method of predicting approximate enlargement factors, the correct value is best determined by two dimensional tests. These consist essentially of two series of experiments the first to determine wave transmission and reflection characteristics at prototype scale and the second to determine the correct size of stone for reproduction of these characteristics in the model.

However due to practical limitations or due to non-existence of the prototype it may not be possible to perform the first investigation. Under such conditions the prototype should be replaced by a model section built on a scale considered sufficiently large to avoid scale effects. Wave transmission characteristics recorded during these experiments may then be considered to be representative of prototype conditions. In the model test series, stone size has to be varied until transmission coefficients are approximately the same. Once the stone size is selected, model breakwaters for three dimensional studies could be constructed. Whalin and Chatham (1974) adopted this technique for a model study of a harbour project at a distorted scale. It is evident that on most occasions this type of detailed experimentation is not feasible on economic considerations. Furthermore exact reproduction is rarely possible because of the variations of transmission coefficients with wave period and height, as an exact correspondence over a range of wave periods is unlikely. Hence much reliance is placed on analytical techniques however approximate they may be.

10.4. Objectives of the present study

To obtain complete similitude between model and prototype for flow through porous media it is required that the hydraulic gradient is same for both. In this study an analytical method is developed, based on the expression for hydraulic gradient under steady flow condition, to evaluate the enlargement factor k. In the initial phase k is expressed in terms of laminar and turbulent resistance

terms, velocity and a characteristic dimension as applicable to both model and prototype. Simplifying assumptions are made to express k in terms of parameters applicable only to the prototype and results from steady flow tests are used to assess the validity of such assumptions. Attention is also focused on the sensitivity of k to variations in porosity. Finally, results from the present study pertaining to scale effects on cylindrical lattice structures and spherical lattice structures are presented for comparison with previous work. The objective is to obtain a clearer understanding of the influence of the key parameters in relation to wave transmission in hydraulic models.

10.5. Analytical development, its application and discussion

10.5.1. Analytical development

The general expression for the hydraulic gradient (I) for steady flow through porous media is of the form

$$I = au + bu^2 \tag{10.2}$$

where a and b are constants dependent on the void characteristics of the medium, the two terms being interpreted as the laminar and turbulent components respectively.

$$I = I_L + I_T \tag{10.3}$$

Of the many expressions developed for flow through porous media, those of Engelund (1953) and LeMehaute (1957) are widely accepted (eq. 2.12 and eq. 2.13).

A more specific expression of the above equations is as follows,

$$I = f_L \frac{\gamma}{gd^2} u + f_T \frac{1}{gd} u^2 \tag{10.4}$$

or

$$I = \left(\frac{2f_L}{Re} + 2f_T\right) \frac{u^2}{2gd} \tag{10.5}$$

in which d is the characteristic dimension
Re is the Reynolds number ($Re = ud/\gamma$)
f_L and f_T are laminar and turbulent resistance coefficients.

Values of f_L and f_T as given by the equations of Engelund (1953) and LeMehaute (1957) are given below.

	f_L	f_T	f_T/f_L	I_T/I_L
Engelund (1953)	$\alpha_o(1-n)^3/n^2$	$\beta_o(1-n)/n^3$	$\beta_o/\alpha_o n(1-n)^2$	$\dfrac{\beta_o Re}{\alpha_o n(1-n)^2}$
LeMehaute (1957)	$c_2/2n^5$	$c_3/2n^5$	c_3/c_2	$c_3 Re/c_2$

TABLE 10.1 STEADY FLOW LAMINAR AND TURBULENT COEFFICIENTS

With regard to LeMehaute's equation it is possible to express the hydraulic gradient (I) in the form

$$I = c\left(\frac{ud}{\gamma}\right)F(n)\,\frac{u^2}{2gd} \qquad (10.6)$$

where c and F are functions of Reynolds number and porosity respectively. It is also observed that the ratio f_T/f_L does not include a porosity dependent term. In the case of Engelund's equation the ratio is a function of porosity but the hydraulic gradient cannot be expressed as separate functions of Reynolds number and porosity.

The term
$$\xi = \frac{I_T}{I_L} - \frac{f_T}{f_L}\,Re \qquad (10.7)$$

plays an important role in assessing the degree of turbulence in flow through porous media, including its dependence on Reynolds number.

In evaluating scale effects for laminar and turbulent flow it is observed that for complete similitude between model and prototype it is necessary to consider the total expression for the hydraulic gradient given by eq. 10.4.

$$I_r = \frac{I_m}{I_p} = \frac{(I_L + I_T)_m}{(I_L + I_T)_p} = 1 \tag{10.8}$$

$$I_r = \left[\frac{f_{Lm} \frac{\gamma}{g d_m^2} u_m + f_{Tm} \frac{1}{g d_m} u_m^2}{f_{Lp} \frac{\gamma}{g d_p^2} u_p + f_{Tp} \frac{1}{g d_p} u_p^2} \right] = 1 \tag{10.9}$$

Using the Froude criterion, $u_r = \sqrt{L_r}$ (10.10)

where L_r is the length scale ratio $L_r = \frac{L_m}{L_p}$

i.e. $u_m = u_p \sqrt{L_r}$

Assuming $d_r \neq L_r$ and that d_r can be expressed as

$$d_r = k\, L_r \tag{10.1}$$

where k (≥ 1) is an enlargement factor, it is possible to introduce eq. 10.10 and eq. 10.1 into eq. 10.9 in order to obtain an expression for k.

It is observed that k is found from the quadratic equation

$$(f_{Lp} + f_{Tp} Re_p) k^2 - (f_{Tm} Re_p) k - \frac{f_{Lm}}{L_r^{3/2}} = 0 \tag{10.11}$$

and is expressed as follows

$$k = \frac{L_r^{3/2} f_{Tm} Re_p + \sqrt{L_r^3 f_{Tm}^2 Re_p^2 + 4 L_r^{3/2} f_{Lm} (f_{Lp} + f_{Tp} Re_p)}}{2 L_r^{3/2} (f_{Lp} + f_{Tp} Re_p)} \tag{10.12}$$

However, if it is assumed that

$$f_{Lm} = f_{Lp} = f_L \qquad (10.13)$$
$$(\text{i.e. } (f_L)_r = 1)$$

and
$$f_{Tm} = f_{Tp} = f_T \qquad (10.14)$$
$$(\text{i.e. } (f_T)_r = 1)$$

eq. 10.12 can be simplified to

$$k = \frac{f_T Re_p + \sqrt{f_T^2\, Re_p^2 + 4(f_L + f_T\, Re_p) f_L / L_r^{3/2}}}{2(f_L + f_T Re_p)} \qquad (10.15)$$

By introducing eq. 10.7 into eq. 10.15, k is further simplified to

$$k = \frac{\xi_p + \sqrt{\xi_p^2 + 4(1 + \xi_p)/L_r^{3/2}}}{2(1 + \xi_p)} \qquad (10.16)$$

where
$$\xi_p = \frac{I_{Tp}}{I_{Lp}} = \frac{f_{Tp}}{f_{Lp}} Re_p \qquad (10.7)$$

subject to conditions specified in eqs. 10.13 and 10.14.

From the above equation it appears that
as $\xi_p \to 0$ the expression for $k \to {}^1/L_r^{\frac{1}{2}}$ (i.e. laminar flow) and
as $\xi_p \to \infty$ the expression for $k \to 1$ (i.e. turbulent flow).

Using these two extreme conditions and substituting in eq. 10.1 then

$$d_r = \sqrt[4]{L_r} \qquad \text{for laminar flow} \qquad (10.17)$$

$$d_r = L_r \qquad \text{for turbulent flow} \qquad (10.18)$$

This indicates that although the turbulent term is correctly represented, the laminar term requires that material should be scaled much larger than the values determined according to the Froude criterion.

It should be noted that the expression for k as given by eq. 10.16 is valid on the assumption that the respective resistance coefficients for the model and prototype are equal. It is observed that the enlargement factor is a function of

the Reynolds number of the prototype (Re_p), the scale ratio of length (L_r) and the ratio of turbulent/laminar resistance coefficients (f_T/f_L).

However, it should be appreciated that it is difficult in practice to determine the Reynolds number of the prototype by measuring the velocity within a porous structure. The largest uncertainty in the use of the above evaluation for model studies of breakwaters is that concerning the magnitude and characteristics of the velocity field in the prototype structure. Under such circumstances it is convenient to replace the Reynolds number by a related parameter whose value could either be measured or evaluated from existing field data. For this purpose it is possible to use the hydraulic gradient ($I = \Delta H/\Delta L$) and relate it to field measurements on wave transmission.

Eq. 10.5 can be expressed as a quadratic equation in terms of the Reynolds number

$$Re^2 + \frac{f_L}{f_T} Re - \frac{Igd^3}{f_T \gamma^2} = 0 \qquad (10.19)$$

the solution being

$$Re = \frac{- f_L \pm \sqrt{f_L^2 + 4Igd^3 \, f_T/\gamma^2}}{2f_T} \qquad (10.20)$$

in which

$$I = \frac{\Delta H}{\Delta L} \qquad (10.21)$$

10.5.2. Evaluation of hydraulic gradient

When applying eq. 10.20 to a practical case, it is necessary to estimate the head loss of a rubble mound breakwater and this has to be obtained from reported values of wave transmission. An analysis of this type is appropriate to successive quasi-steady flows such as long wave interaction with breakwaters. As an initial approximation, ΔH can be taken as the amplitude at the loop in front of the breakwater and ΔL as the average width of the core. $\Delta H/\Delta L$ is the gradient of the head loss through the voids in the core of the breakwater section. The influence of k is more significant if the crest of the core material section is relatively high with respect to the total structure. With reference to the properties

of prototype material, LeMehaute (1965) suggests the use of an effective diameter which is taken to be the "10 percent smaller than" quarry stone from the core material grading curve.

Results from field studies on wave transmission provide further information which is of use for this type of computation. Figs. 10.1.a and 10.1.b relate to the work of Thornton and Calhoun (1972). Results from another study performed by Hattori and Sakai (1973) are presented in Fig. 10.1.c. For a given wave steepness it is possible to evaluate K_t from which the extreme values of ΔH can be computed as

$$\Delta H = (1 \pm K_t)H_i \qquad (10.22)$$

It is evident that the problem is more complicated if it is required to determine the conditions for similitude and scale effects in the case of a breakwater which is subjected to overtopping. Simple relationships cannot be obtained for the combination of overtopping and permeability.

10.5.3. Influence of laminar and turbulent resistance coefficients

On the basis of the above analytical developments, it is possible to assess the influence of some of the important parameters.

The requirement that the respective resistance coefficients are the same for the model and prototype (eq. 10.13 and 10.14) is not fully justified and is assumed valid in the absence of experimental data covering a wide range of materials. Until steady flow tests are performed on a wider spectrum of materials used for breakwater construction the influence of these parameters will remain unclear. The conditions under which Engelund's equation was derived have been already presented.

In the present study the results from tests on cylindrical lattice structures can be used to illustrate this point. Given in Table 10.2, are the resistance coefficients of three structures in which the porosity, the shape of void and the tortuosity remain unchanged. The varying parameter is the size of the void characterized by its dimension which is also equal to the diameter of the cylindrical member.

n = 0.607 Diameter	a and b in $I = au + bu^2$		f_L and f_T in $I = f_L \frac{\gamma}{gd^2} u + f_T \frac{1}{gd} u^2$	
	a (sec/m)	b $(sec/m)^2$	f_L	f_T
15 mm	0.612	3.051	1210.9	0.449
20 mm	0.682	1.338	2400.1	0.263
30 mm	0.642	0.751	5083.5	0.221

TABLE 10.2 STEADY FLOW COEFFICIENTS FOR CYLINDRICAL LATTICE STRUCTURES

It is evident that the values of f_L and f_T for these structures vary quite significantly indicating the influence of the void dimension. Since all parameters except the void dimension (d) are constant it can be assumed that the turbulent parameter is proportional to a certain power of the diameter (d) of the cylinder (i.e. $b \propto d^m$) and it is recalled that m was found to be equal to −1.98 with a correlation coefficient of 0.96, indicating the existence of an inverse square law. Although this value was determined, only on three sets of data it is evident that the overall results do not support the simplifying assumptions made, eqs. 10.13, 10.14, i.e. $(f_L)_r \neq (f_T)_r \neq 1$.

10.5.4. Influence of porosity on the enlargement factor

The analytical development presented earlier can be used to assess the influence of porosity on the modelling of transmission. For this purpose, Engelund's equation is assumed to be valid and ξ_p represented by

$$\xi_p = \frac{\beta_o}{\alpha_o} \frac{1}{n(1-n)^2} Re_p \qquad (10.23)$$

with α_o = 1500.00 and β_o = 3.6 being used for computations. This expression is now substituted in eq. 10.16 to calculate the enlargement factor, k.

Fig. 10.2 is a plot of the enlargement factor, k, versus porosity (n) for various L_T at a prototype Reynolds number, Re_p = 1000. Since the influence of k is important for low flow rates, a Re_p value of 1000 was used for the illustration. Varying Reynolds numbers will be considered in a separate plot.

From Fig. 10.2 it is observed that for a given scale ratio, k reaches a maximum at $n \simeq 0.35$ and for small models the curvature of the plots is pronounced. A reasonable value of porosity for quarry-run core material is in the range 0.35 to 0.40, depending on the grading. In this region the respective curves are reasonably flat and therefore a variation in porosity will not have a significant influence on the value of k. However in other regions the curves have considerable slope and a difference of 0.1 in porosity can change the value of k by approximately 20% or more. This plot clearly illustrates the sensitivity of k to changes in porosity and the importance of assessing the value of the porosity of the prototype in order to obtain an appropriate value of k for correct similitude.

Fig. 10.3 is a plot of the enlargement factor (k) versus porosity (n) for varying prototype Reynolds number at scale ratio $L_r = 1/30$. Two-dimensional studies on breakwaters are typically constructed at scales around this value. It is evident that as flow changes from laminar to turbulent the enlargement factor reduces in magnitude and approaches unity.

Fig. 10.4 is a plot of the enlargement factor (k) versus scale ratio (L_r) for varying prototype Reynolds number at a porosity of 0.4, the latter being a representative value with regard to breakwater studies. The advantage of working with a large model at high Reynolds numbers is clearly evident.

Figs. 10.2, 10.3 and 10.4 illustrate some of the problems associated with modelling flow through porous media with particular attention being focused on the occurrence of laminar flow and varying porosity. In the absence of extensive experimentation it is necessary to use this type of analytical method to evaluate model properties required to compensate for scale effects. Sufficient care should be taken in evaluating prototype properties which are required for this purpose. From the foregoing discussion, it is observed that porosity and the resistance coefficients of both model and prototype play a vital role.

When using an enlargement factor it is important to ensure that it is uniformly applied to the regions concerned and precautionary measures should be adopted in grading the model material and in the construction of the model. It is also very difficult to adjust or to duplicate the voids ratio for a scale model of a breakwater. The relatively large variation of the permeability with a small variation of the void coefficient is the main source of error in this kind of study.

This aspect can be further investigated by analysing the hydraulic characteristics of randomly packed spheres of diameters 19 and 25 mm which are in

the ratio 1:1.32. Table 10.3, given below, illustrates the relevant parameters. Both media consist of spherical elements of different diameter packed in a similar way. The use of this type of element ensures that the void matrix is uninfluenced by the irregularities in shape of the constituent element. Information pertaining to rounded stones is also included for comparison.

	a and b in $I = au + bu^2$		f_L and f_T in $I = f_L \frac{\gamma}{gd^2} u + f_T \frac{1}{gd} u^2$	
	a (sec/m)	b $(sec/m)^2$	f_L	f_T
Spheres D = 19 mm n = 0.350	1.707	14.632	5420.6	2.727
Spheres D = 25 mm n = 0.394	1.454	11.558	7995.7	2.835
Rounded stone D = 34.8 mm n = 0.362	1.120	14.085	11932.2	4.808

TABLE 10.3 STEADY FLOW COEFFICIENTS FOR SPHERES AND ROUNDED STONES

In the case of the spheres it is observed that f_T is approximately the same whereas f_L differs significantly. This illustrates the point that by using material which are slightly different, in this case a change in diameter by a factor 1.32, it is possible to obtain flow coefficients which are different. For example, if the required enlargement factor obtained by using the flow coefficients of the 19 mm spheres is 1.32, this necessitates the use of 25 mm spheres which have different permeability coefficients. This demonstrates some of the limitations of the analytical procedure and further developments can only be achieved by detailed experiments on flow through porous media.

10.6. Scale effect tests on wave transmission and reflection

Experimental investigations on scale effects pertaining to wave transmission are important to obtain information on the reliability of using models to predict prototype performance. Although a given experimental result relates to a certain state of flow, it does not necessarily represent prototype condition nor can it be used to predict prototype behaviour. Hence care must be exercised when

interpreting transmission coefficients obtained under laboratory conditions for application in prototype conditions.

10.6.1. Review of previous studies

Tests to determine the scale effects of wave transmission through porous structures have been reported by Johnson, Kondo and Wallihan (1966), Wilson and Cross (1972) for rubble, Delmonte (1972) for closely packed uniform spheres and Kondo and Toma (1972) for cylindrical lattice structures. In all cases they have used the Froude criterion for scaling and considered the largest structure to be the control model. The structures were placed in flumes at appropriate locations and side effects minimised by extending the test section across the full width of the channel, simulating the condition of an infinitely wide structure. A summary of the experimental structures and relevant results is presented in Table 10.4 and Figs. 10.5.a to 10.5.d.

In the present investigation similar tests were performed on three cylindrical lattice structures and two spherical lattice structures. The details of the investigation are reported in Table 10.5. Before analysing the results of the present study, it is appropriate to comment on the previous investigations.

Fig. 10.5.a refers to tests performed by Johnson, Kondo and Wallihan (1966). It is evident from the dimensionless plots for the three structures that the Froude criterion is not the only factor involved. As the wave steepness increases the three curves tend to converge, with agreement between the control and the smaller model improving at high Reynolds numbers. This is confirmed in the second plot (Fig. 10.5.b) which shows the percentage difference between the control and smaller model values of transmission coefficient for varying Reynolds numbers. Some of the factors which would have affected their results as well as those of Wilson and Cross (1972) are,

(i) rubble sizes not exactly scaled and the absence of any precision in defining a characteristic dimension for the media;

(ii) variation in the porosities of the structures;

(iii) wave interaction and resulting losses due to the presence of an external porous interface to keep the rubble in place;

(iv) experimental errors which may have an influence on the smallest model used for the test.

Results of Delmonte (1972) are presented in Fig. 10.5.c and are very similar to those of Johnson et al. (1966) and, of the above factors, all except the first would have affected the results of the experimental programme. Delmonte (1972) used different parameters for his analysis. The results of Kondo and Toma (1972) are presented in Fig. 10.5.d and of the factors listed, only the last would have any influence on the results. This is an advantage when using a well-defined structural form for this type of experiment. The results indicate a similar trend to those of the other authors.

It should be noted that in all cases the transmission coefficients increased in ascending order of the characteristic dimension of the media and the curves tend to converge at higher values of wave steepness corresponding to higher Reynolds numbers.

10.6.2. Discussion of experimental results

The relevant information pertaining to the present investigation is given in Table 10.5. Using the Froude criterion for scaling and considering the largest structure to be the control model with the smaller units as models, the conditions specified in the table were used for the five structures. At the selected wave period and depth, transmission and reflection coefficients were obtained for different incident wave heights. It is noted that water depths ranging from 15.0 to 30 cm and wave periods ranging from 1.0 to 1.5 seconds were used for this study.

Figs. 10.6.a to 10.6.c show the results from cylindrical lattice structures. From these plots it is observed that scale effects are not particularly dominant for the three structures tested. In the case of K_t and K_d the results can be presented by a single curve with a good degree of correlation. The same cannot be said for the variation of K_r. It was pointed out earlier that K_r did not indicate a definite variation with wave steepness and this was attributed to an inherent deficiency in the method of measurement. This problem has been encountered by all who have performed similar studies.

Fig. 10.7 presents the results for the spherical lattice structure. Unlike the cylindrical lattice structures, the presence of scale effects is clearly observed. The smaller structures exhibited higher transmission, higher reflection and lower loss coefficients in comparison with the control model. A single curve cannot be used

to represent either transmission or reflection for both structures.

A cross-comparison with the work of Delmonte (1972) indicates that he obtained higher transmission for larger structures and this trend is not observed in the present study. This may be due to the fact that the wave period range used by Delmonte varied from 1.90 secs to 0.95 secs, whereas the corresponding range for this study varied from 1.16 secs to 1.00 sec . At shorter periods the energy dissipation is more effective and it increases with the length of the structure resulting in minimum transmission. Hence it is important to realize that due consideration should given to the wave period range when comparing the results of scale-effect studies. It is recommended that for a given set of structures, tests to investigate scale effects be performed for different ranges of wave period and water depth to assess their influence on the phenomenon.

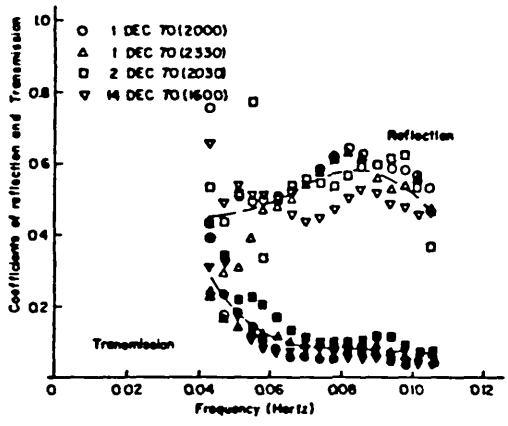
The objectives of this test programme were to investigate the influence of scale effects and their relative magnitude. From the foregoing discussion, it is evident that the results obtained cannot be generalized over a wide range of wave period and their interpretation is strictly limited to the test conditions. It is observed that the experiments are not really representative of typical model-to-prototype relationships. A more detailed study would need to cover scale ratios ranging from $^1/10$ to $^1/100$ for different ranges of wave period. For the selected test conditions in the present study, scale effects were less evident in cylindrical lattice structures than in spherical lattice structures.

Properties of porous media				Conditions specified for scale effect tests		
Details of structures used for the investigation		Dimension (mm)	Porosity	Structure length (cm)	Water depth (cm)	Wave period (sec)
Rubble Johnson et.al. (1966)	control model 1:2 model 1:4 model	33.0 14.2 9.1	0.45 0.49 0.50	60.96 30.48 15.24	60.96 30.48 15.24	1.40 0.99 0.70
Rubble Wilson & Cross (1972)	control model 1:1.8 model 1:4.23 model	34.8 19.4 8.2	0.437 0.411 0.428			
Closely packed spheres Delmonte (1972)	control model 1:2 model 1:4 model	54.0 27.0 13.5	0.40 0.40 0.40	60.96 30.48 7.62	48.77 24.38 12.19	1.90 1.34 0.95
Cylindrical lattice structures Kondo & Toma (1972)	control model 1:1.89 model 1:3.1 model 1:8.5 model	34.0 18.0 11.0 4.0	0.607 0.607 0.607 0.607		50.0 26.5 16.2 5.9	1.80 1.31 1.02 0.62

TABLE.10.4 DETAILS OF SELECTED INVESTIGATIONS ON THE INFLUENCE OF SCALE EFFECTS ON WAVE TRANSMISSION AND REFLECTION

Properties of porous media				Conditions specified for scale effect tests		
Details of structures used for the investigation		Dimension (Diameter in mm)	Porosity	Structure length (cm)	Water depth (cm)	Wave period (sec)
Cylindrical lattice structure	control model	30.0	0.607	45.0	30.00	1.50
	1:1.5 model	20.0	0.607	30.0	20.00	1.23
	1:2 model	15.0	0.607	22.5	15.00	1.06
Spherical lattice structure	control model	51.0	0.476	40.8	26.84	1.16
	1:1.34	38.0	0.476	30.4	20.00	1.00

TABLE.10.5 DETAILS OF THE PRESENT STUDY ON THE INFLUENCE OF SCALE EFFECTS ON WAVE TRANSMISSION AND REFLECTION



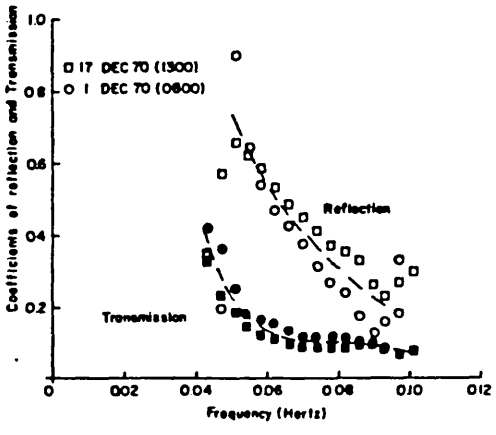


Fig.10.1.a Reflection and transmission coefficients vs Frequency
(Thornton and Calhoun 1972)

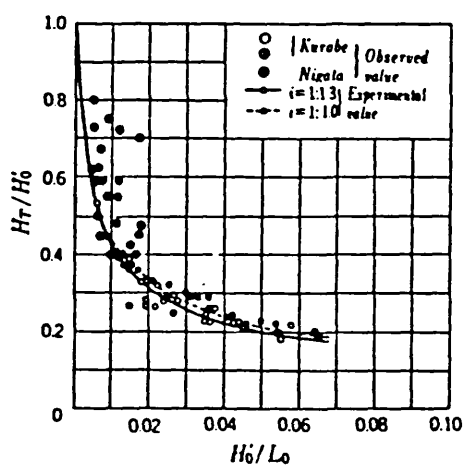


Fig.10.1.b Transmission coefficients vs Steepness
(Hattori and Sakai 1973)

FIG.10.1 RESULTS FROM FIELD STUDIES ON WAVE TRANSMISSION

FIG. 10.2 ENLARGEMENT FACTOR (k) vs POROSITY

$d_m = kL_r d_p$

k=enlargement factor

L_r=scale ratio based on Froudes Criteria

α=1500.0 , β=3.6

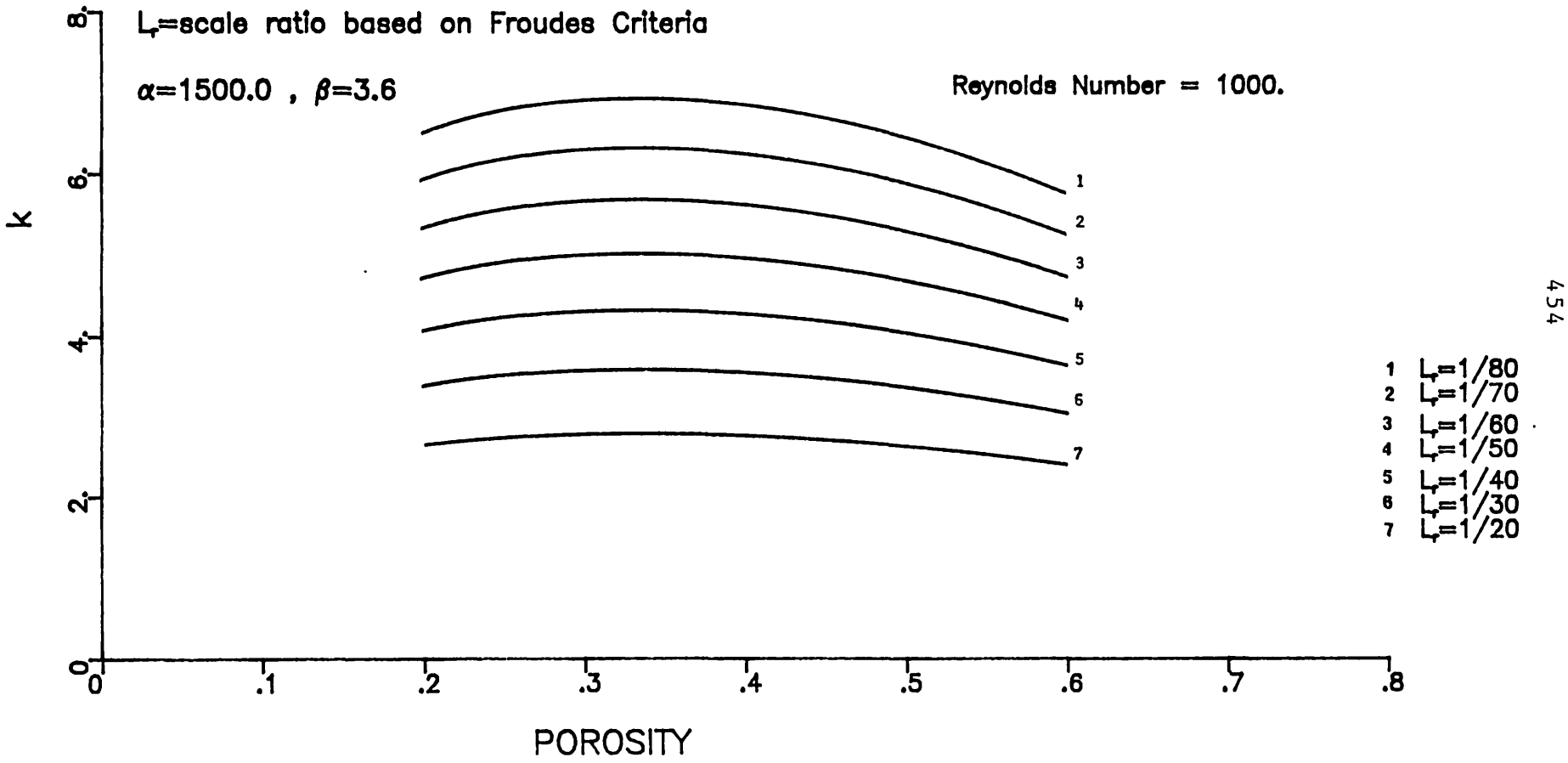


FIG. 10.3 ENLARGEMENT FACTOR (k) vs POROSITY

$d_m = kL_r d_p$

k=enlargement factor

L_r=scale ratio based on Froudes Criteria

α=1500. , β=3.6

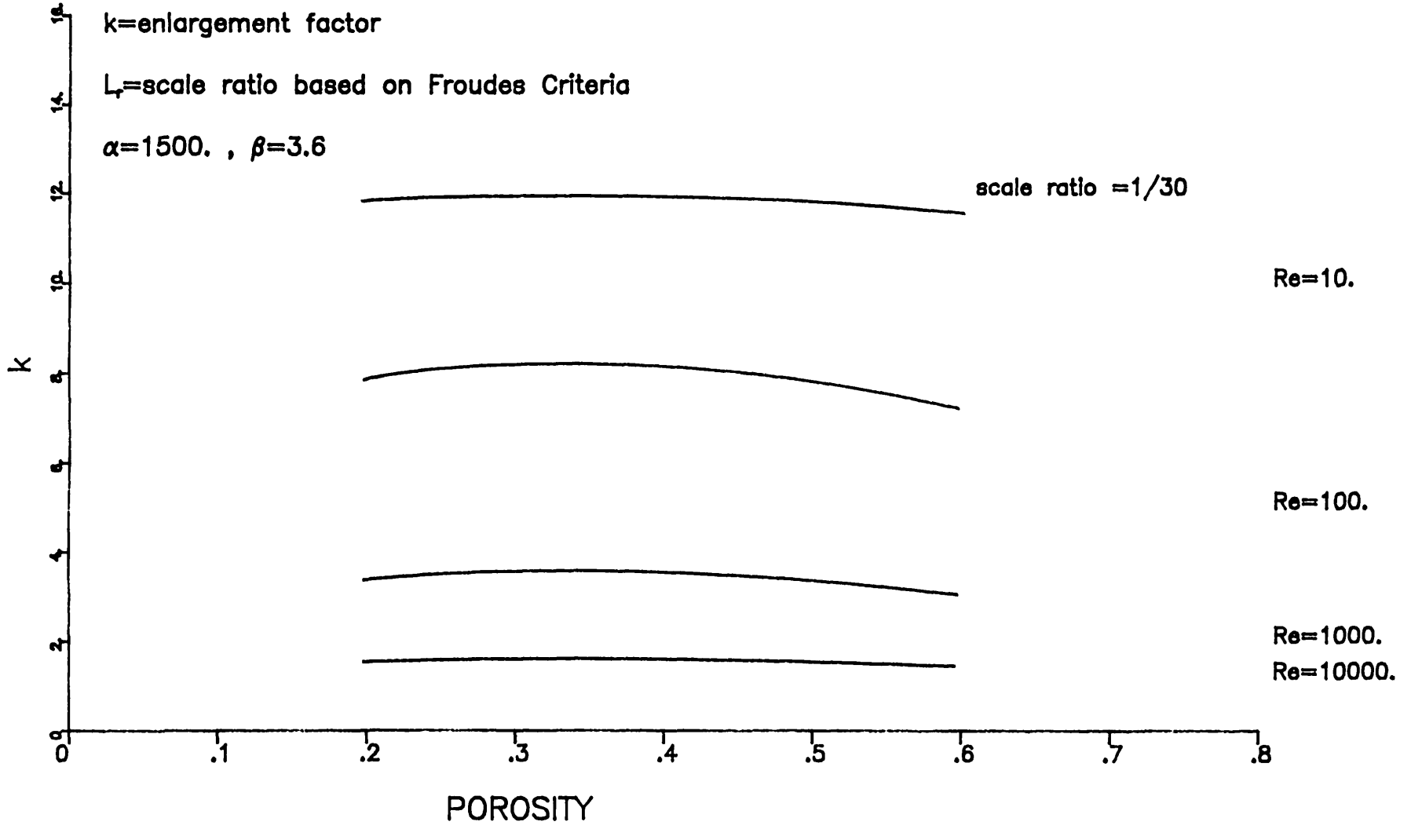


FIG. 10.4 ENLARGEMENT FACTOR (k) vs SCALE RATIO

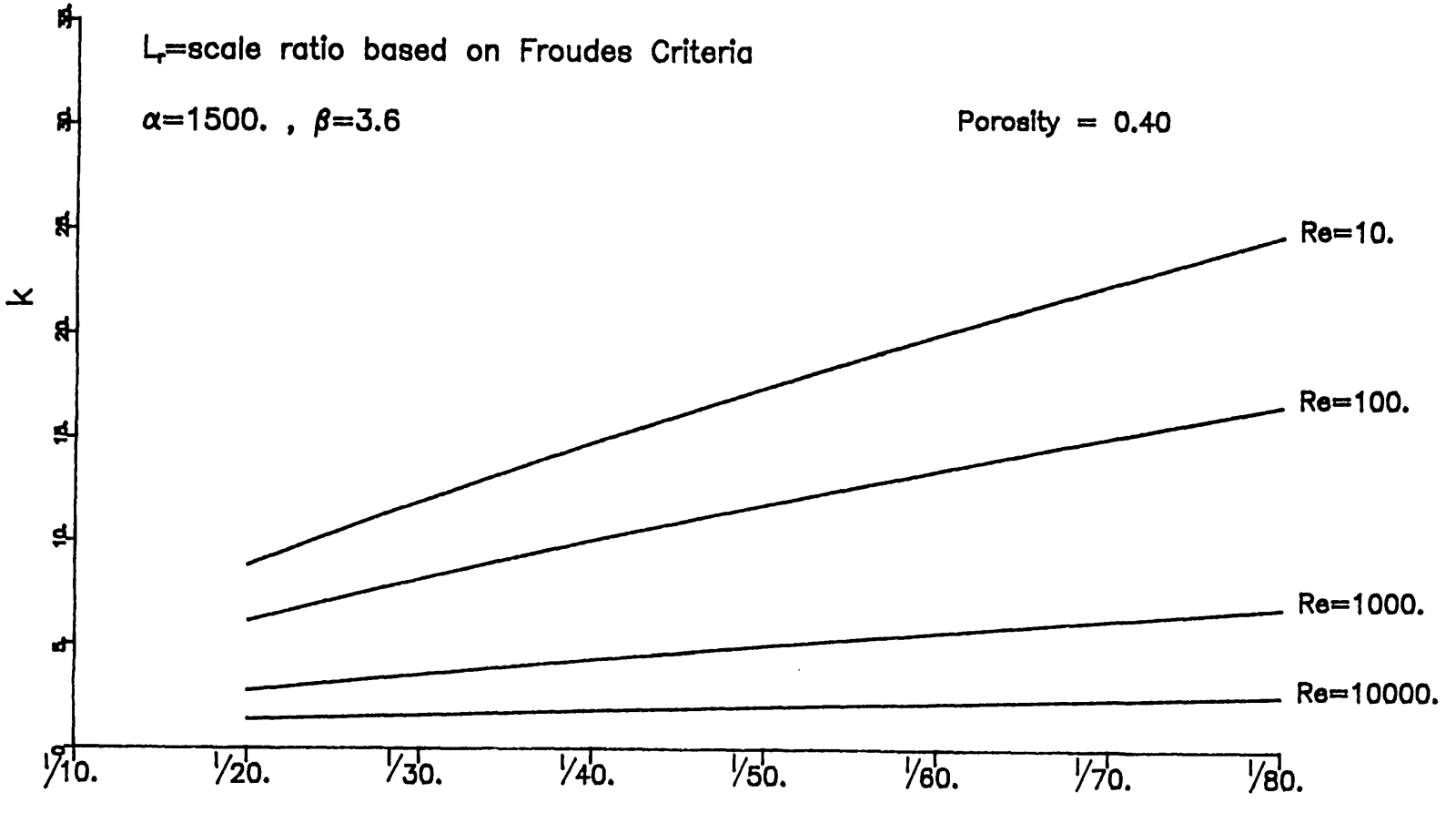
$d_m = k L_r d_p$

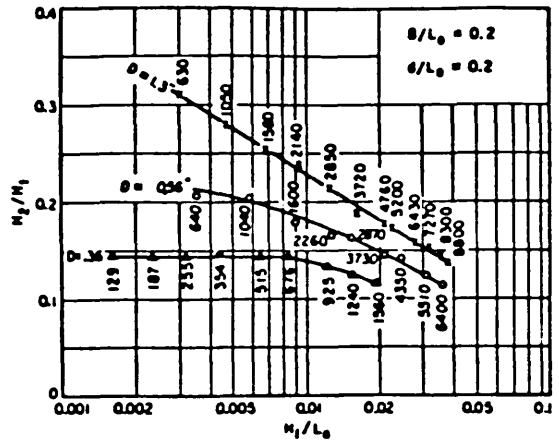
k=enlargement factor

L_r=scale ratio based on Froudes Criteria

α=1500. , β=3.6

Porosity = 0.40





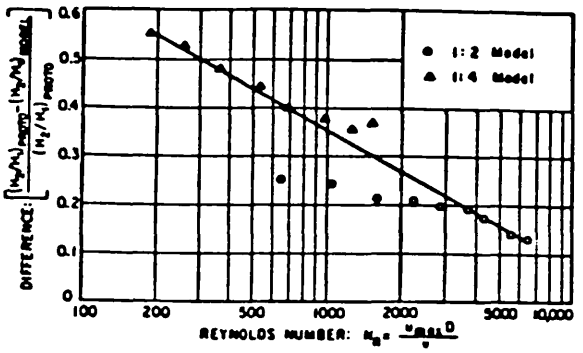


Fig.10.5.a and 10.5.b Variation of transmission coefficients vs Steepness and Reynolds number (Johnson,Kondo and Wallihan 1966)

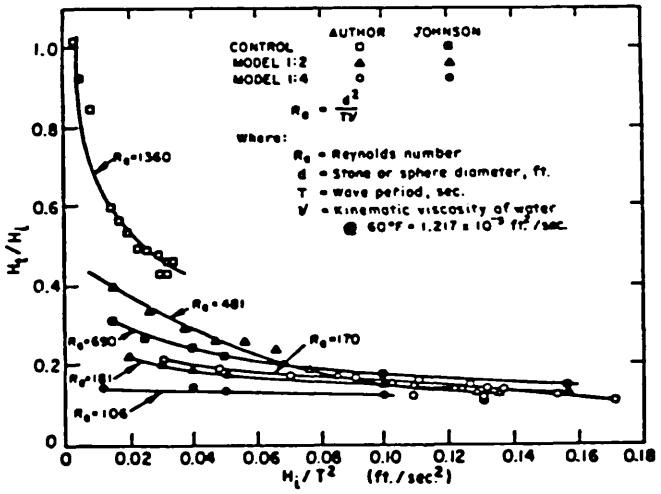


Fig.10.5.c Transmission coefficients vs Steepness (Delmonte 1972)

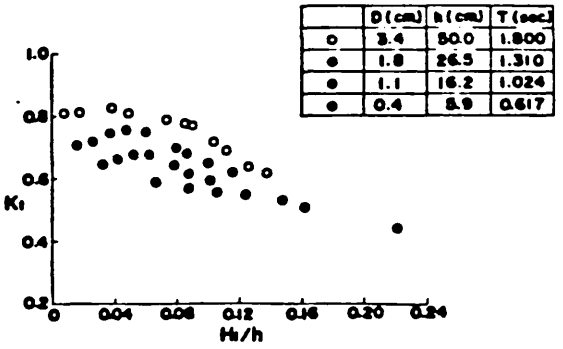


Fig.10.5.d Transmission coefficients vs Steepness (Kondo and Toma 1972)

FIG.10.5 RESULTS FROM PREVIOUS INVESTIGATIONS ON THE INFLUENCE OF SCALE EFFECTS ON WAVE TRANSMISSION

FIG.10.6.A K_T VS STEEPNESS

SCALE EFFECT TESTS FOR CYLINDRICAL LATTICE STRUCTURES

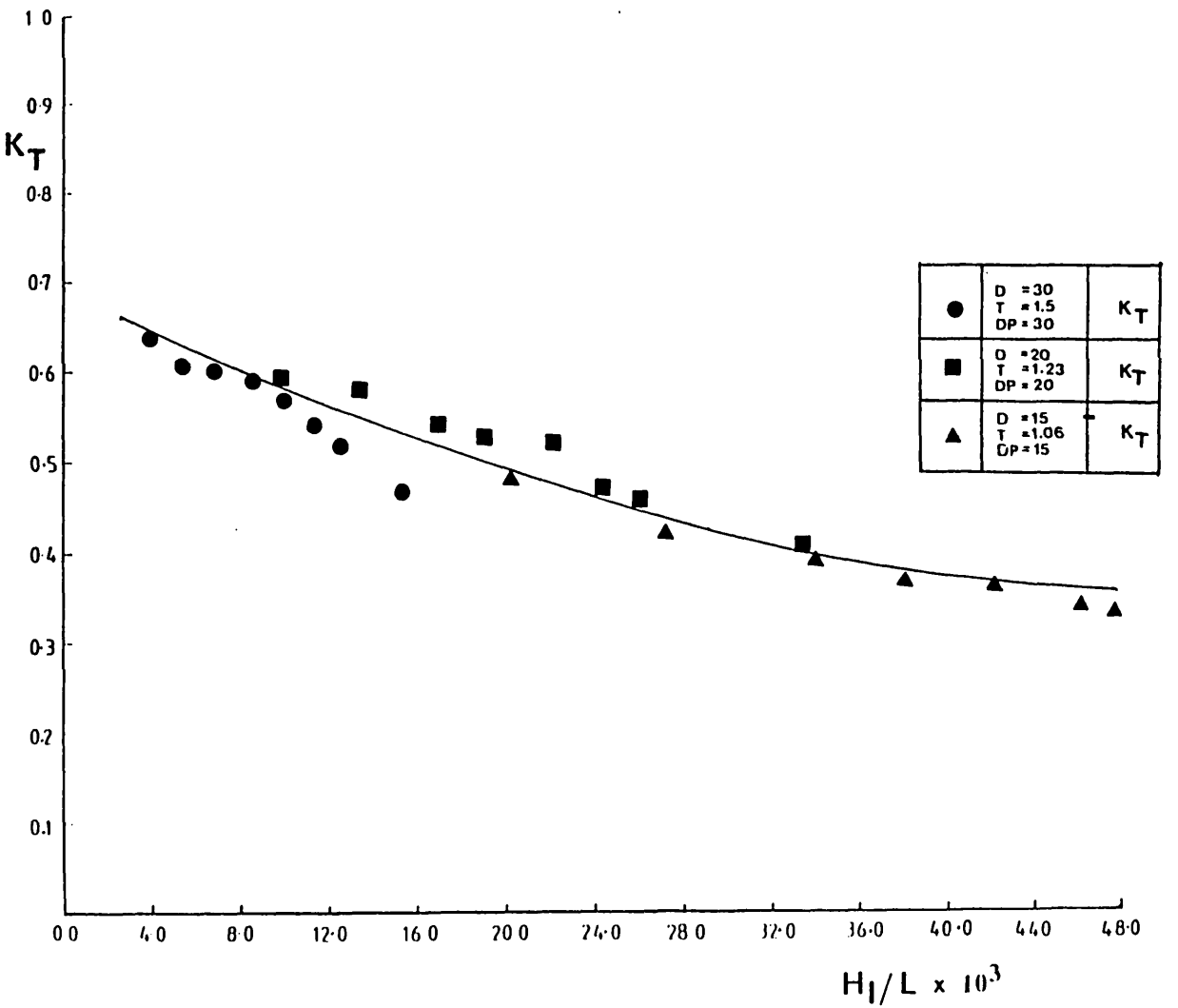


FIG.10.6.B K_R VS STEEPNESS

SCALE EFFECT TESTS FOR CYLINDRICAL LATTICE STRUCTURES

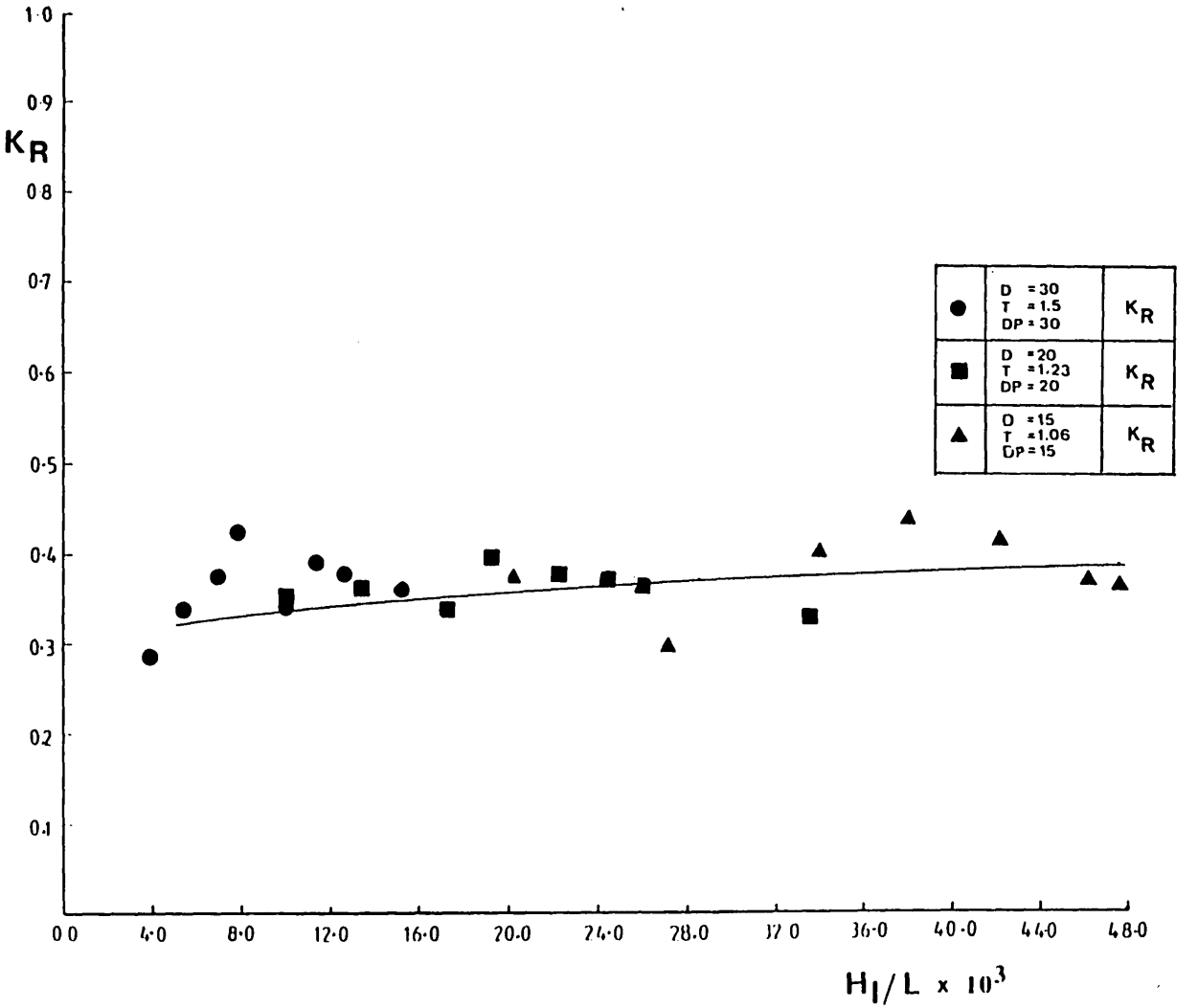


FIG.10.6.C K_D VS STEEPNESS

SCALE EFFECT TESTS FOR CYLINDRICAL LATTICE STRUCTURES

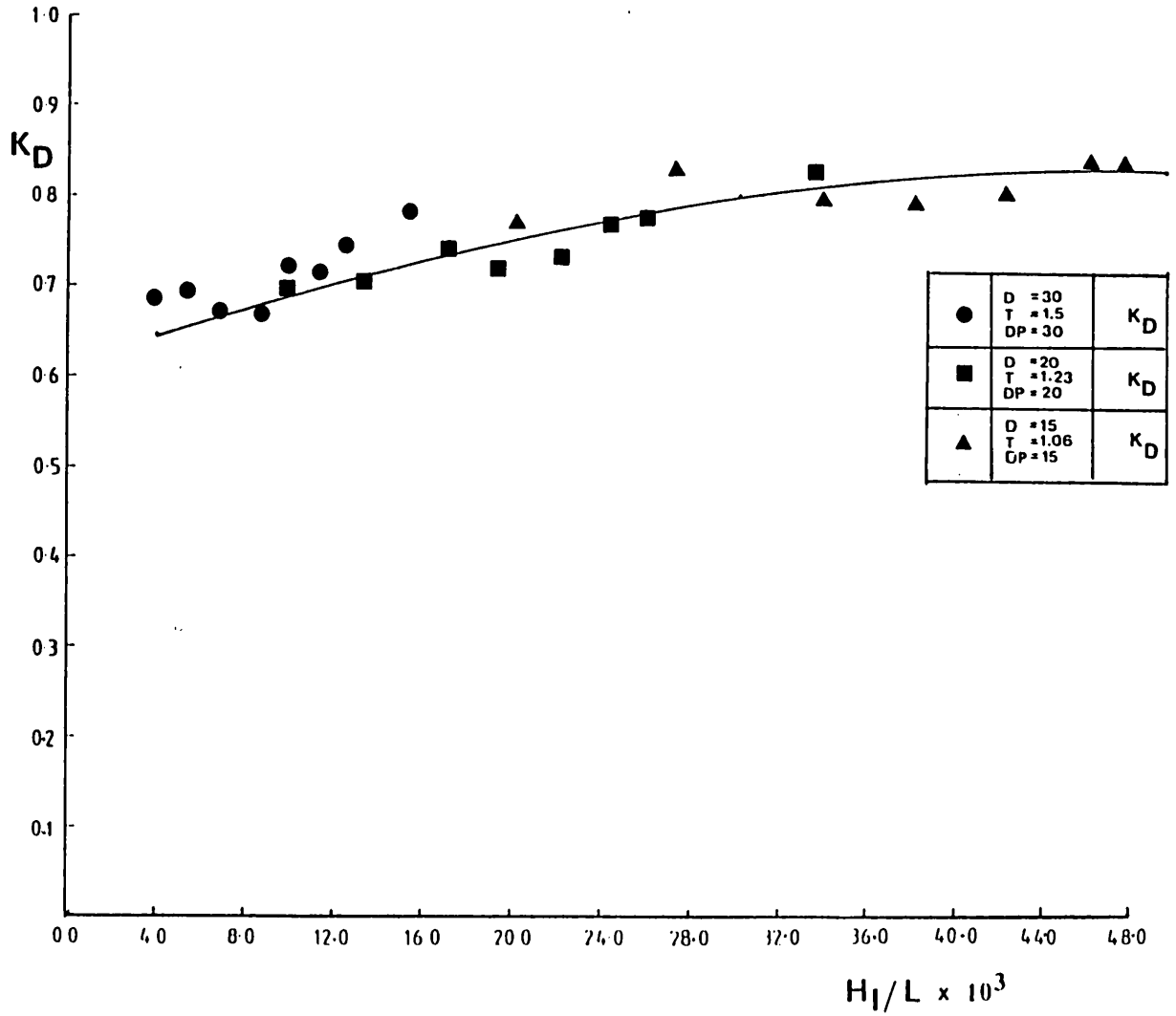
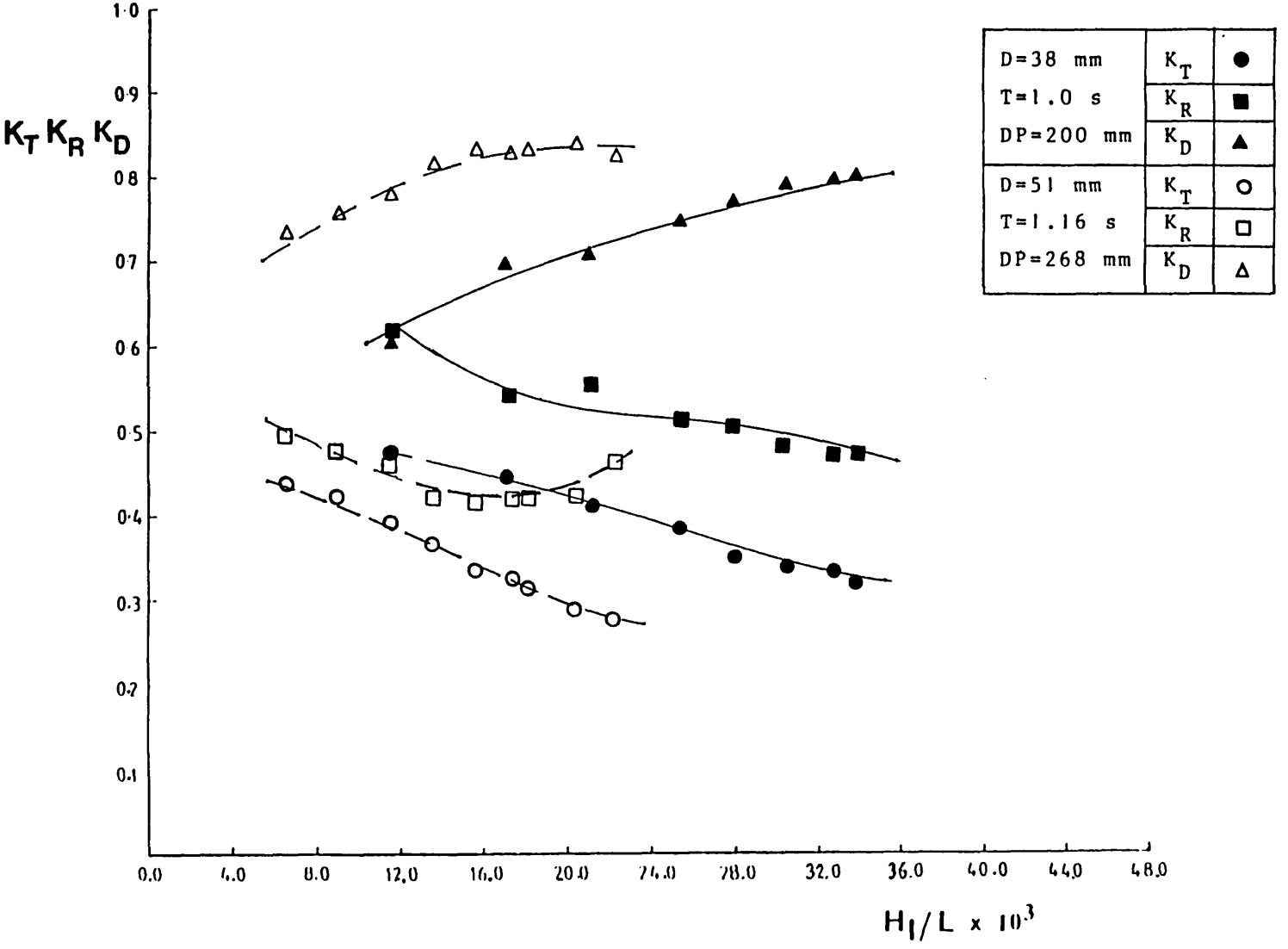


FIG.10.7 K_T,K_R AND K_D VS STEEPNESS

SCALE EFFECT TESTS FOR SPHERICAL LATTICE STRUCTURES



CHAPTER 11 - SUMMARY, CONCLUSIONS AND RECOMMENDATIONS

11.1. Summary

(1) This study presents the results from an extensive investigation into the hydraulic behaviour of porous structures. The main objective was to assess the influence of voids and overall geometry on the performance of porous coastal structures in relation to energy dissipation.

(2) Different types of porous media of varying internal and external configurations were used for the study. Experimental studies were performed under steady, oscillatory and accelerated flow conditions in which either the object to be tested or the surrounding fluid was set in motion in a prescribed manner.

(3) On the basis that the internal configuration of a porous medium consists of an assembly of packed elements, the influence of the geometry of both the constituent elements and the voids matrix on hydraulic behaviour was investigated by the proper selection of experimental media. Variation of the external geometry generated a wide spectrum of porous coastal structures of practical interest.

(4) The different structures investigated were broadly classified as follows:

(i) Vertical faced, rectangular, porous structures containing homogeneous fill. Depending on whether the rear face was permeable or impermeable, two types of structure, the open block and closed block, were identified. Gabion walls and vertical breakwaters built entirely from pre-cast concrete units are the closest prototype structures simulated by these porous media consisting of rock fill and hollow block armour units respectively.

(ii) Sloping structures containing homogeneous fill.

(iii) Conventional trapezoidal breakwaters with layered fill and armoured with hollow block armour units.

(iv) Vertical pile structures with and without horizontal bracings.

(5) The study identified the governing parameters both geometric and hydraulic, required to classify porous media in general and hollow block armour units in particular. The importance of these parameters in relation to wave energy dissipation was investigated by the proper selection of experimental media. The essence of the investigation was to obtain, from structures having a high overall porosity, increased energy dissipation characteristics while optimizing reflection and transmission coefficients. Such structures contribute to economic use of materials and reduce the overall costs for a given design.

(6) Analytical and numerical techniques were developed for the prediction of external and internal transmission coefficients and reflection coefficients for wave action on rectangular porous structures consisting of homogeneous fill. The respective coefficients were predicted in terms of the incident wave conditions and the hydraulic and geometric properties of the porous medium. An assessment was also made on the influence of scale effects on wave transmission through porous structures.

11.2. Conclusions

(1) The results of steady flow permeability tests established that both the Forchheimer and Exponential forms of resistance equations (eqs. 6.1 and 6.2) can be used for the hydraulic gradient – velocity relationship. Use of the Forchheimer form is recommended because it permits the investigation of the on–set of turbulence based on the ratio between turbulent and laminar components of the hydraulic gradient (eq. 6.3). The results also illustrated the sensitivity of the flow coefficients in the resistance equations to changes in the characteristic dimension of the void and interface properties. This information is directly applicable when estimating resistance coefficients for mathematical simulation of flow through porous media. The variability of the respective flow coefficients, when using different experimental apparatus, was evident from a comparison with previous investigations. Studies over a wide range of porous media demonstrated that it was not possible to develop a general formula which accommodates all the variables involved.

(2) Results of oscillatory flow tests on rectangular porous blocks established that provided the wave height exceeds the characteristic dimensions of the porous media, transmission coefficients decrease with increasing steepness – an observation accounted for by increased frictional losses. When the wave height was small in comparison to the characteristic dimension, waves interacted with individual components of the structure in contrast to effective flow through

a porous medium. The reflection coefficients did not display a definite dependence on wave steepness. However, the scatter in the results was not excessive and the order of magnitude could be estimated. It was not possible to relate the hydraulic behaviour of a given structural form to a single parameter such as the characteristic dimension or the overall porosity. The importance of the governing parameters in relation to wave energy dissipation was established from the results of the experimental programme. By proper selection of these parameters it was possible to construct porous structures which exhibit high loss coefficients with minimum reflection and transmission characteristics.

(3) Additional tests under oscillatory flow conditions assessed the influence of the external geometry on selected porous structures.

(i) Comparison of external and internal wave characteristics for vertical porous block structures of varying length, with and without rear impermeable faces illustrated several important design aspects in relation to their hydraulic behaviour. When waves collide against these structures most of the energy was attenuated within a short distance; of the order of about ten times the characteristic dimension from the front interface. This was more pronounced for steeper waves. Waves of long period and lower amplitude were more effectively transmitted through the structure. In the case of closed block structures the location of the rear impermeable face had a dominant influence on internal transmission coefficients and it was found that as the length of a closed block structure increased, its performance was very similar to the equivalent open block structure. This happens earlier with high amplitude waves having a shorter period. Extending the length of the structure beyond a certain value would be uneconomical as additional length did not contribute to significant further reductions in reflection and transmission coefficients. This optimum length was dependent on the dominant incident wave conditions. The reflection coefficients for the closed block structures were found to be lower than for open block structures and they also exhibited increased energy dissipation characteristics mainly due to the increased wave activity induced by the presence of standing waves.

(ii) For submerged porous block structures it was found that as the degree of submergence increased, the energy loss coefficients

decreased with increased wave transmission. However, marginal overtopping did not reduce the efficiency of the structure.

(iii) The introduction of a front slope to an existing vertical-faced, open block structure had a pronounced influence in controlling reflection characteristics. The variation in the transmission coefficients under these conditions was minimal. The reflection coefficients of sloping porous structures were found to be low in comparison with those corresponding to smooth or rough faced impermeable slopes.

(iv) Tests on the trapezoidal homogeneous breakwater and its rectangular equivalents supported the previous conclusion on the influence of sloping configurations. The trapezoidal structure proved to be very effective exhibiting minimum reflection and transmission characteristics.

(v) The front slope and the overall effective length are two important parameters of a porous wave absorber constructed with homogeneous material. Results from the study indicated that wave reflection was more dependent on the front slope whereas wave transmission was greatly influenced by the effective length. It was also evident that these structures perform at their best for wave breaking conditions with relatively short waves having high amplitudes rather than non-breaking long waves of small amplitude.

(4) Results from constant acceleration and velocity tests on a moving porous block identified the relative importance of the drag force and inertia force coefficients under constant acceleration. The drag force corresponding to a given instantaneous velocity within a flow with constant acceleration differed from that for the same constant velocity in a flow with zero acceleration; the former was greater than the latter. As the acceleration increased the corresponding increase in the drag force was greater. In comparison with the significant increase in the drag force, the influence of the inertia force under constant acceleration conditions was small.

(5) Tests on the breakwater section provided information on the mechanics of wave action on the breakwater as a whole and on forces acting on a typical hollow block armour unit.

(i) The energy dissipation characteristics of a hollow block armour slope were dependent to a high degree on the external and internal structure of the individual hollow block armour unit. An armour slope consisting of units having lateral porosity and an interconnected voids matrix with continuous and unobstructed flow paths was found to be more effective in dissipating energy. By the proper selection of governing parameters it is possible to design cost–effective hollow block armour units having increased porosity while optimising reflection, run–up, run–down and transmission. Reflection coefficients decrease with increasing wave steepness and decreasing armour slope. Empirical equations were presented for the prediction of reflection coefficients (eq. 9.5) and a comparison was made with previous studies on hollow block and interlocking types of armour unit (eqs. 9.6 and 9.7). For design purpose an initial estimate of the reflection coefficients can be made by these methods but detailed tests are recommended for the selected structural configuration and design wave conditions. Prediction equations should only be used within the flow range for which they have been developed.

(ii) The study identified the types of loads acting on armour units and in the case of a cubic hollow block type, along–slope and lift forces were considered the characteristic loading criteria. Results from tests using regular waves indicated that for a given armour unit – depending on its relative position and incident wave conditions – impact loads were superimposed on gradually varying or quasi–static loads. For armour units located in the immediate vicinity of the still water level impact loads were observed in both along–slope and normal components corresponding to point of impact. The positive along–slope force was found to be the dominant loading force with impact increasing with increasing wave steepness. The relative magnitude of the positive lift force was found to be within acceptable limits for the experimental conditions used for this study and the hydrodynamic forces were not high enough to extract the unit from the armour slope. In reality this force component will be resisted by frictional forces between adjacent armour units. The introduction of an impermeable underlayer did not cause any significant change in either the lift force or the along–slope force.

(6) The analytical and numerical simulation of wave motion in porous media provided satisfactory agreement with experimental results for a wide range of porous structures. In the comparison, several important aspects of physical significance were identified. The use and validity of steady flow coefficients under unsteady flow conditions and the proper evaluation of interface losses are two of them. To a great extent both were influenced by air entrainment. Sloping porous structures can be analysed using the methods presented by transforming the structure to an equivalent rectangular form. Allowances for wave breaking and losses at the interface have to be incorporated in the solution. The sensitivity of the numerical solution to variations in steady flow coefficients provided information on the possible outcome of improper estimation of these coefficients.

11.3. Recommendations

(1) Steady flow permeability tests over an extensive flow domain covering a wide range of rock fill are required to obtain a better understanding of the hydraulic gradient - velocity relationships for materials used for breakwater construction. It is recommended that these tests be performed in at least three different permeameters to study the variability of the coefficients when using different experimental apparatus.

(2) The effects of air entrainment due to wave-structure interaction and its influence on the effective conductivity of the structure have not been subjected to detailed research. It is recommended that a detailed study including interface losses due to waves breaking on vertical and sloping permeable faces be undertaken to cover a wide range of structures with varying external and internal configurations.

(3) In the absence of field data more detailed experimental information is required on reflection and transmission characteristics of typical trapezoidal breakwaters armoured with different types of armour units and of varying external slope and different internal configurations. The proposed empirical formulae (eqs. 9.5 and 9.6) can be improved from such results. This type of study will also provide information on the influence of the underlayers and the core on the hydraulic behaviour of breakwaters.

(4) Laboratory measurements of forces acting on hollow block armour units under more severe incident wave conditions should be made to obtain information on the relative magnitude of the respective force components. There is also a

need to determine the forces acting on the cap wall and the toe structure.

(5) The wave impact forces observed for both along-slope and normal force have important implications in relation to the capabilities of armour units to withstand such impact. Although dynamic similarity tests on armour units have been developed (Burcharth 1981), there remains a strong need to relate wave induced forces to armour strength.

(6) Full-scale measurements of wave forces and material strain in hollow block armour units are recommended. Results from these studies will provide information on the force domain of prototype units in service conditions.

(7) Evaluation of scale effects on wave reflection and transmission from rubble mound breakwaters and on the forces acting on armour units have not been considered in detail. Hence it is recommended that the series of tests identified in Sections 3 and 4 be performed at different scales and comparison be made with prototype data obtained from studies recommended in Section 6.

(8) The proposed analytical and numerical techniques should be extended to cover layered structures with sloping surfaces. For the analytical method this can be achieved by adopting equivalent rectangular sections whereas for the numerical method this can be achieved by refinements to the computational technique. However to do so it is necessary to obtain a proper estimate of the resistance coefficients and to incorporate quantitative expressions for air entrainment, interface losses and movement of outcrop point for a wide range of flow conditions and different structural configurations and this can only be evaluated by carefully controlled experimental programmes.

REFERENCES

ABBOT, M.B. 1966. An introduction to the method of characteristics. American Elsevier Publishing Co. New York.

ABBOT, M.B., PETERSON, H.M. and SKOVGAARD, O. 1978. On the numerical modelling of short waves in shallow water. Journal of Hydraulic Research. Vol. 16, No.3, pp. 173–204.

AGERSCHOU, H., LUNDGREN, H. and SORENSEN, T. 1984. Breakwater design: Chapter 6 of planning and design of ports and marine terminals. John Wiley and Sons.

AHMED, N. AND SUNADA, D.K. 1969. Non–linear flow in porous media. Journal of the hydraulics division, ASCE. Vol. 95, HY6, pp. 1847–1857.

ALLSOP, N.W. and OJO, S.I.A. 1982. Low–crest rubble mound breakwaters. Proc. of Int. Conf. on Hydraulic modelling of civil engineering structures.

ALLSOP, N.W. 1983. Low–crest breakwaters, studies in random waves. Proc. ASCE Conf. Coastal Structures '83, Virginia, U.S.A.

ARBHABHIRAMA, A. and DINOY, A.A. 1973. Friction–factor and Reynolds number in porous media flow. Journal of the hydraulics division, ASCE, Vol. 99, HY6, pp. 901–911.

AUSTIN, D.I. and SCHLUETER, R.S. 1982. A numerical model of wave–breakwater interactions. Proc. 18th Conf. on Coastal Engineering, Capetown, South Africa, pp. 2079–2096.

BARENDS, F.J., VAN DER KOGEL, H., UIJTTEWALL, F.J. and HAGENAAR, J. 1983. West breakwater, Sines Dynamic–geotechnical stability of breakwaters, Proc. ASCE Conf. Coastal Structures '83, Virginia, U.S.A.

BATTJES, J.A. 1974. Surf similarity. Proc. 14th Conf. on Coastal Engineering, Copenhagen, Denmark, Chapter 26, pp. 466–680.

BENASSAI, E., RAGONE, A. and SCIORTINO, J.A. 1983. Wave attenuation due to a modular porous breakwater. Proc. ASCE Conf. Coastal Structures '83, Virginia, U.S.A., pp. 222–234.

BIESEL, F. 1950. Equations de l'ecoulement non lent en miliesu permeable, application au calcul des filtres a houle. La Houille Blanche, 2.

BRUUN, P. and JOHANNESSON, P. 1976. Parameters affecting the stability of rubble mounds. Journal of waterways, harbour and coastal engineering, ASCE, Vol.102, WW2, pp. 141-164.

BURCHARTH, H.F. 1981. Full-scale dynamic testing of Dolosse to destruction. Coastal Engineering, 4, pp. 229-251.

BURCHARTH, H.F. 1983. Material, structural design of armour units. Proc. seminar on Rubble Mound Breakwaters, Stockholm, Sweden.

BURCHARTH, H.F. and THOMPSON, A.C. 1983. Stability of armour units in oscillatory flow. Proc. ASCE Conf. Coastal Structures '83, Virginia, U.S.A.

CARVER, R.D. and DAVIDSON, D. 1978. Dolos-armoured breakwaters. Proc. 16th Conf. on Coastal Engineering, Hamburg, Germany. Chapter 136, pp. 2263-2284.

COSTELLO, R.D. 1952. Damping of water waves by vertical circular cylinders. Trans. Amer. Geophys. Union. Vol.33, No.4, pp. 513-519.

DAI, Y.B. and KAMEL, A.M. Scale effect tests for rubble mound breakwaters. US Army Engineer. Waterways Experiment Station, Vicksburg, Missisippi. Res. report H-69-2.

DARCY, H. 1856. Les fontaines publiques de la ville de Dijon, Dalmont, Paris.

DATTARI, J., RAMAN, H. and SHANKER, N.J. 1978. Performance characteristics of submerged breakwaters. Proc. 16th Conf. on Coastal Engineering, Hamburg, Germany. Chapter 130, pp. 2153-2171.

DELMONTE, R.C. 1972. Scale effects of wave transmission through permeable structures. Proc. 13th Conf. on Coastal Engineering, Vancouver, Canada. Chapter 105, pp. 1867-1872.

DICK, T.M. and BREBNER, A. 1968. Solid and permeable submerged breakwaters. Proc. 11th Conf. on Coastal Engineering, London, England. Chapter 72, pp. 1141-1158.

DRACOS, T. 1969. Calculation of the movement of the outcrop point. Proc. XIII, Congress of the IAHR, paper D-2, Kyoto, Japan.

DUDGEON, C.R. 1966. An experimental study of the flow of water through coarse granular media. La Houille Blanche. 7. pp. 785-801.

DUDGEON, C.R. 1967. Wall effect in permeameters. Journal of the hydraulics division. ASCE, Vol. 93.

ENGELUND, F. 1953. On the laminar and turbulent flow of groundwater through homogeneous sand. Trans. Danish Acad. Tech. Sci. No. 3.

FALLON, A.R. 1972. Discontinuous composite wave absorber studies. Proc. 13th Conf. on Coastal Engineering, Vancouver, Canada. Chapter 108, pp. 1903-1916.

FORCHHEIMER, P. 1901. Wasserbewegung durch Boden. Zeit. Ver. deutsch. Ing., 45.

FUHRBOTER, A. 1970. Air entrainment and energy dissipation in breakers. Proc. 12th Conf. on Coastal Engineering. Washington D.C., U.S.A. Chapter 24, pp. 391-398.

FUHRBOTER, A. 1986. Model and prototype tests for wave impact and run-up on a uniform 1:4 slope. Coastal Engineering. 10. pp. 49-84.

GARRISON, C.J., FIELD, J.B. and MAY, M.D. 1977. Drag and inertia forces on a cylinder in periodic flow. Journal of the waterway port coastal and ocean division. ASCE. Vol.103, WW2, pp. 193-204.

GIBSON, R.J. and WANG, H. 1977. Added mass of pile group. Journal of the waterway port coastal and ocean division. ASCE. Vol.103, WW2, pp. 215-223.

GODA, Y. and IPPEN, A.T. 1963. Theoretical and experimental investigation of wave energy dissipators composed of wire mesh screens. Massachusetts Institute of Technology, Hydrodynamics Laboratory Report. No. 60.

GOPALAKRISHNAN, T. and TUNG, C. 1980. Run-up of non-breaking waves - a finite element approach. Coastal Engineering. 4. No.1.

GORING, D.G. and RAICHLEN, F. 1979. Forces on block bodies accelerating in still fluid. Journal of the waterway port coastal and ocean engineering. ASCE. Vol. 105, WW2, pp. 171-189.

GRAVESON, H. 1979. Design of caisson breakwaters. Danish Hydraulic Institute. Report 1/79.

GRUNE, J. and KOHLHASE, S. 1974. Wave transmission through vertical slotted walls. Proc. 14th Conf. on Coastal Engineering, Copenhagen, Denmark. Chapter 111, pp. 1906-1923.

GUNBAK, A.R. 1979. Rubble Mound Breakwaters. Division of port and ocean engineering, University of Trondheim, The Norwegian Institute of Technology, Trondheim, Norway. Report No. 1.

GUPTA, R.D. 1985. Angularity of aggregate particles as a measure of their shape and hydraulic resistance. Proc. Inst. Civ. Engrs. Part 2, Vol. 79, pp. 705-716.

HAKKELING, B. 1971. New technique used in Scheveningen breakwater construction. The Dock and Harbour Authority. July, pp. 104-106.

HANNOURA, A.A. and McCORQUODALE, J.A. 1978a. Virtual mass of coarse granular media. Journal of the waterway port coastal and ocean division. ASCE. Vol. 104, WW2, pp. 191-200.

HANNOURA, A.A. and McCORQUODALE, J.A. 1978 b. Air-water flow in coarse granular media. Journal of the hydraulics division. ASCE. Vol. 104, HY7, pp. 1001-1010.

HANNOURA, A.A. and McCORQUODALE, J.A. 1978 c. Unsteady flow in porous media solved by combined finite element method of characteristic model. Proc. 2nd Int. Conf. on Finite Elements in Water Resources, London.

HANNOURA, A.A. and McCORQUODALE, J.A. 1979 a. Wate motion in rockfill embankments. Advances in Water Resources. Vol. 2, pp. 149-152.

HANNOURA, A.A. and McCORQUODALE, J.A. 1979 b. Environmental wave forces on rubble mound breakwaters. Civil Engineering in the Ocean IV. Vol. 1, pp. 367-379.

HANNOURA, A. 1980. A hybrid finite element model applied to unsteady flow problems. Proc. 3rd Conf. on Finite elements in water resources.

HANNOURA, A. and BARENDS, F. 1981. Non-Darcy flow: A state of the art. Flow and transport in porous media. Editors. Verruijt, A., Barends, F., Balkema, A.A., Rotterdam, The Netherlands.

HANNOURA, A.A. and BARENDS, F. 1982. Numerical modelling of rubble mound breakwaters. Proc. 4th Int. Conf. on Finite elements in water resources, Germany.

HANNOURA, A.A. and McCORQUODALE, J.A. 1985 a. Rubble mounds: hydraulic conductivity equation. Journal of waterway port coastal and ocean engineering division. ASCE. Vol. 111, WW5, pp. 783-799.

HANNOURA, A.A. and McCORQUODALE, J.A. 1985 b. Rubble mounds: numerical modelling of wave motion. Journal of waterway port coastal and ocean engineering division. ASCE. Vol. 111, WW5, pp. 800-816.

HATTORI, M. and SAKAI, M. 1973. Experimental study on wave transmission through breakwaters. Proc. 20th Japanese conf. on Coastal Engineering.

HOLMES, P. and CHAPLIN, J.R. 1978. Wave loads on horizontal cylinders. Proc. 16th conf. on Coastal Engineering, Hamburg, Germany. Chapter 147, pp. 2449-2460.

HOWELL, G. 1986. A system for the measurement of the structural response of Dolos armour units in the prototype. Proc. Int. conf. on Measuring techniques of hydraulic phenomena in offshore, coastal and inland waters, London, pp. 177-188.

HUDSON, R.Y. 1959. Laboaratory investigation of rubble mound breakwaters. Journal of the waterways, and harbours division. ASCE. Vol. 85, WW3, pp. 93-119.

HUDSON, R.Y. 1979. Coastal hydraulic models. US Army Corps of Engineers, Coastal Engineering Research Center. Fort Belvoir. Special report No. 5.

HUNT, I.A. 1959. Design of seawalls and breakwaters. Journal of the waterways and harbours division. ASCE. Vol. 85, WW3, pp. 123-152.

HYDRAULICS RESEARCH STATION. 1970. High Island Water Scheme in Hong Kong. A study on the use of dolos armour units for wave protection on the seaward face of the eastern dam. Report EX 532.

HYDRAULICS RESEARCH STATION. 1973. High Island Water Scheme in Hong Kong. Model tests of a Cob block wave protection cover for the inner face of the main dam. Report EX 632.

HYDRAULICS RESEARCH STATION. 1983. The Shed breakwater armour unit, model tests in random waves. Report EX 1124.

IJIMA, T., TANAKA, E. and OKUZONO, H. 1976. Permeable seawall with reservoir and the use of Warock. Proc. 15th conf. on Coastal Engineering, Honolulu, Hawaii. Chapter 151, pp. 2063–2642.

IRIBARREN, C. and NOGALES, C. 1949. Protection des Ports II. Comm 4. 17th Int. Navig. Congr., Lisbon, pp. 31–80.

JENSEN, O.J. and KLINTING, P. 1983. Evaluation of scale effects in hydraulic models by analysis of laminar and turbulent flows. Coastal Engineering. 7, pp. 319–329.

JOHNSON, J.W., KONDO, H. and WALLIHAN, R. 1966. Scale effects in wave action through porous structures. Proc. 10th conf. on Coastal Engineering, Tokyo, Japan. Chapter 59, pp. 1022–1024.

KAMEL, A.M. 1969. Water wave transmission through and reflection by pervious coastal structures. US Army Engineer Waterways Experiment Station. Res. report.. H–69–1.

KEULEGAN, G.H. and CARPENTER, L.H. 1958. Forces on cylinders and plates in an oscillating fluid. Journal of research of the National Bureau of Standards. Vol. 60, no. 5, Res. paper 2857.

KEULEGAN, G.H. 1968. Wave damping effect of screens. US Army Engineer. Waterways Experiment Station. CE. Vicksburg, Missisipi. Res. report. No. 2–12.

KEULEGAN, G.H. 1973. Wave transmission through rock structures, Hydraulic model investigation. US Army Engineer Waterways Experiment Station. Hydraulics laboratory, Vicksburg, Missisipi. Res. report. H-73-1, 75.

KHADER, Abdul, M.H. and RAI, S.P. 1980. A study of submerged breakwaters. Journal of Hydraulic Research. Vol. 18, No. 2, pp. 113-122.

KOGAMI, Y. 1978. Researches on stability of rubble mound breakwaters. Coastal Engineering in Japan. Vol. 21, pp. 76-93.

KONDO, H. 1970. An analytical approach to wave transmission through permeable structures. Coastal Engineering in Japan. Vol. 13, pp. 31-42.

KONDO, H. and TOMA, S. 1972. Reflection and transmission for a porous structure. Proc. 13th conf. on Coastal Engineering, Vancouver, Canada. Chapter 104, pp. 1847-1865.

KONDO, H., TOMA, S. and YANO, K. 1976. Laboratory study on pervious core breakwaters. Proc. 15th conf. on Coastal Engineering, Honolulu, Hawaii. Chapter 152, pp. 2643-2661.

KOUTITAS, C. 1982. A numerical model for rubble mound breakwater stability. Proc. symp. on Eng. in marine environment, Brugge, pp. 21-26.

LEAN, G.H. 1967. A simplified theory of permeable wave absorbers. Journal of Hydraulic Research. Vol. 5, No. 1, pp. 15-30.

LeMEHAUTE, B. 1957. Permeabilite des digues en enrochements aux ondes gravite periodiques. (The perviousness of rockfill breakwaters to periodic gravity waves). La Houille Blanche. No. 6, 1957, pp. 903-916 and Nos. 2, 3, 1958.

LeMEHAUTE, B. 1965. Wave absorbers in harbours. US Army Engineer Waterways Experiment Station. CE, Vicksburg, Miss. Contract report. No. 2-122.

LIGGET, J.A. and CUNGE, J.A. 1975. Numerical methods of solution of the unsteady flow equations. Chapter 4 of Unsteady flow in open channels. (Ed. Mahmood, K. and Yevjevich, V.) Water Resources Publications, Fort Collins.

LIGTERINGEN, H. 1983. Developments in model techniques for breakwaters in deep water. Proc. seminar on Breakwaters, Casablanca.

LIGTERINGEN, H. and HEYDRA, G. 1984. Recent progress in breakwater design. Dock and Harbour Authority. July, pp. 47-50.

LIGTERINGEN, H., MOL, A. and GROENEVELD, R.L. 1985. Criteria and procedures for the structural design of concrete armour units. Proc. conf. on Developments in Breakwaters. Inst. Civil Engrs., London, England.

LOSADA, M.A. and GIMENEZ-CURTO, L.A. 1981. Flow characteristics on rough permeable slopes under wave action. Coastal Engineering. 4, pp. 187-206.

LUDWICK, J.C. et al. 1976. Field performance of permeable breakwaters. Journal of the waterway port coastal and ocean engineering. ASCE. WW3, Vol. 102, pp. 357-368.

MADSEN, O.S. 1974. Wave transmission through porous structures. Journal of the waterways, harbours and coastal engineering. ASCE. Vol. 100. WW3, pp. 169-188.

MADSEN, O.S.and WHITE, S.M. 1976 a. Energy dissipation on a rough slope. Journal of the waterways, harbours and coastal engineering division. ASCE. Vol. 102, WW1, pp. 31-48.

MADSEN, O.S. and WHITE, S.M. 1976 b. Wave transmission through trapezoidal breakwaters. Proc. 15th conf. on Coastal Engineering, Honolulu, Hawaii. Chapter 153, pp. 2662-2676.

MADSEN, O.S., SHUSANG, P. and HANSON, S.U. 1978. Wave transmission through trapezoidal breakwaters. Proc. of 16th conf. on Coastal Engineering, Hamburg, Germany. Chapter 129, pp. 2140-2152.

MADSEN, P.A. 1983. Wave reflection from a vertical permeable wave absorber. Coastal Engineering. 7, pp. 381-396.

MADSEN, P.A. and WARREN, I.R. 1984. Performance of a numerical short-wave model. Coastal Engineering. 8, pp. 73-93.

MASSEL, S.R. and MEI, C.C. 1977. Transmission of random wind waves through perforated or porous breakwaters. Coastal Engineering. 1, pp. 63–78.

MASSEL, S.R. and BUTOWSKI, P. 1980. Wind waves transmission through porous breakwater. Proc. 17th conf. on Coastal Engineering, Sydney, Australia. Chapter 19, pp. 333–346.

MATTSON, A. 1963. Reflections of gravity waves. Proc. of the IAHR congress, London, pp. 319–326.

McCORQUODALE, J.A. 1970. The finite element method applied to non–Darcy flow. 18th Annual Speciality Conference, Hyd. division, ASCE, University of Minnesota.

McCORQUODALE, J.A. 1972. Wave energy dissipation in rockfill. Proc. 13th conf. on Coastal Engineering, Vancouver, Canada. Chapter 107, pp. 1885–1901.

McCORQUODALE, J.A. and NASSER, M.S. 1974. Numerical methods for unsteady non–Darcy flow. Int. symposium on finite element methods in flow problems, Swansea, pp. 545–557.

McCORQUODALE, J.A. and HANNOURA, A.A. 1977. Accelerated flow in porous media. Proc. 6th Canadian Congress of Applied Mechanics, Vancouver, Canada, pp. 611–612.

McCORQUODALE, J.A., NASSER, M.S. and HANNOURA, A.A. 1977. The effect of entrained air on wave action on a porous structure. Proc. 6th Canadian congress of Applied Mechanics, Vancouver, Canada, pp. 541–542.

McCORQUODALE, J.A., HANNOURA, A.A. and NASSER, M.S. 1978. Hydraulic conductivity of rockfill. Journal of Hydraulic Research. Vol. 16, No. 2, pp. 123–137.

MICHE, M. 1951. Pouvoir reflechissant des ouvrages maritimes exposes a L'action de Houle. Annales des Pont et Chaussees, pp. 295–319.

MIZUMURA, K. 1984. Flow analyses in idealized rubble mound breakwater. Journal of waterway port coastal and ocean engineering division. ASCE. Vol. 110, WW3, pp. 344–355.

MORAES, C. 1970. Experiments of wave reflection on impermeable slopes. Proc. 12th conf. on Coastal Engineering, Washington D.C., U.S.A. Chapter 31, pp. 509-521.

NASSER, M.S. and McCORQUODALE, J.A. 1973. Wave propagation in a rockfill dam. Proc. of the IAHR symposium, Istanbul, Turkey, pp. 173-176.

NASSER, M.S. and McCORQUODALE, J.A. 1974. Experimental study of wave transmission. Journal of the waterway harbours and coastal engineering division. ASCE. Vol. 100, WW4, pp. 279-286.

NASSER, M.S. and McCORQUODALE, J.A. 1975. Wave motion in rockfill. Journal of the waterway port coastal and ocean engineering division.ASCE. Vol. 101, WW2, pp. 145-160.

NASSER, M.S. 1977. The outcrop point movement in non-Darcy flow. Proc. 6th Canadian Congress of Applied Mechanics, Vancouver, Canada, pp. 613-614.

NASSER, M.S. 1979. Experimental analysis of wave interaction with rockfill embankments with impervious cores. Proc. Port and ocean engineering under arctic conditions, Norway, pp. 1351-1364.

NG, H.C. 1969. An experimental study of steady non-Darcy flow in crushed rock. MASc. dissertation, University of Windsor, Windsor, Ontario, Canada.

POLUBARINOVA-KOCHINA, P.Y. Theory of the motion of groundwater. Princeton University Press, Princeton, New Jersey.

SANDSTROM, A. 1974 a. Measurement of incident wave height in composite wave trains. Proc. 14th conf. on Coastal Engineering, Copenhagen, Denmark. Chapter 21, pp. 386-391.

SANDSTROM, A. 1974 b. Wave forces on blocks of rubble mound breakwaters. Hyd. Lab., Royal Institute of Technology, Stockholm, Sweden. Bulletin no. 83.

SARPKAYA, T. AND GARRISON, C.J. 1963. Vortex formation and resistance in unsteady flow. Journal of Applied Mechanics. Vol. 30, series E, no. 1, pp. 16-24.

SARPKAYA, T. 1975. Forces on cylinders in a sinusoidally oscillating fluid. Journal of Applied Mechanics. ASME, pp. 32–37.

SARPKAYA, T. and COLLINS, N.J. 1978. Drag and inertia forces on a cylinder in periodic flow. (Discussion of the paper by Garrison, C.J., Field, J.B. and May, M.D. 1977). Journal of the waterway port coastal and ocean division. ASCE, Vol. 104, WW1, pp. 96–98.

SAWARAGI, T. 1966. Scouring due to wave action at the toe of permeable coastal structures. Proc. 10th conf. on Coastal Engineering, Tokyo, Japan. Chapter 61, pp. 1036–1047.

SCHEIDEGGER, A.E. 1974. The physics of flow through porous media. University of Toronto Press.

SCOTT, TURCKE, BAIRD and REDSHAW 1987. A rational design procedure for concrete armour units for breakwaters. The Dock and Harbour Authority. January, pp. 203–208.

SEELIG, W.N. 1983. Wave reflection from coastal structures. Proc. ASCE conf. Coastal Structures '83, Virginia, U.S.A., pp. 961–973.

SHIMADA, T., HIROAKI, Y. and IWASA, N. 1981. Stability against wave, wave reflection factor and transmission factor of Diagonal Frame Caissons. Proc. 28th Japanese conf. on Coastal Engineering.

SHIRAISHI, N., PALMER, R. and OKAMOTO, H. 1976. Quay wall with wave absorber 'Igloo'. Proc. 15th conf. on Coastal Engineering, Honolulu, Hawaii. Chapter 154, pp. 2677–2696.

SHUTO, N. and HASHIMOTO, H. 1970. Hydraulic resistance of artificial concrete blocks. Proc. 12th conf. on Coastal Engineering, Washington D.C., U.S.A. Chapter 97, pp. 1587–1599.

SIGURDSSON, G. 1962. Wave forces on breakwater capstones. Journal of the waterways and harbours division. ASCE. Vol. 88, WW3, pp. 27–60.

SINGH, K.Y. 1968. Stabit – a new armour block. Proc. 11th conf. on Coastal Engineering, London, England. Chapter 52, pp. 797–814.

SMITH, G.D. 1979. Numerical solution of partial differential equations. Oxford University Press, London, 2nd edition.

SOLLITT, C.K. and CROSS, R.H. 1972. Wave transmission through permeable breakwaters. Proc. 13th conf. on Coastal Engineering, Vancouver, Canada. Chapter 103, pp. 1827–1846.

STICKLAND, I.W. 1969. Cob Units – Report on hydraulic model research. Wimpey Laboratory, Ref. no. H/334.

STIVE, R.J.H. 1984. Wave impact on uniform slopes at approximately prototype scale. Proc. symposium on scale effects in modelling hydraulic structures, Esslingen, Germany.

STRAUB, L.G. 1956. Experimental studies of wave filters and absorbers. St. Anthony falls hydraulics laboratory, University of Minnesota. Project report no. 44.

SULISZ, W. 1985. Wave reflection and transmission at permeable breakwaters of arbitrary cross-section. Coastal Engineering. 9, pp. 371–386.

SVENDSEN, I.A. 1976. Reflection of long waves from rubble mound breakwater. Institute of Hydrodynamics and Hydraulic Engineering, Technical University, Denmark. Progress report 38.

TIMCO, G., MANSARD, E.P.D. 1982. Improvements in modelling rubble-mound breakwaters. Proc. 18th conf. on Coastal Engineering. Chapter 122, pp. 2047–2061.

TENG, C.C. and NATH, J.H. 1985. Forces on horizontal cylinder towed in waves. Journal of waterway port coastal and ocean engineering division. ASCE, Vol. 111, WW6, pp. 1022–1040.

THORNTON, E.B. and CALHOUN, R.J. 1972. Spectral resolution of breakwater reflected waves. Journal of the waterways, harbours and coastal engineering division. ASCE. Vol. 98, WW4, pp. 443–460.

URSELL, F., DEAN, R.G. and YU, Y.S. 1960. Forced small-amplitude water waves: A comparison of theory and experiment. Journal of Fluid Mechanics. Vol. 7, no. 3, pp. 33–52.

VAN HIJUM, E. 1985. On modelling from grass to Dolosse. In physical modelling in coastal engineering. Ed. Dalrymple, R.A., Balkerma, Rotterdam.

VAN DE MEER, J.W. 1985. Stability of rubble mound revetments and breakwaters under random wave attack. Proc. conf. on Developments in Breakwaters, Inst. of Civil Engrs, London, England.

VAN WEALE, B.J. and HERBICH, J.B. 1972. Wave reflection and transmission for pile arrays. Proc. 13th conf. on Coastal Engineering, Vancouver, Canada. Chapter 110, pp. 1935–1954.

VERLEY, R.L.P. and MOE, G. 1979. The forces on a cylinder oscillating in a current. UHL report STF 60 A79061. Norwegian Institute of Technology, Norway.

VOLKER, R.E. 1969. Non-linear flow in porous media by finite elements. Journal of the hydraulics division. ASCE. Vol. 95, HY6, pp. 2093–2114.

WARD, J.C. 1964. Turbulent flow in porous media. Journal of the hydraulics division. ASCE. Vol. 90, HY5, pp. 1–12.

WECKMANN, J., BIGHAM, G.N. and DIXON, R.A. 1983. Reflection characteristics of a wave absorbing pier. Proc. ASCE conf. Coastal Structures '83, Virginia, U.S.A., pp. 953–960.

WHALIN, R.W. and CHATHAM, C.E. 1974. Design of distorted wave models. Proc. 14th conf. on Coastal Engineering, Copenhagen, Denmark. Chapter 122, pp. 2102–2121.

WHILLOCK, A.F. 1981. An appraisal of rubble mound breakwaters. The Dock and Harbour Authority. November, Vol. 62, pp. 186–189.

WILKINSON, A.R. and ALLSOP, N.W.H. 1983. Hollow block armour units. Proc. ASCE conf. Coastal Structures '83, Virginia, U.S.A., pp. 208–221.

WILSON, K.W. and CROSS, R.H. 1972. Scale effects in rubble-mound breakwaters. Proc. 13th conf. on Coastal Engineering, Vancouver, Canada. Chapter 106, pp. 1873–1884.